DTIC FILE COPY

AFWAL-TR- 87-4139
VOLUME II

PROCEEDINGS OF THE 1987 TRI-SERVICE CONFERENCE ON CORROSION

Fred H. Meyer Jr., Editor
Air Force Wright Aeronautical Laboratories
Materials Laboratory

MAY 1987

U.S. Air Force Academy, Colorado

AD-A189 660

Approved for public release; distribution unlimited.

DTIC
ELECTE
MAR 0 2 1988
S D
H

MATERIALS LABORATORY
AIR FORCE WRIGHT AERONAUTICAL LABORATORIES
AIR FORCE SYSTEMS COMMAND
WRIGHT-PATTERSON AFB, OHIO 45433-6533

88 3 01 096

NOTICE

When Government drawings, specifications, or other data are used for any purpose other than in connection with a definitely related Government procurement operation, the United States Government thereby incurs no responsibility nor any obligation whatsoever; and the fact that the government may have formulated, furnished, or in any way supplied the said drawings, specifications, or other data, is not to be regarded by implication or otherwise as in any manner licensing the holder or any other person or corporation, or conveying any rights or permission to manufacture use, or sell any patented invention that may in any way be related thereto.

This report has been reviewed by the Office of Public Affairs (ASD/PA) and is releasable to the National Technical Information Service (NTIS). At NTIS, it will be available to the general public, including foreign nations.

This technical report has been reviewed and is approved for publication.

Fred H. Meyer

FRED H. MEYER
Corrosion Control/Non-Destructive
Evaluation Group
Systems Support Division

Thomas D. Cooper by RW

THOMAS D. COOPER, Chief
Materials Integrity Branch
Systems Support Division
Materials Laboratory

FOR THE COMMANDER

Warren P. Johnson by MK

WARREN P. JOHNSON, Chief
Systems Support Division
Materials Laboratory

If your address has changed, if you wish to be removed from our mailing list, or if the addressee is no longer employed by your organization, please notify AFWAL/MLSA, W-PAFB, OH 45433 to help us maintain a current mailing list .

Copies of this report should not be returned unless return is required by security considerations, contractual obligations, or notice on a specific document.

Unclassified
SECURITY CLASSIFICATION OF THIS PAGE

AD-A189660

REPORT DOCUMENTATION PAGE

Form Approved
OMB No. 0704-0188

1a. REPORT SECURITY CLASSIFICATION Unclassified	1b. RESTRICTIVE MARKINGS
2a. SECURITY CLASSIFICATION AUTHORITY	3. DISTRIBUTION/AVAILABILITY OF REPORT Approved for public release; distribution is unlimited.
2b. DECLASSIFICATION/DOWNGRADING SCHEDULE	
4. PERFORMING ORGANIZATION REPORT NUMBER(S)	5. MONITORING ORGANIZATION REPORT NUMBER(S) AFWAL-TR-87-4139, Volume II
6a. NAME OF PERFORMING ORGANIZATION Materials Integrity Branch Systems Support Division 6b. OFFICE SYMBOL (If applicable) AFWAL/MLSA	7a. NAME OF MONITORING ORGANIZATION
6c. ADDRESS (City, State, and ZIP Code) AFWAL/MLSA Wright-Patterson AFB OH 45433-6533	7b. ADDRESS (City, State, and ZIP Code)
8a. NAME OF FUNDING/SPONSORING ORGANIZATION Materials Laboratory 8b. OFFICE SYMBOL (If applicable) AFWAL/MLSA	9. PROCUREMENT INSTRUMENT IDENTIFICATION NUMBER
8c. ADDRESS (City, State, and ZIP Code) AFWAL/MLSA WPAFB OH 45433-6533	10. SOURCE OF FUNDING NUMBERS PROGRAM ELEMENT NO. / PROJECT NO. / TASK NO. / WORK UNIT ACCESSION NO.

11. TITLE (Include Security Classification)
Proceedings of the 1987 Tri-Service Conference on Corrosion

12. PERSONAL AUTHOR(S)
Fred H. Meyer, Jr. (Editor)

13a. TYPE OF REPORT	13b. TIME COVERED	14. DATE OF REPORT (Year, Month, Day)	15. PAGE COUNT
Final	FROM 1/86 TO 5/87	May 1987	466

16. SUPPLEMENTARY NOTATION

17. COSATI CODES			18. SUBJECT TERMS (Continue on reverse if necessary and identify by block number)
FIELD	GROUP	SUB-GROUP	

19. ABSTRACT (Continue on reverse if necessary and identify by block number)
This report is a compilation of the papers presented at the 1987 Tri-Service Conference on Corrosion held at the Air Force Academy, Colorado on 5-7 May 1987.

20. DISTRIBUTION/AVAILABILITY OF ABSTRACT ☒ UNCLASSIFIED/UNLIMITED ☐ SAME AS RPT. ☐ DTIC USERS	21. ABSTRACT SECURITY CLASSIFICATION Unclassified
22a. NAME OF RESPONSIBLE INDIVIDUAL Fred H. Meyer	22b. TELEPHONE (include Area Code) (513) 255-5117 22c. OFFICE SYMBOL AFWAL/MLSA

DD Form 1473, JUN 86 Previous editions are obsolete.

SECURITY CLASSIFICATION OF THIS PAGE
Unclassified

FOREWORD

This report was compiled by the Materials Integrity Branch, Systems Support Division, Materials Laboratory, Air Force Wright Aeronautical Laboratories, Wright-Patterson AFB, Ohio. It was initiated under Task 24180704 "Corrosion Control & Failure Analysis" with Fred H. Meyer, Jr. as the Project Engineer. The 1987 Tri-Service Conference on Corrosion is a follow-up of eight prior conferences held in 1967, 1969, 1972, 1974, 1976, 1978, 1980 and 1983.

This Report (Vol I, Vol II) includes all available papers from the 1987 Tri-Service Conference on Corrosion.

This technical report was submitted by the editor.

Proceedings of Prior Conferences are available in:

1. AFML-TR-67-329 (1967) (AD 826-198)
2. MCIC 73-19 (1972) (AD 771345)
3. AFML-TR-75-42 Vol I, Vol II (1974) (ADA 021053, ADA 029934)
4. MCIC-77-33 (1976) (ADO 49769)
5. MCIC-79-40 (1978) (AD A- 73054)
6. AFWAL-TR-81-4019 Vol I, Vol 2 (1980) (ADA 106803)
   (ADA 115785)
7. 1983 Tri-Service Corrosion Conference Proceeding Naval Ship R&D Center Annapolis, MD 20084.

The purpose of the 1987 Conference was to continue interservice Coordination in the areas of corrosion research and corrosion prevention and control. Specifically, the objectives were to make Department of Defense personnel, contractors and interest individuals aware of the important Corrosion problems in Military equipment, to present the status of significant corrosion research projects currently pursued by the military services and to provide a general forum for exchange of corrosion prevention and control information. (Approved)

DTIC COPY INSPECTED 1

Accession For
NTIS GRA&I ☑
DTIC TAB ☐
Unannounced ☐
Justification
By
Distribution/
Availability Codes
Dist | Avail and/or Special
A-1

TABLE OF CONTENTS

VOLUME II

SESSION A - SPECIAL TOPICS - ARMY..... 1

Hydrogen Embrittlement Susceptibility of High Strength ESR 4340 Steel Alloys for Ballistically Resistant/Tolerant Components..... 3

Politaconic Acid Macromolecule Primer for Adhesive Bonding and Corrosion Control of Aluminum... 16

Environmental Exposure Test of M151A2 Vehicle Bodies..... 29

Corrosion and Corrosion Inhibition of Metals/Alloys in Methyphosphonic Difluoride..... 70

SESSION B - SPECIAL TOPICS - NAVY..... 109

Development of Microencapsulated DNBM Quaternary Ammonium Inhibitors for Paints..... 111

Inadequacies of EMI-Seal Material: A Corrosion Study..... 128

Stress Corrosion Cracking Properties of Al-Li Alloys.... 142

Trends in Underwater Shipboard Paints..... 150

Corrosion of Tungsten Alloys in Marine Environments..... 165

Corrosion and Fatigue Properties of FeCrB/Si Metallic Glass Wires in Aqueous Environments..... 187

SESSION A - SPECIAL TOPICS - II..... 203

Surface Conditioning Products as Tools for Corrosion Removal and Corrosion Prevention..... 205

The Effect of Titanium Reinforcement on the Life of Positive Grids in Lead-Acid Batteries..... 220

NBC Contamination Survivability of Army Material..... 235

Recent Advances in Metallic/Ceramic Coatings for Corrosion Control in Military Applications..... 259

BEST AVAILABLE COPY

TABLE OF CONTENTS

VOLUME II

CONTINUED

Carboxylate Formation at the Interface between a Polyimide Coating and Colbalt. 280

Ion Beam Alloying of Aluminum for Corrosion Resistance 303

Agenda for Advancing Electrochemical Science and Technology 333

SESSION B - Aircraft Corrosion. 341

Water Based Primers for Structural Adhesive Bonding of Aircraft 343

Preventing Aircraft Corrosion by Predictive Corrosion Modeling 359

Vanadic Hot Corrosion of Gas Turbine Blade Coating Materials. 386

Attendance List 413

Late Papers-Received After Deadline 426

The Air Force Corrosion Program - 1987. 427

Validation of Nitronic 33 Stainless Steel in Reinforced and Prestressed Concrete 439

BEST AVAILABLE COPY

SESSION A
SPECIAL TOPICS - ARMY

Chairman
Milton Levy
Army Materials Technology Lab

HYDROGEN EMBRITTLEMENT SUSCEPTIBILITY OF HIGH STRENGTH ESR 4340 STEEL ALLOYS FOR BALLISTICALLY RESISTANT/TOLERANT COMPONENTS

BY
Louis Raymond
L. Raymond & Associates
Newport Beach, CA 92658-7925

and

Albert A. Anctil
Army Materials Technology Laboratory
Wacertown, MA 02172-0001

ABSTRACT

This program focuses on the need to improve the resistance of high strength steels to hydrogen embrittlement or hydrogen stress cracking. Variations in heat treatment and modifications in alloy composition of electroslag remelted 4340 steel at 53 HRC were extensively explored. Target goals were established in terms of threshold stress intensity parameter, and damage tolerance index. In general, all alloy additions improved KIhem. The addition of 0.1% vanadium appears to be the most significant individual modification to ESR 4340 steel in that it alone provides the same gains as the more heavily alloyed ESR 4340 steels. The results must be somewhat qualified because the hardness of ESR 4340V was 50 HRC instead of the intended 53 HRC. Silicon additions of about 1.5% tended to maximize the benefits from alloy modifications. Although within an alloy system the heat treatment effects were minor or secondary relative to alloy additions, the use of an intermediate quench and subzero cooling appeared to maximize the benefits from heat treatment. Increasing the threshold KIhem was not directly related to tempering temperature as anticipated. Overall, KIhem was increased from 10 ksi SQR(in.) to a maximum value of about 15 ksi SQR(in.). Other improvements must be based on nonconventional approaches to thermal processing.

1.0 INTRODUCTION

Ballistically resistant advanced helicopter steel components can use either high-strength or high-hardness (53HRC) ESR-steels, or pay a weight penalty and use thicker, lower-hardeness (43HRC) ESR-steels. Reoccuring hydrogen embrittlement problems in fracture critical members is the reason many designers are making this change and paying the weight penalty. Because of the extensive use of high-strength steels in current designs, the solution of going to lower-strength steels has limited viability, until the weight penalty becomes too severe. These weight penalties can only be avoided by improving the hydrogen embrittlement resistance of high-strength or high-hardness (53$\pm$1HRC) ESR 4340 steel.

The susceptibility to hydrogen assisted stress cracking or hydrogen embrittlement is often measured in terms of a threshold stress intensity parameter under conditions of stress corrosion cracking, KIscc. Implied is testing under conditions of an open circuit potential in an aqueous solution. During test, cathodic charging conditions are used that represent conditions of galvanic coupling often found in a service environment. A -1.2V potential is applied that simulates the sacrificial anodes of a zinc coating on steel. Because of this difference, the threshold stress intensity parameter under conditions that produce hydrogen embrittlement is designated as KIhem for the purpose of this report. Under these conditions, atomic hydrogen is produced on the surface while the sample is under stress.

Other authors report the data as KIscc as a function of potential, but enough data exists to support the contention that they shoud be treated separately. Often KIscc and KIhem are identical, but other times the difference is significant enough to influence alloy selection, as will be illustrated in this report.

The objective of this program is to find an alloy modification or heat treatment that would increase the resistance to hydrogen embrittlement or the hydrogen stress cracking threshold of ESR 4340 steel at 53HRC. Quantitatively, in terms of the threshold stress intensity parameter for hydrogen assisted stress cracking (KIhem), the goals can be identified from the results on a split heat of 4340 steel (Ref 1), where one half the ingot was vacuum arc remelted (VAR) and the other half was electroslag remelted (ESR). Schematically the measured threshold stress intensity results for hydrogen stress cracking, recently presented at a Sagamore conference (Ref 2) are listed in the following table illustrating projected improvements from 10 to 43 ksi. SQR (in) as the hardness is dropped and VAR is used instead of ESR.

THRESHOLD STRESS INTENSITY, KIhem

	53HRC				43HRC	
ESR	- - >	VAR	- - >	ESR	- - >	VAR
10	- - >	15	- - >	29	- - >	43

2.0 TECHNICAL APPROACH

It is the intent of this program to use a selected group of commercially available alloy ESR 4340 type steels that have been relatively well characterized to address the use of alloy modifications or heat treatment to improve the resistance to hydrogen assisted stress cracking instead of melting special heats of steel. A matrix of five materials and four heat treatment conditions were used to evaluate the problem.

The five materials represent two basic alloy steel modifications: (1) increased silicon additions, and (2) increased amounts of carbide formers to affect the secondary hardening characteristics.

Alloying additions were considered because their general effect is to require a higher temperature for a given holding time to secure a given hardness, thus potentially permitting a greater stress relief, when compared to conventional carbon, quenched and tempered steels. The generic guideline being evaluated was that higher tempering temperatures produce increased resistance to stress corrosion cracking for the same hardness level of a tempered martensitic steel.

Modifications in silicon were selected to represent non-carbide forming alloying elements. Increased amounts of silicon are known to improve the resistance of a quenched steel to softening. Amounts varying from as much as °0.5% to 2.0% have been shown to increase the hardness after tempering by as much as 4HRC.

Therefore, three of the five steels selected represent one grouping designed to illustrate the effect of increased amounts of silicon from 0.25%, to 1.5% to 2.5%. Conventional alloy steels of ESR 4340 (baseline), ESR 4340M or ESR 300M, and the new ESR HP310 alloy steels, respectively, were used to represent this variation in silicon content.

The presence of appreciable amounts of strong carbide forming elements, such as chromiun, molybdenum or vanadium may cause softening to be retarded, or may result in an actual increase in hardness when tempered over a certain range of temperatures. This "secondary hardening" effect should provide a greater hardness for a given tempering temperature than would be obtained with a lower alloyed steel (such as 4340 steel). Therefore, a second grouping reflects an increase in the amount of carbide formers from the conventional ESR 4340 to ESR 4340V that has an additional amount of 0.1% vanadium. The third ESR steel in this group is comercially designated as D6Ac steel. In addition to the 0.1% vanadium D6Ac also has an increase in the carbide formers of chromiun and molybdenum, with a concurrent decrease in the amount of nickel. The increase in molybdenum is almost negated by the decrease in nickel, when the effective resistance to softening of these alloying elements is compared.

Four heat treat conditions were evaluated to address the effect of altering either the residual stress or the amount of retained austenite, which might in turn further affect the resistance to hydrogen assisted stress cracking. In addition to the normal quenched and tempered heat treatment, marquenching was used as an alternative design to reduce the amount of residual stress. Since this delayed quenching treatment might also increase the amount of retained austenite, a liquid nitrogen quench was used as a subzero cooling treatment to complete the austenite to martensite transformation. This treatment was applied as an alternative to both the conventional and marquench heat treatments. Retained austenite as a factor that inhibits or accelerates hydrogen assisted stress cracking has not been clearly established.

Abnormal quantities of retained austenite are affected by the combined action of increasing alloying content, and an excessively high quenching temperature. It should also be recalled that coarse grain and the presence of austenite stabilizing elements, such as nickel and manganese, also favors the retention of austenite.

Transformation of retained austenite upon tempering at a given temperature will be in accordance with the isothermal transformation at that temperature level. Treatments to reduce residual stresses tend to increase the amount of retained austenite.

This program addresses the factors affecting susceptibility to hydrogen stress cracking not from a completely research mechanistic analysis, but from a screening survey type program to identify significant processing parameters.

3.0 EXPERIMENTAL PROCEDURES

3.1 Equipment: Instead of the conventional test method to determine the threshold KIhem, a modified, low-cost technique was employed. The proposed method uses the rapid inexpensive, modular (RIM) SCC-testing system. Only a maximum of five Charpy-sized specimens are required to obtain measurment of KIscc instead of 13 or more large size cantilever beam or wedge opening load (WOL) specimens, conventionally used to obtain one measurement of theshold KIscc or KIhem, as per our designation.

The time of test is also 8-hrs for the RIM SCC-testing system as compared to as many as 5,000 hrs per run-out on a conventional cantilever beam or WOL test.

3.2 Specimens: Charpy-sized specimens will be used in all cases. The RIM SCC-test method is described in Ref. 3. The paper provides background detail of the test method utilized to minimize program cost. A machined (crush ground) notched surface was used instead of a fatique precracked notch. The depth of the notch was 2mm (0.078in.). The root radius was about 0.1mm (3-4mils). A 300F stress relief was employed immediately after all grinding operations.

The test specimen orientation was LT in all cases. As per ASTM E399, the specimen orientation is designated by two letters with the first letter (L) designating the direction of the normal to the crack plane and the second letter (T), designating the crack direction, where L, T and S (short transverse) are the orthogonal directions of the ingot.

3.3 Test Methods: To measure KIhem with the RIM SCC-testing system, one specimen is loaded to fracture to obtain the maximum fracture load. If the fracture load is less than the ultimate tensile strength of the material in magnitude; i.e., 250lb for a 250ksi steel, then the specimen is fracture toughness critical. The full scale load on the chart is then adjusted to be slightly more than the fracture load.

A second specimen is then placed in a hydrogen producing environment, which is a 3.5% salt water solution maintained at -1.2 volts vs a saturated calomel electrode. Conventionally, the specimen is then step-loaded until crack initiation occurs. Initial step-loads of 50, 65, 75, 80, 85, 90, 95, and 100% of the fracture load are used. The specimen is held for one hour at each step. A third specimen is then used to refine the value of the crack initiation load, Pi; for example, if the second specimen initially cracked at 75% of the fracture load, then to more accurately measure the crack initiation load, step-loads of 50, 65, 68, 70, 72, 74, 76 and 78% are used.

The threshold KIhem is then estimated as three tenths of the initiation load, Pi.

Since five specimens did not exist for each test condition, the applied step-loads were modified for this program. A large number of small step increments were used with the limited number of samples available. The fewer the samples, the smaller the increments; the larger the number of steps, the longer the duration of the test, which is equivalent to decreasing the strain rate in a slow strain rate tensile.

Fracture toughness per ASTM E399 can be measured either by conventional slow strain rate techniques to measure KIc or dynamically with an instrumented impact test machine to measure the dynamic fracture toughness, KId. Once crack initiation occurs or Pi is measured, the crack can be extended by fatigue to a crack depth ratio of one-half. To insure specimens were free of hydrogen, they were baked prior to fatigue precracking.

4.0 RESULTS

The KIhem results as a function of heat treatment (ultimate tensile strength) are plotted in FIG. 1. The target tensile strength range has been shaded.

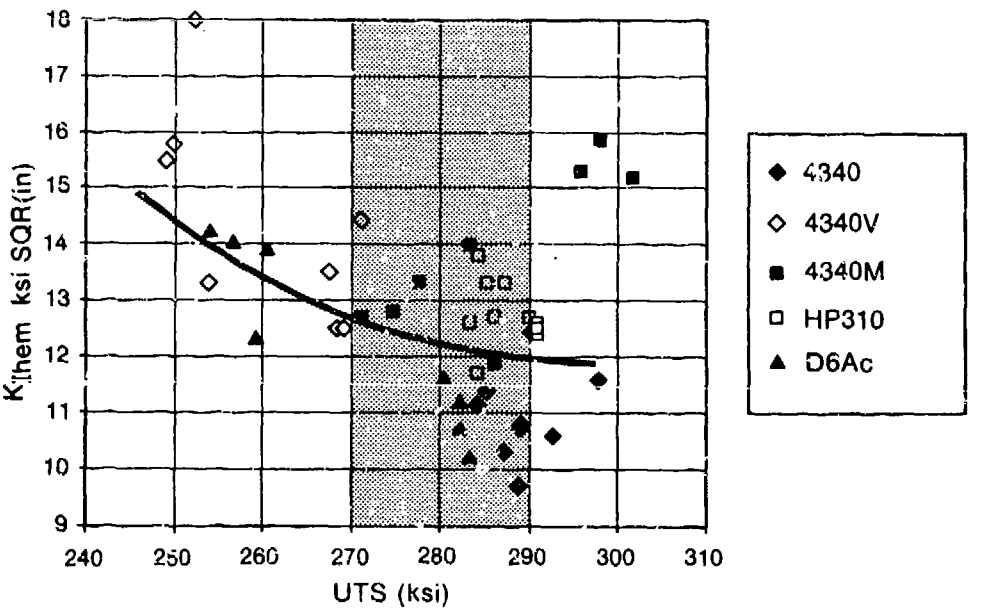

FIG. 1 Threshold KIhem vs Ultimate Tensile Strength.

KIhem, KIc and UTS are plotted in FIG. 2. An overlay of tensile strength illustrates the sensitivity of KIc and KIhem to this parameter. The results are positioned to rank the steels in order of increasing resistance to HEM from left to right.

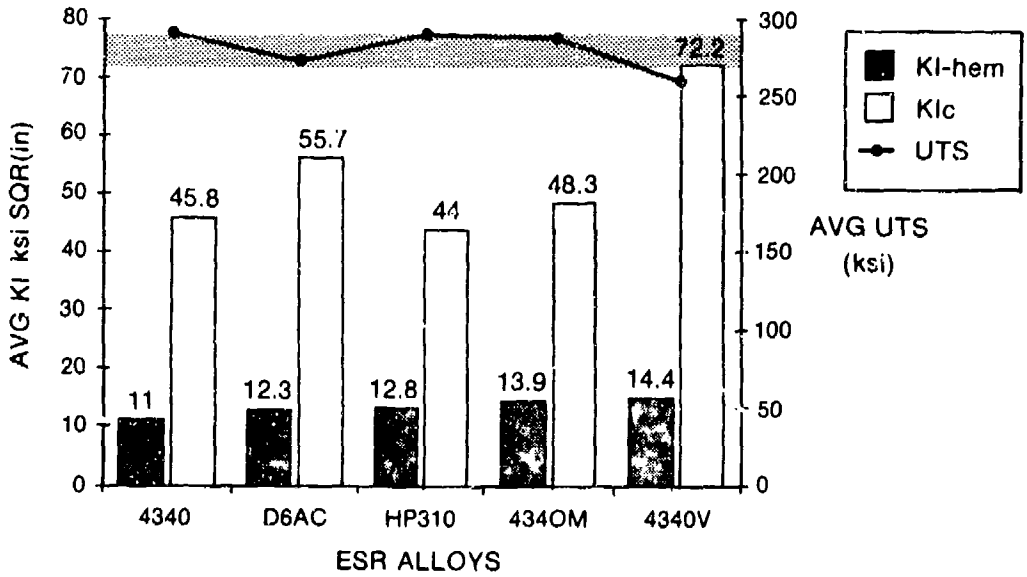

FIG. 2 Relative measures of KIhem and KIc for each alloy with corresponding Ultimate Tensile Strength.

FIG. 3 contains a plot of all of the test results. Superimposed is the trend line (TL) maximum and (TL) minimum taken from the ratio analysis diagram (RAD) developed by Pellini (Ref. 4).

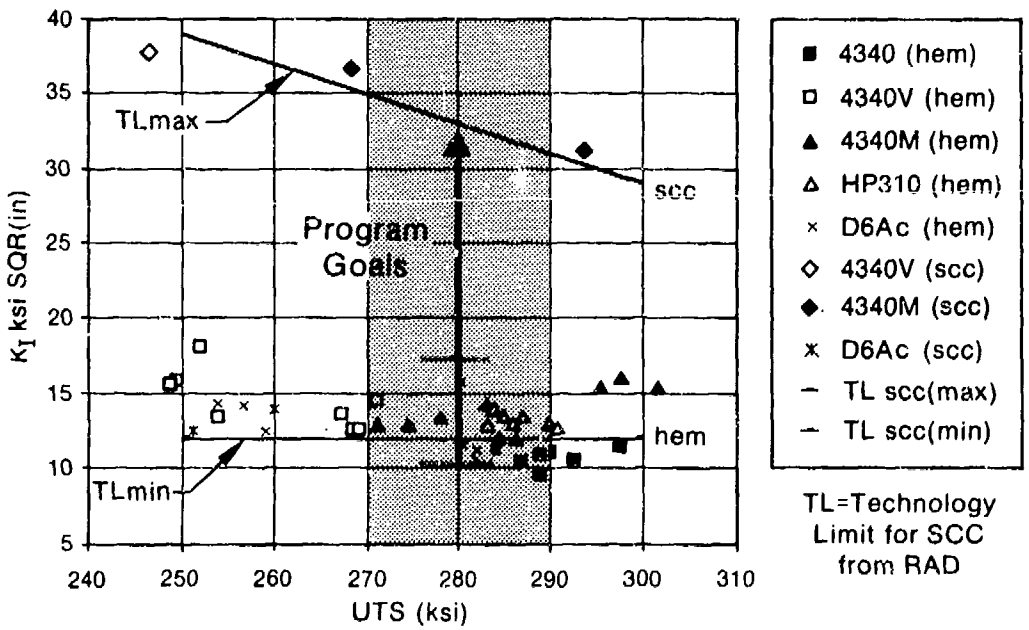

FIG. 3 KIhem and KIscc vs Ultimate Tensile Strength.

Interestingly, the variation in results of this program encompass the min-max range shown in the RAD. This observation suggests that the scatter in the RAD to a large degree, reflects differences in test methods. It should be noted the TLmax for SCC from the RAD coincides with the KIscc or open circuit (-0.6V vs SCE) test results; whereas, TLmin for SCC from the RAD coincides with the KIhem or -1.2V vs SCE test results. The shaded area identifies the target tensile strength range. The program goal is to increase KIscc from a low value of about 10 ksi SQR(in) to TLmax. The horizontal bar at 17ksi SQR(in) reflects the maximum achievements of this program.

4.1 DTI Ratio Analysis: The ratio of the critical stress intensity for fracture (KIc) or for sustained load subcritical crack growth in an environment (KIscc) to the yield strength (YS) is an index of damage tolerance (DTI) because it is related to a critical crack size for fracture or environmentally assisted cracking. In turn, the DTI-ratio is related to the level of nondestructive testing required for quality assurance.

As an example, for a center cracked panel the critcal crack size (a_c) is given by:

$$a_c = 0.25 \text{ o } FS^2 \text{ o DTI-ratio}^2$$

where FS = Factor of Safety or Yield Strength divided by the applied stress.

and DTI-ratio* = KIc of KIscc/Yield Strength (YS)

Obviously, as the factor of safety or DTI-ratio increase, the critical crack size increases, both for fracture, when KIc is used or for environmentally assisted cracking, when KIscc is used in the above equation.

The region of interest in the RAD diagram is above 200ksi yield, or a zone, intersecting with a DTI-ratio for fracture at unity or KIc = YS. The following information can be extracted from the RAD diagram if the estiamte that YS + 40ksi = TS (Tensile Strength) is used.

CRITERIA	UTS = >	240	260	280	300 ksi
	YS = >	200	220	240	260 ksi
Fracture (TL-F)		1.0	0.7	0.5	0.4 SQR(in)
KIc DTI-ratio		31.6	22.1	15.8	12.6 SQR(mil)
(TL-scc)		0.7	0.3	0.15	0.12 SQR(in)
Env DTI-ratio		22.1	9.5	4.7	3.8 SQR(mil)
KISCC/KIC (TL-scc)/(TL-F)		70	43	30	30 %

* For 100% structural integrity, a proof test is required when a_c < .050in or DTI > 1 / (2FS).

4.2 DTI-ratio: Using the previous Table as a guideline to give perspective to the program and establish target properties, the follwing comparisons can be made with regard to properties measured on the ESR steels tested in this program.

With regard to fracture toughness, proposed research programs on innovations to high-strength steel technology have cited DTI-ratio goals of 120/300 (TS) = 120/260 (YS) = 0.4SQR(in) and 60/350 (TS) = 60/310 (YS) = 0.2SQR(in). These goals are consistent with the RAD for they fall on the TL-Fmax curve.

Our target tensile properties are 280±10kis or about 240ksi yield (YS), converted from 53±1HRC. From the RAD, the maximum DTI-ratio for fracture is about 0.5SQR(in) at TL-Fmax.

The measured properties are nominally 50/240 or about 0.2SQR(in) or 40% TL-Fmax, FIG. 4 is a plot of all measured test results.

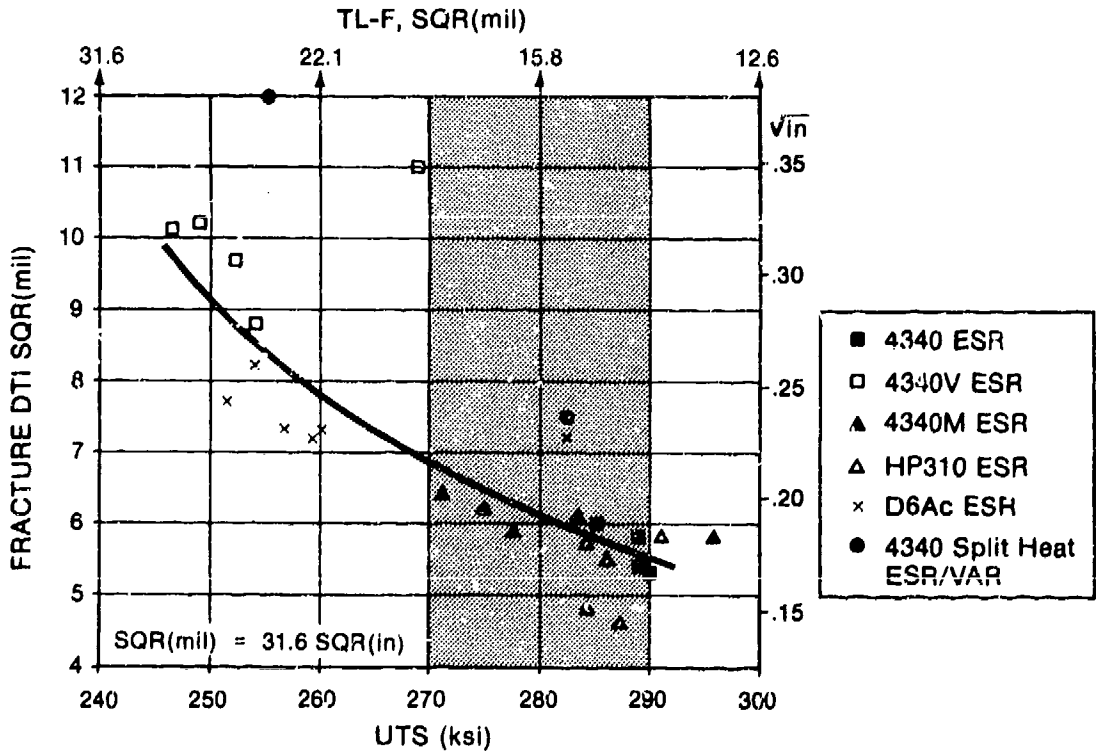

FIG. 4 Average fracture DTI-ratio vs Ultimate Tensile Strength.

With regard to stress corrosion or in our case, hydrogen embrittlement, the target DTI-ratio is 0.15SQR(in) or 4.7SQR(mil) from the RAD TLmax-scc curve. The measured properties averaged 0.05 to 0.06SQR(in) or 1.3 to 2.0SQR(mil) or about 35% TLmax-scc. FIG. 5 is a plot of all measured test results.

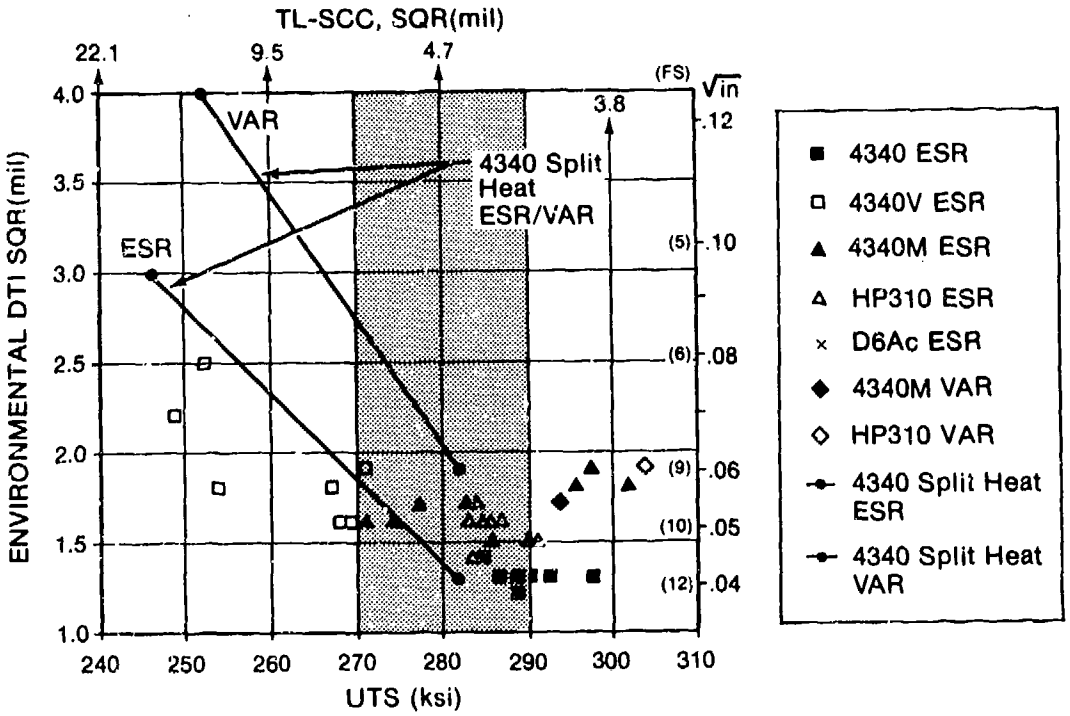

FIG. 5 Average environmental DTI-ratio vs Ultimate Tensile Strength.

FIG. 6 contains average DTI-ratio and UTS for five ESR 4340 alloy steels positioned in order of increasing resitance to hydrogen stress cracking. The shaded band identifies the target tensile properties with 4340V slightly below minimum.

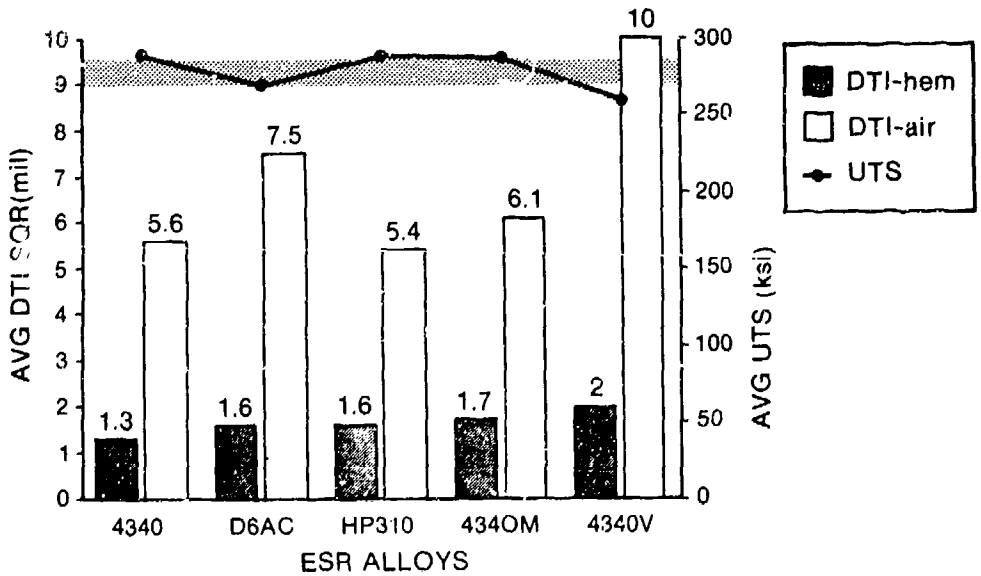

FIG. 6 Relative measures of DTI-hem and DTI-air ratios for each alloy with Ultimate Tensile Strength. DTI in units of SQR(mil) = ($10^{1.5}$) SQR (in) = 31.6 SQR (in)

With regard to the ratio of (KIscc or KIhem)/KIc, a target value is 30% based on TLmax values. The measured properties are about 24% for ESR 4340, 21% for carbide formers, and 30% for silicon additions, primarily reflecting variations in KIc.

5.0 SUMMARY

An increasing number of hydrogen embrittlement failures in ESR 4340 steel at about 53HRC has created a need to improve the resistance of this alloy steel to hydrogen stress cracking. This program was designed to illustrate the effectiveness of alloying and heat treatment on commerical alloys (all ESR) that were selected to represent one group of steels with increasing silicon content and another group with increasing carbide formers. The basis for this selection was the contention that alloying can raise the tempering temperature required to produce a given hardness and thus provide more stress relief. This effect was not found to be true. Above 500F, a decrease is observed.

The objective of this program was quantified by attempting to reach a threshold stress intensity level measured with vacuum arc remelted steels at the same hardness level; i.e., raise KIhem from 10 to 15ksi SQR (in). From this point of view, success was only with 4340M at 300ksi and D6Ac at 250ksi UTS.

Results show that only slight modifications in chemistry, such as the addition of 0.1% vanadium, can sigificantly help to attain the desired vandium goal. Use of 1.5% silicon (4340M, which also has 0.1%V) showed the best promise. Increasing the silicon to 2.5% (HP310) did not perform any better, although both alloy steels performed better than those with additional carbide formers. The gains with the carbide formers were ususally at a sacrifice in strength. The suggestion is that the strength is a more significant variable than the use of a higher tempering temperature.

This program represents a rather exhaustive study that clearly illustrates the difficulty in generating a major advancement such as raising the threshold level to 30-40ksi SQR(in) as with ESR or VAR 4340 steel at 43HRC. The program also clearly illustrates significant differences in stress corrosion testing under an open circuit potential (KIscc) as compared to testing in a cathodically charged hydrogen producing environment, KIhem, which is defintely more severe. This last observation suggests that caution be exercised in using stress corrosion test results for design purposes unless the test conditions are clearly scrutinized. Additional information related to this program may be obtained in REF 5.

6.0 CONCLUSIONS

A large number of possiblilities (five ESR type 4340 alloy steels and four heat treatments) were examined to illustrate that improvements in the resistance of ESR 4340 steel at 280±10ksi ultimate tensile strength, to hydrogen embrittlement are small with conventional variations in heat treatment such as subzero cooling and marquenching. At best, KIhem increases to 15Ksi SQR(in) from 10ksi SQR(in) are obtained. A threshold of fifteen corresponds to a value measured from a split heat of vacuum arc remelted steel at the same strength or hardness (53±1HRC) level.

Silicon additions of 1.5% ESR 4340 steel (300M or 4340M) are more effective than increasing carbide formers, especially if the strength is to be maintained. Additional amounts of silicon to 2.5% (HP310) did not add further improvement to KIscc at this lower strength level. HP310 steel was designed for use at 310ksi ultimate tensile and therefore should also be evaluated at this strength level.

No direct correlation to tempering temperature could be established. Similarly, no distinct advantage was found with marquenching to reduce the severity of the quench or varying the amount of retained austenite by subzero quenching. Although, in general, the least resistant condition of the alloy steels to hydrogen embrittlement appears to be with a conventional quench and temper heat treatment.

The conclusion from observations related to the DTI-ratio is that there is room for improvement in raising KIscc or KIhem to TL-maxscc, and also in raising KIc to TL-Fmax. Focusing on alloy and heat treatment modifications that improve fracture toughness will not necessarily produce concomitant increases in resistance to hydrogen assisted stress cracking.

7.0 REFERENCES

1. Hickey, Jr., C. F. and Anctil A. A., "Split Heat Mechanical Property Comparison of ESR and VAR 4340 Steel," AMMRC TR 83-27, 1983.

2. Raymond, L., "Accelerated KIscc/KIc Testing," Proceedings of the Army Symposium on Solid Mechanics, 1982 - Critical Mechanics Problems in Systems Design, AMMRC MS 82-5, 1982.

3. Raymond, L., "Screening Test for Hydrogen Embrittlement," Proceedings International Symposium for Testing and Failure Analysis, 1981.

4. Pellini, W. S.," Principles of Structual Integrity Technology," Office of Naval Research, p. 188, 1976.

5. Raymond, L., "Study of Effects of Alloying and Heat Treatment on Hydrogen Embrittlement Susceptibility of Electroslag Remelted 4340 Steel," Army Materials Technology Laboratory, MTL TR 86-42, October 1986.

BIOGRAPHY

NAME:
Dr. Louis Raymond

PRESENT AFFILIATION:
L.RAYMOND & ASSOCIATES

TITLE:
Principal Consultant/Owner

FIELD OF INTEREST/RESPONSIBILITIES:
Failure Analysis, Accelerated Corrosion Testing

PREVIOUS AFFILIATIONS/TITLES:
METTEK - Consulting Engineer/Partner
Aerospace Corporation, Materials Science Laboratories - Staff Scientist
Aeronutronic, A Division of the Ford Motor Company - Senior Research Engineer

ACADEMIC BACKGROUND:
Ph.D., Metallurgy, University of California, Berkeley, 1963
M.S., Mechanical Engineering, Carnegie Mellon, 1958
B.S., Mechanical Engineering, Carnegie Mellon, 1956

SOCIETY ACTIVITIES/OFFICES/AWARDS:
Listed: American Men in Science; Who's Who in the West
Member: American Association for the Advancement of Science; Sigma Xi, Pi Tau Sigma (ME honorary); National Academy of Sciences; ASTM; ASM
Awards: NASA Inventors Award; ASTM Testing Award (1978); ASTM Award (1960)

PUBLICATIONS/PAPERS:
Over one hundred and fifty technical publications in the areas of: Stress Corrosion, Hydrogen Embrittlement, Corrosion Fatigue, Fracture Mechanics, Structural Life Cycle, Prediction Analysis and Verification, Failure Analysis, Metal Matrix Composite Materials, Mechanical Metallurgy, Welding and Joining, Manufacturing and Processing, Non-Destructive Inspection, Surface Effects, and Space Processing.

BIOGRAPHY

NAME: Albert A. Anctil

PRESENT AFFILIATION: Army Materials Technology Laboratory

TITLE: Mechanical Engineer

FIELD OF INTEREST/RESPONSIBILITIES: Working in the Metals Research Division and is presently investigating the potential use of specially processed steels in modular armor arrays used to enhance aircraft survivability.

PREVIOUS AFFILIATIONS/TITLES:

ACADEMIC BACKGROUND: Bachelor of Business Administration in Mechanical Engineering and Management from Northeastern University, (June 1960)

SOCIETY ACTIVITIES/OFFICES/AWARDS: Member of ASTM, ASM, ADPA, JTCG/AS chairman Armor/Crew Protection Committee, DoD Certificate of Merit received in 1983.

PUBLICATIONS/PAPERS: Published 34 government technical reports and 20 open literature technical papers.

POLYITACONIC ACID MACROMOLECULE PRIMER FOR ADHESIVE BONDING AND CORROSION CONTROL OF ALUMINUM

T. Sugama, L. E. Kukacka, and N. Carciello

May 1987

Prepared for presentation at the
Tri-Service Corrosion Conference
United States Air Force Academy
Colorado Springs, CO
May 5-7, 1987

PROCESS SCIENCES DIVISION

POLYITACONIC ACID MACROMOLECULE PRIMER FOR ADHESIVE BONDING AND CORROSION CONTROL OF ALUMINUM

T. Sugama, L. E. Kukacka, and N. Carciello

May 1987

Prepared for presentation at the
Tri-Service Corrosion Conference
United States Air Force Academy
Colorado Springs, CO
May 5-7, 1987

PROCESS SCIENCES DIVISION
DEPARTMENT OF APPLIED SCIENCE
BROOKHAVEN NATIONAL LABORATORY
ASSOCIATED UNIVERSITIES, INC.

This work was performed under the auspices of the
U.S. Department of Energy, under contract No. DE-AC02-76CH00016
and supported by the U.S. Army Research Office Program MIPR-ARO-112-87

POLYITACONIC ACID MACROMOLECULE PRIMER FOR ADHESIVE BONDING AND CORROSION CONTROL OF ALUMINUM

T. Sugama, L. E. Kukacka, and N. Carciello
Process Sciences Division
Department of Applied Science
Brookhaven National Laboratory
Upton, NY 11973

ABSTRACT

When polyitaconic acid (PIA) macromolecules are applied as water-soluble primers in polyurethane (PU) adhesive/aluminum adherend joint systems, they interact preferentially with the hydrated oxide aluminum to form hydrogen bonds, and with the isocyanate groups in the adhesive to yield polymer-to-polymer chemical bonding. This chemical coupling between the adhesive and adherend acts significantly to promote interfacial adhesive bonds. The arrangement of a near monolayer of PIA intermediate film plays a key role in governing the adhesion durability of the joint system and the corrosion resistance of the aluminum upon exposure to corrosive fluids. The bond stability and the corrosion resistance are due primarily to the formation of interfacial reaction products which are less susceptible to hydrolysis.

INTRODUCTION

The results from investigations to determine the nature of interfacial interactions which play key roles in promoting adhesive bonding and in improving adhesion durability at interfacial contact zones in PU adhesive/polyacrylic acid (PAA) primer/FPL-etched aluminum (Al) adherend joint systems, have been reported (1). It was concluded that a near monolayer thickness of an intermediate PAA primer film should be applied as a means of occupying all of the available functional groups at the PU adhesive and Al adherend sites. The primer preferentially interacts both with the hydrated oxide of the Al adherend to form hydrogen bonds, and with the isocyanate groups in the PU to yield polymer-to-polymer chemical bonding. The chemical crosslinking resulting from the thin PAA film played a significant role in promoting interfacial adhesive bonds and improved adhesion durability in the joint systems.

When the crosslinking nature and the interplay of polycarboxylic acids were considered on theoretical grounds, it was presumed that PIA macromolecules which have two functional carboxylic acid pendant groups combined to the same backbone carbon atom would be a more effective crosslinking material than PAA which contains a single functional group. The present of a PIA intermediate monolayer will also improve the adhesion bond and its durability at PU/PIA/Al interfacial joints. Therefore, the present study is to report the continuing investigations of the crosslinking nature and the role of the PIA intermediate layer in the PU-to-Al

joint systems. Emphasis was placed on the interface between the carboxylic acid groups of PIA and the PU adhesive or Al adherend. In addition, the nature of the interface produced by intermolecular reactions was studied to determine its role in the corrosion resistance of aluminum upon exposure to corrosive fluids.

Materials

The aluminum used in the experiments was 2024-T3 clad aluminum (Al) sheet containing the following chemical constituents: 92 wt% Al, 0.5 wt% Si, 0.5 wt% Fe, 4.5 wt% Cu, 0.5 wt% Mg, 0.1 wt% Cr, 0.25 wt% Zn, and 0.15 wt% other. The oxide etch of the Al was prepared in accordance with a well known commercial sequence called the Forest Products Laboratory (FPL) process. As the first step in the preparation, the surfaces were wiped with acetone-soaked tissues to remove any organic contamination. They were then immersed in chromic-sulfuric acid ($Na_2Cr_2O_7 \cdot 2H_2O$: H_2SO_4 : Water = 4 : 23 : 73 by weight) for 10 min at 80°C. After etching, the oxide surfaces were rinsed with deionized water at 25°C, and subsequently dried for approximately 15 min at 50°C. For the purpose of comparison with the PIA macromolecule used as a crosslinking primer, three water-soluble polymers, polystyrene-sulfonic acid (PSSA), polyacrylamide (PAM), and polyvinylpyrolidone (PVP), were also employed. All of these macromolecules having an average molecular weight in the range of 40,000 to 120,000, were dissolved in water to prepare a 0.05 to 1.0% polymer solution. In order to deposit these polymer films on the FPL-etched Al surfaces, the Al substrates were immersed for 5 min in the polymer solutions at 25°C, and then dried in an oven at 150°C for 30 min. PU resin was applied as an elastomeric topcoating. Polymerization of the PU was initiated by incorporating a 50% amine curing agent.

RESULTS AND DISCUSSION

The thickness of the primer film deposited on the adherend surfaces was determined using auger electron spectroscopy (AES) in the same manner as was described in our earlier paper (1). The average thickness of the films prepared using macromolecule concentrations of up to 1.0% ranged from approximately 1.0 to approximately 50 nm. With all of the macromolecular species used in this study, a concentration of <0.1% produced a film thickness <4nm. The use of a 0.05% macromolecule concentration produced a near monolayer.

The polyurethane (PU) adhesive was placed onto the adherend surface that was covered with the macromolecule primer, and the PU-coated adherend specimens were then subjected to a 0.1 M NaOH solution at 80°C for 24 hr. All the edges on the adhesive/primer/adherend joints were left unprotected in order to evaluate the degree of susceptibility of the interfacial bonding nature to the hot alkaline solution. This evaluation was accomplished on the basis of data obtained from 180° peel strength tests performed before and after exposure. Some of these data are shown in Figure 1, as a function of macromolecule concentration in the aqueous solution applied on the treated Al surface. The strength value represents the average of three measurements made for each primer concentration.

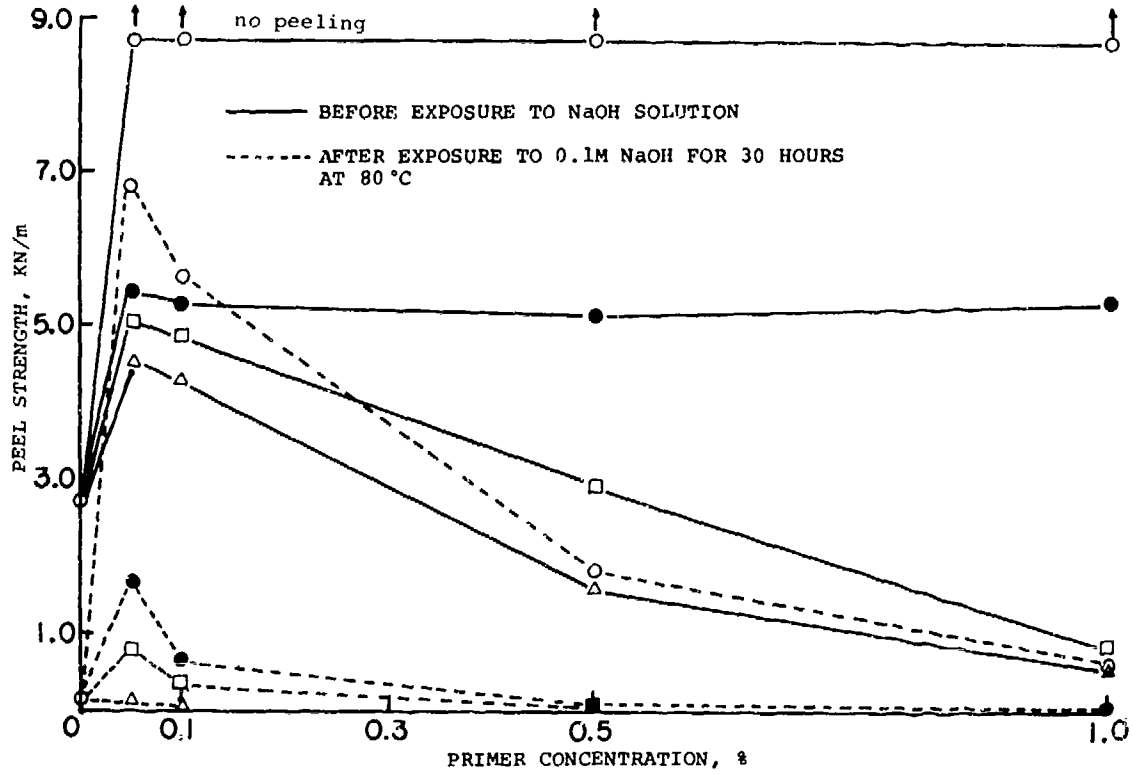

Figure 1. Peel strength as a function of primer concentration for PU/PIA/Al (o), /PVP/ (●), /PAM/ (□), and /PSSA/ (Δ) joint systems before and after exposure for 30 hr to hot alkali at 80°C.

As seen in Figure 1, the peel strength of the unexposed PU/Al control specimens prepared without the use of primers, was increased by more than three times when a PIA intermediate primer layer was applied. When a primer concentration of only 0.05% was used, no peeling occurred, and a strength of at least 8.7 KN/m was attained. This value appeared independent of the primer concentration. In contrast, the use of PVP, PSSA, and PAM primers was less effective. For PVP systems, the use of a primer concentration of 0.05% increased the strength by approximately 90%, and this value also appeared to be independent of concentration. However, the strengths for both the PAM and PSSA joint systems are dependent upon the primer concentration. Increases in strength were attained when concentrations of up to 0.05% were used, but further additions resulted in strength reductions. These can be attributed to the weakness of the primer films.

Sugama, 3

When the joint specimens were exposed to a hot alkali solution, the strength of the control specimen dropped dramatically to a value of 0.05 KN/m, a reduction of 98% from its original strength. A partial separation of the PU film from the Al surface was visually observed.

The durability of PIA-primed joint systems depended mainly on the PIA concentration. The deposition of a thin PIA film (approximately 1.0 nm thickness) derived from the addition of a 0.05% concentration, resulted in a strength reduction of only 22%. The addition of 0.5% PIA which corresponds to a film thickness of approximately 8.5 nm, resulted in a strength retrogression of approximately 80%. Further strength retrogression was noted when a 1.0% concentration (approximately 50 nm thickness) was used. The possible reason for the strength reduction is hydrolytic dissolution of the PIA layer which contains abundant residual hydrophilic carboxylic acid (COOH) groups. This leads to the conversion of the primer from the solid state into a gel state, resulting in increased water absorption, penetration, and swelling phenomena at the interfacial region, and ultimately failure. It is, therefore, obvious that the poor durability of the adhesion bonds is due to failure of the primer. From these observations, it can be concluded that the formation of a thin film of a near monolayer thickness would be much less susceptible to hydrolysis because of the presence of fewer free hydrophilic groups in the intermediate layers. In this case, most of the COOH groups in the monolayers would chemically react with the available reactive groups occupying the outermost interfacial sites on both the PU and Al, and the progression of this interfacial reaction would contribute to the transformation from a hydrolytically unstable interface to a stable one. Producing this transformation at the interfaces is the most important factor in achieving long-term bond durability in chemically aggressive environments.

When compared with the results obtained with PIA primers, the PVP-, PSSA, and PAM- primed joint systems exhibited considerable strength retrogression after exposure to hot alkali. The data also indicated that the rate of strength reduction increased with primer concentration. This trend was quite similar to that obtained from the PIA-primed joint systems.

Based upon these results, it appears that the application of a PIA macromolecule primer with a near monolayer thickness will significantly improve adhesive bonding and the durability of the bond in PU/Al joint systems.

In order to substantiate the nature and mode of the interactions between PIA and Al and Pu, which are responsible for the improvements described above, additional studies were performed. The studies were accomplished using X-ray photoelectron spectroscopy (XPS) and specular reflectance infrared (IR) spectra.

Figure 2 shows the results from XPS high-resolution examinations of the C_{1s} region of a bulk PIA polymer surface and a PIA-Al interface. The C_{1s} peak of the bulk polymer surface (Figure 2-a) was resolved to show the presence of two-carbon species in the binding energy (BE) range of 290.0 to 284 eV. The predominant peak fixed at 285.0 eV as an internal reference, was calibrated with the contribution of the hydrocarbon-type carbon. According to literature data, the component at

BEST AVAILABLE COPY

288.9 eV can be assigned to $-\overset{\overset{\displaystyle O}{\|}}{C}-O-$ in the carboxylic acid of PIA and in the itaconic structure, 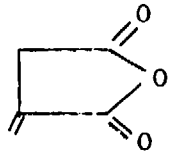 , formed by intra-dehydration reactions between the two adjacent COOH groups located on the same backbone carbon, during the baking process at 150°C (5,6). In the spectrum for the PIA/Al interface (Figure 2-b), attention was given to the COOH group peak shifting to a lower BE. The decrease in BE of 0.4 eV seems to suggest that an intermolecular hydrogen bond is present at the interfaces. Since the FPL treatment not only provides a fresh Al_2O_3 layer covering the Al substrate, but also induces the chemisorbed hydrous layer into the outermost surface sites of Al_2O_3 (7-9), the interaction between the carboxylic acid and the hydrous Al_2O_3 can be predicted as follows.

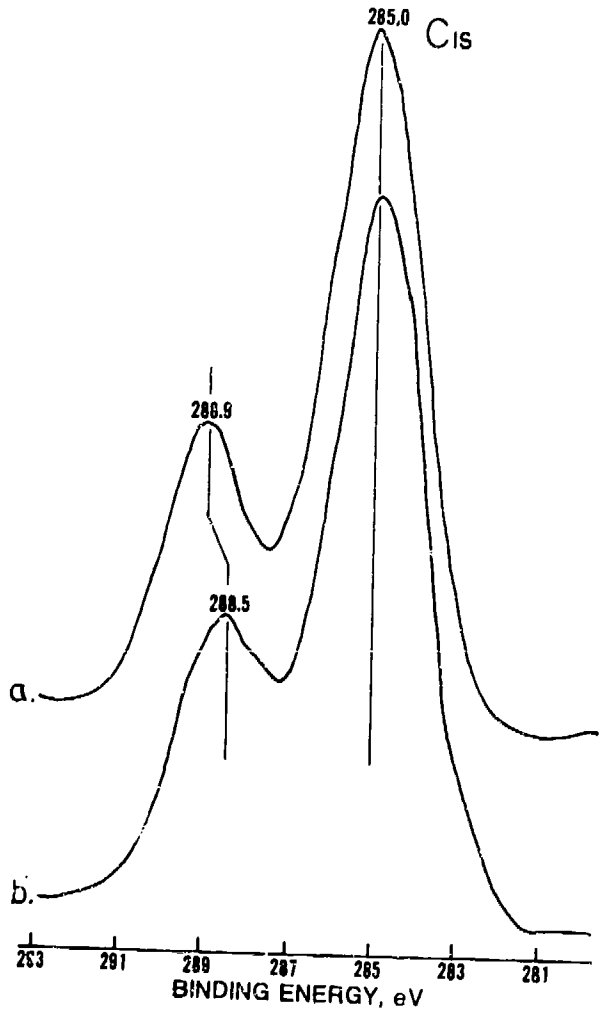

Figure 2. C_{1s} spectra from bulk PIA surface (a) and PIA/Al_2O_3 interface (b).

Sugama, 5

$$- COOH \text{ (proton donor)} + H_2O \text{ --- } O - Al \text{ (proton acceptor)} \rightleftharpoons$$

$$- COO^- \text{ --- } {}^+H_3O \text{ --- } O - Al \xrightarrow{-H_2O} - COO^- \text{ --- } {}^+HO - Al.$$

The nature of this interface produced by a strong ionic interaction serves an essential role in promoting the bond strength at PIA/Al_2O_3 interfaces. Furthermore, the formation of a hydrogen bond provides the maximum resistance to water displacement, thereby improving the adhesion durability in a wet environment.

The most effective crosslinking mechanisms for PIA primers which would promote interfacial bonding and enhance the bond durability, would result from a molecular bridge consisting of a uniform monolayer film containing enough functional groups to occupy all of the available polar sites on both the adhesive and the adherend surfaces. As mentioned earlier, some of the free COOH groups in the PIA macromolecules form a hydrogen bond with the free protons on the hydrated Al_2O_3 surfaces. The other free COOH groups can react with the PU adhesive.

To assess the PIA-PU interfacial bond mechanisms responsible for the improvement of polymer-polymer adhesion, specular reflectance IR analyses were made. The samples were prepared by spin-casting the PU resin onto PIA-primed aluminum mirrors at 4000 rpm, and then curing them in a vacuum oven for up to 3 hr at 110°C. The resultant IR spectra, shown in Figure 3, were recorded over the frequency range of 2500 to 1390 cm^{-1}. The assignments of absorption peaks for the PIA film and the uncured PU resin, marked in Figure 3, are summarized in Table 1. Interesting spectra were obtained from the PU/PIA/Al joint specimens recorded as a function of heating time at 110°C. Of particular interest was the appearance of a new band at 1680 and 1630 cm^{-1} which can be assigned to unsaturated amine, C = N, groups. The C = N peak at 1630 cm^{-1} is due to the conjugation with the neighboring phenyl. The intensity of these new peaks increases conspicuously as the heating time is extended; whereas, that of isocyanate, - N = C = O, groups in the PU resin at 2260 cm^{-1} tends to decrease. This seems to prove that isocyanate groups in PU adjacent to the PIA macromolecules can form a chemical bond with the carboxylic acid of PIA. Therefore, the increasing C = N intensity with extended heat curing time can be explained as a further progression of the intermolecular reaction between the isocyanate of PU and the carboxylic acid of PIA. This interaction mechanism is given below:

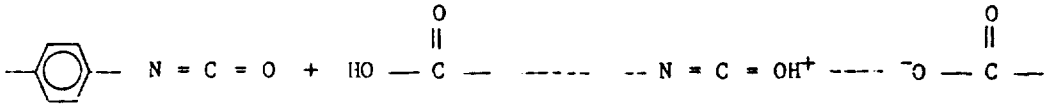

It is believed that this chemical intermolecular reaction is a very important mechanism which greatly enhances the adhesive strength and the bond durability of PU/PIA/Al_2O_3 joints.

Sugama, 6

BEST AVAILABLE COPY

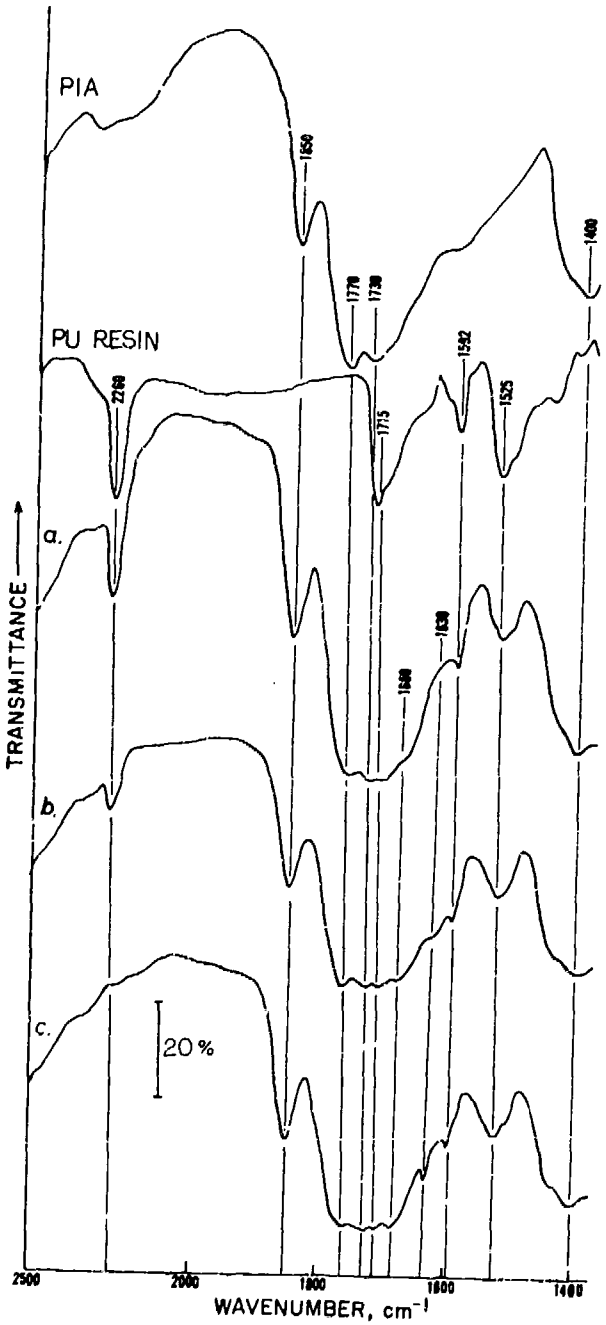

Figure 3. IR spectra of PIA film and PU resin, and PU/PIA interface resulting from various baking times; (a) 0 min, (b) 15 min, and (c) 180 min at 110°C.

Sugama, 7

Table 1. IR Peak Assignments for PIA Film and PU Resin on Al Mirrors

PIA		PU	
Functional group	Frequency (cm^{-1})	Functional group	Frequency (cm^{-1})
Itaconic (-C=O)	1850	-N=C=O	2260
Itaconic (-C=O)	1770	Amide I (-C=O)	1715
-COOH	1730	Phenyl	1592
$-CH_2-$	1400	Amide II (-C=O)	1525

The experimental work was extended further to determine if the interfacial reaction products could be correlated with the results from corrosion testing at Al surfaces in halide-based corrosive fluids. As recently reviewed by Foley (10), the localized corrosion (pitting corrosion) of Al alloys is initiated by the adsorption of the reactive anions such as chloride ions, on the oxide-covered Al surface, and then the adsorbed anions chemically react with the Al ion in the Al_2O_3 lattice or the precipitated Al_2O_3 hydrates. This chemical reaction leads to the transformation of Al_2O_3 and hydrated Al_2O_3 into colloidal transitory Al compounds such as $Al(OH)Cl_2$ and $Al(OH)_2Cl$, and complexes such as $AlCl^{2+}$ and $Al(OH)^{4+}$. The presence of these water-soluble aluminum salts could be related to the nature of the unstable oxide surface. Hence, the adsorption activity of chloride or other aggressive anions can be described as a preliminary step in promoting pitting corrosion on oxide-covered Al.

In an attempt to gain information regarding the effectiveness of the interfacial reaction products as a corrosion protective layer on FPL-etched Al surfaces, the polarization behavior of Al surfaces in PIA/Al and PU/PIA/Al joint systems was determined. The tests were conducted in a deaerated 0.5 M NaCl solution at 25°C. For these tests, the PU deposition on the 3.5-nm thick PIA-coated Al and uncoated Al surfaces was applied by spin-coating at 4000 rpm. The thickness of the deposited PU film was approximately 500 nm. Figure 4 shows the typical polarization curves of log current density vs potential for the FPL-etched Al, PIA/etched Al, PU/etched Al, and PU/PIA/etched Al systems. From the shape of the curves, the potential axis at the transition point from cathodic to anodic is normalized as the corrosion potential, E_C. The anodic polarization side of all specimens was characterized by a rapid increase in the current density at a certain voltage expressed in terms of the critical pit initiation potential, E_{CI} (11,12).

For the etched-Al surface specimens, noteworthy features of the curve are the E_C of -0.75 V, the current peak of 1.2×10^{-1} $\mu A/cm^2$, and the E_{CI} of -0.73 V. A reduction E_C and E_{CI} to less negative potentials was achieved with the thin PIA film overlaid on the Al surface. A possible interpretation for this is that the magnitude of susceptibility to the colloidal nature of hydrated Al_2O_3 was reduced by the formation of hydrogen bonding between the hydroxyl groups of Al_2O_3 hydrates and the COOH groups of PIA. This suggests that the hydrogen bond-based interfacial reaction products have an ability to protect Al surfaces from aggressive corrosive fluids.

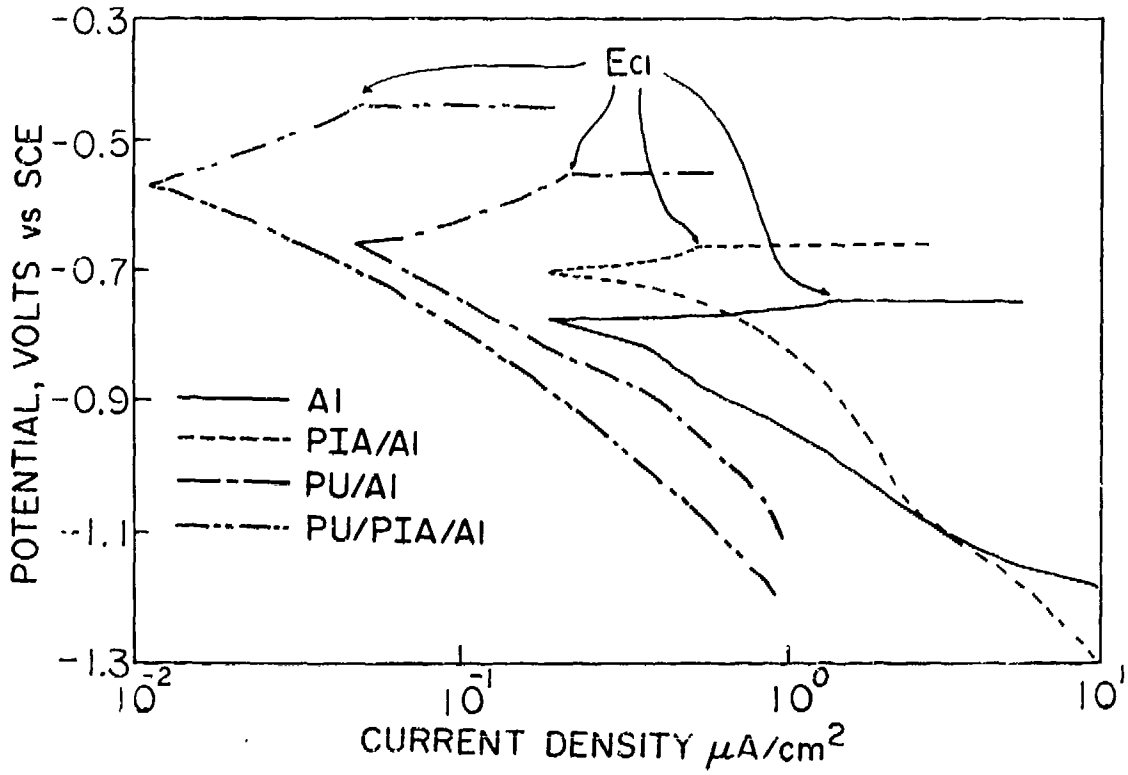

Figure 4. Polarization curves for uncoated, PIA-, PU-, and PU-PIA-coated aluminum immersed in deaerated 0.5 M NaCl solution at 25°C.

On the other hand, an overlay of PU on the Al adherend without PIA primer resulted in a notable reduction in E_C, E_{CI}, and the relative current density at E_C, because of the thick (approximately 500 nm) coating. A further reduction in these elements to less negative potential and current density was obtained with the multiple layer PU/PIA/Al systems.

From the above results, it is apparent that the mechanisms and nature of the reaction products formed in the interfacial region are important factors in protecting Al substrates from corrosion.

CONCLUSION

The use of PIA macromolecules, which contain two functional COOH groups located on the same backbone carbon atom, appear to have great potential as water-soluble primers in PU adhesive/Al adherend joint systems. Preferential reactions between the COOH groups and the hydroxyl groups of hydrated Al_2O_3 and the isocyanate on PU surface sites lead to intermolecular bridging mechanisms which chemically

couple the adhesive and the adherend, thereby promoting interfacial bond strength. A near monolayer thickness of PIA intermediate film is enough to occupy all available functional groups at the adhesive and the adherend surface sites. In addition, the intermolecular reactions contribute significantly to reduce the susceptibility to hydrolysis of the interfacial regions. The nature of this progressive interfacial transformation acts to protect the Al substrate from corrosion.

The use of other hydrophilic macromolecule primers which contain functional $-\overset{\overset{O}{\|}}{\underset{\underset{O}{\|}}{S}}-OH$, $-\overset{\overset{O}{\|}}{C}-NH_2$, and 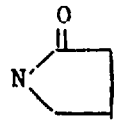 pendant groups seems to be less effective in improving adhesive bonding and durability.

REFERENCES

1. Sugama, T., Kukacka, L. E., Clayton, C. R., and Hua, H. C., "Effects of Polyacrylic Acid Primers on Adhesion and Durability of FPL-Etched Aluminum/Polyurethane Systems," Brookhaven National Laboratory Report, 39300, February 1987 and J. Adhesion Sci. and Tech., (in press).

2. Clark, D. T. and Thomas, H. R., J. Polymer Sci: Polymer Chem., Ed. 14, (1976) 1671.

3. Briggs, D., Brrewis, D. M., and Konieczkre, M. B., J. Mater. Sci., 14, (1979) 1344.

4. Jerome, R., Pireaux, J. J., and Verbist, J. J., Appl. Surface Sci., 27, (1986) 93.

5. Briggs, D. and Seah, M. P., "Practical Surface Analysis by Auger and X-ray Photoelectron Spectroscopy," John Wiley & Sons Ltd., (1985) 385.

6. Dekoven, B. M. and Hagans, P. L., Appl. Surface Sci., 27, (1986) 199.

7. Davis, G. D., Ahearn, J. S., Matienzo, L. J., and Venables, J. D., J. Mater. Sci., 20, (1985) 975.

8. Yanin, A. E., Fin, N., Dodiuk, H., and Klein, I. E., Appl. Surface Sci., 20, (1985) 538.

9. Fin, N., Dodiuk, H., Yanin, A. E., and Drori, L., Appl. Surface Sci., 28, (1987) 11.

10. Foley, R. T., Corrosion, 42, (1986) 277.

11. Foroulis, Z. A. and Thubrikar, M. J., Electrochimica Acta., 21, (1976) 225.

12. Pocius, A. V., in: "Adhesion Aspects of Polymeric Coatings", Mittal, K. L., [Ed.], 173-192, Plenum Press, New York (1983).

BIOGRAPHY

NAME: Toshifumi Sugama

PRESENT AFFILIATION: Brookhaven National Laboratory

TITLE: Associate Chemist

FIELD OF INTEREST/RESPONSIBILITIES: Surface chemistry, corrosion, and interface of ceramic and polymer matrices-based composites.

PREVIOUS AFFILIATIONS/TITLES:

ACADEMIC BACKGROUND: He received his Ph.D. degree in Faculty of Engineering in 1975 from Tokyo Denki University, Japan.

SOCIETY ACTIVITIES/OFFICES/AWARDS: American Chemical Society
Materials Research Society
The Adhesion Society

PUBLICATIONS/PAPERS:

- T. Sugama, L. E. Kukacka, N. Carciello, and J. B. Warren, "Chemisorption Mechanisms and Effect of Polyacrylic Acid on the Improvement in Bond Durability of Zinc Phosphate-to-Polymer Adhesive Joints". J. Materials Sci. 22 (1987) pp. 722-36.
- T. Sugama, L. E. Kukacka, B. G. Galen, and N. B. Milestone, "Characteristics of High Temperature Cementitious Lost-Circulation Control Materials for Geothermal Wells". J. Materials Sci. 22 (1987) pp. 63-75.

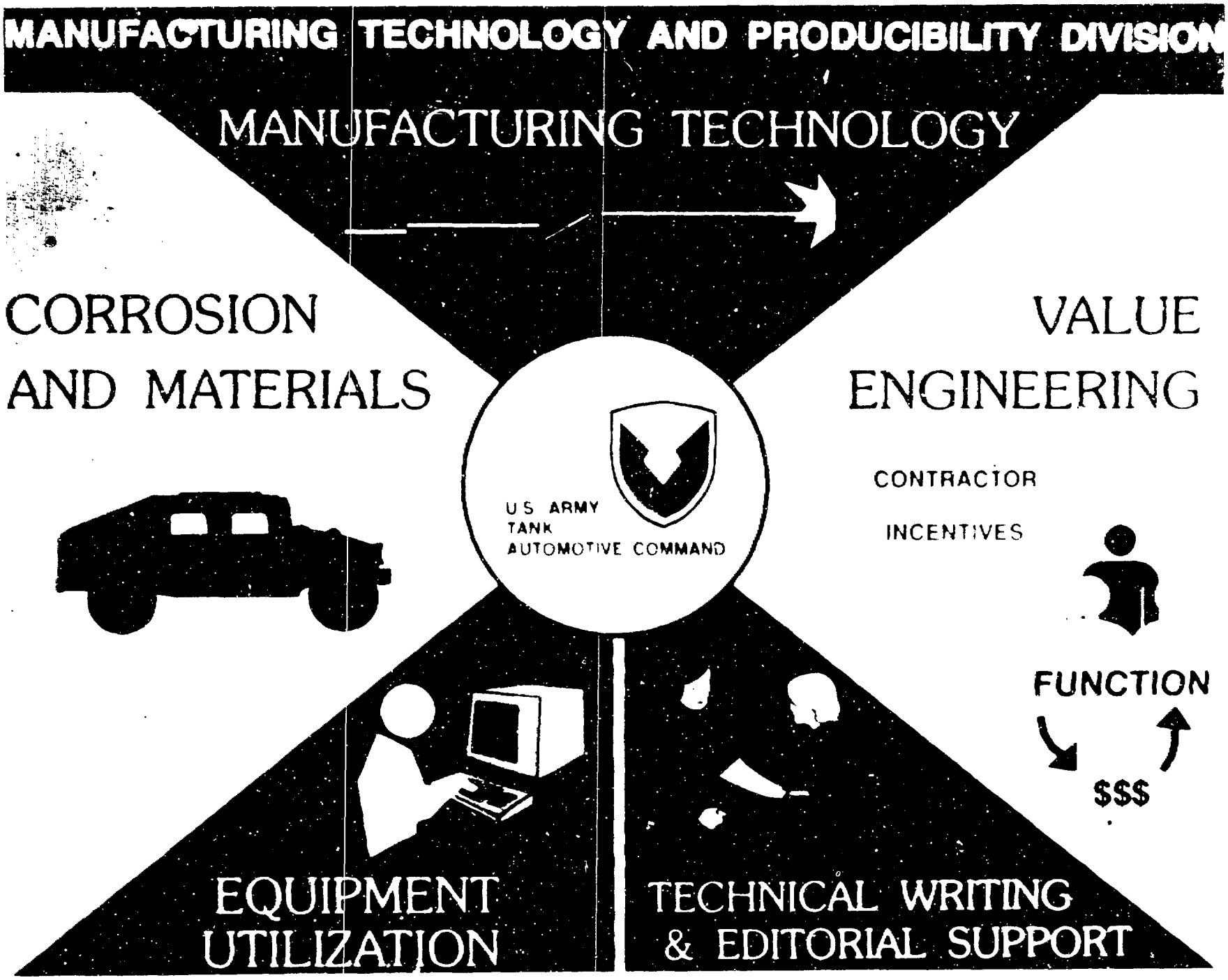
MANUFACTURING TECHNOLOGY AND PRODUCIBILITY DIVISION
MANUFACTURING TECHNOLOGY
CORROSION AND MATERIALS
VALUE ENGINEERING
CONTRACTOR
INCENTIVES
FUNCTION
$$$
U S ARMY
TANK
AUTOMOTIVE COMMAND
EQUIPMENT UTILIZATION
TECHNICAL WRITING & EDITORIAL SUPPORT

ENVIRONMENTAL EXPOSURE TEST OF M151A2 VEHICLE BODIES

SLIDE 1 ON

MY NAME IS GEORGE BUGARIN, I AM CHIEF OF TACOM'S MANUFACTURING TECHNOLOGY AND PRODUCIBILITY DIVISION.

SLIDE 2 ON

TODAY, I WILL PROVIDE YOU AN UPDATE OF OUR ONGOING DOUBLE GALVANIZED BODY EXPOSURE TESTS.

AN OUTLINE OF MY PRESENTATION IS SHOWN ON THIS NEXT CHART.

SLIDE 3 ON

FIRST, I WILL IDENTIFY THE OBJECTIVE OF OUR TEST PROGRAM AND THEN DESCRIBE THE PURPOSE AND THE TYPES OF ENVIRONMENTAL EXPOSURES OF THE PROJECT. THEREAFTER, I WILL INTRODUCE THE TEST VARIABLES, DESCRIBE THE DIFFERENT CONFIGURATIONS AND THEIR PRE-CONDITIONING ASPECTS AND PROVIDE YOU OUR PRELIMINARY RESULTS AND CONCLUSIONS.

ENVIRONMENTAL EXPOSURE TEST OF M151A2 VEHICLE BODIES

SL-2

OUTLINE

- o TEST OBJECTIVE
- o PURPOSE
- o INTRODUCTION
- o TEST PARAMETERS
- o RESULTS
- o CONCLUSION

SL-3

AT THIS TIME I WILL ADDRESS OUR TEST OBJECTIVE AS SHOWN HERE ON THIS NEXT CHART.

SLIDE 4 ON

THE TEST PROGRAM HAS BEEN STRUCTURED TO DETERMINE THE ENVIRONMENTAL EFFECTS OF THE THREE VARIABLES SHOWN.

MOVING ON TO THE PURPOSE OF THE PROGRAM, IT IS SHOWN ON THIS NEXT V-GRAPH.

SLIDE 5 ON

OUR APPROACH IS TO ACCELERATE THE CORROSION EFFECTS BY DIRECT EXPOSURE TO THE FOUR ENVIRONMENTAL ELEMENTS SHOWN HERE.

THE PROGRAM PLAN IS TO EVALUATE COMMERCIAL CORROSION RESISTANT SYSTEMS ON A PRODUCTION BUILT VEHICLE. THE SELECTED DEMONSTRATOR IS THE BODY OF THE M151 A1 JEEP.

TEST OBJECTIVE

DETERMINE ENVIRONMENTAL EFFECTIVENESS OF:

- oo VARIOUS SUBSTRATES
- oo COATINGS
- oo CORROSION PROTECTIVE SYSTEMS

SL-4

PURPOSE

TO ACCELERATE CORROSION/DETERIORATION OF VEHICLE BODIES AND VARIOUS SUBSTRATES BY EXPOSURE TO:

- HI-HEAT
- SUNLIGHT
- HUMIDITY
- SALT AIR

SL-5

SLIDE 6 ON

THESE VEHICLES ARE IDEAL FOR ACCELERATED CORROSION TESTING. BY INCLUSION OF KNOWN CONTROLS, I.E, VEHICLES MANUFACTURED WITH SPECIFIC SUBSTRATE, COATINGS, AND PRESERVATIVES, RELATIVE COMPARISONS OF SERVICE LIFE SHOULD BE PREDICTED. THE VARIABLES WERE CHOSEN FROM PRODUCTS THAT HAVE DEMONSTRATED A HIGH DEGREE OF SUCCESS IN THE COMMERCIAL MARKETPLACE AND EXPOSURE TO ACCELERATED LABORATORY TESTING. THE MAIN VARIABLES SELECTED ARE SHOWN ON THIS NEXT CHART.

SLIDE 7 ON

WE WILL COMPARE THESE VERSUS THOSE CONTROL ITEMS HERE.

THE JEEP BODIES CAME IN TWO DIFFERENT METALLIC CONSTRUCTIONS. WE HAVE APPLIED THESE PRIMERS AND COATINGS. ALSO, WE ARE ASSESSING THE PAYOFF OF APPLYING SPECIFIED RUSTPROOFING COMPOUND.

INTRODUCTION

SL-6

TEST VARIABLES

SUBSTRATE

CONTROL - STEEL
VARIABLE - GALVANIZED STEEL

COATING

CONTROL - ALKYD PRIMER
VARIABLES - EPOXY PRIMER
- CATIONIC EPOXY PRIMER (E-COAT)

CONTROL - ALKYD TOPCOAT
VARIABLES - HIGH-BUILD ACRYLIC
- URETHANE CARC COATING

RUSTPROOFING

CONTROL - WITH RUSTPROOFING MIL-R-46164
VARIABLE - NO RUSTPROOFING

SL-7

NOW TURNING TO THE ACTUAL TEST BODY CONFIGURATIONS. THEY ARE SHOWN ON THIS NEXT CHART.

SLIDE 8 ON

EIGHT (8) VEHICLES WERE PLACED UNDER THIS STATIC TEST PROGRAM. THE DIFFERENCES AND VARIABLES BETWEEN THE TEST ITEMS ARE AS SHOWN.

- FIRST COLUMN IDENTIFIES THE TEST BODIES AND THEIR POSITION BY NUMBER.
- THE SECOND COLUMN SHOWS THE VARIOUS SUBSTRATES.
- THIRD COLUMN DESCRIBES THE PRIMERS APPLIED.
- THE FOURTH COLUMN IDENTIFIES THE SELECTED TOP COATS.
- AND THE LAST COLUMN HAS VEHICLE BODIES WHICH WERE OR WERE NOT RUSTPROOFED.

AS PART OF OUR TEST PLAN ALL TEST ITEMS WERE SUBJECTED TO PRECONDITIONING AS SHOWN HERE:

SLIDE 9 ON

THIS SLIDE SHOWS THE AMOUNT OF MILEAGE PUT ON THE VEHICLE BODIES PRIOR TO START OF OUR TEST. IT IS IMPORTANT TO NOTE THAT THE FIRST SIX (6) BODIES HAD LIMITED ACTUAL OPERATIONAL EXPOSURE. THE TWO VEHICLES (7 & 8) WERE OPERATED FOR 20,000 MILES WITH ACTUAL EXPOSURE TO A MILITARY JEEP ROAD ENVIRONMENT.

SERVICE LIFE PREDICTION

BODY TEST

SITE I.D. NO.	SERVICE LIFE	METAL	PRIMER	TOPCOAT	RUSTPROOF
1	12 YRS.	GALVANIZE	E-COAT	PPG DHT 45323	NO
2	* YRS.	STEEL	EPOXY	CARC	NO
3	12 YRS.	STEEL	E-COAT	PPG DHT 45789	YES
4	7 YRS.	STEEL	ALKYD	ALKYD	NO
5	9 YRS.	STEEL	ALKYD	ALKYD	YES
6	14 YRS.	GALVANIZE	E-COAT	PPG DHT 45323	YES
7	12 YRS.	GALVANIZE	E-COAT	PPG DHT	NO
8	9 YRS.	STEEL	ALKYD	ALKYD	YES

* DUE TO PREMATURE FAILURE OF BODY #2, NO CONCLUSIONS ARE BEING MADE AS TO SERVICE LIFE.

PRECONDITIONING

BODY (1 THRU 6)

PRECONDITIONED FOR 100 MILES

BODY (7 - 8)

PRECONDITIONED FOR 20,000 MILES

SL-9

THIS NEXT CHART DESCRIBES THE ACTUAL PROFILE OF THE 100 MILE PRECONDITION TESTS:

SLIDE 10 ON

O AS NOTED HERE THE VEHICLE WAS WEIGHED, DRIVEN FOR 100 MILES AT 40 MPH OVER GRAVEL ROAD. IT WAS THEREAFTER EXPOSED TO OVERHEAD SALT SPRAY BOOTH, THEN DRIVEN THROUGH A 5% SALT BATH SOLUTION, FOLLOWED BY A DRIVE THROUGH IN A SALT MUD BATH SEVERAL TIMES. THE VEHICLE WAS THEN WEIGHED AGAIN TO DETERMINE PRECISE CHANGES IN WEIGHT.

NOW MOVING TO THE CONDITIONS OF THE 20,000 MILE TEST, THEY ARE SHOWN ON THIS NEXT CHART.

SLIDE 11 ON

VEHICLES 7 & 8 WERE DRIVEN OVER VARIOUS COURSES AND PASSED THROUGH A SALT BATH A MINIMUM OF THREE TIMES PER DAY. THE VEHICLES INCLUDED APPROPRIATE PAYLOADS FOR THE TERRAIN TRAVELED.

100 MILES PRECONDITION TESTS

- o WEIGH VEHICLES
- o 100 MILES GRAVEL ROAD (AT 40 MPH)
- o EXPOSURE OVERHEAD SALT SPRAY BOOTH
- o DRIVE THROUGH SALT BATH SEVERAL CYCLES - 5% SODIUM CHLORIDE SOLUTION.
- o DRIVE THROUGH SALT MUD BATH - SEVERAL CYCLES
- o WEIGH VEHICLE

SL-10

20,000 MILES PRECONDITIONING TEST

- PAVED HIGHWAY (8,000 MILES)
- GRAVEL ROAD (5,400 MILES)
- CROSS-COUNTRY - LEVEL (5,000 MILES)
- CROSS-COUNTRY - HILLY (1,200 MILES)
- COBBLESTONES (400 MILES)
- SALT BATH FORDING PIT (450 CYCLES)

SL-11

FOR MILEAGE ACCUMULATION, THEY WERE DRIVEN OVER FIVE DIFFERENT TEST COURSES AND TRAVELED THRU ASPECIAL SALT BATH FORDING PIT. EVERY 1,000 MILES, WHICH WAS A TEST CYCLE, THE VEHICLES WERE DRIVEN 400 MILES ON PAVED HIGHWAY, 270 MILES ON GRAVEL ROAD, 250 MILES ON CROSS-COUNTRY LEVEL, 60 MILES ON CROSS-COUNTRY HILLY, 20 MILES ON COBBLESTONES, AND THEN PASSED THROUGH THE SALT BATH.

ORIGINALLY, THE 2 VEHICLES (7 & 8) WERE NOT INTENDED TO BE INCLUDED IN OUR STATIC TEST PROGRAM, BUT BECAUSE OF THE MINOR AMOUNTS OF CORROSION DETERIORATION NOTED AFTER 20,000 MILES, IT WAS DECIDED TO FURTHER EXPOSE THESE BODIES AS PART OF OUR PROJECT.

NOW I WILL TURN MY ATTENTION TO THE COATING REQUIREMENTS. THE COATINGS APPLIED TO THE TEST VEHICLES WERE AS SHOWN ON THIS NEXT CHART.

SLIDE 12 ON

THE BODIES WERE PRE-TREATED USING THE SPECIFIED PRIMER. ADDITIONAL PRIMERS AND TOPCOATS WERE APPLIED AND INCLUDED CHEMICAL AGENT RESISTANT COATING, ELECTRO-DEPOSITED PRIMER, ALKYD AND ACRYLIC PAINT. COATING THICKNESSES ARE INDICATED WITHIN THE LAST COLUMN.

COATING THICKNESS REQUIREMENTS

COATING TYPE	SPECIFICATION	THICKNESS
I. PRE-TREATMENT	P-15328 (BLUE WASH PRIMER)	0.3-0.5 MIL
II. PRIMER	CARC MIL-P-53022 (EPOXY)	1.0-1.5 MIL
	ELECTRO-DEP	0.8-1.2 MIL
	ALKYD TT-P-636	1.0-1.5 MIL
III. TOP COAT	CARC MIL-C-46168	1.8-3.0 MIL
	ALKYD MIL-E-2798	1.8-3.0 MIL
	ACRYLIC PPG-DHT-45323	1.8-3.0 MIL
IV. RUSTPROOFING	MIL-C-62218	10 MIL MINIMUM
V. GALVANIZING	G-90	~ 0.8 MIL

SL-12

AFTER THE VEHICLES WERE MANUFACTURED AND PRECONDITIONED, THEY WERE SHIPPED TO THEIR LOCATION AT CAPE CANAVERAL, FLORIDA.

SLIDE 13 ON

THE SITE IS A BEACH FRONT APPROXIMATELY 200 FEET FROM THE OCEAN. ALL EIGHT (8) BODIES WERE INSTALLED ON WOODEN RAILROAD TIES TO THE SAME HEIGHT AS AN ACTUAL VEHICLE WITH WHEELS. THESE BODIES ARE ROTATED 90 CLOCKWISE EVERY FOUR MONTHS DURING THEIR INSPECTION CYCLE.

THE NEXT TWO (2) CHARTS ARE PHOTOS OF A TEST BODY. I WILL DESCRIBE EACH PHOTO AS SHOWN.

SLIDE 14 ON

THIS PHOTO OF BODY(#1) SHOWS ITS INSTALLATION TO THE ACTUAL TEST FIXTURE.

CAPE CANAVERAL FLORIDA TEST SITE

- o BEACH FRONT
- o CLOSE PROXIMITY TO OCEAN

SL-13

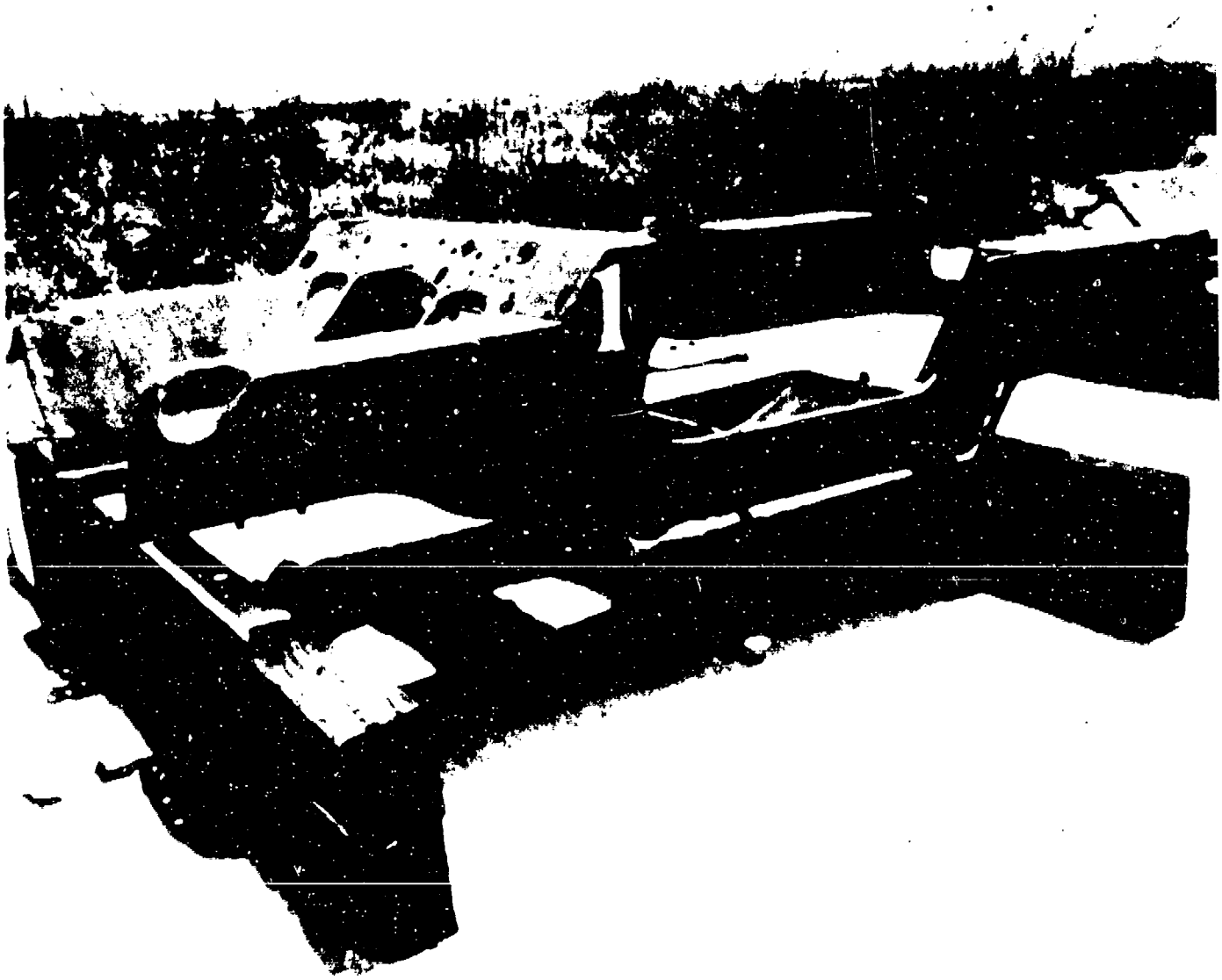

SLIDE 15 ON

THIS PHOTOALSO, OF BODY(#1) IN CLOSE UP, SHOWS THE NICKS AND SCRATCHES THAT WERE NOTED PRIOR TO THE START OF THE TEST. ALL OTHER BODIES WERE INSPECTED IN THIS MANNER PRIOR TO TEST INITIATION.

THE RESULTS TO DATE OF THIS TEST WILL BE PRESENTED HEREAFTER, USING PHOTOS OF THE TEST ITEMS. THESE FIRST RESULTS WERE NOTED AFTER 12 MONTHS OF EXPOSURE IN THE MARINE ENVIRONMENT.

50

SLIDE 16 ON

THIS PHOTO OF BODY 1 REVEALS THAT THE DOUBLE GALVANIZED AND ELECTROCOATED PRIMED BODIES WITH AN ACRYLIC TOP COAT APPEARS SUPERIOR IN CORROSION RESISTANCE.

SLIDE 18 ON

BODY 3 HERE WAS NEXT BEST. THIS ITEM IS THE STEEL BODY WITH THE E-COAT PRIMER AND ACRYLIC TOP COAT WITH RUST-PROOFING COMPOUND APPLIED.

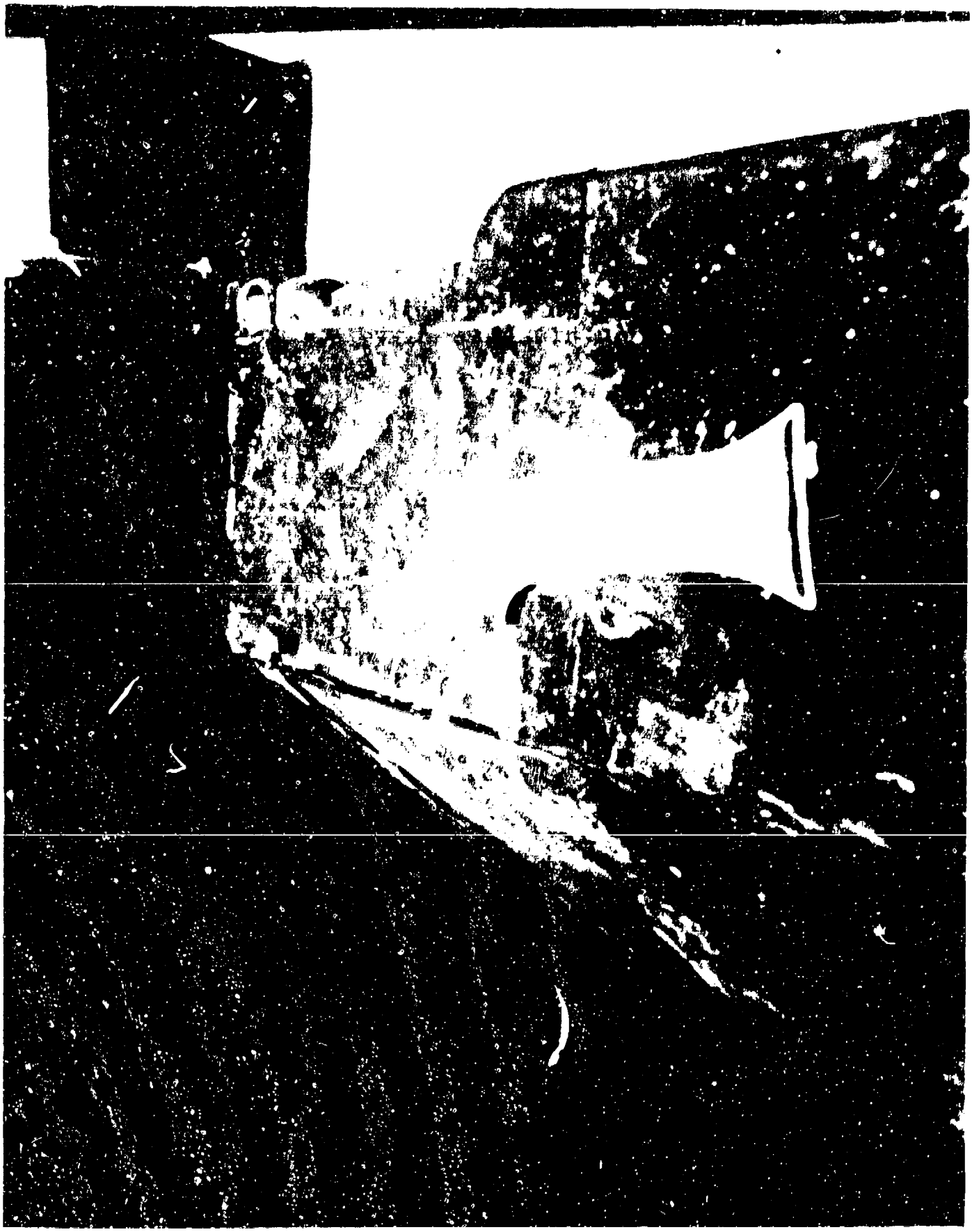

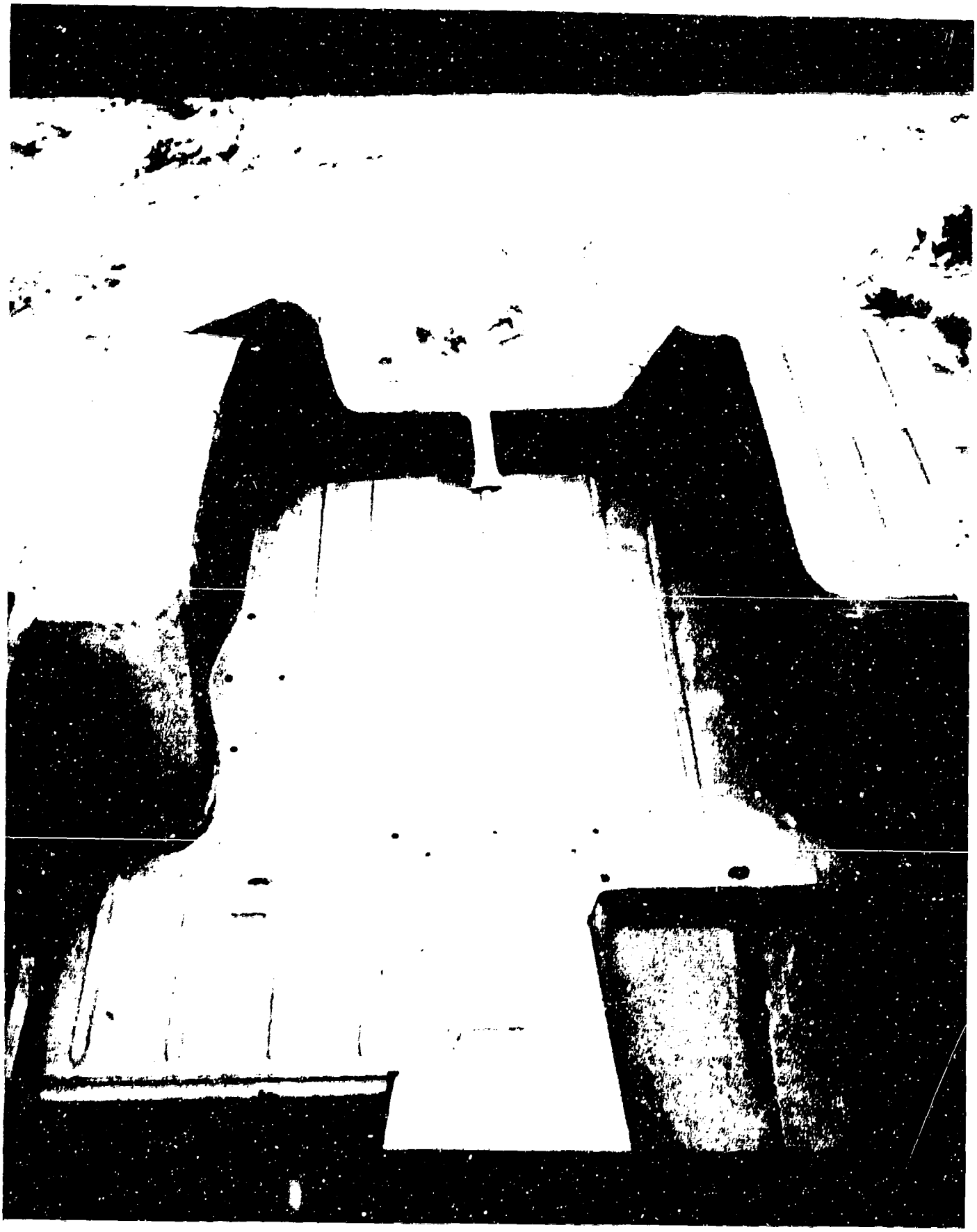

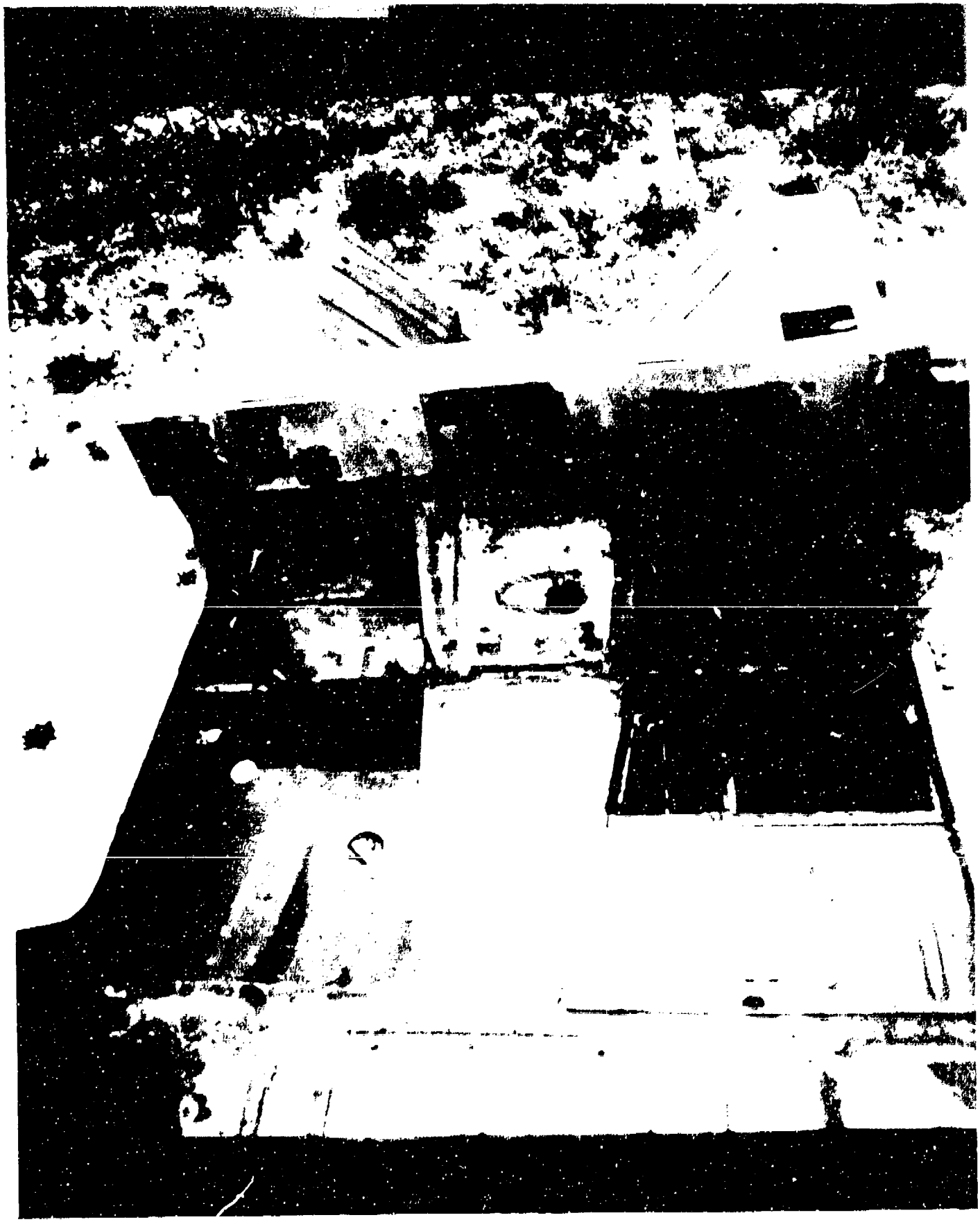

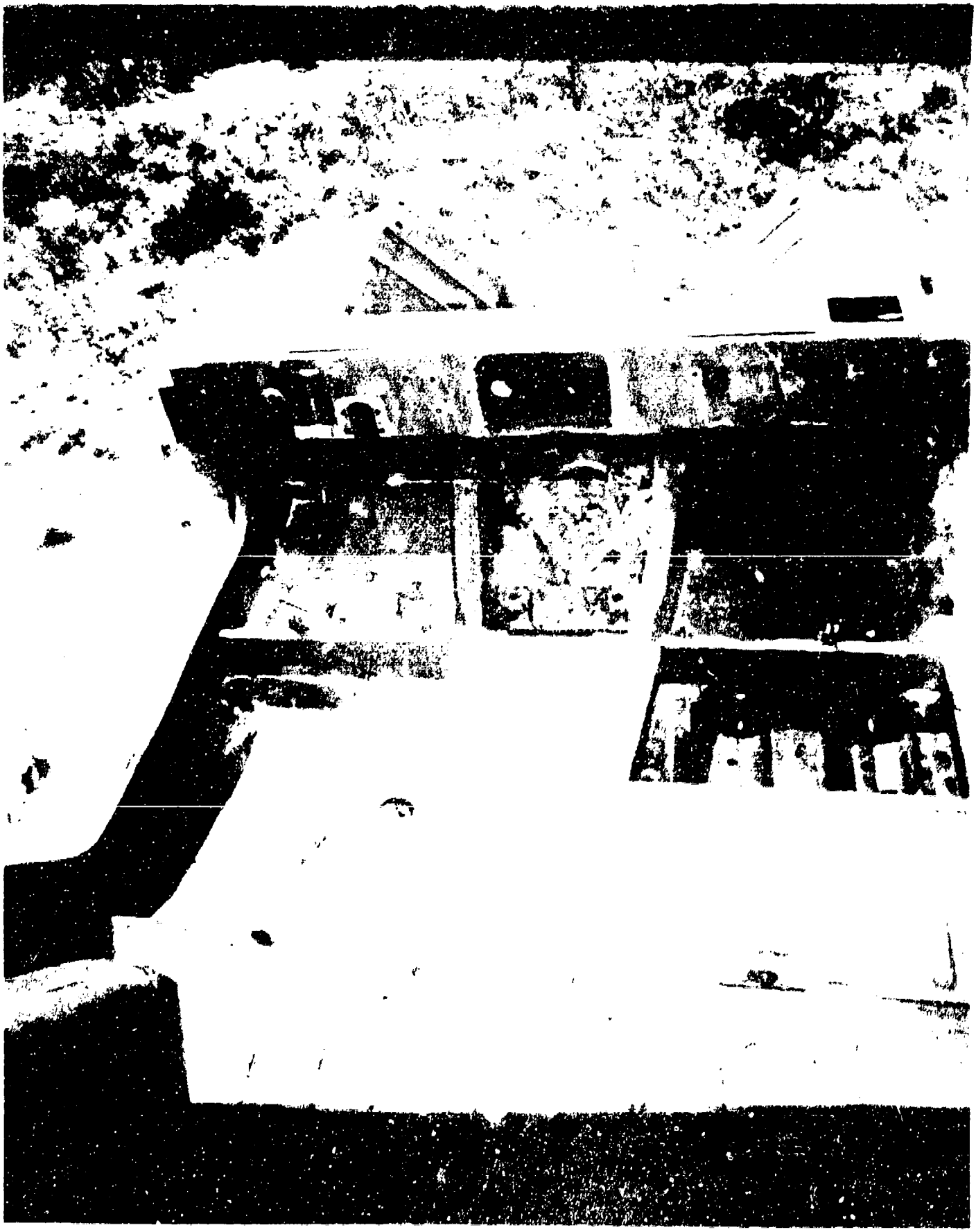

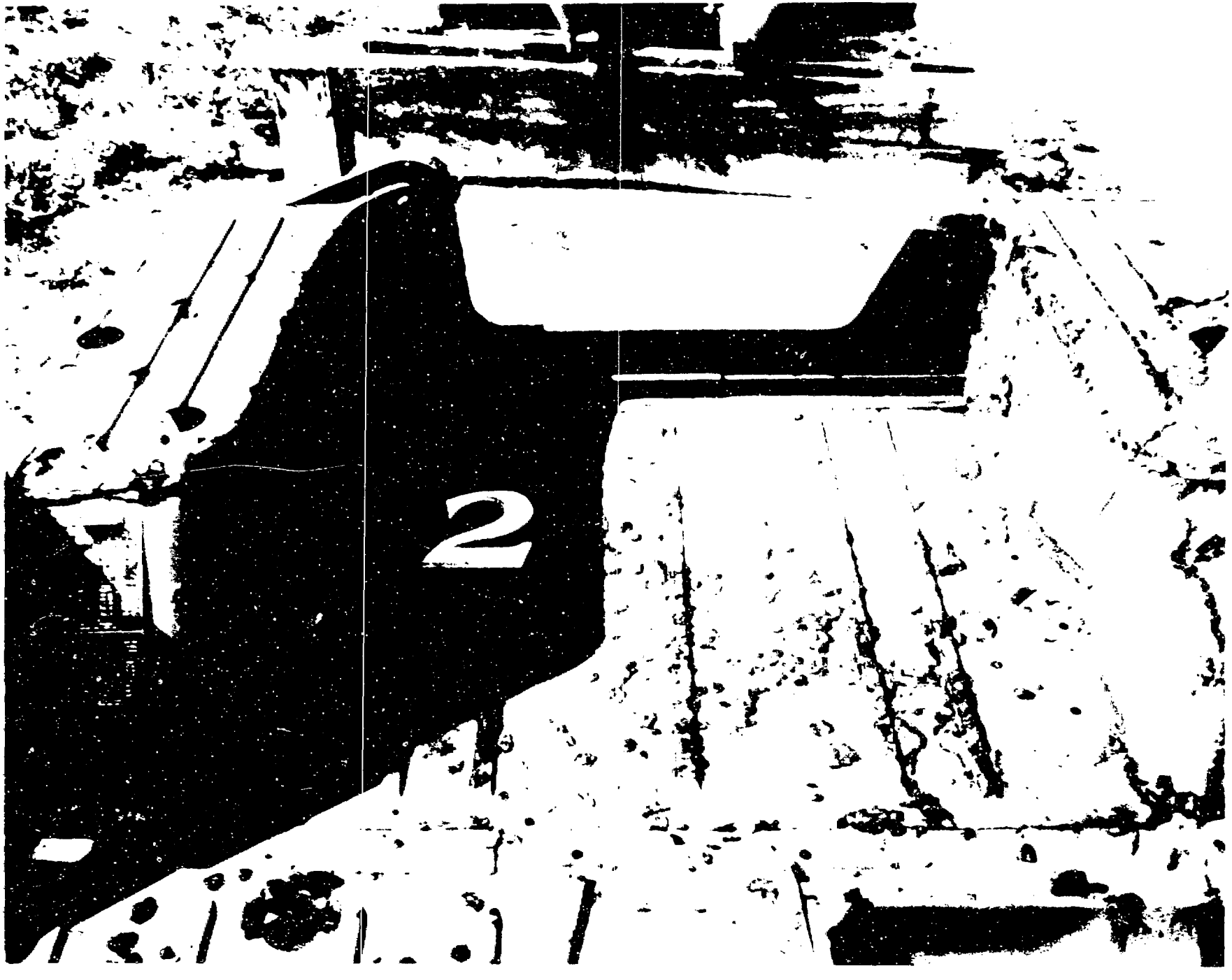
2

THE PREMATURE FAILURE OF THIS BODY SHOWS UP MAINLY IN THE FAILURE OF THE ADHESION OF THE SPRAY-ON EPOXY PRIMER WHICH LIFTED OFF THE PRIMER AND RESULTED IN CREVICE CORROSION. THE CAUSE HAS BEEN IDENTIFIED AS IMPROPER PRETREATMENT BEING APPLIED.

NOW MOVING TO THE RESULTS AT THE 18 MONTH INTERVAL, WHICH WAS THAT OF LAST DEC 86. THEY SHOW ESSENTIALLY THE SAME PATTERN AS THAT ESTABLISHED DURING THE FIRST YEAR, WITH THE EXCEPTION OF BODY #2 WHICH IS SHOWN HERE.

SLIDE 23 ON

WHICH HAS DETERIORATED EXTREMELY FAST DURING THIS TIMEFRAME--TO WHERE WE NOW HAVE STAGE #4 CORROSION ON VARIOUS LOCATIONS OF THE VEHICLE. THIS AGAIN STRESSES THE IMPORTANCE OF CLEANING AND PRETREATING. UNLESS ALL DUST, DIRT AND OTHER CONTAMINANTS ARE REMOVED PRIOR TO PRIMING, MARGINAL PERFORMANCE OF A CARC APPLIED PAINT SYSTEM CAN BE EXPECTED.

SLIDE 24 ON

NOW LOOKING AT THE TEST RESULTS:

RESULTS

ALTHOUGH LABORATORY TESTING MAY INDICATE THE PREFERRED PRODUCT OF CHOICE, IT DOES NOT TOTALLY DEMONSTRATE THE PERFORMANCE OF THESE SYSTEMS IN A FIELD ENVIRONMENT. HOWEVER, THE LABORATORY TESTS ARE IMPORTANT IN SELECTING PREFERRED CANDIDATES BUT IT SHOULD NOT BE USED AS THE SOLE CRITERIA IN JUDGING THE ULTIMATE PERFORMANCE OF A CORROSION-RESISTANT SYSTEM.

SLIDE 25 ON

THE EXPOSURE TESTING PARALLELED FINDINGS CONDUCTED WITH COMMERCIAL VEHICLES. THEIR FINDINGS, AS WELL AS THIS STUDY, STRONGLY INDICATE THE IMPORTANCE OF EVALUATING THE COMBINATION OF SUBSTRATES, COATINGS AND PRETREATMENT APPLIED UNDER PRODUCTION CONDITIONS.

THE PERFORMANCE OF TOPCOATS DOES NOT APPEAR TO BE AN ISSUE IN THIS STUDY, SINCE THE CARC PAINT IS THE ONLY TOP COAT WHICH NOW MEETS THE SPECIFIED REQUIREMENTS FOR PROVIDING LIVE AGENT RESISTANCE. ALSO, THE TOPCOAT IS GENERALLY NOT AS CRITICAL AS ONE MAY ASSUME, BECAUSE 90% OF THE CORROSION PROTECTION IN MOST PAINT SYSTEMS IS THE RESULT OF SUBSTRATE, I.E., ITS PRETREATMENT, GALVANIZING AND APPLIED PRIMER COAT. THE TOP COAT SERVES MAINLY AS AN ADDED PHYSICAL BARRIER AGAINST MOISTURE PENETRATION AND ABRASION.

RESULTS CONTINUED

- CAPE CANAVERAL TEST RESULTS PARRALLEL COMMERCIAL VEHICLE TEST.
- TOP COATS ARE NOT AT ISSUE.
- 90% OF PROTECTION FROM CORROSION IS BASED ON SUBSTRATE.
- RUSTPROOFING VS NO RUSTPROOFING INCONCLUSIVE UNDER STATIC CONDITIONS.

SL- 25

THE PAY OFF EFFECTS OF RUSTPROOFING VS NO RUSTPROOFING ARE NOT TOTALLY CONCLUSIVE AT THIS TIME.

HOWEVER, OUR CAPE CANAVERAL TEST DOES SHOW THERE APPEARS TO BE AN ADVANTAGE IN USING RUSTPROOFING COMPOUND ON PLAIN STEEL BODIES WITH ALKYD PAINTS. SECONDLY, THE RUSTPROOFING COMPOUNDS DID NOT ADD OR DETRACT FROM THE CORROSION PROTECTION OFFERRED BY THE DOUBLE GALVANIZED AND E-COATED SYSTEMS.

WE PRESENTLY HAVE AN ON-GOING DYNAMIC TEST WITH A QUANTITY OF 149 M151 JEEPS LOCATED IN THE TROPICS, SUCH AS: HAWAII, PANAMA & PUERTO RICO THAT SHOULD RESOLVE THIS ISSUE.

SLIDE 26 ON

A WEALTH OF DATA HAS BEEN GENERATED AS A RESULT OF THIS STUDY. THESE EIGHT (8) VEHICLES WILL REMAIN UNDER TEST THROUGH CALENDAR YEAR 88 AT CAPE CANAVERAL AND SHOULD GENERATE FURTHER DATA. IN ADDITION, METALLURGICAL AND PHOTO MICROGRAPHIC TEST OF SAMPLES FROM EXPOSED VEHICLES ARE BEING EVALUATED BY TACOM, MTL, AND AN INDEPENDENT LABORATORY.

CONCLUSIONS

NOW MOVING TO A SYNOPSIS OF OUR PRELIMINARY FINDINGS, THEY ARE SHOWN ON THE FOLLOWING SLIDE:

SLIDE 27 ON

DOUBLE GALVANIZED STEEL APPEARS TO OUTPERFORM COLD ROLLED STEEL

DOUBLE GALVANIZED STEEL WITH ELECTRO-DEPOSITED PRIMER WITHOUT RUSTPROOFING APPEARS TO OFFER EXCELLENT PROTECTION AGAINST RUST.

STEEL BODIES WITH ALKYD SYSTEMS APPEAR TO BENEFIT FROM RUSTPROOFING APPLIED TO THE UNDERSIDE OF THE VEHICLE BODY.

E-COATED PRIMER APPEARS TO OUTPERFORM BOTH ALKYD AND SPRAY EPOXY PRIMERS.

THE SPRAY EPOXY PRIMER WITH CARC TOP COAT FAILED PREMATURELY DUE TO APPARENT LACK OF STRINGENT SURFACE PREPARATION NEEDED IN SUCH A SYSTEM.

BEST COLOR RETENTION OF THE TOP COATS IS AS SHOWN ON THIS CHART WITH CARC THE BEST

O THE PAY OFF OF RUSTPROOFING VS NO RUSTPROOFING AS MENTIONED EARLIER IS INCONCLUSIVE UNDER THE STATIC CONDITIONS OF THIS TEST. AS I HAVE STATED WE HAVE AN ON-GOING TEST IN THE TROPICS TO GATHER MORE DATA IN THIS REGARDS.

CONCLUSIONS

- GALVANIZED STEEL OUTPERFORMS C.R.S.
- GALVANIZED STEEL + E.D. PRIMER - RUSTPROOFING
- C.R.S. + ALKYD PRIMER + RUSTPROOFING
- E.D. PRIMER > ALKYD
- E.D. PRIMER > SPRAY EPOXY
- EPOXY PRIMER + CARC TOPCOAT = PREMATURE CORROSION FAILURE
- BEST COLOR RETENTION = CARC
  THEN = ACRYLIC
  THEN = ALKYD
- RUSTPROOFING VS NO RUSTPROOFING = INCONCLUSIVE UNDER STATIC TEST

SL-27

AS ALREADY MENTIONED, WE WILL CONTINUE THESE TESTS FOR ANOTHER 1 1/2 YEARS AND SUPPLEMENT THIS INFORMATION WITH OUR ONGOING TROPIC FIELD TEST RESULTS. WE ARE HOPING THAT THE DATA GENERATED WILL BE BENEFICIAL AND ENABLE US TO MAKE SERVICE LIFE PREDICTIONS UNDER THESE ACCELERATED CONDITIONS.

THIS COMPLETES MY BRIEFING.

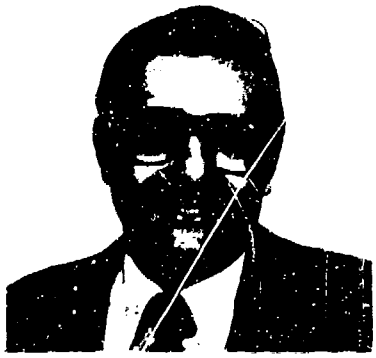

BIOGRAPHY

NAME: GEORGE J. BUGARIN

PRESENT AFFILIATION: Employed as Supervisory Mechanical Engineer at the US Army Tank Automotive Command, Warren Michigan.

TITLE: Mr. Bugarin is presently Chief of the Manufacturing Technology and Producibility Division within the Directorate For Design and Manufacturing Technology.

FIELD OF RESPONSIBILITIES: As Division Chief his assigned mission includes directing TACOM's Value Engineering, Manufacturing Technology, Producibility and Corrosion Prevention and Control Programs.

PREVIOUS AFFILIATIONS/TITLES: As a result of his 29 1/2 years of employment at TACOM, Mr. Bugarin has acquired an extensive background in tactical wheeled vehicle programs. He has been a Command appointed Weapon System Manager of several major truck projects. Mr. Bugarin was previously assigned as Chief of the Tactical Systems, Tactical Systems Support and the Components and Materials Divisions.

ACADEMIC BACKGROUND: Mr. Bugarin has two academic degrees. He is a graduate of the University of Detroit with a Bachelor's Degree in Mechanical Engineering. Also, he has received a Master's Degree in Business-Major in Administrative Management from Wayne State University.

SOCIETY ACTIVITIES/OFFICES/AWARDS: Mr. Bugarin is a Registered Professional Engineer in the State of Michigan. He has received numberous TACOM achievement certificates/awards.

PUBLICATIONS/PAPERS: Mr. Bugarin has authored a Fuel Conservation publication and has presented several papers on TACOM's Corrosion Prevention and Control Program.

BIOGRAPHY

NAME: Saul Isserow

PRESENT AFFILIATION: Corrosion Center of Excellence, Army Materials Technology Laboratory, Watertown, MA 02172 (Since 1971)

TITLE: Metallurgist

FIELD OF INTEREST/RESPONSIBILITIES: Corrosion Prevention and Control

PREVIOUS AFFILIATIONS/TITLES: Nuclear Metals Inc., Concord, MA (1954-1970)

ACADEMIC BACKGROUND: B.A. Brooklyn College, M.S. and PhD, Physical Chemistry, Pennsylvania State University

SOCIETY ACTIVITIES/OFFICES/AWARDS: Member of ASM, ACS, APMI, ASTM, and International Materials Reviews Committee (ASM)

PUBLICATIONS/PAPERS: Assorted publications, including chapters in books on corrosion, powder metallurgy, and materials for nuclear reactions.

BEST AVAILABLE COPY

CORROSION AND CORROSION INHIBITION OF METALS/ALLOYS IN METHYPHOSPHONIC DIFLUORIDE

CHESTER V. ZABIELSKI AND MILTON LEVY
ARMY MATERIALS TECHNOLOGY LABORATORY
WATERTOWN, MA 02172-0001

ABSTRACT

Electrochemical potentiodynamic polarization studies have been carried out for a variety of ferrous and non-ferrous metals in methylphosphonic difluoride. Studies of the effect of organic inhibitors on the corrosion rate of 1020 steel, 316 and 304 stainless steel and magnesium in methylphosphonic difluoride were also carried out.

INTRODUCTION

Binary munitions in which two different constituents are kept in separate compartments until activation will constitute a significant fraction of the chemical weapons in the United States. Because these munitions will be used under extreme circumstances, they must be stock piled over very long periods of time up to 30 years and still be able to operate reliably when the need arises. A very high reliability of the storage container is essential to the subsequent activation of and availability of this weapon system. The failure of the storage container is a hazard in itself because of the toxic nature of one of the constituents.

The principal cause of failure will be the corrosion of the storage container by the highly corrosive methylphosphonic difluoride (DF).

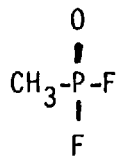

This compound will react with alcohol in the weapon system to form the active agent (GB). The hygroscopic DF interacts with the minor amounts of water which may be present, to form hydrogen fluoride. DF is not used in pure form but contains significant amounts of chlorides and cathodic impurities such as iron, copper and nickel which further increase the corrosion rate of most metals/alloys. Although polymeric liners are being used, they may slowly interact with HF in the DF and the substrate metal/alloy must be able therefore to withstand corrosion and pitting attack. Pitting attack could lead to rapid perforation of the container.

The objectives of this program are: to investigate the kinetics and mechanisms of corrosion of Al 6061 T6 and candidate metal alloys in methylphosphonic difluoride (DF); to establish effective corrosion inhibitors, and to ultimately incorporate or immobilize inhibitors into coatings which can provide protection above the liquid line. Vapor phase (thin electrolyte film) corrosion has been shown to be the primary failure mode in GB munitions and is prevalent in DF systems. DF is a major constituent of GB. Electrochemical studies for metals/alloys in methylphosphonic difluoride were initiated under a joint MTL-CRDC program.

EXPERIMENTAL PROCEDURE

MATERIALS:

The DF for this study was utilized in two purities 97.1% and 99.8%. The complete compositions are shown in table 1. Neutral aqueous fluorides and dilute acidic fluorides solutions were also studied. Potential organic inhibitor materials were added to DF to determine their effects on the corrosion processes and to provide a means for protecting the alloys against corrosion.

A variety of metals/alloys were utilized. Nominal compositions for the ferrous and non-ferrous metals/alloys are contained in tables 2-6.

Test Specimen and Procedures

The corrosion cell was a modified polarographic trielectrode cell constructed from teflon[1]. The reference electrode in the DF solution was a silver wire in 0.1M silver nitrate in acetonitrile. The working electrode was an alloy cylinder, 1.2cm^2 surface area. The counter electrode was a spiralled 40 gauge platinum wire. In order to describe the anodic and cathodic processes, anodic and cathodic polarization measurements were made utilizing the potential sweep method of potentiostatic polarization. The electrode potential was continously changed at a constant rate of 5000mv/hr and current simultaneously recorded. Corrosion rates in mils per year were generally determined by extrapolation of the cathodic portion of the polarization curve and pitting scans were performed to elucidate mechanisms of passivation or pitting. One hour potential-time data were obtained for all alloys in all environments in order to determine the corrosion potentials. In addition selected cylindical specimens e.i. modified polarization specimens 1.2-4.5 cm^2 were exposed up to 180 days at room temperature to DF-22 vapor by positioning the specimen above DF-22 solution with and without added organic inhibitors.

ELECTROCHEMICAL RESULTS

Selected Alloys

Potential-time curves for a group of alloys in both DF-2 and DF-22 solutions are shown in figures 1 and 2 respectively. Generally equilibrium potentials were obtained within 30 minutes. Except for Hastelloy B and Hastelloy C which contain chromium and molybdenum, the corrosion potentials of the other metals/alloys were more active e.i. negative in DF-22 the higher purity solution. The corrosion potential range for the metals/alloys was (+0.71V to -0.644V) in DF-2, the 97.1% solution and (+.254V to -1.100V) in DF-22, the 99.8% solution

Polarization curves in DF-2 and DF-22 for Hastelloy B, Hastelloy C, titanium, Al 6061 T6 and 1020 steel are shown in figure 3 and for Ta-10W, Monel, Ta, and 1020 steel in figure 4. All the metals/alloys exhibited lower corrosion current densities in DF-22, the higher purity 99.8% solution

than in DF-2 (97.1%) solution. Current densities in the passive region were less than 100ua/cm^2 with the exception of 1020 steel.

Pitting scans for Ta-10W in DF-2 and DF-22 solution are shown in figure 5, and in figure 6 for Al 6061- T6 in DF-2 solution and Hastelloy C in DF-22 solution. Pitting tendency as determined from potentiodynamic pitting scans disclosed that pitting did not occur for any metal/alloy in the DF-2 solution but that pitting was evident in DF-22, the higher purity solution for Monel, Ta-10W and Hastelloy B and C. The chromium content of Hastelloy B and Hastelloy C and the tungsten content in Ta-10W may impart susceptibility to pitting in the purer DF-22 solution. DF-22 vapor exposure data, also shows that Hastelloy B, Hastelloy C and Ta-10W undergo pitting.

The polarization curves for 1020 steel in aqueous fluoride solutions are shown in figure 7. The curve for .2% HF and 0.1M (NH_4) HF_2 have similar current densities. The addition of .2% NaCl to .2% HF displaces the curve toward significantly higher current densities. The curves for .1M NaF and .1M KF in comparison to the .2% HF_2 solutions show lower current densities and more active or negative potentials.

The corrosion rates of the metals/alloys in DF-2 shown in table 7 were significantly higher than those in DF-22. The impurities in the DF-2 solution cause an increase in the corrosion rate. 1020 steel had the highest corrosion rate in both solutions. Al 6061- T6, Hastelloy C and Ta-10W have corrosion rates <1 mpy in both solutions.

The corrosion rates for 1020 steel in acidic fluoride solutions were higher than those for neutral fluoride solutions. The corrosion rates in mils per year were 14.9 for .2%HF and 17.0 for .1M (NH_4) HF_2. These corrosion rates were similar to the value of 17.5 obtained in the higher purity DF-22 solution. The corrosion rate in 0.2%HF + 0 .2% NaCl solution was 173.5 mpy which exceeded the value of 99.2 mpy in DF-2, the solution which contains .22% chloride.

Aluminum Alloys

Polarization curves for aluminum alloys are compared for DF-2 (97.1%) and DF-22 (99.8%) solutions in figure 8. The polarization curves for aluminum alloys in DF-22 solution are characterized by lower current densities. Al 7075, Al 5083, Al 6061 and Al 2090 develop passive regions in both solutions with current densities less than 20 ua/cm^2. Table 8 lists the corrosion rates determined from the extrapolation of the cathodic and anodic Tafel slopes. Four aluminum alloys, Al 7075, Al 5083, Al 6061 and Al 2090 have corrosion rates <1 mpy in both DF-2 and DF-22 solutions. Pitting scan data in table 3 for the DF-22 solution indicates that Al 5083 which contains 4.5% magnesium and Al 2090 which contains 2.4% lithium undergo pitting. Visual examination of the polarization specimens after completion of the pitting scans confirmed the occurrence of pitting in Al 5083 and Al 4043. DF-22 vapor exposure data in table 8 revealed pitting in Al 5083 and Al 6061 T6.

Copper Alloys

Polarization curves for selected copper alloys are compared for DF-2 (97.1%) and DF-22 (99.8%) solutions in figures 9 and 10 respectively. The polarization curves for copper alloys in DF-22 show lower passive current densities (100 a/cm^2) than in DF-2 solution. The addition of zinc to pure copper displaces the curves toward more negative potentials. Table 8 lists the corrosion rates in DF-2 and DF-22 solutions determined from the extrapolation of cathodic and anodic Tafel slopes. The corrosion rates in DF-2 solution for pure copper and the copper alloy containing 38% Zn, 2%Pb (this alloy was machined from a brass valve used in a one ton GB agent container) exceed 20 mpy and are significantly higher than those for the copper alloys in DF-22 solution. The corrosion rates in DF-22 solution were between 1.53 and 3.06 mpy, except for Cu (38% Zn, 2%Pb) which had a rate of .28 mpy. Pitting scan data in table 8 for the DF-22 solution disclosed that pitting occurs. Visual examination of the polarization specimens after the completion of the pitting scans confirmed that pitting does indeed occur. DF-22 vapor exposure data showed that Cu (30% Zn) undergoes severe pitting.

Magnesium, Uranium Alloys

The polarization curves for commercially pure magnesium and DU-0.75%Ti (warm worked) are compared in DF-22 solution in figure 11 with Al 6061 T6 and Al 2017. Magnesium and DU-0.75 Ti exhibit more active corrosion potentials and higher current densities but passive current densities don't exceed 100ua/cm^2. Passive current densities for the Al alloys are between 5 and 10 ua/cm^2. The corrosion rates in DF-22 solution listed in table 8 show that commercially pure magnesium and DU-.75%Ti significantly exceed the rates for Al 6061 and Al 2017 but are lower than that for 1020 steel. Pitting scan data in table 8 for DF-22 solution indicates severe pitting occurs on commercially pure magnesium and slight pitting occurs on warm worked DU-.75%Ti. Visual examination of the polarization specimens after completion of the pitting scans confirmed the occurrence of pitting in commercially pure magnesium. DF-22 (99.8%) vapor exposure data in table 8 also shows severe pitting of magnesium

Stainless and Other Ferrous Alloys

Polarization curves for stainless and other ferrous alloys in DF-22 (99.8%) solution are shown in figure 12. The increase in chromium and nickel content displaces the stainless steels curves (in comparison to 1020 steel) toward more noble potentials and lower current densities. The corrosion rates for the stainless steels in DF-2 and DF-22 solutions (table 9) were 1 mpy or less. The corrosion rates for 304SS and 317L SS in DF-2 solution markedly exceeded those in DF-22 solution but were lower than the corrosion rates for 1020 steel. Pitting scan data in table 9 for the DF-22 solution indicated that slight pitting occured on 304SS and 430SS. Visual examination of polarization specimens after completion of pitting scans disclosed slight pitting for 430SS, 304SS, and 316L SS. The DF-22 vapor exposure data in table 9 indicated severe pitting of 304SS and no pitting of 316L SS.

Nickel Alloys

Polarization curves for nickel alloys in DF-22 solution are shown in figure 13. In comparison to the curve for pure nickel, addition of chromium and molybdeum to nickel displaces the curves for Hastelloy B and C toward more noble potentials and lower current densities. The addition of copper to pure nickel shifts the curve for Monel toward more negative or active potentials. The corrosion rates in DF-22 solution in order of increasing rates were Hastelloy C (0.08 mpy, Hastelloy B (0.68 mpy) commercially pure nickel (1.38 mpy) Monel (1.81 mpy) and Ni 200 (2.40 mpy). The corrosion rates in DF-2 solution were somewhat higher than in DF-22 for Hastelloy C (.19 mpy) and Hastelloy B (2.06 mpy) and markedly higher for Monel (14.97 mpy). Pitting scan data in table 9 for the DF-22 solution indicate that the nickel alloys Hastelloy C, Hastelloy B, Ni 200, Monel and commercially pure nickel undergo pitting. The visual examination of polarization specimens after completion of the pitting scans revealed pitting of Ni 200 and commercially pure nickel. DF-22 vapor exposure data in table 8 indicated pitting of Hastelloy B and Hastelloy C.

Inhibitor Studies

1020 Steel

Table 10 lists the percent cathodic and anodic inhibition efficiencies for .025 molar organic inhibitor additions to DF-2 (97.1%) based on corrosion rates determined from cathodic and anodic Tafel slope extrapolations. Sulfanilimide was found to have the highest cathodic and anodic inhibiting efficiencies of 74.3 and 84.2. Benzonitrile, benzothiazole, benzotriazole additions provided cathodic and anodic inhibiting efficiences greater than 50%. Sulfanilimide, benzonitrile and benzotriazole are N-containing additives while benzothiazole is an S-containing additive. These species may chemically absorb on the surface to inhibit corrosion by acidic fluorides (HF) and acidic chlorides (HCL). The remaining organic inhibitor additions NLS (Na salt), NLS (free acid), benzimidazole,N-containing additives and 2-benzothiazole- ethiol, 1-phenyl-2-thiourea,S- containing additives had cathodic and anodic inhibiting efficiencies lower than 50% .

316L Stainless Steel

Table 11 lists the percent cathodic and anodic inhibiting efficiencies for .025 molar organic inhibitor additions to DF-2 (97.1%). Benzotriazole was found to have the highest cathodic and anodic inhibiting efficiences of 97.5 and 98.6% respectively. Pitting scan data indicated that pitting occurred. Visual examination of specimens after completion of the pitting scan revealed the presence of pitting. Exposure in DF-2 liqu d and vapor however, did not confirm the presence of pitting . NLS (Free acid) gave the next highest cathodic anodic inhibiting efficiencies of 40.8 and 73.8% respectively.

304 Stainless Steel

Figure 14 shows a comparison of anodic polarization curves for 304 SS in DF-22 with and without a .025M benzothiazole addition. The inhibitor addition shifted the curve toward more negative potentials and lower current densities. Table 12 compares the efficacy of the four different inhibitors.

Benzotriazole had the highest cathodic inhibiting efficiency of 76.4 percent followed by benzothiazole and sulfanilimide (greater than 50 percent) and n-lauroyl sarcosine (Na salt) (below 50 percent). Pitting data scan in table 12 showed that all the inhibitor additions eliminated pitting. Visual examination of the polarization specimens confirmed the elimination of pitting by the four inhibitor additions. Figure 15 shows that 304 stainless specimens exposed to the vapor above the DF-22 (99.8%) solution with .025 molar benzothiazole were free of pitting.

Commercially Pure Magnesium

Figure 16 compares anodic polarization curves for commercially pure magnesium in DF-22 (99.8%) with and without .025M benzothiazole. The addition of the inhibitor shifted the curve toward more noble potentials, showed an active-passive transition and reduced the critical current for passivity from 100ua/cm2 to 10ua/cm2. Table 13 shows that benzothiazole had a higher cathodic inhibiting efficiency (87.5%) than benzotriazole (71.5%). The pitting scan data in table 13 showed that both inhibitors eliminated pitting. Visual examination of the polarization specimens from pitting scans, however, revealed that slight pitting was evident. Figure 17 shows that commercially pure magnesium exposed to DF-22 (99.8%) vapor containing .025 molar benzothiazole significantly reduces the magnitude of pitting.

SUMMARY

The corrosion rate of the metals/alloys in 97.1% DF were significantly higher than in 99.8% DF. The Cl, Fe and other impurities in the 97.1% solution cause an increase in the corrosion rate.

1020 steel had the highest corrosion rate in both solutions. Hastelloy C, Ta-10W, Al 6061 T6, Al 5083, Al 2090, Al 7075-T6 have corrosion rates <1 mpy in both solutions.

The corrosion potentials of the metals/alloys were generally more active in the higher purity solution except for Hastelloys C and B, stainless steels 304 and 316L, Al 2090, Al 2017, and Cu (38%Zn,2%Pb).

Pitting tendency as determined from potentiodynamic pitting scans disclosed that pitting did not occur for any metal/alloy in the 97.1% solution but that pitting was evident in the higher purity 99.8% solution for high nickel content alloys, pure Cu, Cu(5%Zn), Cu(30%Zn), Cu (38%Zn,2%Pb), stainless steels 304 and 316L, Al 5083, Al 2090, Al4043, Mg, and warm-worked DU-0.75%Ti.

Inhibiting efficiencies determined from reductions in potentiondynamic polarization corrosion rates based on cathodic and anodic Tafel slope extrapolations respectively for 0.025 molar additions of organic inhibitors were highest in:

97.1% DF for sulfanilimide (74.3% and 84.2%) and 1020 steel and for benzotriazole (97.5% and 98.6%) with 316L stainless steel;

99.8% DF for benzotriazole (70.5% and 76.4%) and 304 stainless steel and for benzothiazole (87.5%) and Mg.

Potentiodynamic pitting scans for 304SS in 99.8% DF solution with 0.025 molar additions of benzotriazole, benzothiazole, sulfanilimide and N-lauroylsarcosine (Na salt) and for Mg with benzothiazole and benzotriazole showed that these inhibitors reduced or eliminated pitting.

Visual observation of 304 stainless steel and Mg specimens after long term exposure to vapor above 99.8% DF disclosed that an addition of 0.025 molar benzothiazole to the liquid phase greatly reduced the extent of pitting.

Acknowledgement

The methylphosphonic difluoride utilized in this investigation was provided by Pascal A. Tarantino of the U.S. Army Armament, Munitions and Chemical Command, Aberdeen Proving Ground, Maryland 21010.

REFERENCES

1. P.A. Tarantino and M.M Decker "Use of Electrochemical Techniques To Study The Corrosion of Selected Alloys By DF" CRDC-TR-8403 July 1984.

2. C.V. Zabielski and M. Levy "Corrosion of Metals/Alloys in Methylphosphonic Difluoride," Extended Abstracts, Electrochemical Society, 86-7, 347 (1986).

Table 1

ANALYSIS AND PURITY OF DF

ANALYSIS	SAMPLES DF-2	SAMPLES DF-22[a]
METALS (ppm)		
Fe	120	7
Cu	10	10
Ni	18	22
Cr	4	1
Zn	18	2
Mo	2	2
TOTAL METALS (wt %)	0.017	0.004
Cl (wt %)	0.22	0.01
PURITY (mole %)		
F.P. DEPRESSION	97.1	99.8
NMR	96.8	99.9
IMPURITIES (mole %)		
PERCENT ACCOUNTABLE	0.237	0.0014
PERCENT NOT ACCOUNTABLE	2.763	0.249

(a) REPRESENTS DF THAT WAS PURIFIED BY DISTILLATION IN HASTELLOY B EQUIPMENT TO PRODUCE HIGH PURITY MATERIAL.

Table 2

COMPOSITION OF NON FERROUS ALLOYS

ALLOY	NOMINAL COMPOSITION (%)				
	Ta	W	Ti	U	Mg
Pure Ta	99.9	--	--	--	--
Ta (10%W)	90	10	--	--	--
Pure Ti	--	--	99.9	--	--
Pure Mg	--	--	--	--	99.9
DU (warm worked)	--	--	0.75	99.25	--

Table 3

COMPOSITION OF STAINLESS STEEL ALLOYS

	NOMINAL COMPOSITION (%)						
ALLOY	Fe	Ni	Cr	Mn	Mo	Si	Cu
20Cb-3	35	35	20	2	2.5	1	3.5
317L SS	60	12	19	2	3.5	1	--
316L SS	65	12	17	2	2.5	1	--
304 SS	68	10	19	2	--	--	--
430 SS	80	0.8	17	1	--	1	--
1020	99	--	--	0.5	--	--	--

Table 4

COMPOSITION OF NICKEL ALLOYS

	NOMINAL COMPOSITION (%)					
ALLOY	Ni	Cr	Mo	Fe	Cu	W
Hast. C	59	16	16	5	--	4
Hast. B	61.2	1	28	5	--	--
Monel	66.5	1.3	--	--	31.5	--
Ni 200	99.5	--	--	--	--	--
Pure Ni	99.9	--	--	--	--	--

Table 5

COMPOSITION OF ALUMINUM ALLOYS

ALLOY	NOMINAL COMPOSITION (%)							
	Al	Si	Mg	Cu	Fe	Mn	Zn	Li
Al 2017	93	0.6	0.6	4	0.7	0.7	--	--
Al 2090	93.4	--	--	2.8	--	0.8	--	2.4
Al 4043	93	5.3	--	--	0.8	--	--	--
Al 5083	98	0.5	4.5	--	0.5	0.7	--	--
Al 6061-T6	96	0.6	1	--	0.7	--	--	--
Al 7075-T6	90	0.5	2.5	1.6	0.5	--	5.6	--

Table 6

COMPOSITION OF COPPER ALLOYS

ALLOY	NOMINAL COMPOSITION (%)			
	Cu	Zn	Ni	Pb
Cu (38%Zn, 2%Pb)	60	38	--	2
Cu (30%Zn)	70	30	--	--
Gilding Metal	95	5	--	--
Pure Cu	99.9	--	--	--

Table 7

CORROSION RATES IN MILS PER YEAR

ALLOY	DF-2	DF-22
1020	99.2	17.5
MONEL	15.0	1.8[sp]
Ta	9.1	<.1
Ti	3.3	0.2
HASTELLOY B	2.0	2.0[sp]
Ta: 10% W	0.8	0.5[sp]
Al 6061-T6	0.1	<.1
HASTELLOY C	<.1	<.1[sp]

CORROSION RATES OF 1020 STEEL

SOLUTION	MPY
0.2% HF + 0.2% NaCl	173.5[p]
0.1M $(NH_4)HF_2$	17.0
0.2% HF	14.9
0.1M KF	2.1
0.1M NaF	1.5

[p] Pitting
[sp] Slight Pitting

Table 8

POTENTIODYNAMIC CORROSION RATES AND PITTING OBSERVATIONS FOR NON FERROUS ALLOYS IN DF-2 (97.1%) AND DF-22 (99.8%) AT 25°C

	CORROSION RATE (MPY)				PITTING IN DF-22		
	DF-2		DF-22		polarization		vapor
ALLOY	cathodic	anodic	cathodic	anodic	scan	visual	exposure
AL 7075	0.40	nd	0.06	0.07	N	N	nd
AL 5083	0.42	0.49	0.07	0.07	P	nd	PP
AL 2090	0.49	0.59	0.09	0.08	SP	SP	N
AL 2017	0.04	0.08	0.62	1.39	N	N	nd
AL 6061	0.59	0.39	0.03	0.04	N	nd	PP
AL 4043	3.09	1.11	0.64	1.47	N	HP	N
Pure Cu	67.6	39.22	1.53	1.90	P	PP	nd
Cu (5%Zn)	nd	nd	2.00	2.82	P	nd	nd
Cu (30%Zn)	nd	nd	1.60	1.69	SP	SP	nd
Cu (38%Zn, 2%Pb)	23.64	45.62	0.28	3.06	P	PP	nd
Pure Mg	nd	nd	10.94	16.81	HP	P	HP
U (0.75%Ti) (warm worked)	nd	nd	5.01	5.36	SP	N	nd

Key For Pitting Data:

nd = no data
N = no pitting
PP = possible pitting
SP = slight pitting
P = pitting
HP = heavy pitting

Table 9

POTENTIODYNAMIC CORROSION RATES AND PITTING OBSERVATIONS FOR FERROUS AND NICKEL ALLOYS IN DF-2 (97.1%) AND DF-22 (99.8%) AT 25°C

ALLOY	CORROSION RATE (MPY) DF-2 cathodic	DF-2 anodic	DF-22 cathodic	DF-22 anodic	PITTING IN DF-22 polarization scan	polarization visual	vapor exposure
20Cb-3	nd	nd	0.30	0.22	N	N	nd
317L SS	nd	nd	1.20	1.17	N	N	nd
316L SS	36.94	77.00	0.27	0.33	N	PP	N
304 SS	43.47	44.15	0.16	0.24	SP	PP	HP
430 SS	nd	nd	0.73	0.91	PP	SP	nd
1020	98.66	135.90	17.50	20.79	N	nd	N
Hastelloy C	0.19	0.23	0.08	0.05	P	nd	PP
Hastelloy B	2.06	2.24	0.68	1.58	SP	nd	SP
Monel	14.97	36.77	1.81	2.45	PP	nd	nd
Ni 200	nd	nd	2.40	2.58	SP	PP	nd
Commercially Pure Ni	nd	nd	1.38	0.88	P	PP	nd

Key For Pitting Observations:
nd = no data PP = possible pitting P = pitting
N = no pitting SP = slight pitting HP = heavy pitting

US ARMY
LABORATORY COMMAND
MATERIALS TECHNOLOGY
LABORATORY

Table 10

POTENTIODYNAMIC CORROSION RATES AND PERCENT INHIBITING EFFICIENCIES (I.E.%) OF 1020 STEEL IN DF-2 (97.1%) WITH .025 MOLAR ORGANIC INHIBITOR ADDITIONS

INHIBITOR ADDITION (.025M)	CATHODIC MPY	CATHODIC I.E.%	ANODIC MPY	ANODIC I.E.%
DF-2	98.7	---	135.9	---
SULFANILAMIDE	25.4	74.3	21.5	84.2
BENZONITRILE	33.7	65.8	42.7	68.6
BENZOTHIAZOLE	35.9	63.6	50.2	63.1
BENZOTRIAZOLE	43.5	56.0	63.1	53.6
NLS* (Na SALT)	55.1	44.2	82.7	39.1
NLS* (FREE ACID)	55.9	43.4	98.6	27.4
2-BENZOTHIAZOLETHIOL	58.2	41.0	106.5	21.6
BENZIMIDAZOLE	----	----	117.9	13.2
1-PHENYL-2-THIOUREA	71.8	27.2	136.0	0.0

* N-LAUROYLSARCOSINE

Table 11

POTENTIODYNAMIC CORROSION RATES AND PERCENT INHIBITING EFFICIENCES (I.E. %) OF 316L STAINLESS STEEL IN DF-2 (97.1%) WITH .025 MOLAR ORGANIC INHIBIOR ADDITIONS

INHIBITOR ADDITION (.025M)	CATHODIC		ANODIC	
	MPY	I.E.%	MPY	I.E.%
DF-2	43.5	---	44.2	---
BENZOTRIAZOLE	1.08	97.5	0.63	98.6
NLS* (FREE ACID)	25.7	40.8	11.6	73.8
NLS* (Na SALT)	30.3	30.4	13.9	68.6
BENZOTHIAZOLE	31.0	28.6	20.5	63.6

* N-LAUROYLSARCOSINE

Table 12

POTENTIODYNAMIC CORROSION RATES AND PERCENT INHIBITING EFFICIENCIES (I.E.) OF 304 STAINLESS STEEL IN DF-22 WITH ORGANIC INHIBITORS ADDED

INHIBITOR	INHIBITOR EFFICIENCY				PITTING OBSERVATIONS			
	ANODIC		CATHODIC		polarization		exposure	
	MPY	I.E. (%)	MPY	I.E. (%)	scan	visual	liquid	vapor
No Inhibitor	0.329	---	0.270	---	SP	PP	HP	HP
0.025M Benzotriazole	0.097	70.5	0.064	76.4	N	N	nd	nd
0.025M Benzothiazole	0.096	70.8	0.083	69.6	N	N	N	N
0.025M Sulfanilamide	0.164	50.2	0.130	52.0	N	N	nd	nd
0.025M N-lauroylsarcosine(Na salt)	0.185	43.8	0.163	39.9	N	N	nd	nd

KEY-FOR PITTING OBSERVATIONS

N = no pitting
PP = possible pitting
SP = slight pitting
P = pitting
HP = heavy pitting
nd = no data

Table 13

POTENTIODYNAMIC CORROSION RATES AND PERCENT INHIBITING EFFICIENCIES (I.E.) OF COMMERCIALLY PURE Mg IN DF-22 WITH ORGANIC INHIBITORS ADDED

	INHIBITOR EFFICIENCY				PITTING OBSERVATIONS		
	CATHODIC		ANODIC		polarization		exposure
INHIBITOR	MPY	I.E. (%)	MPY	I.E. (%)	scan	visual	vapor
No Inhibitor	10.94	---	16.81	---	P	HP	HP
0.025M Benzothiazole	1.37	87.5	nf	nf	N	SP	P
0.025M Benzotriazole	3.09	71.7	3.78	77.5	N	SP	nd

KEY FOR PITTING OBSERVATIONS

N = no pitting
SP = slight pitting
P = pitting
HP = heavy pitting
nd = no data
nf = not found

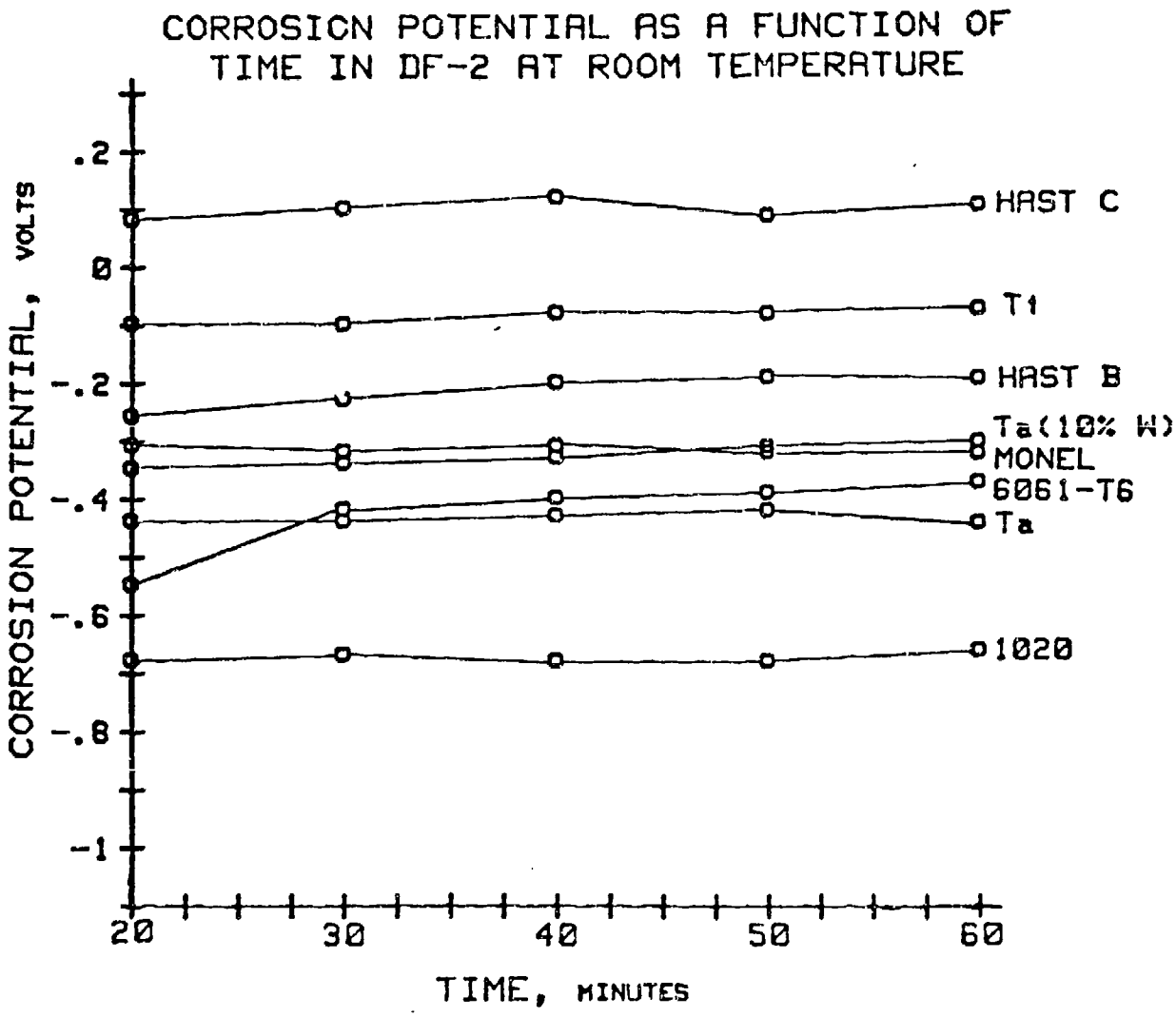
CORROSION POTENTIAL AS A FUNCTION OF
TIME IN DF-2 AT ROOM TEMPERATURE
CORROSION POTENTIAL, VOLTS
.2
0
-.2
-.4
-.6
-.8
-1
20
30
40
50
60
TIME, MINUTES
HAST C
Ti
HAST B
Ta(10% W)
MONEL
6061-T6
Ta
1020

Figure 1

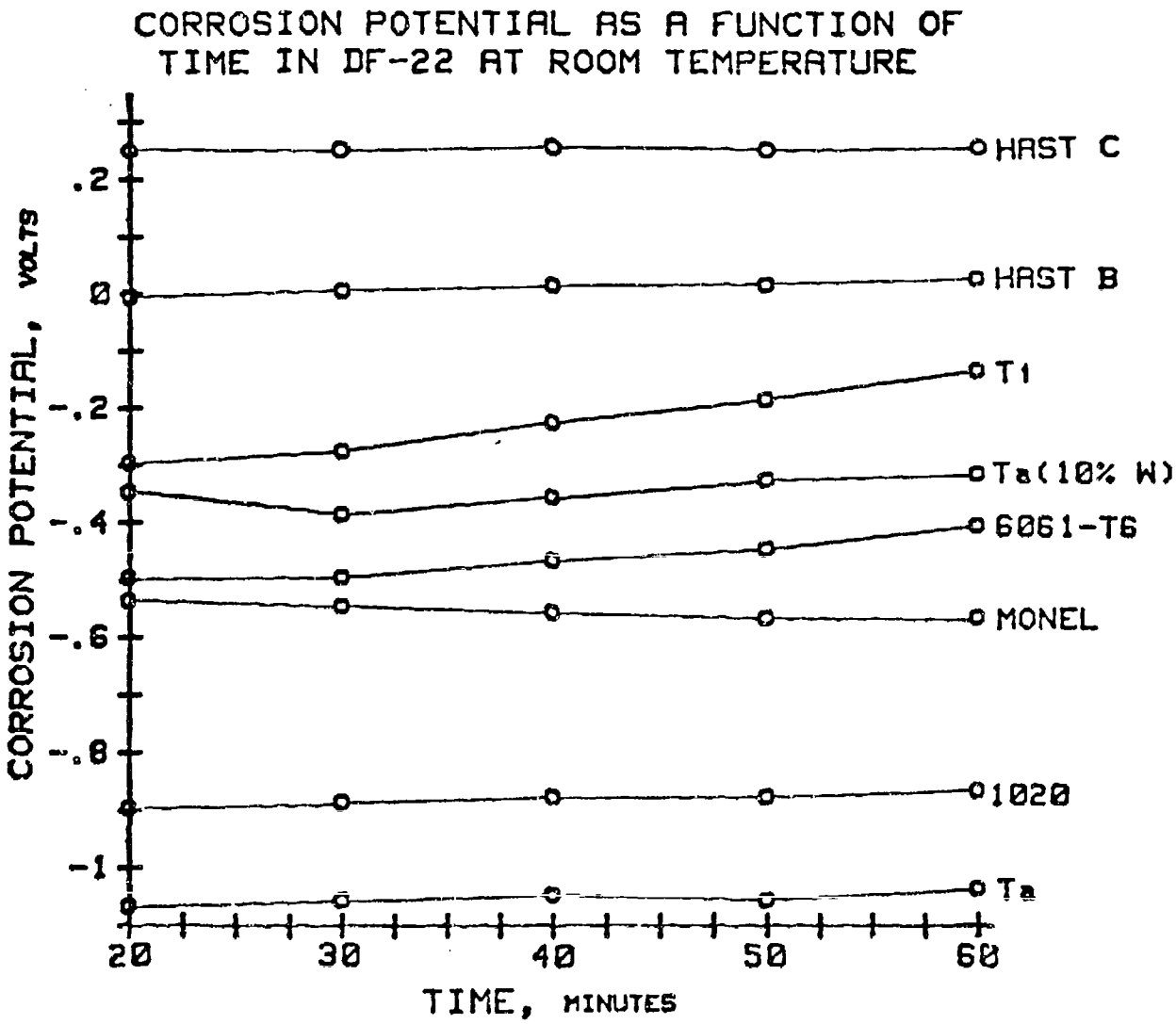
CORROSION POTENTIAL AS A FUNCTION OF
TIME IN DF-22 AT ROOM TEMPERATURE
CORROSION POTENTIAL, VOLTS
.2
0
-.2
-.4
-.6
-.8
-1
HAST C
HAST B
Ti
Ta(10% W)
6061-T6
MONEL
1020
Ta
20
30
40
50
60
TIME, MINUTES

Figure 2

POTENTIODYNAMIC POLARIZATION CURVES IN
DF-2 (97.1%) AT 25°C, SCAN RATE: 1.388 mv/sec

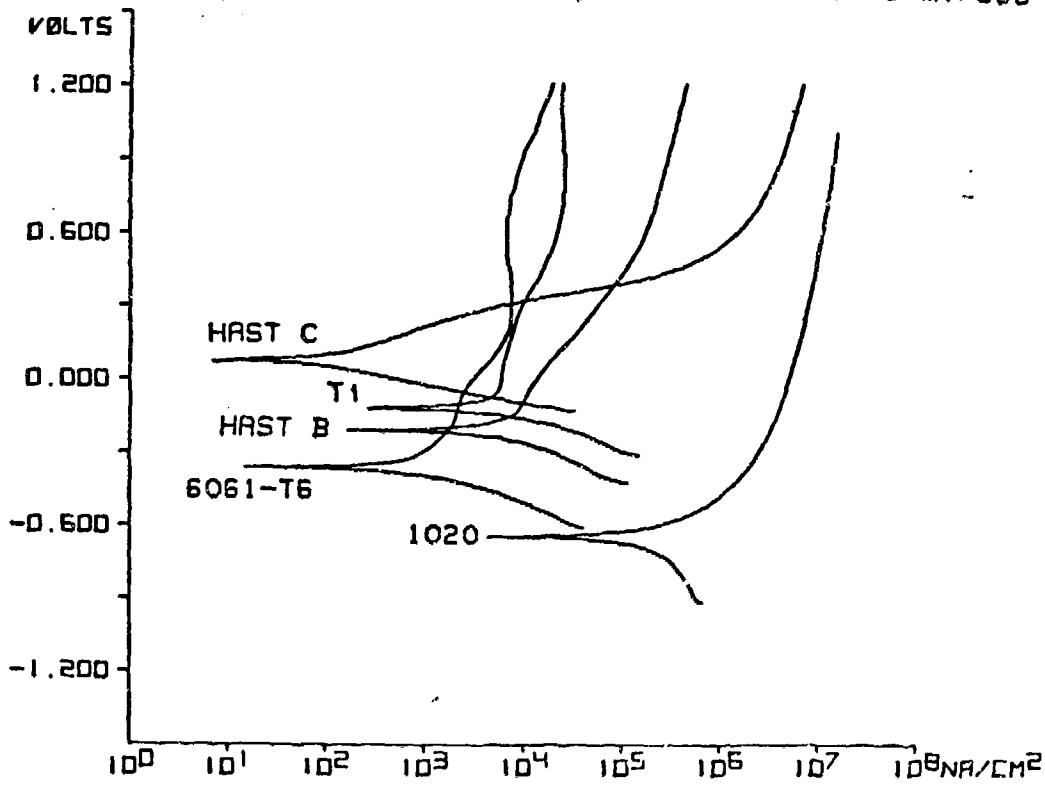

POTENTIODYNAMIC POLARIZATION CURVES IN
DF-22 (99.8%) AT 25°C, SCAN RATE: 1.388 mv/sec

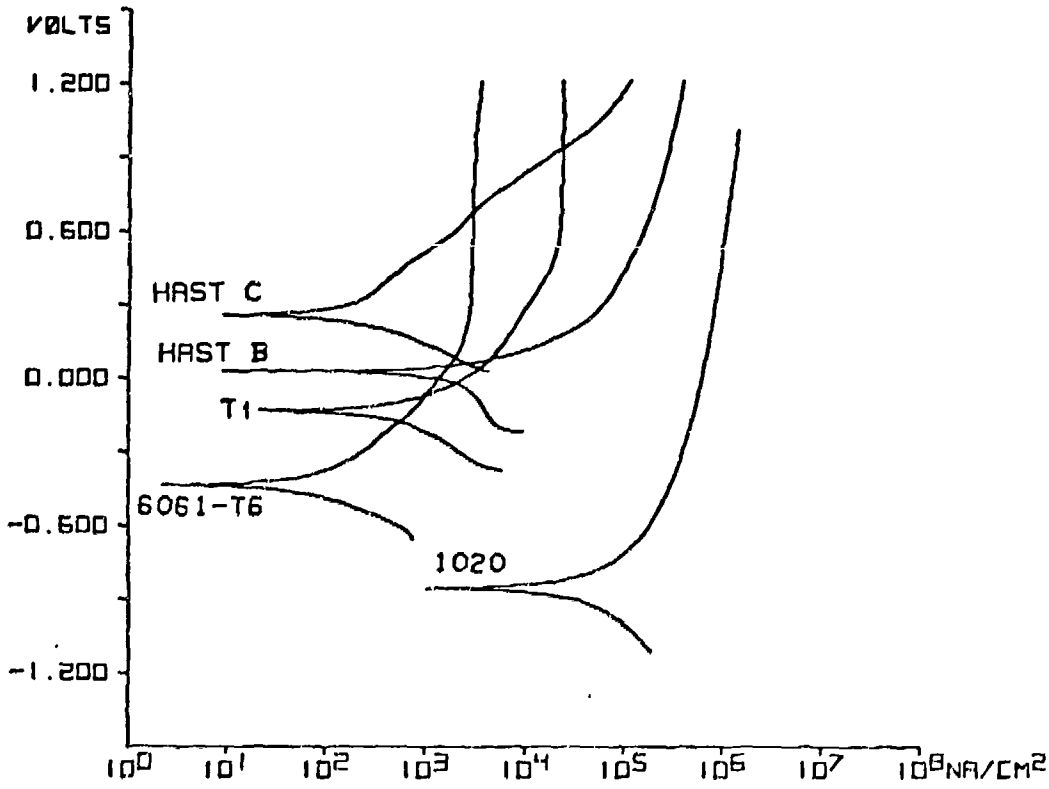

Figure 3

POTENTIODYNAMIC POLARIZATION CURVES IN
DF-2 (97.1%) AT 25°C, SCAN RATE: 1.388 mv/sec

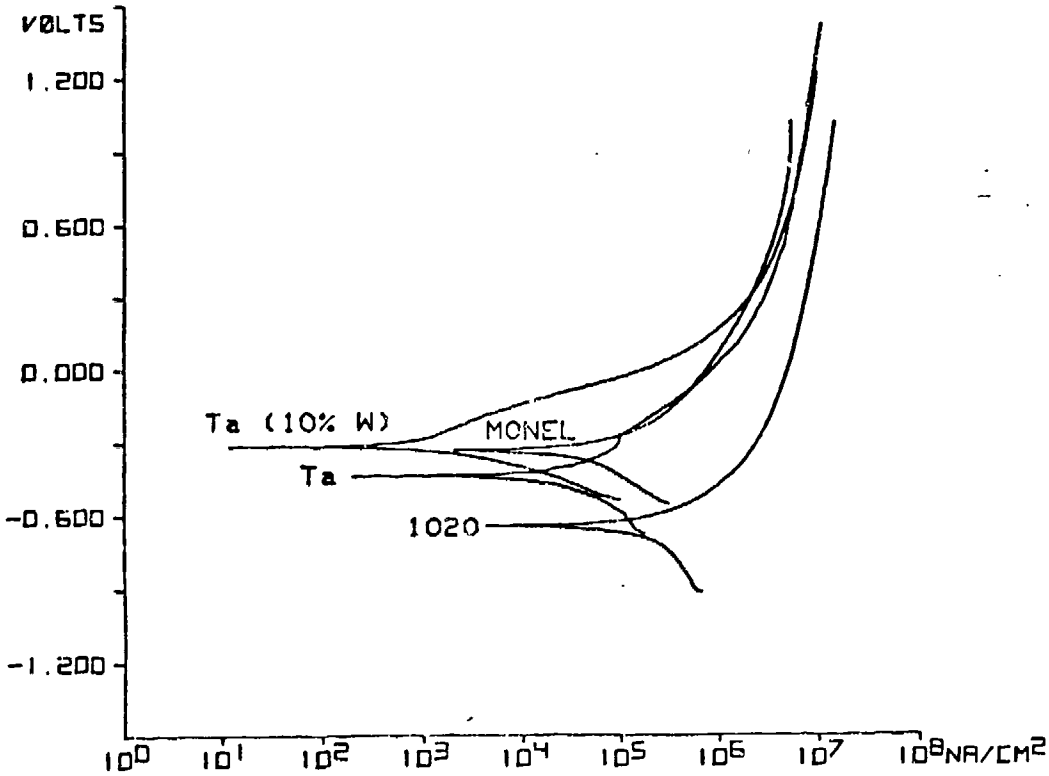

POTENTIODYNAMIC POLARIZATION CURVES IN
DF-22 (99.8%) AT 25°C, SCAN RATE: 1.388 mv/sec

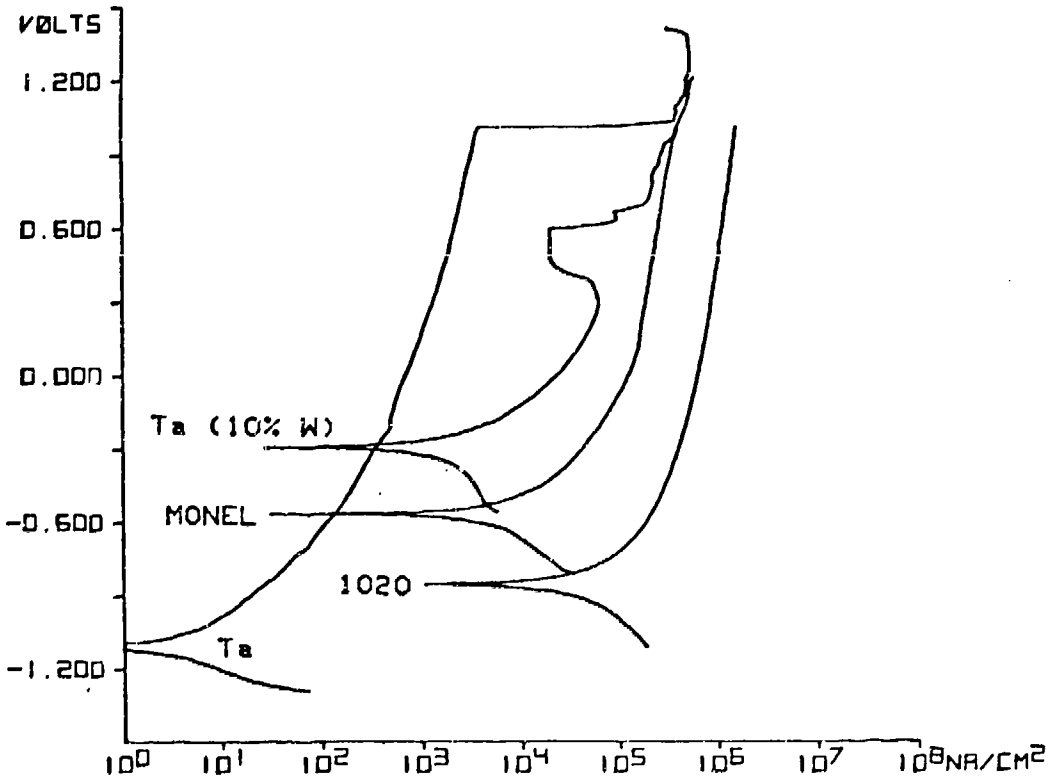

Figure 4

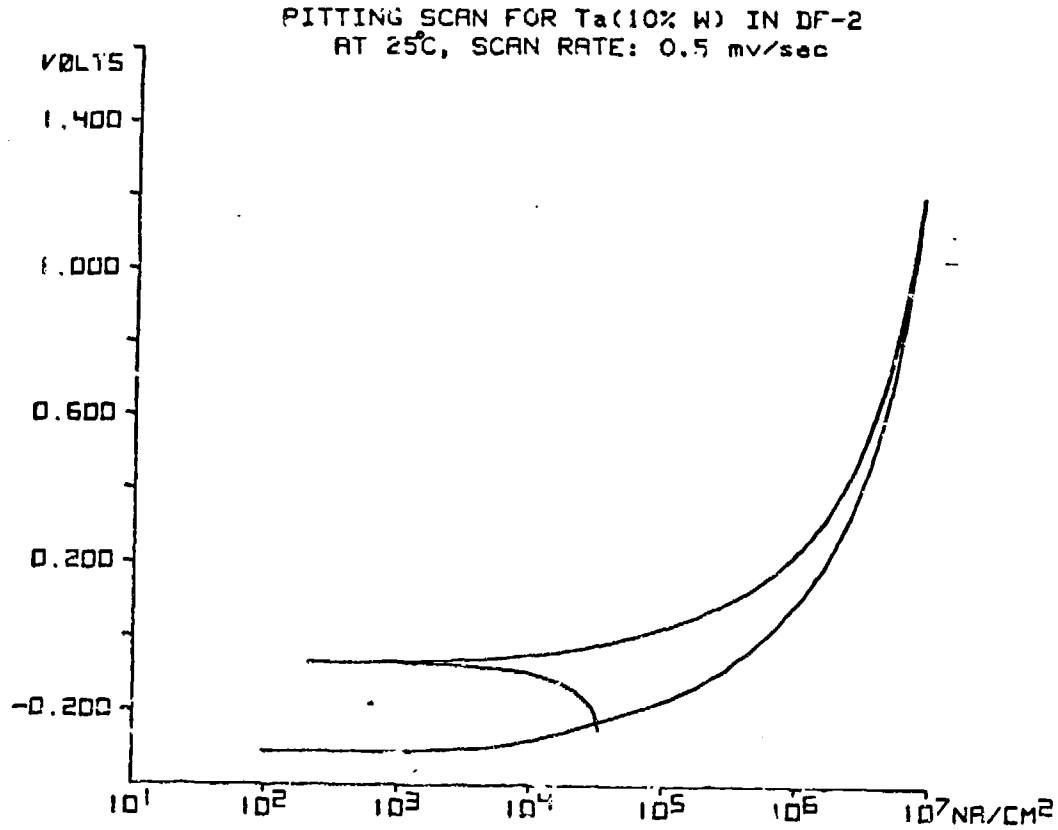
PITTING SCAN FOR Ta(10% W) IN DF-2
AT 25°C, SCAN RATE: 0.5 mv/sec
VOLTS
1.400
1.000
0.600
0.200
-0.200
10¹
10²
10³
10⁴
10⁵
10⁶
10⁷NA/CM²

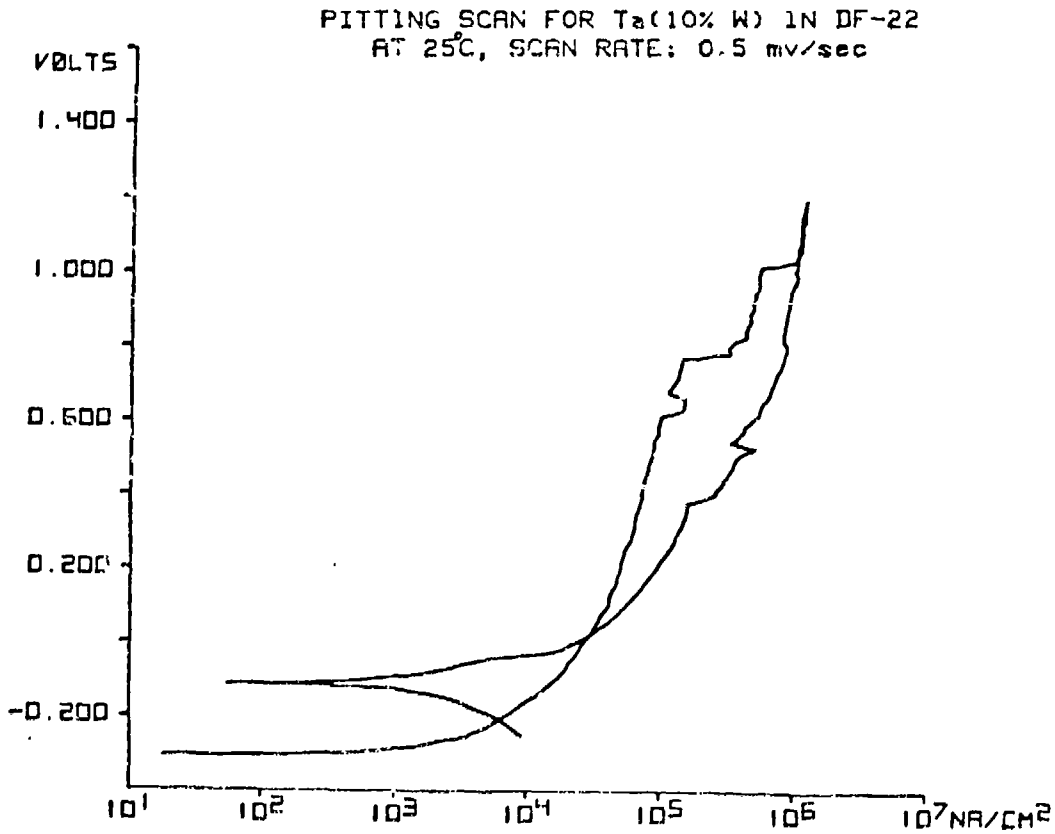
PITTING SCAN FOR Ta(10% W) IN DF-22
AT 25°C, SCAN RATE: 0.5 mv/sec
VOLTS
1.400
1.000
0.600
0.200
-0.200
10¹
10²
10³
10⁴
10⁵
10⁶
10⁷NA/CM²

Figure 5

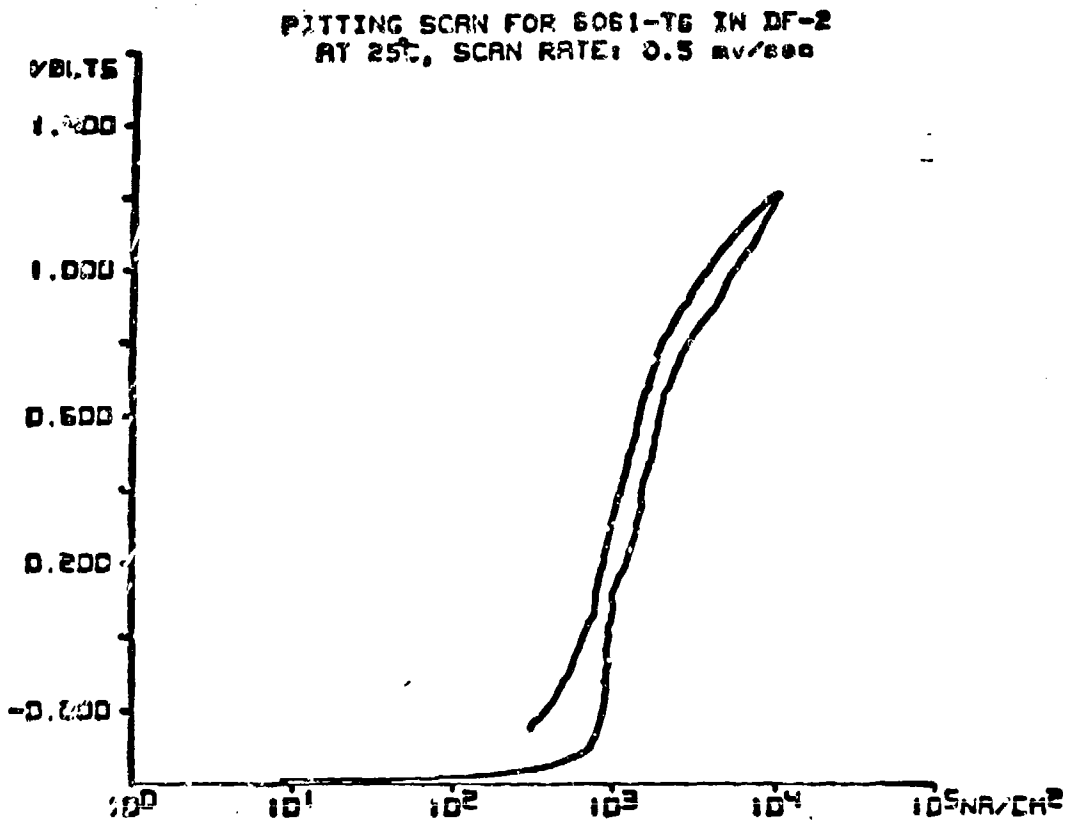
PITTING SCAN FOR 6061-T6 IN DF-2
AT 25°C, SCAN RATE: 0.5 mv/sec
VOLTS
1.400
1.000
0.600
0.200
-0.200
10^0
10^1
10^2
10^3
10^4
10^5 NA/CM^2

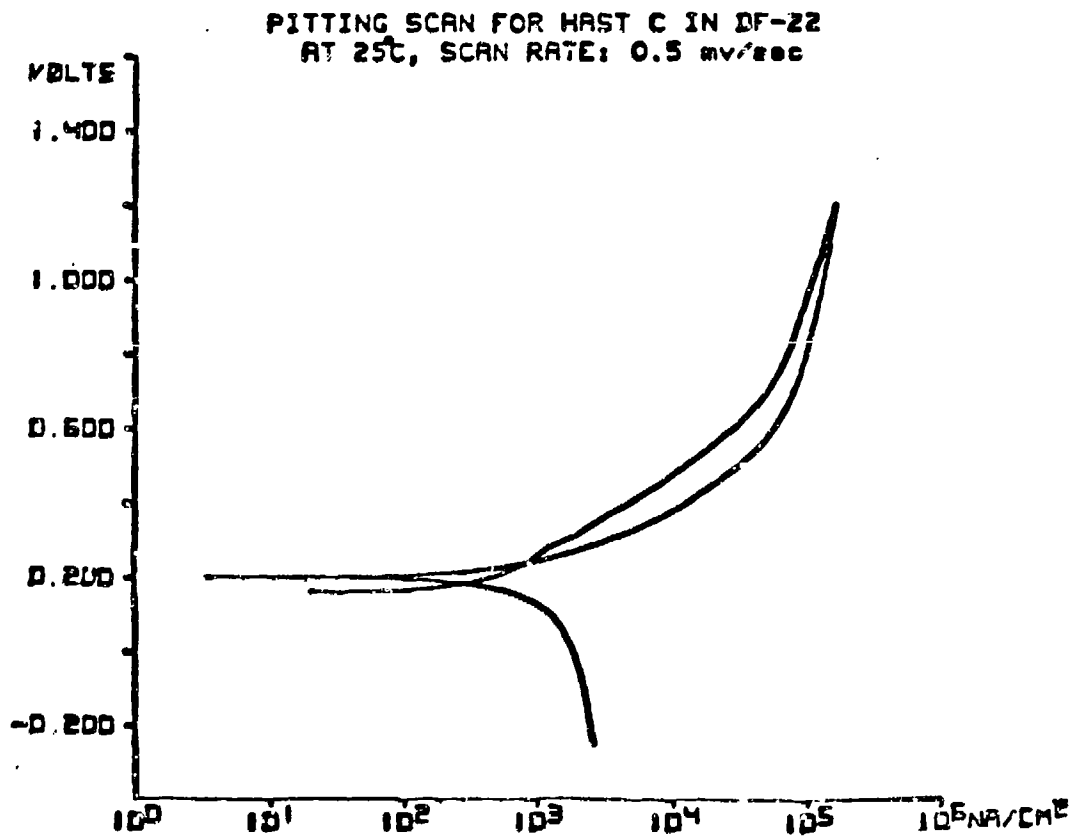
PITTING SCAN FOR HAST C IN DF-22
AT 25°C, SCAN RATE: 0.5 mv/sec
VOLTS
1.400
1.000
0.600
0.200
-0.200
10^0
10^1
10^2
10^3
10^4
10^5
10^6 NA/CM^2

Figure 6

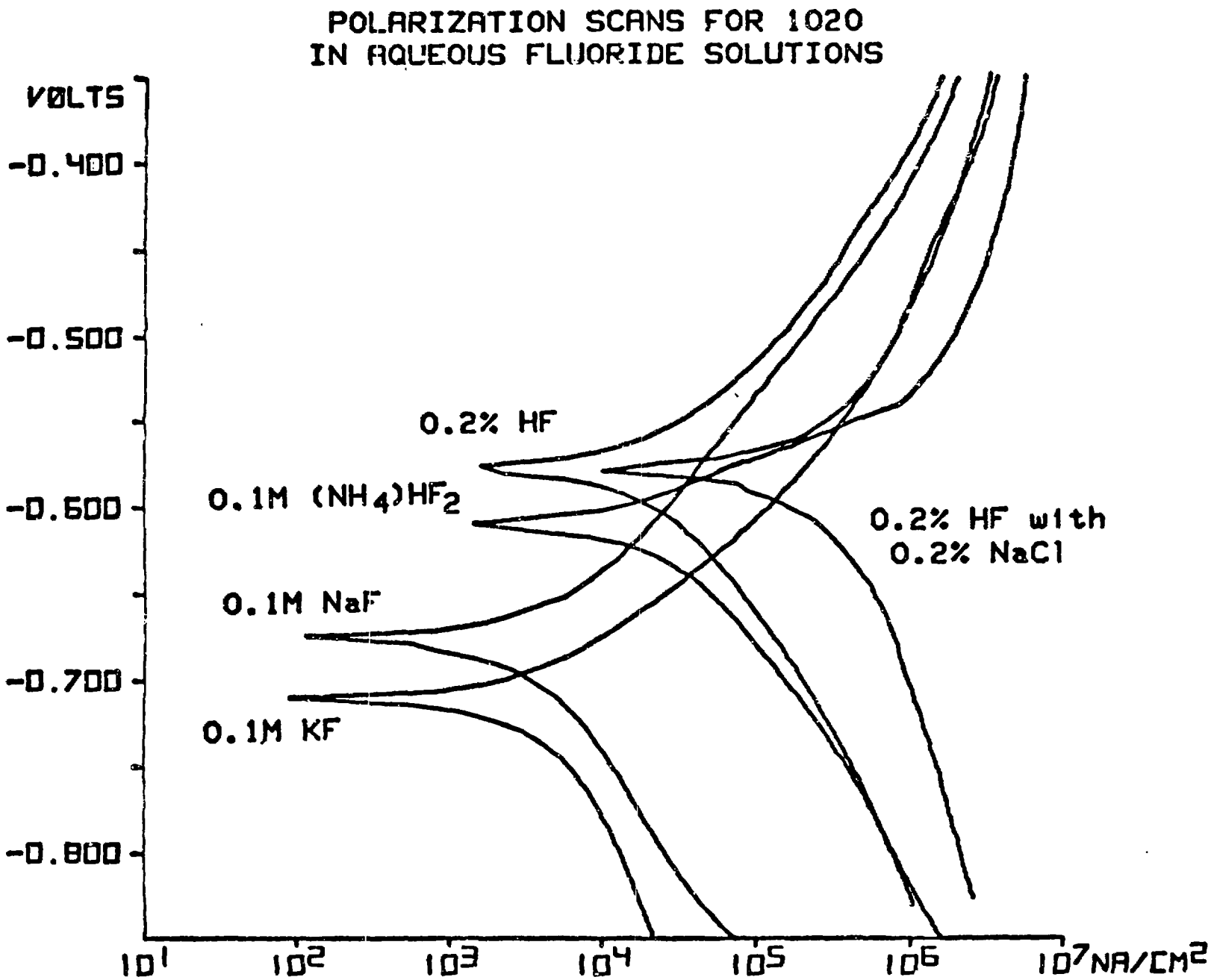
POLARIZATION SCANS FOR 1020
IN AQUEOUS FLUORIDE SOLUTIONS
VOLTS
-0.400
-0.500
-0.600
-0.700
-0.800
0.2% HF
0.1M (NH4)HF2
0.1M NaF
0.1M KF
0.2% HF with
0.2% NaCl
10^1
10^2
10^3
10^4
10^5
10^6
10^7 NA/CM^2

Figure 7

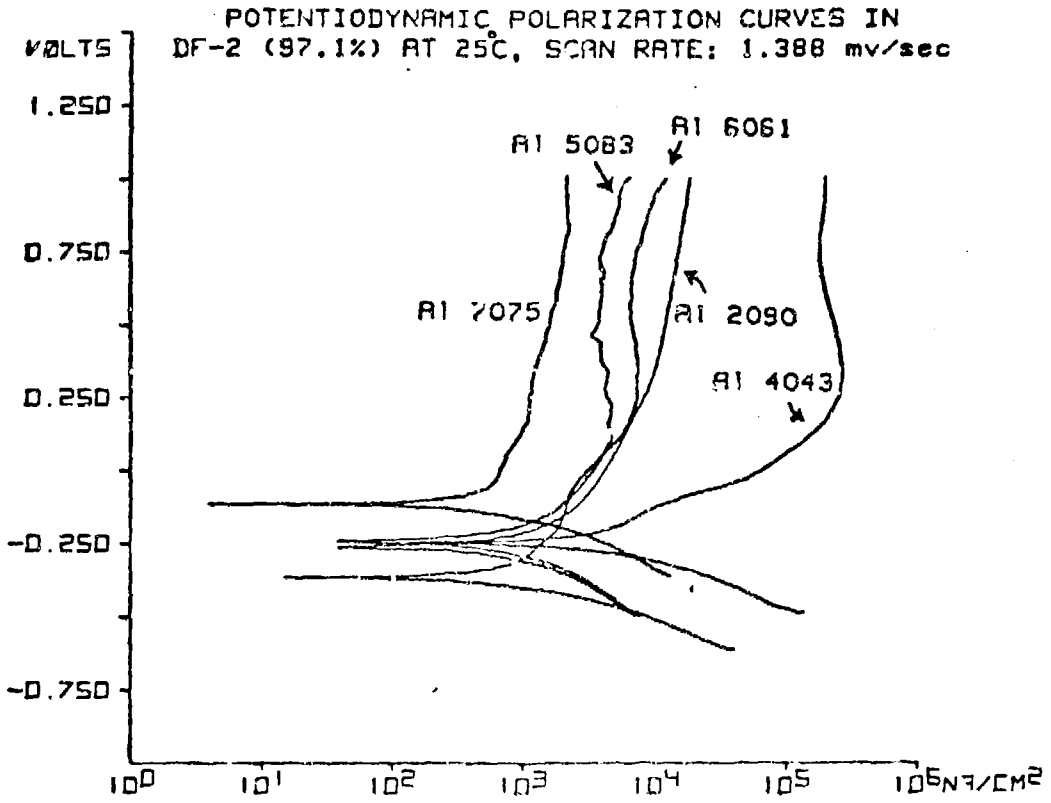
POTENTIODYNAMIC POLARIZATION CURVES IN
DF-2 (97.1%) AT 25°C, SCAN RATE: 1.388 mv/sec
VOLTS
1.250
0.750
0.250
-0.250
-0.750
Al 5083
Al 6061
Al 7075
Al 2090
Al 4043
10^0
10^1
10^2
10^3
10^4
10^5
10^6 NA/CM^2

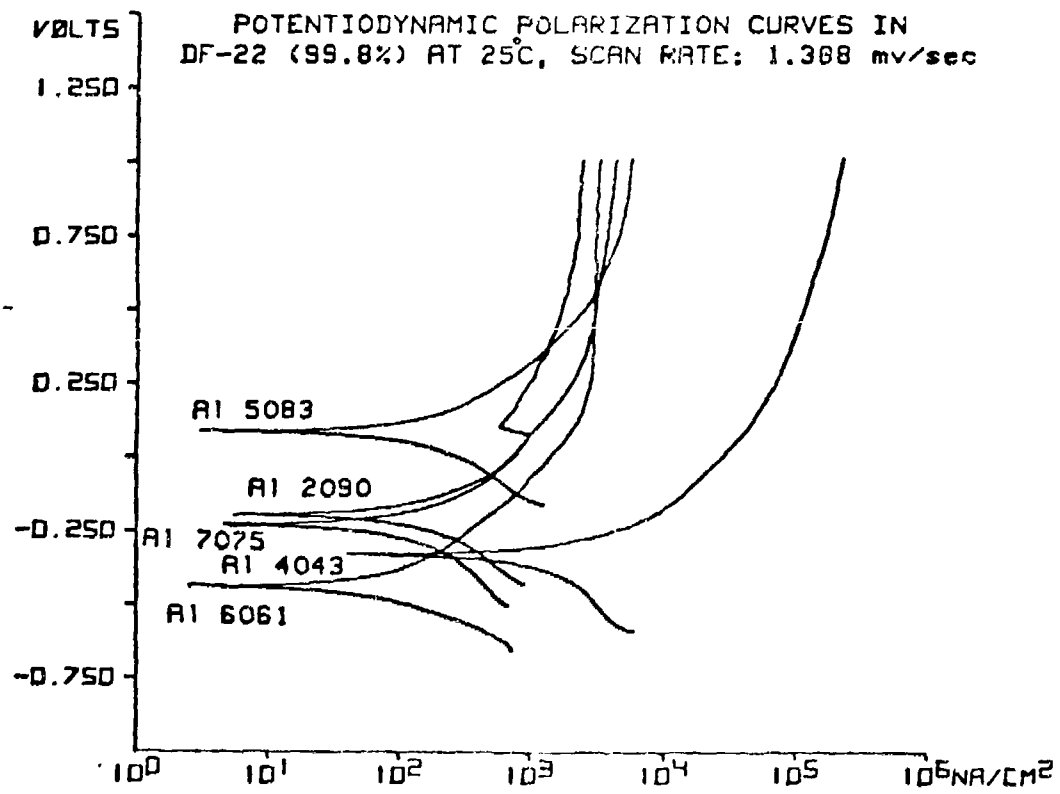
POTENTIODYNAMIC POLARIZATION CURVES IN
DF-22 (99.8%) AT 25°C, SCAN RATE: 1.388 mv/sec
VOLTS
1.250
0.750
0.250
-0.250
-0.750
Al 5083
Al 2090
Al 7075
Al 4043
Al 6061
10^0
10^1
10^2
10^3
10^4
10^5
10^6 NA/CM^2

Figure 8

101

Figure 9

COMPARISON OF COPPER AND BRASS POTENTIODYNAMIC POLARIZATION CURVES IN DF-2 (97.1%) AT 25°C, SCAN RATE: 1.388mv/sec

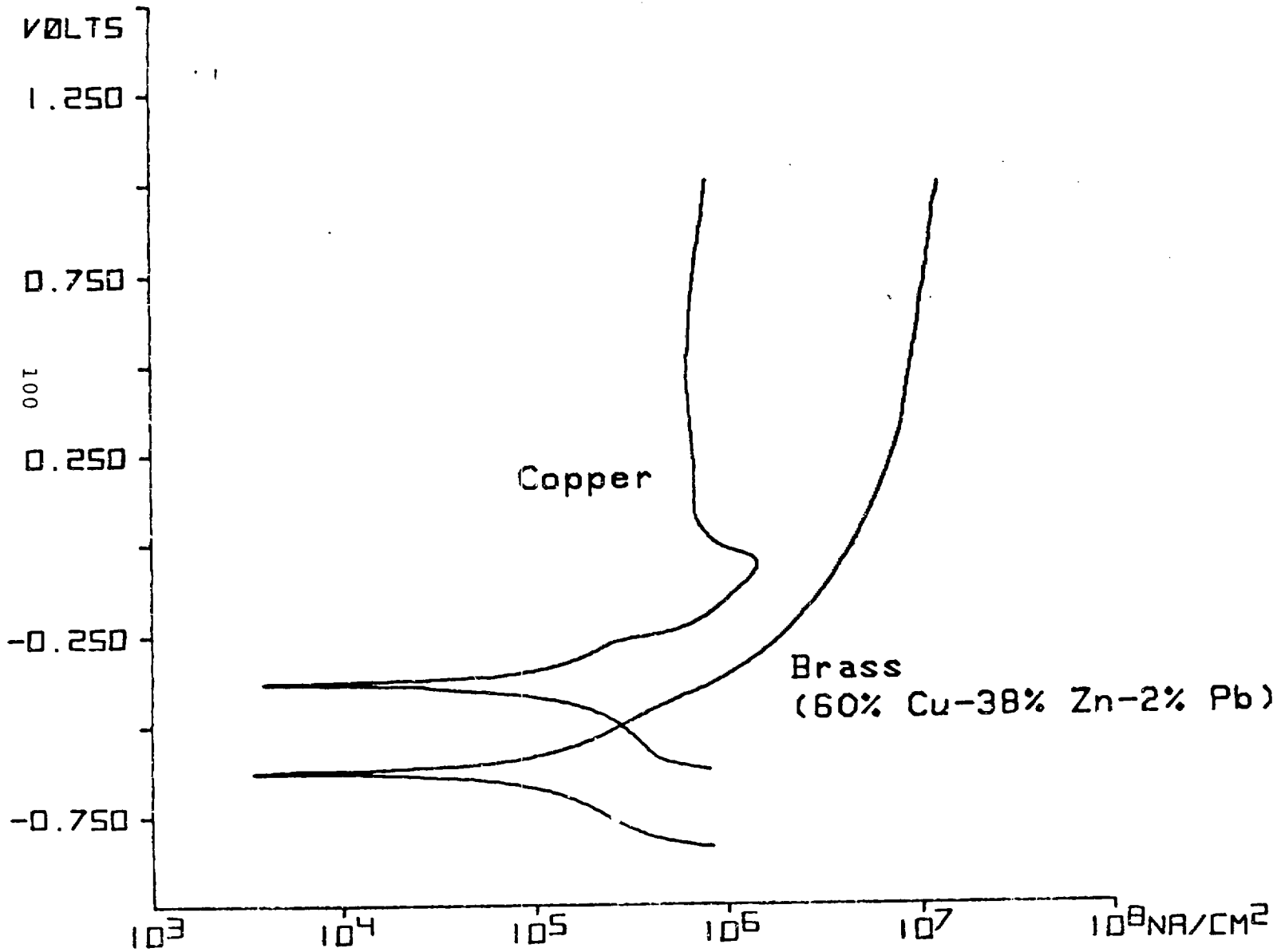

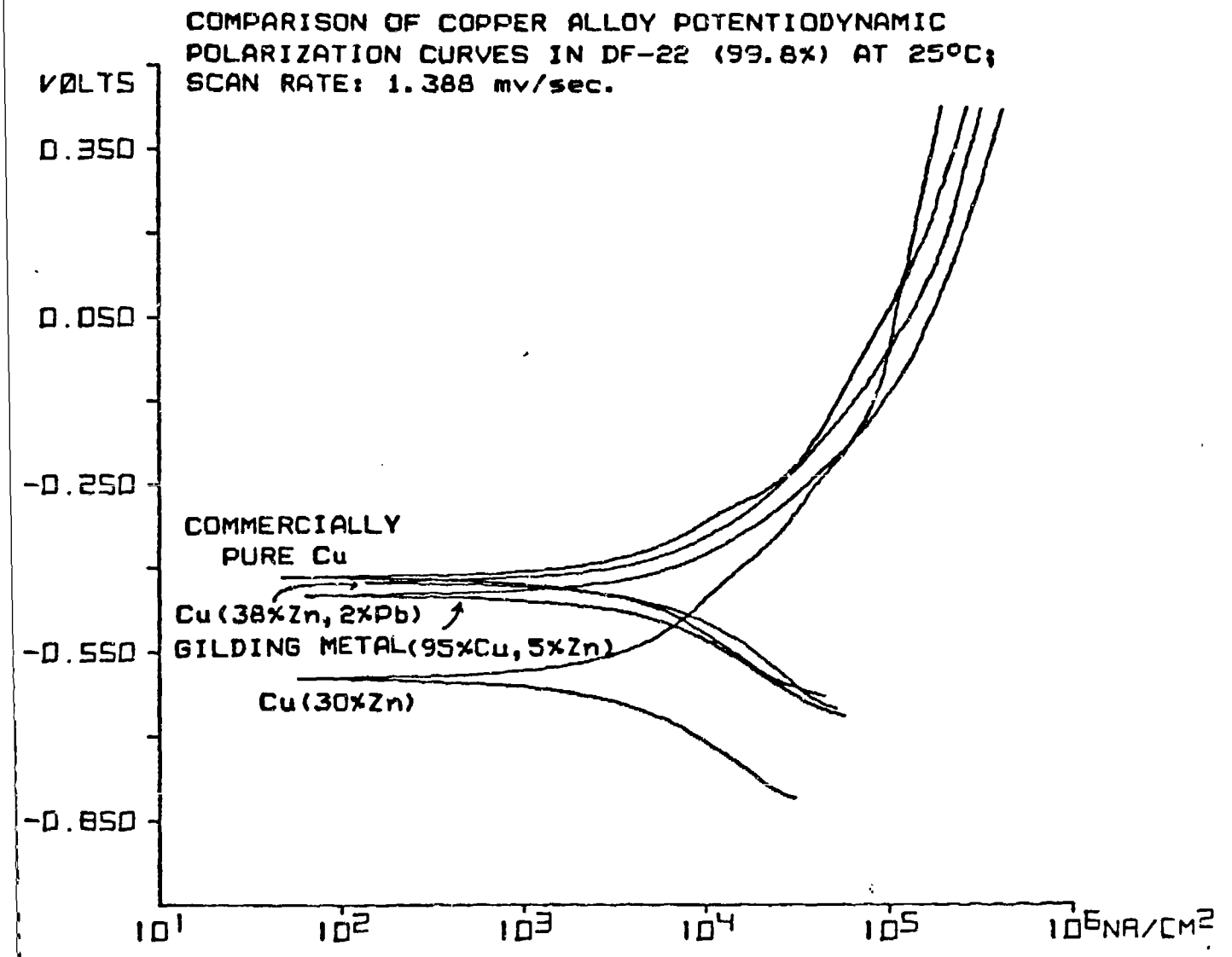
COMPARISON OF COPPER ALLOY POTENTIODYNAMIC
POLARIZATION CURVES IN DF-22 (99.8%) AT 25°C;
SCAN RATE: 1.388 mv/sec.
VOLTS
0.350
0.050
-0.250
-0.550
-0.850
COMMERCIALLY
PURE Cu
Cu(38%Zn, 2%Pb)
GILDING METAL(95%Cu, 5%Zn)
Cu(30%Zn)
10¹
10²
10³
10⁴
10⁵
10⁶NA/CM²

Figure 10

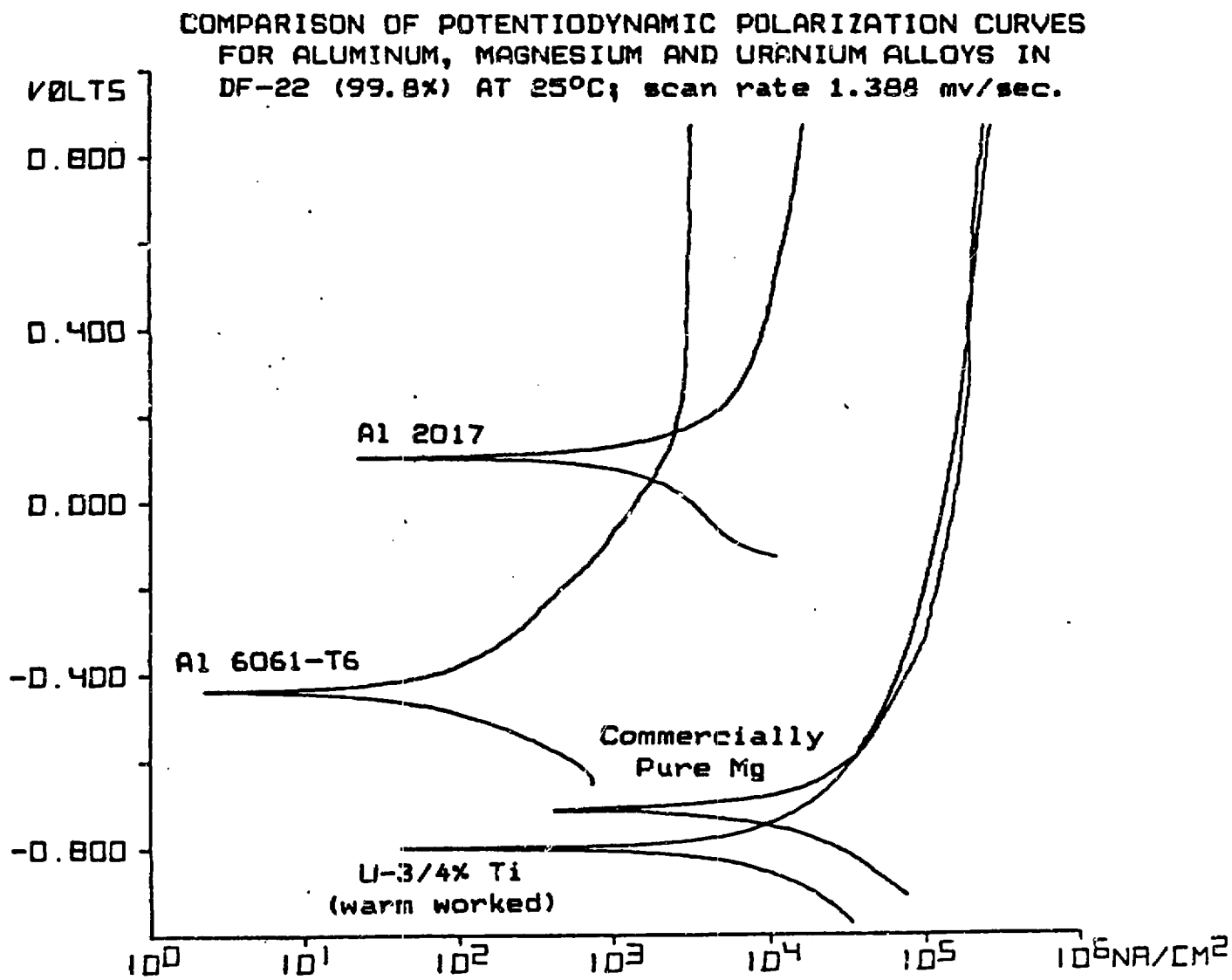

Figure 11

US ARMY
LABORATORY COMMAND
MATERIALS TECHNOLOGY
LABORATORY

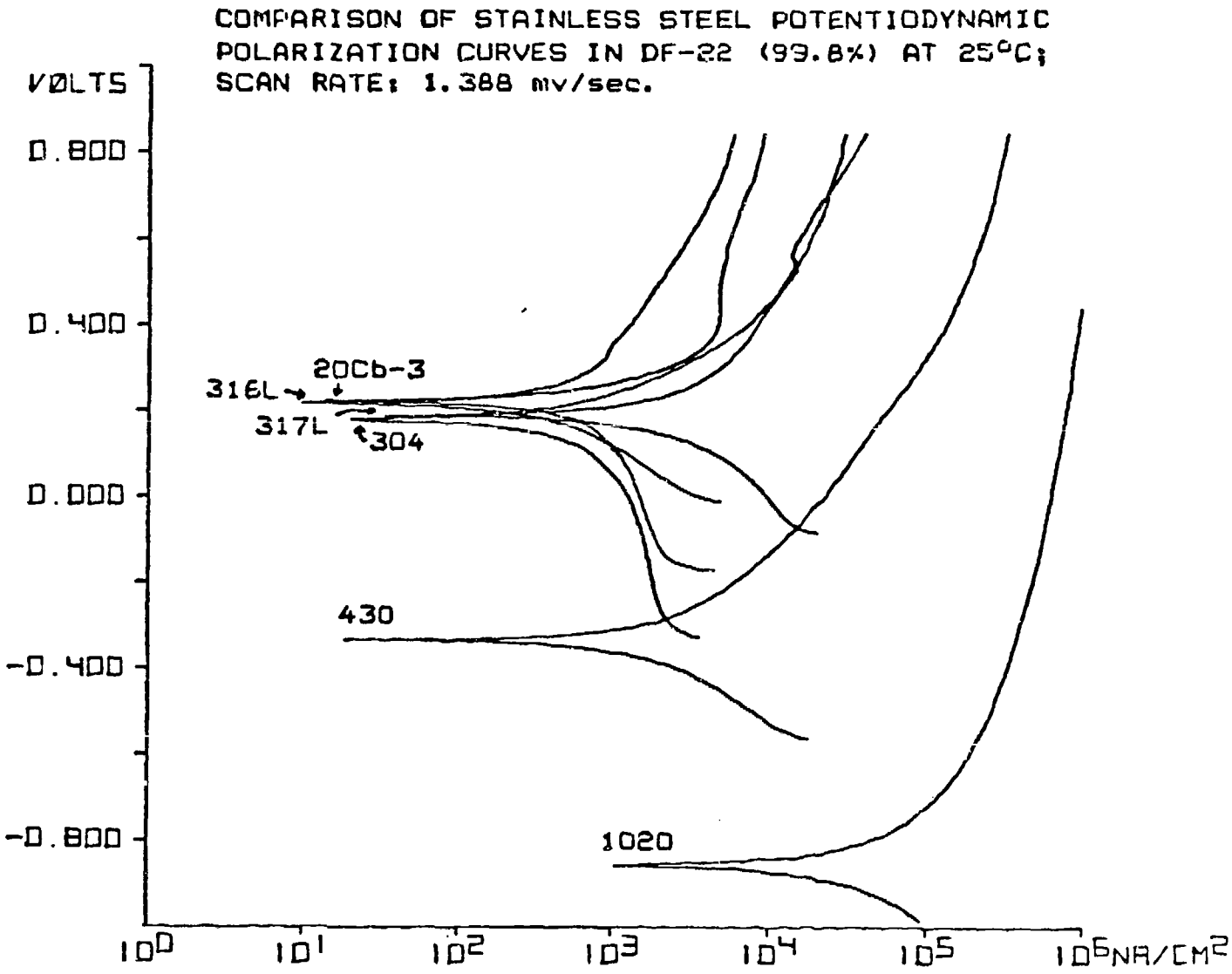
COMPARISON OF STAINLESS STEEL POTENTIODYNAMIC
POLARIZATION CURVES IN DF-22 (99.8%) AT 25°C;
SCAN RATE: 1.388 mv/sec.
VOLTS
0.800
0.400
0.000
-0.400
-0.800
316L
20Cb-3
317L
304
430
1020
10^0
10^1
10^2
10^3
10^4
10^5
10^6 NA/CM^2

Figure 12

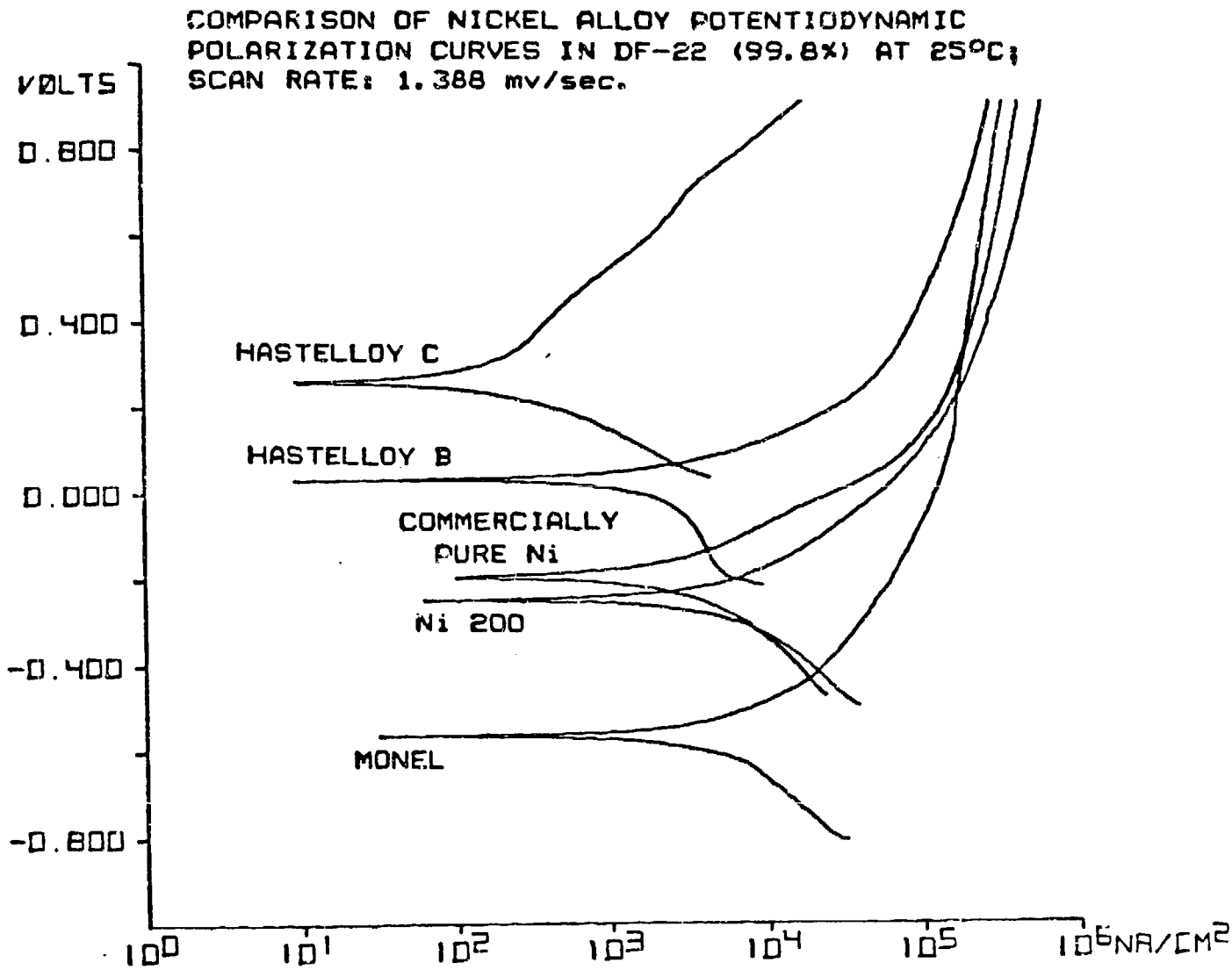
COMPARISON OF NICKEL ALLOY POTENTIODYNAMIC
POLARIZATION CURVES IN DF-22 (99.8%) AT 25°C;
SCAN RATE: 1.388 mv/sec.
VOLTS
0.800
0.400
0.000
-0.400
-0.800
HASTELLOY C
HASTELLOY B
COMMERCIALLY
PURE Ni
Ni 200
MONEL
10^0
10^1
10^2
10^3
10^4
10^5
10^6 NA/CM^2

Figure 13

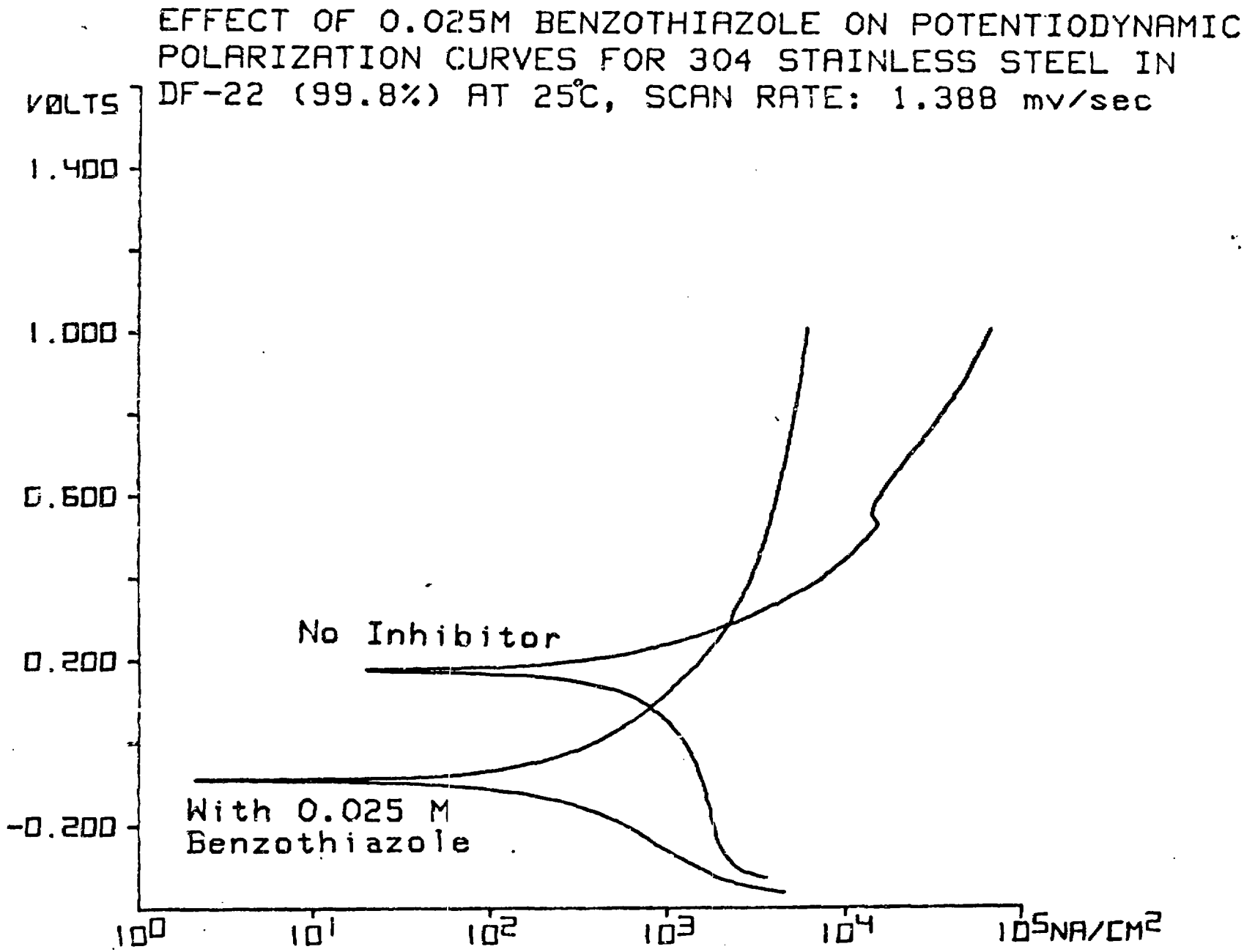
EFFECT OF 0.025M BENZOTHIAZOLE ON POTENTIODYNAMIC POLARIZATION CURVES FOR 304 STAINLESS STEEL IN DF-22 (99.8%) AT 25°C, SCAN RATE: 1.388 mv/sec
VOLTS
1.400
1.000
0.600
0.200
-0.200
No Inhibitor
With 0.025 M Benzothiazole
10^0
10^1
10^2
10^3
10^4
10^5 NA/CM^2

Figure 14

ELIMINATION OF PITTING OF 304 STAINLESS STEEL EXPOSED TO DF-22 VAPOR FOR 30 DAYS BY ADDITION OF 0.025M BENZOTHIAZOLE

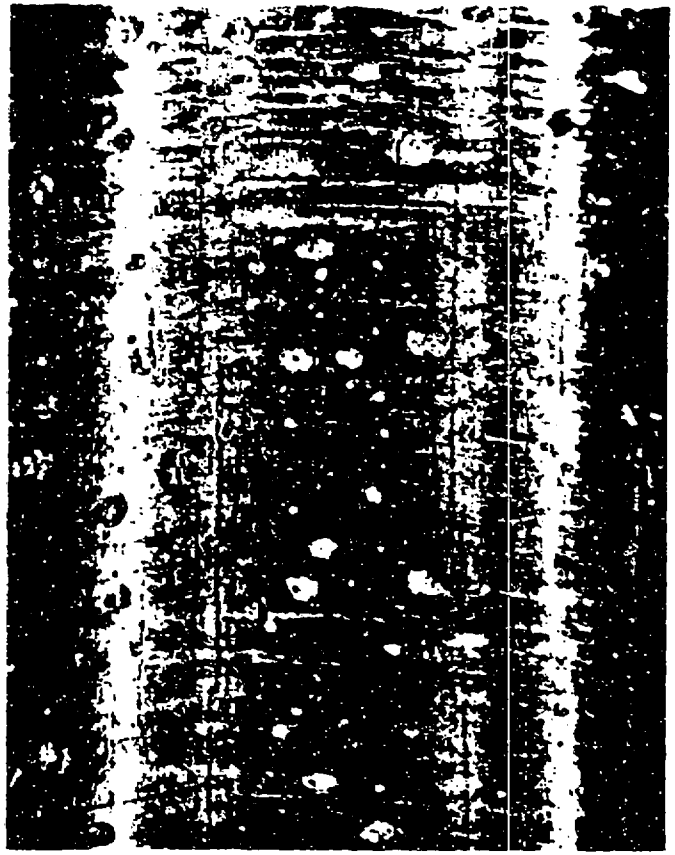

Magnification: 40X

304 STAINLESS STEEL IN DF-22 VAPOR

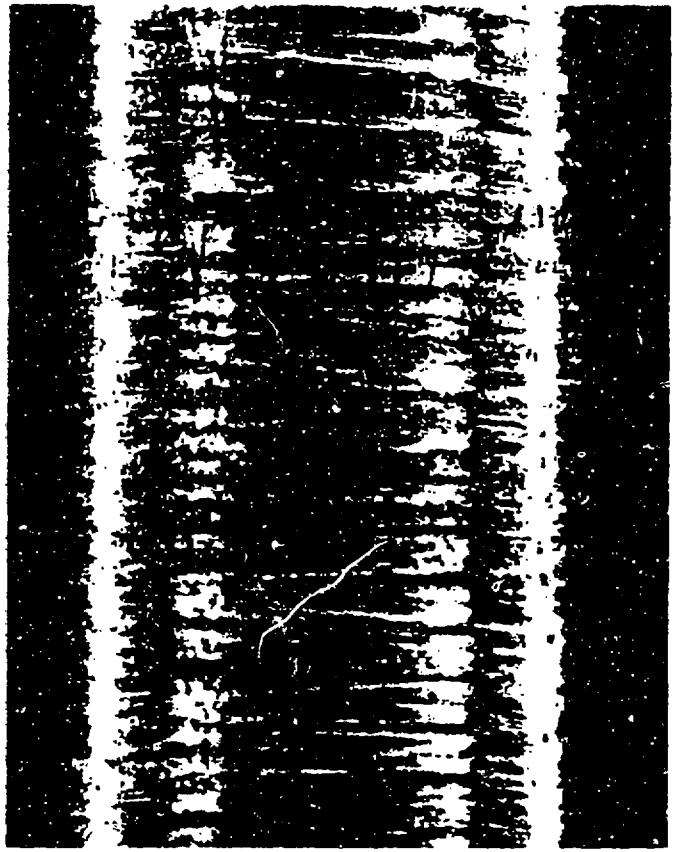

Magnification: 40X

304 STAINLESS STEEL IN DF-22 VAPOR WITH 0.025M BENZOTHIAZOLE

Figure 15

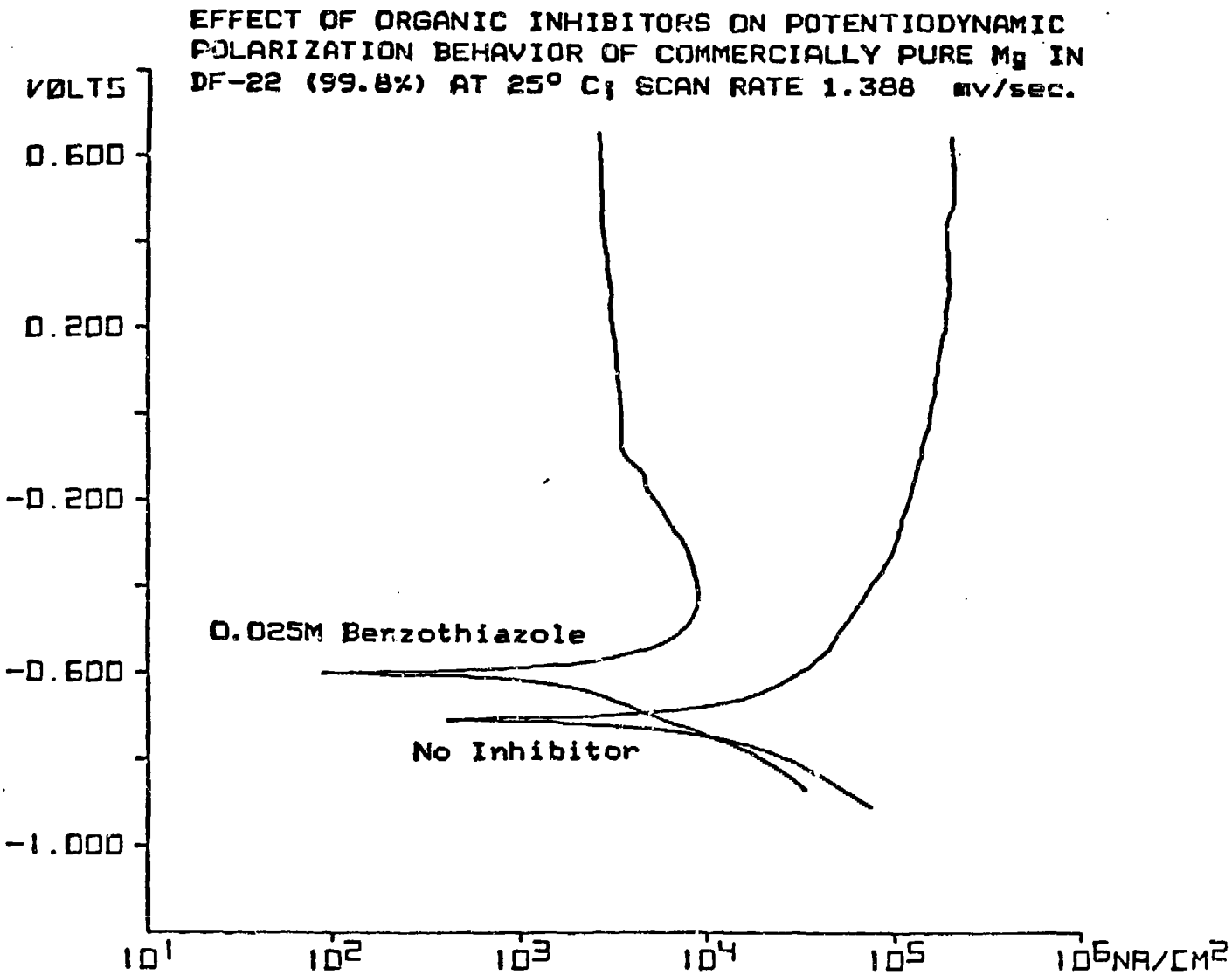
EFFECT OF ORGANIC INHIBITORS ON POTENTIODYNAMIC POLARIZATION BEHAVIOR OF COMMERCIALLY PURE Mg IN DF-22 (99.8%) AT 25° C; SCAN RATE 1.388 mv/sec.
VOLTS
0.600
0.200
-0.200
-0.600
-1.000
0.025M Benzothiazole
No Inhibitor
10¹
10²
10³
10⁴
10⁵
10⁶NA/CM²

Figure 16

REDUCTION OF PITTING OF COMMERCIALLY PURE Mg EXPOSED TO DF-22 VAPOR FOR 15 DAYS BY ADDITION OF 0.025M BENZOTHIAZOLE

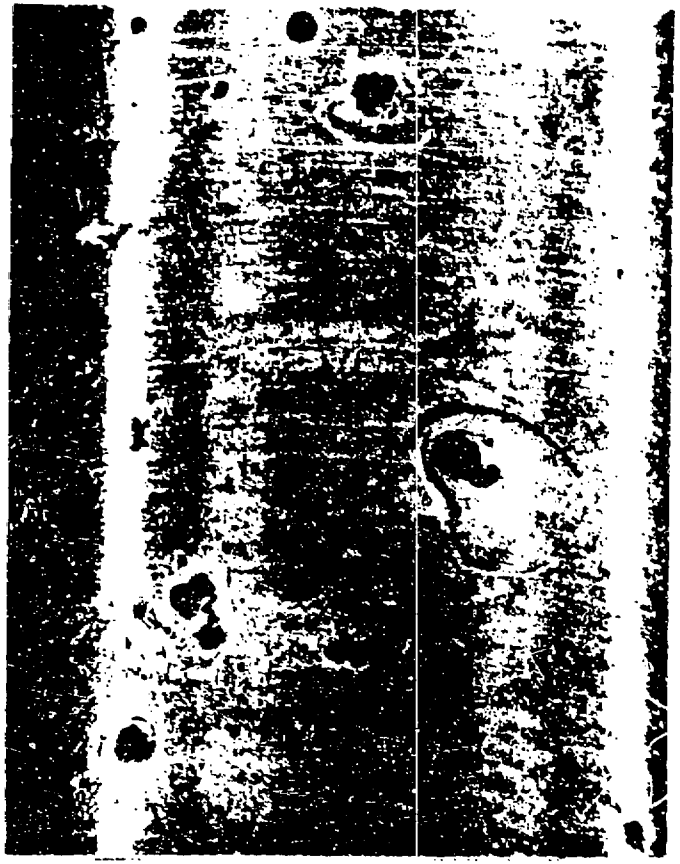

Magnification: 40X

COMMERCIALLY PURE Mg
Mg IN DF-22 VAPOR

Magnification: 40X

COMMERCIALLY PURE Mg IN DF-22
VAPOR WITH 0.025M BENZOTHIAZOLE

Figure 17

SESSION B
SPECIAL TOPICS - NAVY

Chairman
Vinod Agarwala
Naval Air Development Center

DEVELOPMENT OF MICROENCAPSULATED DNBM QUATERNARY AMMONIUM INHIBITORS FOR PAINTS

L.J. Bailin[1] and V.S. Agarwala[2]

Abstract

The microencapsulation of DNBM quaternary ammonium corrosion inhibitors (dichromate, nitrite, borate, and molybdate) for use in epoxy polyamide primers on naval aircraft has been accomplished using a cellulose ether as the outer shell with a deactivating step applied to render the shell impermeable to the primer solvents during cure. The microcapsules are in the 5-30μm (micron) particle size range, and have been prepared to contain 30, 55, and 70% DNBM. These inhibitors were developed to retard corrosion fatigue and stress corrosion cracking in high strength steels and aluminum alloys. Corrosion testing is underway at Lockheed and the Naval Air Development Center, Warminster.

Introduction

The sudden, catastrophic damage caused by environmentally related failures of high strength steel and aluminum alloy naval aircraft parts has long been recognized as a major material problem. Early emphasis focused on improving mechanical properties of the alloys to compensate for these defects. However, it was soon realized that increasing the strength of the steels also increased their susceptibility to environmental cracking or fatigue failures. Subsequent studies concentrated on the interplay of corrosion processes occurring at crack tips or areas of high stress concentrations. To minimize the corrosion processes associated with fatigue cracking, several exploratory studies were carried out based on the feasibility of developing new inhibitor compounds, such as quaternary ammonium salts and crown ether complexes, to be applied in situ for the arresting of crack propagation (Ref. 1, 2). Organic amine chromate salts were also investigated previously as potential inhibitors, and were found to be generally more effective than the common inorganic primer chromates (Ref. 3); however, instability to heat and/or light has precluded their continued development.

Several of the new compounds that have been successful in retarding corrosion fatigue and stress corrosion cracking are described in a recent summary of corrosion inhibition in high strength aerospace materials, including Type 4340 and 300M steels, and 7075-T6 aluminum

(1) Lockheed Palo Alto Research Laboratory, Research and Development Division, Lockheed Missiles & Space Co., Inc., Palo Alto, California

(2) Aero Materials Division, Naval Air Development Center, Warminster, Pennsylvania

alloy (Ref. 4). These materials have been named DNBM, an acronym for a dark brown, high viscosity, 100 percent solids mixture of quaternary ammonium dichromate, nitrite, borate, and molybdate. The properties of these compounds are such that they act to:

(a) inhibit moisture entry at the crack tip, thereby inhibiting corrosion

(b) modify the interfacial chemistry such that atomic hydrogen is removed immediately, thereby impeding its entry into the metal

(c) create a chemical barrier (passive film) at the crack surface

DNBM Materials Development

As originally evaluated for corrosion inhibition, the individual DNBM compounds were prepared in gram quantities that were adequate for application to a crack tip or similar surface. Except for the borate quaternary, however, none was available in quantities required for paints. One objective of the development program, therefore, was to prepare the D, N, and M salts in kilogram size lots. Following initial investigative synthesis and laboratory trials, this was achieved through a commercial supplier. At this time, scaleup to the pilot level, in multikilogram quantities, is in the planning stages.

To illustrate the double exchange reaction, a block diagram of the synthesis is shown in Fig. 1. The nitrite and molybdate salts were prepared by a similar mechanism. The resultant molybdate quaternary was a monosubstituted salt, $CH_3(C_8\text{-}C_{10})_3N\cdot NH_4Mo_2O_7$, determined from the analytical data on Mo content and non-reacted starting material. Table I contains percent analyzed vs. theoretical data for Cr, NO_2, B and Mo, the results having been obtained from kilogram batches of the salts. To maintain chloride levels as low as possible, the sulfate salt was used as the quaternary ammonium starting material.

The DNBM mixture was prepared by adding equal numbers of Cr and Mo atoms. Nitrite was added as if it were a single unit in ~30% excess, and the borate quaternary was added in the same and double the number of Cr atoms.

The 100% DNBM mixture was stable in laboratory light with no change in color or formation of Cr(III) over a period of several weeks. In the presence of solvents, e.g. toluene, isopropanol, a marked change from dark brown, Cr(VI), to green, Cr(III), was observed in several hours to days, depending on the solvent concentration, when exposed to laboratory light. In the case of toluene-DNBM mixtures, GC-MS analysis indicated the formation of benzoic-acid, benzaldehyde, and benzyl alcohol, illustrative of the oxidative activity of the dichromate quaternary salt toward this solvent.

DNBM Solubility in Nonaqueous Solvents and Equilibria in Aqueous Media

The dichromate quaternary has been observed to be almost universally soluble in aliphatic, aromatic, and chlorinated solvents. This is also true for the nitrite, borate, and molybdate salts, with the

exception that the borate is less soluble in acetonitrile; and the molybdate is less soluble in low molecular weight aliphatics, such as petroleum ether.

Of direct consequence to the performance of the inhibitor are the following observations:

a) The salt is insoluble in distilled (ion free) water.

b) The addition of quaternary starting material does not cause any change in solubilization in distilled water.

c) The addition of aqueous sodium chloride or other water soluble ions causes an orange color, Cr(VI), to develop in the aqueous layer.

This evidence supports the concept of reversibility of the exchange equilibria, as well as the integrity of the quaternary functionality shown in Fig. 1.

The probable mechanism for DNBM corrosion inhibition is therefore release of the inorganic inhibitor anions in the presence of seawater, which, under adverse conditions, will make its way through the coating to the substrate that is to be protected. In addition to the hydrolysis reactions, there will form free quaternary ammonium cations, the hydroxide, or chloride, that can act as a separation barrier at aluminum or steel substrates. Non-dissociated DNBM can also serve as a barrier film.

pH of DNBM Quaternary Ammonium Salt Mixtures in Seawater

An additional requirement for practical application of the DNBM inhibitor mixtures is that the pH of DNBM in saltwater will be near neutral. To determine the pH values of DNBM-seawater mixtures, four samples were prepared. The salt water was natural, filtered Pacific Ocean seawater of pH 7.9. The readings were determined after mild stirring or contact for two arbitrary periods of 3 and 15 min. Two levels, excess quaternary and excess seawater, were chosen as conditions that could occur at a primer-substrate interface in the process of failure. Stirring was slow, sufficient to maintain contact between the two phases during the two time periods. See Table II. The borate salt appeared to have less effect on pH than anticipated; however, this may have been caused by a hydrolysis rate effect that could result in somewhat higher pH readings later on.

Formulation of DNBM Inhibitors in Paints

The preferred, and most obvious location for a corrosion inhibitor in an organic coating that is used to protect a metal surface is the position closest to the corrodible substrate. In the case of naval aircraft coatings, it is the epoxy polyamide primer. Fig. 2 shows a cross section of the system, which for aluminum utilizes an aliphatic polyurethane top coat; and for steel, an epoxy or polyurethane top coat. If the DNBM mixture is added directly to the epoxy primer system, the DNBM will dissolve in the solvents of the formulation,

and, depending on the quantity added, may change the cure rate, water resistance, or other properties that can be affected by the presence of a non film-forming, solvent-soluble organic additive. When added to part A of the epoxy formulation (diglycidyl ether of bisphenol A resin, solvents, pigments, etc.), the dichromate quaternary will slowly oxidize the solvents or the hydroxyl bonds of the glycidyl ether branch, with concurrent reduction and loss of the DNBM Cr(VI) content in the presence of light to Cr(III). Therefore, the DNBM inhibitor should be separated from the primer components during the period of formulation, drying and cure. The process of microencapsulation was selected as the means to carry out this function.

Microencapsulation of DNBM for Epoxy Polyamide Primers

The purposes of microencapsulation are specific. The DNBM inhibitor must be protected from contact with the solvents and uncured polymers of the epoxy system. In so doing, the mixture is held in reserve in the primer coat, such that when called for, e.g., as the result of environmental damage to the top coat and primer, the DNBM mixture is released into the area needed. At the same time, the shell of the microcapsule must be sufficiently hydrophilic or water susceptible that when seawater penetrates the primer by diffusion or through cracks, the microcapsules will allow the water to pass through, thereby releasing the DNBM inhibitor from the shell. Since the shell characteristics must be controlled, a shell deactivation process is required in order to accommodate the different penetration/release rates required of the microcapsules.

The criteria used for selection of the microcapsule shell polymers are listed as follows:

a) Non-solubility in coating solvents
b) Non-reactivity with DNBM or coating components
c) Well-established polymer properties
d) Amenable to commercial formulation and production with DNBM

The primary requirement is that the encapsulant polymer resist all solvents, resins, additives, etc., that are present in the primer formulation. The solvents that are used in epoxy polyamide coatings are general solvents, including methyl ethyl ketone, isopropyl alcohol, isobutyl alcohol, butyl cellosolve, cellosolve acetate, with, possibly, small amounts of toluene and xylene. The Mil-T-81772, Type II (epoxy) diluent contains methyl ethyl ketone, methyl isobutyl ketone, and ethylene glycol monoethyl ether or propylene glycol methyl ether. The coating polymers that are insoluble in these solvents and that are also water soluble/dispersible belong to the family of cellulose ethers. Of these, methyl cellulose, hydroxyethyl methylcellulose, and hydroxypropyl methylcellulose were the principal test candidates. Polyvinyl alcohols, derived from hydrolyzed polyvinyl acetate, have similar properties, and were included also.

Basic Microencapsulation Mechananisms

The basic mechanism involves several steps, described as follows for the DNBM-cellulose ether system. The initial step is formation of a stable oil-in-water emulsion of DNBM in an aqueous colloidal solution of the cellulose ether. Methyl cellulose (MC) or one of the alternate polymer candidates is first dissolved in deionized water to form a stable colloidal emulsion. Next, core material is added, and high shear high speed mixing is applied to disperse the DNBM. It was noted experimentally that the ionic salt impurities (e.g. chloride, sulfate, acetate, etc.) in the polymer commodities, particularly the polyvinyl alcohols, were detrimental to the stability of the emulsions; this was observed when the DNBM mixture - reacting prematurely with the impurities - produced yellow-colored aqueous solutions of Cr(VI) ion with a corresponding loss in stability of the colloid.

The objective at this point was to separate the water layer from the stable colloid dispersion. Several methods were available, and were claimed to be relatively simple to perform in the laboratory (Ref. 5). Following preliminary coacervation and phase separation experiments, which were only partially successful, spray drying encapsulation techniques were applied, and these were found to give reproducible results under defined conditions of nozzle size, flow rate, core content, and polymer shell concentration. The advantages of spray drying applied to DNBM-methylcellulose is the ability to handle the labile DNBM materials during the short contact time in the dryer, and the economy of operation (Ref. 6). Two photomicrographs illustrate the 30% core microcapsules. Fig. 3 illustrates in dark and bright field the microcapsules produced in a laboratory-size spray dryer using the D salt, quaternary ammonium dichromate, as the core material. Particle size was mainly 5 to 30 μm (microns). Fig. 4 shows 30% core microcapsules that contain DNBM prepared in a pilot scale spray dryer (commercial operator). The capsules are in the same particle size range, but there are more 30μm particles than in Fig. 3. It may be noted that some of the Fig. 4 microcapsules contain little or no core material as evidenced by a lack of opacity. This is attributed to extraction by the hydrocarbon immersion oil that is used to disperse the particles for photomicrography. Similar phenomena occur if the microcapsules are added directly to the epoxy polyamide formulation without initially deactivating the shell surfaces.

Deactivation of Microcapsule Surfaces

To prevent uncontrolled diffusion of the primer solvents through the cellulose ether shell of the microcapsules, a means to deactivate the shell surface was developed. Alkoxy silanes were applied to the capsules by a method that is the same as that used to apply silanes to waterproof the thermal insulation tiles on the Space Shuttle (Ref. 7) Short chain siloxanes are produced, not silicones that would contaminate paints (or optical surfaces on the Shuttle).

A photomicrograph of silanized microcapsules that contain 55% DNBM is shown in Fig. 5 Except for size distribution, the particle size range

of 5 to 30μm is similar to those in Fig. 3 and 4. Microcapsules containing 70% DNBM (not shown) were also prepared having a similar size and size distribution. Fig. 6 drawings portray the geometry of the three capsules.

It is likely that several silane treatment levels will be required to achieve different diffusion or disintegration rates when the treated particles are added to a working epoxy polyamide primer. This conclusion is based on NaCl and water diffusivity studies in the same epoxy system that indicate a relatively short diffusion time, a few weeks to months, for the NaCl-H_2O system to pass through the epoxy polyamide primer coat to the substrate (Ref. 8).

Development of Optimum Size for DNBM Microcapsules

The standard epoxy polyamide primer used on naval aircraft is controlled by Mil-P-23377, Primer Coatings: Epoxy-Polyamide, Chemical and Solvent Resistant. The principal corrosion inhibitor pigment is strontium chromate, an inorganic solid that is effectively insoluble in the coating. As a result of restrictions caused by the presence of the inorganic pigment, the range of dry film thickness is specified from 0.6 to 0.9 mils or 15 to 23 microns. Upon initial consideration the same requirement would seem to apply to the DNBM microcapsules. However, the microcapsules are liquid cores surrounded by a thin shell of deactivated cellulose ether. Thus it is likely that the thickness restriction will not be directly applicable, since the microcapsules are less brittle or friable than the $SrCrO_4$ particles and should have a lower (less negative) effect on cohesion than the solid inorganic particles. The epoxy polyamide coatings may therefore be useful at greater than 1 mil; and particle sizes greater than 23 microns, from 25 to 50 microns, may be acceptable. The optimum size remains to be determined through formulation and test.

Current particle size development is directed at 20-40 μm, with a minimum number of particles below 15 μm. The latter restriction results from calculation of the wall thickness for a 15 μm or less particle that contains 70% by weight DNBM. The calculated wall thickness, utilizing the following equations, is 0.84 μm, assuming the density of the polymer wall and core to be equal to 1.0.

$$W = r_1 - r_2$$

where W = wall thickness, r_1 = capsule radius, r_2 = radius of encapsulate.

$$W = \sqrt[3]{\frac{3V_1}{4\pi}} - 3\sqrt{\frac{100 - \%\ \text{wall}}{100}\left(\frac{3V_1}{4\pi}\right)}$$

where V_1 = volume of capsule. (Ref. 5). This is too thin to obtain shell and silanization uniformity.

Corrosion Testing of DNBM Microcapsules in Epoxy Polyamide Coatings

Corrosion testing is underway at Lockheed and the Naval Air Development Center, Warminster. The MIL-P-23377 epoxy polyamide primer is the control, and DNBM is being formulated as a replacement for the standard $SrCrO_4$ inhibitor. Tests include -

a) Accelerated neutral salt spray (fog)
b) Copper accelerated acetic acid salt spray (fog)
c) Accelerated weather resistance (xenon arc)
d) Corrosion fatigue (electrochemical)

plus coating evaluations to determine the effect, if any, of the DNBM microcapsules on the working properties of the primer.

Acknowledgement

This work is supported by the Naval Air Development Center, Warminster, Pennsylvania, under Contract No. 62269-85-C-0218.

References

1) Clark, K.G. and J. Ohr, "The Chemistry and Applications for the Solubilization of Chromate Salts in Nonpolar Organic Media - Part III," Report No. NADC-78017-60, 23 Mar 1979. AD A072922

2) Agarwala, V.S. and J.J. DeLuccia, "New Inhibitors for Crack Arrestment in Corrosion Fatigue of High Strength Steels," NACE, 36, 208-12 (1980)

3) Rice, K.K., S.L. Lehmann, D.K. Klapprott, C.L. Mahoney, "Exploratory Development of Corrosion Inhibiting Primers," AFML-TR-77-121, 11 Jul 1977. AD B026652.

4) Agarwala, V.S. and J.J. DeLuccia, "Inhibition of Corrosion Fatique and Stress Corrosion Cracking in High Strength Aerospace Materials," Paper No. 258, Extended Abstracts, 170th National Meeting, The Electrochemical Society, San Diego, CA, Oct 19-24, 1986.

5) Patwardhan, S.A. and K. G. Das, "Microencapsulation" Ch. 5, in Controlled-Release Technology, Ed. K.G. Das, Wiley-Interscience, 1983.

6) "Microencapsulation" in Kirk-Othmer Encyclopedia of Chemical Technology, , 3d ed. Vol. 15, pp 470-93 (1981).

7) Manufacturing Process, Lockheed Missiles & Space Co., Inc., Sunnyvale, CA.

8) Ruggeri, R.T. and T.R. Beck, "Application of Electrochemical Engineering Methods and Theory to Solving Corrosion and Adhesion Problems with Organic Coatings," Report No. NADC-84107-60, April 1984. AD-A147799.

- BASIC EXCHANGE EQUILIBRIA

$$2[CH_3(C_8 - C_{10})_3N \cdot Cl] + Na_2Cr_2O_7 \underset{XSNaCl}{\overset{XSCr_2O_7^{2-}}{\rightleftharpoons}} \text{QUATERNARY AMMONIUM DICHROMATE } [CH_3(C_8 - C_{10})_3N]_2^+ \cdot Cr_2O_7 + 2NaCl$$

- PROCESS

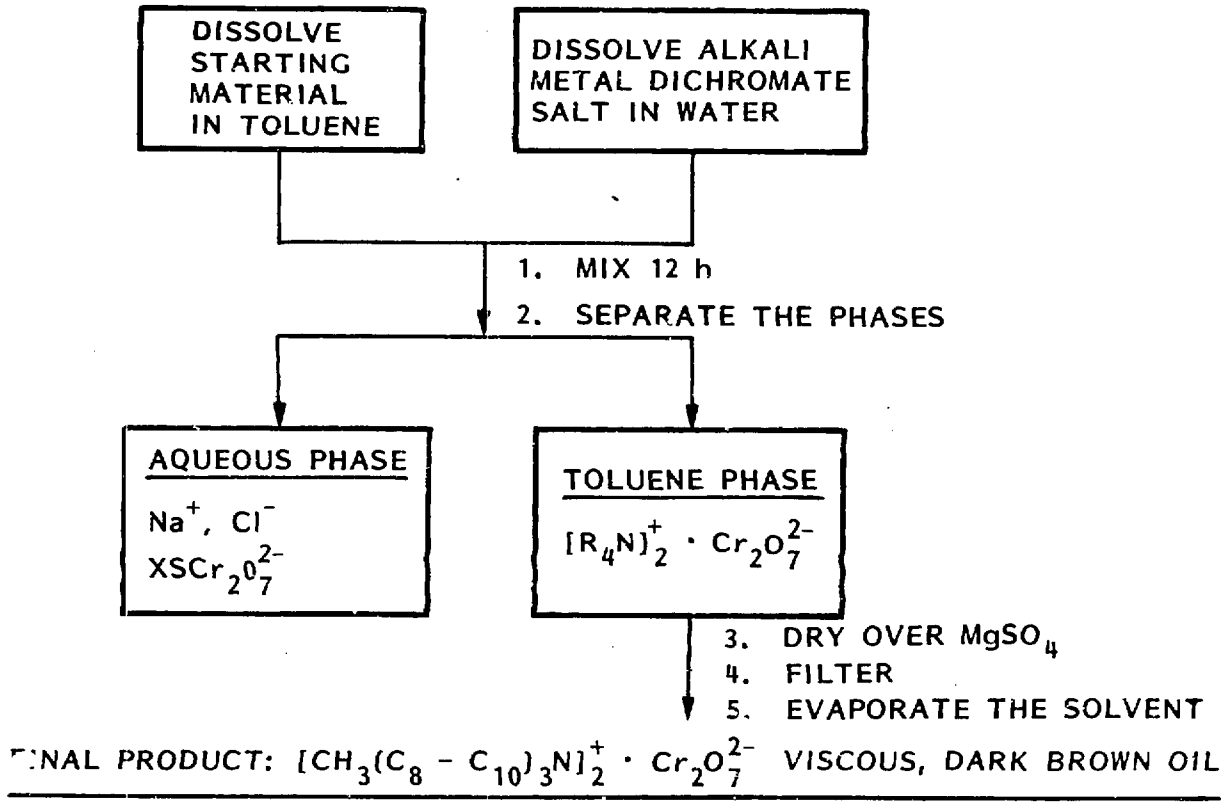

FIGURE 1. SYNTHESIS OF QUATERNARY AMMONIUM DICHROMATE "D"

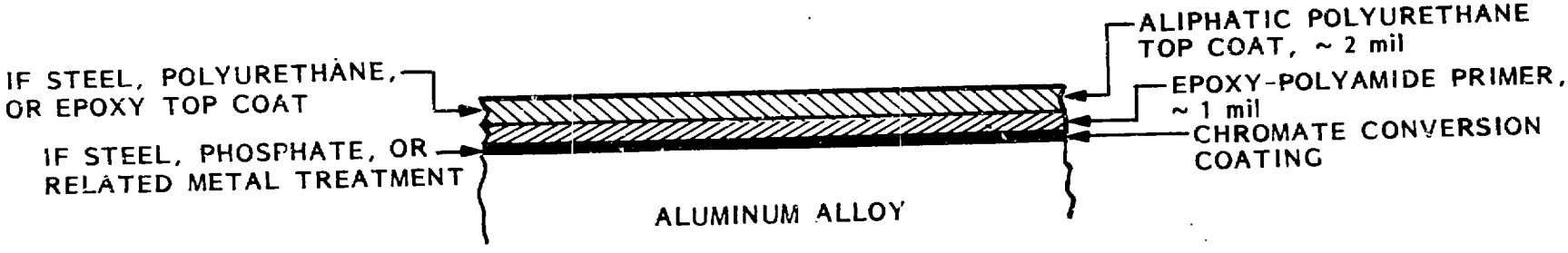

FIGURE 2. PLACEMENT OF DNBM INHIBITOR IN PAINTS

200X OPTICAL MICROGRAPH, SAMPLE NO.7-864

30% CORE, SPRAY DRIED

10μm

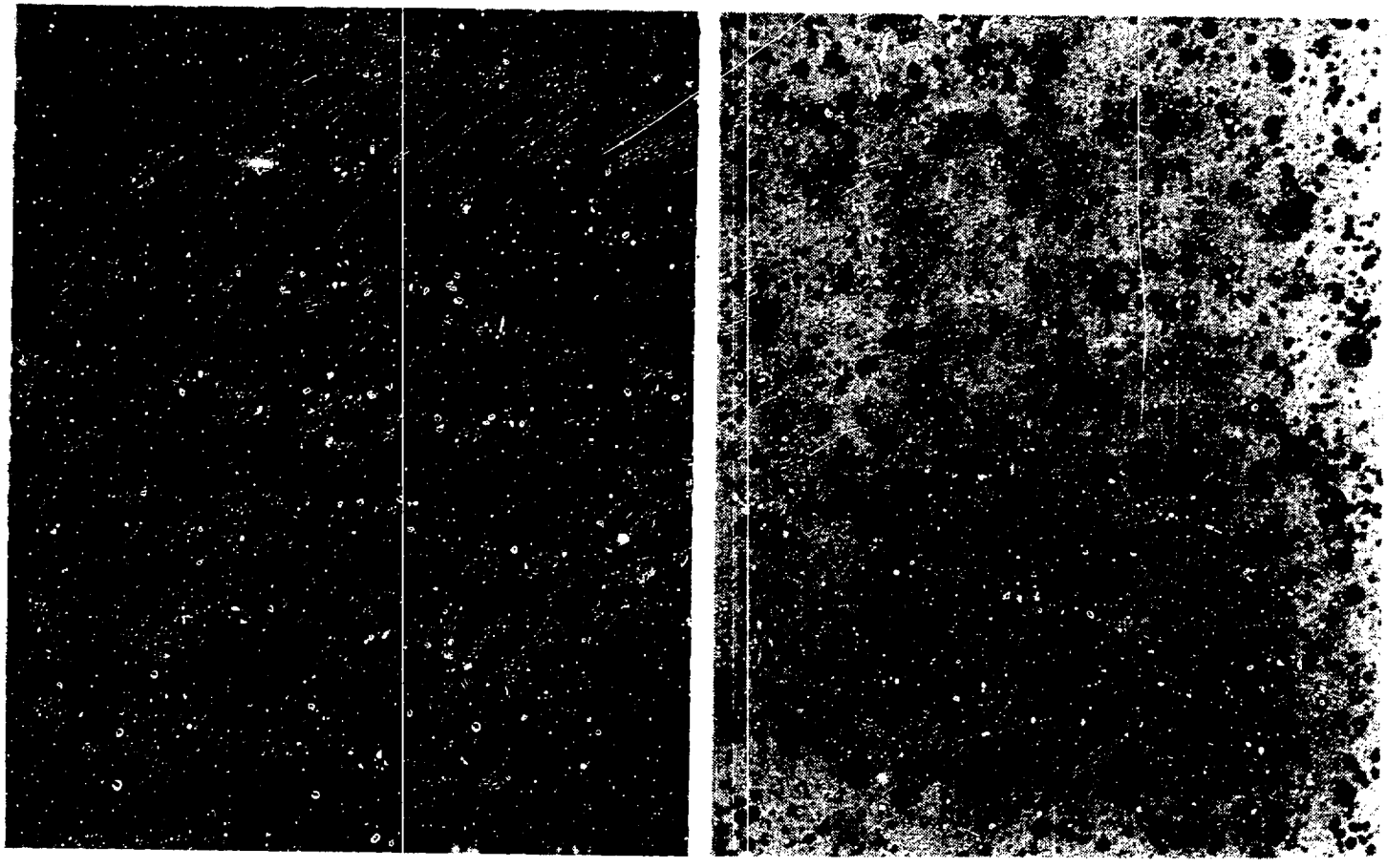

FIGURE 3. D (DICHROMATE) LABORATORY EMULSIFICATION AND SPRAY-DRY PROCESS

200X OPTICAL MICROGRAPH, SAMPLE NO.7-968

30% CORE, SPRAY DRIED

10μm

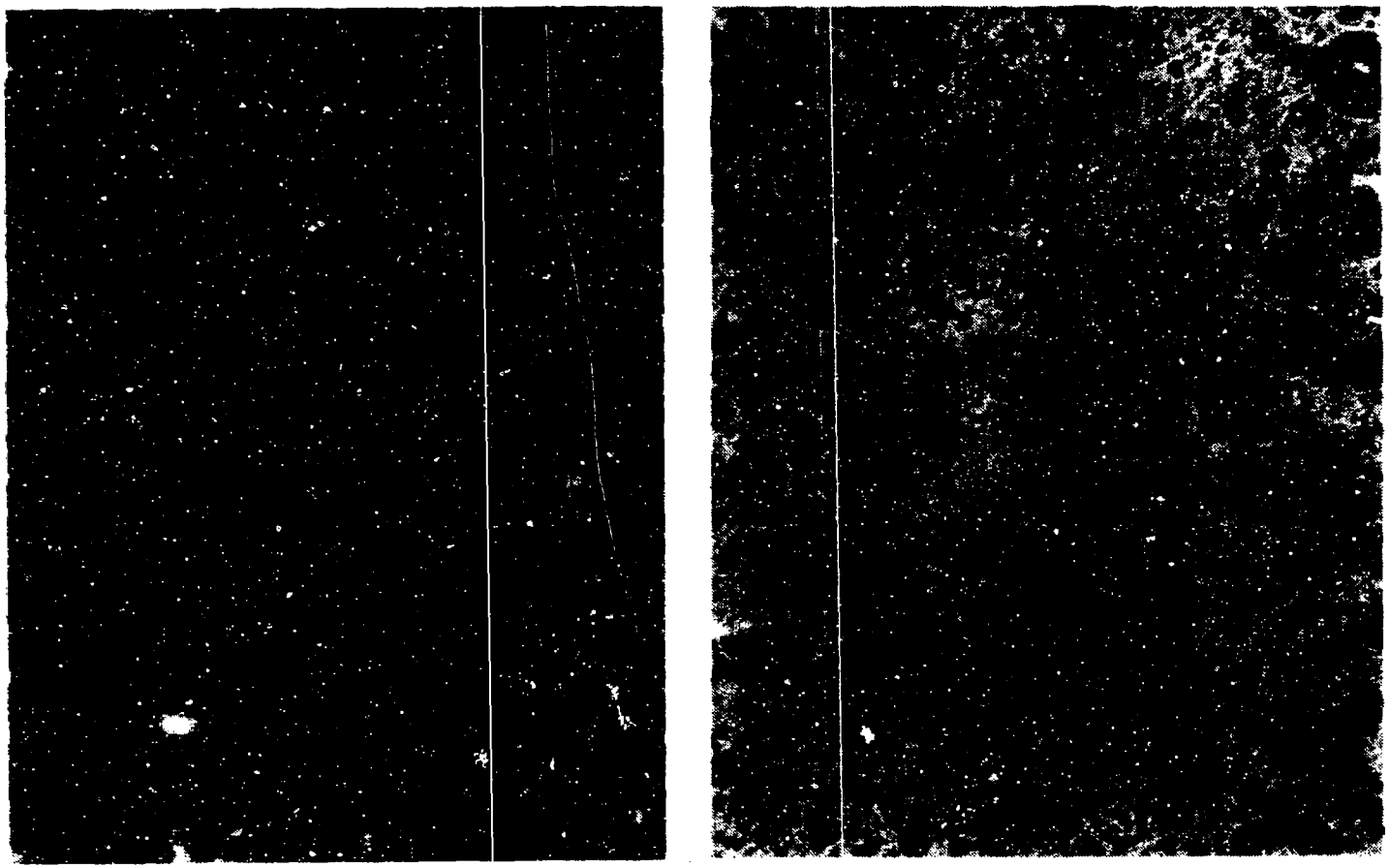

FIGURE 4. DNBM MICROENCAPSULATION SCALE UP

200X OPTICAL MICROGRAPH, SAMPLE NO. 8-082

55% CORE, SPRAY DRIED, SILANIZED

10μm

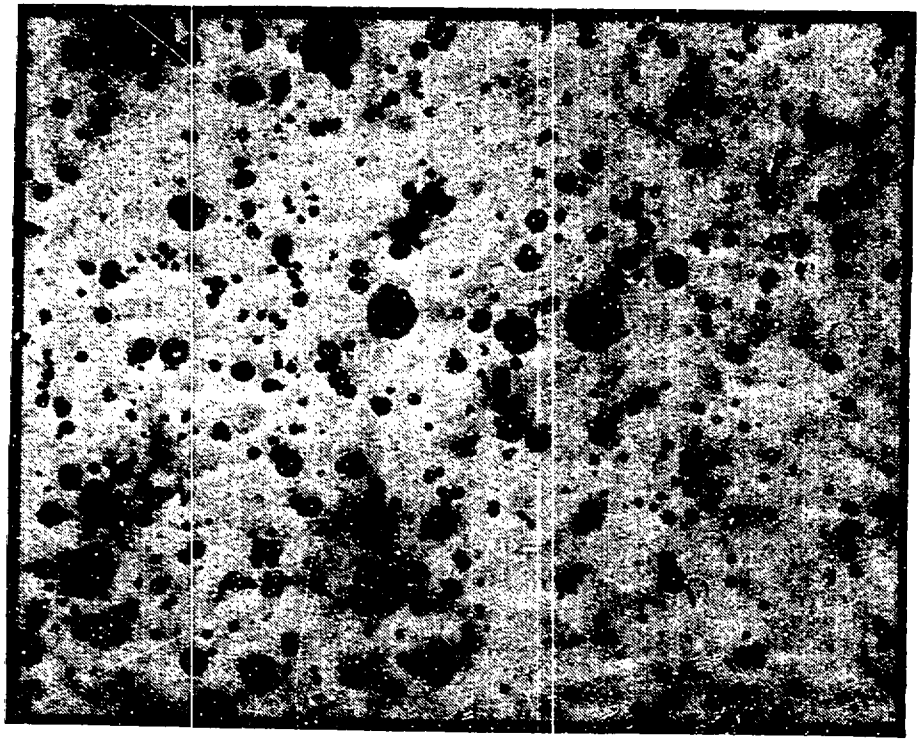

FIGURE 5. DNBM MICROENCAPSULATION SCALE UP

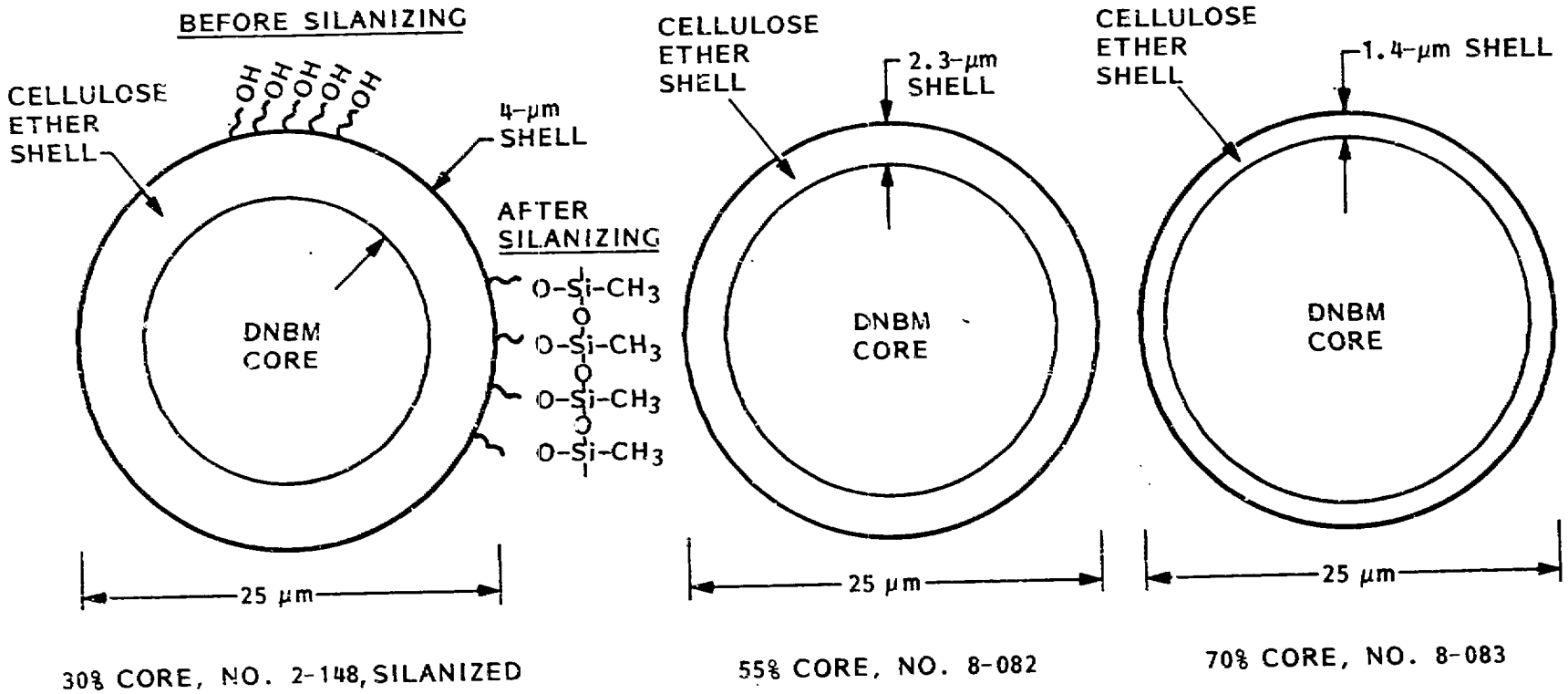

FIGURE 6. MICROENCAPSULATED DNBM INHIBITOR PARTICLES

TABLE I. ANALYSIS OF INDIVIDUAL KILOGRAM QUANTITY DNBM QUARTERNARY AMMONIUM SALTS

SALT	PERCENT ANION		THEORETICAL	PERCENT YIELD	CHLORIDE ppm
D DICHROMATE, 150-149	Cr (VI)	9.4	10.16	92.5	47
N NITRITE, 150-160	NO_2^-	7.8	10.23	76.2	102
B BORATE, RD 5444A [90% SOLIDS, 10% ISOPROPANOL]	B	1.36	1.51 (AS $H_2BO_3^-$ SALT)	90.1	22
M MOLYBDATE, 150-150 [61% SOLIDS, 39% TOLUENE]	Mo	24.9	26.37 (MONOSUBSTITUTED SALT)	94.4	37

TABLE II. pH OF DNBM – NATURAL SEAWATER MIXTURES AFTER MILD STIRRING

					pH READINGS			
	DICHRO-MATE	NITRITE	BORATE	MOLYBDATE	EXCESS QUATERNARY 10/1		EXCESS SEAWATER 10/3.5	
			(IPA REMOVED)	(61% SOLIDS 39% TOLUENE)	3 min	15 min	3 min	15 min
10990-89	29.0 g	41.4	31.7	32.9	6.59	6.77	6.20	6.26
10990-92	30.0	42.4	78.0	34.6	7.04	7.06	6.54	6.60
RD5444A, BORATE ——— 100% ———					10.4	—	9.16	9.21
NATURAL SEAWATER (PACIFIC OCEAN, HALF MOON BAY, CA) 5/86. FILTERED					7.9			

BIOGRAPHY

NAME: Dr Vinod S. Agarwala

PRESENT AFFILIATION: Surface Interaction Research Group at Naval Air Development Center, Warminster, PA.

TITLE: Materials Technical Specialist and Leader

FIELD OF INTEREST/RESPONSIBILITIES: Principal areas of research are corrosion mechanism and inhibition, corrosion assisted cracking, hydrogen embrittlement, alloy development and environmental corrosion monitoring.

PREVIOUS AFFILIATIONS/TITLES:

ACADEMIC BACKGROUND: Educated at Banaras Hindu University, India, and Massachusetts Institute of Technology, Cambridge, MA. Holds a bachelors's, two master's and a doctorate degrees in physical chemistry, metallurgy and corrosion.

SOCIETY ACTIVITIES/OFFICES/AWARDS: A fellow of the Council of Scientific & Industrial Research, India, the National Research Council of Canada, and the National Research Council of the National Academy of Sciences. An honorary member of the M.E.I. Faculty of the ASM and adjunct professor at Drexel University College, Philadelphia, PA.

a Recipient of Navy's 1981 Scientific Achievement Award and Capt Walter S. Diehl Award for Excellence in Science and Engineering in the Navy.

PUBLICATIONS/PAPERS: Has published extensively and holds two patents on inhibitors.

BIOGRAPHY

NAME: Lionel J. Bailin

PRESENT AFFILIATION: Chemistry Department at Lockheed Palo Alto Research Laboratories.

TITLE: Staff Scientist

FIELD OF INTEREST/RESPONSIBILITIES: Directs and conducts research and development on inorganic and organic coatings for major Lockheed programs. During the past 8 years, he has been actively engaged in the study of corrosion on high strength (7000 series) aluminum alloys and the means to alleviate pitting via improved formulations and applications of chromate conversion coatings. Also serves as consultant to engineering groups on solicone and epoxy coatings as well as inorganic materials used in specialized applications.

PREVIOUS AFFILIATIONS/TITLES: In earlier work at Lockheed, he formulated and tested refractory oxide filled inorganic silicate and silicon coatings for refractory oxide filled inorganic silicate and silicone coatings for thermal control surfaces.

E.I. DuPont De Nemours and Co., Wilmington, Delaware, Pigments Dept.

ACADEMIC BACKGROUND: PhD in Chemistry from Tulane University in heavy metal chemistry, nonaqueous solvents, and complex ions.

SOCIETY ACTIVITIES/OFFICES/AWARDS: Member of Electrochemical Society

PUBLICATIONS/PAPERS: Presented and Authored papers in the area of refractory oxide filled inorganic silicate and silicone coatings for thermal control surfaces.

BEST AVAILABLE COPY

INADEQUACIES OF EMI-SEAL MATERIAL: A CORROSION STUDY

Vinod S. Agarwala
Richard C. Paciej
James J. Thompson
Naval Air Development Center
Warminster PA 18974

ABSTRACT

Electromagnetic interference(EMI) seals are mandatory for all structural joints in naval aircraft because of the high electromagnetic environment present on aircraft carriers. Currently, a major component used in these seals is a 20% Zn/Sn coating arc-sprayed onto an Al alloy substrate. This coating was found to causing major structural damages when exposed to naval environments. Pits up to 35 mils deep on the Al alloy have been observed under the seal after one year of service on F/A-18 aircraft. A study of this material, 20% Zn/Sn arc-spray coating, has been reported here in terms of its compatibility with the substrate metal in naval environments.

INTRODUCTION

All naval aircraft require protection from the high electromagnetic environment present on aircraft carriers. The electromagnetic interference (EMI) seals used in joints for this purpose prevent the reception as well as broadcast of the electromagnetic energy. The seals are vital for the proper functioning of avionics and for lightning strike protection. Poor designs of earlier seals have produced severe galvanic incompatibility. Seals made from silver-filled epoxy (adhesive material) and Ferrex braid system, have shown excessive corrosion damages on substrate structures, aluminum alloys. Due to the severity of the carrier environment, the corrosion damages have been reported to be beyond the means of simple corrective maintenance efforts. During an Age Exploration Program Depot (AEPD) inspection in 1984, extensive corrosion and pitting, pits up to 70 mils deep (the maximum correctable depth is 10 mils), were found in the aluminum alloy structural materials. A quick solution was instituted to replace the silver-filled epoxy in the EMI seal with a 20% Zn/Sn arc-spray coating. Schematic diagrams of both the old and new seal designs and an unexposed Zn/Sn/Ferrex seal are shown in Figure 1. The use of 20% Zn/Sn coating in the design was to protect the structural aluminum alloy cathodically. However, within six months of carrier exposure, structural corrosion damages associated with the new EMI seal were reported (1,2). Figure 2 shows an example of corrosion under the EMI seal and water intrusion on the F/A-18 Radar Nosedome Bulkhead. Additionally, the combination of corrosion and aircraft vibrations caused corrosive wear (dark areas in Figure 2) of the Zn/Sn coating. The formation of corrosion products may also reduce the effectiveness of the EMI seal since most oxides are insulators and create a non-conductive path. Thus, a study of this Zn/Sn coating material was made and its corrosion behavior with respect to the substrate metal was investigated.

Recently, a corrosion inspection of F/A-18 aircraft (AEPD, Dec 1985) was performed after one carrier deployment (3). It was reported that the Dorsal Longeron/EMI installation of the F/A-18 revealed large accumulation of powdery residue, a corrosion product. Corrosion pits were noted in areas that were covered by the metal spray coating. The deepest pits measured were about 0.020 to 0.035 inch. The inspection report concluded that, one year after the application of the Zn/Sn coating and one carrier deployment, the new EMI

BEST AVAILABLE COPY

installation did not perform as expected.

The method used for depositing the Zn/Sn coating was electric arc-spray. The material used for this spray process was in the form of wire. Metal coatings deposited using different thermal spray techniques are very similar in structure and properties. A high quality, dense, well bonded coating can be produced by these processes. However, changes in processing parameters may cause an increase in coating porosity (voids) and oxide content (4). Figure 3 shows a schematic of a cross sectional view of such a coating with possible defects. No matter what the processing parameters are, there will be always some porosity involved with these coatings. The amount of porosity in a typical coating can range from 10 to 15% of the total volume of the coating. It has been shown that porosity leads to an increase in corrosion susceptibility of a coating and also of the substrate (4,5).

The methods to reduce porosity in coatings are increasing the thickness and/or thermo-mechanical treatment of the coating after spraying. A technique used to reduce porosity is glass bead blasting of the coated surface. However, there is an inherent danger of coating de-adhesion and increase in corrosion susceptibiltiy of the substrate with this process. Another common method to counteract coating porosity problems is to apply a sealant to the coating which covers coating defects and reduces interfacial breakdowns due to corrosion. However, candidate sealants must be conducting to allow EMI protection. In this study, pre-treatments like glass bead blasting and a corrosion preventative compound, MIL-C-81309, have been tested for corrosion control.

EXPERIMENTAL PROCEDURE

MATERIALS:

The materials studied were: Al 7075-T6 panels, 20% Zn/Sn wire and arc-sprayed chips, pure Sn and Zn metal sheets, and Zn/Sn coated 7149 Al panels. The Zn/Sn materials and EMI seal assemblies (cf. Figure 1) used in this study were provided by McDonnell Aircraft Corporation.

TESTS:

A shipboard exposure test of the 20% Zn/Sn arc-sprayed coating was performed by exposing a number of specimens to the carrier environment on the USS CONSTELLATION for six months. Salt spray (5% NaCl/SO_2) tests were performed on both the Zn/Sn/Monel and Zn/Sn/Ferrex braid EMI seal assemblies, as shown in Figure 1. Also tested were 7149 Al panels with a 20% Zn/Sn coating pretreated with (1) a glass bead blast, (2) a coating of MIL-C-81309, (3) a combination of (1) and (2) and (4) no pretreatment. A chemical analysis of the corrosion product, removed from the seal assemblies, was made after a five-day exposure to SO_2/salt spray. The electrochemical tests consisted of the corrosion potential, galvanic corrosion current and potentiodynamic polarization measurements. All electrochemical tests were performed in a 3.5% NaCl (pH2) solution. No special surface cleaning treatments were applied to the coating before testing.

RESULTS AND DISSCUSION

Shipboard Exposure:

The 20% Zn/Sn arc-sprayed coating on the 7149-T7 Al alloy showed severe pitting and general corrosion of the substrate after a six-month exposure on the carrier, USS CONSTELLATION. Both the unexposed and exposed test specimens from the carrier were as shown in Figure 4. During the carrier's deployment in the Indian Ocean, pitting corrosion had penetrated through the coating and into the substrate. A cross section of an exposed carrier specimen, in Figure 5, shows pits in the aluminum substrate up to 12 mils deep and, the area of the panel where the Zn/Sn coating was removed.

BEST AVAILABLE COPY

SO_2/Salt Spray Chamber Test:

Figure 6 shows severe corrosion of the Zn/Sn coating in the EMI seal assembly after exposure for five days in 5% NaCl/SO_2salt spray. The corrosion product analyzed indicated almost 98% leaching of zinc from the Zn/Sn coating leaving the EMI seal enriched in Sn.

A 7149 Al panel coated with Zn/Sn, which was glass bead blasted and then coated with MIL-C-81309 and exposed to SO_2/salt spray is shown in Figure 7. Note that only half of this specimen was sprayed with MIL-C-81309. This specimen was exposed for approximately 60 hours. Specimens with only the MIL-C-81039 compound and no bead-blasting were kept 24 hours longer in the SO_2/salt spray chamber. In all cases, MIL-C-81309 compound appeared to increase the length of time before blistering occurred. As shown on the right half of Figure 7, glass bead blasting was very detrimental as it blistered the coating readily. But where the MIL-C-81309 coating was applied on the left half of specimen in Figure 7, blisters were observed to form at a much slower rate compared to the Zn/Sn coating without any pretreatment. If the blisters on the test specimens were touched by a pin, they would collapse implying gas (bubble) formation during corrosion. This suggests the ingress of corrosive environment into the coating either along the oxide layers (cf. Figure 3) or through pores within the coating. A cross sectional view of the Zn/Sn arc-spray coating on the Al panel, shown in Figure 8, illustrates such pathways.

Electrochemical:

The corrosion potential measurements of the coating material were and compared with 7075-T6 Al alloy. It was found that the Zn/Sn arc-spray material was highly active and closer to the open circuit potential for Zn (-0.95 V vs. SCE). However, because Zn is highly electrochemical active its depletion from the coating is highly possible. The loss of Zn from the Zn/Sn coating during the salt spray exposure tests (cf. Figure 6) confirms this result. Depletion of Zn means that the sacrifical protective properties of the coating is lost as its potential reaches closer to that of Sn (-0.65 V), thus becomes a cathode instead. In other words coatings is enriched with Sn.

A potential of -0.90 volts was applied to the Zn/Sn coated 7149 panel until the anodic current (dissolution current for Zn) reached zero. At this potential Sn will not corrode as it will be a cathode and Zn will selectively dissolve away leaving the Zn/Sn coating mostly rich in Sn. Figure 9 shows a cross sectional view of such a panel after the controlled potential test.

Galvanic Couples:

A galvanic couple between the 7075-T6 Al and Zn/Sn arc-spray coated material was made. The galvanic current between the two specimens of equal surface area was measured using a zero resistance ammeter and recorded as a functon of time. It was found that high initial galvanic corrosion current (500 $\mu A/cm^2$) decreased to less than half of the value in about two hours of exposure. This indicated that the Zn component of the Zn/Sn arc-spray coating is sacrificed very rapidly, thus, limiting the coating's ability to protect the Al alloy substrate. However, a galvanic couple made up of 7075-T6 Al and Zn/Sn wire(material used for arc-spraying) showed a significantly lower initial corrosion current (10 $\mu A/cm^2$) and continued to protect the Al alloy component even after long exposures at a steady protection corrosion currrent of approximately 20 $\mu A/cm^2$. Dezincification of the Zn/Sn arc-spray coating in the former couple will result in a Sn rich coating which will act as a cathode and corrode the aluminum, instead of protecting it. Additionally, the corrosion product formed during the selective oxidation of zinc, which is in the EMI seal installation, will result in the loss of EMI protection (electrical continuity) of the structure. This agrees well with the failures observed on F/A-18

BEST AVAILABLE COPY

specimens(cf. Figure 6).

Electrochemical Polarization:

A potential range of -1.3 to -0.7 volts with respect to a S.C.E. reference electrode and a scan rate of 0.166 mv/sec was selected for potentiodynamic polarization measurements. Before the start of the polarization scan , the steady-state open circuit corrosion potential was determined. Potentiodynamic polarization diagrams for Zn/Sn arc-spray and wire material were as shown in Figure 10. The anodic polarization curve for the Zn/Sn arc-spray material was at a slightly higher potential(less active) than the Zn/Sn wire indicating a lower dissolution rate for the arc-spray coating. The anodic polarization plot for the Zn/Sn arc-spray coating at potentials more positive than -950 mV showed a decrease in the current due to depletion of Zn or enrichment of Sn; this curve represented the behavior of pure Sn. If there was no depletion of Zn, the anodic polarization curve for the Zn/Sn arc-spray coating would appear as the extrapolated part as shown in Figure 10. The current densities for the Zn/Sn wire material were slightly higher than for the arc-spray material, indicating that certain changes have occured in the Zn/Sn material during the arc-spray process.

CONCLUSIONS

The sacrifical corrosion protection properties of the Zn/Sn arc-spray coating are very temporary in nature. From the laboratory tests, it was estimated that the protective nature of the Zn/Sn coating may last upto 6 months. Initially, the coating offers a high degree of protection but only for a short period of time. This condition changes very quickly because the coating becomes primarily rich in Sn and acts as a cathode, thereby causing the substrate, Al alloy, to corrode. The carrier exposure tests have confirmed the limited protective ability of the Zn/Sn arc-spray, because Al alloy panels exhibited general corrosion and pitting during long exposures.

The interfacial corrosion between the coating and the Al alloy substrate caused blistering and created corrosion pathways; porosity in the arc-spray coating, was the responsible factor. Glass bead blasting after the arc-spraying caused severe debonding of the Zn/Sn coating and accelerated the rate of blister formation. Use of Corrosion Preventative Compound, MIL-C-81309, reduced the ingress of environment into the coating, thus enhanced the time before blistering could be observed.

ACKNOWLEDGEMENT

The contributions of Dr.R.C. Paciej and Mr.J.J. Thompson are gratefully acknowledged in these investigations.

REFERENCES

1. STRFITRON ONE ONE THREE 040808Z May 85.
2. COMCARAIRWING FOURTEEN 020508Z Jun 85.
3. NAVAIRREWORKFAC 251646Z Feb 86.
4. "Metallized coatings for Corrosion Control of Naval Ship Structures and Components", National Materials Advisory Board, NMAB Report No. 409 (1983).
5. Shaw, B.A., "Corrosion Barrier Coatings - Investigation of Thermal Spray Coating Characteristics", David Taylor Naval Ship R&D Center, Report No. DTNSRDC/SME-83/89.

BEST AVAILABLE COPY

F/A-18 EMI SEAL

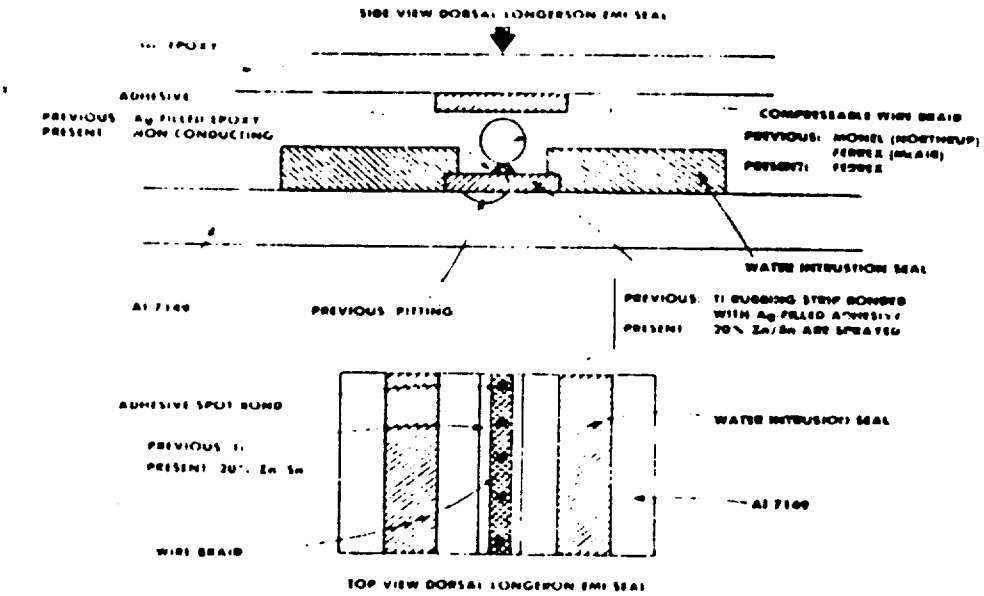

SCHEMATIC DIAGRAM OF SEAL

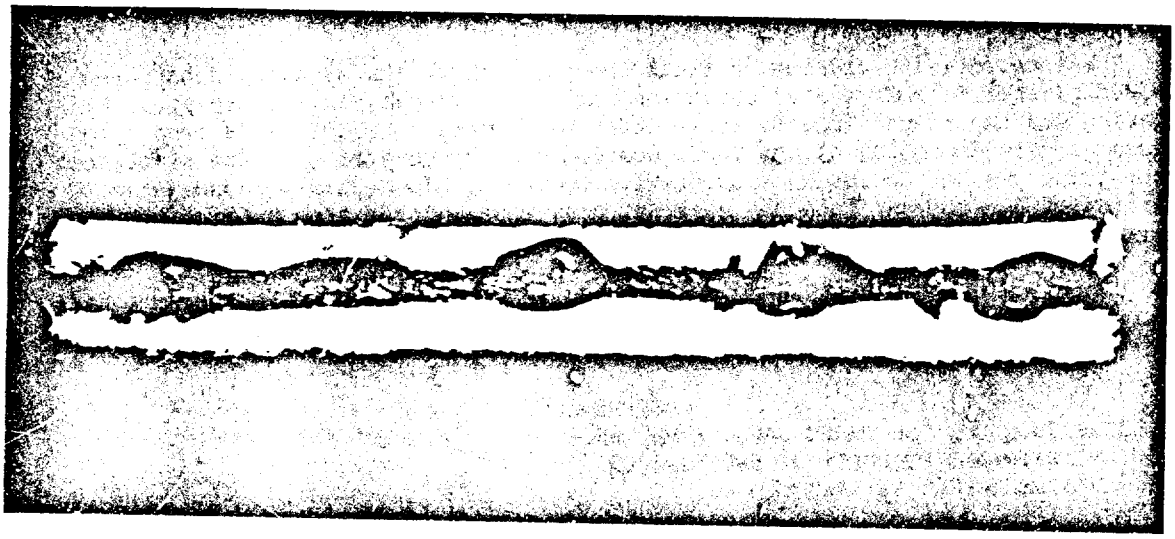

UNEXPOSED SPECIMEN

Figure 1 - Schematic of the F/A-18 EMI-seal and a photograph of the specimen used.

BEST AVAILABLE COPY

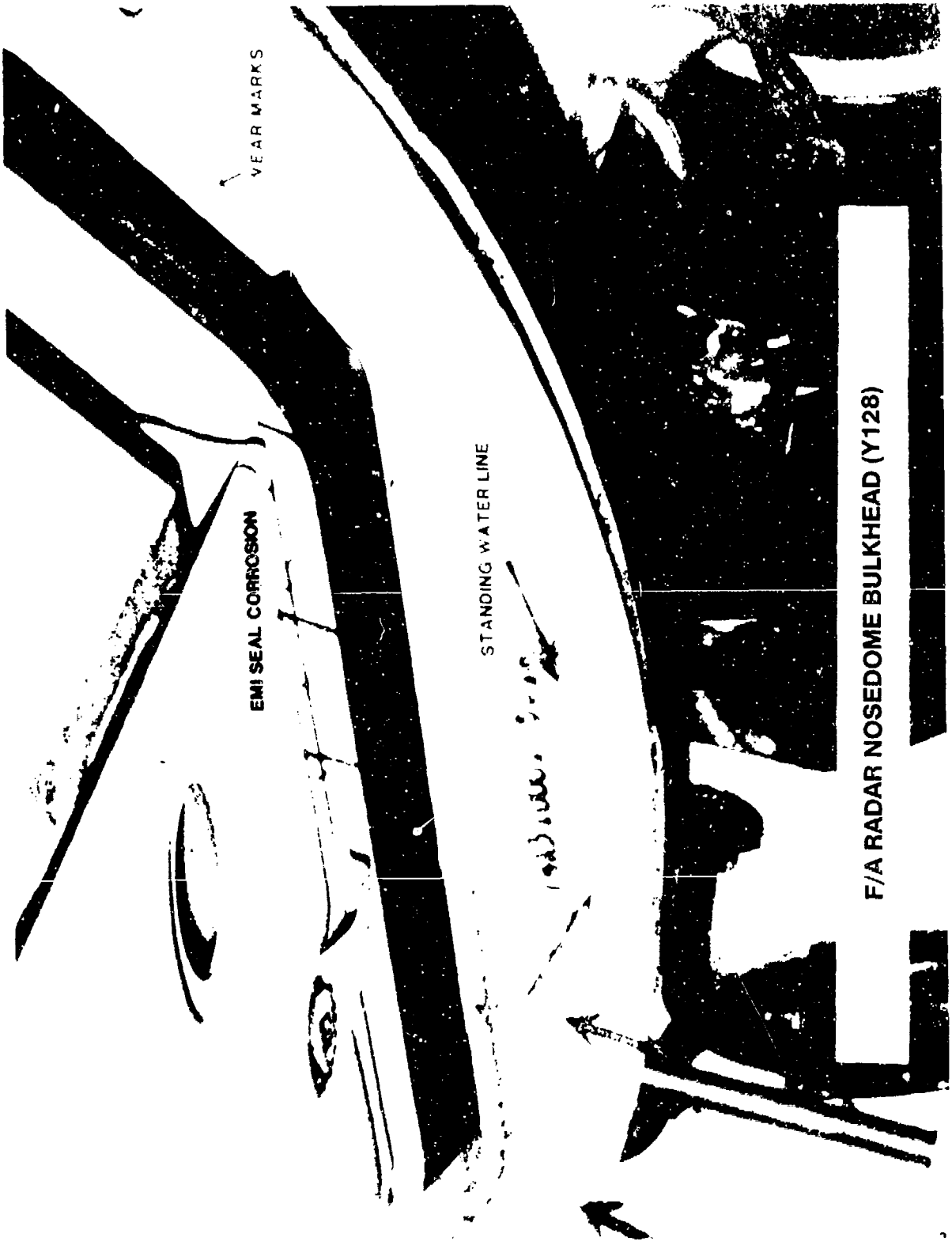

Figure 2 - Corrosion under the EMI-seal area in the F/A-18 Radar Nosedome Bulkhead (Y128).

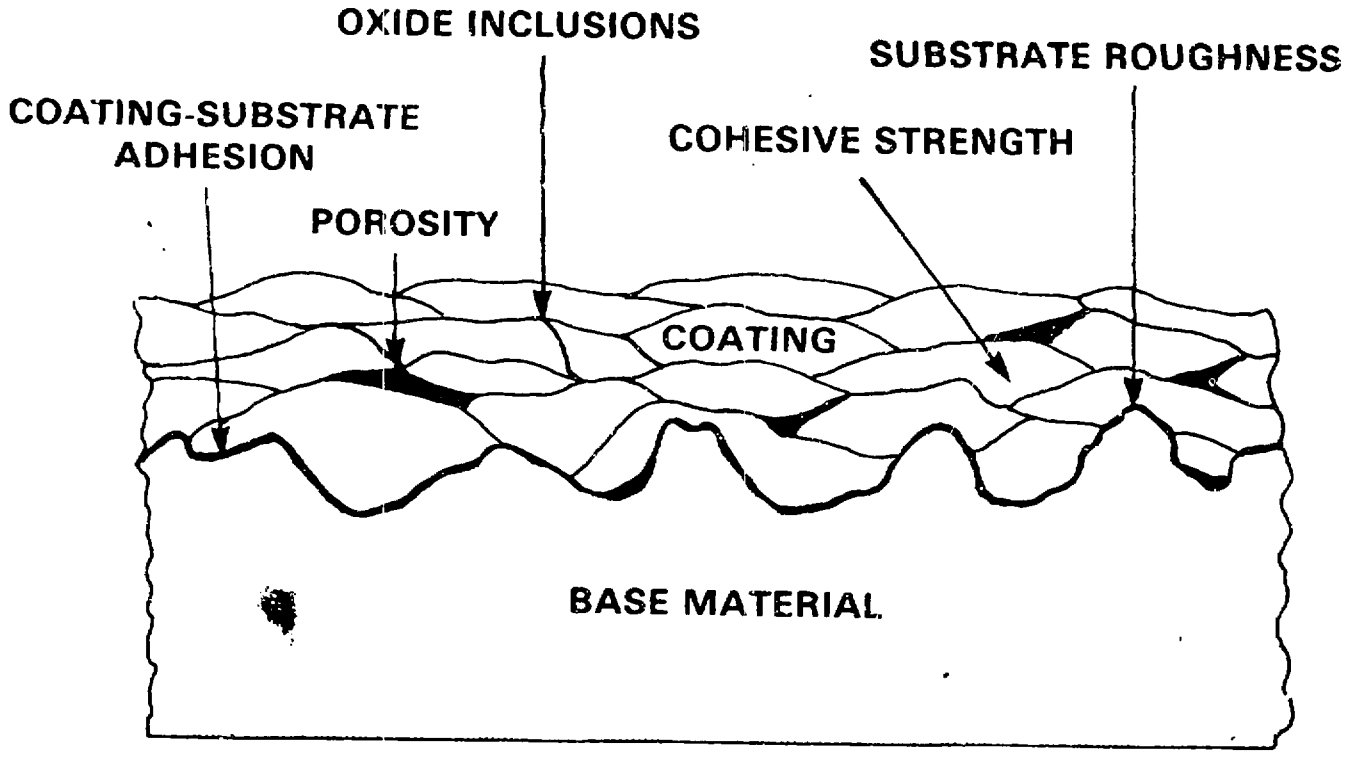

Figure 3 - Cross sectional view of the metal spray coating.

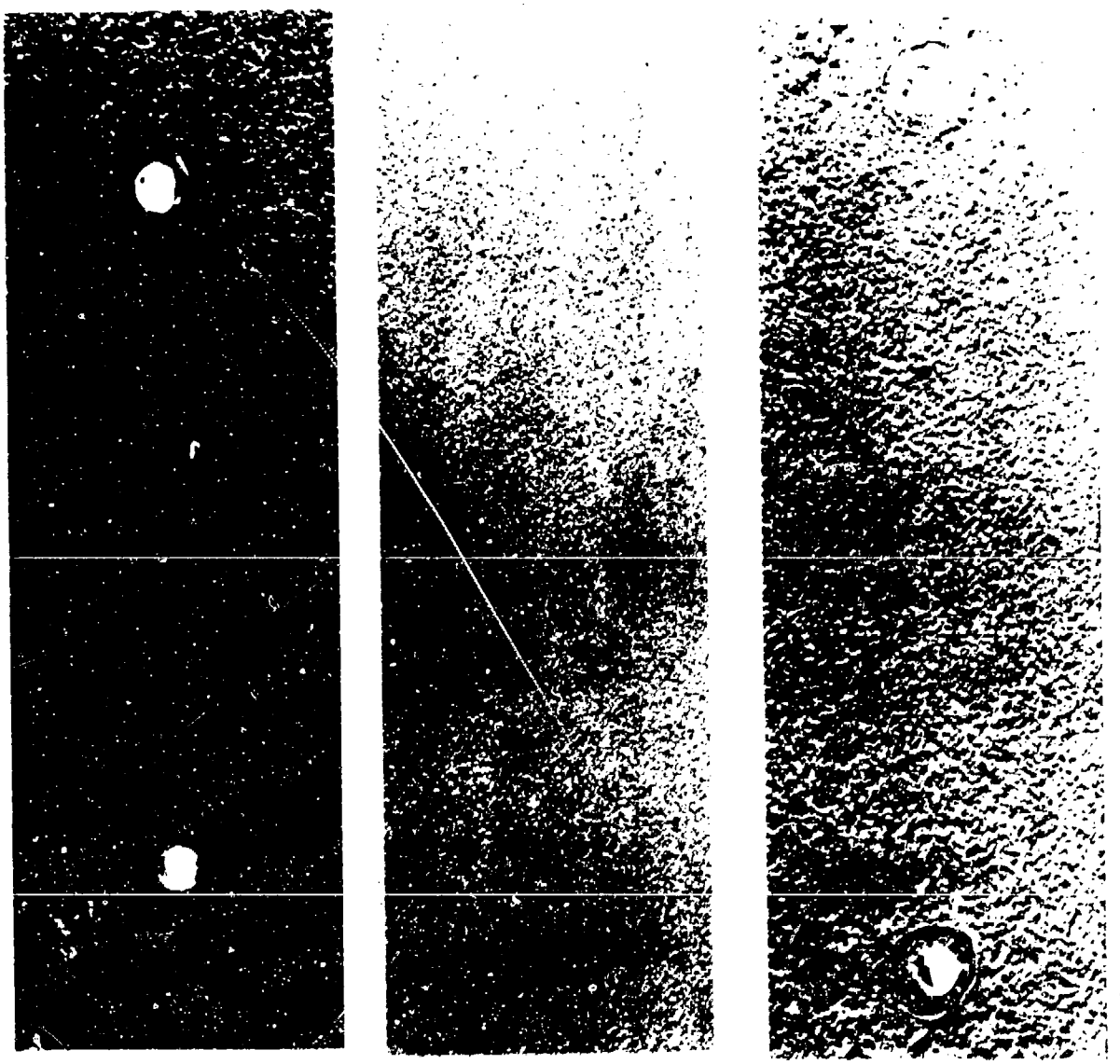

EXPOSED UNEXPOSED EXPOSED

EXPOSED TO CARRIER ENVIRONMENT FOR 6 MONTHS

Figure 4 Corrosion of arc-sprayed Zn/Sn coating on 7149-T7 Al in a carrier environment.

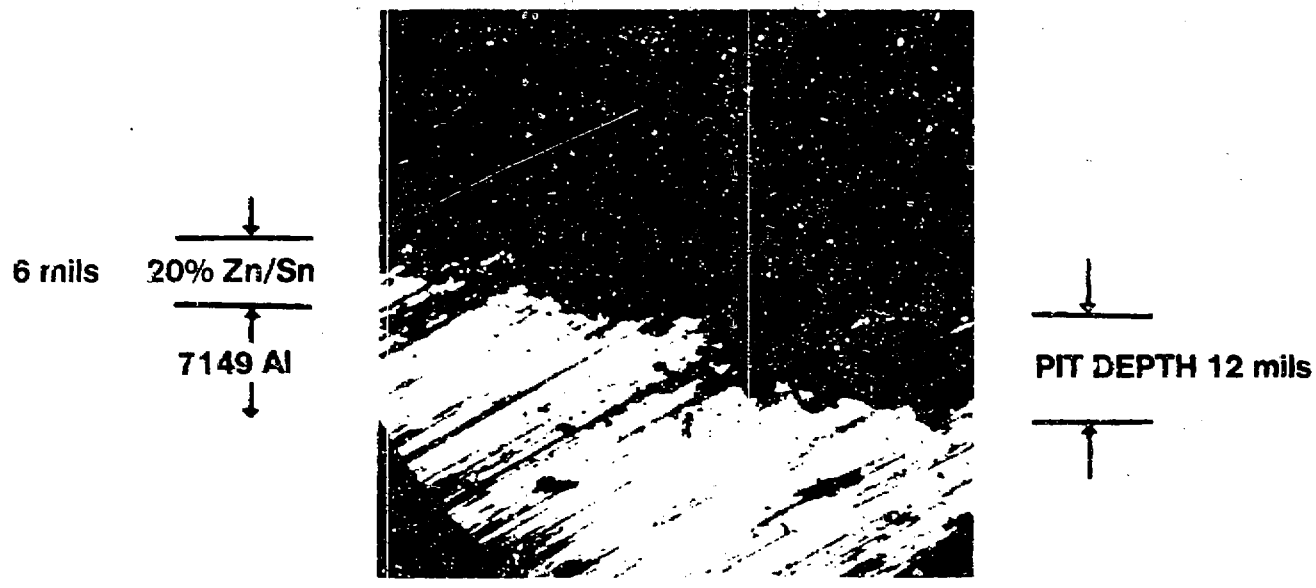

EXPOSED 6 MONTHS TO CARRIER ENVIRONMENT

Figure 5 Cross-section view of Figure 4.

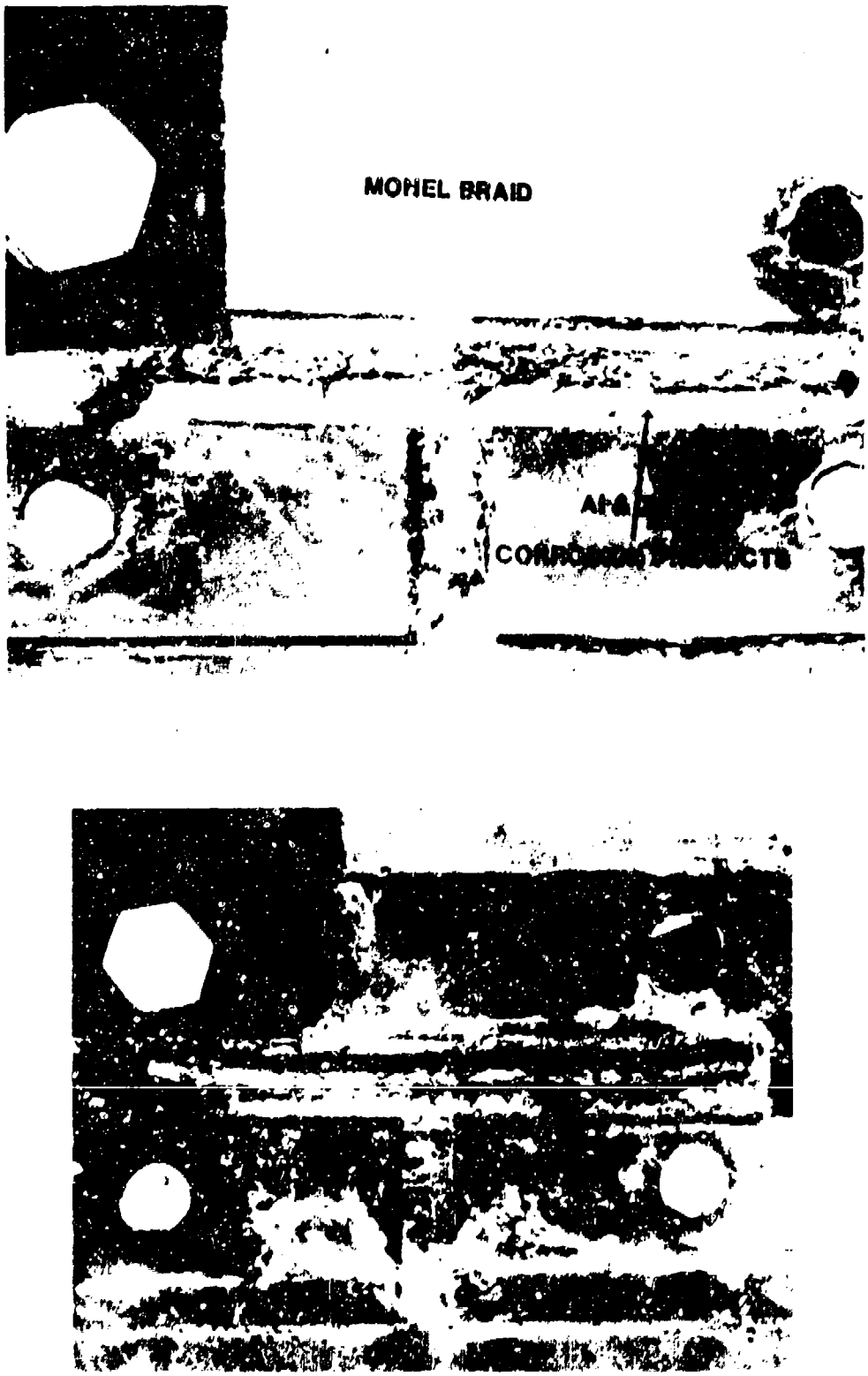

Figure 6 Corrosion of F/A-18 EMI-seal specimens exposed to $NaCl/SO_2$ spray chamber for five days.

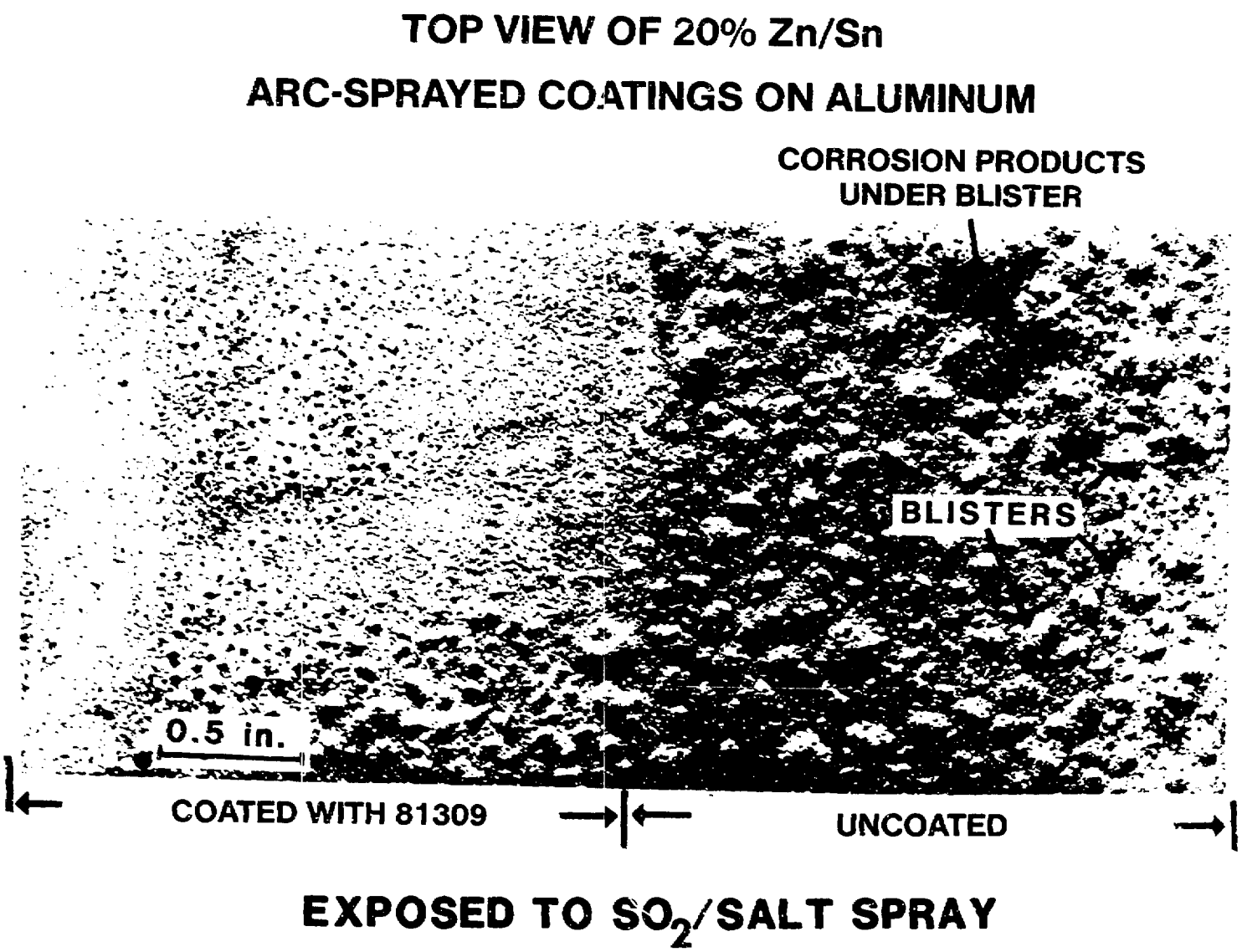

Figure 7 Corrosion behavior of post-treated Zn/Sn arc-sprayed coating with Corrosion Preventative Compound and glass bead beading.

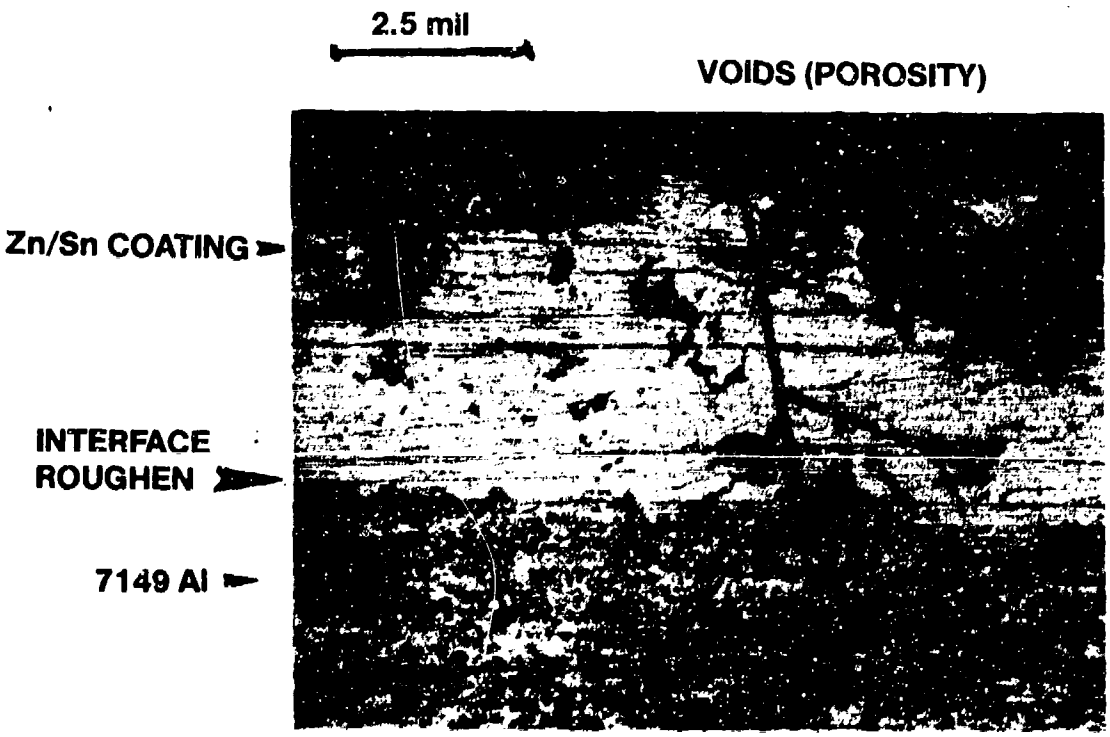

Figure 8 Cross sectional view of the Zn/Sn coating on 7149-T7 Al panel.

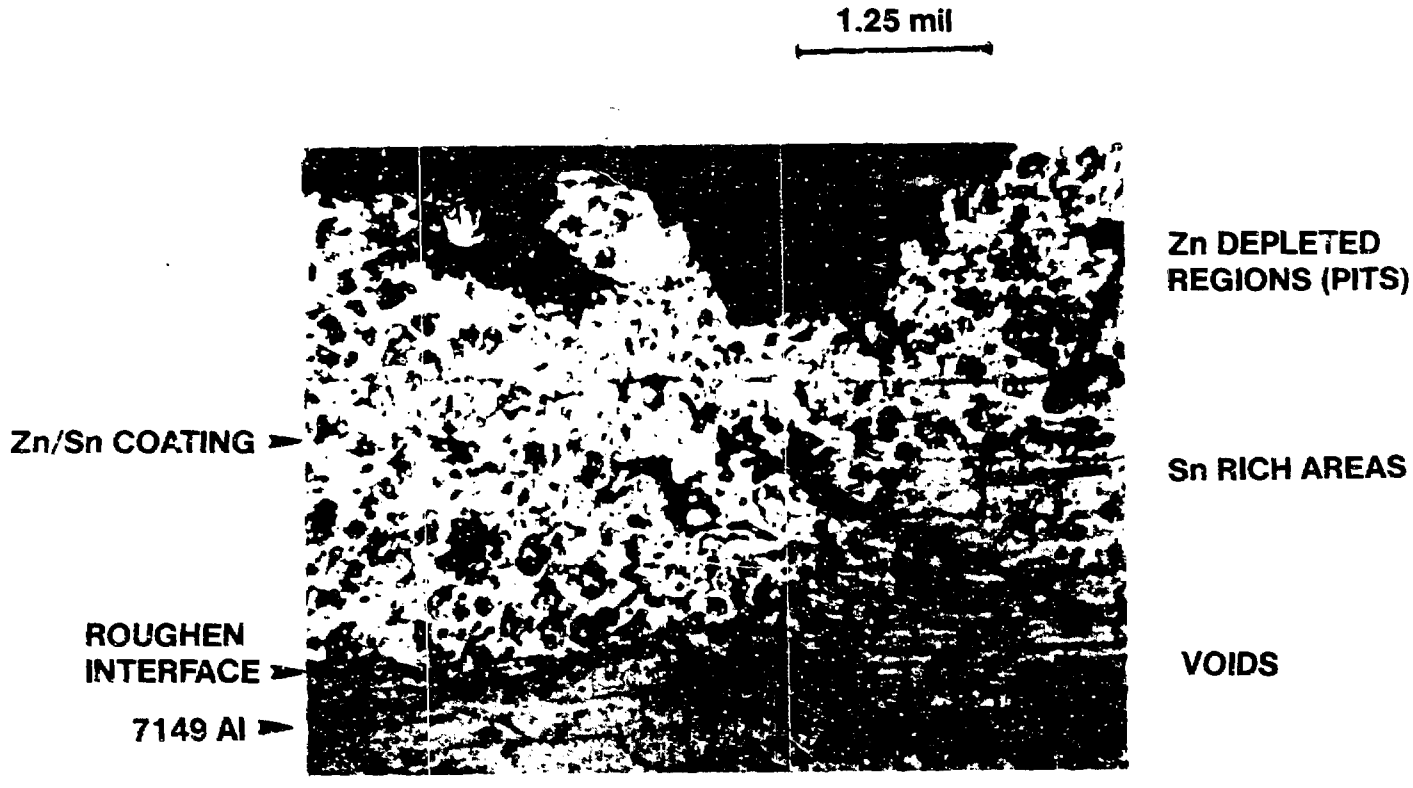

Figure 9 Cross sectional view of corroded Zn/Sn coating on 7149-T7 Al after controlled potential test.

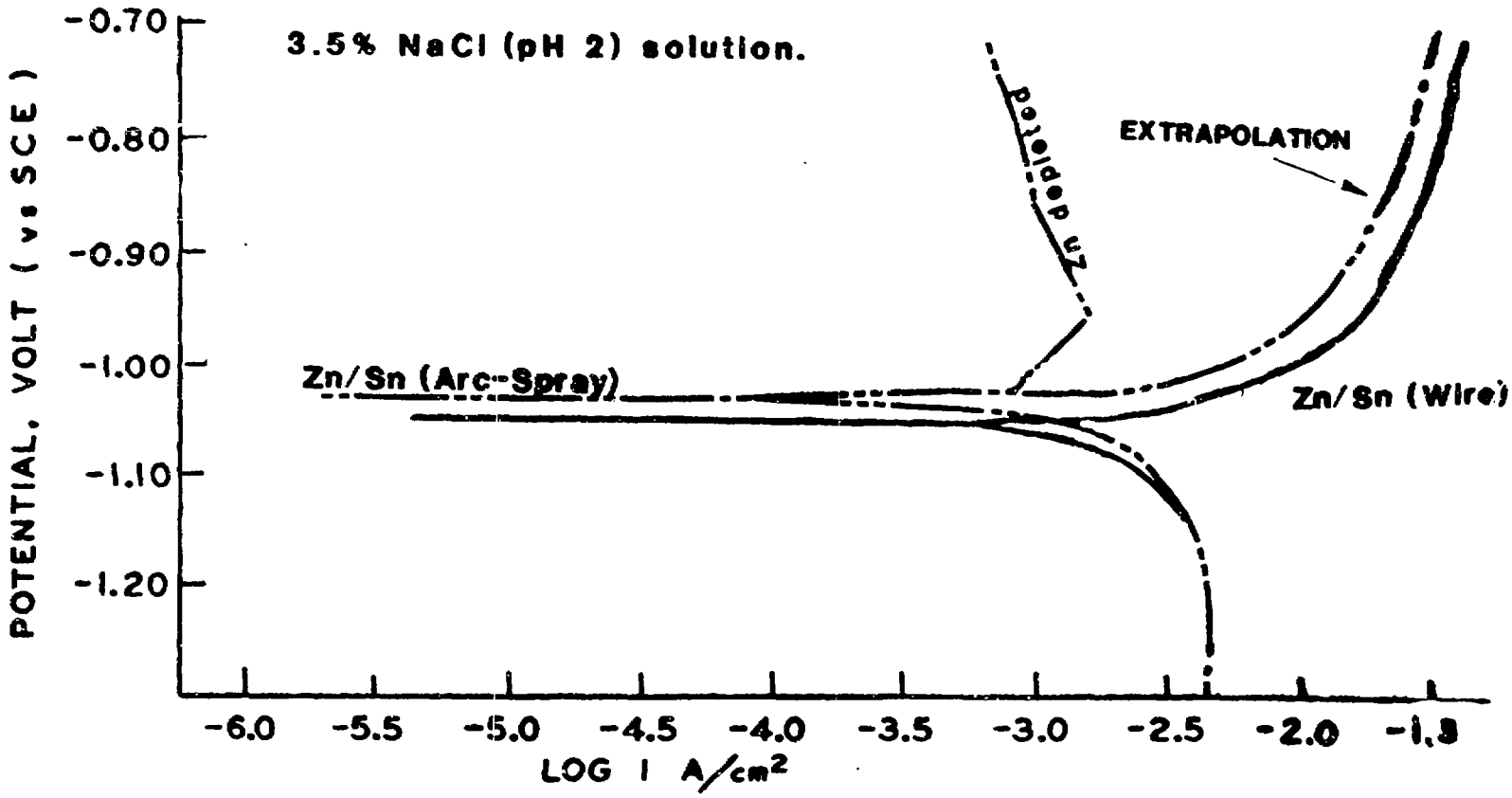

Figure 10 Polarization diagrams for Zn/Sn material in a 3.5% solution (pH 2).

STRESS CORROSION CRACKING PROPERTIES OF Al-Li ALLOYS

J.B. Lumsden and A.T. Allen

Rockwell International Science Center
1049 Camino Dos Rios
Thousand Oaks, CA 91360

Introduction

Aluminum-lithium alloys have received much attention recently [1,2] because of their potential for weight savings, with increased stiffness, in many types of aerospace vehicles. Conventional aluminum alloys can fail by intergranular stress corrosion cracking (SCC) in specific environments, which has necessitated the development of alloy compositions and heat treatments to increase SCC resistance. Although experience with conventional Al alloys suggests SCC could be a potential problem in Al-Li alloys, the environmental effects for this family of alloys have been measured only to a limited extent [3]. This work was undertaken to assess the SCC behavior of Al-Li alloys exposed to choride solutions, examining the effects of strain rate, aging treatments and potential.

Experimental

The material used in this work was British ALCAN Aluminum 8090 in the form of rolled plate 24.4 mm-thick and a 43 mm-thick rolled plate of Alcoa 2090. The compositions are shown in Table 1. The as-received condition of the 8090 was solution-treated and stretched 2%, and that of 2090 was the T8E41 condition. Microstructural examination of the two alloys revealed pancake-shaped grains produced during hot working. Tensile specimens were machined from the 8090 alloy in both the longitudinal and short transverse directions having gauge lengths of 14 mm. Following machining, the specimens were aged in an air-circulating oven. The aging conditions were 170°C for 4 h, 170°C for 64 h and 230°C for 4 h. These thermal treatments correspond to the underaged, peak aged and overaged conditions, respectively. Tensile specimens having a 14 mm gauge length were machined from the 2090 material in the short transverse

Table 1

Alloy Compositions

Alloy	Li	Cu	Mg	Zr	F3	Si	Al
8090	2.5	1.2	0.68	0.07	0.11	0.08	Balance
2090	5.6	3.0	0.25	0.15	0.12	0.1	Balance

direction and tested in the as-received condition. Tensile specimens were also machined from 7475-T6 in the short transverse direction and tested for comparison purposes.

The SCC properties were evaluated using the constant extension rate technique [4]. Specimens were dynamically strained while polarized potentiostatically in a deaerated 0.5 M NaCl solution. The solution in the enclosed 500 ml cell was continuously refreshed, since preliminary experiments indicated that dissolution of the Al-Li alloys during an experiment could raise the pH of a stagnant solution as much as 3 pH units.

Pitting potentials were determined in a deaerated 3.5 M NaCl solution. The measurements were made by scanning the potential from -1400 mV (SCE) at 20 mV/min at room temperature.

Results and Discussions

Table 2 shows the electrochemical parameters obtained from the polarization curves. The Al-Li alloys have a higher pitting potential than the conventional aluminum alloy 7475-T6, and their passive current density is typically 0.5-1.5 $\mu A/cm^2$ less. Also, the extent of the passive range, the difference between the pitting potential and the corrosion potential, is greater for the Al-Li alloys. The passive region of the advanced alloys ranges from 230 mV for 8090 to 360 mV for 2090, compared to 220 mV for 7475-T6.

Table 2

The Corrosion Potential, E_{corr} the Passivation Current Density, i_{pass}, and the Pitting Potential, E_{pit}, for Al Alloys

Alloy	Aging Conditions	E_{corr} (SCE)	I_{pass}	E_{pit} (SCE)
Al 7475	T6	-1010 mV	2 μA/cm^2	-790 mV
Al 8090	170°C/4 h	-960 mV	0.7 μA/cm^2	-680 mV
Al 8090	170°C/64 h	-945 mV	0.9 μA/cm^2	-715 mV
Al 8090	230°C/4 h	-970 mV	1.5 μA/cm^2	-715 mV
Al 2090	T8E41	-1020 mV	1.5 μA/cm^2	-660 mV

Table 3 shows the slow strain rate results for the Al 8090 alloy polarized at -700 mV (SCE). The elongation to failure for the three aging conditions is compared to that in air for the tensile axis laying both in the short transverse and the longitudinal directions. The strain rate was 10^{-7} s^{-1}. The elongation is substantially reduced by exposing the alloy to the NaCl solution. There is no effect of aging on SCC resistance. This SCC behavior contrasts with that of many conventional aluminum alloys, in which precipitation hardening (aging) at ambient or higher temperatures can have pronounced effects on SCC susceptibility [5]. Maximum susceptibility often occurs in the underaged condition and overaging can substantially improve SCC resistance.

Figure 1 shows the effect of potential on the normalized elongation-to-failure, which is the ratio of the strain-to-failure in solution at the indicated applied potential to the strain-to-failure in air, for 8090 in the underaged condition, 2090-T8E41, and 7475-T6. The tensile axis of all alloys was in the short transverse direction. The 8090 alloy has a critical potential for SCC, -750 mV, below which there is no change in ductility (no susceptibility to SCC). Above -750 mV, there is a rapid decrease in the elongation-to-failure of 8090 as the applied potential is more anodic, indicating high susceptibility to SCC. The SCC behavior of 7475-T6 is reverse that of the Al-Li alloy. The conventional alloy is more suceptible to SCC below a critical potential (-790 mV), which corresponds to the pitting potential, and more resistent to SCC above this potential. The SCC

Table 3

Aging Treatments and Stress Corrosion Cracking Properties of 8090

	Short Transverse		Longitudinal	
Aging	Elongation (Air)	Elongation (-700 mV)	Elongation (Air)	Elongation (-700 mV)
170°C/4 h	4.2%	0.4%	8.9%	1.1%
170°C/64 h	3.9%	0.2%	6.2%	1.1%
230°C/ 4 h	3.7%	0.5%	7.1%	1.3%

Fig. 1 Potential dependence of the ratio of strain-to-failure of 8090 aged 170°C for 4 h, 2090-T8E41 and 7475-T6.

behavior of 2090-T8E41 is different from that of 8090 and 7475-T6 in that an abrupt change in SCC susceptibility is not observed, although there is a slow decrease in the elongation ratio as the potential becomes more anodic between -800 and -625 mV. Using

the elongation ratio as a measure of the SCC susceptibility, 2090-T8E41 is more susceptible to SCC in the passive range of potentials than 8090 in the underaged condition. However, near and at the pitting potential, 8090 is much more susceptible to SCC than 2090-T8E41.

Fractography was performed on all specimens. The fracture surface of the short transverse and longitudinal tensile specimens of the Al-Li alloys were the same for all aging conditions. The short transverse specimens had flat, nearly featureless fracture surfaces with vertical steps, suggesting an intergranular fracture. The step height, measured by stereo imaging, corresponds to the short transverse grain size. The steps on the fracture surface correspond to transitions of the crack front from one grain boundary plane to an adjacent one. Fracture surfaces of specimens with the tensile axis in the longitudinal direction had numerous secondary cracks parallel to the tensile axis. The distance between the secondary cracks were comparable to the grain size in the short transverse direction. There was no evidence that SCC cracks initiated at pits.

Further work must be performed to determine if a hydrogen mechanism or slip dissolution mechanism applies to the Al-Li alloys. The differences in the SCC behavior of 8090 and 7475-T6 both as a function of potential and artificial aging suggest that the cracking mechanisms are different for the two alloys. These differences in behavior may arise because the crack tip chemistry is dominated by lithium in the Al-Li alloys, the result of which is a basic crack tip solution and not an acidic one, as in the case of conventional alloys. The observed potential dependence of SCC susceptibility above the pitting potential and SCC resistance below the pitting potential for the 8090 can be explained both by invoking either a hydrogen mechanism or a slip-dissolution mechanism. Hydrogen is generated inside a growing crack by the hydrolysis of dissolving metal ions, which could adsorb on the unfilmed crack tip surface and penetrate the metal. Cracking by slip dissolution most often occurs in a potential region of film instability such as the pitting potential. SCC by slip dissolution is usually arrested at potentials above the pitting potential by crack blunting as was the case for 7475-T6.

Acknowledgement

This work was supported by the Rockwell International Science Center IR&D program.

References

1. T.H. Sanders, Jr., and E.A. Starke, Jr., Eds., Aluminum Lithium Alloys I, The Metallurgical Society of AIME, Warrendale, PA, 1981.
2. T.H. Sanders, Jr., and E.A. Starke, Jr., Eds., Aluminum Lithium Alloys II, The Metallurgical Society of AIME, Warrendale, PA, 1983.
3. N.J.H. Holroyd, A. Gray, G.M. Scamans and R. Hermann, Aluminum Lithium Alloys III, Eds., C. Baker, P.J. Gregson, S.J. Harris and C.J. Peel, Institute of Metals, London, 1986, p. 310.
4. G.M. Ugiansky and J.H. Payer, Eds., Stress Corrosion Cracking - The Slow Strain Rate Technique, The American Society for Testing and Materials, Philadelphia, PA, 1979.
5. M.O. Speidel, Met. Trans. 6A, 631 (1975).

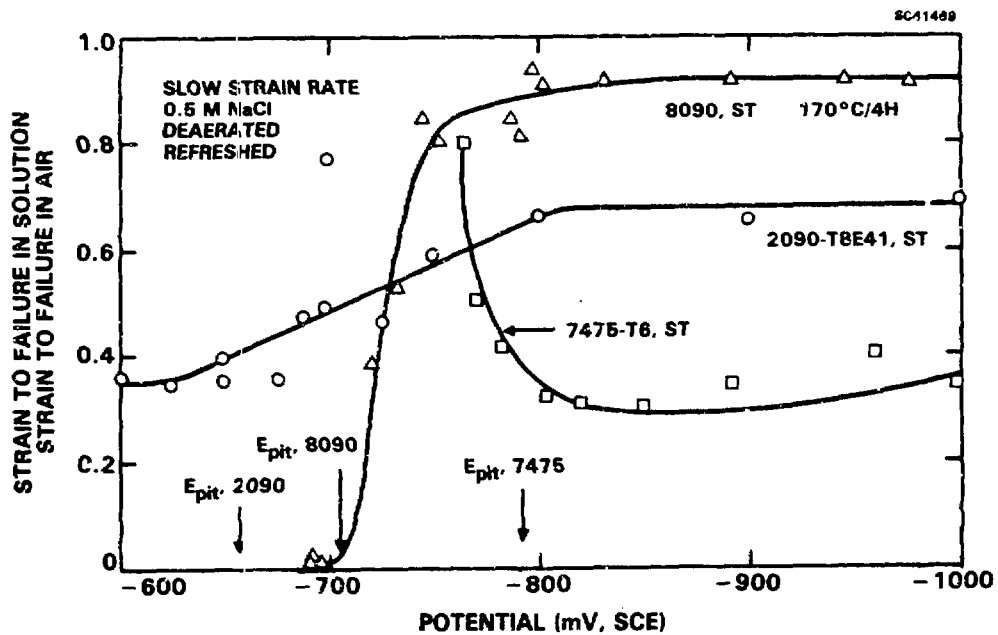
SC41469
SLOW STRAIN RATE
0.5 M NaCl
DEAERATED
REFRESHED
8090, ST
170°C/4H
2090-T8E41, ST
7475-T6, ST
E_{pit}, 8090
E_{pit}, 2090
E_{pit}, 7475
STRAIN TO FAILURE IN SOLUTION
STRAIN TO FAILURE IN AIR
1.0
0.8
0.6
0.4
0.2
0
-600
-700
-800
-900
-1000
POTENTIAL (mV, SCE)

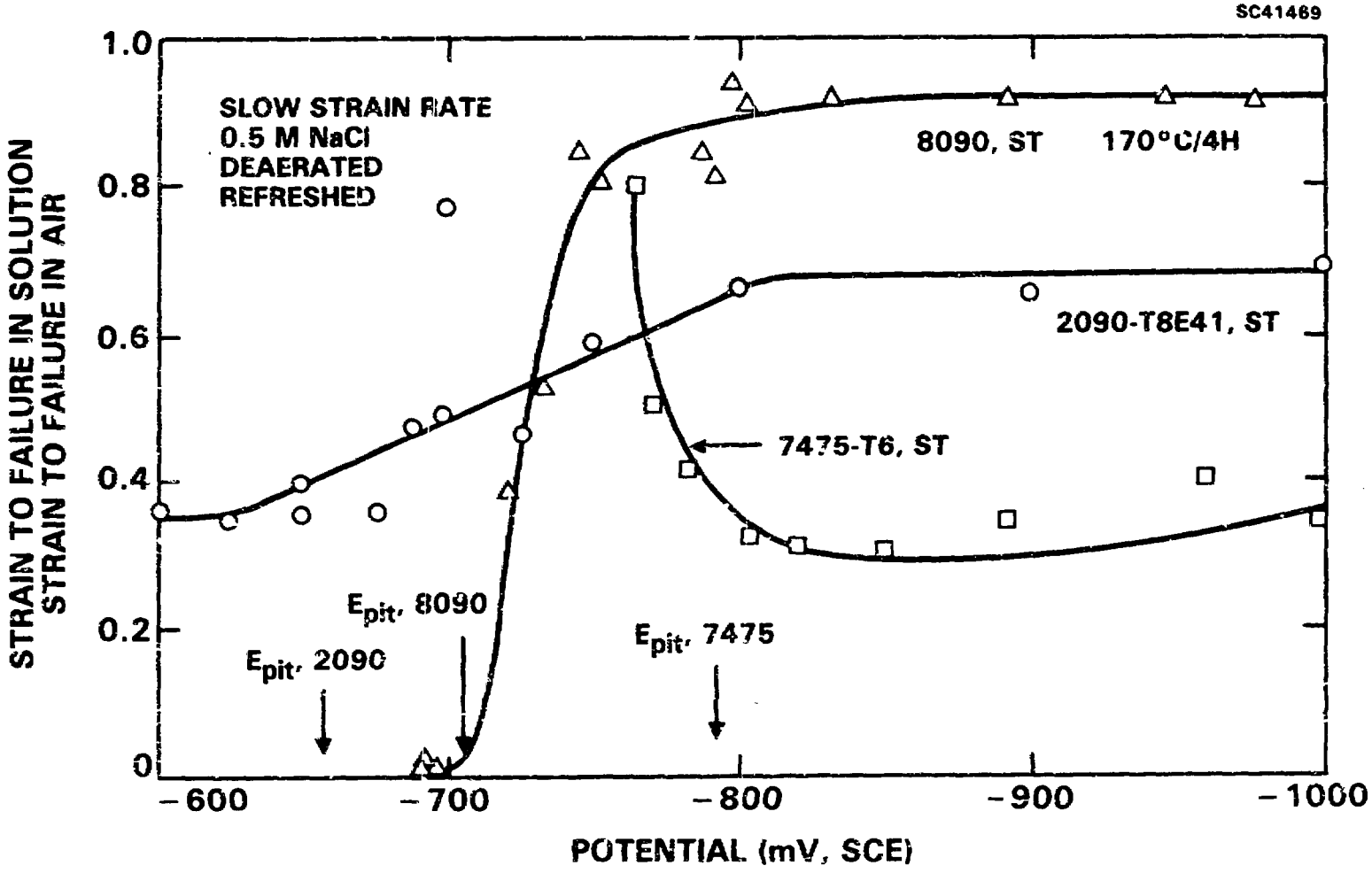
SC41469
SLOW STRAIN RATE
0.5 M NaCl
DEAERATED
REFRESHED
8090, ST
170°C/4H
2090-T8E41, ST
7475-T6, ST
E_{pit}, 8090
E_{pit}, 2090
E_{pit}, 7475
STRAIN TO FAILURE IN SOLUTION
STRAIN TO FAILURE IN AIR
1.0
0.8
0.6
0.4
0.2
0
−600
−700
−800
−900
−1000
POTENTIAL (mV, SCE)

TRENDS IN UNDERWATER SHIPBOARD PAINTS

by

Karen M. Poole
Gerard S. Bohlander
George I. Loeb, Ph. D.

Current high performance paints, both antifouling and anticorrosion, offer the potential for long term marine service. The primary benefit of long life paints to the Navy is to reduce life cycle and maintenance costs, such as fuel consumption, labor costs for application and surface preparation, removal and disposal costs, and underwater maintenance.

ANTICORROSIVE COATINGS

Reducing the tendency of paints to blister has been a major research objective in improving anticorrosive coatings. Paint blistering indicates paint deterioraration and can lead to corrosion problems if the blisters are broken. This is of particular concern to the Navy because the underwater hull cleaning apparatus used to rejuvenate the standard Navy copper based antifouling paint system can rupture blisters. Because these blisters occur at the paint-substrate interface, bare metal is exposed. In severe cases of blistering, it is conceivable that increased exposure of bare metal could overstress the ship's cathodic protection system.

The two specifications for shipboard underwater anticorrosive hull coatings are MIL-P-24441, which describes two series of epoxy-polyamide formulations that differ in solvent system and include primer and topcoats, and MIL-P-23236, which is a performance specification for proprietary coatings. The series of formulations originally employed in MIL-P-24441 are the Type I coatings, which contain normal butanol and super hi flash naphtha. The second series of formulations, Type II, were added to the specification in 1980 as a result of air

pollution requirements described in California Rule 66; these coatings contain ethylene glycol monoethyl ether, ethylene glycol monobutyl ether, and paint thinner (mineral spirits).

Current research at David Taylor Naval Ship R&D Center (DTNSRDC) to improve anticorrosive coating systems has been primarily concerned with blistering of the Type II coating. Poor surface preparation and application procedures are known causes of blistering. However, even with strict control over these variables, blistering occurs, suggesting that there may be variables within the paint that should be controlled. These variables include choice of solvents, choice of raw material supplier, combination of raw materials from various suppliers, and blending procedures.

Osmotic blistering occurs because hydrophilic solvents, such as glycol ethers, collect at localized areas of the paint/substrate interface. They absorb water that has permeated the film, creating an osmotic pressure difference which swells these regions. As oxygen and cations permeate the film, corrosion reactions occur and produce hydroxyl ions that cause further delamination of the film.[1] Osmotic blistering is accelerated in the laboratory using hot water immersion tests. Elevated temperatures and dilute immersion solutions (less than 20 microsiemens conductivity) accelerate the blistering process. The source of cations can be in the paint; for example, epoxy resin contains sodium ions that remain after manufacturing.

The performance of the Type I, Type II, and proprietary coatings was compared using a hot water immersion test. A three-coat system of the green primer (F-150 only) and a three coat system of the green primer and the light gray and dark gray topcoat (F-150, F-151 and F-154) were evaluated for both Type I and Type II. For the proprietary coatings, the systems recommended by the

manufacturer were used. The Type I and Type II coatings were obtained from seven suppliers approved on the MIL-P-24441 Qualified Products List. A coating approved for use as a standard in the specification hot water immersion test was also evaluated.

The test procedure was to immerse 3- x 5-inch steel Q-panels coated with the various paint systems in 180°F deionized water for two weeks. The panels were evaluated for blistering at 3-hour intervals using a blister rating scheme based on ASTM D714. To avoid any thermal shock to the coating, the test apparatus was designed to allow the panel to remain completely immersed during inspection. Blister size and blister density were rated on a scale from zero to ten in increments of one, a value of ten indicating no blisters. The two values were then combined mathematically using the following formula to obtain the blister resistance rating:

$$\text{Blister resistance} = (\text{blister size} \times \text{blister density})^{1/2}$$

Blister resistance is dependent on both blister size and blister density. The above formula allows both factors to be incorporated into a single rating between one and ten.

The results are illustrated in Figs. 1, 2, and 3. The Type I coatings were more blister resistant than the Type II coatings as indicated by the number of Type I coatings with blister resistance ratings greater than nine, while the Type II coatings all have ratings below eight. Of the five proprietary coatings tested, only one performed better than the Type II coatings. The variation in performance within each type of coating suggests that there are more than just solvent effects. A proposed cause of this variation was poor quality control. The following specification tests were performed on each of the Type I and Type II coatings to ensure quality: fineness of grind, percent volatile content,

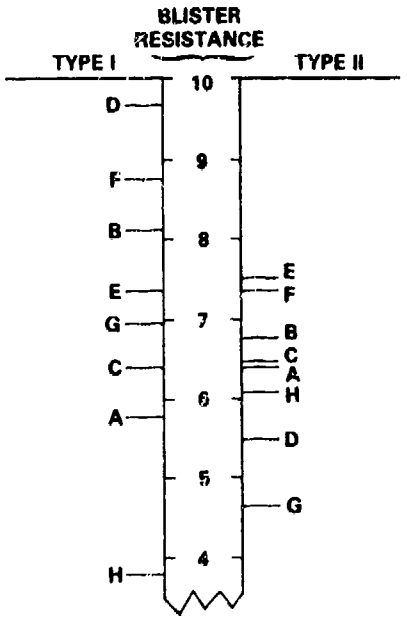

Fig. 1. Comparison of type 1 and type II coating systems from different vendors (F150/151/154). Letters identify numbers.

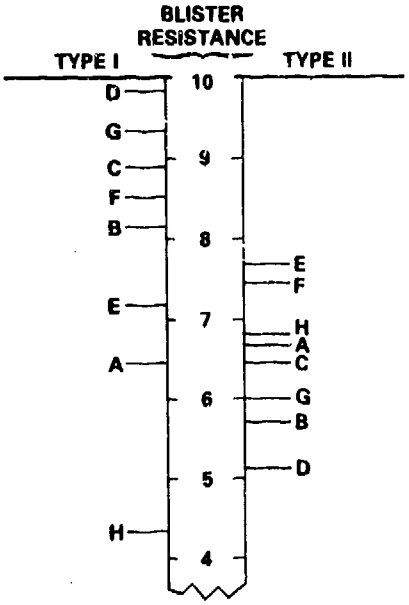

Fig. 2. Comparison of type I and and type II coating systems from different vendors (3 coats of F150). Letters identify vendors.

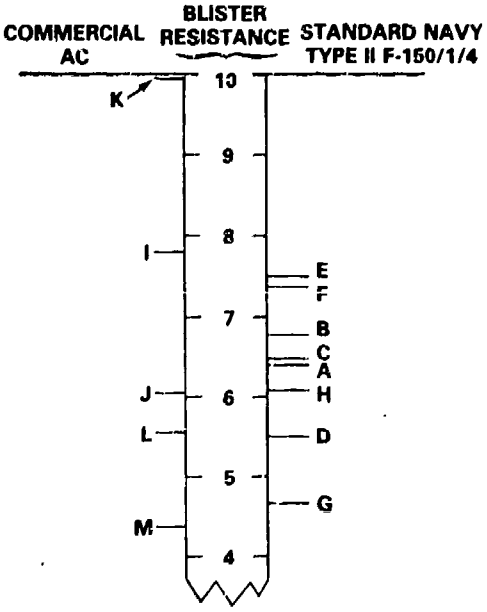

Fig. 3. Comparison of commercial anti-corrosive coatings with Navy type II F150 series from different vendors. Letters identify vendors.

weight per gallon, and sag resistance. All of the paints deviated from specification requirements for at least one of the tests; however, no correlation was found between nonconformance to the specification and blister performance.

Another series of blister tests involved studying the effect of using various combinations of MIL-P-24441-approved raw material suppliers for the major ingredients -- epoxy resin, polyamide resin, polyamide adduct, and solvents. The raw materials selected are from a representative number of suppliers presented in Table 1. An experiment was designed using analysis of variance to facilitate testing of the twenty-seven paints that resulted from combination of the major ingredients. The results of this study indicated that choice of raw material supplier is significant for polyamide and polyamide adduct and that certain combinations of major ingredients improve performance.

Table 1. Raw material suppliers for major ingredients.

Polyamide	Polyamide Adduct
Epotuf SF7791	Epotuf SF7792
Genamid 2000	Versamid 280B75
Unirez 2810	Unirez 2180B75

Epoxy Resin
Epon 828
Araldite 6010
Der 331

Ethylene Glycol Monoethyl Ether	Ethylene Glycol Monobutyl Ether
Union Carbide	Union Carbide
Eastman	Eastman
Shell	

Paint Thinner
Varsol 18
Chevron 350-H

In the above series of tests, three alternative solvent systems for use as substitutes for the Type II system were also evaluated. The purpose of evaluating these solvent systems was for possible replacement of the Type II solvent system because prohibition of ethylene glycol monoethyl ether and ethylene glycol monobutyl ether has been proposed. The solvent systems are:

a. n-butanol, super hi-flash naphtha, isobutyl isobutyrate;

b. propylene glycol monomethyl ether, propylene glycol monomethyl ether acetate, paint thinner;

c. propylene glycol monomethyl ether acetate, super hi flash naphtha.

These solvent systems were also evaluated with the combinations of raw materials tested with the Type II solvent systems. The results indicated that choice of solvent system was also significant. The alternative solvent systems also provided coatings with blister performance superior to Type II if the combinations of raw materials were selected based on the blister test performance.

The conclusions from these studies are that: a) choice of raw material supplier for polyamide and polyamide adduct has a significant effect on blister performance, b) certain combinations of polyamide and polyamide adduct improve blister performance, c) choice of solvent system has a signficant effect on blister performance.

ANTIFOULING COATINGS

Research in antifouling coatings has been directed at high performance coatings with lifetimes exceeding 5 years. The standard Navy antifouling paint, F-121, is a conventional cuprous oxide coating which typically prevents fouling for 7 to 24 months. Toxicant release in F-121 occurs in two steps. First, the soluble rosin matrix dissolves and exposes the cuprous oxide pigment to seawater. Then the cuprous oxide is dissolved and the cuprous

complexes oxidized to cupric complexes, producing the toxic cupric ion. Eventually, pores are created from the insoluble vinyl matrix as the soluble components of the paint dissolve. The proposed mechanism of failure is the formation of insoluble cupric salts on the surface and in the pores that block diffusion of the cupric ion. Programs are underway at DTNSRDC to evaluate commercial coatings that remain fouling-free longer than the standard Navy paint. These new coatings are primarily ablative, or renewable surface type paints, and organotin copolymer coatings. Ablative paints slowly dissolve as a function of water velocity and temperature providing a fresh surface for release of toxicant. The toxicant is usually cuprous oxide or an organotin compound. The organotin copolymer coatings, developed at DTNSRDC, effectively control release rate of organotin by chemical bonding of the toxicant to the binder. When immersed in seawater, the bond is slowly hydrolyzed and the toxicant released.

There are currently twelve antifouling (AF) paints under evaluation on ship hulls, both commercial products and Navy formulations, and other formulations are being evaluated by static exposure panels and panels attached to bilge keels. The paints under evaluation on ship hulls include organotin copolymer, organotin/cuprous oxide ablative, cuprous oxide ablative (tin-free), and F-121 modified with ammonium sulfate. The addition of ammonium sulfate to standard F-121 is proposed to inhibit formation of insoluble copper salts. The current status of these trials is summarized in Table 2. The DTNSRDC organotin copolymer and the commercial cuprous oxide ablative formulations exhibit excellent (>99% fouling free) performance against hard fouling and soft fouling. The commercial cuprous oxide ablative coating has been under evaluation for 6 months. The DTNSRDC organotin copolymer coating is

Table 2. Current status of ship trials of antifouling paints.

Paint	Service To Date	Control Against Hard Fouling	Control Against Soft Fouling	Other
Organotin Copolymer Ablative	70 mos.	Excellent*	Some slime and algae	Release rate unacceptable
TBTO & Cuprous Oxide Ablative	60 mos.	Excellent	Some slime and algae	
Organotin Copolymer & Cuprous Oxide Ablative	30 mos.			
Organotin Copol ymer (DTNSRDC)	75 mos.	Excellent	Excellent	Reformulation to optimize release rates
Cuprous Oxide Ablative	39 mos.	Excellent	Excellent	Paint has been reformulated. New formulation-- 6 mos. evaluation
Ammonium Sulfate Modified F-121	New trial			

* Excellent = 99% fouling free performance.
Acceptable release rate $\leq 0.1\ \mu/cm^2/day$ utilizing parallel plate method.

currently being reformulated to optimize release rates of organotin to comply with environmentally acceptable release rates of $<0.1\mu/cm^2/day$ utilizing a parallel plate analysis method. The commercial organotin copolymer ablative and TBTO (tributyltin oxide)/cuprous oxide ablative coatings are excellent against hard fouling; however, some soft fouling (algae and slime) is present. The release rate of the organotin copolymer ablative coating exceeds the maximum acceptable value for organotin. The evaluation period for the commercial organotin copolymer/cuprous oxide ablative coating is still in an early phase. The ammonium sulfate modified F-121 trial began in November 1986.

As calcareous foulers come under control, marine microbial biofilms (slime), macroalgae (grass), and the roughness of the paint itself are now becoming the limiting frictional factors for ship performance. A study was performed to assess the possible effects of microbial biofilms upon hydrodynamic drag under hydraulic conditions that reflect realistic ranges of vessel operation. A friction disc machine, Fig. 4, was used to measure increase in hydrodynamic friction created by microbial films under various conditions of fluid flow, represented by the rotational Reynold's number R_R, which is proportional to rotational speed. The moment coefficient, C_m, is proportional to drag on the disk at a given speed, and is calculated from measurements of the torque required to rotate a disk at constant angular velocity. A plot of C_m versus R_R relates drag to hydrodynamic flow conditions. The percent increase in drag is $100\ (C_m - C_o)/C_o$, where C_m is the moment coefficient of a disk covered with a biofilm, and C_o is the moment coefficient for a clean disk. In order to relate the data derived from friction disk experiments to realistic situations, a procedure developed by Granville[3] can be used.

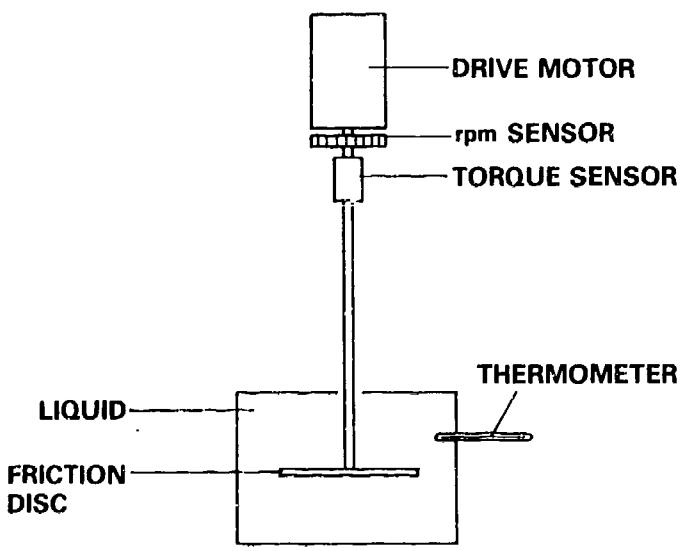

Fig. 4. Hydrodynamic friction disc apparatus.

This method makes use of semi-empirical theory to relate the frictional drag experienced by a disk having a particular surface character to a large plate of the same surface character. The flow about the spinning disk is characterized by the rotational Reynold's number. However, the flow past the flat plate is characterized by a different but related Reynold's number. Thus, the result of the Granville transformation yields results over a different speed range for the plate than for the disk. The size of the plate or vessel is important in the calculation. Table 3 illustrates the drag of biofilms. The speeds for the two plate lengths are obtained from from Granville transformations of the friction disk experimental data and correspond to the percent drag increase from the biofilm. Figure 5 illustrates the effect of biofilm thickness to increase the relative drag coefficient at high speed for the rotating disk experiment. Figure 6 illustrates the percent increase in drag from bacterial and algal films as predicted for flat plates. There are considerable differences in drag due to film thickness and type of film.

Table 3. Drag change due to biofilm on smooth surface.

Drag Increase due to Biofilm (%)	Speed (knots) of filmed plated*	
	110-m plate	140-m plate
2.2	22	17
5.0	28	22
8.0	35	27
10.0	44	34
12.0	55	43
14.0	70	54

* Hypothetical speed determined using Granville transformations[3] of data from frictional disk experiments.

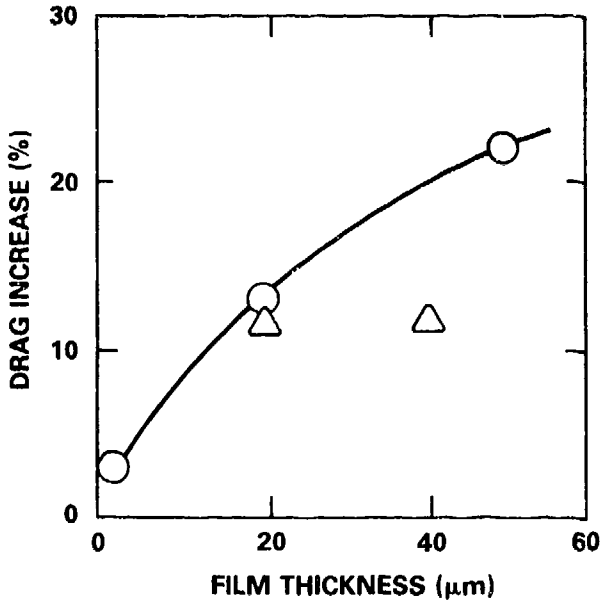

Fig. 5. Effect of film thickness on relative drag coefficient at high speed. ○ = bacterial flow cultures, △ = algal stirred cultures.

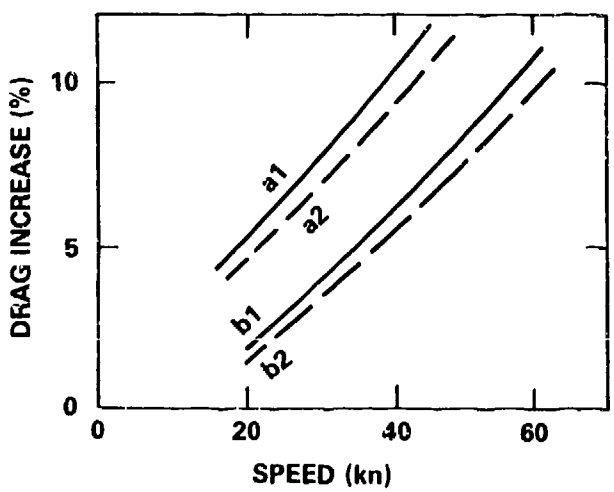

a1 = 50 μm BACTERIAL FILM, 110-m PLATE LENGTH;
a2 = 50 μm BACTERIAL FILM, 220-m PLATE LENGTH;
b1 = 40 μm ALGAL FILM, 110-m PLATE LENGTH;
b2 = 40 μm ALGAL FILM, 220-m PLATE LENGTH.

Fig. 6. Percent increase in drag on filming: predicted for flat plates from rotating disc experiments.

The conclusions from tests on antifouling coatings are as follows: a) AF coatings are available, both commercially and as Navy formulations, that provide long term performance against calcareous fouling organisms, and in some cases inhibit slime and algae, b) frictional increments of the order of 10% are caused by microbial biofilms. Further research is needed in the areas of roughness and viscoelastic properties of the biofilms, their tenacity on different types of surfaces, and methods to control these properties.[2]

1. Funke, W. "Blistering of Paint Films," in: Corrosion Control by Organic Coatings, Edited by H. Leidheiser, Jr., National Association of Corrosion Engineers, Texas (1981), pp. 97-102.

2. Loeb, G.I., D. Laster, and T. Gracik, "The Influence of Microbial Fouling Films on Hydrodynamic Drag of Rotating Discs," in: Marine Biodeterioration: An Interdisciplinary Study, Edited by J.D. Costlow and R.C. Tipper, Naval Institute Press, Maryland (1984).

3. Granville, P.S. "Similarity Law Characterization Methods for Arbitrary Hydrodynamic Roughness, David Taylor Naval Ship Research and Development Center Report (DTNSRDC-SPD 815-01, Bethesda, Md (1978).

BIOGRAPHY

NAME: Karen M. Poole

PRESENT AFFILIATION: Paints and Processes Branch at the David Taylor Naval Ship Research and Development Center

TITLE: Chemist

FIELD OF INTEREST/RESPONSIBILITIES: Development of anticorrosive and anti-fouling coatings

PREVIOUS AFFILIATIONS/TITLES:

ACADEMIC BACKGROUND:

SOCIETY ACTIVITIES/OFFICES/AWARDS:

PUBLICATIONS/PAPERS:

BEST AVAILABLE COPY

BIOGRAPHY

NAME: Gerard S. Roblanco

PRESENT AFFILIATION: Paints and Processes Branch at the David Taylor Naval Ship Research and Development Center.

TITLE: Materials Engineer

FIELD OF INTEREST/RESPONSIBILITIES: Fouling, corrosion control, and hull roughness

PREVIOUS AFFILIATIONS/TITLES:

ACADEMIC BACKGROUND: Masters degree in Ocean Engineering from Catholic University of America

SOCIETY ACTIVITIES/OFFICES/AWARDS:

PUBLICATIONS/PAPERS:

BEST AVAILABLE COPY

BIOGRAPHY

NAME: George I. Loeb

PRESENT AFFILIATION: Paints and Processes Branch at the David Taylor Naval Ship Research and Development Center working in the Environmental Sciences Division.

TITLE: Research Scientist

FIELD OF INTEREST/RESPONSIBILITIES: Biological Attachment and Surface Modification

PREVIOUS AFFILIATIONS/TITLES:

ACADEMIC BACKGROUND: PhD from Cornell University

SOCIETY ACTIVITIES/OFFICES/AWARDS:

PUBLICATIONS/PAPERS:

BEST AVAILABLE COPY

CORROSION OF TUNGSTEN ALLOYS IN MARINE ENVIRONMENTS

K. L. Vasanth and C. M. Dacres
Naval Surface Weapons Center
10901 New Hampshire Avenue
Silver Spring, MD 20903-5000

ABSTRACT

Tungsten alloys are important for Navy applications because of their high density and strength. Very little information is available about the corrosion behavior of these alloys, although tungsten is known to be corrosion resistant. The corrosion behavior of five tungsten alloys in 3.5% NaCl has been characterized using electrochemical and gravimetric tests. Laboratory results are compared to results obtained from exposure to natural sea water. The uniform corrosion rate of the alloys considered were found to be under 2 mils per year. However, alloys designated S1 and S2 exhibited preferential local attack. The corrosion in these alloys occur between tungsten particles where matrix alloy precipitated. Such an attack affects the strength of these alloys leading to fracture, particularly under the conditions of impact and load.

INTRODUCTION

In recent years, tungsten has found application in many weapon systems. In the form of a liquid phase sintered alloy (W-Ni-Fe or W-Ni-Cu) it is commonly used as the armor piercing core of medium to large caliber (>20 mm) kinetic energy ammunition (1). Recently tungsten alloys have also been used as preformed fragments in various anti-craft and anti-missile warheads (1). The cited application uses a dense penetrator core, of either tungsten carbide or more recently, liquid phase sintered tungsten alloy, surrounded by a ballistic sheath for aerodynamic purposes. The industrial applications of tungsten alloys include counter balances, gyroscope rotors, and radiation shields.

The Navy requires high density materials for armor piercing ammunition. Of the materials with densities over 15 gm/c.c, only two are readily available and economical - tungsten and uranium. The latter, though an attractive option, its use is restricted because of health hazards due to radiation. In addition, uranium alloys are known to be susceptible to stress corrosion cracking (SCC) in a variety of environments (2,3). SCC in PHALANX penetrators during long-term storage in humid air has been reported, and the presence of oxycarbide inclusion was identified as the cause of the observed cracking (4).

Until recently, the corrosion of tungsten alloys was not considered a problem. Andrew, et al. (5) reported that a 90% W, 7.5% Ni, 2.5% Co alloy readily corrodes when exposed to air saturated with water vapor. Levy and Chang (6) studied some tungsten heavy alloys and reported that 97 W-2 Ni-0.7 Fe-0.3 Co alloy was most corrosion resistant in solutions containing chloride ions. The tungsten alloys containing nickel and iron, considered here have not been characterized for their corrosion behavior. The Navy's interest is to get an estimate of the strength and shelf life in an uncontrolled environment.

EXPERIMENTAL

ELECTROCHEMICAL

Discs with a diameter of 1.2 cm and a thickness of about 0.4 cm were cut from the alloy samples using a diamond disc saw. Specimens were mounted in epoxy and wet polished with 320A, 400A and 600A silicon carbide, rinsed with distilled water, acetone degreased, air dried and immediately used for electrochemical investigations.

The solution used for polarization resistance measurements and potentiodynamic scans was 3.5 % NaCl. 3.5 % NaCl was prepared using laboratory reagent grade sodium chloride and distilled water. All the electrochemical investigations were made using a software driven EG&G Model 351 Corrosion Measurement System and Potentiostat/Galvanostat Model 273. The open circuit potential (initial corrosion potential) was obtained for each system, by allowing the specimen to stand in 3.5 % NaCl for a period of 30 minutes to an hour. The open circuit potential stabilized during this period (see Table 1). The potentials were measured using a standard calomel electrode.

Polarization resistance measurements. Polarization resistance (Rp) measurements were made using a three electrode assembly. A + 10 mV potential range was applied to the sample surface at the equilibrium corrosion potential (Ecorr). A scan rate of 0.1 mV/sec was used.

Calculation of corrosion rates using Rp values are difficult because of the inherent uncertainty in the change of Tafel constants with time. However, it is an elegant technique used to predict the trends in the corrosion rate with time.

Potentiodynamic polarization measurements. Potentiodynamic polarization scans were made for the tungsten alloy samples to better characterize the corrosion behavior. Alloy samples were allowed to stabilize for one hour prior to testing. The polarization scans were run at a scan rate of 0.5 mV/sec beginning at Ecorr at intervals of 1, 96 and 168 hours.

IMMERSION TEST

The washed and degreased tungsten alloy samples were painted at the bottom with AMERCOAT 90, epoxy paint, to prevent crevice corrosion. The paint was allowed to dry in air for about 48 hours. The weight of each specimen was recorded and then kept immersed in 400 ml of 3.5 % NaCl. The specimens were removed from test environment after 5 months, and rinsed under running tap water, ultrasonically cleaned in distilled water for ten minutes. Finally, the specimens were rinsed with acetone, air dried and weighed.

FIELD TESTS

16 samples of each alloy have been exposed to three types of test environments at the NSWC/Ft.Lauderadale Corrosion test site:

a) Continuous immersion in sea water
b) Alternate immersion in sea Water
c) Atmospheric exposure to marine environment

For the continuous immersion test, pre-weighed specimens were mounted on sample racks and immersed in a flume containing sea water. Fresh sea water is circulated at a rate of 0.5 gallon per minute.

For alternate immersion tests, the specimens were immersed in sea water for one day and for six days kept exposed to the marine atmosphere. This test is designed to determine the combined effect of sea water immersion and marine atmospheric exposure.

The atmospheric exposure test involves a continuous exposure of the specimens to the marine atmosphere. In these field tests, the specimens of each alloy type will be taken out at specified intervals, weighed and photographed. The first set of samples were taken out of the continuous and alternate immersion tests after 2 months, cleaned as described in Reference 5, air dried and weighed. The weight-loss data was used to compute the corrosion rates and are given in Table 2. The weight-loss data and calculated corrosion rates obtained from the laboratory immersion tests in 3.5 % NaCl, are given in Table 3 along with some observations. The red-brown and yellow color of the residue indicates the formation of WO_2 and WO_3 respectively (see Table 4) (7). The red-brown corrosion product might have also come from the corrosion of iron present in the matrix alloy between tungsten particles.

ENERGY DISPERSIVE X-RAY ANALYSIS (EDAX) AND SCANNING ELECTRON MICROSCOPY (SEM)

Five sintered tungsten alloys have been investigated. These were subjected to EDAX in the "as received" condition and after sawing the machined surface. This was done for identifying any difference between the surface and the bulk of the alloys. The results of EDAX analysis are given in Table 5. The EDAX spectra of the machined and sawed surface in all cases except type S2 are similar, and showed the presence of iron and nickel as alloying elements, the bulk element being tungsten. The spectrum of "as received" machined surface of S2 showed traces of potassium and calcium (Figure 1 a) in addition to the alloying elements iron and nickel, while the sawed surface of the sample (Figure 1b) indicated no such impurities. Potassium and calcium that were found only on the machined surface and not in the bulk alloy could be attributed to the use of soap and/or chalk powder in the machine shop while handling these samples.

RESULTS AND DISCUSSION

POLARIZATION RESISTANCE MEASUREMENTS

Polarization resistance measurements were made for each of the five types of tungsten alloys in 3.5 % NaCl over a period of about 35 days. Polarization resistance versus time plots are shown in Figure 2. The alloys S1, S2, T1 and T2 show an increase in the corrosion rate up to 48 hours after which the corrosion rate reaches an approximate limiting value. On the other hand K1 shows a higher corrosion rate up to 12 hours but from 0.5 day to 12 days the corrosion rate decreases and eventually reaches a limiting value. This may be attributed to the building or thickening of the oxide film which reaches a constant value with time.

Polarization resistance versus time plots for S2, T1 and T2 show flat plateau regions approximately from 3 to 7 days, 9 to 26 days and 28 to 34 days. Between these plateau regions the plots show a dip indicating increased corrosion rate. The corrosion rate remained almost constant in the plateau regions. This corrosion trend indicates that an oxide film growth occurs on the samples which occassionaly breaks down exposing the fresh surface leading to corrosion.

A visual examination of the specimens after polarization resistance studies at 35 days, showed that S1 and S2 were attacked at preferential sites, T1 and T2 showed intense uniform corrosion with a reddish-brown layer of corrosion product on their surface and K1 showed moderate uniform corrosion. The preferential corrosion could be due to a) inhomogeneity of the alloy and /or b) dissolution of iron from the precipitated alloy in grain boundaries. Assuming that the dissolution mechanism is

predominant in these cases, equation 1 as suggested by Ammar, et al. (7), and presently proposed reactions 2 and 3 may be occurring in addition to the corrosion of iron to iron oxide :

$$1)\quad 2\,OH^- + WO_3 = WO_4^{\,2-} + H_2O$$

$$2)\quad H_2O + WO_3 = H_2WO_4$$

$$3)\quad 2\,NaCl + H_2WO_4 = Na_2WO_4 + 2\,HCl$$

From 2 and 3, $2NaCl + WO_3 + H_2O = Na_2WO_4 + 2\,HCl$

POTENTIODYNAMIC STUDIES

Potentiodynamic scans were run for all the five types of tungsten alloys in 3.5 % NaCl solution. The epoxy mounted polished specimens were allowed to stabilize for about an hour in 3.5 % NaCl. Potentiodynamic measurements were made at 1, 96 and 168 hour intervals. Alloys K1, S1 and S2 showed a decrease in corrosion rate while T1 and T2 were still corroding at 96 hours. A typical scan for T2 in 3.5% NaCl after one hour is shown in Figure 3. The alloy exhibits an active-passive transition. Koger (9) has attributed the two distinct "knees" nearest to the equilibrium corrosion potential to pure tungsten.

For the purpose of comparison, a bar chart of corrosion rates computed from 1 hour potentiodynamic measurements is shown in Figure 4. It can be seen that alloy type K1 has the lowest corrosion rate and T2 the highest among the five types considered for study. These results are correlated well with the corrosion trends observed in the polarization resistance measurements (Figure 2).

WEIGHT-LOSS MEASUREMENTS

Photographs of alloy samples immersed in 3.5 % NaCl taken after 72 days and 5 months are shown in Figures 5 and 6 respectively. It is evident that the intensity of corrosion of these samples increased as a function of time of immersion.

The corrosion rates calculated based on the weight-loss data in 3.5 % NaCl immersion test also showed that alloy K1 had the lowest corrosion rate. Visual observation indicated that both T1 and T2 had uniform and intense corrosion with a brown corrosion layer on their surfaces while S1 and S2 showed corrosion at selected/preferential sites. The weight loss data from 3.5 % NaCl immersion tests showed that though S2 suffered only preferential corrosion, it exhibited slightly higher weight-loss than T1 and T2.

SEM and EDAX

The samples used for polarization resistance measurements were immersed in 3.5 % NaCl for more than 35 days. These corroded samples were carefully taken out of the epoxy mounting and subjected to SEM and EDAX examination. Cut of five alloys. K1, T1 and T2 exhibited corrosion all over the exposed surface as shown in the SEM of alloy T1 in Figure 7a. For alloys S1 and S2, only some areas of the exposed surface were attacked as shown in the SEM of alloy S1 in Figure 7b.

The SEM photographs and EDAX spectra of the corroded samples are given in Figures 8-12. The common feature in these alloys is that the structure consists of rounded tungsten particles surrounded by a matrix alloy of Fe-Ni-W.

The EDAX examination of the precipitated matrix alloy between the tungsten particles in sample K1 showed the presence of W, Fe and traces of Ni,Zn,Na and Cl (Figure 8b). Na and Cl have obviously come from the NaCl solution in which the sample was immersed. The EDAX of the corrosion products that appear as lumps on tungsten particles in the SEM photograph (Figure 8a) also showed to contain the same elements in almost similar amounts. It can be seen from Figure 8a that the tungsten particles appear intact but some what loosened due to the corrosion of the precipitated matrix alloy between the tungsten particles.

For alloy S1, the corrosion was observed at preferential local sites. The SEM photograph in Figure 9a shows one such attacked area. The attacked area consists of two shaded regions : light and dark gray. The dark gray shaded region on the top side in Figure 9a is due to thick corrosion products on the surface. The light gray region appeared shiny and showed selective attack between the tungsten particles. The shiny appearance of the area indicated that the corrosion film had fallen off exposing the fresh surface (see Figure 7b). This was confirmed by the EDAX of the light grey region which was found to show mostly W with traces of Fe and Ni. On the other hand, the thick corrosion product was found by EDAX to contain predominantly Fe, some W with traces of Ni and Cl as shown in Figure 9b.

The SEM photograph for S2 in Figure 10a clearly shows the rounded tungsten particles and matrix alloy precipitated between these particles. The sample showed preferential localized corrosion as observed in immersion tests. The EDAX of the corrosion products showed mostly Fe, some W and traces of Ni and Cl (Figure 10b). Similar results were obtained for S1. This shows that S1 and S2 as observed visually in immersion tests and by SEM, corroded in a similar manner.

The SEM photograph for alloy T1 in Figure 11a shows that the surface was attacked uniformly. Some "hilly" spots of thick corrosion products were found on the surface. EDAX analysis of these spots showed very little of W, more Ni than Fe and a large proportion of Cl (Figure 11b). The high content of Ni was also found in the fresh sample as shown in Table 4, and appears to have concentrated in the matrix alloy between the tungsten particles.

The results of SEM and EDAX for alloy T2 (Figure 12 a and b) are similar in nature to those found for T1 except that the corrosion product contained large proportion of Fe and only traces of Ni. Both alloys T1 and T2 showed uniform corrosion all over the surface unlike S1 and S2, where only some areas of the surface were attacked.

SUMMARY

1. The laboratory immersion tests in 3.5% NaCl showed that the alloy K1 has the lowest corrosion rate and the alloy S2 the highest.

2. The lowest corrosion rate observed for alloy K1 may be attributed to the high content of tungsten and low content of iron as indicated by EDAX analysis.

3. The alloys K1, T1 and T2 exhibited uniform corrosion, and preferential corrosion was observed in the case of S1 and S2.

4. The SEMs of corroded alloys showed corrosion at the matrix alloy precipitated between rounded tungsten particles.

5. The EDAX analysis showed that all the alloys contained Fe and Ni as alloying elements to start with.

6. The magnitude of corrosion rate for the five tungsten alloys is less than 2 MPY.

ACKNOWLEDGMENT

The authors express their thanks to Dr. M. K. Norr of this Center for his cooperation in producing the SEM micrographs and EDAX scans.

List of Illustrations

1. a) EDAX Spectrum of the Machined Surface of S2.
   b) EDAX Spectrum of the Sawed Surface of S2.
2. Polarization Resistance versus Time Plots for Tungsten Alloys.
3. Potentiodynamic Scan for T2 in 3.5% NaCl.
4. Bar Chart of Corrosion Rates for Tungsten Alloys.
5. Tungsten alloys after 72 days in 3.5% NaCl.
6. Tungsten alloys after 5 months in 3.5% NaCl.
7. a) SEM of alloy T1 (8X) showing uniform corrosion.
   b) SEM of alloy S1 (8X) showing localized corrosion.
8. a) SEM of alloy K1 (500X) after 35 days immersion in 3.5 % NaCl.
   b) EDAX of corrosion product on tungsten particle in K1
9. a) SEM of local corroded area in alloy S1 (100X).
   b) EDAX of dark gray corrosion product.
10. a) SEM of alloy S2 (1000X) showing rounded tungsten particles and the matrix alloy in between.
   b) EDAX of the matrix alloy in between tungsten particles.
11. a) SEM of alloy T1 (500X) showing uniform corrosion.
   b) EDAX of the corrosion product on the surface of alloy T1.
12. a) SEM of alloy T2 showing uniform corrosion.
   b) EDAX of the corrosion product on the surface of alloy T2.

List of Tables.

1. Corrosion Potentials in 3.5% NaCl.
2. Results of 2 Months Immersion in Sea Water.
3. Results of 5 Months Immersion in 3.5% NaCl.
4. Tungsten oxides.
5. EDAX Analyses Summary of Tungsten Alloys.

References

1. P. N. Jones, "The Use of Tungsten in Armament Related Products," Proc. of 2nd Intl. Tungsten Symposium, San Francisco, June 1-5, 81, 1982.

2. C. A. W. Peterson, "A Stress Cracking Study of a Gamma Extruded U-8 wt% Mo-0.05 wt% Ti Alloy," UCRL-14132, April 1965.

3. N. J. Magnani, "The Effects of the Environment on the Cracking Behavior of Selected Uranium Alloys," Corrosion/72 National Association of Corrosion Engineers, Houston, Texas, 1972.

4. S. G. Fishman and W. N. Wishard, "The Effect of High Temperature and Humidity Storage on the Ballistic Properties of Close-in Weapons System Penetrators," NSWC/DL TR-3235, January 1975.

5. J. F. Andrew, M. T. Baker, H. T. Heron., "Corrosion and Protection of Sintered Tungsten Alloy Ammunition Components," Proceedings of 2nd Charlottesville Conference on High Density KE Penetrator Materials, Oct 1980.

6. Milton Levy and Frank Chang, "Corrosion Behavior of High Density Tungsten Alloys," Proc. 2nd Int. Conf. on Environmental Degradation of Engineering Materials," Sept. 21-23, 33-42, 1981.

7. Richard F. Horsnail, "The geology of Tungsten," Proc. 1st Int. Tungsten Symposium, Stockholm, Sept. 5-7,19, 1979.

8. I.A.Ammar, S. Darwish and M. W. Khalil., "An Approach to the mechanism of Corrosion of Tungsten in Alkaline Solutions," Zeitschrift Fver Werkstofftechnik, vol. 13, No.5, May 1982.

9. J. W. Koger, "Corrosion of Tungsten-3.5 Nickel-1.5 Iron and its Constituent Phases in Aqueous Chloride Solutions," No. 42, Corrosion/75, NACE, Houston, TX, 14,1975.

TABLE 1

CORROSION POTENTIALS FOR TUNGSTEN ALLOYS IN 3.5% NaCl

ALLOY	E_{CORR} VS SCE (V) START	E_{CORR} VS SCE (V) END OF 1 HOUR
K1	-0.360	-0.338
S1	-0.355	-0.318
S2	-0.345	-0.312
T1	-0.330	-0.292
T2	-0.359	-0.320

TABLE 2

RESULTS OF 2 MONTHS IMMERSION IN SEA WATER

ALLOY TYPE	WEIGHT-LOSS (g)	CORR. RATE (MPY)
K1	0.205	1.461
S1	0.107	0.771
S2	0.095	0.685
T1	0.195	1.402
T2	0.260	1.838

TABLE 3

RESULTS OF 5 MONTHS IMMERSION IN 3.5% NaCl

ALLOY TYPE	WEIGHT LOSS (g)	CORR. RATE (MPY)	OBSERVATIONS		
			SOLUTION	CORROSION	RESIDUE
K1	0.090	0.289	CLOUDY	UNIFORM	RED & YELLOW
S1	0.110	0.586	CLEAR	PREFERENTIAL	RED-BROWN
S2	0.110	0.781	CLOUDY	PREFERENTIAL	RED & YELLOW
T1	0.180	0.357	CLOUDY	UNIFORM	RED-BROWN
T2	0.240	0.351	CLOUDY	UNIFORM	RED-BROWN

TABLE 4

TUNGSTEN OXIDES

PHASE	AVERAGE O/W	FORMULA	COLOR
ALPHA	3.00	WO_3	YELLOW
BETA	2.90	$W_{20}O_{58}$	BLUE-VIOLET
GAMMA	2.72	$W_{18}O_{49}$	REDDISH-VIOLET
DELTA	2.00	WO_2	BROWN
BETA-W	0.33	W_3O	GREY

TABLE 5

EDAX ANALYSES SUMMARY OF TUNGSTEN ALLOYS

	WEIGHT %		
ALLOY	TUNGSTEN	IRON	NICKEL
K1	98.5	0.6	0.9
S2	98.3	0.6	1.1
S1	94.8	1.9	3.4
T1	94.5	1.8	3.8
T2	93.5	1.9	4.6

EDAX SPECTRA OF TUNGSTEN ALLOY S2

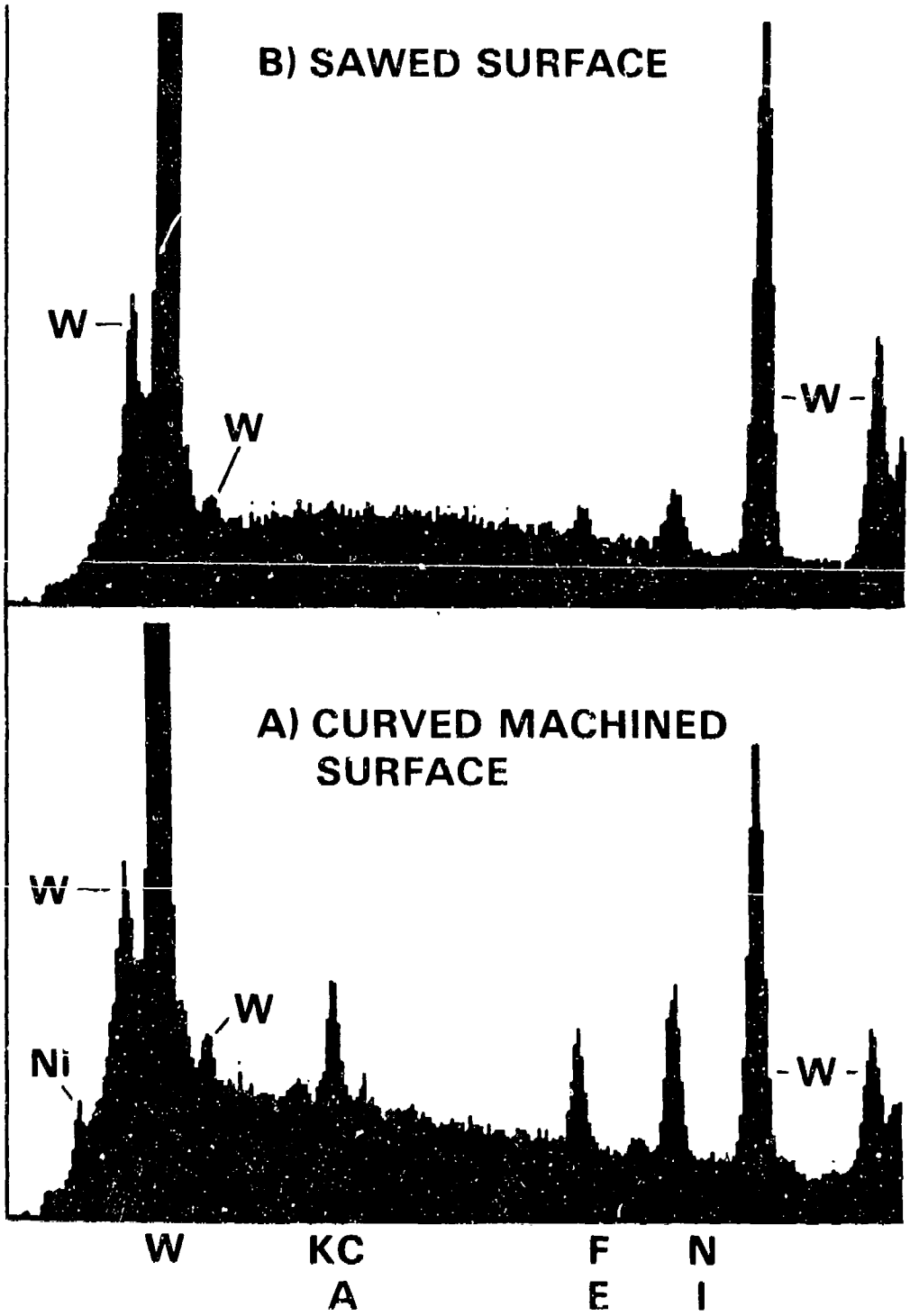

Figure 1

POLARIZATION RESISTANCE VS TIME

TUNGSTEN ALLOYS IN 3.5% NaCl

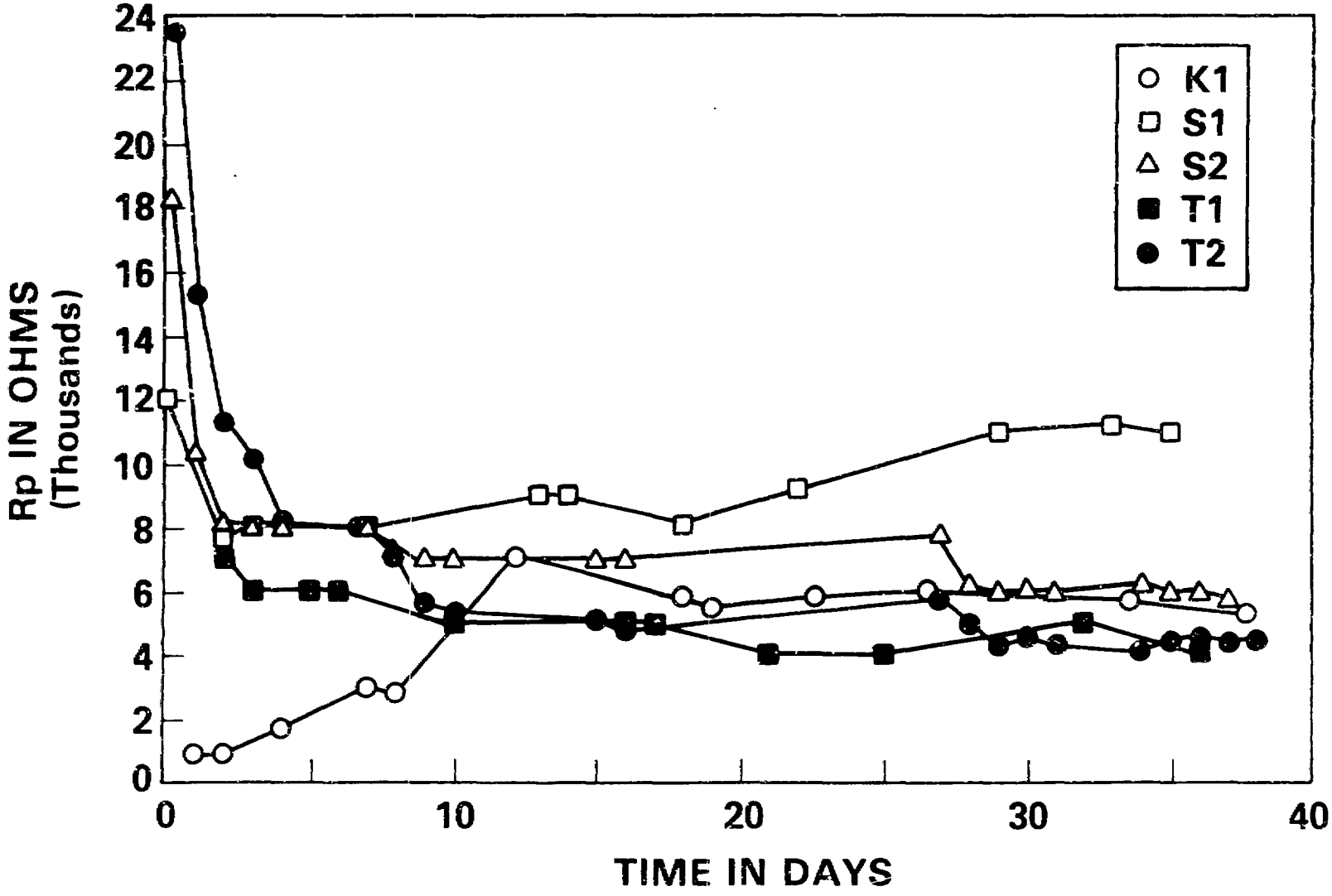

Figure 2

POTENTIODYNAMIC SCAN FOR ALLOY T2 IN 3.5 % NaCl

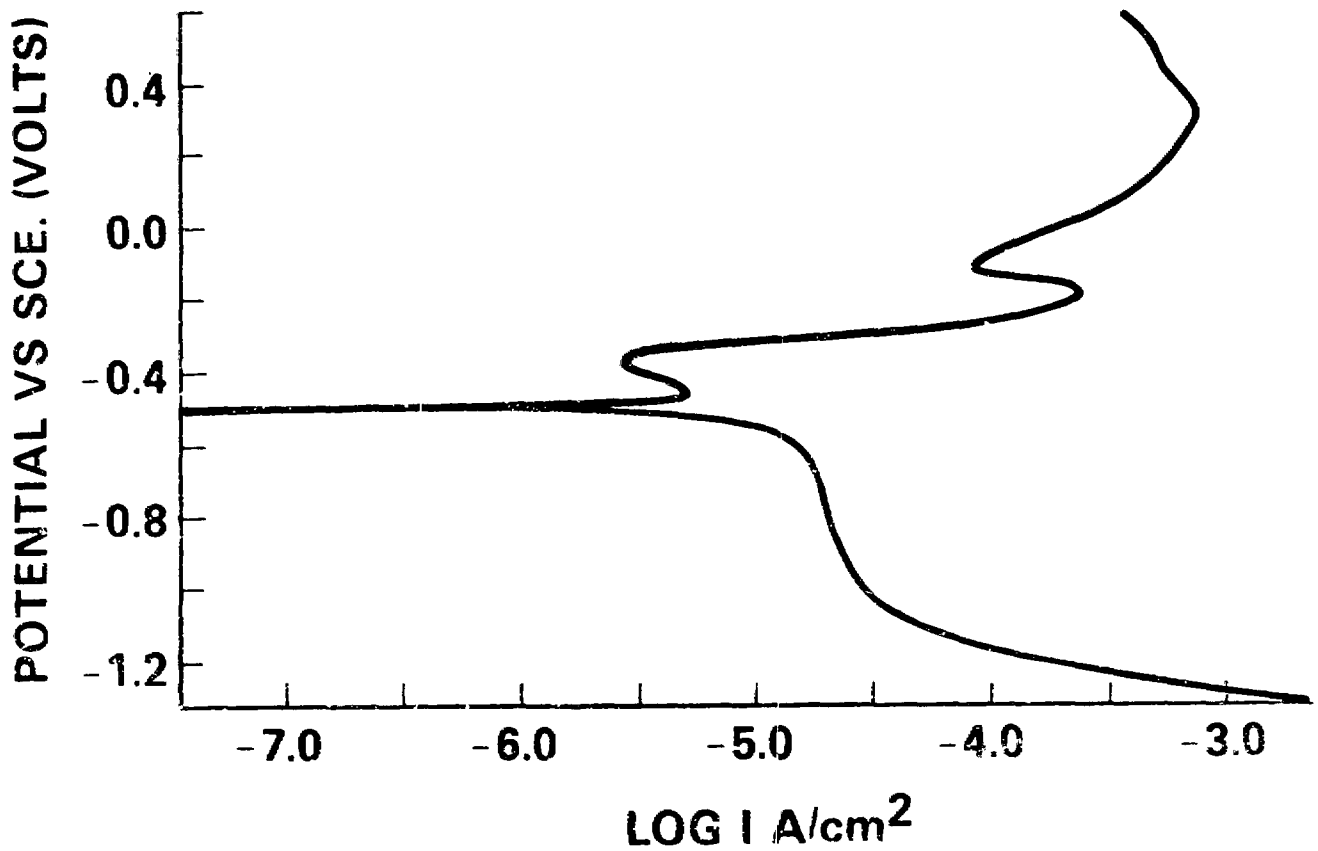

Figure 3

CORROSION RATE IN 3.5 % NaCl
(1 HR POTENTIODYNAMIC DATA)

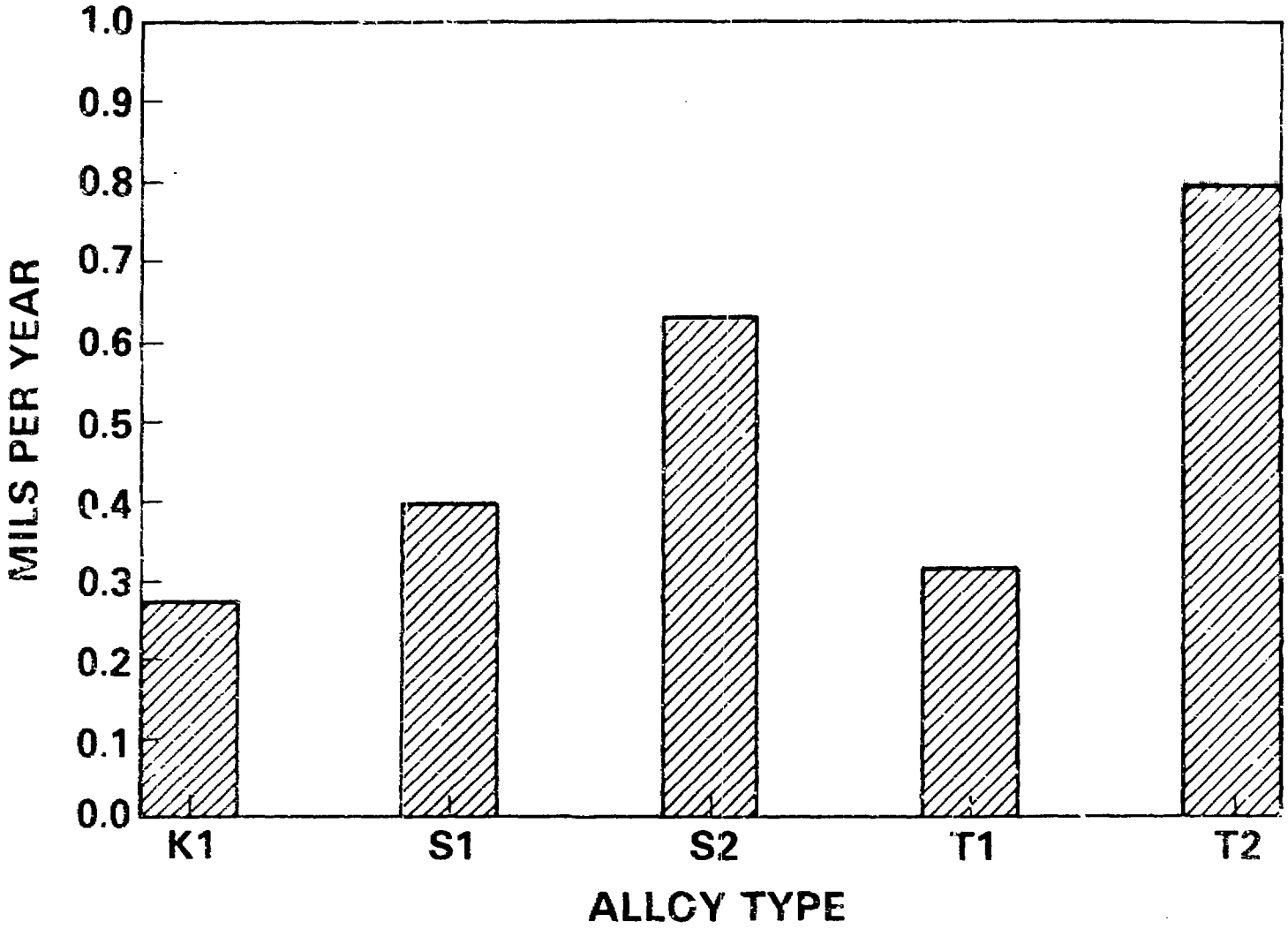

Figure 4

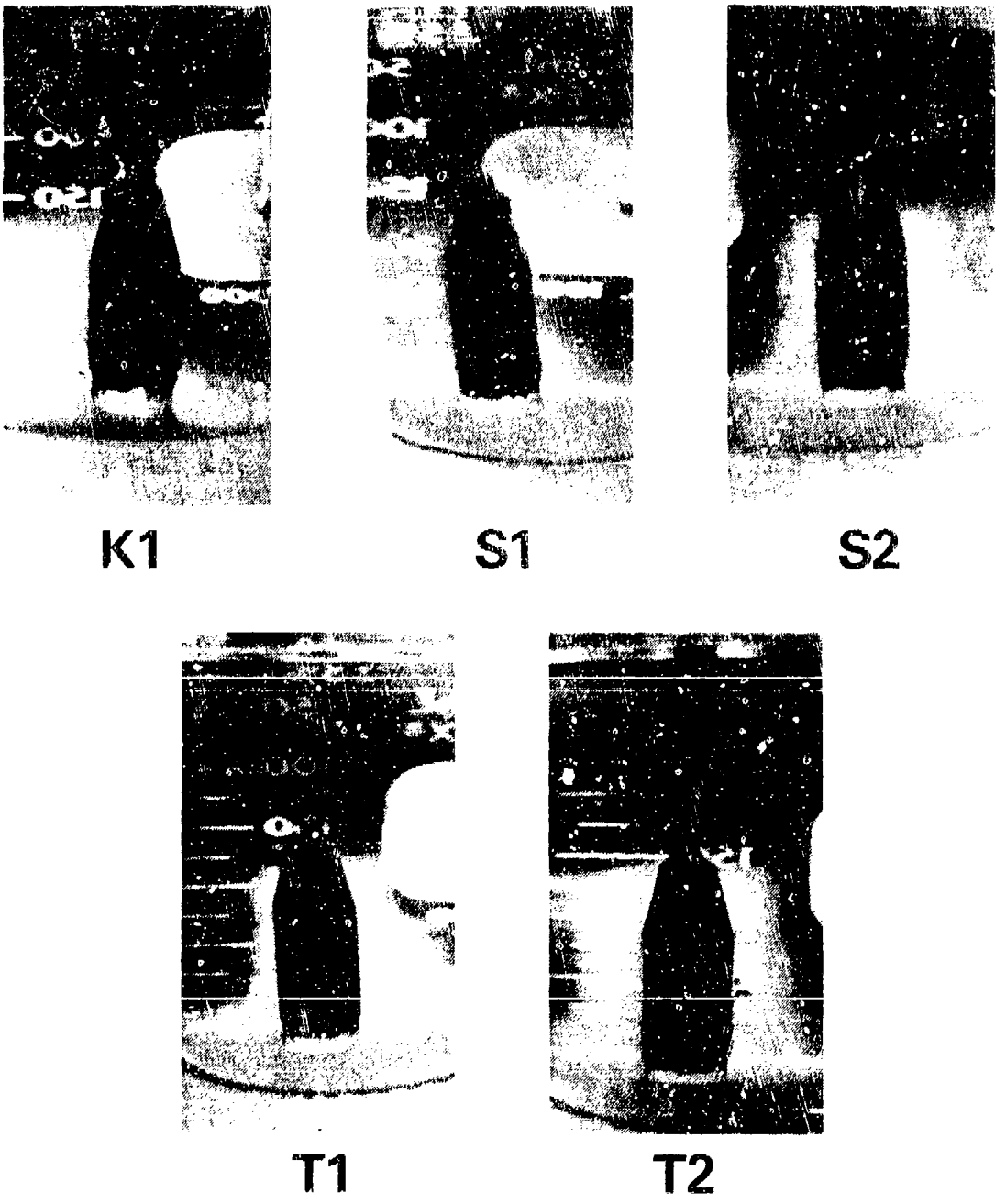

FIGURE 5. TUNGSTEN ALLOYS AFTER 72 DAYS IN 3.5% NACL.

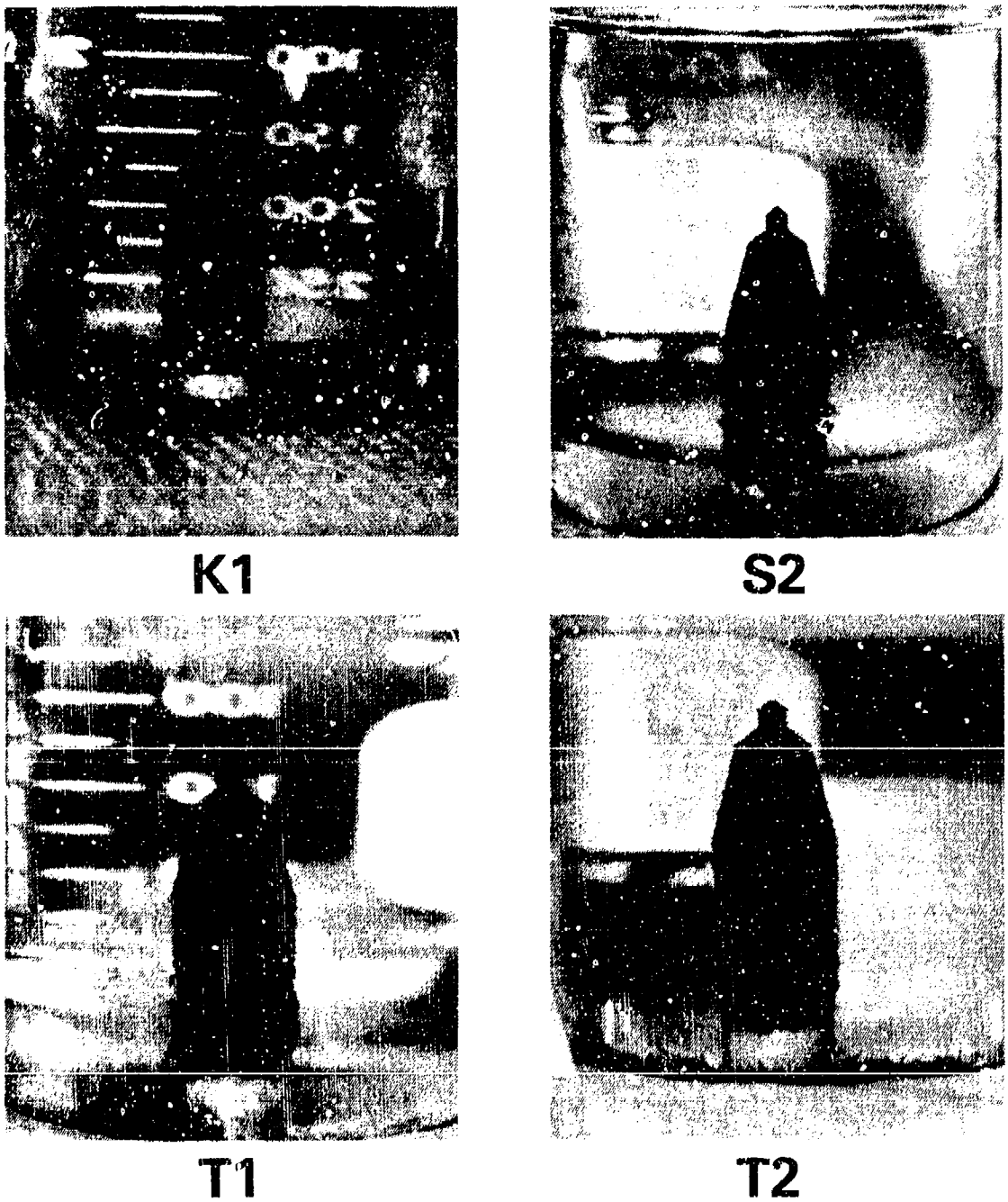

FIGURE 6. TUNGSTEN ALLOYS AFTER 5 MONTHS IN 3.5% NACL.

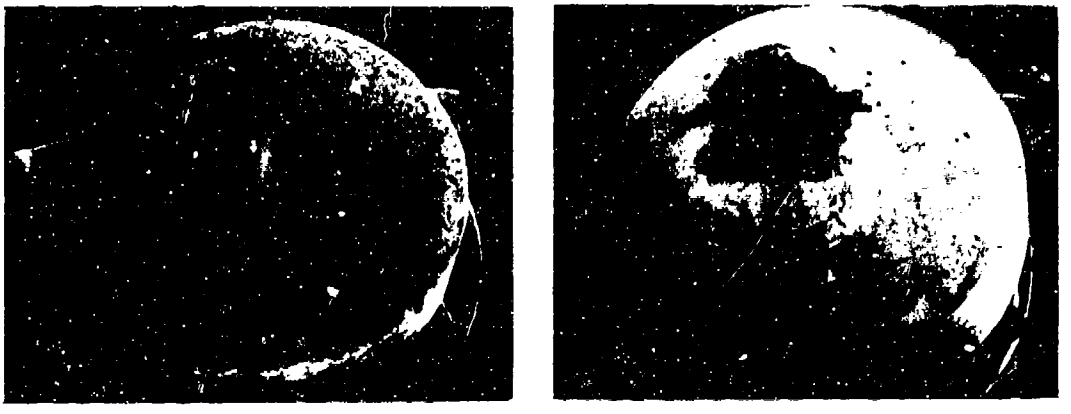

a. b.

a.) SEM OF ALLOY T1 (8x) SHOWING UNIFORM CORROSION.
b.) SEM OF ALLOY S1 (8x) SHOWING LOCALIZED CORROSION.

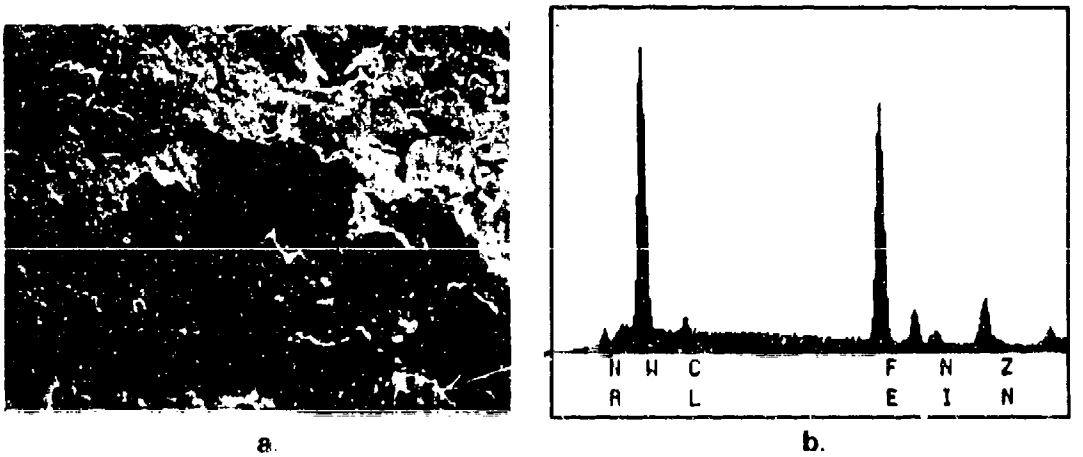

a. b.

a.) SEM OF ALLOY K1 (500x) AFTER 35 DAYS IMMERSION IN 3.5% NaCl.
b.) EDAX OF CORROSION PRODUCT.

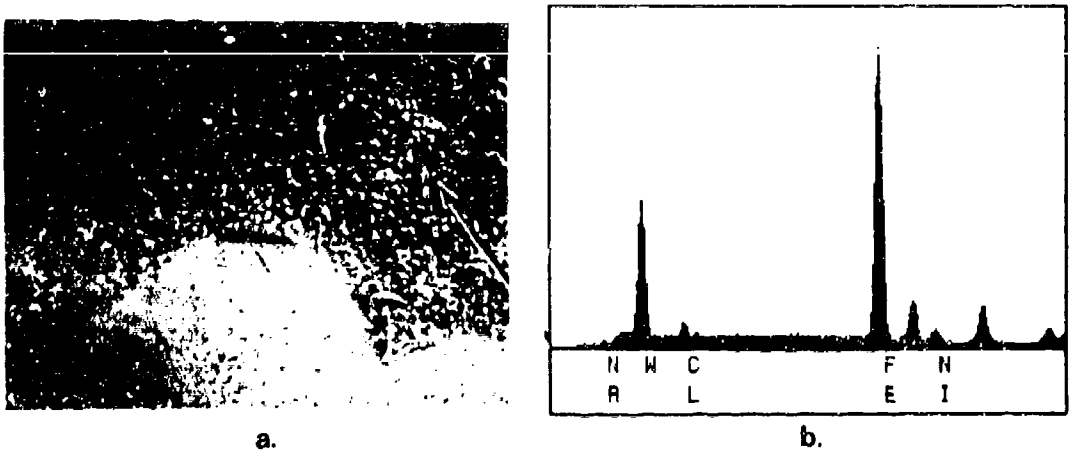

a. b.

a.) SEM OF ALLOY S1 (100x) AFTER 35 DAYS IMMERSION IN 3.5% NaCl.
b.) EDAX OF DARK GRAY CORROSION PRODUCT ON S1.

FIGURES 7 (TOP), 8 (CENTER) AND 9 (BOTTOM).

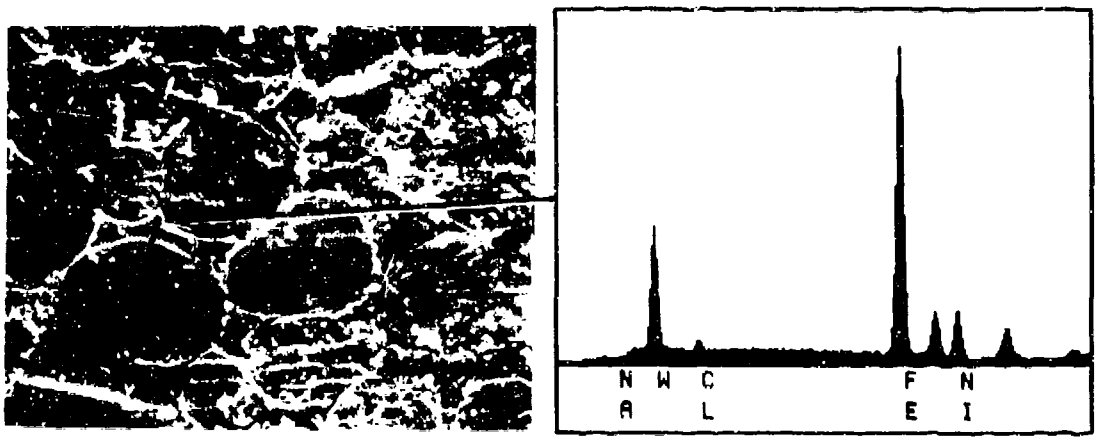

a. b.

a.) SEM OF ALLOY S2 (1000x) AFTER 35 DAYS IMMERSION IN 3.5% NaCl.
b.) EDAX OF MATRIX ALLOY BETWEEN TUNGSTEN PARTICLES.

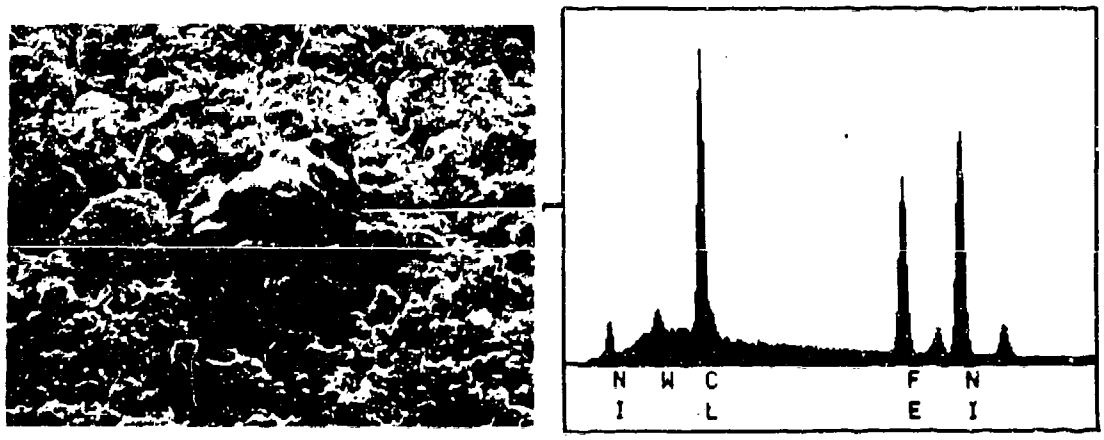

a. b.

a.) SEM OF ALLOY T1 (500x) AFTER 35 DAYS IMMERSION IN 3.5% NaCl.
b.) EDAX OF THICK "HILLY" SPOT OF CORROSION PRODUCTS.

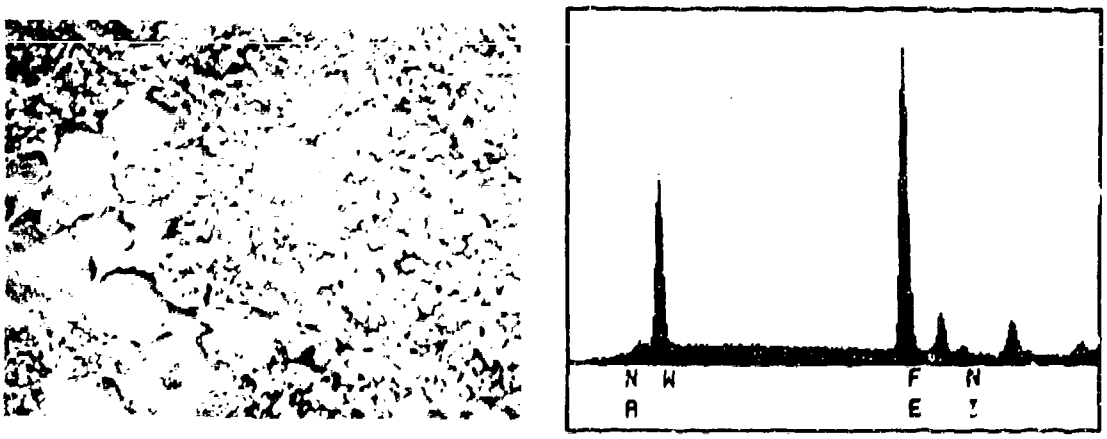

a. b.

a.) SEM OF ALLOY T2 (500x) AFTER 35 DAYS IMMERSION IN 3.5% NaCl.
b.) EDAX OF THICK CORROSION PRODUCTS.

FIGURES 10 (TOP), 11 (CENTER) AND 12 (BOTTOM).

CORROSION AND FATIGUE PROPERTIES OF FeCrB/Si METALLIC GLASS WIRES IN AQUEOUS ENVIRONMENTS

Anh H. Le and Lawrence T. Kabacoff
Naval Surface Weapons Center, White Oak
10901 New Hampshire Avenue
Silver Spring, Maryland 20903-5000

ABSTRACT

Measurements have been made of the corrosion and fatigue properties of metallic glass wires of composition $Fe_{75-X}Cr_XB_{15}Si_{10}$(X = 5, 8, 11) in air, deionized water, 3.5 w/o NaCl and 1.0 N H_2SO_4. A clear inverse relationship was observed between the corrosion rate and the number of cycles to failure. Fatigue limits were observed for those cases where spontaneous passivation occurs (all compositions in air and deionized water, and 8 and 11 a/o Cr in chloride solution). It was found that the mechanism for the fatigue failure of specimens which spontaneously passivate differs from that of metallic glasses in acidified chloride environment where active/passive behavior is observed. A model is proposed to explain this observation.

INTRODUCTION

Transition metal-metalloid metallic glasses containing principally Fe and Cr have long been known to exhibit high strength and toughness (1), as well as remarkable resistance to corrosion (2). In spite of these outstanding properties, commercial development of these materials has been confined to magnetic applications, most notably power distribution transformers and transducers. Early on, fatigue measurements clearly showed that the metallic glasses then available were unsuitable for such structural applications as tire cord and flywheels (1).

All of these fatigue measurements were made on metallic glass ribbons which were produced by some form of continuous chill block casting. Such ribbons tend to have irregular surfaces and large local variations in ribbon thickness. Recently, a new fabrication technique has been developed in which a stream of melt is injected into a moving layer of a water solution (3,4). The moving water layer is established on the inside of a rotating drum. The speed of the melt, the speed of the water, and the angle of entry are matched in such a way that the melt stream solidifies into a smooth, uniform wire with a round cross section. The quench rate achievable by this technique is quite high, and wires of, for example, amorphous Fe-B-Si have been produced with diameters as high as 160 microns (4).

A number of fatigue measurements have been made on metallic glass wires, mostly in an environment of either moist air or deionized water (5). The results may be summarized as follows: (1) the fatigue properties of the metallic glass wires are greatly superior to those of ribbons of similar

composition; (2) the fatigue limit is clearly a function of the corrosion rate regardless of whether the implicit parameter is composition or corrosiveness of the environment; (3) Fe-based metallic glass wires with a moderate amount of Cr have fatigue properties in deionized water superior to those of 304 stainless steel. Based on the dependence of the fatigue properties on corrosion rate, and on the results of stress corrosion measurements made on metallic glass ribbons in an acidic chloride environment, it was proposed that fatigue failure resulted from hydrogen accumulation. The difference in fatigue properties between wires and ribbons was attributed to the better surface smoothness of wires.

In this report we extend the corrosion and fatigue measurements to include 3.5 weight percent (w/o) NaCl and 1.0 N H_2SO_4 and present evidence that the failure mechanism in the chloride solution is substantially different from that has been observed previously for wires in an acidic environment containing chloride. The compositions selected were $Fe_{75-X}Cr_XB_{15}Si_{10}$ (x = 5, 8, 11).

EXPERIMENT

Potentiodynamic and pitting scans were obtained utilizing an EG&G Corrosion Measurement Console (Model 350A). The three-electrode-cell consisted of a working electrode, a graphite counter electrode and a SCE (saturated calomel electrode) reference electrode. Solutions of 3.5 w/o NaCl and 1.0 N H_2SO_4 were prepared from analytical grade chemicals and deionized water. Measurements were made at room temperature in aerated solutions. The initial potential for potentiodynamic curves was set at 250 mV below the open circuit potential. The scan rate was 1 mV/sec.

Bending fatigue measurements were made on wire specimens of each composition immersed in either 3.5 w/o NaCl or H_2SO_4. In addition, selected measurements were made in air (65% RH) and deionized water in order to compare our results with those previously reported. The apparatus used is illustrated in Figure 1 and is similar to that used by Hagiwara etal. (5). The strain is produced by passing a wire specimen over a pulley, which is immersed in the medium of interest. The maximum strain is controlled by the diameter of the pulley and is determined by the relation:

$$\lambda = d/(d + D)$$

where the d is the diameter of the wire and D is the diameter of the pulley. The measurements were made at room temperature in aerated solutions using the same solutions that were used for potentiodynamic measurememts. The repetition rate was four passes over the pulley per second.

In order to investigate the role of hydrogen in fatigue failure of these metallic glass wires in a seawwater environment, wires with 8 and 11 a/o Cr (which exhibit a fatigue limit in the chloride solution) were subjected to bending fatigue in the 3.5 w/o NaCl solution as described above except that the application of strain was interrupted prior to failure. Some wires were then baked out in an oven at 125^{0}C for 15 minutes (which is sufficient to remove any accumulated hydrogen but insufficient to produce structural relaxation, as determined by ductility tests (6). The other wire specimens were also removed from the pulley, but allowed to sit in the solution instead

of being baked out. The wires were then returned to the pulley and the application of cyclical strain was continued. The pulley diameter was chosen such that failure could be expected to occur in forty or thirty-eight minutes (for 8 and 11 a/o Cr respectively) if the application of bending strain were not interrupted. The baking (or "resting" time) was fifteen minutes, as was the time for application of cyclical strain. Thus, the time sequence was fifteen minutes "on" and fifteen minutes "off", cycled repeatedly.

RESULTS AND DISCUSSION

Figure 2 shows polarization curves for amorphous wires in 3.5 w/o NaCl solution. The wires containing 5 a/o Cr display an active/passive behavior, while the 8 and 11 a/o Cr specimens exhibit complete passivity. As expected, the corrosion current density and, therefore, the corrosion rate decreases with increasing Cr content. All three compositions exhibited active/passive behavior in 1.0 N H_2SO_4 as illustrated in Figure 3. Once again, the corrosion current decreased with increasing a/o Cr.

Pitting potentials varied only slightly as a function of composition in the NaCl solution (1.20 V/SCE for 5 and 8 a/o Cr and 1.170 V/SCE for 11 a/o Cr). This is illustrated in Figures 4, 5 and 6, which show pitting scans for 5, 8 and 11 a/o Cr in 3.5 w/o NaCl, respectively. It is also apparent from these figures that the hysteresis is extremely small, indicating a very low rate of crevice corrosion. In 1.0 N H_2SO_4 all of the pitting potentials were the same (0.966 V/SCE).

Figures 7, 8 and 9 illustrate the number of cycles to failure as a function of maximum bending strain for 5, 8 and 11 a/o Cr, respectively. Fatigue limits were observed for each composition in air and deionized water, and for 8 and 11 a/o Cr in 3.5 w/o NaCl. Our data on moist air and deionized water agree very well with previously published data by Hagiwara et. al.(7). Comparison of Figures 2 and 3 with Figures 7, 8 and 9 clearly show the relationship between corrosion rate and fatigue limit (or number of cycles to failure), and that failure occurs through a corrosion fatigue mechanism.

The results of the experiment in which the cyclical application of bending strain was periodically interrupted were somewhat surprising. As described in the preceding section wire specimens in 3.5 w/o NaCl were subjected to cyclical bending strain for fifteen minutes, then baked for fifteen minutes. Without interruption, failure would, for the strain chosen, occur after forty minutes. This was repeated (fifteen minutes on, fifteen off) for eight hours without failure (a total of four hours of strain application). This is consistent with the hypothesis that failure is due to accumulation of hydrogen. What was surprising is that the control specimens, which were not baked but were, rather, kept in the chloride solution during the "rest" period, also experienced no fatigue failures. In both cases, after the eight hours testing, cyclical strain was applied without interruption until failure. The time to failure in both cases was approximately the same as would be obtained for a "virgin" specimen. Since the control specimens remained in the solution, there was no removal of hydrogen. Thus, the bulk accumulation of hydrogen could not have been the cause of the fatigue failure in this case.

Extensive work has been done by Hashimoto et. al.(7,8) on the mechanical

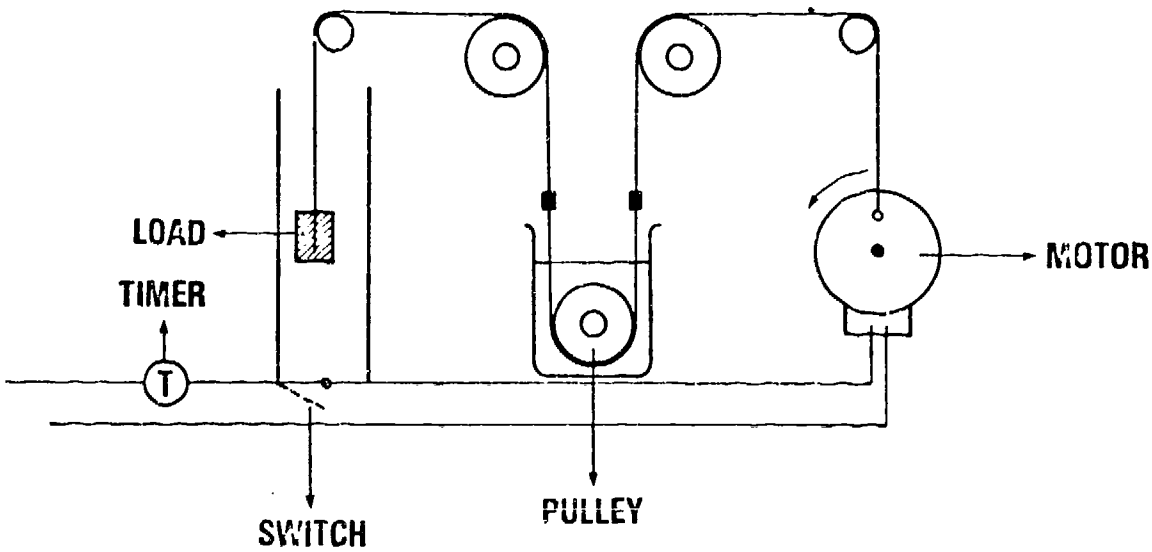

FIGURE 1. SCHEMATIC DIAGRAM OF THE APPARATUS USED TO MEASURE FATIGUE DUE TO CYCLICAL BENDING STRAIN

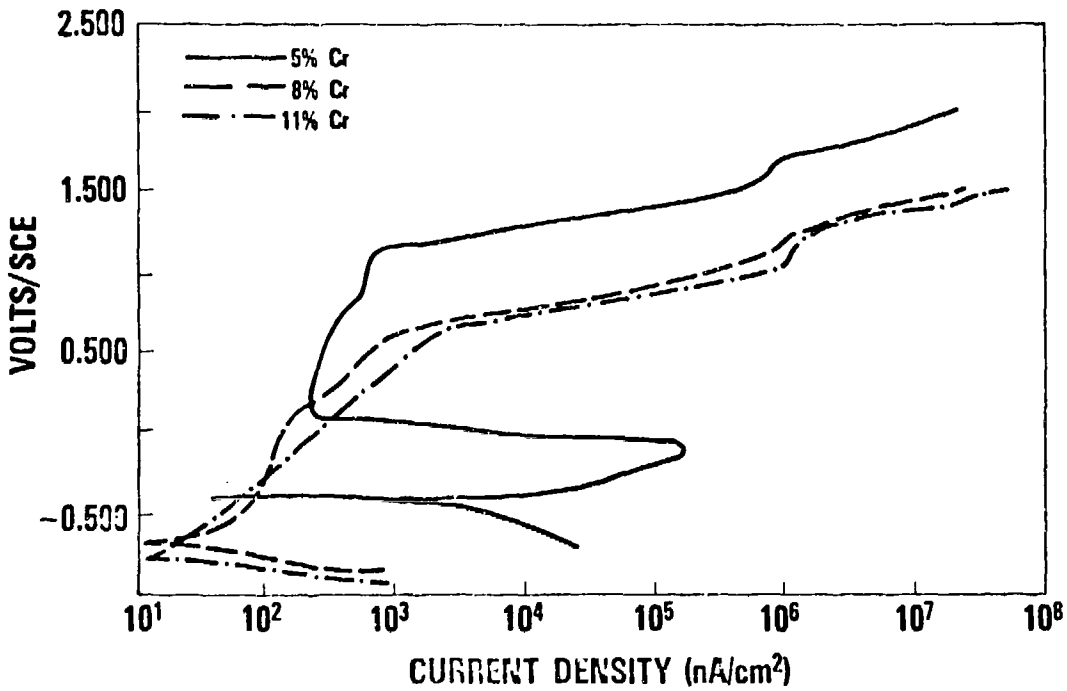

FIGURE 2. POTENTIODYNAMIC CURVES OF AMORPHOUS $Fe_{75-X}Cr_XB_{15}Si_{10}$ IN 3.5% NaCl

35

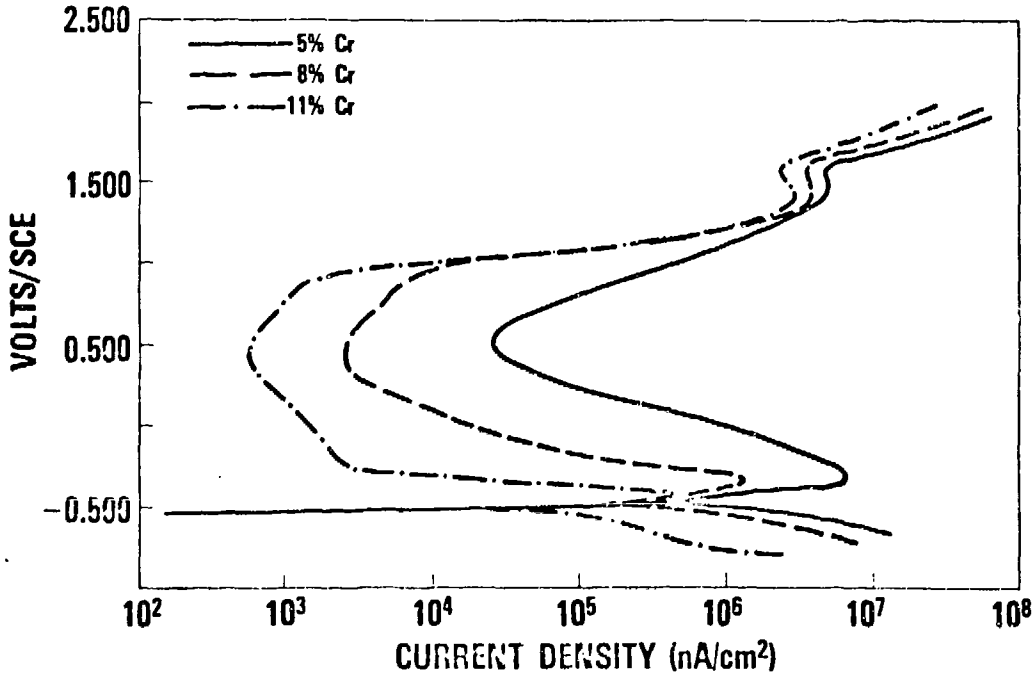

FIGURE 3. POTENTIODYNAMIC CURVES OF AMORPHOUS $Fe_{75-X}Cr_XB_{15}Si_{10}$ IN 1.0 N H_2SO_4

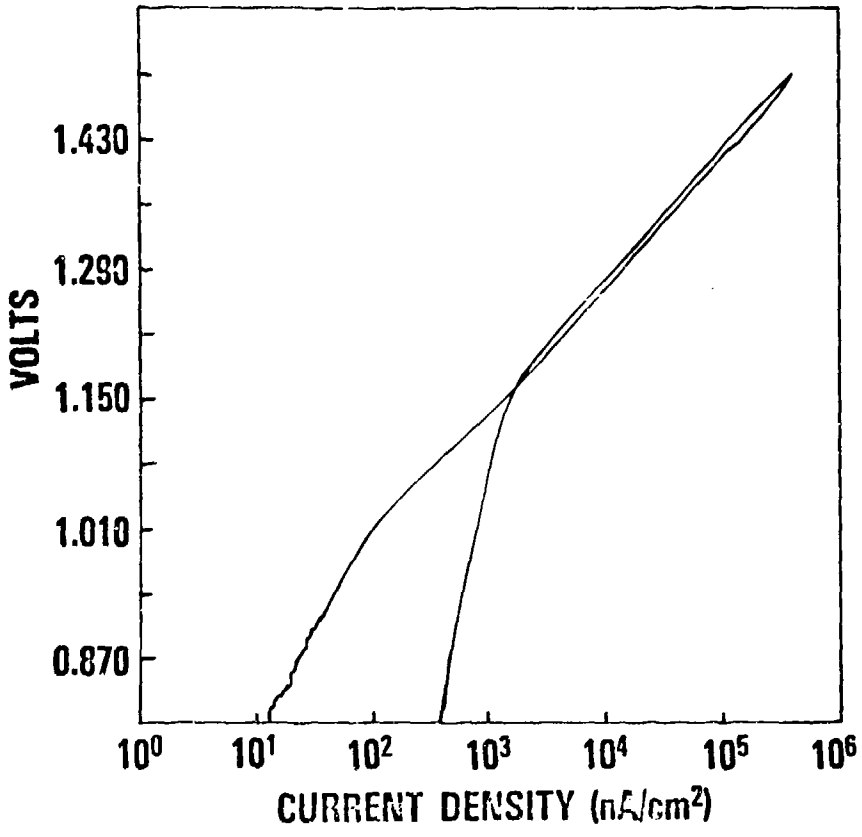

FIGURE 4. PITTING SCAN OF AMORPHOUS $Fe_{70}Cr_5B_{15}Si_{10}$ IN 3.5% NaCl

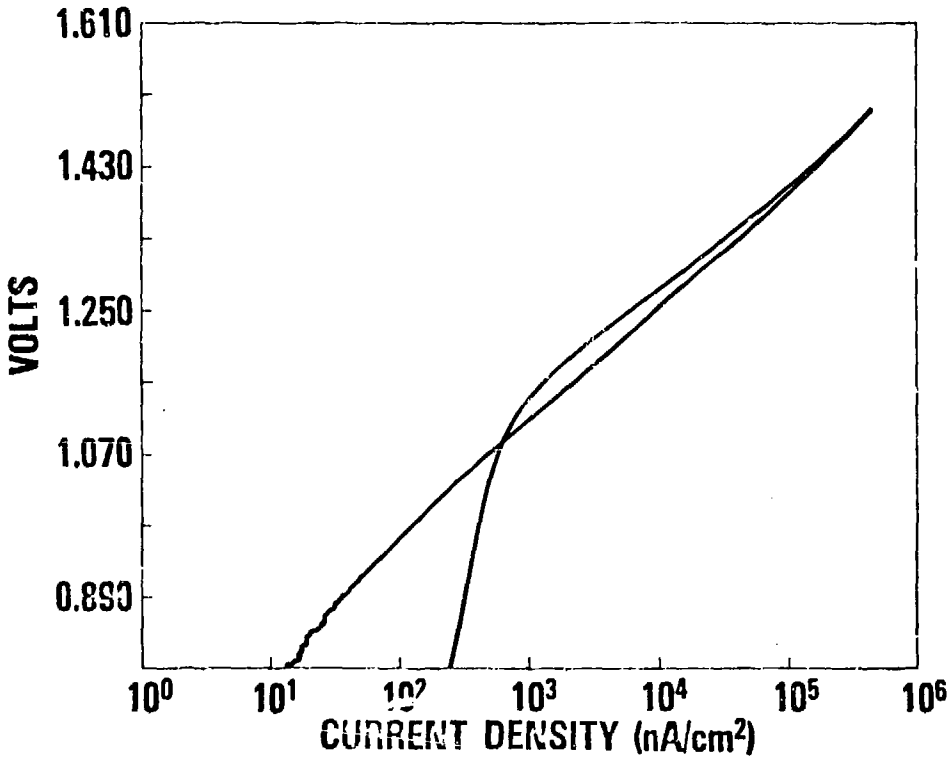

FIGURE 5. PITTING SCAN OF AMORPHOUS $Fe_{67}Cr_8B_{15}Si_{10}$ IN 3.5% NaCl

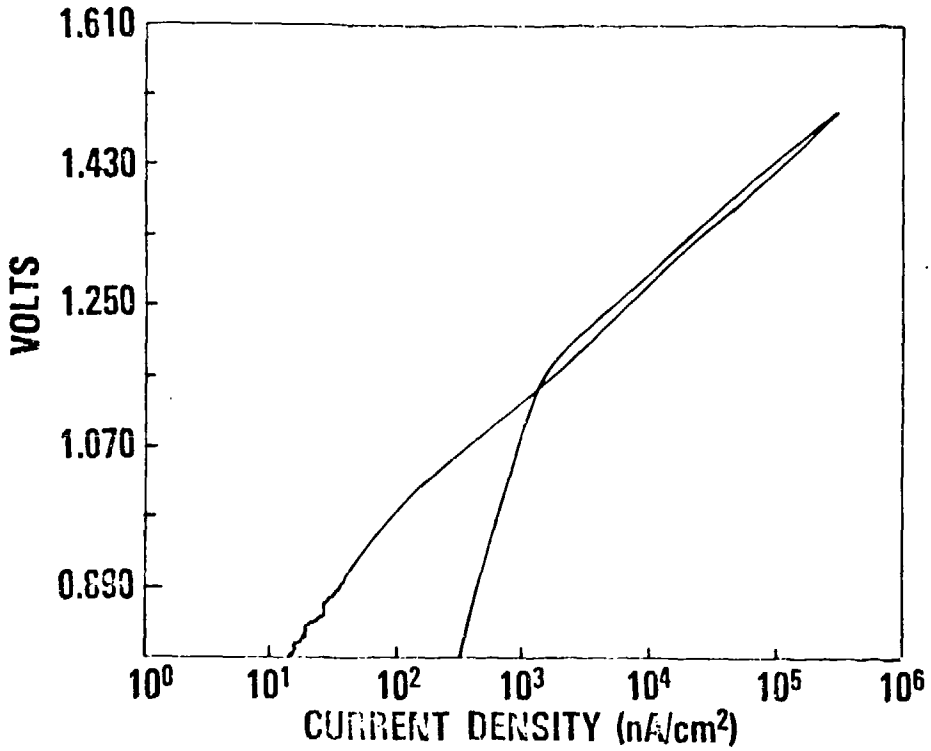

FIGURE 6. PITTING SCAN OF AMORPHOUS $Fe_{64}Cr_{11}B_{15}Si_{10}$ IN 3.5% NaCl

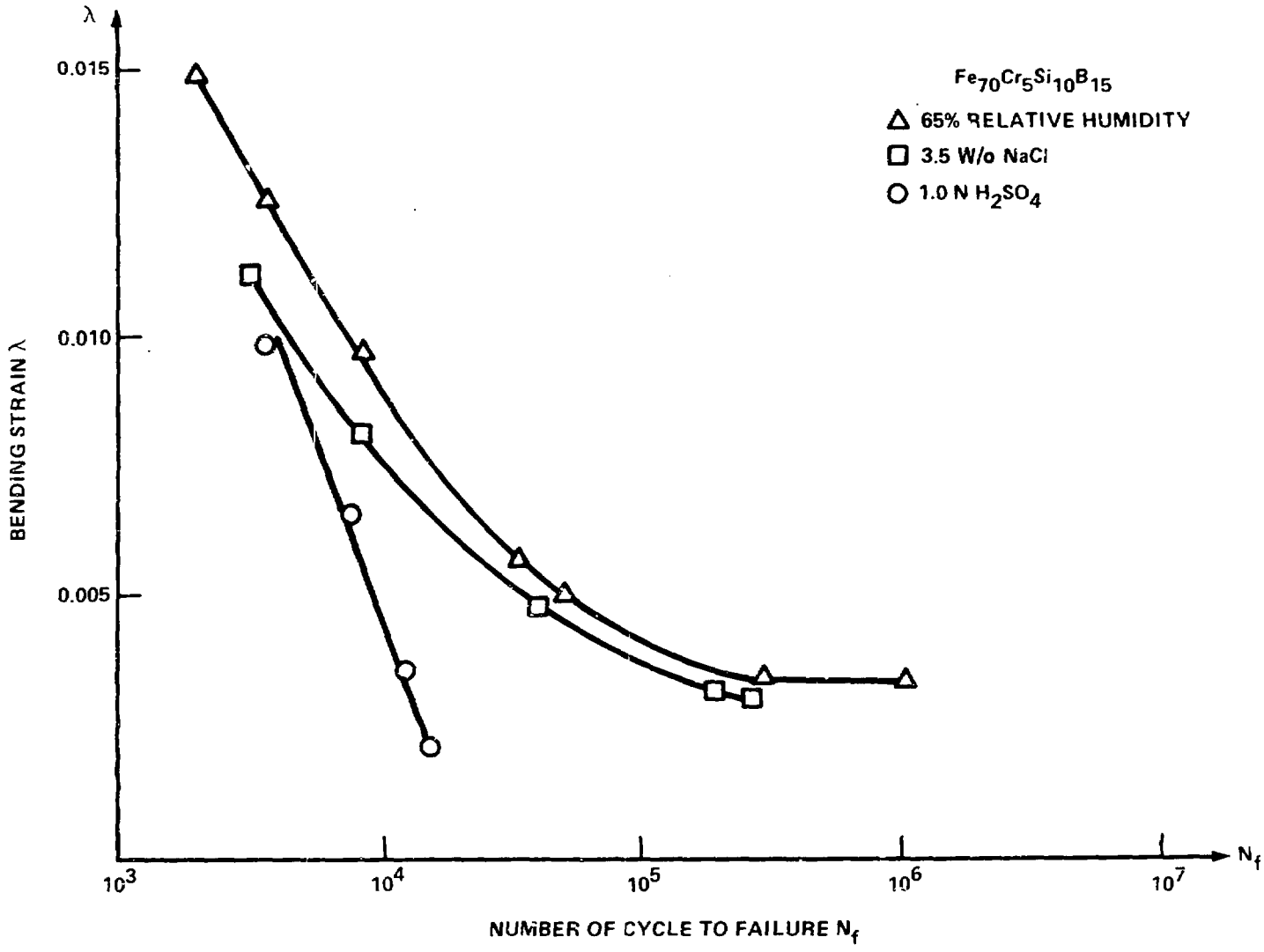

FIGURE 7. NUMBER OF CYCLES TO FAILURE AS A FUNCTION OF BENDING STRAIN FOR THE COMPOSITION $Fe_{70}Cr_5Si_{10}B_{15}$

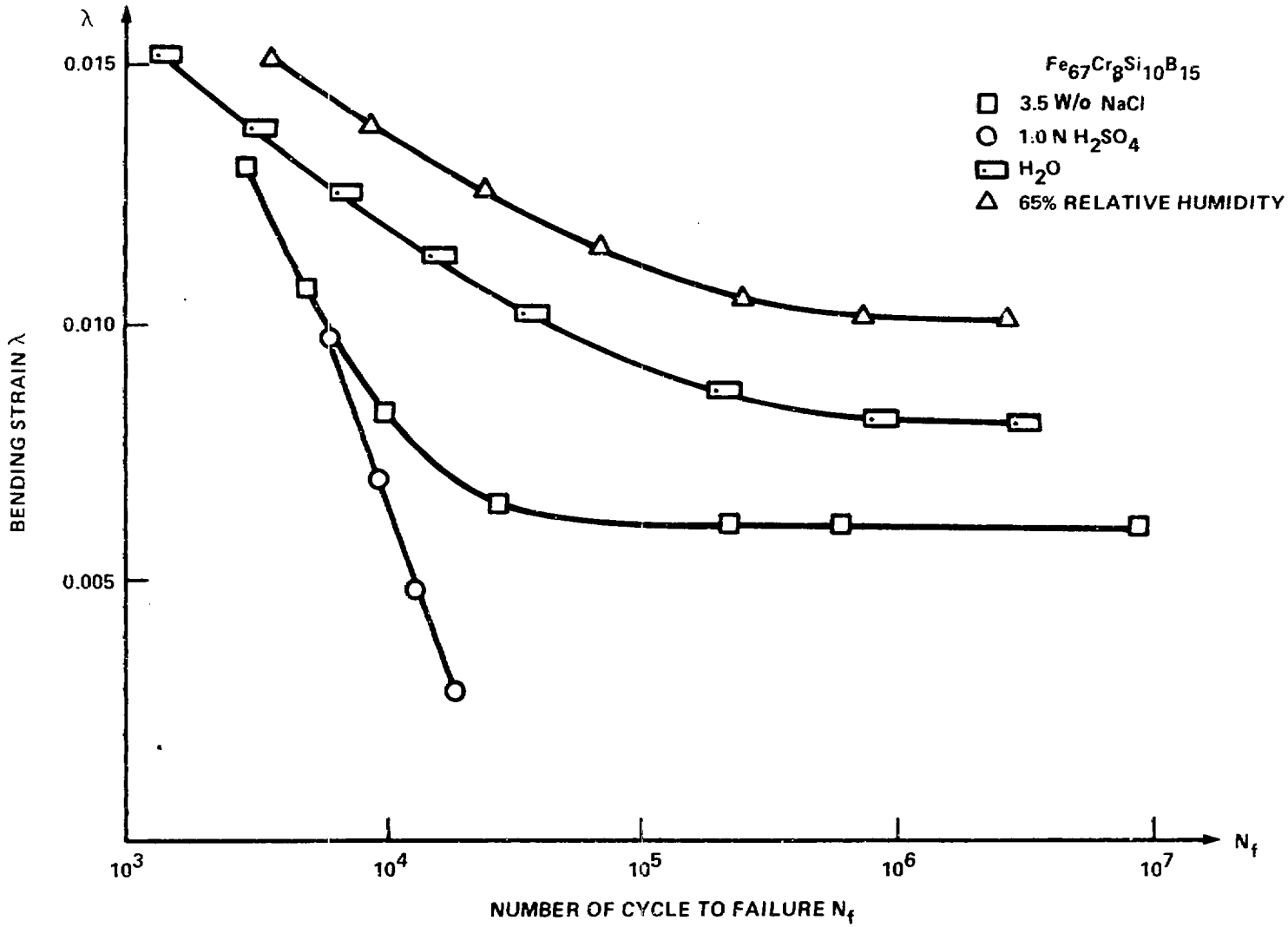

FIGURE 8. NUMBER OF CYCLES TO FAILURE AS A FUNCTION OF BENDING STRAIN FOR THE COMPOSITION $Fe_{67}Cr_8Si_{10}B_{15}$

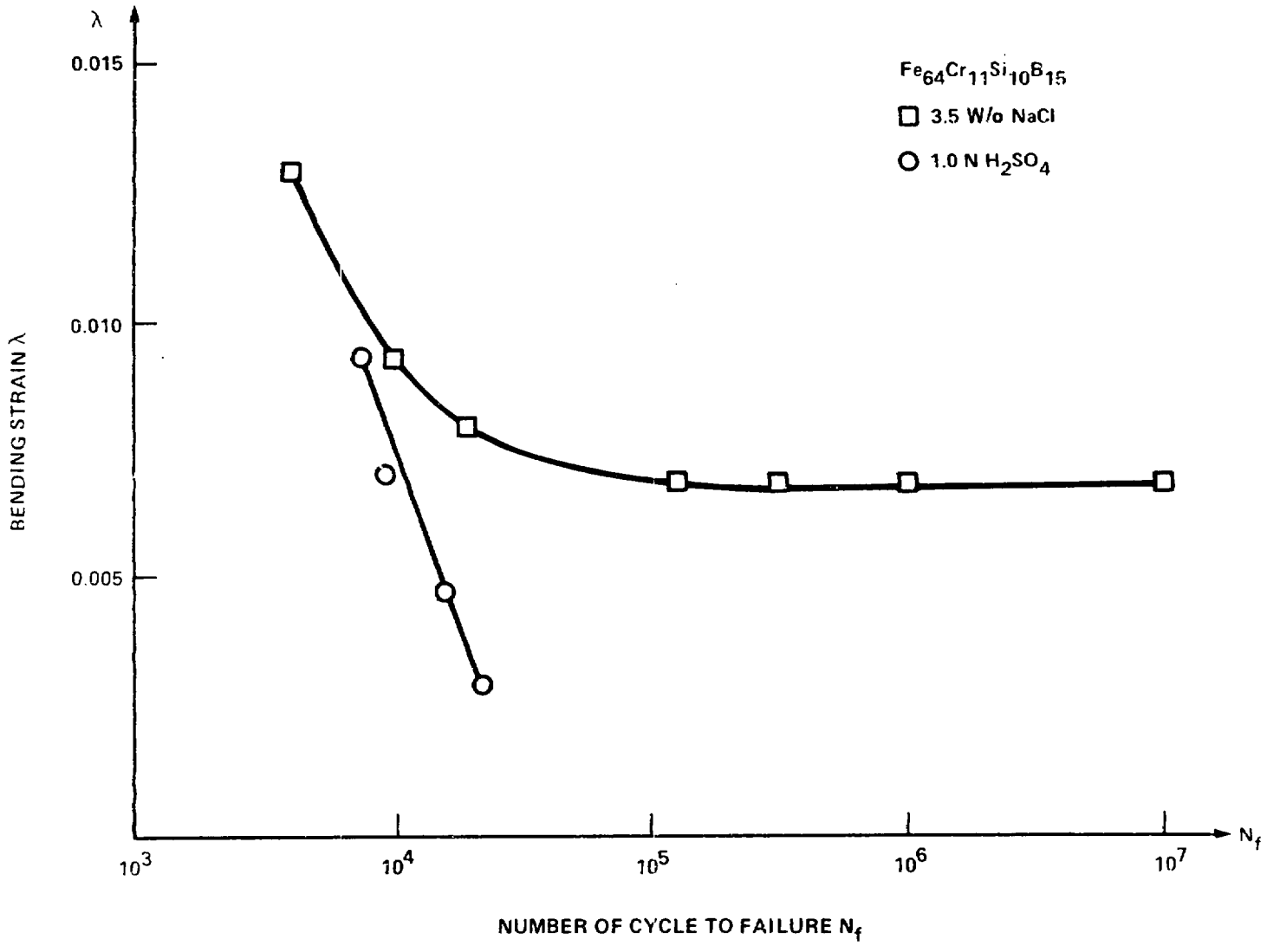

FIGURE 9. NUMBER OF CYCLES TO FAILURE AS A FUNCTION OF BENDING STRAIN FOR THE COMPOSITION $Fe_{64}Cr_{11}Si_{10}B_{15}$

failure of metallic glass ribbons in acidic chloride environment. This work includes tensile testing in a corrosive environment (with interruptions and baking similar to what was done in the present study) and examination of the fracture surfaces. The evidence for brittle failure in an acidic environment due to bulk accumulation of hydrogen is convincing. It is interesting to note, however, that fracture surfaces produced by failure in a neutral chloride environment differed from those produced in an acidified environment. It should also be noted that fatigue limits were observed only in cases of spontaneous passivation. In the case of an acidic environment or low chromium content in a neutral chloride environment, the general corrosion rate is relatively high, with hydrogen formed uniformly over the surface. In the case of spontaneous passivation, corrosion occurs primarily in cracks created in the passive film by the application of strain. Thus, it is reasonable to assume that the failure mechanism in the two cases will be substantially different.

A reasonable hypothesis for fatigue failure in the case of the spontaneously passivating specimens is that cracks in the passive film admit solution to the bare metal surface resulting in very rapid dissolution and formation of a "crevice". This bare surface repassivates very quickly with the new passive film thickening over a period of time. If strain is again applied while the passive film in the crevice is still thin, a new crack will form in the crevice. Repeated application of strain will result in the growth of this crevice. Failure occurs when a critical size is reached. Since the pH in the crevice can be much lower than in the bulk solution (9), it is possible that some local accumulation of hydrogen occurs. If the cyclical application of strain is interrupted, the new passive film in the crevice thickens until it is no longer the weakest point and the next application of strain does not necessarily form a crack in the passive film at that site. If local hydrogen accumulation is a contributing factor to failure, the interruption in application of strain allows diffusion of hydrogen away from the site. More data will be needed in order to determine the validity of this hypothesis, including measurement of the kinetics of passive film formation, rates of hydrogen diffusion in these metallic glasses, and a closer examination of the effects of composition and pH on both the fatigue properties and passive film formation. Experiments to obtain this information are in progress.

ACKNOWLEDGMENT

This work was begun under the Independent Exploratory Development Program of the Naval Surface Weapons Center and principally supported by I. Caplen and R. Hardy of the David Taylor Naval Ship Research and Development Center Ship and Submarine Materials Block Program. The authors are indebted to Dr. Robert Shull of the National Bureau of Standards for invaluable discussions on stress corrosion cracking in metallic glasses.

REFERENCES

1. L. Davis, Metallic Glasses, edited by J. Gillman and H. Leamy (American Society for Metals, Metals Park, 1978), p. 190.

2. K. Hashimoto and T. Masumoto, Glassy Metals: Magnetic, Chemical and Structural Properties, edited by R. Hasagawa (CRC Press, Boca Raton, 1983), p. 235.

3. A. Inoue, M. Hagiwara and T. Masumoto, Met. Tran. 13, 373 (1982).

4. A. Inoue, M. Hagiwara and T. Masumoto, J. Mater. Sci. 17, 580 (1982).

5. M. Hagiwara, A. Inoue and T. Masumoto, Rapidly Quenched Metals, edited by S. Steeb and H. Warlmont (Elsevier Science Publishers, New York, 1985), p. 1779.

6. L.Kabacoff, Unpublished Data.

7. A. Kawashima, T. Sato, and K. Hashimoto, J. Non-Cryst. Sol. 70, 55 (1985).

8. A. Kawashima, K. Hashimoto, and T. Masumoto, Corr. Sci. 16, 935 (1976); Corrosion 36, 577 (1980).

9. B. Brown, C. Fujii, and E. Dahlberg, J. Electrochem. Soc. 116, 218 (1969).

BIOGRAPHY

NAME: Anh H. Le

PRESENT AFFILIATION: Naval Surface Weapons Center/White Oak Lab
Electrochemistry Branch R33 Corrosion Technology Group

TITLE: Research Chemist

FIELD OF INTEREST/RESPONSIBILITIES: Corrosion/Battery

PREVIOUS AFFILIATIONS/TITLES:

ACADEMIC BACKGROUND: Physical Chemistry, PhD (1977)

SOCIETY ACTIVITIES/OFFICES/AWARDS: Member of Electrochemical Society

PUBLICATIONS/PAPERS:

BEST AVAILABLE COPY

SESSION A
SPECIAL TOPICS II

Chairman
John Sedriks
Office of Naval Research

Preceding Page Blank

BEST AVAILABLE COPY

SURFACE CONDITIONING PRODUCTS AS TOOLS FOR CORROSION REMOVAL AND CORROSION PREVENTION

BY

JOSEPH J. CLAUS
SPECIALIST
3M
ST. PAUL, MN

ABSTRACT

3-dimensional abrasive products have a long history of use in corrosion prevention and corrosion repair. Not only do they generate better surfaces for painting and coating, thus offering better protection, but they are used for stress control and to remove corrosion and deteriorated coatings.

This paper describes the ability of these products to perform in corrosion related situations. Specific application areas, such as munitions reclaimation, airframe maintenance, ground vehicle repair and plant refurbishing, are highlighted. Additionally, the chemical nature of a surface together with its physical characteristics are shown to be the foundation for corrosion prevention.

Presented at the Tri-Service Corrosion Conferences, May, 1987, Colorado Springs, Colorado.

Preceding Page Blank

SURFACE CONDITIONING PRODUCTS AS TOOLS FOR CORROSION REMOVAL AND CORROSION PREVENTION - by Joseph J. Claus, Specialist, 3M, St. Paul, Minnesota

Abstract:

3-dimensional non-woven abrasive products have a long history of use in corrosion prevention and corrosion repair. Not only do they generate better surfaces for painting and coating thus offering better protection, but they are also used for stress control and to remove corrosion and deteriorated coatings.

This paper describes the ability of these products to perform in corrosion related situations. Specific application areas, such as munitions reclamation, airframe maintenance, ground vehicle repair, and plant refurbishing are highlighted. Additionally, the chemical nature of a surface together with its physical characteristics are shown to be the foundation of corrosion prevention.

A few years ago the National Bureau of Standards estimated that corrosion costs in the United States exceeded 70 billion dollars annually. Although that amount may have changed some the last year or so, the enormity of the bill is staggering. Perhaps few people are as aware of corrosion's insidious effects as are those in the Armed Forces. Vehicles, ammunition, equipment, buildings, and other goods are exposed to the widest variety of environments possible. Exposure

Everything deteriorates. Whether it is a wooden fence post in the ground, or a plastic component of an automobile, or one of the noble elements, say gold, as a finger of a printed circuit board, some type of degradation of the material is taking place. The term corrosion has been used to identify some of the more common and visible types of deterioration that occurs around us. Other examples: red rust in a pile of scrap metal; crazing, cracking, color fading of plastic containers; the cable clamps on the terminal of a battery. One of the laws of nature is that materials tend to return to their least energetic state. In that process of returning it is the corrosion that manifests itself to us as evidence of the return to that state.

Since corrosion most always initiates at the interface or outer surface of materials, a brief review of the nature of surfaces seems appropriate at this point. While the model that is presented here is primarily for metals, the analogy can also be transferred to other materials as well.

The surface can be considered a multi-layered transition region between a gas and a solid. Figure 1 depicts a conceptualized cross-sectional view of the transition region of a metal surface. The layer directly above the bulk material is a segregated region which is enriched in alloying elements that are driven to the outer boundaries from the bulk by thermodynamic forces in the natural process of energy minimization. When elements of the segregated layer, as well as the

to these environments is often under less than favorable conditions. Even with the best of preventive measurements, deterioration of parts, components, and all systems is experienced due to the effects of poor protection, constant exposure, or even ordinary use.

The purpose of this paper is to facilitate an awareness of a family of products that have been successfully used for the preparation of materials for corrosion prevention, and which have shown themselves to be effective in the removal of the bi-products of corrosion. 3-dimensional abrasive products and rotary peening materials surface condition the metals, wood, plastics, glass, etc. which are used to manufacture the goods and equipment that are used almost daily. These surface preparation products work because of their open, non-loading, durable properties.

3-dimensional nonwoven abrasive products are composed of three materials; fiber, resin and mineral. The fiber forms the backbone to which the mineral is held with a resin system. When used properly the product gives controlled cut, that is, it will remove surface materials without dangerously undercutting or gouging. In many instances the products are ideal for spot repair and for feathering areas adjacent to old, intact coatings. Depending on the construction and use of the product, a wide variety of aggressiveness can be selected: one form of these products will not even scratch glass, another form will be so aggressive that abrasion of a hardened steel surface can occur.

material of the base metal, combine with oxygen from the atmosphere, the reaction products form what is identified as the oxidized layer. On top of this develops the chemisorbed layer which contains compounds which are formed from chemicals in the surrounding environment and which are strongly bonded to the substrate. Finally, on top of this, exists a region of weakly bound materials from the environment. This outer most or physisorbed layer is easily removed, even by imaging, but in the process new material is immediately available to take its place. Actually, the surface is an intermixing of these layers.

A typical metal surface, such as that found on steel, and depicted in Figure 2, has important chemical and topigraphical characteristics. The bulk consists of iron, along with alloying and trace elements (Li, C, Na, Mg, Al, S, Mn). The surface region (some 10-80 angstroms deep) includes the layers previously identified which are composed of iron oxides, segregated element oxides, and compounds of Ca, Na, Cl, S, P.

Surface irregularities are also typical of most steel surfaces, such as scratches, gouges, fissures, and dents, in which rolling oils, processing fluids, and other environmental contaminants can be trapped. Finally the physisorbed layer contains water, carbon dioxide, oxygen, dust, dirt, fingerprints, etc., and other contaminants.

It is clear then that metal surfaces have a chemical nature that is very different from the bulk metal. Frequently these chemical

differences are detrimental and must be removed by a cleaning process for optimum performance in coating, bonding, and other surface sensitive application areas.

Analogously what is true of metal surfaces can also be extended to the surfaces of most other materials. In other words, there is a region of contamination on the exterior of most materials, which makes it difficult, and sometimes impossible, to adequately protect, bond, weld, coat, or make proper use of.

Ideally, in preparing new materials for operation in normal or severe environments, adequate preparation of their surfaces for the protective system is important as a way to postpone the effects of corrosion. Similarly, in the repair of contaminated areas the removal of the products of the contamination also is paramount if there is any hope of restoring a system to a protective state.

Of course there are numerous ways in which the surfaces of materials can be prepared. However, our 3-dimensional abrasive products offer some unique characteristics in being able to condition surfaces for both corrosion protection and for the removal of the products of corrosion.

CORROSION PREVENTION:

Removal of contamination from new materials is certainly important in

preparing them for the application of protective coatings or for good bonding or other surface sensitive application areas. Contamination can come from two sources as can be seen from the following examples: In one case, aluminum sheets with the surfaces in the "as received" condition cannot reliably be resistance spot welded on a production bases. However, sheets whose surfaces have been abraded with 3-dimensional abrasive products passed the "Weld Reliability Test" and were able to do so even after 90 days of plant storage. Analysis of the surface chemistry of the 5182-T0 Alloys was useful in determining the differences in the surface chemistry for the "as received" and "brushed" aluminum. Figure 3 compares the elemental composition of the two surfaces. Specific notice is to be made of the magnesium dominant in the "as received" material over the brushed specimen. This suggests a heavy MgO layer on the "as received" sample which is removed by brushing the surface. It is evident that a magnesium-aluminum-oxygen composition occupies the outer surface of the "as received" sample for a thickness of nearly 200 angstroms. After brushing, the oxide layer grows to a depth of only 25 angstroms.

It is the high electrical resistance of the Mg-Al-O compound (1700 micro ohms which causes the poor weldability of the "as received" alloy and therefore promotes poor tip life. The thin oxide layer of the brushed metal has a low resistance (250 micro ohms) and contributes to the improved weldability and extended tip life.

In the second case, the poor performance of a paint system over steel caused excessive corrosion. Many may remember the corrosion problems on our automobiles during the mid and late 70s. The poor protection

of the paint system was eventually traced back to a layer of carbon on the surface of the steel that prevented good bonding between the steel substrate and the paint coats. Investigation of the surface of the steel revealed that the carbon was deposited on the surface during the annealing process. The hydrocarbons in the rolling and protective oils and also in the annealing gases would bake out on the surface of the steel and could be removed most effectively only by mechanical means. Figure 4 reviews Auger scans of the surface of "good" and "bad" steel showing that the bad steel has considerably more carbon on the outer surface. Figure 5 compares the distribution of the surface carbon (the white area) on a bad steel surface and that same surface after it has been cleaned with the 3-dimensional abrasive product. Greater care in the annealing practices and the brushing of the steel surface as part of the application of such protective coatings as Zincrometal, has encouraged the automakers to the point where they now offer 5 and 7 year warranties against perforation type corrosion.

These two examples are cited so that it is clear that contamination is can come from two distinct sources: from the exterior environment that the surfaces see, or from the migrating or segregating of material from within the bulk itself. In either case it has been shown that processing the surface with a 3-dimensional abrasive product produces a substrate which is free from the detrimental contaminants and which promotes subsequent processing for improved performance.

Surface conditioning abrasives remove contaminants and produce an active surface with uniform, predictabile chemistry while removing

only a small amount of the base material. The resulting surfaces allow coating systems and bonded areas to have optimum adhesion and corrosion protection. To further demonstrate better corrosion protection and better coating adhesion, examples of steel panels were selected. (Figure 6) One was cleaned with only an alkaline cleaner. The second was alkaline cleaned and conditioned with a 3-dimensional abrasive product. Both panels were coated with a zinc phosphate and a 0.5 mil acrylic enamel. Next the panels were scribed to bare metal Both surfaces were then subjected to salt spray tests.

Note that corrosion has crept under the paint in surface "A" and blistering has appeared, while there is virtually no corrosion or blistering under the paint of surface "B" which has been processed with the 3-dimensional abrasive product.

CORROSION REPAIR

Materials will and do corrode. Repair of these materials is not difficult if the effect of corrosion is caught early in the initial stages. Spot repair of areas effected is often easier than allowing a whole unit to become corroded. 3-dimensional abrasive products lend themselves very admirably to spot repair of corroded areas. The following examples serve well to illustrate the effectiveness of the 3-dimensional abrasive materials:

- On aircraft aluminum skins, corrosion can be removed with flap brushes on straight shaft portable tools, or with non-woven discs on right angle grinders. Residual paint can be readily removed without noticeable loss of Alclad surface.

These surface conditioning abrasives have been approved for use on many types of military aircraft to clean and control corrosion as is spelled out in Air Force T.0.1-1-1 and Navy Corrosion Manual NAVAIR-509.

- On ship bulkheads, corrosion areas and old coatings can be removed with either non-woven discs or unitized wheels. Spot repair and feathering into the old intact coatings makes for an easy maintenance operation.

- Utilizing extra coarse grade discs and wheel products has demonstrated superior corrosion and paint removal on 155 mm munitions over wire brushes, leaving a cleaner surface in a shorter time period while not damaging the brass or fiberglass components. Renovation of Ordnance has been recently demonstrated at both Tully and the Mieseau Army Depots.

- For heavy deck corrosion and coatings removal, rotary peening products are more effective than needle guns, disc sanders or deck crawlers, leaving a 1 mil or greater profile required to repaint U.S. Naval ships.

- To reduce the possibility of stress corrosion cracking on critical surfaces, specialized rotary peening products can be utilized to return the surface to the desired Almen intensity.

SUMMARY:

Surface contamination or corrosion of materials is a common concern of the military and industry. There exists a family of products whose 3-dimensional abrasive nature makes their use possible for the removal of contamination for the application of protective coatings and also for the removal of the effects of corrosion, without significant stock removal, damage to the material, and which can leave the surface, at least initially, free of residual inhibiting material reflecting the materials bulk composition. These materials are easy to use, effective, and very versatile. They work because they remove contamination and corrosion for only a micron or so of a material's surface, thus creating a region which can be coated with a protective material. Thus, whether it is to prepare a surface for the application of a protective coating, or to remove the products of a corroded area so that new protection can be applied, these 3-dimensional abrasive products can be used to stop the inroads which corrosion is making today.

ENVIRONMENT

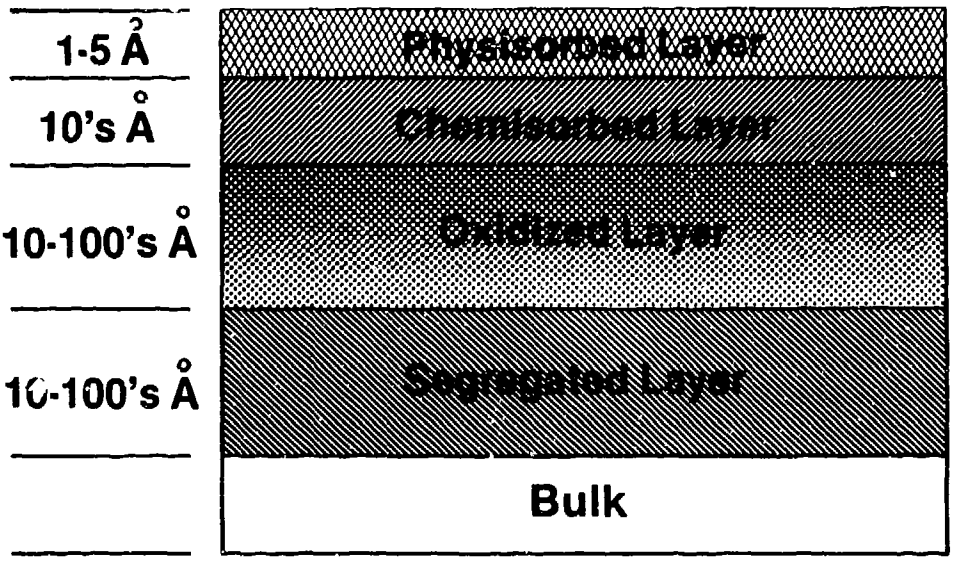

Figure 1.
Conceptualized cross-section view of transition region of a metal surface.

BAD STEEL SURFACE

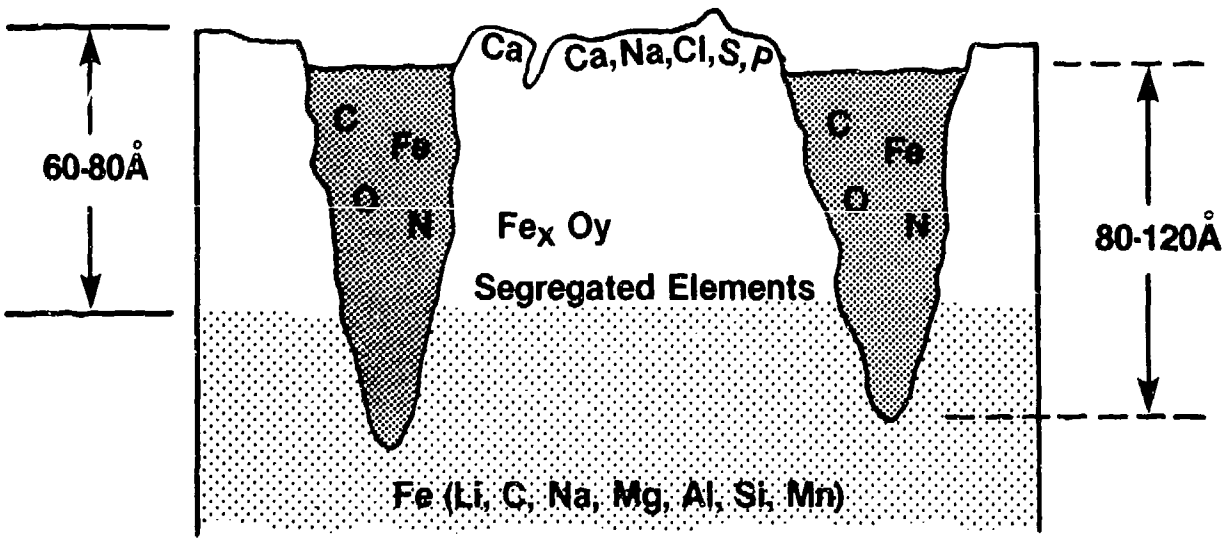

Figure 2.
Conceptualized cross-section of cold rolled auto body steel surface.

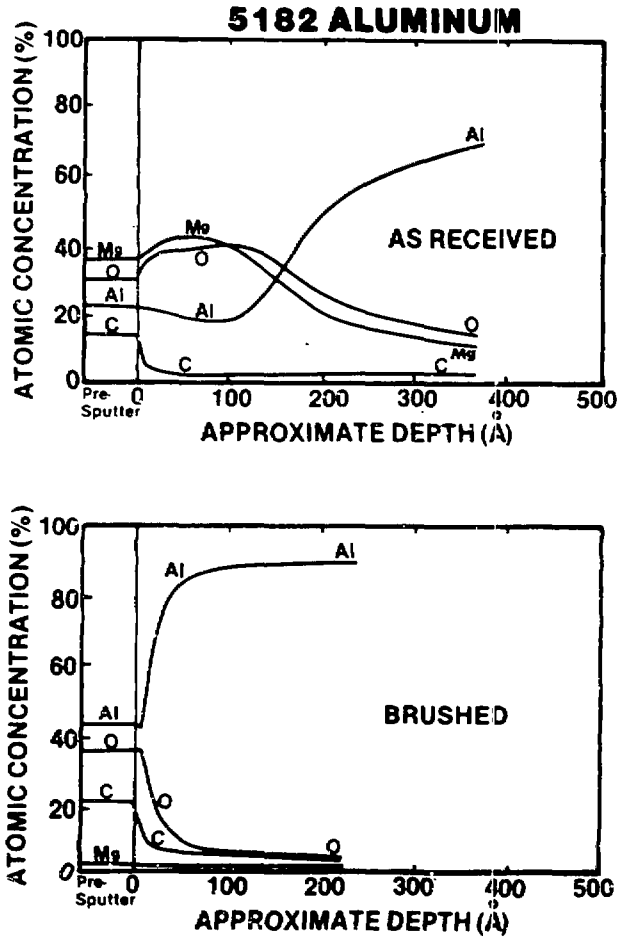

Figure 3 – Auger Depth Profiles of 5182-0 aluminum in "as received" and "brushed" states.

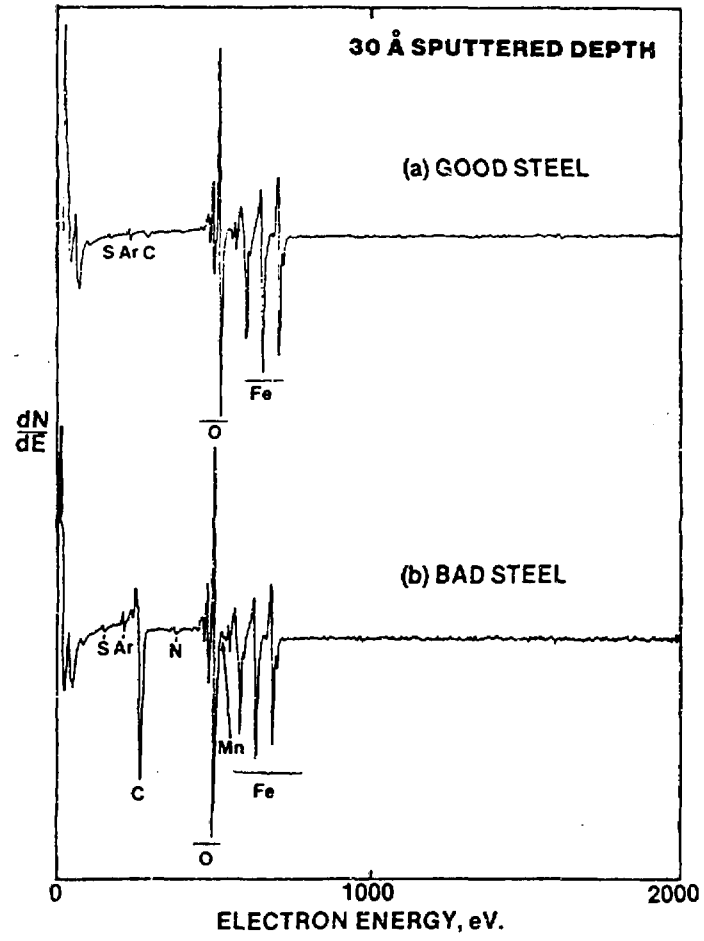

Figure 4 - Auger Spectra of "good" and "bad" steel surfaces.

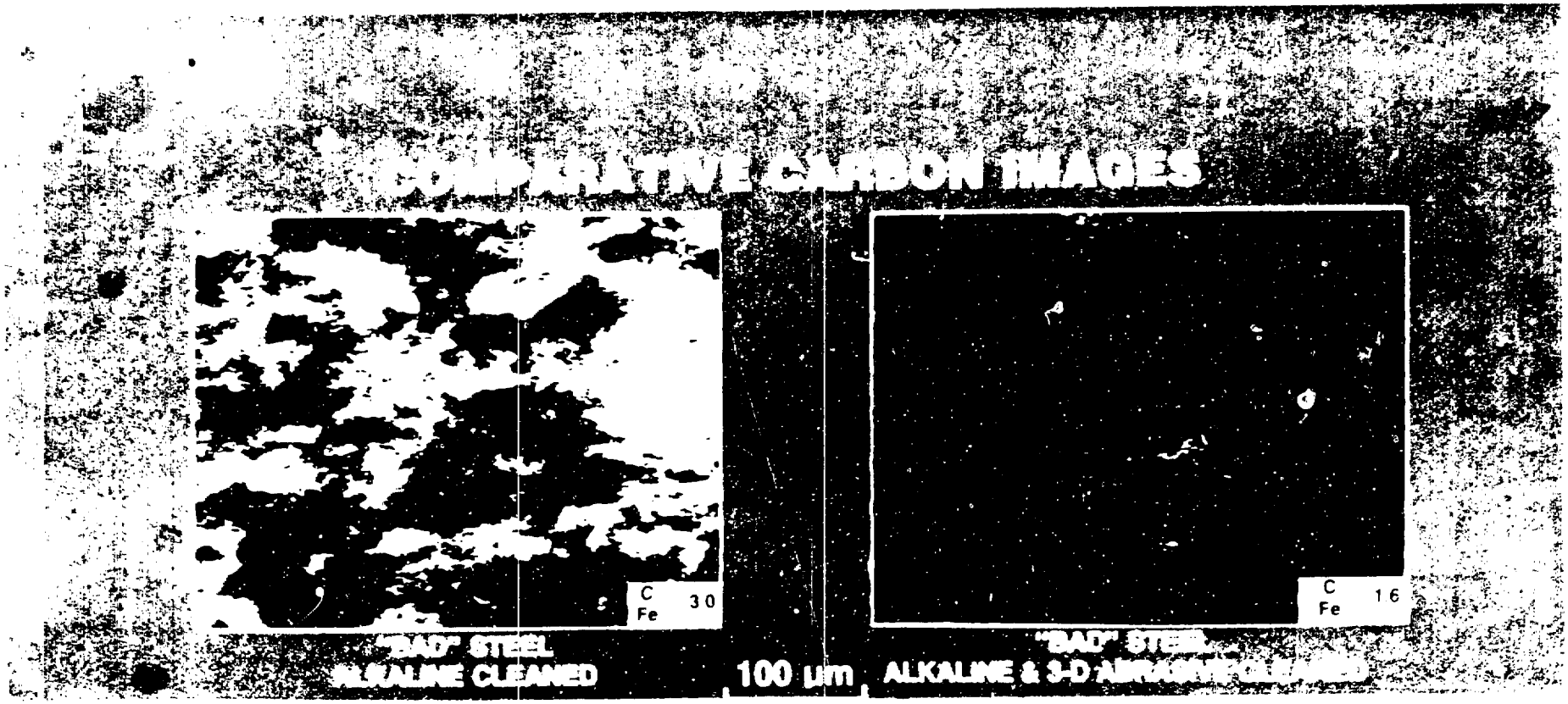

Figure 5 - Comparison of carbon distribution (white area) on alkaline cleaned only (left) and alkaline plus abraded (right) steel surfaces.

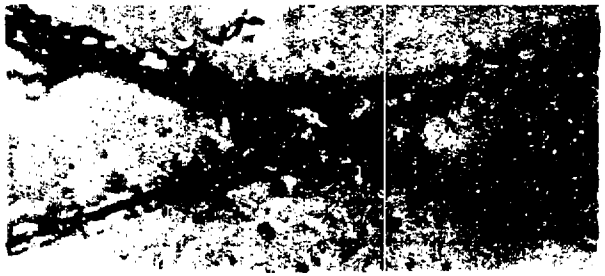

Surface "A"

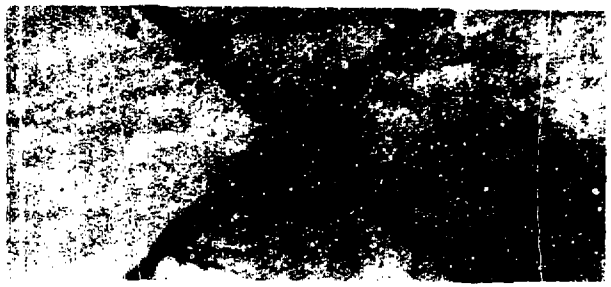

Surface "B"

Figure 6 - Surface "A" - Alkaline cleaned only after 240 hours salt spray.
Surface "B" - Alkaline plus abrasive cleaned after 720 hours salt spray.

BIOGRAPHY

NAME: Joseph J. Claus

PRESENT AFFILIATION: 3M
Building Service & Cleaning Products
15 Years

TITLE: Technical Service Specialist
Certified Manufacturing Engineer

FIELD OF INTEREST/RESPONSIBILITIES: Surface Science, Application Development, Corrosion and Contamination Control, Surface Preparation

PREVIOUS AFFILIATIONS/TITLES:

ACADEMIC BACKGROUND: BS, St. Louis University

SOCIETY ACTIVITIES/OFFICES/AWARDS:

Society of Automotive Engineers; National Coil Coaters Assn.; Steel Structures Painting Council; Boy Scouts of America

PUBLICATIONS/PAPERS: Author or co-author of over 25 papers.

1 Atch

THE EFFECT OF TITANIUM REINFORCEMENT ON THE LIFE OF POSITIVE GRIDS IN LEAD-ACID BATTERIES

by

W. A. Ferrando and K. L. Vasanth
Corrosion Technology Group
Naval Surface Weapons Center, White Oak
Silver Spring, MD 20903-5000
(202) 394-3527

Abstract

Positive grid failure by various corrosion mechanisms is an important life-limiting factor in lead-acid secondary batteries. A 5-6 year life cycle is currently typical for such batteries in both commercial and military use. Significantly increased ship availability and cost savings to the Navy can be anticipated with the incorporation of batteries of reinforced positive grid design into its vessels.

This paper presents the results of comparative data on titanium wire reinforced and unreinforced large lead alloy positive grids under an accelerated positive potential float corrosion test. We report on uniform and intergranular corrosion and grid growth. These studies have provided a reliable estimate of reinforced grid service life. In turn, a confident projection of at least a 10 year cell operational life can be made.

Introduction

Current lead-acid secondary batteries in both civilian and Naval use typically achieve a 5-6 year service life. Replacing a battery set is a costly and time consuming operation, often requiring a prolonged port call for the ship involved. A battery lifetime of at least 10 years, therefore has been set as a goal by the Navy. This achieved, the battery overhaul schedule can be made to coincide with other required major docking maintenance. Substantial cost savings will be realized. In addition, higher volumetric energy density eventually may be required in future system batteries to handle greater power demands which can occur on the modern ships during reactor emergencies. Cells fabricated with thinner electrodes, made possible using the reinforced grid

construction might help attain this increased energy density in the near term, until other advanced battery systems are developed.

Background

The most prevalent failure modes experienced in lead-acid batteries can be attributed to corrosion reactions taking place in the positive grids. At the cell operating potential, the positive grid is subject to both uniform and intergranular corrosion in the electrolyte at operating potential.

Uniform corrosion acts to thin the grid cross section. The grid gradually weakens and its current carrying capability decreases. Often, the active material pellets loosen and lose electrical contact. Although this type of corrosion cannot be eliminated, it can be reduced substantially by auspicious choice of grid alloy. Pure lead itself exhibits the lowest uniform corrosion rate, but is too soft for long term grid stability. Alloying produces a stronger grid, but at the penalty of an increased rate of uniform corrosion.

Intergranular corrosion, being a preferential corrosive attack along metallic grain boundaries, is abetted in battery grids by aggregation of alloying species in these regions. Practical effects of intergranular corrosion product accretion in the lead-acid battery grid are at least twofold: (1) gradual grid embrittlement to the point of extreme fragility and (2) physical growth of the grid due to spreading of the grain boundary regions by wedging action of the corrosion products.

The addition of a suitable reinforcement to the lead alloy grid has been found virtually to arrest intergranular corrosion. In addition, since the reinforcement significantly strengthens the grid, cell failure due to positive electrode shape change is largely eliminated. This becomes especially important after several years service. Moreover, the reinforced electrodes, being stronger, might be constructed thinner in future cell design. This will lead to a higher volumetric energy density.

Experimental

Corrosion of The Titanium Reinforcement

Figure 1 shows the components of a 75X size (5.5" X 16.25" X 0.125") lead-acid cell employed in an accelerated corrosion test. This work is concerned with corrosion processes taking place in the titanium reinforcement (A) and positive grid (B). The reinforcement preform is made of commercially pure 40 mil titanium wire laser welded at all intersections. This preform is sized and positioned to be cast in the center of the lead alloy grid. The corrosion rate for pure titanium in the H_2SO_4 electrolyte as a function of potential is shown in Figure 2. This indicates a rate of about 0.02 mm./year (0.75 mils/year) in the PbO_2 positive electrode operating potential range. At this corrosion rate, even an exposed portion of the titanium preform will far exceed the 10-12 year lifetime requirement. Previous reports (1) and (2) have explored some metallurgical and corrosion effects in grid alloys and titanium reinforcement.

Test Cell Construction/Data Acquisition

We present here the results of comparative accelerated corrosion tests on both reinforced and unreinforced (control) MFX lead alloy (Pb-1.45%Sb-1.45%Cd, GNB, Inc., Langhorne, PA, proprietary alloy) grids of the above described type. Two sets of 21 test cells, each containing four reinforced or unreinforced positive grids, respectively, were constructed with daramic separators and five Pb-Ca negative grids. After filling with 1.28 gram/cc. specific gravity H_2SO_4 electrolyte, they were immersed, seven each, in temperature baths at 50°C, 60°C and 70°C, respectively. One cell from the unreinforced and reinforced groups each was removed from each temperature bath every month.

Specific comparative data has been obtained on: (1) uniform corrosion by weight loss, (2) grid growth and (3) intergranular corrosion. While real time cell cycling and other tests still must be performed, the accelerated methods enable cell design modifications to be incorporated as rapidly as possible. Three months accelerated testing at 70°C as described above is approximately equivalent, corrosion wise, to six years of ambient temperature tests. Data available at the three temperatures allows Ahrrenius type corrosion rate versus temperature relationships to be plotted.

Grid Corrosion under Accelerated Test

Using geometrically calculated grid electrode areas and weight loss values, corrosion rates were determined. Figure 3 shows these computed rates for the reinforced (top) and unreinforced (bottom) grids, respectively, versus immersion time at the three test temperatures. Corrosion rates in the range of about 1-10 mils/year (mpy) are observed for both grid sets. This result indicates a lack of influence of the reinforcement upon uniform grid corrosion. In each case, the data show an initial decline in corrosion rate with time, followed by an increase after several months immersion. One explanation for this could be the initial formation of a partially protective corrosion product layer. In time the layer thickens and loses its adherence. As this falls away, the metal surface becomes again more completely exposed and the corrosion rate rises.

Figure 4 shows the data at 4 months immersion replotted as corrosion rate (mpy) versus temperature (^{o}C). A linear dependence has been drawn above 50°C. The curved, dotted portion below 50°C indicates that a nonlinear relationship exists at lower temperature, allowing for the observed ambient temperature corrosion rate. The reinforced and unreinforced grids show virtually the same uniform corrosion rate behavior.

Grid Growth and Intergranular Cracking

Up to this point, the presence of reinforcement apparently has little effect on the grid corrosion properties. We will observe such a conclusion to be premature. A small fraction of the weight loss, heretofore recorded as uniform, is in fact due to intergranular corrosion. This corrosion component, while having only a minor impact on weight loss, contributes substantially to growth and aging fragility of the grid. The corrosion products act as wedges between the metallic grains, driving them apart and decreasing ductility. The intergranular corrosion mechanism is abetted in the presence of tensile stresses in a structure, as is the case with the battery grids.

The reinforcement must encompass all grid members, being fabricated in the form of a one piece welded wire mesh or preform. It previously has been reported[2], that isolated wire reinforcement has only a limited ability to control grid growth due probably to insufficient bonding strength at the Ti wire-lead alloy interface. The welded Ti preform, by contrast, locks the grid members at each intersection point

and does not rely upon the interfacial bonding for its efficacy. Use of the preform, therefore, produces a type of pseudo-composite. It is a rather special case of the application of structural reinforcement.

Figure 5 shows the grid measurement points employed in these tests. A sufficient number was chosen to assure reasonable accuracy. Figure 6 shows the measured average vertical (top) and horizontal (bottom) grid member growth of the preform reinforced and unreinforced grids, respectively, versus time in the accelerated immersion test. Growth of both the vertical and horizontal members proceeds in the same way. The unreinforced grids show an exponential type of growth over the test period. It is noteworthy that, despite the rapid increase in growth rate, the ~0.5% end of test growth is quite small, recalling that a maximum growth of about 2% is allowable to maintain a reasonably low probability of cell failure by electrode edge shorting. This indicates that MFX is among the better performers as a positive grid alloy.

Discernible growth of the reinforced grids begins only at about 5 months into the test. Their growth of ~0.1% at 6 months testing or about 12 years service is virtually negligible. Electrodes fabricated from these grids simply will not fail by grid growth over the anticipated life of the cell.

Figure 7 shows cross-section photographs of the unreinforced control MFX alloy grid members as they undergo corrosion in the immersion test at 70°C. The sequence begins at lower right with the grid member prior to immersion (the dark surrounding area is a portion of the plastic cold mount). It proceeds counterclockwise, showing grid members immersed for 2,4 and 6 months, respectively. The metallic grain boundaries are visible especially in the 2 and 4 month samples. Already at 2 months, corrosion is evident around its perimeter clearly following the grain boundaries. At 4 months, corrosion has proceeded deeply along the boundaries leaving long, finger-like protrusions around the perimeter. Finally, by 6 months, the protrusions have corroded away. The intergranular corrosion continues, isolating outer grains and significantly reducing grid strength and electrical conductivity.

Figure 8 gives some visual comparison of the extent of corrosion in the reinforced and unreinforced grids immersed at 70°C for 6 months. A reinforced member cross-section prior to immersion is shown at top right. The Ti wire has

floated during casting in the research mold, causing it to lie off-center in the grid. Such will not be the case with production grids, as preform a special guide wire system has been devised to assure proper alignment.

A reinforced grid member cross section after 6 months immersion at 70°C is shown at top right (in this case, titanium wire of a somewhat larger diameter has been used). The arrows indicate the extent of corrosion at the grid-wire interface and at the grid surface. Some intergranular corrosion is evident. Although this can scarcely be termed superficial, it, however, has not sent cracks deeply into the cross-section interior. Grid integrity and current carrying capability are quite well maintained. The unreinforced grid (lower left), at this stage, is characterized by deep cracks (arrows) which continue to penetrate the grid cross-section along the grain boundaries. The relieved tensile condition achieved by reinforcement, in a sense, allows the metal grains to remain tightly together, retarding the intergranular corrosion.

Summary

(1) A welded titanium wire preform reinforcement cast into lead alloy positive battery grids will be very effective in extending grid service lifetime from the present 5-6 years to more than 10 years, even in the case of partial exposure of the wire to the electrolyte.

(2) Uniform grid corrosion is unaffected by the addition of reinforcement. The rate of uniform corrosion probably will set the ultimate limit on reinforced grid lifetime for a particular lead alloy.

(3) Deep penetrating intergranular corrosion has been sharply reduced by the addition of the reinforcement.

(4) As a consequence of reinforcement, the average growths of both horizontal and vertical grid members have undergone at least a five-fold reduction. The accelerated test indicates a negligible grid growth through at least 10 years service.

(5) Overall grid durability and end-of-life fragility have been improved dramatically by the presence of the preform reinforcement.

Technical References

(1) Otto, N. C., Gould, Inc. Report #N60921-81-C-0231-7, 10 Aug 1984, Gould Research Center, Rolling Meadows, IL 60008.

(2) Ferrando, W. A. and Vasanth, K. L., "Metallographic and Corrosion Studies of Partially Reinforced Pb-1.45%Sb-1.45%Cd Alloy Battery Grids," Proceedings 32nd Power sources Symposium, Cherry Hill, N.J., Jun 9-12, 1986.

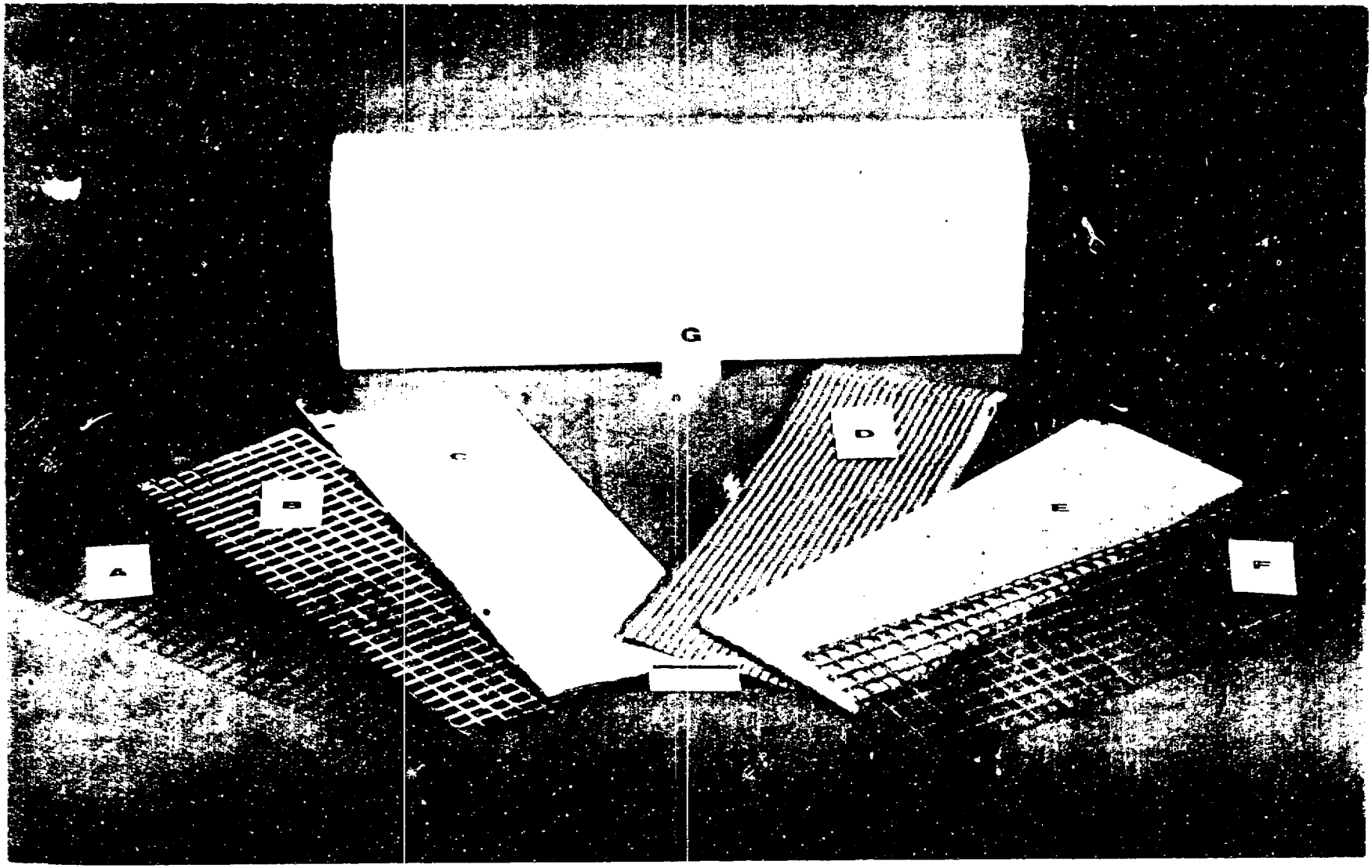

FIGURE 1. COMPONENTS OF A 75X SIZE REINFORCED LEAD-ACID CELL: TITANIUM REINFORCEMENT "PREFORM" (A), CAST MFX ALLOY POSITIVE GRID (B), PASTED POSITIVE ELECTRODE (C), DARAMIC SEPARATOR (D), PASTED NEGATIVE ELECTRODE (E) AND NEGATIVE LEAD ALLOY GRID.

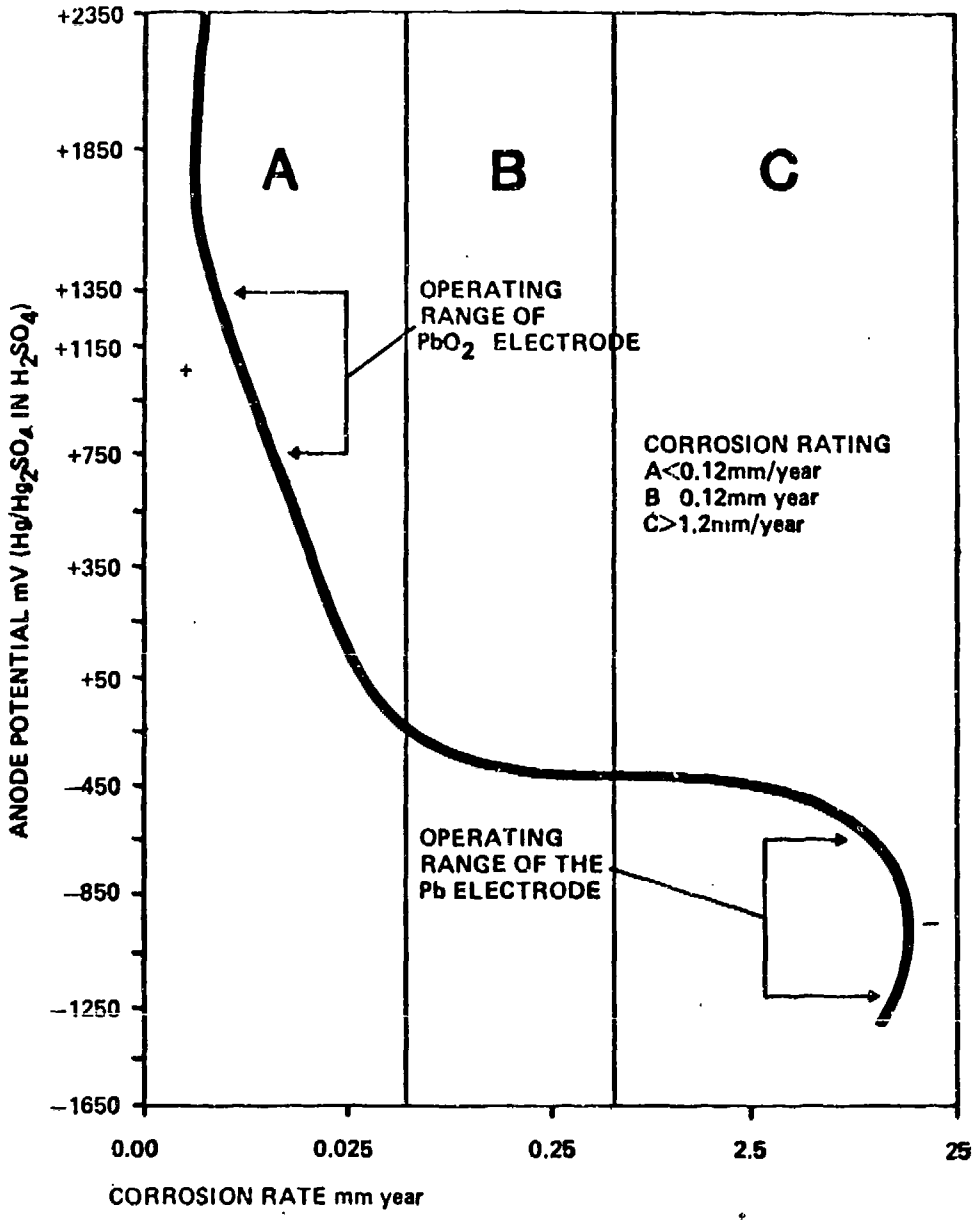

FIGURE 2. CORROSION RATE VERSUS APPLIED POTENTIAL FOR TITANIUM IN 40% SULFURIC ACID AT 60°C. TAKEN FROM REFERENCE(1).

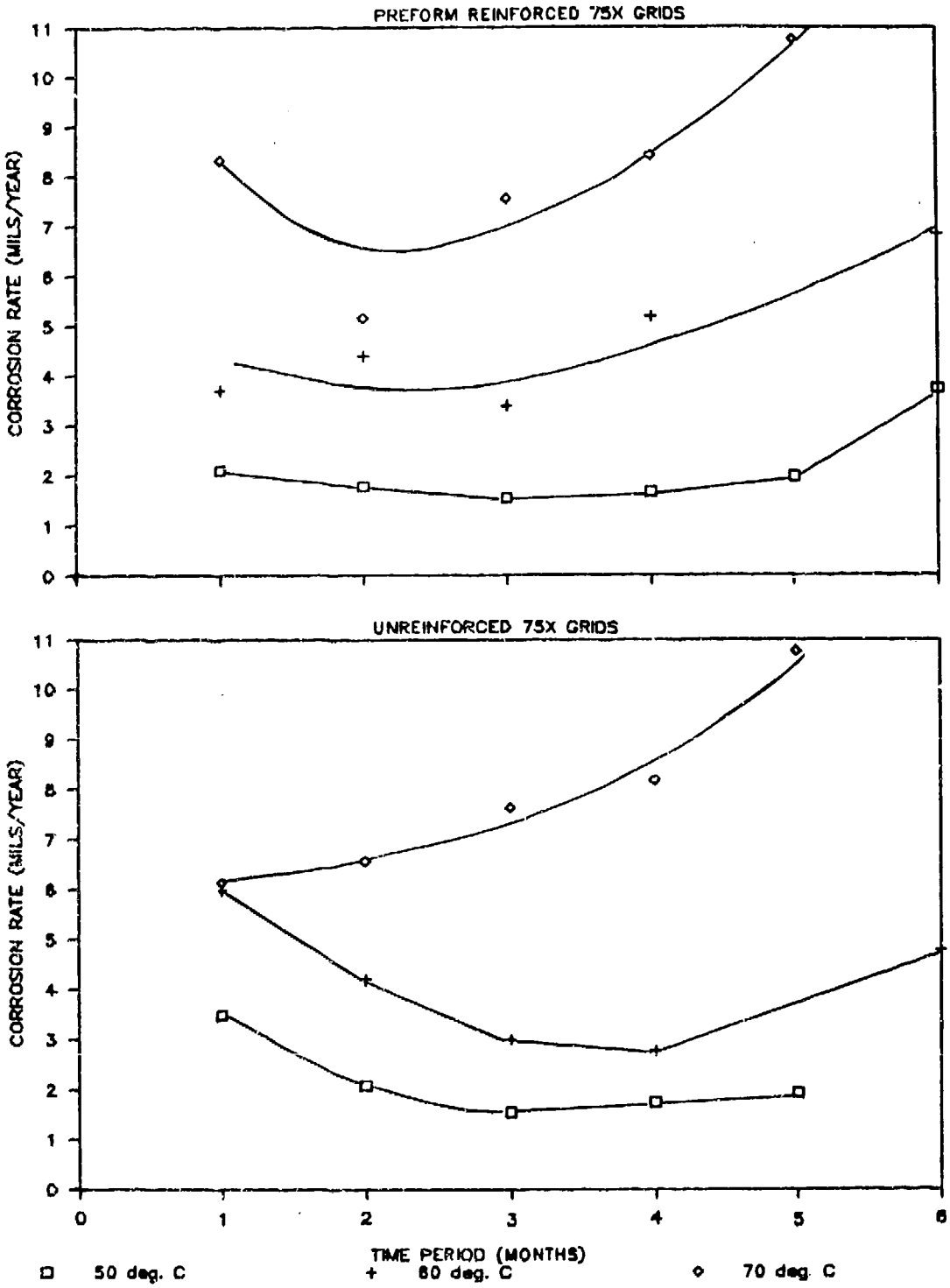

FIGURE 3. CORROSION RATE FROM WEIGHT LOSS MEASUREMENT VERSUS IMMERSION TIME FOR REINFORCED (TOP) AND UNREINFORCED (BOTTOM) MFX ALLOY GRIDS, RESPECTIVELY.

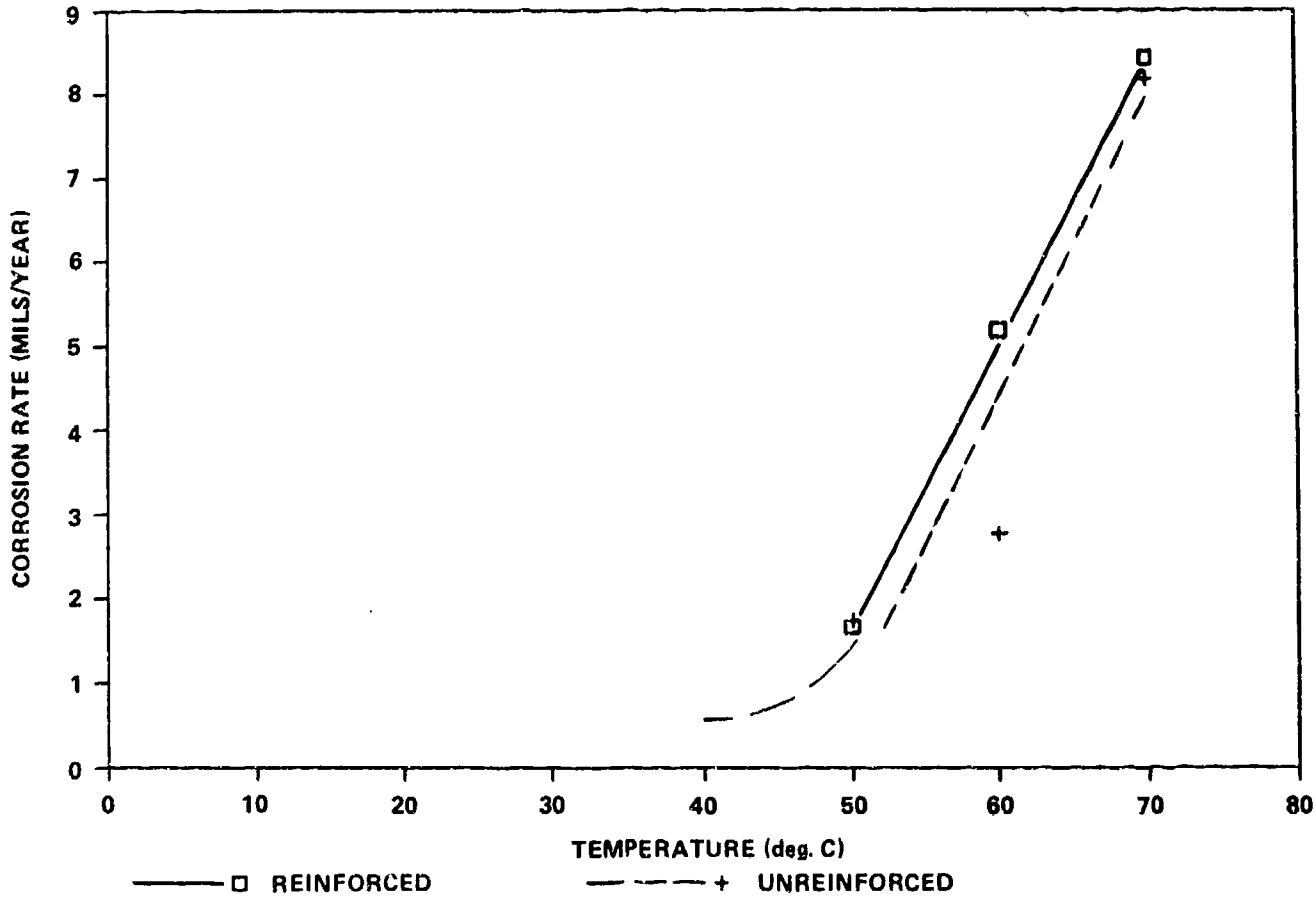

FIGURE 4. CORROSION RATE FROM WEIGHT LOSS MEASUREMENT VERSUS TEMPERATURE FOR REINFORCED AND UNREINFORCED MFX ALLOY GRIDS AFTER 4 MONTHS IMMERSION.

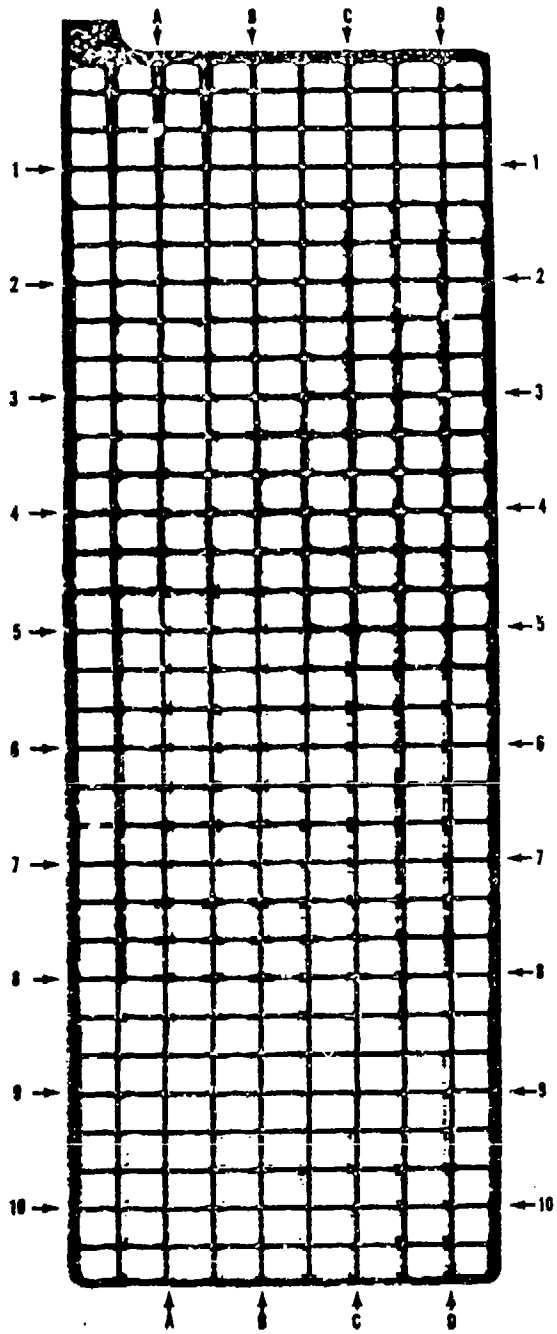

FIGURE 5. 75X GRID MEASUREMENT POINTS USED IN IMMERSION TEST, VERTICAL MEMBERS (A-D) AND HORIZONTAL MEMBERS (1-10).

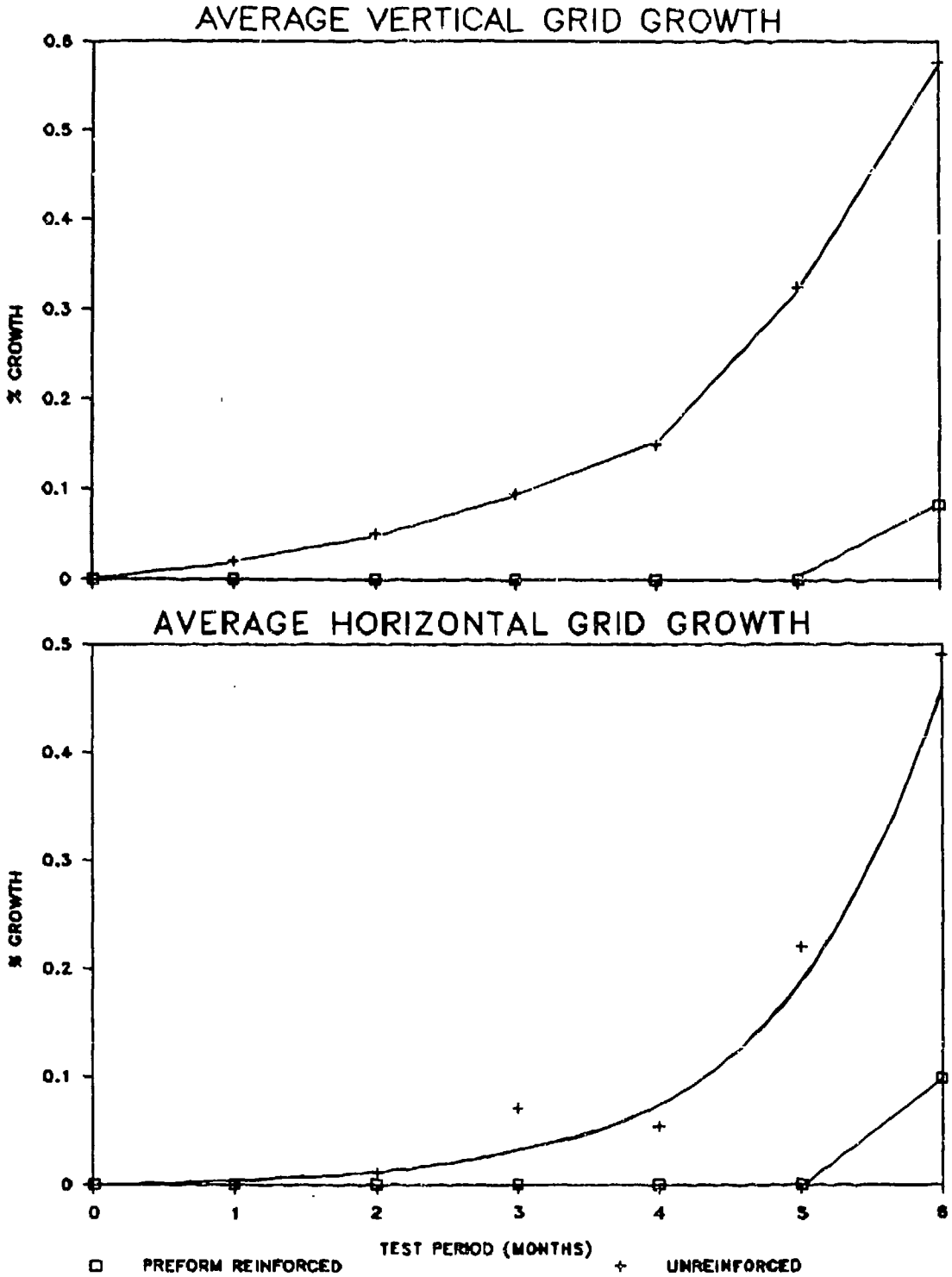

FIGURE 6. AVERAGE VERTICAL AND HORIZONTAL GRID MEMBER GROWTH VERSUS IMMERSION TIME AT 70°C FOR REINFORCED (SQUARES) AND UNREINFORCED (CROSSES) MEMBERS.

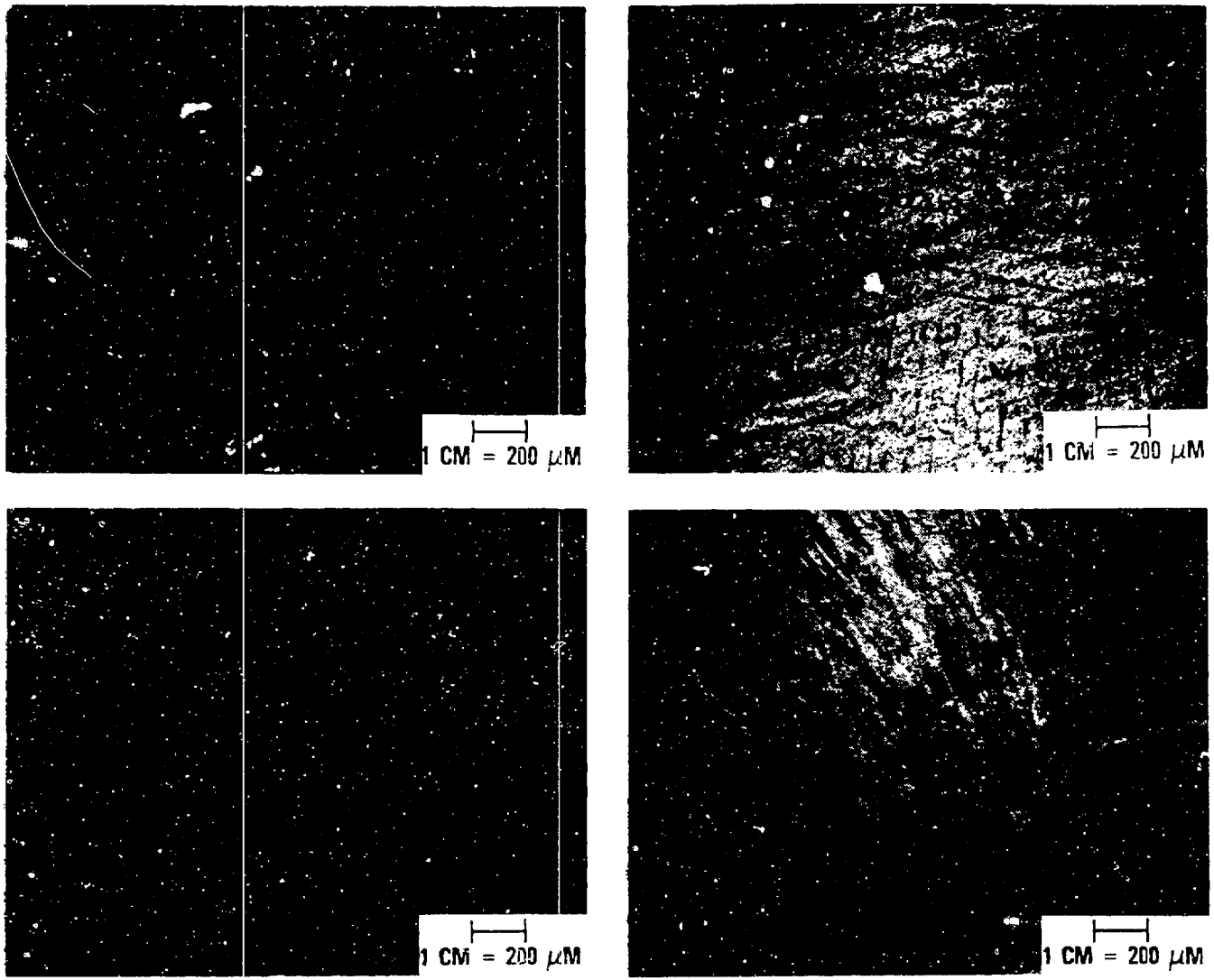

FIGURE 7. CROSS-SECTIONAL VIEWS OF AN UNREINFORCED MFX ALLOY GRID IMMERSED IN 1.28 GRAM/CC SPECIFIC GRAVITY H_2SO_4 AT 70°C, +1.25 V. VERSUS Hg/Hg_2SO_4 STANDARD. COUNTERCLOCKWISE FROM LOWER RIGHT: PRIOR TO AND AFTER 2, 4 AND 6 MONTHS IMMERSION, RESPECTIVELY.

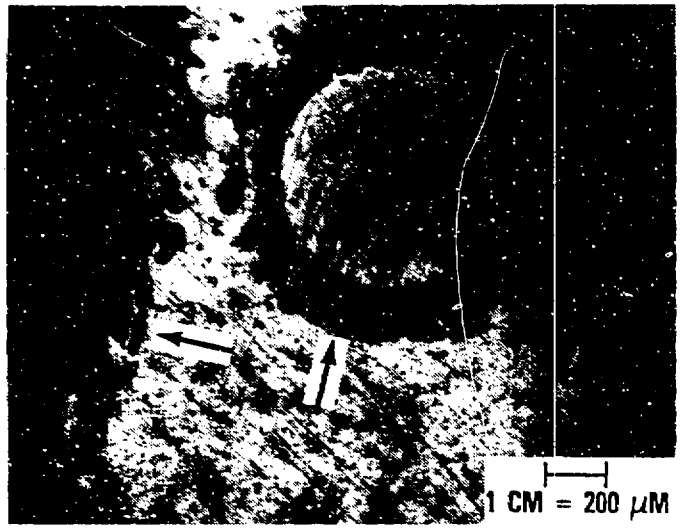

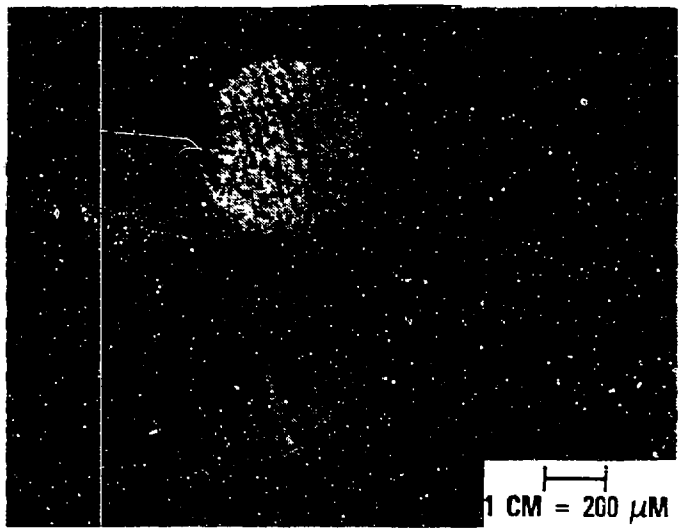

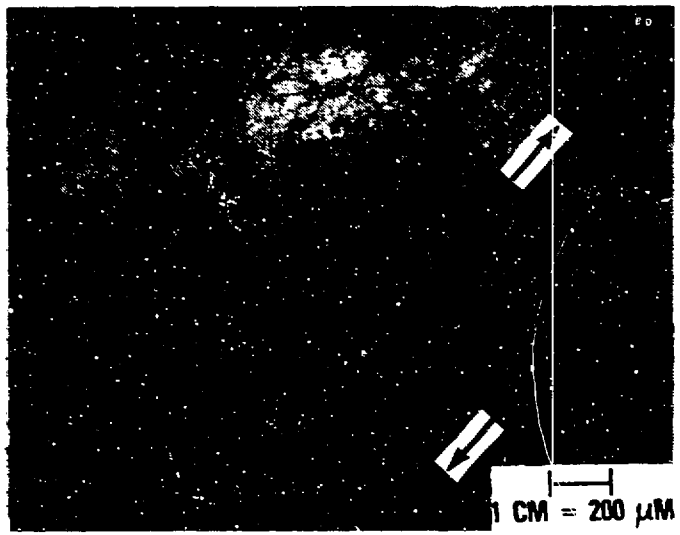

FIGURE 8.
MFX ALLOY GRIDS IMMERSED IN 1.28 g/cc SPECIFIC GRAVITY H_2SO_4, +1.25 V. VERSUS Hg/Hg_2SO_4 STANDARD AT 70°C, CROSS-SECTIONAL VIEWS. ABOVE: REINFORCED, BEFORE IMMERSION; UPPER LEFT: REINFORCED, AFTER 6 MONTHS IMMERSION; LOWER LEFT: UNREINFORCED, AFTER 6 MONTHS IMMERSION.

US ARMY
ARMAMENT
MUNITIONS
CHEMICAL COMMAND

CHEMICAL RD&E CENTER

NBC CONTAMINATION SURVIVABILITY

OF ARMY MATERIEL

BY DR. JOSEPH J FEENEY

SMCCR-NB
Area Code (301) 671-3420
Autovon (584) 3420

235

NBC DEFINITIONS

NUCLEAR

- RESIDUAL RADIOLOGICAL CONTAMINATION
  - FALLOUT
  - NEUTRON-INDUCED GAMMA ACTIVITY

BIOLOGICAL

- INFECTIOUS MICROORGANISMS
- BIOCHEMICALLY DERIVED TOXINS AND VENOMS
- BIOREGULATORS
- OTHER NOVEL BW AGENTS

CHEMICAL

- ALL KNOWN CW AGENTS
  - BLOOD (AC)
  - NERVE (VX, GB, GD, TGD)
  - BLISTER (HD, HL)

A0332- AA7 2814-06

SMCCR Form 38, 1 April 1985

COMMON CHEMICAL AGENTS

TYPE	NAME	SYMBOL	PHYSICAL PROPERTIES			
			BOILING POINT (C)	VOLATILITY 25 C MG/M^3	VAPOR DENSITY*	HEAT OF VAPORIZATION (CAL/GM)
BLISTER	MUSTARD	HD	228	920	5.50	94.0
BLOOD	-	AC	26	1,075,000	0.93	210.0
NERVE	SARIN	GB	158	22,000	4.86	80.0
	SOMAN	GD	198	3,900	6.30	72.4
	-	VX	298	10.5	9.20	72.8

*AIR VAPOR DENSITY = 1

A0332-S7092104

CHEMICAL REACTIVITY OF SOME CHEMICAL AGENTS

MILITARY SYMBOL	CHEMICAL FORMULA	CHEMICAL BY-PRODUCTS FROM REACTIONS WITH: CAUSTICS	MINERAL ACIDS	OXIDIZING MINERAL ACIDS
HD	$(CLCH_2CH_2)_2S$	CHLORIDE SALTS, THIODIGLYCOL	HCL, THIODIGLYCOL	HCL, SO_2, CL_2CO HALOGENATED COMPOUNDS
GB	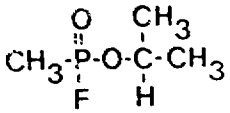	FLUORIDE SALTS, ISOPROPYL ALCOHOL METHYLPHOSPHONATE SALTS	HF	HF, OXIDES OF N.P. AND S
GD	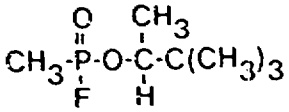	FLUORIDE SALTS, PINACOLYL ALCOHOL METHYLPHOSPHONATE SALTS	HF	HF, OXIDES OF N.P. AND S
VX	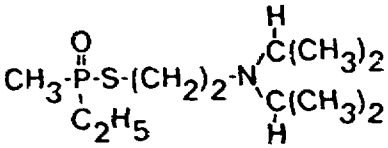	COMPLEX SERIES OF BY-PRODUCTS	H_2S, OXIDES OF S	H_2S, OXIDES OF N.P. AND S

A0332- S7092105

CURRENT STANDARD DECONTAMINANTS

	DS2	STB
COMPOSITION:	DIETHYLENETRIAMINE, METHYLCELLUSOLVE, NaOH	$Ca(OCl)_2$ AND $Ca(OH)_2$
USED:	NEAT	MIX WITH H_2O
USED ON:	PAINTED SURFACES	UNDERCARRIAGE, TERRAIN, PERSONAL EQUIPMENT
DISADVANTAGE:	"PAINT REMOVER", *LOGISTICS*	CORROSION, *SUPPLY PROBLEMS*

AGENT EFFECTS ON MATERIALS

★ AGENTS CAN ALTER PROPERTIES OF MATERIALS

★ TYPICAL AFFECTED PROPERTIES

- MECHANICAL - TENSILE STRENGTH, COMPRESSION SET, etc.
  - HD REDUCES TENSILE STRENGTH 25-40% ON MOST ELASTOMERS
- CHEMICAL - PERMEABILITY, DIFFUSION RATE, etc.
  - ACRYLICS, SILICONES, EPOXIES, URETHANES SHOW INCREASED PERMEABILITY ON EXPOSURE TO HD
- FIELD - DIELECTRIC CONSTANT, INDEX OF REFRACTION, etc.
  - HD CAUSES SWELLING, HAZING, SLIGHT CRAZING ON STRETCHED ACRYLIC; RESISTIVITY IS REDUCED

F5123508

CORROSION RESISTANCE OF METALS TOWARD CB

METAL	CORROSION EFFECT
STEEL 1020	CONSIDERABLE ATTACK
AL ALLOY - 3S	CONSIDERABLE ATTACK
AL ALLOYS - 4S, -17S, -24S	MODERATE ATTACK
AL ALLOYS - 52S, -A54S, -61S	VERY SLIGHT ATTACK
COPPER	SLIGHT ATTACK
BRASS (62% CU, 37% ZN)	SLIGHT ATTACK
MAGNESIUM ALLOY FS-1	SEVERE PITTING
CADMIUM-PLATED STEEL	CADMIUM PLATING ATTACKED AND REMOVED AFTER 3 MONTHS
NICKEL ALLOYS INCONEL, K-MONEL	NEGLIGIBLE EVIDENCE
LEAD	SLIGHT ATTACK
TIN	VERY SEVERE ATTACK
INDIUM	SOME PITTING
SOLDER (LEAD-TIN)	SURFACE ATTACK, PROBABLY REMOVAL OF TIN

A0332- S7092101

INFLUENCE OF CW ENVIRONMENTS ON METALS

ENVIRONMENT	METAL ALLOYS 2024-T351 AL	6061-T6 AL	7075-T65 AL	7079-T6 AL	AISI-4340 STEEL	AZ31 MG
VX	N	N	N	N	N	N
GB	N	N	N	N	P	N
HD	S	N	S	S	S	N
DS2	N	C	N	N	S	N
VX/DS2	N	N	N	N	N	N
GB/DS2	P	N	N	P	N	N
HD/DS2	N	N	N	N	N	N
NAOCL	S	C	C	C	S	N
VX/NAOCL	P	P	P	P	N	S
GB/NAOCL	S	N	N	S	P	S
HD/NAOCL	S	N	S	S	C,N	S

N - NO EFFECT
S - STRESS CORROSION CRACKING
C - GENERAL SURFACE CORROSION
P - POSSIBLE EMBRITTLEMENT (FAILURE AT POINT OF ENVIRONMENT APPLICATION); IMPLIES SOME DEGREE OF SURFACE CORROSION
C,N - SURFACE CORROSION, BUT FAILURE OCCURRED AT A POINT REMOVED FROM CORRODED AREA

A0332-S7092102

INFLUENCE OF CW ENVIRONMENTS ON NONMETALS

ENVIRONMENT	POLYSULFIDE SEALANTS PS 890	PR 1221	PR 1422	RTV 88	PLEXIGLASS	TIRE
VX	B	B	B	T	N	N
GB	N	G	G	N	N	N
HD	(S)G	(S)G	(S)G	(S)G	T	N
DS2	N	N	N	N	N	(S)G
VX/DS2	B	B	B	N	N	T
GB/DS2	(S)G	G	(S)G	P	N	T
HD/DS2	T	T	T	N	T	T
NAOCL	(S)G	N	N	(S)G	N	(S)G
VX/NAOCL	B	B	B	(S)G	G	T
GB/NAOCL	N	G	(S)G	(S)G	G	T
HD/NAOCL	N	N	(S)G	N	T	(S)G

N - NO EFFECT
T - SOFTENED
B - BLISTERED
(S)G - SLIGHT - GENERAL ATTACK OR DETERIORATION OF PROPERTIES
P - POSSIBLE EMBRITTLEMENT (FAILURE AT POINT OF ENVIRONMENT APPLICATION); IMPLIES SOME DEGREE OF SURFACE CORROSION

A0332- S7092103

DECONTAMINATION EFFECTS

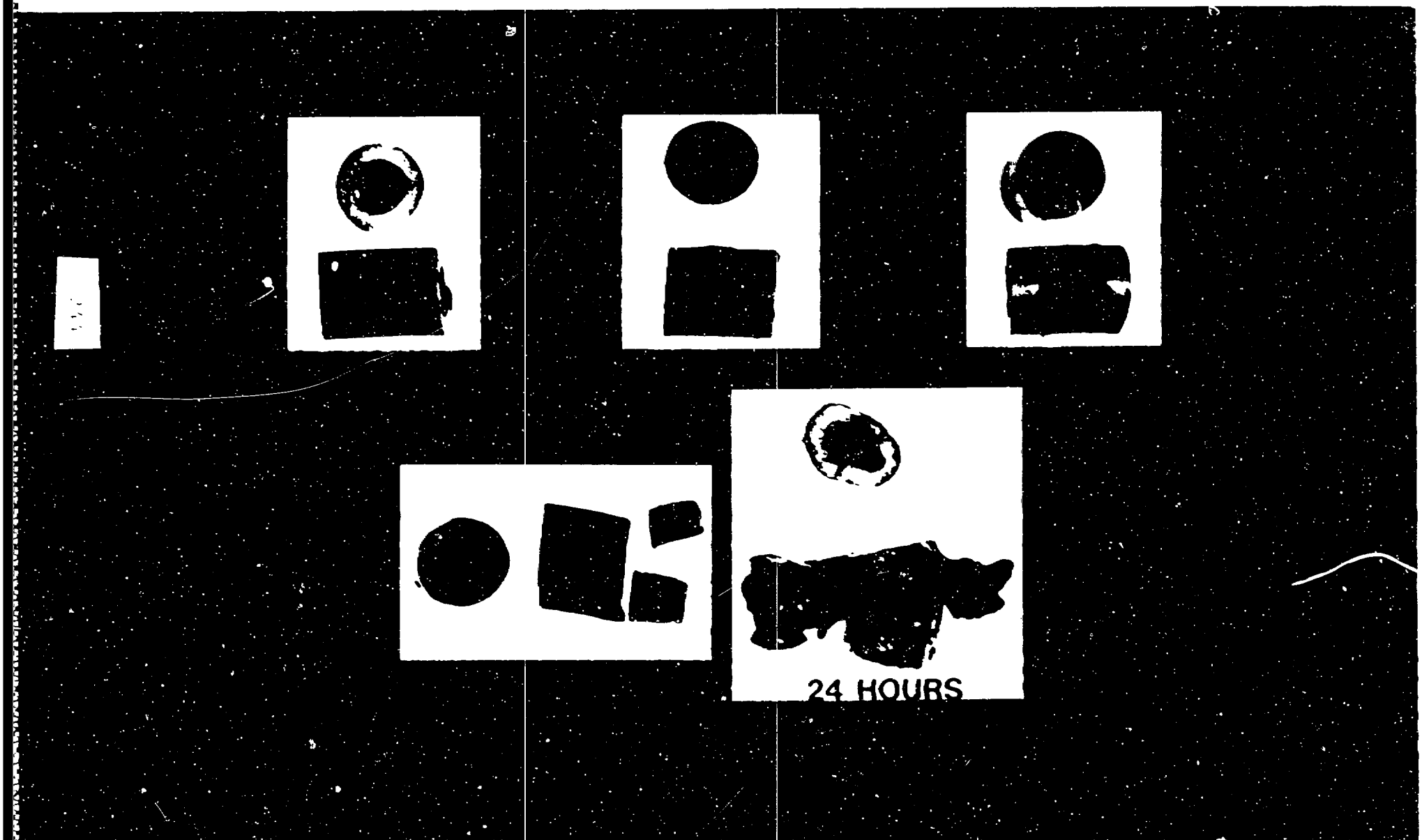

DIETHYLENETRIAMINE ON LEXAN (POLYCARBONATE) AT 50°C

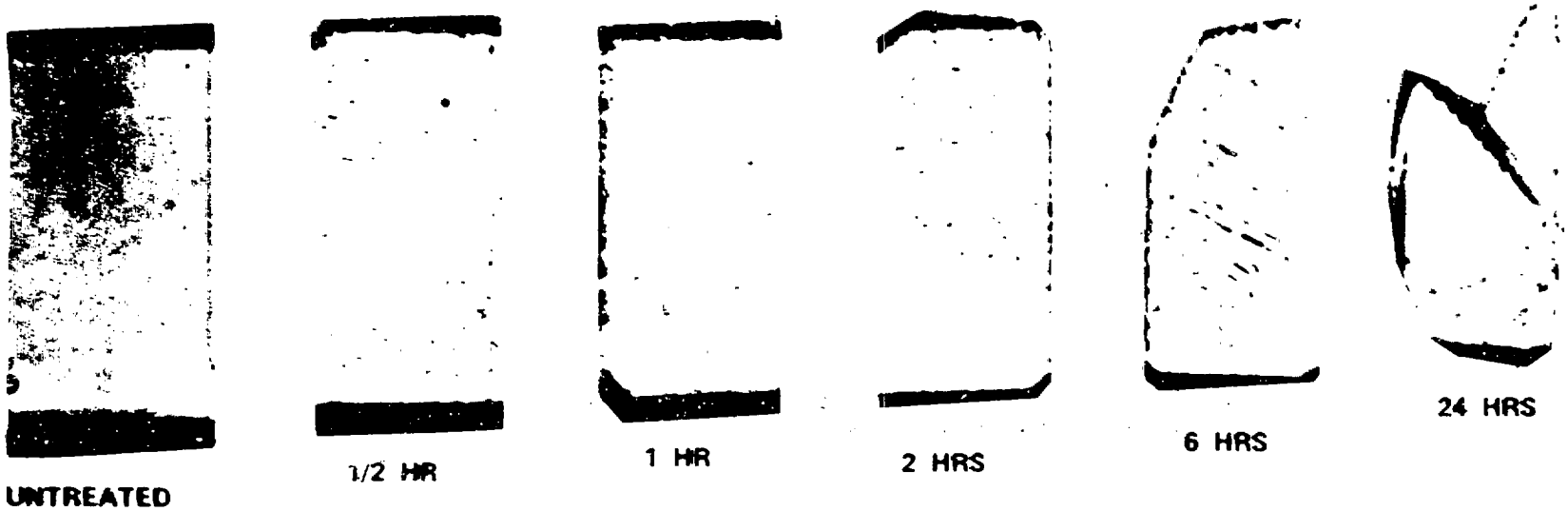

18% WEIGHT LOSS IN 1/2 HOUR
78% IN 24 HOURS

(POLYVINYLIDENE FLUORIDE) AT 50°C

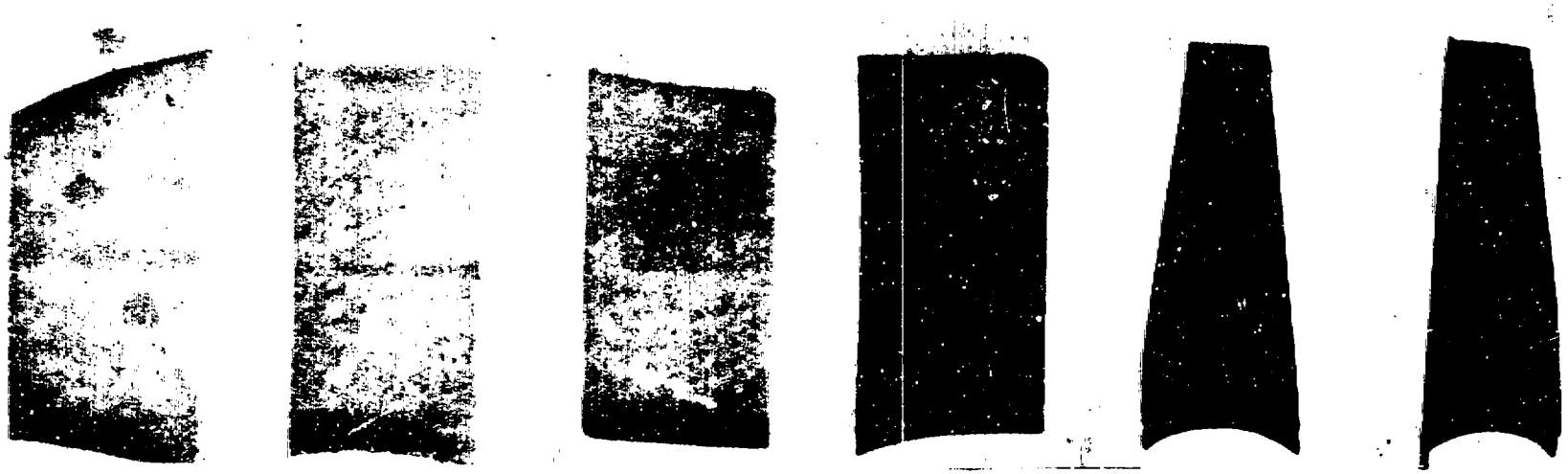

UNTREATED 1/2 HR 1 HR 2 HRS 6 HRS 24 HRS

COLOR CHANGED FROM CLEAR TO REDDISH BROWN

GENERIC EFFECTS
PLASTICS AND POLYMERS

AGENTS MECHANISM OF FAILURE IS SOFTENING DUE TO SORPTION; H & V TYPES ATTACK RUBBER AND ELASTOMERS, FLUOROELASTOMERS GENERALLY GOOD: POLYETHYLENES FAIR; TEFLONS, POLYVINILIDENE CHLORIDES AND POLYACRYLONITRILES SEEM TO BE GOOD

DECONTAMINANTS SWELLING, CRACKING, DISSOLUTION ARE COMMON EFFECTS WITH DS-2 OR STB; POLYETHYLENE, KEL-F VITON, BUTADIENE-STYRENE GENERALLY GOOD

GENERIC STATEMENTS HAVE SHORTCOMINGS

- SOME FLUOROELASTOMERS MAY FAIL; SOME SARANS GOOD, ACRYLICS VARY

A0332-885281407-01

SMCCR Form 38, 1 April 1985

AGENT EFFECTS ON ELECTRONICS

- AGENTS CAN ALTER ELECTRICAL CHARACTERISTICS OF ITEMS
- PRINCIPAL MODES FOR EFFECTS
  - ELECTROLYTIC PROCESSES
    - POSITIVE CIRCUIT ELEMENTS CORRODE (TURN BLACK) WHEN EXPOSED TO HD, VX, GD, AT APPROXIMATELY 20 VOLTS
  - ALTERATION OF DIELECTRIC PROPERTIES
    - RESISTIVITY OF ACRYLIC CONFORMAL COATING REDUCED BY 10^5 – BECOMES CONDUCTIVE

F5123509

CONTAMINATION AVOIDANCE SUPPRESSION

MATERIALS ASPECTS

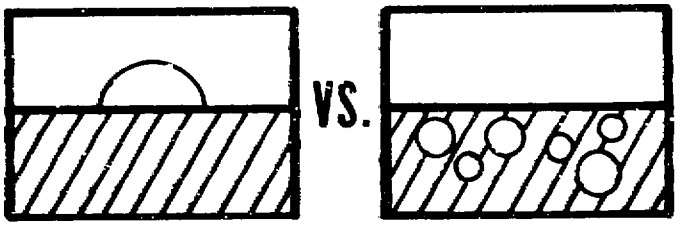

DESIGN ASPECTS

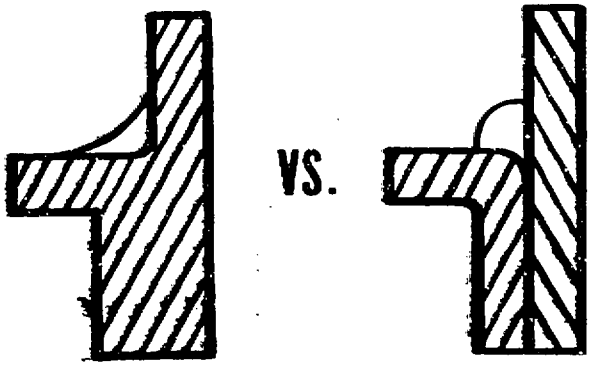

AR 70 - 71

NBC CONTAMINATION SURVIVABILITY

THE CAPABILITY OF A SYSTEM AND ITS CREW TO WITHSTAND AN NBC-CONTAMINATED ENVIRONMENT, INCLUDING DECONTAMINATION, WITHOUT LOSING THE ABILITY TO ACCOMPLISH THE ASSIGNED MISSION

- DEPARTMENT OF ARMY PROPONENT – DEPUTY CHIEF OF STAFF FOR RESEARCH, DEVELOPMENT AND ACQUISITION (DCSRDA)
- STAFF MANAGER – UNITED STATES ARMY NUCLEAR CHEMICAL AGENCY (USANCA)

A0332- F5123504

NBC CONTAMINATION SURVIVABILITY AR 70-71

POLICIES

- ALL MISSION ESSENTIAL EQUIPMENT MUST BE NBC CONTAMINATION SURVIVABLE.
- NBC CONTAMINATION SURVIVABILITY:
  - WILL BE CONSIDERED IN ALL REQUIREMENTS DOCUMENTS (I.E., LOA, ROC, LR).
  - WILL BE ESTABLISHED DURING PROGRAM INITIATION PHASE AND REFINED.
  - WILL BE MANAGED THROUGHOUT MATERIEL LIFE CYCLE.
  - WILL BE REVIEWED AT ALL IPR'S, ASARC'S AND DSARC'S.
  - CHANGES OR WAIVERS WILL BE AJUDICATED ONLY BY THE NUCLEAR AND CHEMICAL SURVIVABILITY COMMITTEE.

A0332-Y4094402-01

SMCCR Form 38, 1 April 1985

NBC CONTAMINATION SURVIVABILITY QUALITATIVE STANDARDS

DECONTAMINABILITY

- THE EQUIPMENT MUST BE CAPABLE OF BEING DECONTAMINATED USING STANDARD NBC DECONTAMINANTS AND PROCEDURES AVAILABLE IN THE FIELD, TO THE POINT THAT THE CONTAMINANT POSES NO CASUALTY-PRODUCING HAZARD TO UNPROTECTED PERSONNEL EXPOSED DURING NORMAL MISSION PROFILE OF THE EQUIPMENT

HARDNESS

- THE EQUIPMENT MUST BE RESISTANT TO THE MATERIEL-DAMAGING EFFECTS OF NBC CONTAMINANTS AND THE DECONTAMINATION AGENTS AND PROCEDURES REQUIRED TO REMOVE THE CONTAMINATION

COMPATIBILITY

- THE EQUIPMENT MUST BE CAPABLE OF BEING OPERATED, MAINTAINED, AND RESUPPLIED BY PERSONNEL WEARING THE FULL NBC PROTECTIVE ENSEMBLE

A0332- 2V6 2938-03

DECONTAMINABILITY CRITERION

FOR CHEMICAL CONTAMINANTS

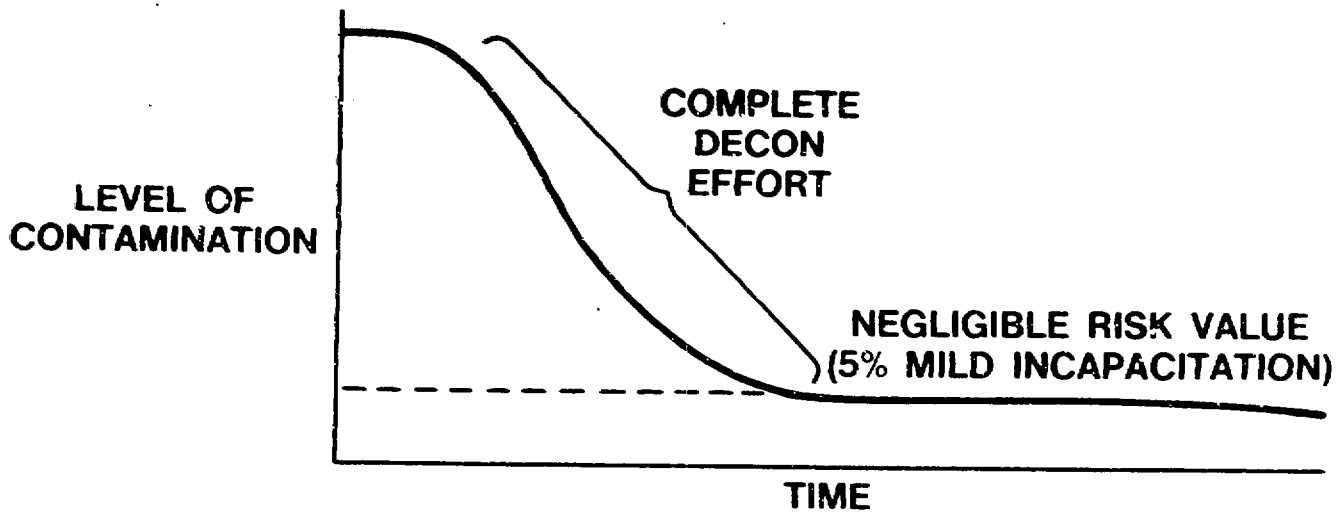

- EXTERIOR SURFACES INITIALLY CONTAMINATED WITH 10 G/M^2 OF CHEMICAL AGENTS; INTERIOR SURFACES, 1 G/M^2
- DECONTAMINATION OCCURS 1 HOUR AFTER CONTAMINATION USING STANDARD FIELD DECONTAMINANTS, EQUIPMENT, AND PROCEDURES
- EXPOSURE PERIOD FOLLOWING DECONTAMINATION IS BASED ON NORMAL MISSION PROFILE, BUT NOT TO EXCEED 12 HOURS

A0332- 2V6 2938-04

HARDNESS STANDARD (QUANTIFIED)

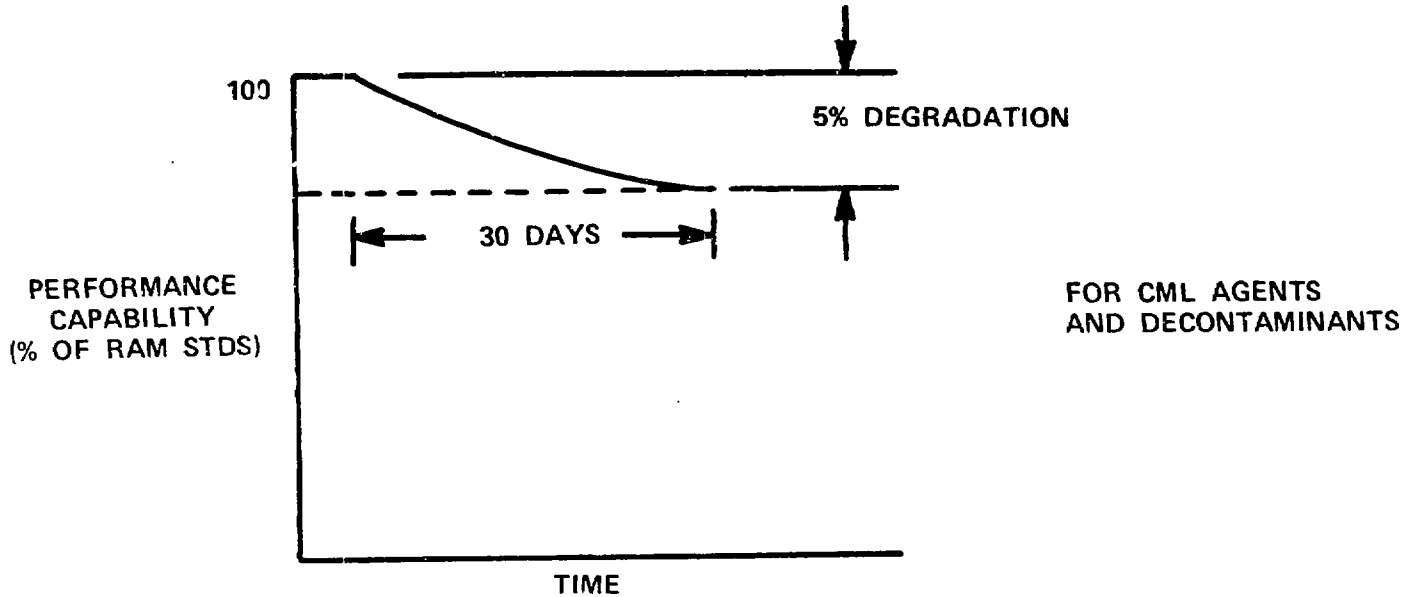

- MISSION ESSENTIAL EQUIPMENT AND MATERIEL SHALL BE HARDENED TO ENSURE THAT DEGRADATION OVER A 30-DAY PERIOD OF NO MORE THAN 5 PERCENT IN SELECTED QUANTIFIABLE ESSENTIAL CHARACTERISTICS IS CAUSED BY 5 EXPOSURES TO NBC CONTAMINANTS, DECONTAMINANTS, AND DECONTAMINATING PROCEDURES ENCOUNTERED IN THE FIELD.

SMCCR Form 38, 1 April 1985

COMPATIBILITY CRITERION (QUANTIFIED)

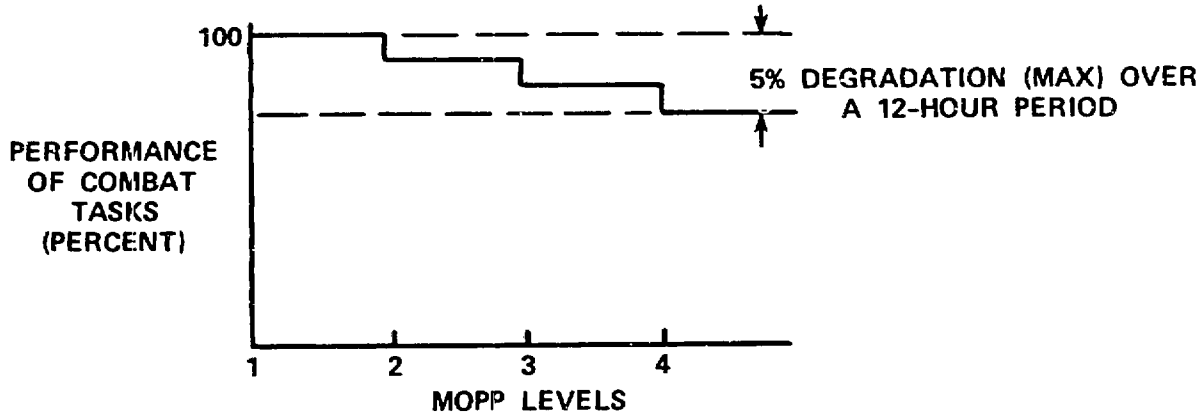

THE DESIGN OF MISSION-ESSENTIAL EQUIPMENT AND MATERIEL SHALL TAKE INTO CONSIDERATION THE COMBINATION OF EQUIPMENT AND EXISTING AND ANTICIPATED NBC PROTECTION. THE COMBINATION OF EQUIPMENT AND NBC PROTECTION SHALL PERMIT PERFORMANCE OF MISSION-ESSENTIAL OPERATIONS, COMMUNICATION, MAINTENANCE, RESUPPLY, AND DECONTAMINATION TASKS BY TRAINED AND ACCLIMATIZED TROOPS FOR A TYPICAL 12-HOUR MISSION PROFILE IN A CONTAMINATED ENVIRONMENT:

- IN METEOROLOGICAL CONDITIONS OF AREAS OF INTENDED USE
- WITH NO DEGRADATION OF CREW PERFORMANCE GREATER THAN 5 PERCENT BELOW LEVELS SPECIFIED FOR TASKS ACCOMPLISHED IN A NON-NBC ENVIRONMENT

1-28

SUMMARY AR 70-71

CRITERIA

- DECONTAMINABILITY (HAZARD REDUCTION)
  - EQUIPMENT DESIGN (PROMOTE RUNOFF, ELIMINATE COLLECTION POINTS)
  - MATERIALS SELECTION (RESIST SORPTION, SELECT IMPERMEABLE MATERIALS)
- HARDNESS (RESISTANCE TO AGENT/DECONTAMINANT DAMAGE)
  - MATERIALS SELECTION (AGENT/DECONTAMINANT COMPATABILITY)
  - DESIGN TO ELIMINATE CONTAMINANT ENTRAPMENT
- COMPATIBILITY (MINIMAL DEGRADATION WHEN OPERATING IN MOPP)
  - EQUIPMENT DESIGN (HUMAN ENGINEERING – MAN-PROTECTIVE CLOTHING/EQUIPMENT INTERFACE)
  - COLLECTIVE PROTECTION

A0332- E60201-05.01

NBC SURVIVABILITY GUIDANCE HANDBOOKS

AVAILABLE FROM THE DEFENSE TECHNICAL INFORMATION CENTER

- NBC (NUCLEAR, BIOLOGICAL AND CHEMICAL) CONTAMINATION SURVIVABILITY: A HANDBOOK FOR DEVELOPMENT/MANAGEMENT OF MATERIEL PROGRAMS
  - DTIC NO. B098033
- GUIDELINES - DESIGN TO MINIMIZE CONTAMINATION AND TO FACILITATE DECONTAMINATION OF MILITARY VEHICLES AND OTHER EQUIPMENT: INTERIORS AND EXTERIORS
  - DTIC NO. A149088
- NBC MATERIALS HANDBOOK
  - DTIC NO. B079397

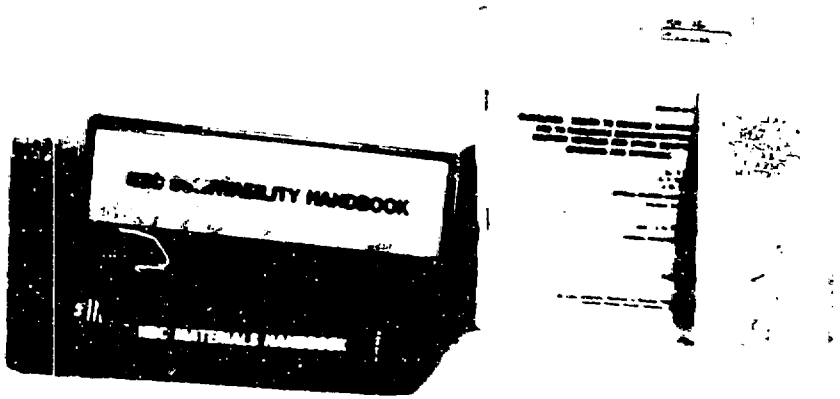

A0332

SMCCR Form 38, 1 April 1985

NBC CONTAMINATION SURVIVABILITY

CRDEC POINTS OF CONTACT

● MAILING ADDRESS	COMMANDER, CHEMICAL R D & E CENTER ATTN: APG, MD 21010-5423
● CRDEC GENERAL POINT OF CONTACT	DR. WILLIAM S. MAGEE, JR. (301) 671-3420, SMCCR-NB
● DESIGN GUIDELINES ON CONTAMINATION AVOIDDANCE AND DECONTAMINATION	MR. JOSEPH THOMPSON (301) 671-3234, SMCCR-PPD
● MODELING	MR. RICHARD SAUCIER (301) 671-4241, SMCCR-ST
● MATERIALS DATA BASE	DR. JAMES BAKER (301) 671-2532, SMCCR-PPD
● SIMULANT DATA BASE	MR. PHILIP A. COON (301) 671-3546, SMCCR-RSP
● TECHNICAL INDUSTRIAL LIASON	MR. RICHARD DIMMICK (301) 671-2031, SMCCR-OPP

A0332- 2V6 2938 15

RECENT ADVANCES IN METALLIC/CERAMIC COATINGS FOR CORROSION CONTROL IN MILITARY APPLICATIONS

Mark F. Mosser

Sermatech International Inc.

ABSTRACT:

This paper describes recent advances in metallic/ceramic coatings meeting the MIL-C-81751B specification and related corrosion/oxidation resistant chromate/phosphate finishes. A brief history of the generic coating family is followed by detailed descriptions of the improved coating processes.

Coating advances are described in three general areas. In the first, improved sealed coating systems are presented. These sealed coatings have superior corrosion resistance and improved erosion resistance when compared to conventional coatings. Test documentation is included and examples are given in which these coatings are described in applications on turbine compressor components, fasteners, and marine hardware.

The second area of coating improvement relates to coating processes designed for gun barrels and other ordnance hardware. These emissive coatings are shown to provide the thermal shock resistance, corrosion protection, and lateral heat transfer necessary for improved barrel life.

The third area described includes coatings specifically designed for operation in harsh acid rain environments including SO_x, NO_x and acid halide exposure conditions. To simulate these exposure conditions, test results are presented in which coatings are evaluated in several acidic test environments including CASS (ASTM D-368). Test results include heat cycling and acid exposure data on several alloys used in turbine compressors.

INTRODUCTION:

Metallic/ceramic coatings such as are described in this paper have been in use for over twenty five years. In 1969 the original coating system based on this technology was incorporated into a military specification, MIL-C-81751. This coating, known as SermeTel W*, became the Type I coating described by this specification. At the time the specification was written little was known about the chemistry of the coating. Since then, the environment has worsened and military/aerospace hardware has changed. It is not surprising that improvements in the coating system have also occurred. Before reviewing the improvements, it is necessary to review the original coating and describe the various processing steps used to produce the different classes.

Type I coatings within this specification are generically unique paint-on slurry coatings. First described by Charlotte Allen [1], these inorganic coatings consist of a pigment, aluminum powder, and a binder material. This binder material is an acidic solution consisting of metallic phosphates and dichromates. After the coating has been applied, usually by spray painting, it is given a thermal treatment by heating to about 650°F (343°C). At this temperature, the dichromates and phosphates undergo a series of chemical reactions that produce a well bonded glassy inorganic polymer matrix with aluminum pigmentation. The binder material becomes a ceramic-like structure during the curing process. It is amorphous and insoluble in most solvents, including boiling water.

Although this coating binder matrix contains acidic chromates and phosphates, the chemical reactions involved in coating formation are completely different from the reactions that produce a wide variety of common metal pretreatments based on phosphates and chromate/dichromate chemistry. Common phosphate coatings use specific formulations to produce iron, zinc, manganese and other phosphate layers on steel as well as on other metals. These phosphate layers can have fair corrosion resistance but are widely used as paint pretreatments. These coating layers usually are formed by the reaction of an acidic

* A registered trademark of Teleflex Inc. and a product of Sermatech International Inc.

phosphate and an oxidizer with a ferrous metal. The resulting phosphate layer is alkaline in nature, highly crystalline and has a limited temperature resistance. Similarly, chromate pretreatments are used on zinc, aluminum, magnesium, ferrous metals as well as on phosphate layers. In each case, the coatings formed are a result of the chemical reaction between the chromate ion and the substrate metal. The corrosion resistance of such films is fair; the coatings being primarily used as bases for paint.

In contrast to the coatings just described, the Type I metallic-ceramic coating can be applied to most metallic substrates. Little or no surface reaction occurs other than bonding reactions. As a result, the coating can be applied to carbon steels, stainless steels, nickel alloys, cobalt alloys, refractory metals, aluminum alloys, glass, ceramics, organic polymers, composites, and other materials which can be exposed to the prescribed cure temperature, which can be as low as 375°F (191°C).

MIL-C-81751 divides the Type I coating into four classes. Note that these four classes are based on exactly the same coating slurry, but use different processing steps. The classes are shown in Table I.

TABLE I

MIL-C-81751 Classification of Type 1 Coatings

1.2 Classification - Metallic-ceramic coatings shall be furnished in the following Types and Classes, as specified (see 6.2):

Type I - Class 1 - Coating cured at 650 ± 25°F

Class 2 - Coating cured at 650 ± 25°F and post treated at elevated temperature

Class 3 - Initial coat(s) cured at 650 ± 25°F, and burnished prior to applying top coat that is cured at 650 ± 25°F

Class 4 - Coating cured at 650 ± 25°F and post treated by burnishing

To understand the coating and its various classes, it is useful to review the various coating structures. Figures 1 through 4 are SEM photomicrographs showing the surface of each coating class. In Figure 2 the individual aluminum particles are visible, each surrounded by the bonding layer of chromate/phosphate polymer.

The classes are described as follows:

1) Class 1 - Two (or more) coating layers are applied and cured according to the following procedure:

   a. Vapor degrease
   b. Dry or wet blasting with 100-250 mesh abrasive grit
   c. Spray application followed by 175°F oven dry for 15 minutes
   d. Cure at 650°F for 15 minutes minimum
   e. Repeat steps 3 and 4

2) Class 2 - The coating that has been applied per the Class 1 requirements is exposed to a temperature between 950 and 1050°F (510-566°C). This heat treatment, or post cure as it is often called, causes a reaction to occur between the aluminum particles and the encapsulating chromate/phosphate layer producing the reactive ionic compound, aluminum phosphide. Since this compound is semiconductive, electrical conductivity is established across the coating surface and throughout the coating volume. This occurs without disruption of the coating structure or diffusion of aluminum into the base metal. Note that the coating structure (Figures 1 and 2) remains unchanged.

3) Class 3 - One coating layer is applied and cured per the Class 1 procedure. The coating is then mechanically abraded or "burnished" with abrasive media such as alumina or silica. This causes compression of the coating layer and particle to particle welding of the aluminum pigment. The coating layer produced resembles that shown in Figure 3. It is electrically conductive. The layer is then topcoated with a second coating layer, dried, and cured at 650°F. The final surface structure is the same as shown in Figures 1 and 2 since the final layer is not burnished.

4) Class 4 - The coating is applied and cured in the manner of a Class 1 coating; typically two coats are applied and cured. Use of alumina or silica abrasive at low pressure in a blast cabinet produces the burnished surface shown in Figure 3. If glass beads are used, the surface of the coating shows the orange peel appearance

shown in Figure 4. Figures 2 through 4 clearly show the extent of surface changes caused by impingement of particles on the surface of cured Class 1 coatings. The surfaces are severely cold worked in Figures 3 and 4, but no weight loss is observed as a result of the processing and all the coatings treated in this way are electrically conductive.

Taking one coating slurry and producing four different classes of coated products cause complication and confusion. These classes are necessary because the additional processing steps produce other coatings with other desirable properties. All classes share the following properties:

Temperature resistance	-	up to 1600°F
Thermal shock	-	1175°F to water quench
Heat cycle/salt spray	-	16 hrs. 1000°F/32 hrs. S/S for six cycles
Bond strength	-	>8000 psi
Solvent Resistance	-	Resistant to water, oils, greases and organic solvents

Other general coating properties are listed in MIL-C-81751. Certain properties vary with the coating class. As previously described, Class 2 and Class 4 coatings exhibit surface and volume electrical conductivity. Class 3 coatings show the same conductivity until overcoated. It has been found that these classes of coatings are not just electrically conductive, they are also galvanically active, sacrificial aluminum-rich coatings. Because of this property scribed coatings of Classes 2,3 or 4, when applied to steel substrates, will show no red rust after 1000 hours of ASTM B117 salt fog exposure. Little difference has been seen in the performance of Class 2, Class 3 or Class 4 coatings when compared in salt spray testing. A table of comparative galvanic potentials is given in Table 2. Results are in agreement with literature values such as those reported by Mansfeld (3).

TABLE II

Galvanic Series [2]

Material	Millivolts
Zinc plating	975-990
Cadmium plating	760- 765
Type 1 Class 2,3,4 coating	730-760
AA3003 Aluminum	720-745
AA2024T3 Aluminum	590
1010 Steel	565

Potentials were measured at 20°C in aerated 3.4% NaCl against a saturated calomel electrode.

A summary of the differences in the Type 1 coating classes is given below in Table III.

TABLE III

MIL-C-81751B TYPE I COATING CLASS DIFFERENCES

Property	Class 1	Class 2	Class 3	Class 4
Thickness	1.5-4 mils (38-102 μm)	Same	Same	Same
Electrically Conductive on surface	No	Yes	No	Yes
Sacrificial	No	Yes	Yes	Yes
Surface Finish	35-60R_A	35-60R_A	35-60R_A	25-70R_A
Erosion resistance/ (liters/mil per ASTM D968)	>100	>200	>100	>100

This coating system is unique - combining sacrificial action, high temperature resistance and good erosion characteristics. These properties make the various classes of this coating ideal candidates for steel components in a wide variety of applications. Of the four classes, Class 4 has the broadest range of uses. This coating class is used on fasteners, turbine compressor hardware,(e.g., blades, vanes, cases, etc.,) aircraft landing gear and a wide variety of other airframe components. The Class 2 coating is often used on large turbine components, such as engine cases that are exposed to high temperature. In many applications, the coating has replaced silicone aluminum paint and diffused nickel/cadmium plating because of improved performance in high heat applications coupled with corrosive environments. No other paint-on coating system offers similar performance.

High performance protective films such as these coatings require care in application to achieve best results. Because the coating material is a water borne slurry and is highly filled with aluminum pigment, it has the inherrent problems of a water borne coating. Without humidity and temperature control during application, applied coatings will vary in thickness and surface roughness. Additionally, since an inorganic slurry is being applied, great care must be taken to assure complete absense of oil, grease and other organic contaminants. These concerns become of greater importance as surface smoothness and thickness control become more important.

Improved Coating Systems - When the military specification for this coating was written, the coating process had been in use for about eight years. At that time, the Class 1 coating was predominant, with Class 2 and Class 4 coatings becoming more widely used. By 1970 these coating systems had been specified by most turbine and airframe manufacturers in the world and were being applied in many countries.

Information from users is essential for product improvement. To answer the question, "How can this coating be improved?", four lines of development work were followed:

1. Improvement of surface finish
2. Creation of a topcoat system

3. Decrease in coating porosity
4. Addition of corrosion inhibitors

During the decade of the 1970's, two of these lines of coating improvement/development were followed. One area of development related to application of smoother coatings; the other had to do with sealed coatings having greater corrosion resistance. These developments were mandated by customers facing the fossil fuel crisis of the early 1970's and the growing acid rain problem, respectively.

Surface Finish Improvements

Development work in surface finish improvement resulted in the introduction of a new smooth processed coating for turbine compressor applications, SermeTel Process 5375®. Although the coating process met the requirements of MIL-C-81751B Type 1 Class 4, it also provided enhanced compressor performance through improved surface finish on airfoils thereby reducing fuel consumption and turbine exhaust gas temperatures. Additionally, the corrosion protection properties of the original coating were maintained by the new process providing sacrificial protection in corrosive environments without extensive formation of white corrosion products. Excessive corrosion products would have caused surface roughness which would have resulted in efficiency loss. Eventually, surface finish profiles of 16-25 microinches AA were produced by this process. Actual profile was dependent on part geometry. This process saw extensive use on a wide variety of turbine compressor components, since it was specifically designed as a coating process for airfoils and was not applicable to marine hardware or general airframe components. Although the enhanced surface finish improved corrosion resistance slightly, the improvement was not dramatic; corrosion resistance was similar to other Class 4 coatings. The surface was still primarily aluminum metal.

Sealed Coatings

Coincident to the development of smoother coatings conforming to this specification, another line of development sought further improvement in the corrosion resistance of the aluminum coating.

TABLE IV

CORROSION RESISTANCE OF COATING CLASSES

Class	Hours to Red Rust (ASTM B-117)
1	< 168
2	> 1000
3	> 1000
4	> 1000

Substrate - mild steel

The data presented in the above table IV indicates that a Class 1 coating is not sacrificial and is only a fair barrier against penetration by the corrosive test solution. Classes 2, 3 and 4 show superior resistance to the salt spray environment, because the coatings are galvanically active, but white corrosion products can be seen on coated surfaces. Corrosion of the base metal has been replaced with corrosion of the coating as is always seen in sacrificial coatings. This corrosion decreases the life of the coating system. Clearly, sealing the coatings by topcoating should result in improved anti-corrosion properties by combining additional barrier protection with sacrificial protection.

Figure 5 shows a metallographic transverse section of a 2 mil (50 m) thick Class 4 coating at 500X magnification. Figure 6, like Figure 1, shows an SEM photomicrograph of the coating surface of a Class 1 coating at 1000X magnification. By studying these figures, it is clear that the coating structure is open and porous, susceptible to moisture absorption and corrosion attack.

While many film-formers could be used to topcoat this porous coating structure, a specific group of topcoats was devised which utilize the same basic chromate/phosphate chemistry as the basecoat material. By using this approach, virtually all the requirements of MIL-C-81751B Type I can be met by a topcoated system. By utilizing similar chemistry, the same application equipment and cure conditions can be employed.

Sermatech International has developed several of these topcoats. SermeTel 570A was the first topcoat developed. This coating continues to be widely used. SermeTel 842 has the same properties as 570A but is black in color. SermeTel TCS is used as a topcoat sealant for certain proprietary coating systems and produces a superior surface finish.

The topcoats are usually applied over grit burnished, Class 4, basecoated surfaces. After topcoat application, the coating surface is no longer electrically conductive, yet the conductive layer, which is covered and sealed in these topcoated systems, will still supply galvanic protection to steel components in saline environments. When coupled to a calomel electrode, the galvanic potential remains at 750 millivolts, the same as the basecoat material (See Table II). Because of the sealing effects, little white corrosion is seen after long term salt spray exposure.

SermeTel 570A applied over a Class 4 coating is shown in Figure 7 in a SEM photomicrograph at 1000X magnification. This coating combination is known as SermeTel 725. Figure 8 shows a SEM photomicrograph of the same coating system in transverse section. The 570A topcoat seals the surface and fills all available coating porosity at or near the surface with a hard corrosion resistant layer. The topcoat is 0.1 - 0.3 mils (2.5 - 7.5 μm) thick.

Use of the topcoated systems began in 1977 on the PT6 T400 Twin Pack helicopter engine[4]. While the specific basecoat, SermeTel 709, does not meet the military specification, it is a generically similar system designed to have superior corrosion resistance and to be very thin. Specification approvals of these coatings followed on a variety of turbines including the LM2500, LM5000, T700, T64 and J85. Additional widespread use of these coating systems was seen on power generation turbines and for overhaul of other non-specified components. In 1980 Wanhill et al[5] described the successful evaluation of these coatings on helicopter compressors in acidified environments attesting to the corrosion protection supplied by these coatings even under extreme conditions. The use of the topcoat sealer extended the range of uses for the basecoat material.

The performance of these topcoated systems led to evaluation in several marine environments. In one series of tests reported by Jankowsky[6], SermeTel 725 was a candidate coating for 17-4 PH steel and 4130 steel. During an eleven month exposure on the USS America of which seven months were in the Indian Ocean, coated samples were exposed to a high humidity/high salt fog environment. The SermeTel 725 coating system was rated best of coatings tested on these alloys.

Additional tests were conducted by NAVSSES and reported by Rogus and Vapniarek[7]. In these tests, simulated valve shaped specimens were exposed to a seven day schedule which included two

eight hour exposures to 925°F, a total of 32 hours of cool down time and 120 hours of salt fog. Additional stud/nut specimens were also coated and tested. SermeTel 725 was among the candidate coatings for both valves and stud/nut assemblies. The tests were run for 146 days. At the end of that time period, the SermeTel 725 coating was the sole survivor of the fastener coatings tested and the only coating recommended for fastener use. As a coating for the valve simulations performance was rated "satisfactory", but not equivalent to sealed wire sprayed aluminum. The wire sprayed aluminum was significantly thicker (4-24 mils) making comparisons difficult.

Based on these tests and others, the SermeTel 725 System has been specified on the following U.S. Navy hardware:

(1) Nelson type and clamp type pipe hangers (CG47 class cruisers).
(2) Bolts, nuts, studs and washers conforming to MIL-S-1222G.
(3) SUBSAFE level 1 bolting.
(4) Threaded fasteners for steam valves
(5) Boat davit systems.
(6) Other weather deck hardware.

Ten years of experience with these coatings has allowed the following general conclusions to be drawn:

1. Sealed coatings have improved atmospheric corrosion resistance against saline environments and acid rain conditions.
2. Sealed coatings have improved barrier properties eliminating white corrosion products, but maintaining galvanic activity of the basecoat.
3. Sealed coatings have superior resistance to corrosion induced by galvanic couples.
4. Sealed coatings have smoother surface profiles.
5. Sealed coatings allow thinner total coating systems to be applied.

Sealed Coatings for Gun Barrels - A logical application for these sealed coatings, such as SermeTel 725, is on gun barrels. Severe corrosion problems exist on 20 mm and 30 mm cannon systems since they are exposed to rapid heating, thermal shock and saline environments. These problems are seen on naval guns as well as those that are aircraft mounted.

To evaluate the performance of candidate coatings, Robbins Air Force Base conducted a test on 20 mm Vulcan cannon barrels.

Three coatings were evaluated (1) SermeTel 725, (2) MIL-C-46010 Corrosion Inhibiting Dry Film Lubricant, and (3) Phosphate and paint. The exteriors of two barrels were coated with each coating before assembly into the six barrel gun.

The test consisted of firing 200 round bursts from the gun at the rate of 4000/6000 rounds/minute cycled with salt spray exposure. During the firing, muzzle temperatures reached about 700°F, in the coolest area of the barrel. Other areas reached temperatures exceeding 1000°F. After 31,000 rounds had been fired through each barrel, the gun was disassembled.

Upon examination, the barrels coated with dry film lubricant and the phosphate/paint system were severely corroded. The SermeTel 725 coating had darkened but showed no red rust or adhesion loss.

A further coating benefit was observed when the barrel bores were examined. Although 31,000 rounds had been fired through each barrel the barrels coated with SermeTel 725 showed little bore erosion. It was estimated that although 47,000 rounds is considered maximum barrel life, the barrels coated with SermeTel 725 still had another 40,000 rounds of life. Presumably, the dense aluminum filled coating not only protected the outside of the barrel against corrosion and oxidation, but provided improved lateral heat transfer eliminating hot spots and keeping the barrel cooler, thus slowing the softening rate of the chromium plating in the bore.

These sealed coatings have been specified on the GE Goalkeeper gun system.

Further Coating Improvements - The introductions of smoother coatings and sealed coatings conforming to MIL-C-81751B were the first two lines of coating process development work completed. A further development combined the best features of the improved processes to result in a coating system that is both smooth, like SermeTel Process 5375® and sealed like SermeTel 725. The resulting process, SermeTel Process 5380®, has an extremely smooth surface finish (10 microinches AA at 0.10 cutoff) and because of the topcoat/sealer layer can maintain that smooth surface through long term exposure to saline environments and thermal cycling. An additional benefit of the coating system is the improved erosion resistance designed into the coating by pigment selection.

The concept of pigment selection is essential to the third area of coating improvements. That improvement centers around

methods of decreasing the porosity of coatings that conform to MIL-C-81751B Type I. It was reasoned that by reducing porosity internally in addition to adding a sealant topcoat layer, coating performance could be further improved. This was done experimentally by eliminating the conventional atomized aluminum powder generally used in the coating and substituting a specially prepared aluminum powder having improved particle size, shape and particle size distribution.

The results of these evaluations indicated that by proper pigment selection improved coatings could be produced. These improved coatings have greater uniformity in pigment packing resulting in improved particle to particle bonding, improved surface finish and decreased porosity. The result is improved corrosion resistance. Use of this improved basecoat which conforms to MIL-C-81751B Type 1 Class 4 with topcoat/sealer layers has resulted in a further improvement in smooth sealed coatings for turbine compressor airfoils. The new coating system, SermeTel Process 5380® D.P. not only has all the properties of preceeding sealed coatings, but also has improved erosion resistance and surface finish. This data is summarized in Tables V and VI.

TABLE V

EROSION RESISTANCE COMPARISON
(ASTM D968)

Coating System	Erosion Coefficient (liters/mil)
MIL-C-81751B Type I Class 4	100
Process 5380	300
Process 5380DP	> 500

TABLE VI

SERMETEL SURFACE FINISH PROGRESSION

Date	Process	Surface Finish (Microinches AA at 0.10 cutoff)
1970	MIL-C-81751B Type I Class 4	55*
1973	Process 5375	35

1977	Process 5375	15-25
1980	Process 5380	10
1985	Process 5380DP	3-5

*Measured on individual blades, values may vary depending on part geometry.

This advanced coating system results from 15 years of development work, each incremental step resulting in some improved coating property. This development work is still continuing.

Coatings for Acidic Environments - One last area of coating development relates to improved coatings for severe environments. In the last quarter century, acid rain has increased corrosion rates significantly. The presence of sulfur and nitrogen in fossil fuels results in SO_2 and NO_x after combustion. These gases readily dissolve in water forming acidic condensation having pH values as low as 3.5. Conditions on fossil fuel powered ships and in turbine engines are worse causing severe pitting damage to a wide variety of hardware. This pitting failure is of particular concern when failure occurs in applications where coatings normally resistant to salt fog are being used.

An area of concern in any development program is acceptable test methods for evaluating candidate coatings. In evaluating coatings for acidic rain conditions, standard salt spray testing is not a useful tool. Figure 9 shows results of standard salt spray testing of four coated samples on mild steel panels. The four coatings listed are 1) W4 (SermeTel W Class 4, conforming to MIL-C-81751B Type 1 Class 4), 2) 725 (SermeTel 725 - as W4 but sealed with SermeTel 570A), 3) 2241 (SermeTel Process 2241 - an improved smoother sealed coating with a basecoat conforming to MIL-C-81751B Type 1 Class 4), and 4) STS-EF-1 (a coating specifically formulated for acidified environments.) Note that all coatings tested resist neutral salt spray and show no base metal corrosion after 1000 hours. The conclusion is that the salt spray test is not a good tool for sorting these candidate coatings.

A list of accelerated test methods taken from a recent publication[8] is shown in Table VII. Unlike the other acidified test methods, the copper accelerated acetic acid salt spray or CASS test (ASTM B368) is standardized, repeatable and widely used. A conventional salt spray chamber is used. However, the test method does not model any specific environment.

TABLE VII

ACCELERATED TESTING METHODS

Test	pH	Salinity	Temp.	Contaminants
Neutral salt spray (ASTM B117)	6.5-7.2	5% NaCl	35°C	None
CASS (ASTM B368)	3.1-3.3	5% NaCl	49	Acetic acid, $CuCl_2$
Kesternich (DIN 50018)	1.0-2.0	None	40	SO_2 and other gases
SO_2/salt spray	4.0	5% NaCl	36	SO_2(aqueous)
HCl/salt spray	1.0	9% NaCl	36	HCl(1%), $FeCl_2$(0.1%)
H_2SO_3/NaCl immersion	4.0	5% NaCl	76	H_2SO_3, O_2 (.32 atm)

Panels representing the same four coating systems were tested in the CASS environment. Results are shown in Figure 10. Note that, unlike salt spray test results, failure can occur in less than 100 hours and that the coatings divide into three groups: (1) a sacrificial aluminum coating exposed to the environment fails first, (2) a pair of sealed coating systems performs significantly better, (3) a coating specifically designed to operate in the acidified environment is best.

These results are consistant with the nature of the acidic environment. At the pH of the CASS test there is no sacrificial action possible. Aluminum does not sacrifice, it corrodes rapidly. The sealed coatings have no aluminum pigment exposed to the acidic environment, but eventually through porosity or condensation the top coat film is compromised and corrosion occurs.

The STS EF1 coating is designed to utilize the best of the developments previously described. It utilizes a topcoat sealer to reduce corrosive attack on the aluminum pigment. It utilizes aluminum pigments selected for maximum pigment density and packing to eliminate pinholes and porosity. Further, it

incorporates corrosion inhibitors to neutralize any corrosive media that penetrates the topcoat/sealer.

Because the greatest corrosion problems observed have included both acid rain exposure and heat cycling, two additional tests were performed that combined these features. Figures 11 and 12 illustrate the performance of the four coatings under these conditions. Figure 11 shows results after heat cycling to 400°F for 6 hours, 2 hours cooling and 16 hours in CASS. This cycle is repeated up to ten times. Similarly, Figure 12 shows a heat cycle CASS test in which the cycle temperature is 850°F. Note the rapid failure of all systems except the coating specifically designed for the acid rain condition.

The STS EF-1 coating is a new system. It is undergoing extensive testing in a wide variety of acidic environments. Unfortunately, the coating does not meet the military specification because the additional performance requirements make modifications of the basic composition necessary.

Conclusion

Coatings designed to meet MIL-C-81751 have been in use for a quarter century. During this period the coatings have been improved as conditions of operation have changed. Now, topcoated systems are almost universally used because of superior performance. Work continues to extend the possible uses of this adaptable coating system.

SEM PHOTOMICROGRAPHS OF MIL-C-81751B

TYPE I COATING CLASSES (SERMETEL W)

Figure 1: Class 1, 2 and 3 Coatings, 300X, 45° angle.

Figure 2: Class 1, 2 and 3 coatings, 1000X, 45° angle.

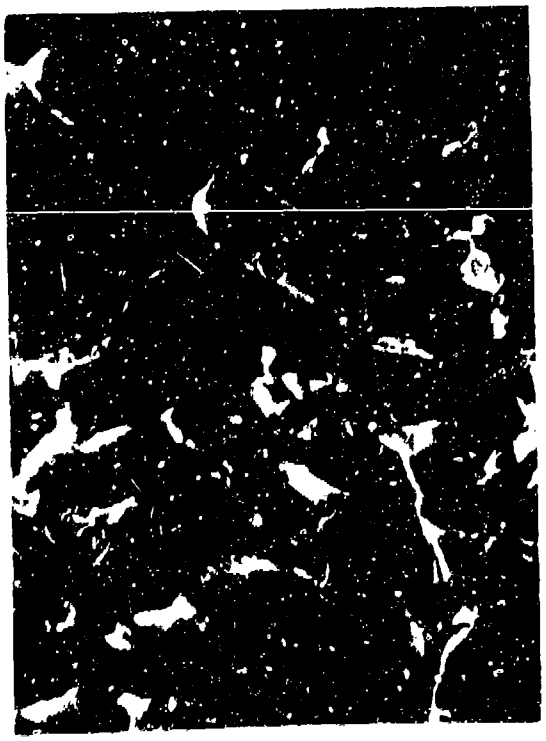

Figure 3: Class 4 coating, grit burnished, 1000X, 45° angle.

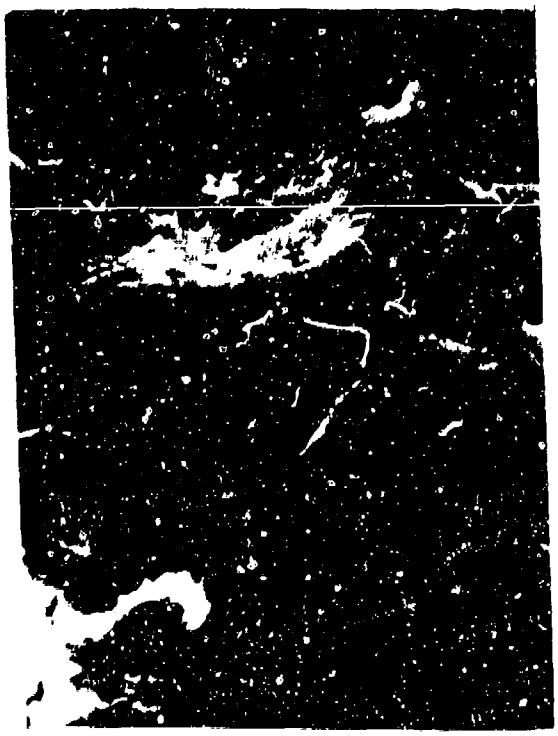

Figure 4: Class 4 coating, glass bead burnished, 1000X 45° angle.

171

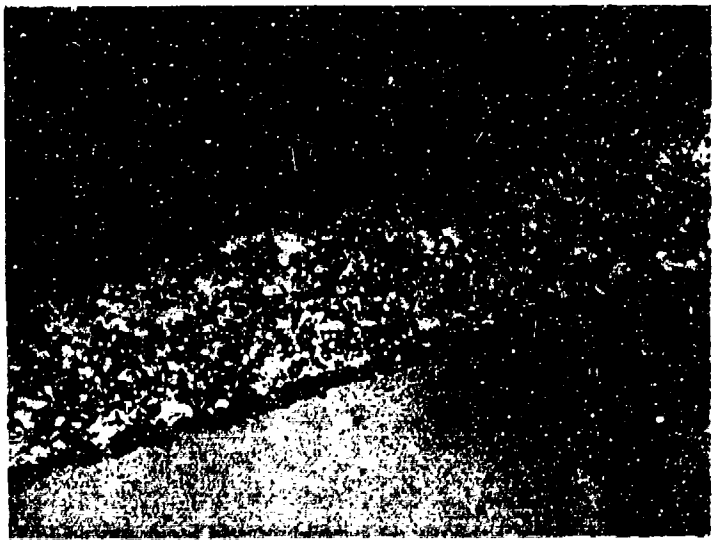

Figure 5: Cross Section optical photomicrograph of a Class 1 coating (SermeTel W) 500X

Figure 6 SEM Photomicrograph of a Class 1 coating surface 1000X

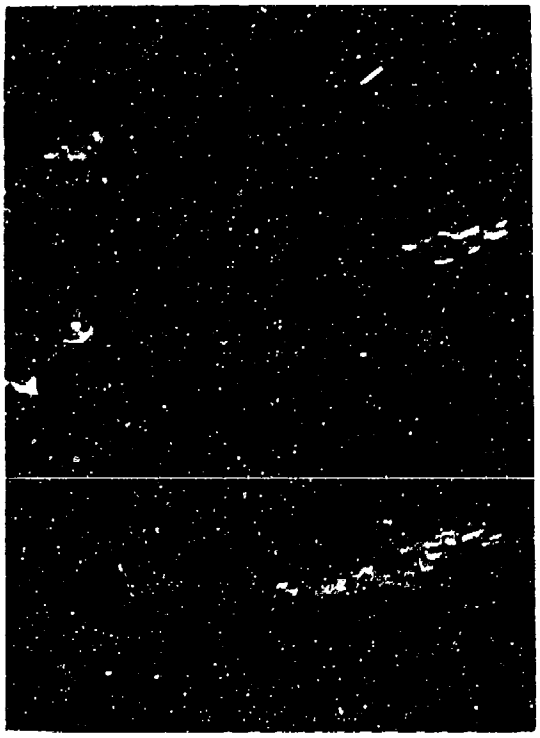

Figure 7: SEM Photomicrograph of the Surface of a Sealed Class 4 coating (SermeTel 725) 1000X

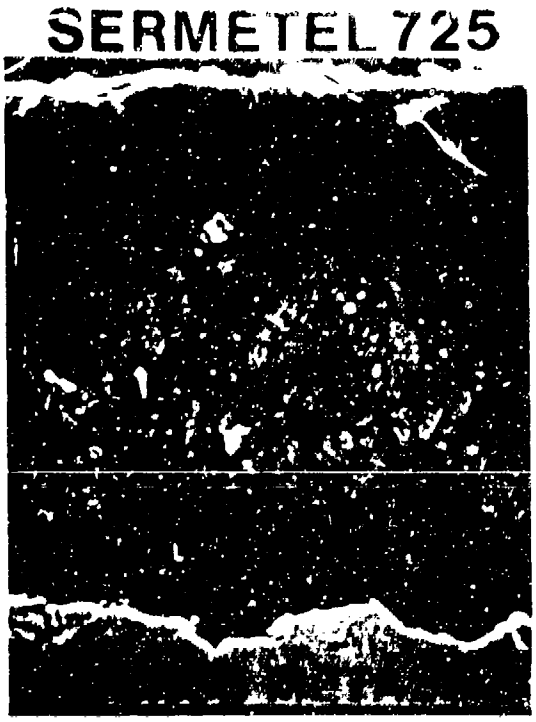

Figure 8: SEM Photomicrograph of a cross section of a sealed Class 4 coating (SermeTel 725) 1500X

COMPARATIVE PERFORMANCE OF VARIOUS SERMETEL COATING SYSTEMS IN ENVIRONMENTAL TESTS

FIGURE 9

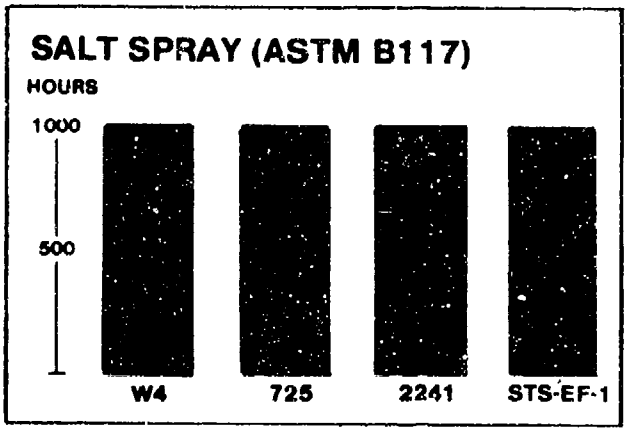

FIGURE 10

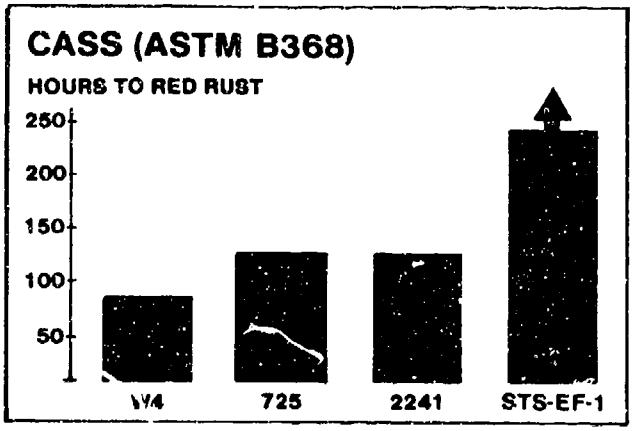

FIGURE 11

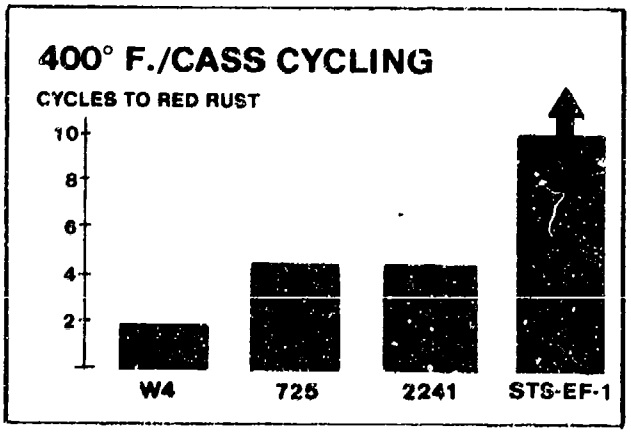

FIGURE 12

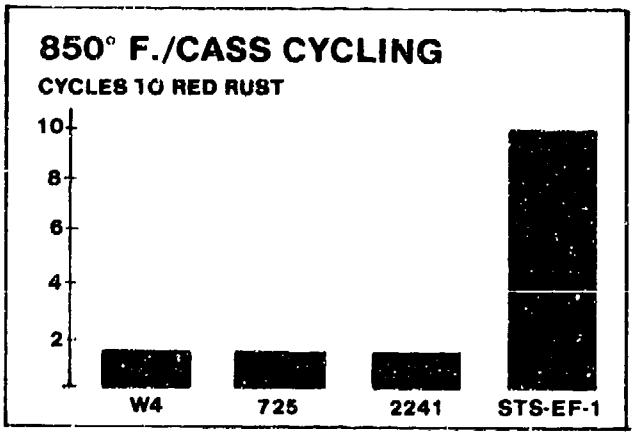

References

(1) Allen, C (1966) U.S. Patent 3,248,251

(2) Mosser, M. F. and McMordie, B. G., "Evaluation of Aluminum Ceramic Coatings on Fasteners to Eliminate Galvanic Corrosion". SAE Technical Paper 860112, taken from SP-64. Corrosion: Coatings and Steels; Presented at the SAE International Congress and Exposition, Detroit, Michigan - February 24-8, 1986.

(3) Mansfeld, F., Galvanic Corrosion of Al Alloys Coupled to Coated PH 13-8 Mo Stainless Steel", Corrosion, Vol. 29, No. 7, July, 1973, p. 277.

(4) Newhart, J. E., "Evaluation of SermeTel 735 in a T400-CP-400/402 Full Scale Salt Corrosion Test", NAPTC Report LR-77-22.

(5) Wanhill, R. J. H., Kolkman, H. J., Mom, A. J. A., van Gestel, F. G. J. A., "Prevention of Corrosion and Fatigue Failure of Helicopter Gas Turbine Compressors", Presented at the Sixth European Rotorcraft and Powered Lift Aircraft Forum, September 16-19, 1980 Bristol, U.K.

(6) Jankowsky, E. J., "Shipboard Exposure Testing - USS America", Progress Report NADC-82101-60 Naval Air Development Center, Warminster, PA.

(7) Rogus, B. J. and Vapniarek, F. J., " Testing of External Coating Systems for the Corrosion Control of Steam Valves", Naval Ship Systems Engineering Station, Philadelphia, PA., in Proceedings of the 1980 Tri-Service Conference on Corrosion.

(8) McMordie, B. G., and Mosser, M. F., "Evaluating Turbine Compressor Coatings for Acidified Environments", ASME 86-GT-290, Presented at the International Gas Turbine Conference and Exhibit, Dusseldorf, West Germany, June 8-12, 1986.

CARBOXYLATE FORMATION AT THE INTERFACE BETWEEN A POLYIMIDE COATING AND COBALT

Richard D. Granata, Philip D. Deck and Henry Leidheiser, Jr.

Department of Chemistry and the
Zettlemoyer Center for Surface Studies
Sinclair Laboratory #7
Lehigh University
Bethlehem, PA 18015

Tri-Services Corrosion Conference
US Air Force Academy
Colorado Springs, CO
May 5-7, 1987

ABSTRACT

The interfacial region between a polymer coating and a metal substrate was studied using three techniques. Each technique permitted interface integrity and was performed under normal atmospheric pressure conditions. Infrared analysis of the polymer at the interface was accomplished by using an internal reflectance technique through an optically thin metal film. A second infrared technique employed photoacoustic spectroscopy of thin polymer films on high surface area metal substrates. Emission Mössbauer spectroscopy, made surface sensitive by depositing less than a monolayer of ^{57}Co on a cobalt substrate, permitted evaluation of the chemical changes occurring on the cobalt substrate as a result of polymer coating application and cure. Each technique revealed the presence of metal carboxylates within the interfacial region. These carboxylates may provide primary bonding between coating and substrate.

INTRODUCTION

One of the major uses of polymer coatings is metal substrate protection against corrosion. Protective organic coatings have intimate contact between coating and metal. Such contact may yield chemical interactions between the organic and metal components which may beneficially or adversely affect the utility of the polymer/metal system.

BEST AVAILABLE COPY

The research described herein is part of a program designed to understand better the protection provided by organic coatings to metal substrates. A focus of this research is to understand the chemistry of the interface between coating and substrate and to predict its influence on coating performance. One of the polymers under study, polyimide (PI), is of current interest because of its applications in the fabrication of electronic devices. Polyimide is a tough polymer with outstanding thermal and electrical properties. The results described herein may be applicable to other polymer systems that have intrinsic or latent carboxylate moieties.

This paper describes some of the methods selected to probe the chemistry of the interface and presents data for polyimide and poly(acrylic acid) on cobalt, copper and zinc, as well as our current hypothesis for the interfacial chemistry.

BACKGROUND

Acquiring information on the interfacial region between coating and metal substrate is no trivial task. Because the interface represents the junction between two dissimilar bulk materials, shown schematically in Figure 1, experimental methods suitable for one component may not be suitable for the study of the other. Further, direct experimental access to the interface is hindered by the two components which make up the interface. This second problem has been eliminated in the study of coating/substrate interfaces by a number of investigators by peeling the coating from the substrate and then carefully analyzing both halves of the interface separately. Such techniques suffer from the disadvantage that the subject of interest, the interface, has been destroyed.

We have chosen to keep the interface intact during our analyses. Indeed, fulfilling the following criteria would constitute an ideal study of the interface.

1) The method should be interface-specific.

2) In keeping with criterion #1, the method should provide information on both the coating and the substrate.

3) The method should be non-destructive.

4) The method should be widely applicable to many systems.

5) The method should allow for concurrent analyses and/or environmental control.

The techniques we have chosen to analyze the coating/metal interface are internal reflection infrared spectroscopy, photoacoustic IR spectroscopy and emission Mössbauer spectroscopy. By sampling through an optically thin metal substrate into the coating using the internal reflection technique we are able to identify chemical moieties in the coating at the interface and draw conclusions as to the coating chemistry at the interface. The photoacoustic technique allows similar sampling through a thin coating on a high surface area substrate. The Mössbauer technique is made interface-sensitive by electrodepositing a monolayer of the active cobalt species onto the sur-

BEST AVAILABLE COPY

face of a cobalt substrate. The Mössbauer spectra obtained provide information on the chemical state of the cobalt in contact with the coating, thus enabling us to draw conclusions about the reactivity of cobalt with the coating.

None of these techniques alone fulfills all the criteria cited for an ideal interfacial study. However, together they complement each other to yield chemical information at the coating/substrate interface without its disruption.

EXPERIMENTAL

Internal Reflection FTIR -Internal reflection infrared spectroscopy permits analysis of a sample to depths of a fraction of the incident radiation wavelength (for IR techniques, depths of several microns). Control of the sampling depth, d_p, can be made by choice of the refractive index ratio between sample, n_2, and internal reflecting element, n_1, and the angle of incidence, θ, (see Figure 2) as given by Harrick [1],

$$d_p = \frac{\lambda}{2\pi n_1 [\sin^2\theta_1 - (n_2/n_1)^2]^{1/2}}$$

As an example, a KRS-5 prism ($n_1 = 2.35$) in contact with a polymer of refractive index of 1.5 and an incident angle of 45°, the sampling depth ranges from 0.5 μm at 4000 cm^{-1} to 4.0 μm at 500 cm^{-1}.

Such sampling depths are far in excess of interfacial specificity; however, by applying the coatings to ultra-thin transparent metal films, we can obtain spectra at both the coating/air interface and the coating/metal interface. Calculation of the difference spectra provide information specific to the metal/polymer interface. Approximately 50 Å thick film of cobalt (99.99% purity) was evaporated at 10^{-6} torr onto a carbon-sputtered glass slide. The slide is carbon-sputtered prior to metal deposition to facilitate easy removal of both metal and organic coating from the slide. Poly(amic acid) (PAA) in N-methyl 2-pyrrolidone is then spin-coated onto the metallized slide. The first stage cure (A-stage) consists of stoving the material at 85°C for 12 min to drive off the solvent. The polymer film at this stage is still PAA. The B-stage cure requires 20 min at 200°C and results in an imidized material. Nominal polyimide (PI) coating thicknesses were 12±2 μm.

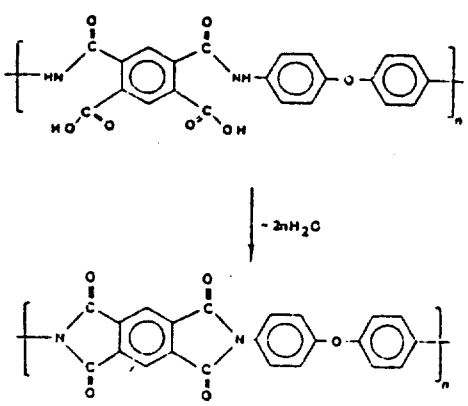

BEST AVAILABLE COPY

After either A- or B-stage cure, the polymer and metal were peeled from the slide as shown in Figure 3. The sample was mounted onto a foam strip with metal side down or metal side up to allow sampling through either the coating/air or the coating/metal interface.

Spectra were obtained at 4 cm^{-1} resolution on a Mattson Sirius 100 Fourier Transform Infrared Spectrometer. The sample spectra were ratioed against a background spectrum obtained for the KRS-5 prism alone. Direct comparison of the spectra obtained from the air versus metal side of the coating was made by a spectral subtraction technique.

Photoacoustic Spectroscopy - The internal reflection technique used to determine the interfacial interactions has the disadvantage of excess sampling depth (0.5-4 μm) into the polymer. Thus, chemistry that is specific to the interface will be represented in the resulting spectra only as a minor component. Another mode of IR sampling was desired to provide additional support for the results obtained with the internal reflection technique.

The wide variety of sample configurations adaptable to this technique permitted us to analyze an ultra-thin polymer film on a high surface area metal sample. The sample was prepared by stirring metal powder in a 1% polymer solution. The powder was removed from the solution and the solvent allowed to evaporate. For polyimide, curing times were decreased 50% relative to 10 μm thick polymer films. After curing, any excess polymer film was removed and the powder was collected. No attempt was made to determine the fraction of metal covered with polymer.

Figure 4 shows a schematic of the PAS IR/sample interaction and signal detection. A sample is placed in the sample cup and sparged with helium gas. A modulated IR beam is directed onto the sample through a NaCl window. At frequencies where no absorption occurs, the incident radiation is either reflected or transmitted. However, at those frequencies where absorption occurs, the infrared energy is converted to thermal energy. The thermal energy creates a pressure wave within the cup cell which is detected by a sensitive microphone. Signals to the detector arise only where absorption of that particular frequency occurs. The Fourier transform technique allows for repeated modulation so that the resulting signals can be summed to increase the signal-to-noise ratio.

The metal powder with polymer was placed in the sample cup of the PA FTIR spectrometer, IBM Model 97, and the spectrum recorded. The spectrum was ratioed against a background spectrum obtained for the metal powder alone.

Since poly(amic acid) was believed to react with certain metals to form metal carboxylate species, poly(acrylic acid) (PAC) was used to determine the possibility that a polymer group chemically reacts with a metal substrate. PAC has a much higher density of acid groups and is more flexible than PAA. In addition, the acid group is the only functional group on PAC, simplifying the resulting spectra and eliminating other complications.

Mössbauer Spectroscopy - This nuclear resonance technique provides detailed information on the electronic state of metals. In emission geometry, the sample serves as the source of gamma rays (Figure 5). The sample

is made the source by doping the sample with the Mössbauer active nuclide or its precursor (^{57}Co in these experiments) into the sample.

An electrodeposition method based on the technique of Deszi and Molnar [3] using $^{57}CoCl_2$ in a hydrazine and an ammonium citrate bath was utilized to form a thin layer of radioactive cobalt. Deposition times ranged from 4 to 8 h to ensure a sufficient concentration of the nuclide on the surface. The surface concentration was estimated to be 10^7 Bq. Although this concentration amounts to less than a monolayer of cobalt deposited by weight, it must be borne in mind that the deposit exhibited an island-like morphology as revealed by electron microscopy. An ^{57}Fe-enriched stainless steel foil was used as the absorber.

Mössbauer spectra were recorded at room temperature after cobalt deposition and following subsequent polymer castings and cures. In this way the chemistry of the surface of the cobalt was monitored by spectral changes occurring as a consequence of polymer coating or cure. In addition to PI, PAC was also used as a coating. A linear combination of the Lorentzian function was used for evaluation of the spectra.

RESULTS

Internal Reflection FTIR - There exist no notable differences between polymer at the metal or air interface for PAA as seen in the spectra in Figure 6. Both spectra reveal the characteristic stretching and bending modes expected for PAA. The carbonyl stretch region reveals a number of species: a benzanilide moiety is represented as a medium peak at 1717cm^{-1} and the overlapping peaks at 1638 and 1605 cm^{-1} are given the assignments of intramolecularly H-bonded acid and secondary amide, respectively. The band at 1539 cm^{-1} is assigned to the N-H bending mode. The aromatic ether C-O stretch (1229 cm^{-1}) overlaps with the C-N stretch at 1211 cm^{-1}. An aromatic C-C stretch is found at 1497 cm^{-1}.

The difference spectrum (metal less air interface) shown in Figure 7 reveals chemical bonds more prevalent at the metal interface. The most prominent feature of this spectrum is the band at 1377 cm^{-1} which is given the assignment of a symmetric C=O stretch of a carboxylate ion. The asymmetric stretch is found at 1576 cm^{-1}. Further support for these assignments is given by the decrease in the O-H bending mode at 1410 cm^{-1}. The frequency difference between the asymmetric and symmetric carboxylate stretches provides a basis for the identification of the nature of the carboxylate present. For PAA/Co this difference is 199 cm^{-1}, which is of the order of ionic carboxylates (copper(II) formate has a $\Delta\nu$ = 181 cm^{-1}[4]).

After B-stage cure, the IR spectrum (Figure 8) reflects the imidization of PAA to PI. The emergence of a peak at 1777 cm^{-1} is representative of the carbonyl stretch for a coupled imide. The benzanilide C=O stretch at 1717 cm^{-1} has increased substantially as has the C-N stretch at 1370 cm^{-1}. The bands at 1638, 1605, and 1539 cm^{-1} have all decreased in intensity indicative of the decrease in acid and 2° amide functionalities in the imidized polymer. The peaks at 1495 (aromatic C-C) and 1229 cm^{-1} (aromatic ether C-O) remain virtually unchanged. Differences in the two spectra obtained for PI are subtle, but nevertheless indicative of further polymer/substrate interaction. The spectrum obtained for PI at the cobalt

interface reveals a shoulder at about 1670 cm^{-1} and the emergence of a small peak at 1530 cm^{-1}.

These and other differences are revealed more clearly in the difference spectrum (Figure 9). The difference spectrum reveals peaks at 1584 and 1397 cm^{-1}; similar peaks were observed in the PAA difference spectrum and assigned as the asymmetric and symmetric stretches of a carboxylate carbonyl, respectively. These peaks in the PI difference spectrum are given the same assignments since one would expect these species to exist in the imidized polymer. Moreover, one observes an enrichment of N-H bonds (positive peak at 1300 cm^{-1}) and a depletion of C-N bonds (negative peak at 1370 cm^{-1}) at the PI/cobalt interface. These data provide further evidence of the presence of interfacial carboxylates.

The most prominent feature of this difference spectrum is the strong band at 1647 cm^{-1}. An assignment to this absorbance is not easily made. In fact, two different assignments seem equally plausible. The peak may arise from complexation of the imide oxygen with cobalt. Rollinson and White [5] have shown that such complexation with chromium(III) lowers the frequency for the amide C=O stretch by 10 to 70 cm^{-1}. The shift observed for the present case is 64 cm^{-1}, within the range cited. Alternatively, one may propose a unidentate coordinated carboxylate forming between the PI and the cobalt. Such a species would require C-N bond scission. Unidentate coordinated carboxylates give rise to a larger $\Delta\nu$ value than the ionic carboxylates, as the asymmetric stretch is shifted to higher and the symmetric to lower frequencies [6]. Hence, the large peak at 1647 cm^{-1} could be given the assignment of the asymmetric stretch and the peak at 1339 cm^{-1} assigned as the symmetric C=O stretch.

Photoacoustic Spectroscopy - The photoacoustic infrared spectra for PAC on copper, cobalt and zinc are shown in Figure 10. The spectrum for PAC on copper shows the $\nu_{C=O}$ for a carboxylic acid at 1720 cm^{-1}. For PAC on cobalt and zinc, the major band for $\nu_{C=O}$ is found at ~1580 cm^{-1} which is indicative of the asymmetric stretch for a carboxylate anion. In addition, a peak is observed at 1360 cm^{-1} indicative of the symmetric carboxylate stretch. These bands compare well with the tentative carboxylate assignments given for the internal reflection data with PAA. A comparison of the bands is given in Table 1.

Thus the IR data indicate the existence of a chemical interaction between PAA, PAC or PI with cobalt. Moreover, we have proposed, based on these data, that the interaction results in the formation of an ionic cobalt carboxylate species in PAA and PAC. Upon imidization, in addition to the presence of the ionic carboxylates, the IR data suggest further interaction, either through a complexation of the imide oxygen or the formation of a unidentate coordinated carboxylate. To confirm or refute our tentative assignments in the IR and to provide us with some sort of mechanistic approach to the chemical interaction occurring at the interface, we now consider the previously published Mössbauer data [2].

Emission Mössbauer Spectroscopy - Figure 11 shows a representative Mössbauer spectrum of a ^{57}Co electrodeposit on a cobalt foil. The spectrum reveals that the deposit is largely Co^{3+}. The hyperfine parameters suggest the compound, CoOOH. The spectrum also indicates the presence of metallic cobalt and $Co(OH)_2$. After coating this same electrodeposit with PAA and

curing at 85°C, the spectrum shown in Figure 12 is obtained. It is readily apparent that the metallic cobalt has been totally consumed to yield an increase in the Co^{2+} fraction. Closer inspection of this Co^{2+} fraction indicates a change in the hyperfine parameters, namely δ = -1.20 mm/s and ΔE = 2.03 mm/s. These values more closely match those given by Grant and coworkers for bulk $FeC_2O_4 \cdot 2H_2O$ (δ = 1.20 mm/s, ΔE = 1.72 mm/s) and bulk $FeCO_3$ (δ = 1.24 mm/s, ΔE =1.80 mm/s) [7] and by Friedt and Asch for bulk $CoC_2O_4 \cdot 2H_2O$ (δ = 1.28 mm/s, ΔE = 1.72 mm/s) and bulk CoC_2O_4 anhydride (δ = 1.27 mm/s, ΔE = 1.55 mm/s) [8] than for $Co(OH)_2$ (δ = -1.34 mm/s, ΔE ranges from 2.32 to 2.80 mm/s) [9]. These data are tabulated in Table 2. Upon B-stage cure (Figure 13), the fraction of Co^{2+} in the deposit continues to increase, however, now at the expense of the Co^{3+} component rather than the metallic cobalt. Still, the hyperfine parameters were consistent with Co-O-C bonding rather than an oxide or oxy-hydroxide. This same trend has been observed in another experiment in which the electrodeposit initially showed mostly metallic character with no Co^{2+} component.

Because the literature values quoted represent bulk samples of these compounds, some degree of inaccuracy is to be expected. To alleviate some of the burden of relying too heavily on these values, a ^{57}Co electrodeposit was coated with poly(acrylic acid) cast from a methanol solution. The Mössbauer spectra obtained prior to and after PAC coating are shown in Figure 14 and reveal the significant increase in the Co^{2+} fraction at the expense of the metallic cobalt fraction. The hyperfine parameters of this Co^{2+} fraction, as shown in Table 2, support the hypothesis of cobalt carboxylates at the interface.

The Mössbauer data also provide us with a mechanistic approach to the formation of these carboxylates. Of the three components which make up the ^{57}Co electrodeposit, the metallic cobalt is observed to be the primary reactant with the acid moieties of PAA.

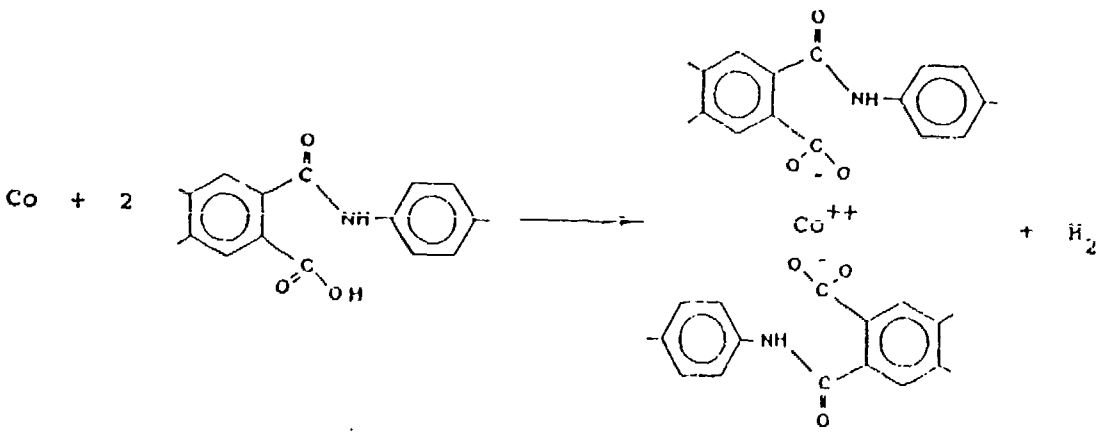

Cobalt has also been observed to react with PAC to form carboxylates. A modest increase in the Co^{3+} fraction at this stage may be rationalized in terms of a competing reaction with cobalt metal and water from the imidization reaction during cure.

$$4\ Co + 2H_2O + 3O_2 \rightarrow 4CoOOH$$

In addition, the CoOOH may also react with the PAA.

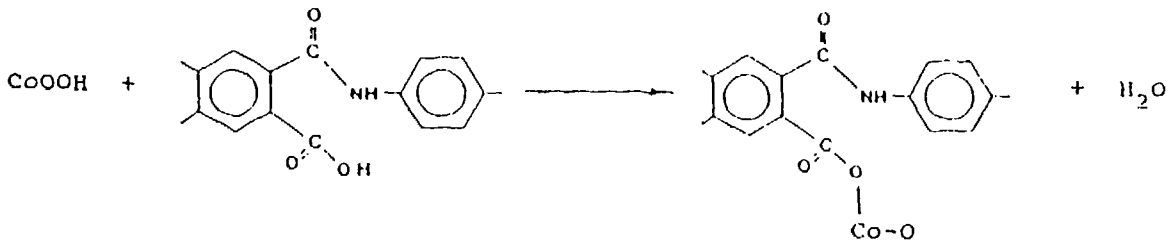

After imidization, further decreases in the Co^{3+} fraction with concomitant increases in the complexed Co^{2+} fraction indicate that CoOOH may react with the PI.

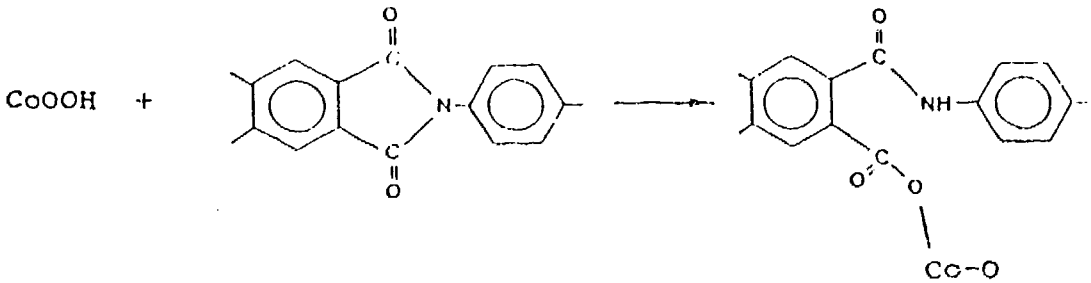

SUMMARY

The infrared and Mössbauer techniques revealed the existence of cobalt carboxylates formed at the interface. It has been shown that the metallic cobalt was reactive with the acid groups of PAA. Cobaltous ions act as cross-linking sites through carboxylate anions in the polymer. In addition, the carboxylates may provide a mode for cobalt cation transport into the polymer. The presence of these carboxylates was observed in the imidized polymer.

Upon imidization, another interaction between cobalt and PI is observed; the IR data suggest either a unidentate coordinated carboxylate or imide complexation with cobalt. Either of these species may promote adhesion of the coating to the substrate through the incorporation of primary bonding between coating and substrate.

Photoacoustic infrared spectroscopy provided useful corroborative information of internal reflection IR band assignments and an alternative sample preparation method.

It is the goal of our continuing research to understand better the effects of these interfacial interactions and their relationship to the development of organic coatings with greater protective properties.

ACKNOWLEDGEMENTS

The authors are grateful for the support provided by the Office of Naval Research for this study.

REFERENCES

1) N. J. Harrick, "Internal Reflection Spectroscopy", Interscience, New York (1967).

2) A. Vértes, I. Czakó-Nagy, P. Deck and H. Leidheiser, Jr., J. Electrochem. Soc. 134, 1628 (1987).

3) J. Deszi and B. Molnar, Nuclear Instruments and Methods 54, 105 (1967).

4) A. M. Heyns, J. Molecular Structure 127, 9-20 (1985).

5) C. L. Rollinson and R. C. White, Inorganic Chemistry 1, 281-285 (1962).

6) G. B. Deacon and R. J. Phillips, Coordination Chem. Rev. 33, 227-250 (1980).

7) R. W. Grant et al., J. Chem. Phys. 45; 1015 (1966).

8) J. M. Friedt and L. Asch, Radiochimica Acta 12, 208 (1969).

9) G. W. Simmons in "Passivity of Metals", R. P. Frankenthal and J. Kruger, eds., The Electrochemical Society, Inc., Princeton, NJ, 1978, pp. 898-917.

Table 1

Comparison of IR Bands for PAC and PAA

Polymer	Cobalt	Bands (cm^{-1}) Zinc	Copper
PAC	1360[a]	1360[a]	----
	1580[a]	1580[a]	----
	----	----	1720[b]
PAA	1377[a]	1377[a]	----
	1576[a]	1576[a]	----
	----	----	1717[b]

a - Carboxylate asymmetric C=O stretch.
b - Free acid band.

Table 2

Mössbauer Hyperfine Parameters for Co^{2+} Component

Sample	A (%)	δ (mm/s)	ΔE (mm/s)	ref.
Co-57 dp*	13.5	-1.21	2.40	2
PAA	34.7	-1.20	2.03	2
PI	46.0	-1.17	2.10	2
Co-57 dp*	0.0	---	---	2
PAA	10.5	-1.35	1.92	2
PI	15.8	-1.22	1.94	2
Co-57 dp*	1.7	-0.65	2.74	-
PAC	85.1	-1.06	1.83	-
α-$Co(OH)_2$	bulk	-1.34	2.32-2.80	9
$FeC_2O_4 \cdot 2H_2O$	bulk	1.20	1.72	7
$FeCO_3$	bulk	1.24	1.80	7
$CoC_2O_4 \cdot 2H_2O$	bulk	1.28	1.72	8
CoC_2O_4	bulk	1.27	1.55	8

* - dp (electrodeposited on cobalt)

4F

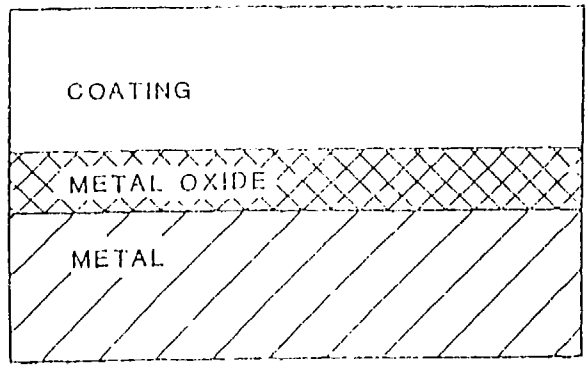

Figure 1. Schematic profile of an organic coating on a metal substrate.

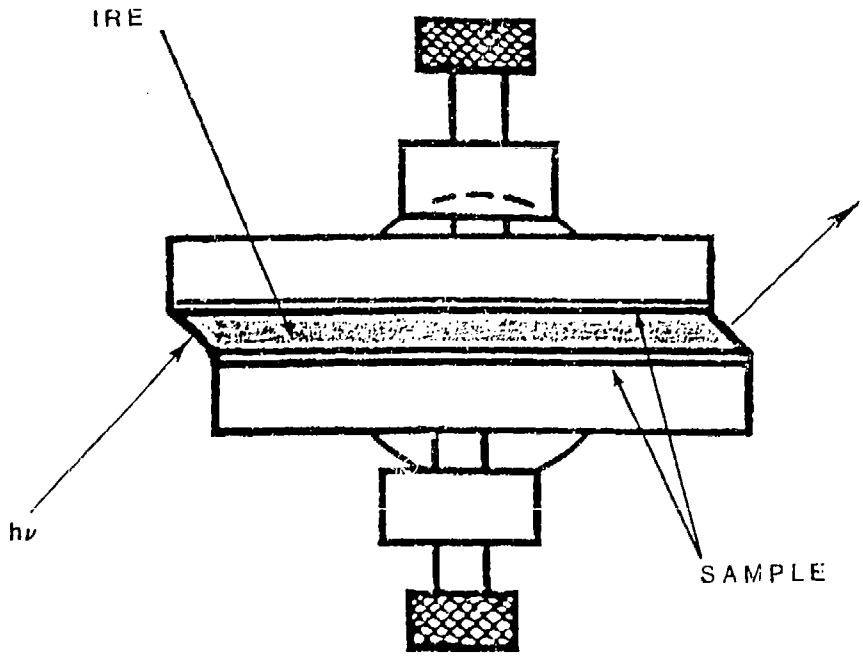

Figure 2 Sampling geometry for internal reflectance infrared spectroscopy. The infrared beam is incident upon the face of the internal reflecting element (IRE) and is internally reflected the length of the prism, penetrating into the sample a fraction of a wavelength upon each reflection.

SAMPLE PREPARATION

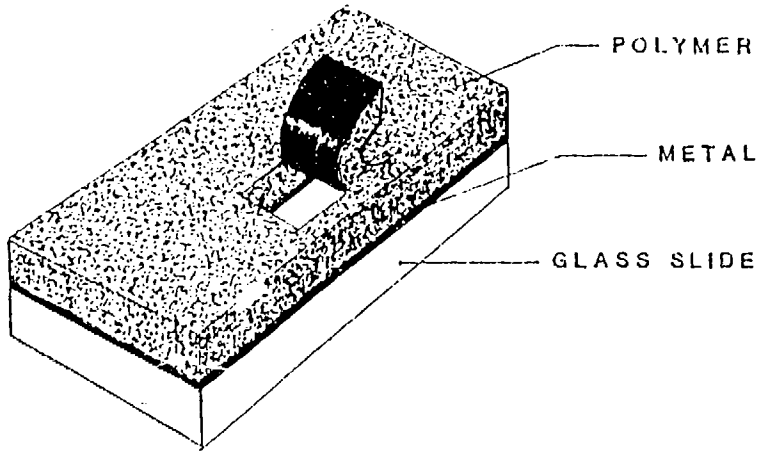

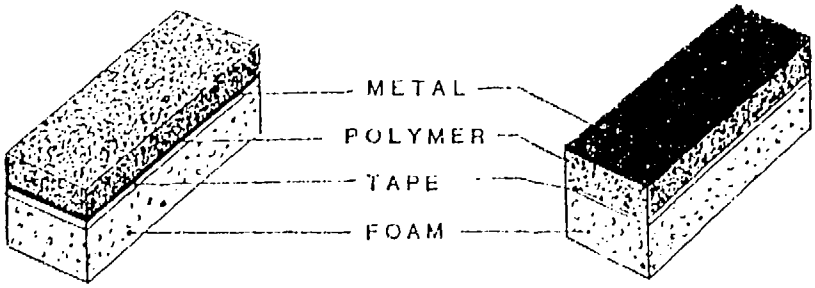

Figure 3. Specimen preparation for sampling the polymer through both the polymer/air and polymer/metal interfaces. The metal film thickness is about 50 Å.

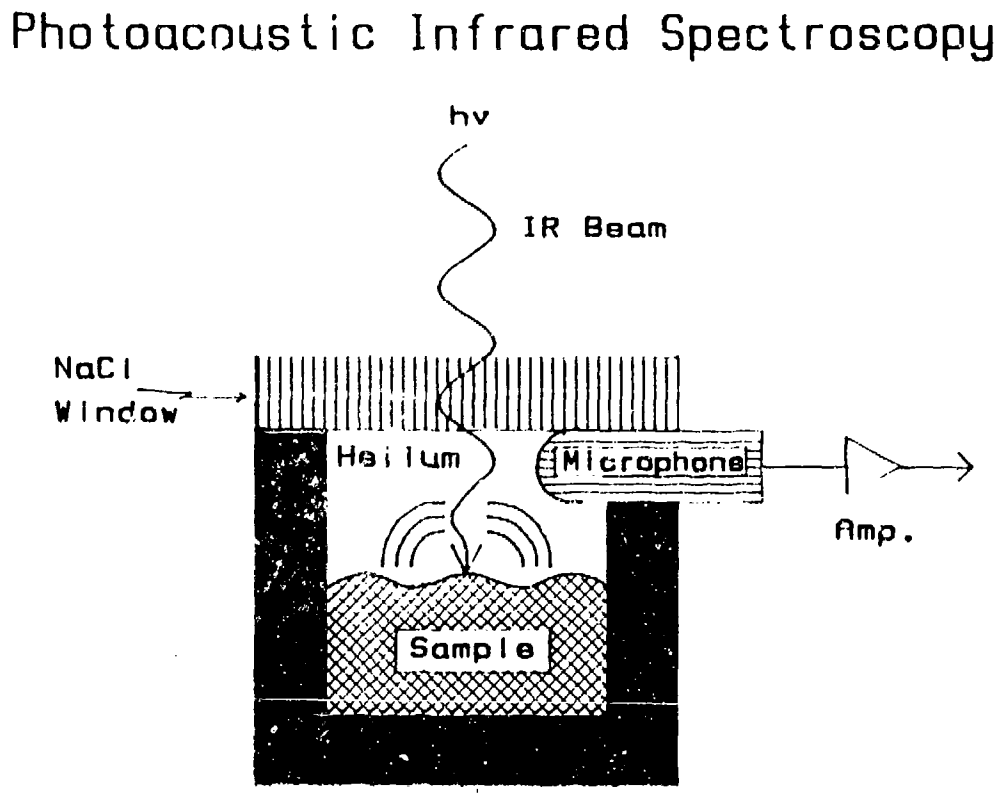

Figure 4. Schematic of the photoacoustic technique.

MÖSSBAUER SPECTROSCOPY

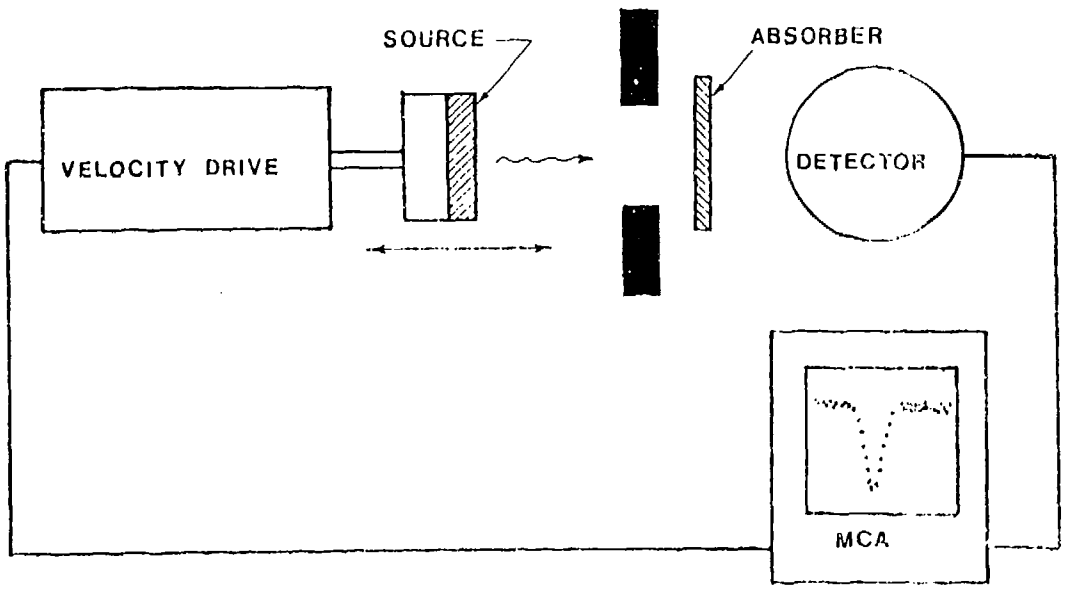

Figure 5. Schematic diagram of the set-up for a Mössbauer experiment. In emission geometry the sample serves as the source of gamma rays.

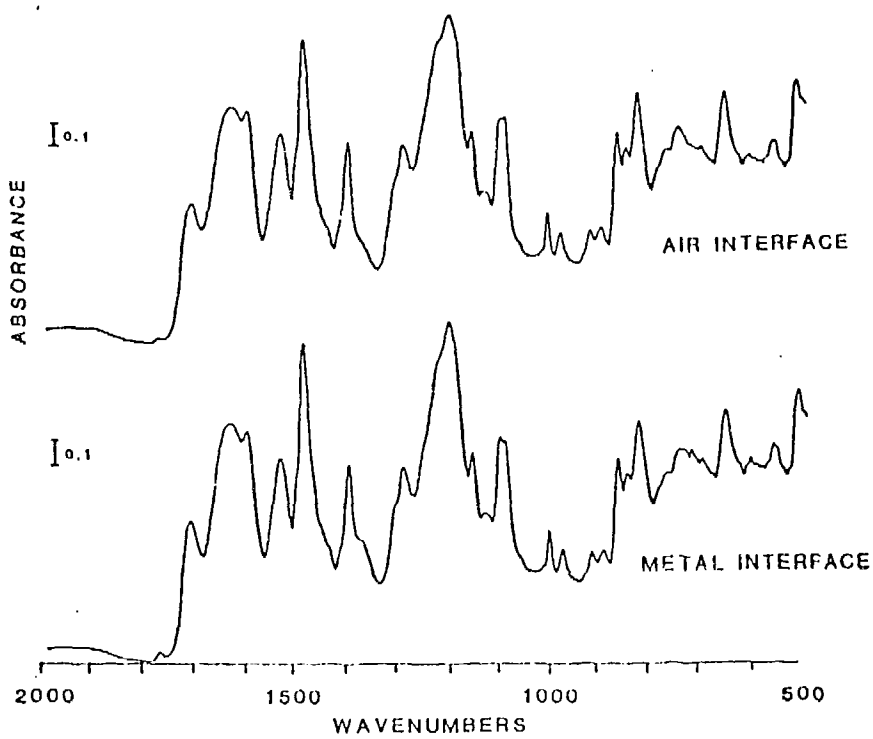

Figure 6. Infrared spectra for poly(amic acid) on cobalt at the a) polymer/air interface and b) polymer/metal interface.

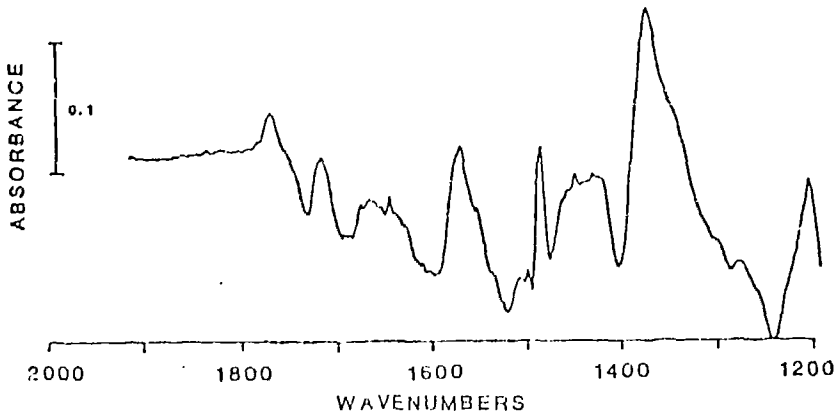

Figure 7. Infrared difference spectrum of poly(amic acid) on cobalt at the metal interface and at the air interface.

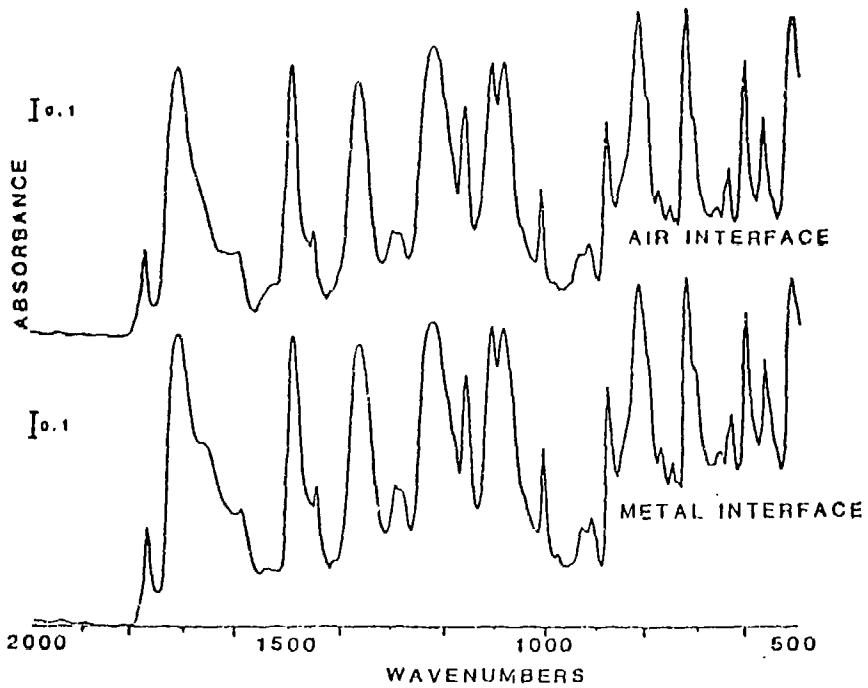

Figure 8. Infrared spectra for polyimide on cobalt at the a) polymer/air interface and b) polymer/metal interface.

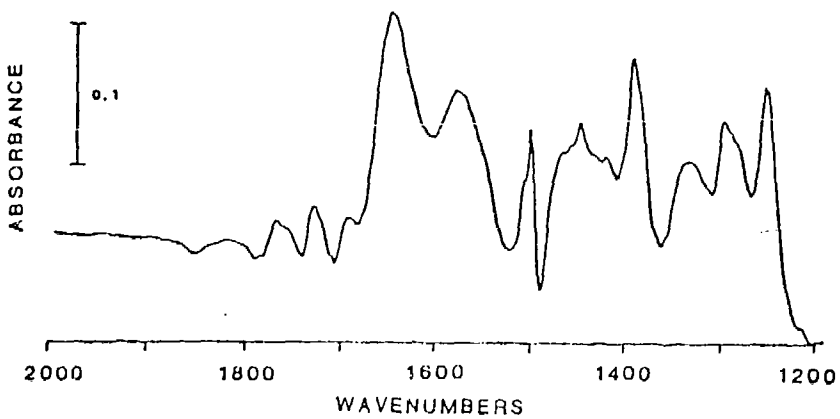

Figure 9. Infrared difference spectrum of polyimide on cobalt at the metal interface and at the air interface.

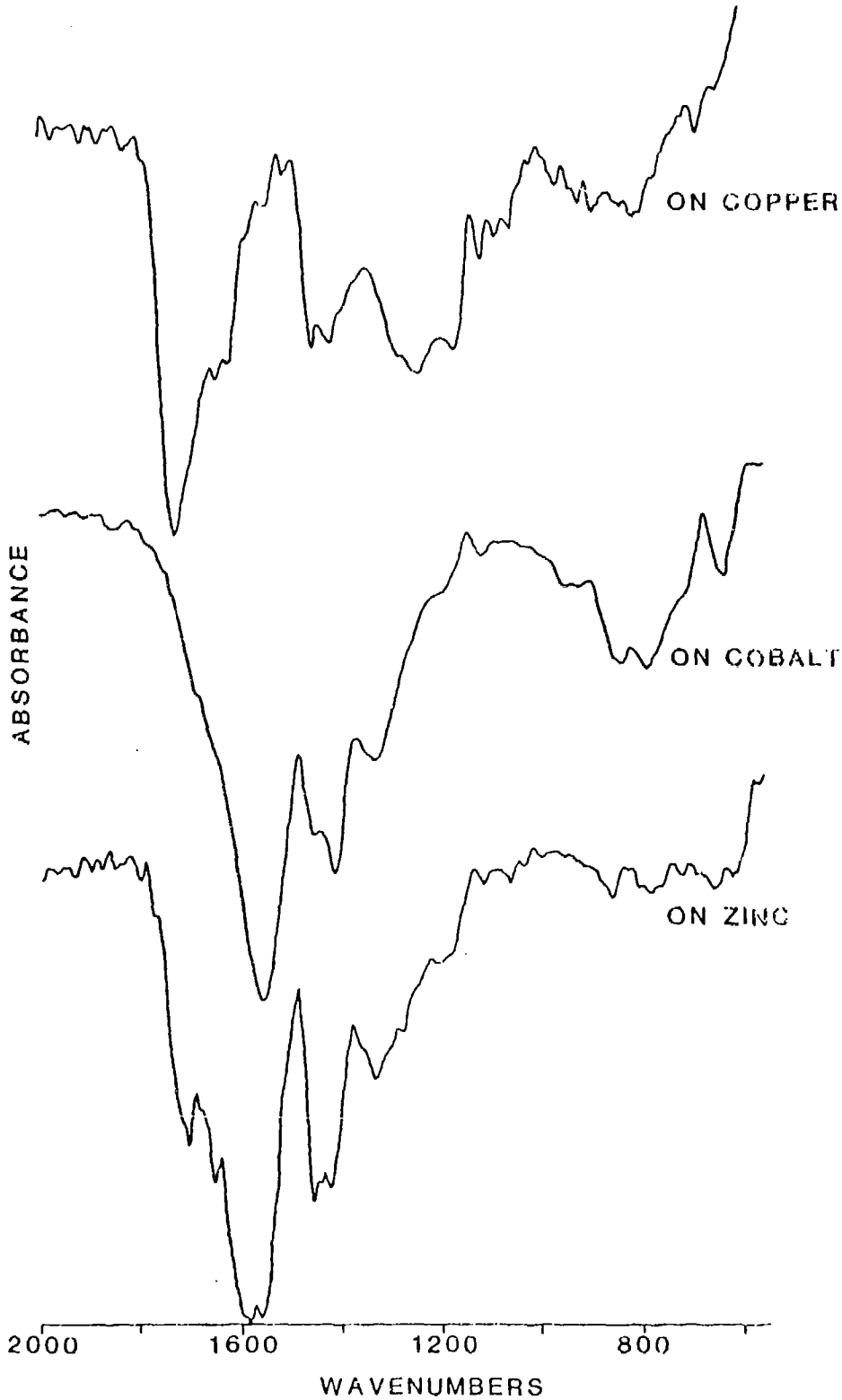

Figure 10. Spectra of poly(acrylic acid) on copper, cobalt or zinc substrates obtained using the photoacoustic technique.

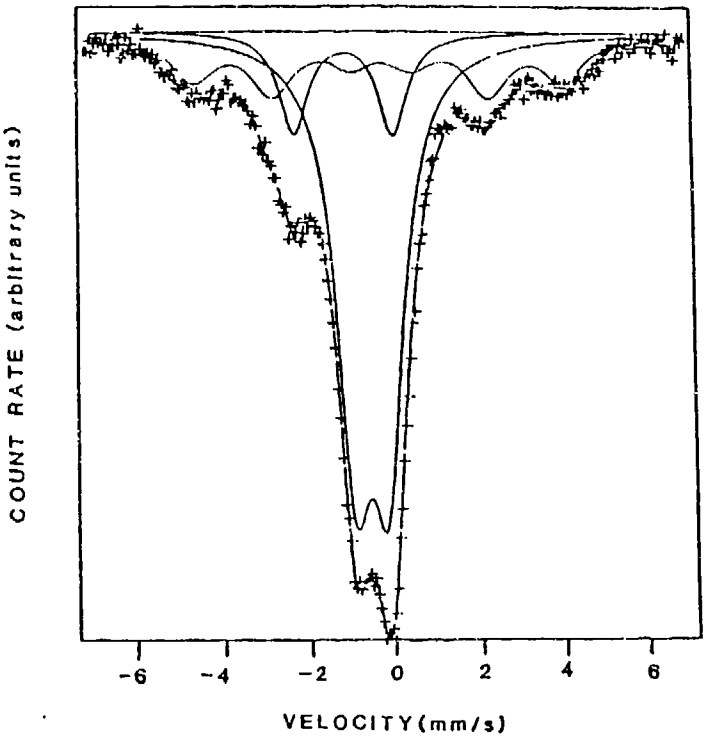

Figure 11. Emission Mössbauer spectrum for ^{57}Co electrodeposited on cobalt foil. Spectrum recorded at room temperature using an ^{57}Fe-enriched stainless steel foil absorber. Reproduced from ref. [2].

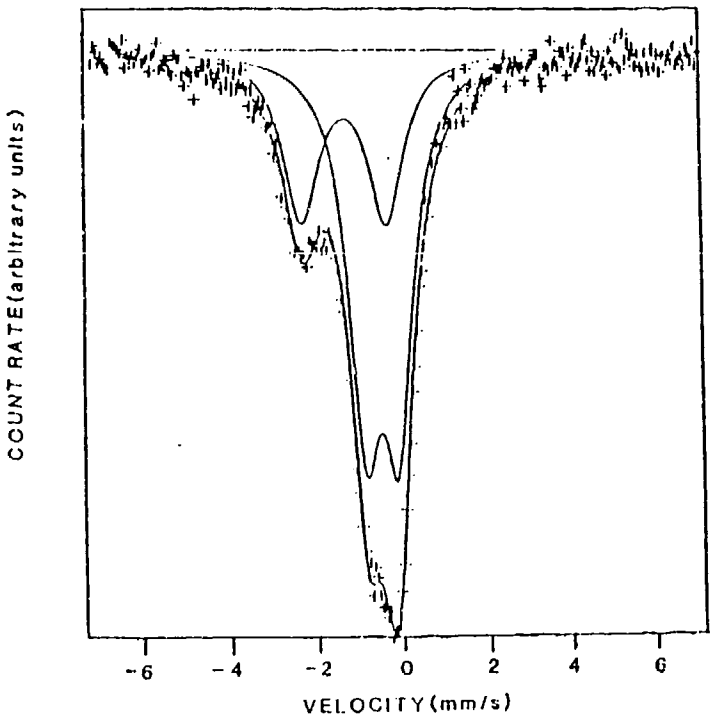

Figure 12. Emission Mössbauer spectrum obtained after poly(amic acid) deposition and A-stage cure. Reproduced from ref. [2].

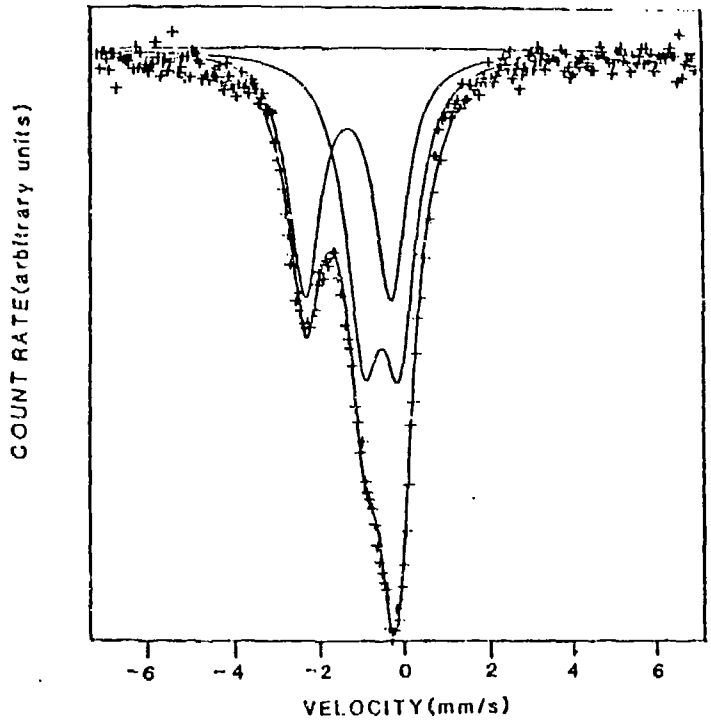

Figure 13. Emission Mössbauer spectrum obtained after B-stage cure (polyimide). Reproduced from ref. [2].

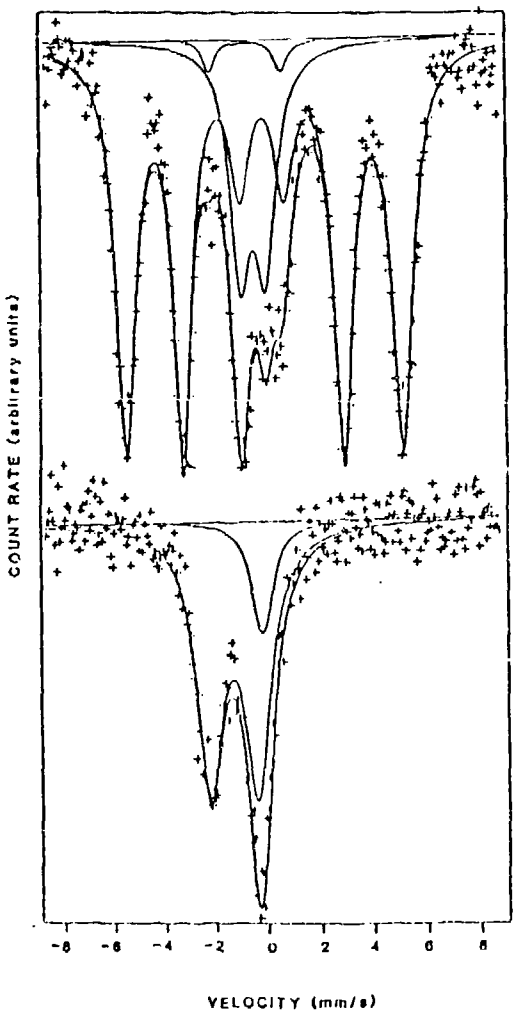

Figure 14. Emission Mössbauer spectra obtained for a) ^{57}Co electrodeposit on cobalt foil and b) that same electrodeposit after poly(acrylic acid) deposition.

BIOGRAPHY

NAME: Philip D. Deck

PRESENT AFFILIATION: Lehigh University
Chemistry Department and
Zettlemoyer Center for Surface Studies

TITLE:
Research Assistant

FIELD OF INTEREST/RESPONSIBILITIES

PREVIOUS AFFILIATIONS/TITLES

ACADEMIC BACKGROUND

B.S., Chemistry, Millersville University, 1983

SOCIETY ACTIVITIES/OFFICES/AWARDS:

ACS

PUBLICATIONS/PAPERS:

"Emission Mössbauer Study of the Interface between a Cobalt Substrate and a Polyimide Coating," A. Vértes, I. Czakó-Nagy, P. D. Deck and H. Leidheiser, Jr., J. Electrochem Soc., July 1987.

BIOGRAPHY

NAME: Richard D. Granata

PRESENT AFFILIATION: Lehigh University

TITLE: Research Scientist, Zettlemoyer Center for Surface Studies
Associate Director, Corrosion Laboratory

FIELD OF INTEREST/RESPONSIBILITIES

Corrosion, organic coatings, batteries and fuel cells, electrochemical impedance.

PREVIOUS AFFILIATIONS/TITLES

Research Scientist, Carnegie-Mellon Institute of Research, 1977-79

ACADEMIC BACKGROUND

B.S. Chemistry, The American University, Washington, D.C.
Ph.D., Chemistry, The American University, Washington, D.C.

SOCIETY ACTIVITIES/OFFICES/AWARDS:

ACS, ECS, NACE, ASTM
Philadelphia Society of Coatings Technology,
FSCT (Corrosion Committee)

PUBLICATIONS/PAPERS:

25 publications

BIOGRAPHY

NAME: Henry Leidheiser, Jr.

PRESENT AFFILIATION: Lehigh University

TITLE: Alcoa Foundation Professor;
Professor, Department of Chemistry;
Director, Corrosion Laboratory

FIELD OF INTEREST/RESPONSIBILITIES

Corrosion, organic coatings, metallic coatings, electrochemical impedance

PREVIOUS AFFILIATIONS/TITLES

Research Associate, University of Virginia, 1946-49
Director, Chief Executive Officer, Virginia Institute for Scientific Research, 1949-60
Lehigh University, 1960 - present

ACADEMIC BACKGROUND

B.S., Chemistry, University of Virginia
M.S., Chemistry, University of Virginia
Ph.D., Chemistry, University of Virginia

SOCIETY ACTIVITIES/OFFICES/AWARDS:

Please see attached

PUBLICATIONS/PAPERS:

235 publications; author or editor of 7 books

Awards for research include:
Young Author's Award, The Electrochemical Society, 1948

J. Shelton Horsley Research Award, Virginia Academy of Science, 1948

Oak Ridge Institute of Nuclear Studies Research Award, 1949

Westinghouse Signal and Brake Award of Institute of Metal Finishing, 1954

NATO Fellow to Cambridge University, England, 1969

Co-authored papers with authors who won the Melvin Romanof Prize of the National Association of Corrosion Engineers in 1972, 1974 and 1978

Silver Medal, American Electroplaters' Society, 1978

Arch T. Colwell Award, Society of Automotive Engineers, 1979

Whitney Award, National Association of Corrosion Engineers, 1983

Humboldt Senior Scientist Award, 1985

Elected Fellow of American Association for the Advancement of Science, 1985, for research in corrosion

Tambour Award, 11th World Congress on Metal Finishing, 1984

Silver Medal, South African Corrosion Institute, 1986

Research Award, Electrodeposition Division of The Electrochemical Society, 1986

Libsch Research Award, Lehigh University, 1987

ION BEAM ALLOYING OF ALUMINUM FOR CORROSION RESISTANCE

P. M. Natishan, E. McCafferty, and G. K. Hubler
Naval Research Laboratory
Washington, DC 20375-5000

ABSTRACT

Ion beam alloying techniques overcome many of the problems associated with conventional alloying. Novel aluminum surface alloys were prepared by ion implanting aluminum with Si, Zr, Nb, Cr, Mo, Zn, or Al at nominal concentration of 4 or 12 atomic percent. The results showed that implantation with Cr, Si, Mo, Zr, and Nb produced surface alloys that were more resistant to pitting than aluminum, and that implantation with Zn produced a surface alloy that was less resistant to pitting attack. The implantation of aluminum into aluminum had no effect on the pitting potential, indicating that the increased and decreased pitting potentials observed for the other implants was a chemical effect. The increased and decreased pitting resistance of the surface alloys was related to the surface charge character of the oxide film. The pit morphology indicated that blister formation and rupture, caused by gas production at the oxide/metal interface, was an important part of pit propagation.

INTRODUCTION

In recent years there has been much interest [1-5] at the Naval Research Laboratory in improving the corrosion behavior of metals and alloys by modification of their surfaces using directed energy beams. Two areas of research involve the processing of metal surfaces by ion beams or by high energy lasers. These surface alloying techniques provide a method of conserving scarce, expensive, or critical materials by concentrating them in the surface where they are required for applications such as corrosion protection, wear resistance, or catalytic performance.

This communication will discuss surface alloying in regards to ion implantation. Some distinct advantages of ion implantation as used in corrosion science are that special alloys which inhibit corrosion may be formed at the surface of a metal without the alteration of desired bulk properties. The fact that ion implantation is a non-equilibrium technique permits the formation of surface alloys which can exceed the solid solubility limits of the implanted species. Metastable phases and amorphous alloys produced in this manner are unattainable by conventional alloying techniques. There is no problem with adhesion of the surface layer as there is with deposited coatings since there is no abrupt interface present between the implanted-alloy layers and the substrate. These and other advantages of the ion implantation method are summarized in Table 1. Table 2 contains the various parameters that can be used to tailor the composition of a surface.

Aluminum Alloys and Surface Alloys

The major corrosion problem with aluminum is the localized breakdown of the passive film, which leads to the initiation and growth of corrosion pits. Improvements in the localized corrosion resistance of aluminum by conventional alloying techniques are limited in two regards. First, alloying additions are normally based on strength considerations; but the resulting intermetallic phases generally disrupt the passive film and are detrimental to corrosion resistance (6). Second, most alloying elements which are known to impart improved corrosion properties have a limited solubility in aluminum. In contrast, surface modification techniques such as ion implantation are non-equilibrium processes and offer a means of producing solid solution surface alloys which can exceed the solid solubility limits of the implanted species.

In order to deal with corrosion prevention in a systematic fashion, it is important to understand the mechanisms involved in passivity and its breakdown. In particular how and why alloying elements enhance or degrade the resistance to corrosion. To cause pitting, an anion such as chloride must first adsorb at the oxide/solution interface. Little attention has been given to this first step, largely because of the difficulty in the experimental determination of adsorption isotherms for small area samples. However, as noted by Hoar (7), "Adsorption is the primary act in every heterogeneous process at the metal/ solution interface, and the nature and subsequent fate of the metal adsorbate "complex" determines whether metal dissolution or passivation occurs".

An important parameter controlling the surface charge, and therefore, the adsorption characteristics of an oxide covered metal, is the pH of zero

charge of the oxide (8,9). In the absence of specific adsorption the pH of zero charge of an oxide, pH_{pzc}, is the pH at which the surface of the oxide has no net charge. See Figure 1. At pH's lower than the pH_{pzc} the surface has a net positive character, and anions such as chloride are electrostatically attracted to the surface and can become incorporated in the oxide. When the pH is higher than the pH_{pzc}, the surface has a net negative charge, and anion adsorption is inhibited.

In this investigation, ion implantation was used to produce binary aluminum surface alloys using elements whose oxides were of known pH_{pzc}. In particular, it will be shown that implanted elements chosen because of the low pH_{pzc} of their oxides (Si, Cr, Zr, Nb, and Mo) produced binary surface alloys that had higher (more positive) pitting potentials than aluminum. The implant chosen because of the high pH_{pzc} of its oxide (Zn) produced a binary surface alloy that had a pitting potential that was lower than that of aluminum.

Oxide Blistering

As in the study of fracture surfaces, the morphology of pits can produce valuable information on their mode of failure. Investigators studying the pitting behavior of ion implanted iron, stainless steels and aluminum have observed: undermining of the oxide film (5,10,11), pits that were still covered by the oxide film (12), or blistering of the oxide (13-15). Therefore, it would seem that an understanding of the events that produce oxide covered pits or blisters would lead to a better understanding pitting corrosion. Bargeron and Givens (13,14) described blister formation and rupture on anodized aluminum and on aluminum with an air-formed oxide films. Their results suggest that blister formation

and growth, caused by gas evolution at the oxide/metal interface, occurs before the end of the initiation period and is therefore, an important step in pit initiation. This communication will describe the phenomenon of blister formation and rupture on ion implanted aluminum as marking the beginning of pit propagation rather than pit initiation.

Experimental Procedures

After polishing, samples were implanted with a selected ion (Cr, Si, Zr, Nb, Mo, Zn, or Al) at a nominal angle of incidence of 0°. The samples were implanted at two energies calculated to produce a depth concentration profile that had a nominal peak concentration of 4 or 12 a/o at the surface and that extended 500 angstroms (Å) into the bulk before decreasing.

The pitting potentials for implanted and unimplanted samples were determined potentiostatically in a deaerated 0.1M NaCl solution using a conventional two compartment cell. After polarization above the pitting potential, the samples were lightly rinsed with distilled water and the varnish was carefully removed using a razor blade. The samples surfaces were observed with a light microscope or a scanning electron microscope.

RESULTS

Implantation Profiles

The implantation parameters were selected to achieve the desired depth concentration profile shown in Figure 2a. The actual concentration profiles, as determined by RBS, were different than those desired. The RBS profile presented in Figure 2b is for a molybdenum 4 a/o implanted aluminum sample, Mo(4 a/o)Al. The concentration of Mo at the surface is less than 2 a/o with the peak concentration of 3.7 a/o occurring at 350

Å. It was assumed that the discrepancy between the desired and actual profiles resulted from radiation enhanced diffusion (RED), ion beam mixing (IBM), or ion channeling during implantation in the rather large grains, 0.005 inches.

Surface Analysis of Oxide Films

Figure 3 presents a post pitting XPS profile for a Si(12 a/o)Al sample. The Si concentration at the surface was approximately 8 a/o. Similiar XPS profiles for Mo(12 a/o)Al and Zr(12 a/o)Al showed surface concentrations of 1 to 2 a/o and 3 to 4 a/o, respectively. These profiles confirmed the presence of the implant material in the oxide film and at the surface of the oxide.

Anodic Polarization

Figure 4 shows anodic polarization curves for Zn(12a/o)Al, Si(12 a/o)Al and unimplanted aluminum. The important characteristic of each curve is the pitting potential, i.e., the electrode potential at which there is a sudden increase in current density due to the initiation of corrosion pits. At potentials below (less positive than) the pitting potential, pits do not initiate: but above the pitting potential, pits initiate and grow. A higher (more positive) pitting potential represents an increased resistance to pitting corrosion. Thus, ion implantation with Si increases the pitting potential of Al by 450 mV, whereas implantation with Zn decreases the pitting potential by 250 mV. It should be noted that implantation of Al into Al has no effect on the pitting potential, see Table 3. This fact indicates that the physical effects of implantation are unimportant and that improvements in pitting potential from the implantation of the various ions can be attributed to chemical

effects. Table 3 lists pitting potentials in de-aerated 0.1M NaCl for aluminum implanted with Mo, Nb, Zr, Si, Zn, Cr, and Al.

Oxide Blistering

Sample handling after anodic polarization was important to the observation of the blisters as the ruptured oxide films were delicate and easily removed. Ultrasonic cleaning or vigorous gas evolution from a pit can destroy the remnants of a ruptured blister leaving only the exposed pit, see Figure 5.

The following series of photos, taken after anodic polarization above the pitting potential, show blisters in various stages of development. For illustrative purposes, blister growth is described as occuring in four stages. Stage 1 is characterized by blisters with no visible cracks or pores, see Figure 6. These unruptured blisters are similar to those observed by Bargeron and Givens (13,14). The unruptured blisters are usually circular or oval in shape. Blisters that have visible cracks were described as being Stage 2, see Figure 7. Stage 3 blisters are characterized by the formation of a secondary region at the periphery of the primary circular/oval region. This secondary region differs from the primary region in that there appears to be a crystallographic etching beneath the oxide, see Figure 8. Ruptured blisters were designated as Stage 4; an example is presented in Figure 9.

A survey of the area of failure showed that the blisters ruptured in the center twice as often as at the edge. These results differed from those of Bargeron and Givens (13,14) that showed that blisters ruptured at the edge.

DISCUSSION

Pitting of Ion Implanted Aluminum

In order to explain the effect of the implanted species on the pitting resistance of the substrate, it is helpful to first examine the events leading to the formation of a pit. To cause pitting, an anion such as chloride must, in turn: 1) adsorb at the oxide/solution interface, 2) penetrate or dissolve through the oxide film, and 3) react locally with the underlying metal.

It is unlikely that ion implantation will have an effect on the second or third pitting steps outlined above. The native passive film on aluminum is already amorphous (16,17), so that implantation would not be expected to improve the resistance of the film to penetration by Cl^- ions. After corrosion pits initiate on aluminum, their rate of propagation is so rapid that implanted ions will probably not be effective in interfering with their growth.

As noted earlier, the pH_{pzc} effects the surface charge and the adsorption characteristics of an oxide. Therefore, the pH_{pzc} should also, to some degree, influence the susceptibility of an oxide covered metal to pitting. If the pH_{pzc} does affect pitting, then it might be possible to predict the pitting behavior of an oxide covered metal from the pH_{pzc}. Figure 10 shows the surface charge character in the range of pH 0 to 14 and the pH_{pzc} of two oxides, Al_2O_3 and Ta_2O_5. In neutral solutions, pH 7, one would predict that an oxide covered metal whose oxide had a pH_{pzc} lower than 7, such as Ta_2O_5 (pH_{pzc} 2.8) (18), would be more resistant to pitting than an oxide covered metal whose oxide had a pH_{pzc} higher than 7, such as Al_2O_3 (pH_{pzc} 9.1) (8,19,20). In fact,

tantalum is very resistant to pitting attack (21), whereas aluminum is susceptible to pitting attack (22,23). In terms of the pH_{pzc}, the pitting resistance of tantalum at pH 7 is explained by the basic nature (negatively charged surface) of the oxide which inhibits anion adsorption. Aluminum is susceptible to pitting attack because the acidic nature (positively charged surface) of the oxide at pH 7 promotes anion adsorption. Figure 11 (2) shows the relationship between the pitting potential of several oxide covered metals in nearly neutral, 1M Cl^- solutions and the pH_{pzc} of their hydrated oxides. The information presented in Figure 11 is for metals with air formed oxide films. It can be seen that the pitting potential increases as the pH_{pzc} decreases.

The results of this investigation showed that the implantation of Cr, Zr, Nb, Mo, and Si (low pH_{pzc}) increased the pitting potential of aluminum whereas Zn (high pH_{pzc}) decreased the pitting potential. Therefore, it appears that ion implantation offers the possibility of inhibiting or enhancing Cl^- ion adsorption by changing the pH_{pzc} of the interface. As shown in Figure 3, the implanted ions are contained in the surface oxide film; so that the effect of ion implantation is to replace a portion of the surface aluminum-oxygen bonds with bonds formed between oxygen and that of the implanted ions.

Blister Formation and Rupture

The physical appearance of the blisters observed in this investigation support a modified version of the sequence of events proposed by Bargeron and Givens (13,14). Cracks of various size were observed to radiate from the centers of the blisters and were present

before total rupture. These cracks, refered to as secondary cracks, are believed to initiate at and propagate from a primary crack or pore leading from the solution to the oxide/metal interface and are the result of stresses caused by the build-up of hydrogen pressure at the oxide/metal interface. The secondary cracks propagate perpendicular to the initial imperfection and finally, when the pressure is great enough the bubble ruptures the oxide film.

The initial crack (primary crack) could be the result of anion induced cracking of the oxide (24-27) or an existing imperfection in the oxide film (10). The small crack or pore provides a path for the solution to reach the oxide/metal interface. When the potential is above the pitting potential, metal dissolution and hydrogen production occur at the base of the crack. The dissolution of the metal and hydrogen production mark end of pit initiation and the beginning of pit propagation.

The blisters that rupture at the center, as seen in Figure 9, are the result of secondary cracks propagating from the primary crack. The blisters that rupture near the edges are the result of secondary cracks propagating from some other imperfection or a second primary crack.

SUMMARY

The approach taken in this investigation was to examine the effect of ion implantation on the pitting behavior of aluminum and to study the morphology of the pits that developed. The results are summarized below:

1. All the binary surface alloys produced from elements (Si, Cr, Zr, Nb, and Mo) that were chosen because of the low pH_{pzc} of their oxide had

higher pitting potentials than aluminum, indicating an increased resistance to pitting corrosion.

2. The binary surface alloy produced from Zn, chosen because of the high pH_{pzc} of its oxide, had a lower pitting potential than aluminum, indicating a decreased resistance to pitting corrosion.

3. Due to the differences in the surface concentrations of samples receiving the same apparent implantation dose, it was not possible to quantitatively correlate increases or decreases in the pitting potentials of the surface alloys to the pH_{pzc} of the oxides of the implanted species.

4. Gas production at the oxide/metal interface is responsible for blister formation and rupture, and the eventual propagation of the pit into the bulk.

ACKNOWLEDGMENTS

The authors gratefully acknowledge the financial support and technical interaction of A. John Sedriks, Office of Naval Research, Arlington, Virginia. The authors also wish to thank Linda D. Terrell for her skill and patience in the preparation of this manuscript. XPS surface analyses were performed by Surface Science Laboratories, Mountain View, California.

REFERENCES

1. E. McCafferty and P. G. Moore, J. Electrochem Soc., 133, 1090 (1986).

2. P. M. Natishan, E. McCafferty, and G. K. Hubler, J. Electrochmem. Soc., 133, 1061 (1986).

3. P. M. Natishan, E. McCafferty, and G. K. Hubler, in "Surfaces, Inhibition, and Passivation", E. McCafferty and R. J. Brodd, Eds., p. 437, The Electrochemical Society, Pennington, NJ (1986).

4. E. McCafferty, G. K. Hubler, P. M. Natishan, P. G. Moore, R. A. Kant, and B. G. Sartwell, Mater. Sci. Eng., 86, p. 1 (1987).

5. G. K. Hubler, P. P. Trzaskoma, E. McCafferty, and I. L. Singer, in "Ion Implantation into Metals", p. 23, V. Ashworth, W. A. Grout, and R. P. M. Proctor, Eds., Pergamon Press, New York, NY (1982).

6. "Aluminum", J. E. Hatch, Ed., p. 279, ASM, Metals Park, Ohio (1984).

7. T. P. Hoar, J. Electrochem. Soc., 117, 17c (1970).

8. G. S. Parks in "Chemical Oceanography", J. R. Riley and G. Skirrow, Eds., Vol. 1, 2nd Edition, p. 241, Academic Press, New York, NY (1975).

9. S. R. Morrison, "Electrochemistry at Semiconductor and Oxidized Metal Electrodes", Plenum Press, New York, NY (1980).

10. G. C. Wood, W. H. Sutton, J. A. Richardson, T. N. K. Riley, and A. G. Malherbe, in "Localized Corrosion", R. W. Staehle, B. F. Brown, J. Kruger, and A. Agrawal, Eds., p. 526, Houston, TX (1974).

11. K. Videm, Kjeller Report No. KR 88, Institute for Atommenergi (1966).

12. J. Yahalom, L. K. Ives, and J. Kruger, J. Electrochem. Soc., 120, 385 (1973).

13. C. B. Bargeron and R. B. Givens, J. Electrochem Soc., 124, 1845 (1977).

14. C. B. Bargeron and R. B. Givens, Corrosion, 36, 618 (1980).

15. C. D. S. Tuck, G. M. Scamans, and M. A. Lunn, in "Workshop on Electrochemistry of High Energy Density Light Metals in Aqueous Solutions", Belgrade, Yugoslavia, 222 (1982).

16. F. P. Fehlner and N. F. Mott, Oxidation Met., 2, 59 (1970).

17. R. S. Alwitt in "Oxides and Oxide Films," J. W. Diggle and A. K. Vijh, Eds., Vol. 4, p. 169, Marcel Dekker, Inc., New York, N.Y. (1976).

18. G. A. Kokarev, V. A. Kolesnikov, A. F. Gubin, and A. A. Korobanov, Elektrokhimiya, 18, 466 (1982).

19. J. A. Yopps and D. W. Fuerstenau, J. Colloid Sci., 19, 61, (1964).

20. H. Sadek, A. K. Helmy, V. M. Sabet, and Th.F. Tadros, J. Electroanal. Chem. 27, 257 (1970).

21. M. F. Abd Rabboh and P. J. Boden, in "Localized Corrosion," R. W. Staehle, B. F. Brown, J. Kruger, and A. Agrawal, Eds., p. 653, NACE, Houston, TX (1974).

22. J. R. Galvele and S. M. de De Micheli, Corrosion Sci., 10, 795 (1970).

23. W. J. Rudd and J. C. Scully, Corrosion Sci., 20, 611 (1980).

24. T. P. Hoar, Corrosion Sci., 7, 341 (1967).

25. L. C. Archibald and J. S. L. Leach, Corrosion Sci., 22, 15 (1977).

26. L. C. Archibald and J. S. L. Leach, Corrosion Sci., 22, 21 (1977).

27. J. S. L. Leach and B. R. Pearson, Electrochimica Acta, 29, 1263 (1984).

28. S. F. Bubar and D. A. Vermilyea, J. Electrochem. Soc., 113, 892 (1966).

29. D. L. Douglass, Corrosion Sci., 5, 255 (1965).

TABLE 1. Advantages of ion implantation

1. No sacrifice of bulk properties.
2. Low temperature process.
3. Solid solubility limit can be exceeded.
4. Alloy preparation independent of diffusion constants.
5. No coating adhesion problems since there is no interface.
6. No change in sample dimensions.
7. Depth concentration distribution controllable.
8. Composition may be changed without affecting grain sizes.
9. Precise location of implanted area(s).

TABLE 2. Ion implantation parameters

Implanted elements	- Virtually any element from hydrogen to uranium can be implanted.
Ion energies	- Normally 2 to 200 keV. Energies up to 5 MeV may be obtained with the Van de Graaff accelerator.
Implantation depths	- Vary with ion energy, ion species and host material. Ranges normally 100 angstroms to 10,000 angstroms.
Range distribution	- Approximately Gaussian. Choice of energies allow tailored depth distribution profiles.
Concentration	- From trace amounts up to 50% or more.
Host material	- Any solid material can be implanted, including metals, semi-conductors, and insulators.

Table 3: Pitting Potentials of the Ion Implanted Aluminum Surface Alloys in 0.1M NaCl.

Unimplanted Al: $-0.700V_{sce}$ (pH_{pzc} 9.1)

Implanted Ion	4 a/o	12 a/o	pH_{pzc} of the Oxide of the Implanted Species	Oxide for Listed pH_{pzc}
Mo	-0.560	-0.545	1.8 - 2.1 [15,16]	MoO_3
Si	-0.640	-0.340	1.8 - 2.2 [5]	SiO_2†
Nb	-0.680	-0.585	2.8 [11]+	Nb_2O_5
Zr	-0.660	-0.410	5.5 - 6.3 [17,18]	ZrO_2†
Cr		-0.565	6.3 - 7.0 [22]	Cr_2O_3
Al		-0.700*	9.0 - 9.4 [5,7,10,13]	Al_2O_3†
Zn		-0.950	9.2 - 10.3 [5]	ZnO

+The pH_{pzc} of Nb_2O_5 is similiar to that of Ta_2O_5.

*Nominal concentration of 8 a/o.

†Oxide composition confirmed by XPS.

FIGURE CAPTIONS

Figure 1. The pH dependence of the surface charge character of an oxide: positive ($pH<pH_{pzc}$), neutral ($pH=pH_{pzc}$) and negative ($pH>pH_{pzc}$).

Figure 2. (a) Desired and (b) actual depth-concentration profiles for Mo(4a/o)Al with a 25-95 keV implantation energy sequence.

Figure 3. XPS depth-concentration profile of Si(12a/o)Al.

Figure 4. Anodic polarization curves for Zn(12a/o)Al, Al, and Si(12a/o)Al.

Figure 5. Pit that is partially covered by the oxide a) before ultrasonic cleaning; b) after ultrasonic cleaning.

Figure 6. Stage 1 blister formation: no visible sign of cracks on the blister.

Figure 7. Stage 2 blister formation: cracks are visable on the blister.

Figure 8. Stage 3 blister formation: blister is cracked and crystallographic etching is observed under the blister.

Figure 9. Stage 4 blister formation: the blister is ruptured.

Figure 10. Surface charge character of Al_2O_3 and Ta_2O_5 between pH 0-14.

Figure 11. Pitting potentials for oxide covered metals vs. the pH_{pzc} of the oxide.

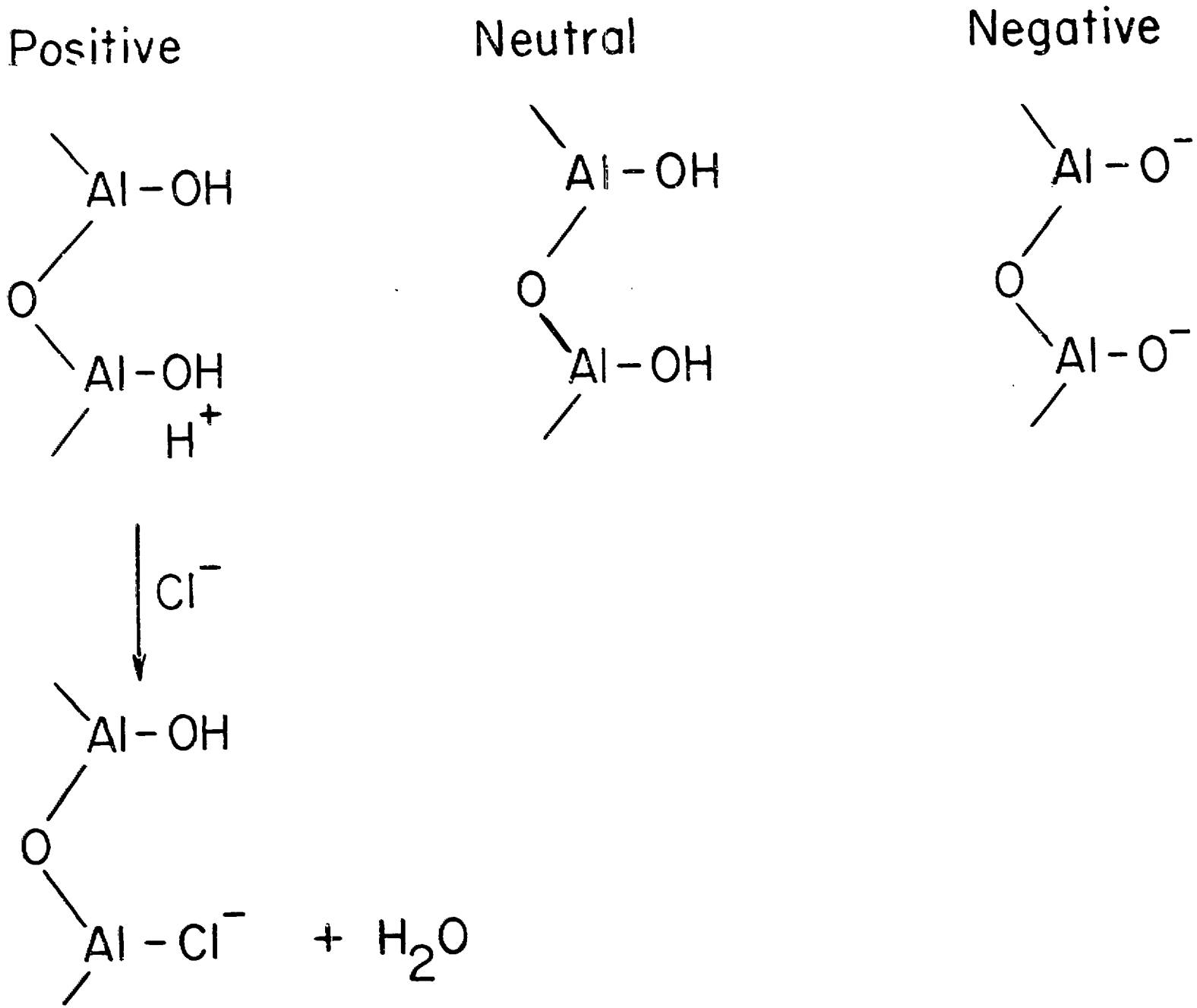
Positive
Neutral
Negative
Al-OH
O
Al-OH
H+
Al-OH
O
Al-OH
Al-O−
O
Al-O−
Cl−
Al-OH
O
Al-Cl−
+ H2O

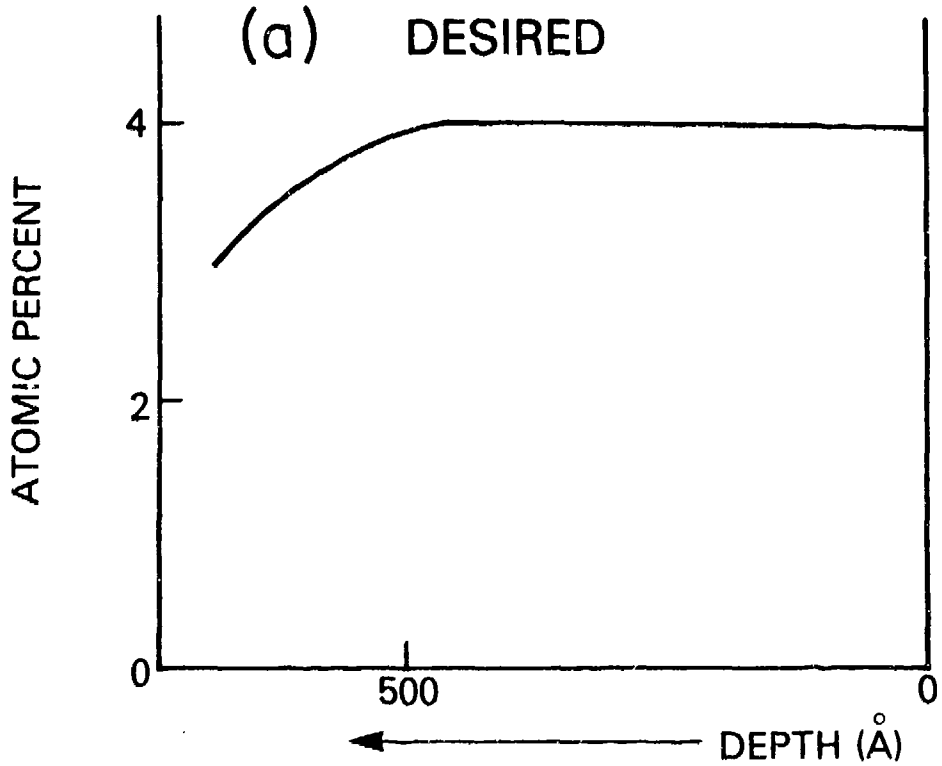
(a) DESIRED
ATOMIC PERCENT
4
2
0
500
0
DEPTH (Å)

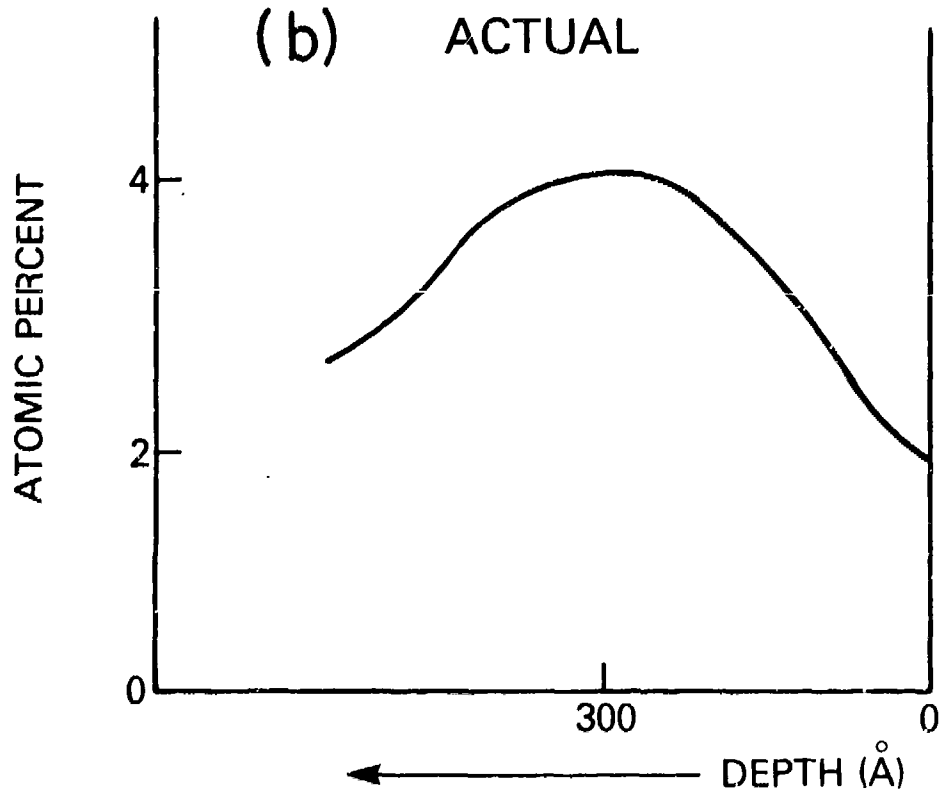
(b) ACTUAL
ATOMIC PERCENT
4
2
0
300
0
DEPTH (Å)

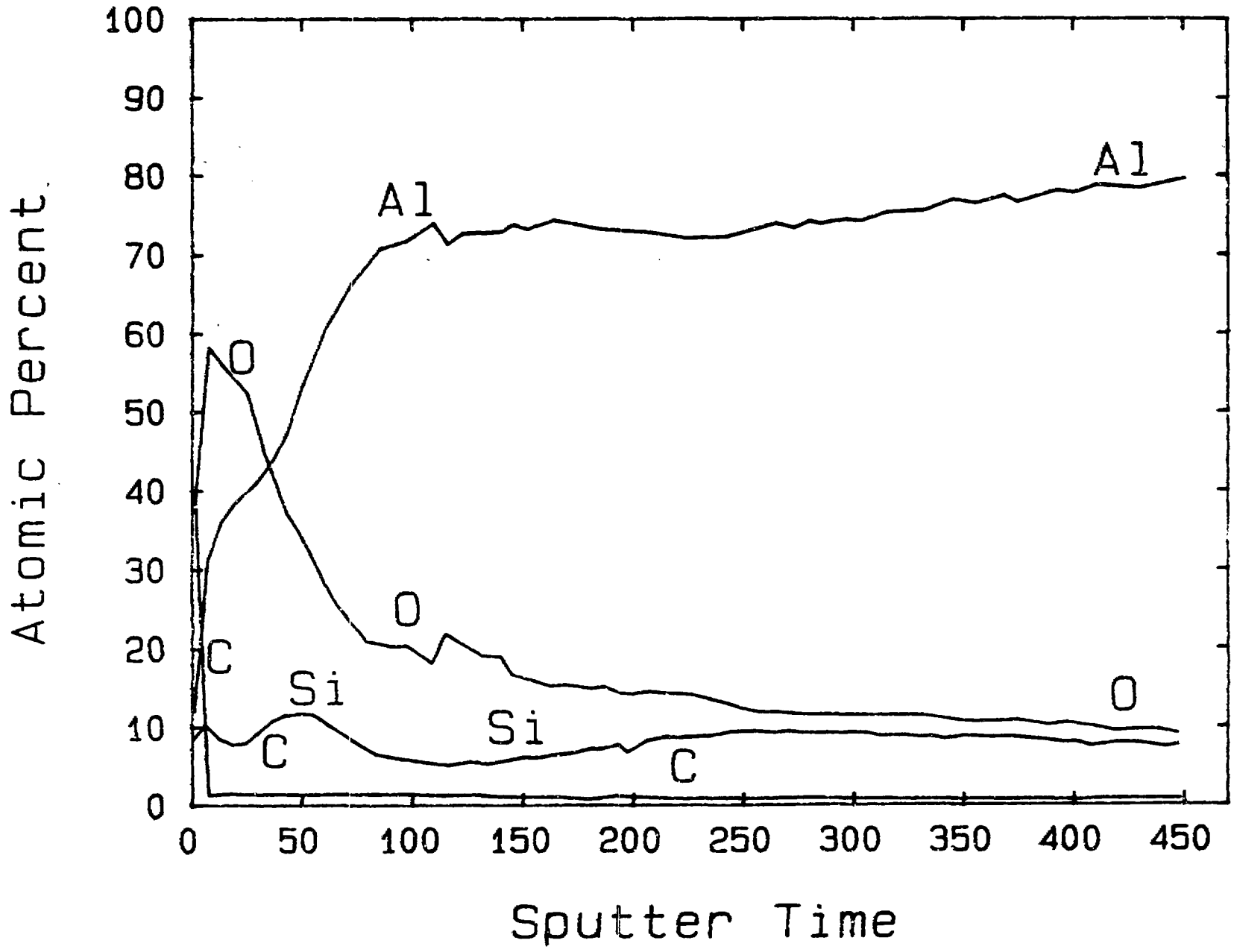
Atomic Percent
100
90
80
70
60
50
40
30
20
10
0
0
50
100
150
200
250
300
350
400
450
Sputter Time
Al
Al
O
O
O
C
C
C
Si
Si

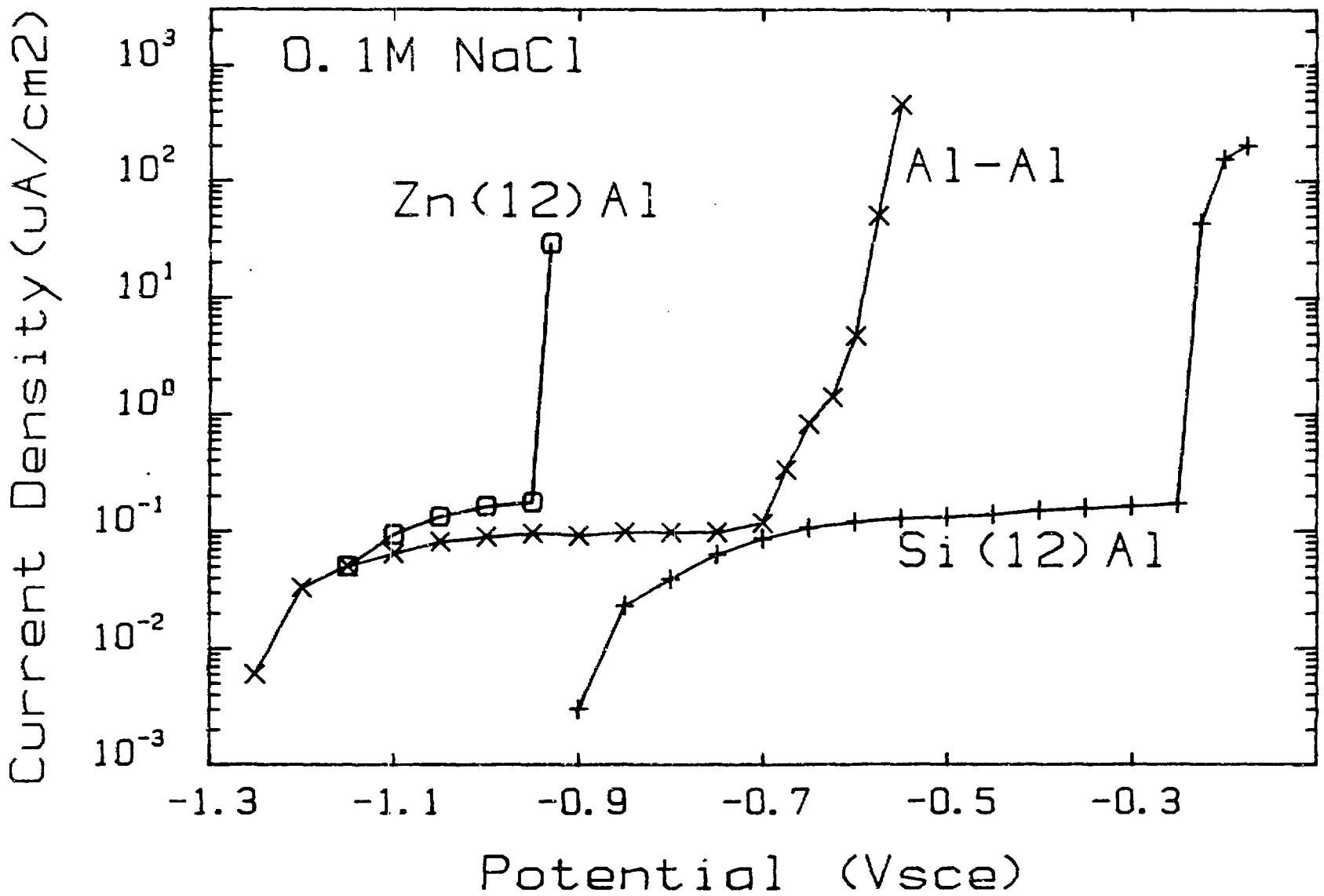
0. 1M NaCl
Zn(12)Al
Al-Al
Si(12)Al
Current Density(uA/cm2)
10^3
10^2
10^1
10^0
10^{-1}
10^{-2}
10^{-3}
-1.3
-1.1
-0.9
-0.7
-0.5
-0.3
Potential (Vsce)

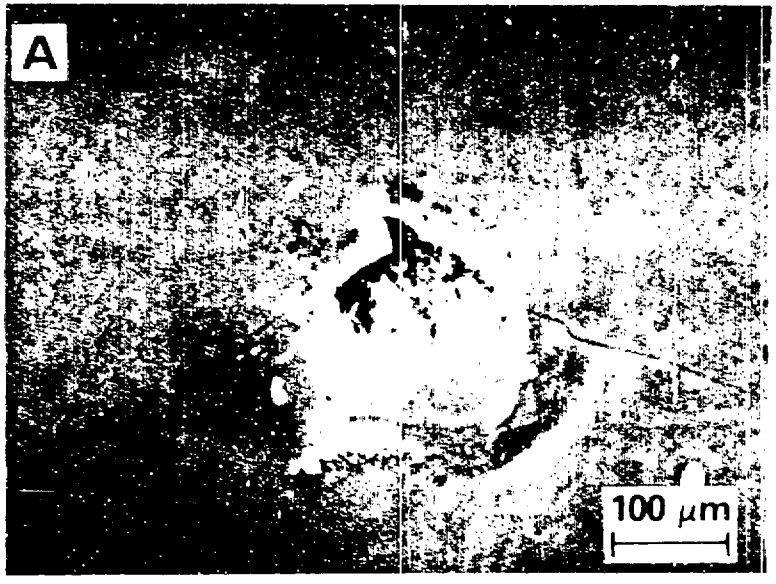
A
100 μm

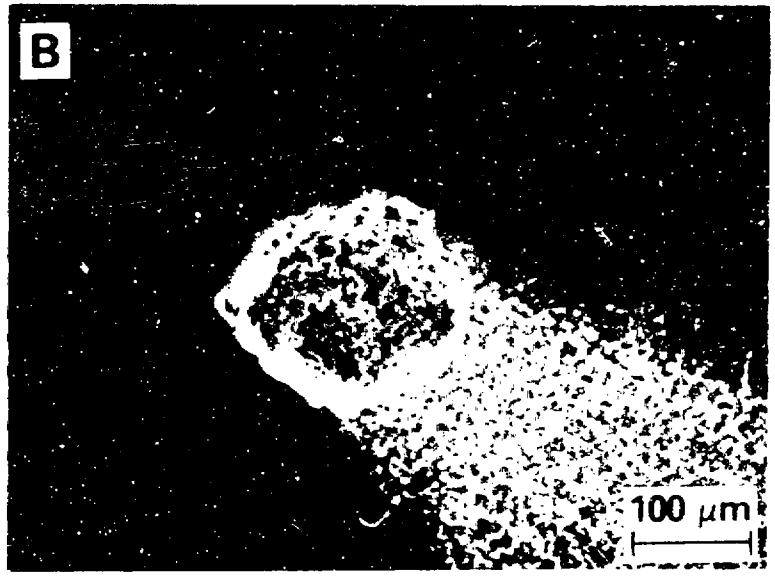
B
100 μm

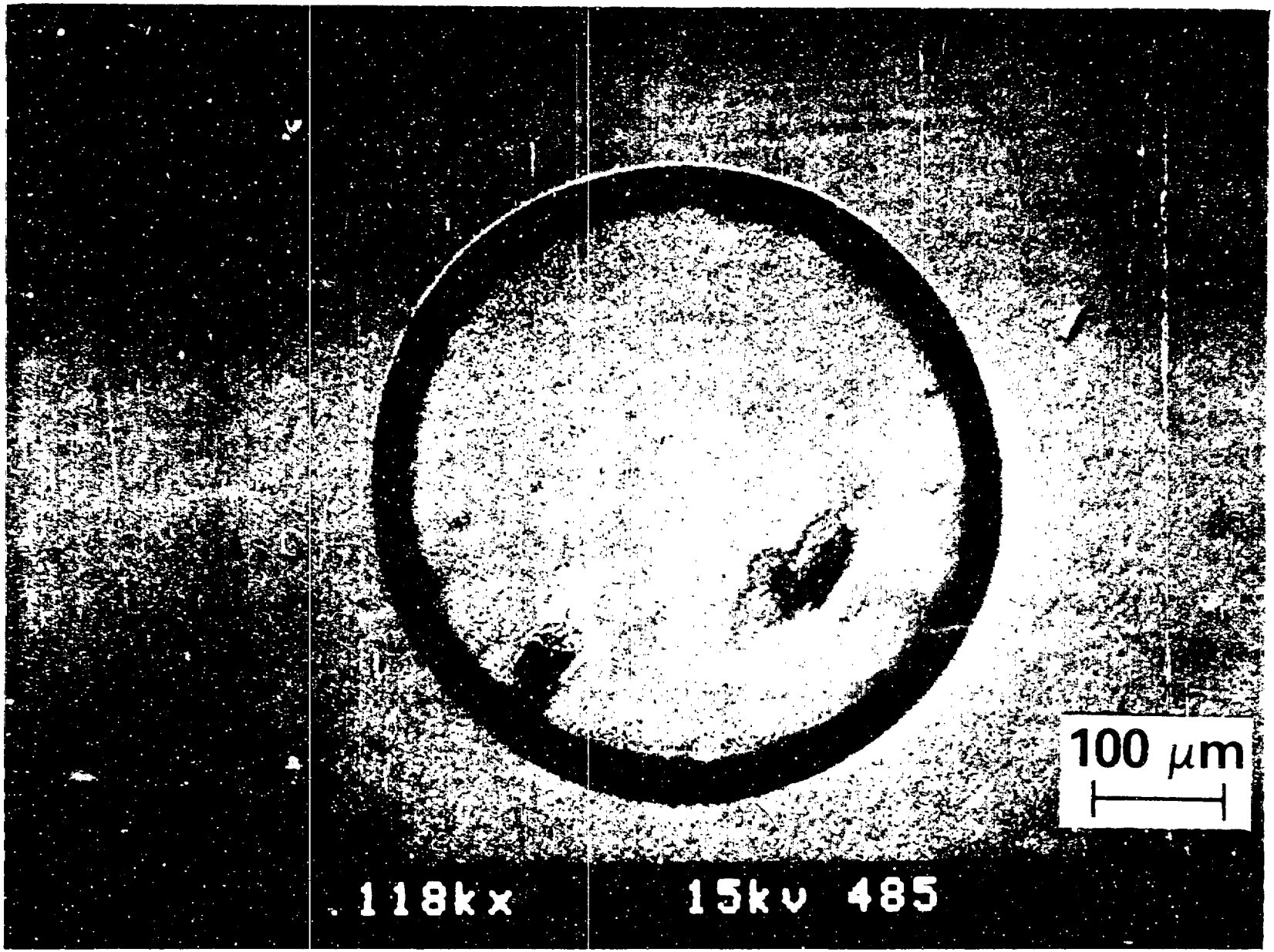
100 μm
118kx
15kv 485

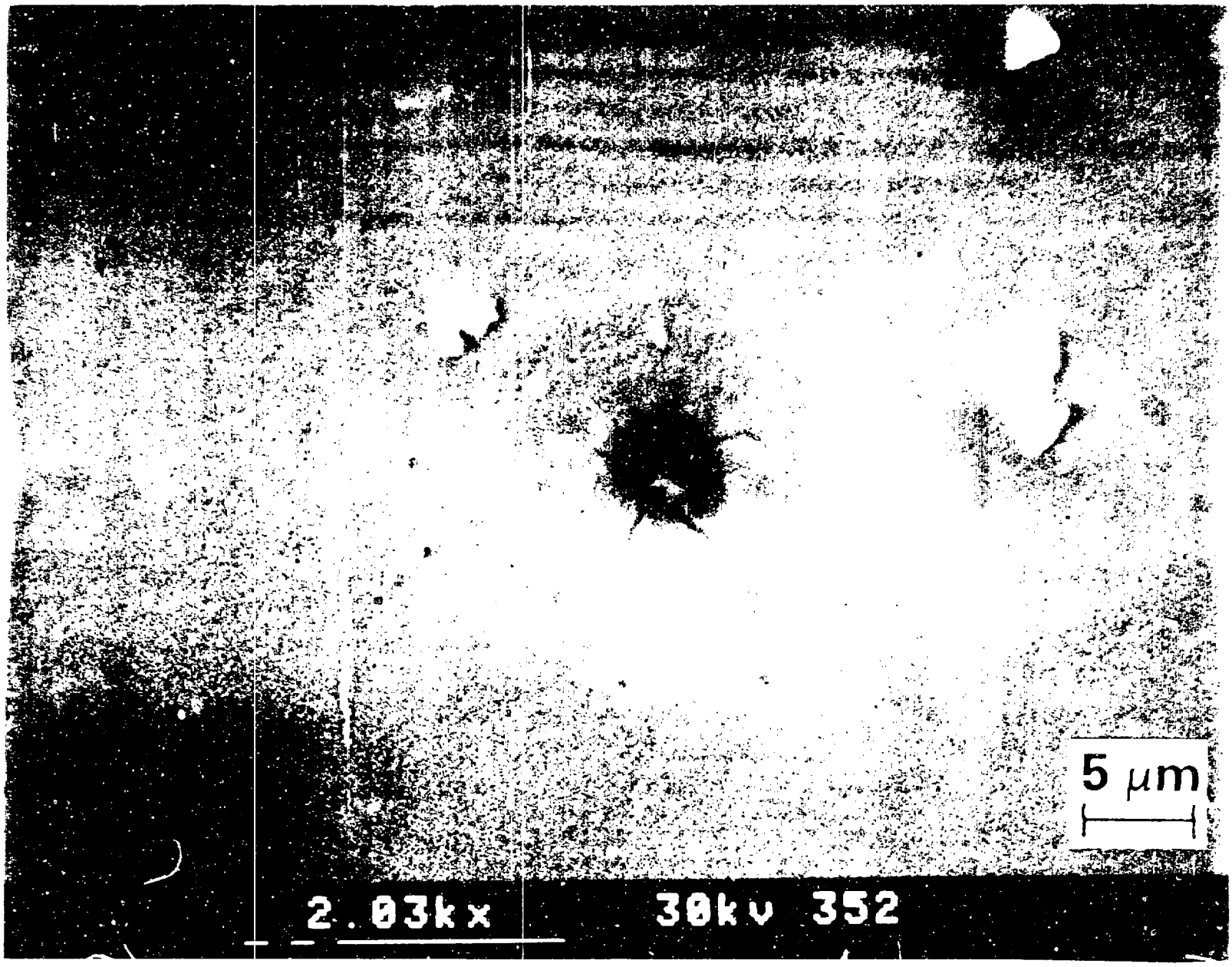
5 μm
2.03kx 30kv 352

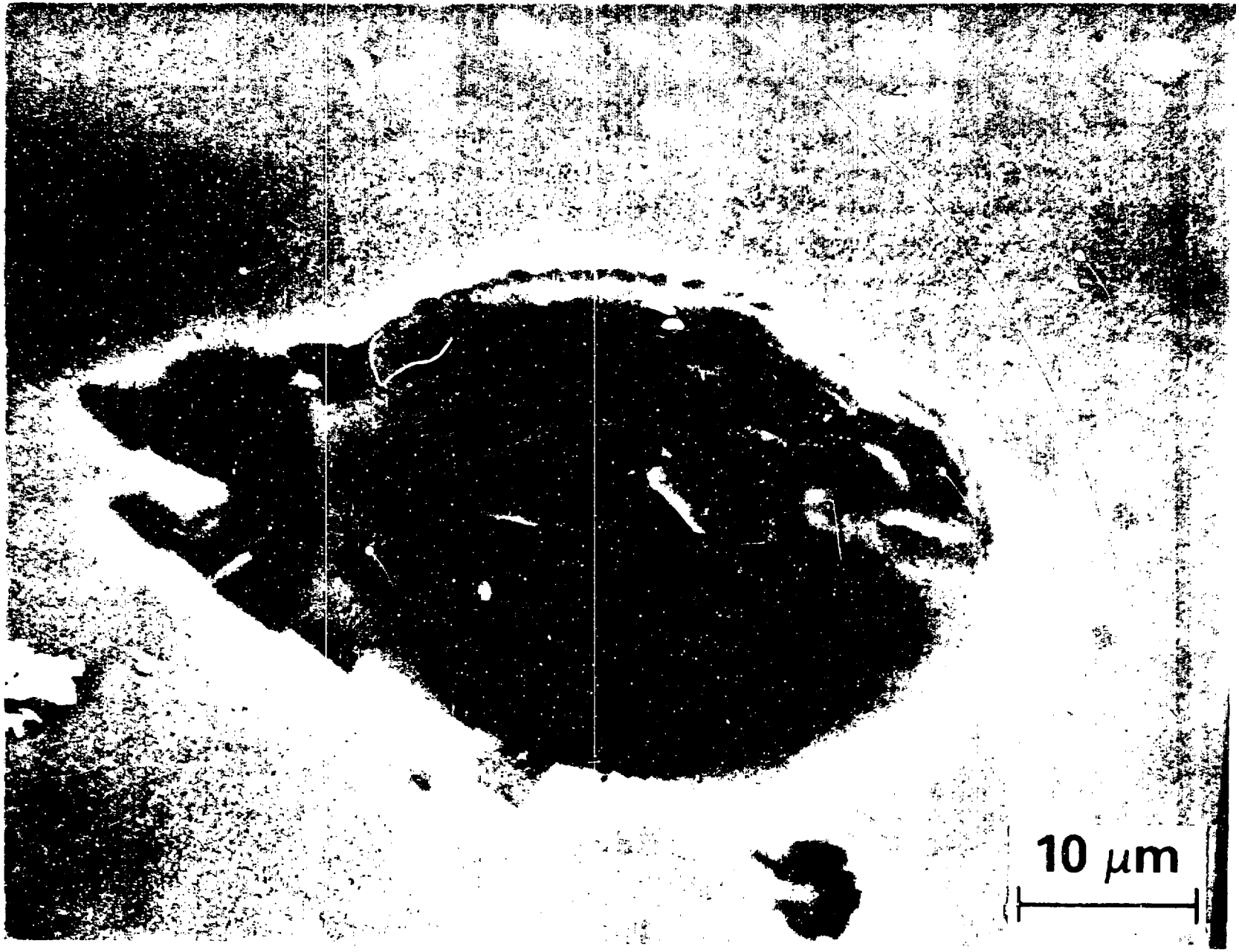
10 μm

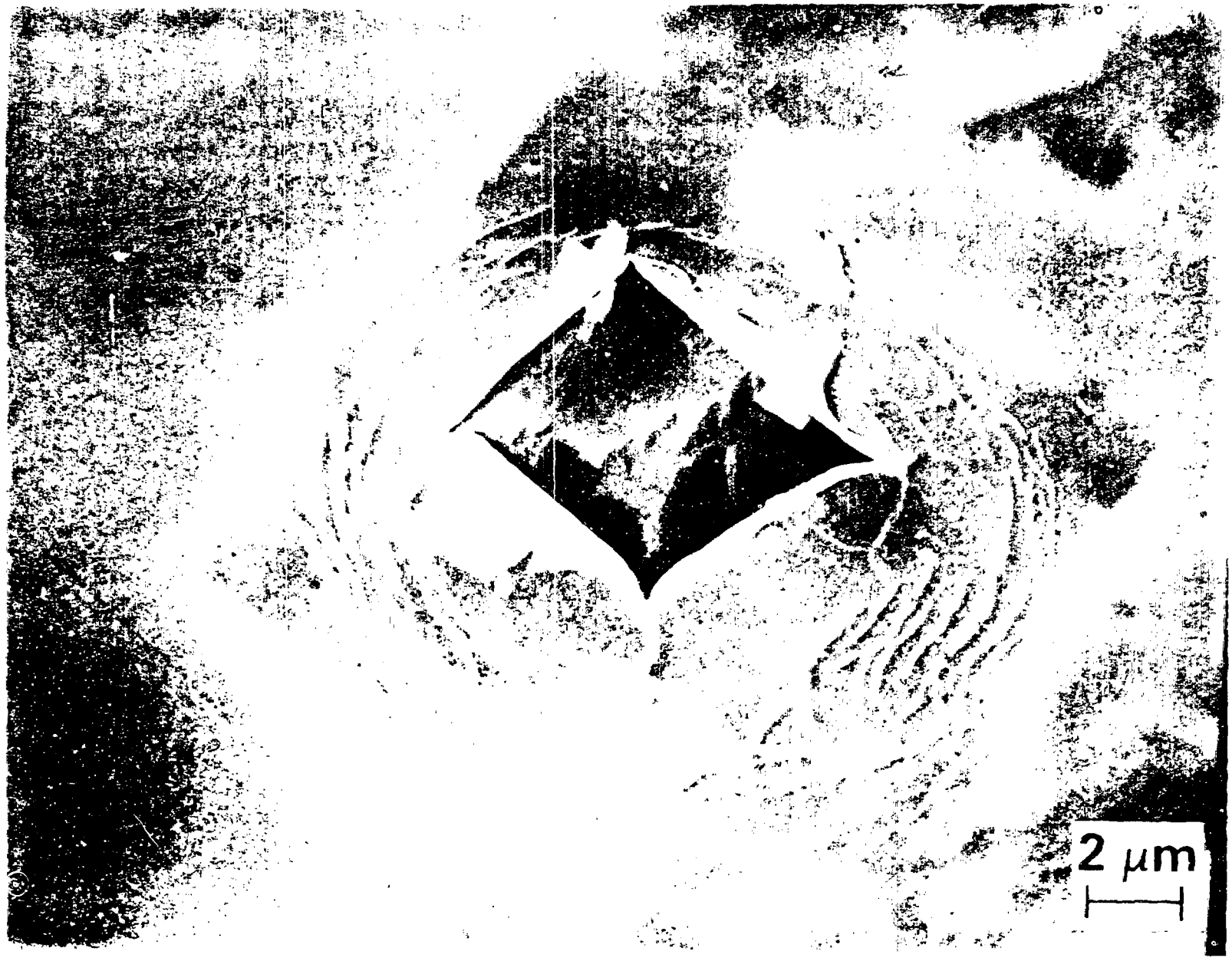
2 μm

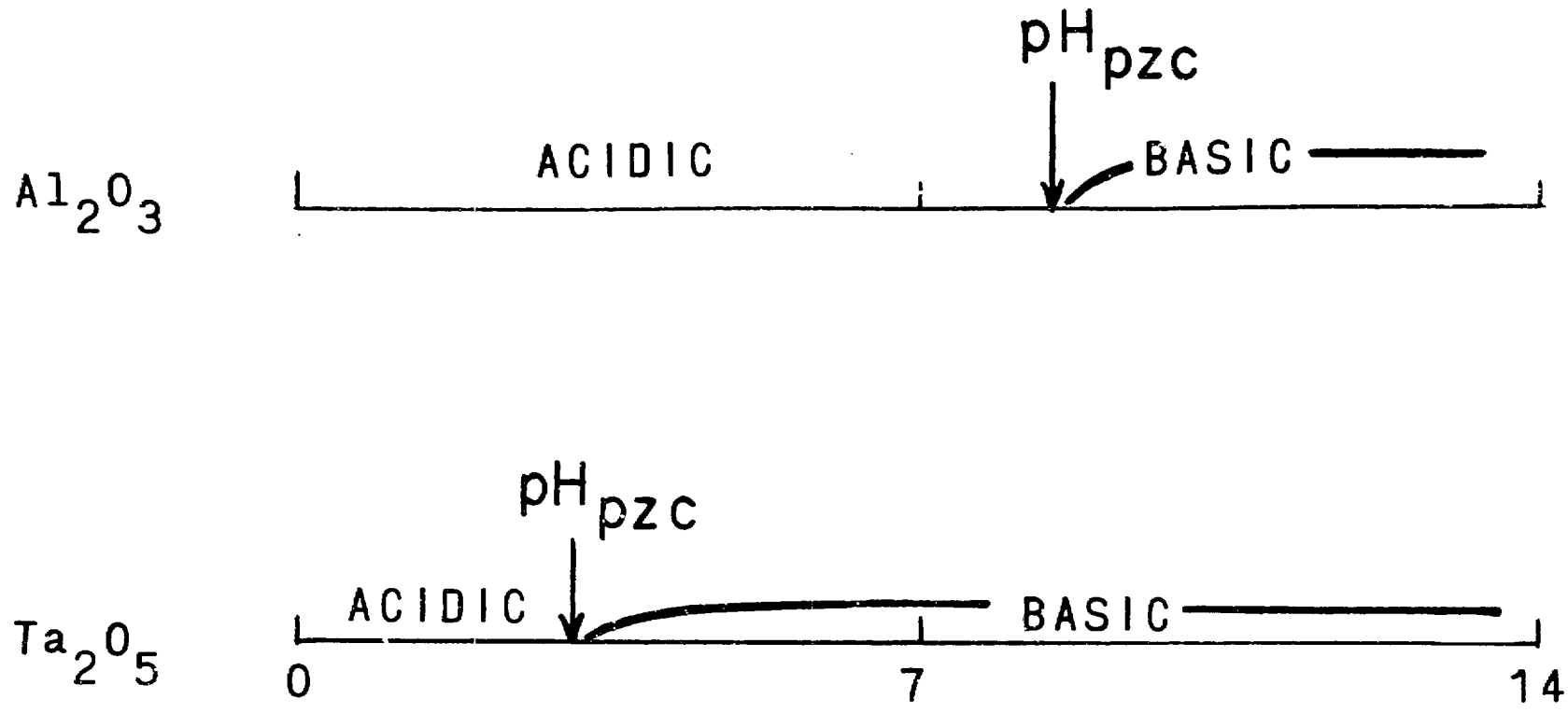
Al_2O_3
ACIDIC
pH_{pzc}
BASIC
Ta_2O_5
ACIDIC
pH_{pzc}
BASIC
0
7
14

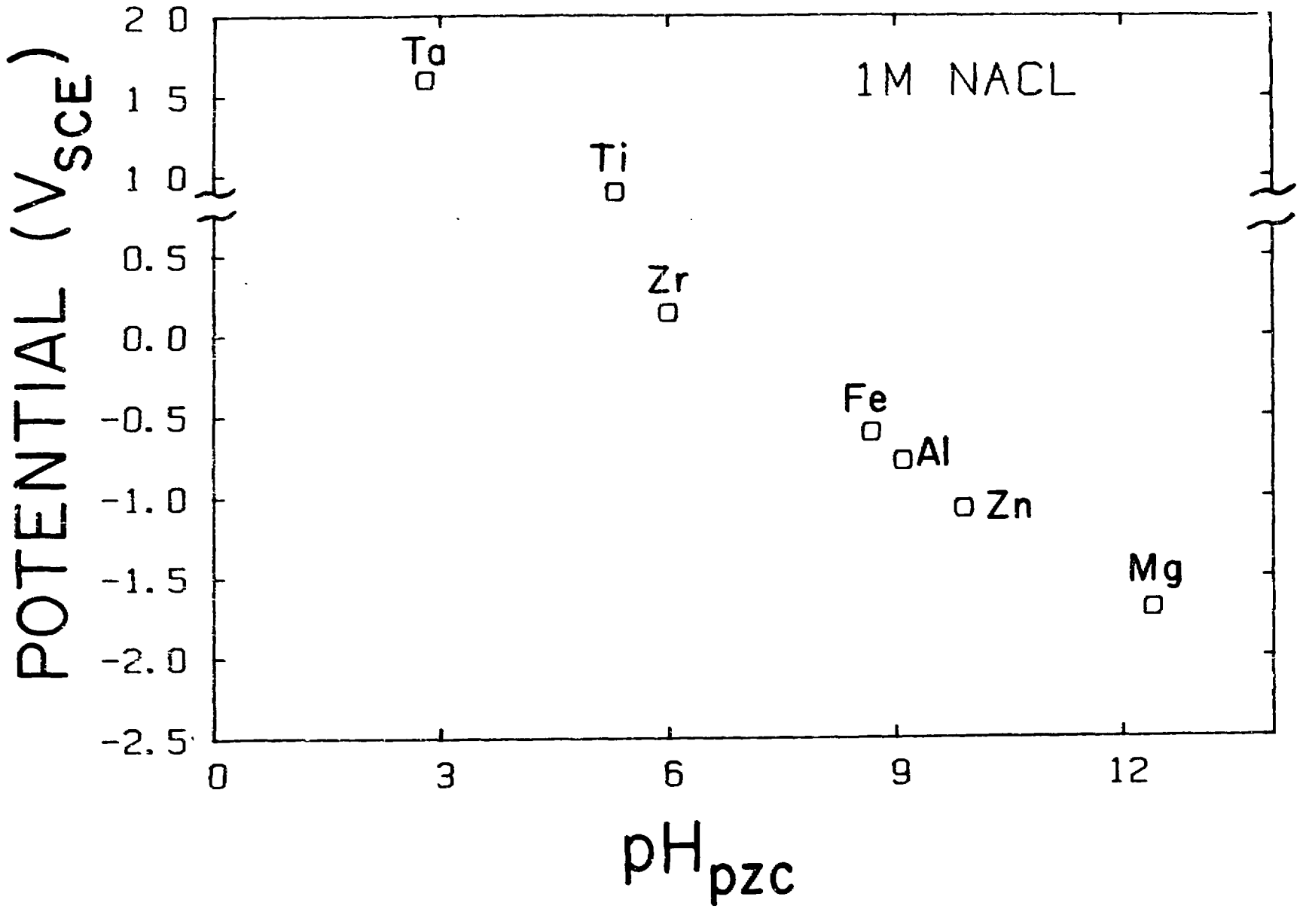
1M NACL
Ta
Ti
Zr
Fe
Al
Zn
Mg
POTENTIAL (V_{SCE})
2.0
1.5
1.0
0.5
0.0
-0.5
-1.0
-1.5
-2.0
-2.5
0
3
6
9
12
pH_{pzc}

BIOGRAPHY

Name:

Paul M. Natishan

Present Affiliation:

Environmental Effects Branch
Code 6314
Naval Research Laboratory
Washington, DC 20375
(202)-767-1344

Title:

Research Metallurgist

Field of Interest/Responsibilities:

Localized corrosion of metals and alloys. In particular, the study of passive films and the breakdown of these films.

Previous Affiliation/Titles:

NRL/NRC Research Associate
Oct. 1983 - Oct. 1985

Academic Background:

PhD. (Materials Science) University of Virginia, Charllotesville, Va., 1983.
M.S. (Materials Science) University of Virginia, Charlottesville, Va., 1979.
B.S. (Biology) Wilkes College, Wilkes-Barre, Pa., 1975.

Society Activities/Offices/ Awards:

National Research Council Associateship Award, 10/83 - 10/85.

Representative to the Individual Membership Committee, The Electrochemical Society, 1986-

Session Vice Chairman, Electrochemical Society, San Diego, Ca. 1986.

Presentations:

11 presentations have been delivered at universities, technical societies, and research centers.

Invited lectures have been presented at:

Aluminum Company of America, Alcoa Center, Pa., May 1986.
University of Virginia, Charlottesville, Va., November 1985.
Johns Hopkins University, Baltimore, Md., February 1985.
Dow Chemical Company, Midland, Mi., February 1982
Wilkes College, Wilkes-Barre, Pa., April 1980.

Publications:

"The Pitting Behavior of Ion Implanted Aluminum Surface Alloys", P.M. Natishan, E. McCafferty, and G.K. Hubler in "Surfaces, Inhibition, and Passivation", E. McCafferty and R.J. Brodd, Eds., The Electrochemical Society, Pennington, N.J., (1986).

"Naval Research Laboratory Surface Modification Program: Ion Beam and Laser Processing of Metal Surfaces for Improved Corrosion Resistance", E. McCafferty, G.K. Hubler, P.M. Natishan, P.G. Moore, R.A. Kant, and B.D. Sartwell, Materials Science and Engineering, (in press).

"Graphite Composite Electrodes in the AC Disinfection of Latex", P.M. Natishan, G. E. Stoner, G. L. Cahen, Jr., and L.L. Scribner, I/EC Process Design and Developement, (accepted for publication 8/86).

"The Effect of the pH of Zero Charge on the Pitting Potential", P.M. Natishan, E. McCafferty, and G.K. Hubler, Journal of the Electrochemical Society, 133, 1061, (1986).

"Corrosion Protection by Ion Beam or Laser Processing", E. McCafferty, P.M. Natishan, P.G. Moore, G.K. Hubler, R.A. Kant, and B.D. Sartwell in "Proceedings of the 1985 Tri-Service Conference on Corrosion", Battelle Laboratories (in press).

"The Use of Composite Electrodes for the Electrochemical Disinfection of Recirculating Fluids", Ph.D. Dissertation, University of Virginia, (1983).

"Fluoride Determination in Dental Alloys", M.S. Thesis, University of Virginia, (1979).

AGENDA FOR ADVANCING ELECTROCHEMICAL SCIENCE AND TECHNOLOGY

by

W. S. Smyrl, S. M. Wolf, and A. H. Landgrebe

Authors' note: This paper is based on a study of the same title, and details of its findings will be available after the report is published.[1] The conclusions and recommendations in this paper are those previously published.[2]

INTRODUCTION

The economic cost of corrosion in the United States has been estimated[3] to be about $120 billion (in 1982). This staggering figure amounts to about 4 percent of the gross national product, or more than $500 per person annually in the United States. The broad categories examined are shown in Table 1 along with the losses that could be avoided by implementation of known corrosion control technology. It is noteworthy that new technology will be required to avoid most of the costs.

TABLE 1. Estimated 1982 Corrosion Costs for the United States

Category	Cost ($ billion)	Avoidable Cost ($ billion)
Energy industries	67.5	1.4
Electric power	6.6	0.2
Material production	13.9	0.4
Government operations	17.8	4.5
Personally owned automobiles	16.2	10.5
Total	122.0	17.0

The federal government has made major commitments to support certain aspects of electrochemical science and engineering. Information on the level of federal support of basic research and of applied research and development (i.e., classifications 6.1 and 6.2/6.3/6.4, respectively, in Department of Defense terminology) was obtained from managers in the Departments of Commerce, Defense, Energy, Interior, and Transportation, the National Science Foundation, the National Aeronautics and Space Administration, and the National Institutes of Health. Corrosion was identified by most agencies as part of their electrochemistry programs. Total basic and applied funding for corrosion was about $9 million and $7 million, respectively.

CONCLUSIONS AND RECOMMENDATIONS

The study led to the conclusion that a new approach to corrosion science and corrosion engineering is not only necessary but possible. The required capabilities are becoming available in the scientific ability to model surfaces and interfaces, in the electrochemical and surface science techniques for studying interfaces in situ, in the computational facilities for modeling, and in materials processing technology. An approach is required that builds on existing multidisciplinary capabilities of individuals and institutions. Further, this approach must provide a mechanism that integrates multidisciplinary activities into a framework that brings coherence to complex phenomena and yields a comprehensive basis for understanding them. Six central recommendations were identified on theory and modeling, experimental probes, lifetime prediction, investigation of advanced materials, multidisciplinary efforts, and education.

- *Theory and Modeling: Greater emphasis on modeling and theory is recommended for both elementary corrosion processes and their interactions in complex macroscopic systems. Given the opportunities and need in the next decade for this field to adopt advances made in other disciplines, the study concluded that greater support of theory and modeling is justified even if the total support of this field remains constant.*

Two complementary areas for theory and modeling have been identified—elementary processes and macroscopic systems. Regarding elementary processes, new theoretical approaches for characterizing electrolytes are in hand and are being applied to dielectric-solvent surfaces. Just emerging are theoretical treatments for the physics of electrons at metal-electrolyte interfaces. The incorporation of understanding from both these areas in theories to describe the elementary processes at metal-electrolyte interfaces is possible, even for the complex interfaces encountered in corrosion systems. Extension of this work to include interfacial films will provide a fundamental physical understanding of metallic corrosion capable of predicting corrosion behavior from first principles.

Descriptions of individual corrosion processes can be assembled and used to predict materials degradation in macroscopic systems. However, the computations required are usually so lengthy and complex as to require access to large scale computational facilities. Expansion of this approach to the analysis and prediction of corrosion behavior on a wider scale requires the development of more efficient mathematical techniques and algorithms and of methods for simplifying the calculations without loss of significant factors.

- *In Situ and High Resolution Experimental Probes: The active support now given to the development of probes to measure corrosion processes in situ and with the spatial resolution needed for studying local corrosion phenomena should be continued. Of particular importance is the use of probes where possible as sensors for on-line monitoring of corrosion of components in technologically important systems.*

Over the past decade, a revolution has occurred in the field of electrochemistry with the development of in situ and ex situ surface analysis techniques capable of resolving important phenomena on both microscopic and short time scales. These techniques should be adapted and utilized to characterize local physicochemical corrosion events in situ. In addition, in situ techniques should be extended to provide on-line monitoring of real-world systems where reliability often requires detecting the onset and progress of corrosion phenomena (e.g., pit depth and crack length) as a function of time.

- *Lifetime Prediction in System Applications: Quantitative methodologies for predicting lifetimes should be developed, coupling advanced models with identification and measurement of critical parameters and with computer-based expert systems. This effort will necessitate generating physicochemical data bases to support systems analysis as well as using advances in theory and experimental techniques discussed above.*

A major objective of corrosion science and engineering is to permit selection of materials giving corrosion resistance compatible with system design in specific service environments. Even for the simplest case, general corrosion of metals, present lifetime prediction strategies are qualitative or nonexistent because of the lack of (a) realistic models, (b) understanding of critical parameters, (c) test data, or (d) suitable coupling between the models and the experimental results. These factors must be addressed if materials are to be selected for reliable and economic service.

Currently available thermodynamic and kinetic data bases are incomplete to support quantitative modeling of many corrosion systems, particularly those where predictions of behavior under extreme conditions or over extended periods of time are desired. Because the unavailability of data limits the use of models, a critical need exists to upgrade and expand the sources of information on the thermodynamic properties of chemical species, exchange current densities, activity coefficients, rate constants, diffusion coefficients, and transport numbers, particularly where concentrated electrolytes under extreme conditions are involved. Many of these data are obtained in disciplines that traditionally have been on the periphery of corrosion science, so it will be necessary to encourage interdisciplinary collaboration to meet the need.

A number of proprietary expert systems are being developed for corrosion engineering, specifically for materials selection in marine environments, in pressurized water reactor steam generators, and for high strength aluminum alloys. The availability to designers of computer-based expert systems for corrosion engineering will improve the performance and reliability of new structures and systems. Knowledge of corrosion and related phenomena for specific materials under consideration for use is an important input to the materials selection process in the early stages of design, where problems can be dealt with most effectively and without compromising design intent. This knowledge is at present gained principally through practical experience and so is held by "experts". Codifying their knowledge for wider accessibility and utility will lead to improved corrosion resistant designs.

- *Corrosion Resistance of Advanced Materials: The corrosion behavior and limits of chemical stability of newly developed materials should be determined as an integral part of materials development in order to indicate where more detailed modeling and experimental efforts are warranted.*

New engineering materials, evolved through chemical synthesis or advances in processing, require study to determine the limits of their corrosion resistance in service environments. Baseline investigations on advanced materials are a prerequisite if their corrosion properties are to be characterized sufficiently to allow them to be introduced reliably into engineering systems. For example, some metallic glasses appear to be remarkably inert and have commercial appeal. In contrast, metal-matrix composites are being pursued for structural applications but in many cases appear to lack corrosion resistance. The use of ceramics in electrochemical systems as separators, electrodes, electrolytes, and containment vessels emphasizes the importance of understanding and enhancing reliability while maintaining attractive chemical, electrical, and other properties in new service environments.

- *Multidisciplinary Activities and Education in Corrosion Science and Engineering: Industry, government, and academia should foster multidisciplinary research approaches. These will draw upon advances made in related fields of physics, mathematics, and electrochemistry, among others, and must build on the strengths of individual participants and facilities in these several fields.*

Advances in the stabilization of interfaces will benefit from enhanced multidisciplinary approaches in education, in research, and in application. Because corrosion science incorporates elements of physics, chemistry, electrochemistry, materials science, mathematics, and engineering, it is essential that scientists and engineers skilled in these disciplines be encouraged to contribute to this field, i.e., to its concepts and theories, predictive methods, and experimental techniques. The panel concluded that industry and government should provide this encouragement by expanding support of collaborative efforts. The panel further concluded that an essential part of the development of this field will be improved undergraduate and graduate education in this field in universities; this is needed to provide trained engineers and scientists capable of contributing to advances called for in efforts recommended in this report.

- *Instruction in Corrosion Practice: Improved education must be provided on a continuing basis to engineers responsible for materials selection.*

A broader knowledge of corrosion on the part of the users of materials in design will result in major reductions in the corrosion- related costs of maintenance, repair, and replacement. The correct selection and usage of materials to withstand the corrosive environ- mental influences that cause degradation and failure must be based on an appreciation of these influences and the ways in which they can affect materials and structures. Such knowledge can be supplied by utilizing existing resources for continuing education and should be a part of the background of all those who are concerned with design. However, the education of engineers at the bachelor level is deemed inadequate with respect to corrosion—it will probably be limited to a single course in a materials curriculum. Efforts should be made to include more laboratory experience in corrosion in conjunction with lecture courses at this level.

REFERENCES

1. Panel on Electrochemical Corrosion of the Committee on Electrochemical Aspects for Energy Conservation and production. Agenda for Advancing Electrochemical Corrosion Science and Technology. NMAB 438-2. National Materials Advisory Board. Washington, D.C., National Academy Press, to be published, 1987.

2. Committee on Electrochemical Aspects of Energy Conservation and production. New Horizons in Electrochemical Science and Technology. NMAB 438-1. National Materials Advisory Board. Washington, D.C., National Academy Press, 1986.

3. R. E. Meredith. The Cost of corrosion and the Need for research. Report to Office of Energy systems. U.s. Department of energy, Washington, D.C., 1983.

BIOGRAPHICAL SKETCHES

ALBERT R. LANDGREBE received a B.S. degree in chemistry from Fordham University and a Ph.D. degree from the University of Maryland. After graduating, he spent five years at the National Bureau of Standards, then became a staff member at the Atomic Energy Commission, Energy Research and Development Administration and the Department of Energy. His research interest include electrochemistry, radiochemistry, chemical separations and corrosion.

WILLIAM H. SMYRL is a Professor of Chemical Engineering and Materials Sciences and Associate Director of the Center for Corrosion Research at the University of Minnesota. He received his Ph.D. (chemistry) at the University of California, Berkeley, and spent 3 years at the Boeing Scientific Research Laboratories and 11 years at Sandia National Laboratories. He joined the faculty of the University of Minnesota in 1984. His research interests are modeling of corrosion processes, in situ techniques for metal-metal oxide interface studies, digital impedance for faradaic analysis, stress corrosion cracking, polymermetal interfaces, and electrochemical processes.

STANLEY M. WOLF is a Senior Staff Scientist in the National Materials Advisory Board in the Commission on Engineering and Technical Systems of the National Research Council. His current studies address the role of materials science and engineering in various technologies in an industralized society. Before joining the National Research Council in 1985, Dr. Wolf spent 22 years with the federal government conducting and managing materials research programs, including high temperature and electrochemical corrosion. He received his education at Massachusetts Institute of Technology, Cornell University, and Virginia Polytechnic Institute and State University.

SESSION B
AIRCRAFT CORROSION

Chairman
Richard Kinzie
Warner Robins Air Logistics Center

Preceding Page Blank

WATER BASED PRIMERS FOR STRUCTURAL ADHESIVE BONDING OF AIRCRAFT

A. V. Pocius and T. H. Wilson, Jr.
Adhesives, Coatings and Sealers Division
3M
St. Paul, Minnesota 55144-1000

ABSTRACT

Physical characteristics, coating characteristics and performance characteristics of three new primers useful for structural adhesive bonding of aircraft are discussed. The most evident characteristic of these new primers is that they are primarily water vehicled primers in contrast to today's primers which are primarily solvent vehicled. Thus, these primers meet the stricter pollution control regulations now found in many states. Two of these primers, XB-3982, and XB-3983, can be spray applied using conventional methods and provide performance characteristics equivalent to today's solvent vehicled primers. Thus, these new primers can directly replace their solvent based analogs. The third primer, XA-3995, is a cathodic electrophoretically applied structural adhesive bonding primer. This primer is primarily water vehicled and provides good high temperature performance. In addition, the cathodic electrophoretic application method allows for uniform, reproducible application of thin coatings of primer with very efficient utilization of material.

1. INTRODUCTION

Currently aircraft adherends are primed with corrosion-inhibiting primers which are generally, organic solvent thinned, epoxy and phenolic based, cured at 121°-176°C and which contain an organic insoluble, slightly water-soluble corrosion-inhibiting pigment (usually a chromate salt). The performance characteristics that a structural adhesive bonding primer must have are listed in Table 1. Although present day materials have these necessary characteristics, they suffer from several drawbacks:

Preceding Page Blank

- They are organic solvent thinned and do not comply with new, stricter pollution control regulations;
- They are applied by "line-of-sight" methods and cannot be used to coat inaccessible portions of complex parts (e.g. the interior of a honeycomb cell); and
- Solvent-based primers are relatively brittle (in comparison to the adhesive). If the primer is applied too thick, bond performance can be reduced[1].

The new pollution control regulations mentioned above shall limit future utilization of organic solvent thinned structural bonding primers. For example, California Rule 1124 limits the amount of organic solvent that a structural adhesive bonding primer can contain to 375 grams/liter of organic solvent as applied, less water. Virtually all of the presently used structural adhesive bonding primers far exceed this organic solvent content. Thus the necessity for development of water thinned structural adhesive bonding primers.

This paper describes the physical characteristics, coating characteristics and performance characteristics of 3M's new water thinned structural adhesive bonding primers and compares them to their solvent based analogs. The data contained herein demonstrate that water thinned primers can perform as well as solvent thinned materials and still meet pollution control regulations.

2. Spray Applied Primers

a. Experimental

I. Metallic Adherends and Surface Preparation.

The metals used in this study were two alloys of aluminum; bare 2024-T3 and bare 7075-T6. "Bare" indicates the absence of cladding. The surface preparation was phosphoric acid anodization. The phosphoric acid anodization process that we used is shown in Table 2.

II. Primer Application and Curing

All of the primers were applied by means of a Binks Model 62 Spray Gun equipped with a siphon. The air cap was a #66S while the fluid tip and needle were #66. The distance from the panel was 9 ± 3 inches. The spray gun line pressure for application of EC-3960, EC-3917 and XB-3982 was 30 psi but was 50 psi for XB-3983. The primers, after application were air dried at ambient temperature for 1/2 hour and then cured in a forced air oven at 250°F (121°C) for 1 hour. The resulting cured primer thickness as measured by a Förster Isometer

was 0.003 ± 0.0001 cm (0.12 ± 0.04 mils).

III. Adhesive Bonding and Physical Characterization

The film adhesives used in this work were AF-163-2K (0.06 lb./sq. ft.) and AF-143 (0.075 and 0.04 lb./sq. ft.) all products of 3M. The adhesives were cut into the appropriate shapes and laid up by hand at ambient laboratory temperature. The cure schedule for AF-163-2K was a rise rate of 4-5°F/min. to 250°F (121°C) under a positive pressure of 35 psi. The bonds were held at 250°F (121°C) for one hour. The cure schedule for AF-143 was a rise rate of 4-5°F/min. to 350°F (177°C) under a positive pressure of 45 psi. The bonds were held at 350°F (177°C) for 1 hour. After the bonds were cooled to room temperature, they were sawn into the appropriate shapes. Ultimate strength characteristics were measured on an Instron Tensile Tester rated for 10,000 lbs. force. The rate of crosshead displacement for lap shear tests (ASTM D1002) was 0.1 inch/min. (0.25 cm/min.) while the crosshead displacement rate for the floating roller peel test (ASTM D3167) was 6 inches/min. (15.2 cm/min.) for AF 163-2K while for AF-143 it was 12 inches/min. (30.5 cm/min.). For elevated and reduced temperatures from ambient, the samples were conditioned to temperature and tested in a Missimers Environmental Cabinet.

IV. Durability Testing

Durability of bond made with adherends primed with the primers discussed above was estimated by two methods. The first method is described by Pocius, et. al.[2]. It involves exposing lap shear specimens of a certain type to a high temperature (140°F (60°C)), condensing humidity (95-100% RH) environment while maintaining a sustained load on the specimen. The combination of high temperature, high humidity and high stress is thought to be the most deleterious to bond durability[3]. The stress applied to the joints was either 1200 psi (8.27 MPa) or 1800 psi (12.4 MPa). The time to failure was then recorded.

The second method used to gauge durability was the wedge test. This test is described in Reference 4 and is essentially a uniform thin adherend double cantilever beam fracture test in which the Mode I load is applied by means of driving a wedge into the end of a 1 inch wide specimen. The crack opened specimen is then placed in a high humidity, high temperature chamber (140°F

(60°C)/95-100% RH) and the growth of the crack is determined.

V. Salt Fog Testing

Samples of surface prepared and primed metal were scribed with an "X" by means of a razor blade and were then placed in a salt fog cabinet maintained under the conditions specified in ASTM B117. In addition floating roller peel specimens were exposed to the same environment to determine the extent of corrosion in the bondline under the salt fog conditions.

VI. Electron Microscopy

Samples of uncured, partially cured and completely cured primers that had been coated on aluminum were examined by means of a JEOL Model 840 Scanning Electron Microscope having a resolution of 100Å. Two types of images were obtained. A topographical view of each surface was obtained by secondary electron imaging while an elemental contrast image was obtained by backscattered electron imaging.

b. Results and Discussion

Table 3 shows some important characteristics of XB-3982 and XB-3983. Notable in these characteristics is the low content of organic solvents and the much increased flashpoint. More important are the strength characteristics of adhesive bonds made with these primers. Tables 4 and 5 show lap shear performance comparing XB-3982 and XB-3983 to their solvent thinned counterparts, EC-3960 and EC-3917. It is evident that the primers all provide the same level of performance, as is desired. In Tables 6 & 7 the peel performance of bonds made with adherends primed by these materials is compared. Once again the performance of the water thinned materials equates that for the solvent thinned materials.

Having demonstrated that physical performance is not degraded by the use of a water thinned primer, it remains to be shown that resistance of adhesive bonds to adverse environment is not severely degraded by the use of a water thinned primer. Needless to say, the greatest concern is the resistance of a primed adhesive bond to moisture and salt fog especially in light of the fact that the primer itself was applied from water. The resistance of primed floating roller peel specimens to a salt fog environment is shown in Tables 8 and 9. Once again, the water thinned primers are compared to their solvent thinned counterparts. As can be seen, the

performance of the bonds is unaffected by the type of primer. Most importantly when the bonds were peeled open, no corrosion was found internal to the adhesive bond. As discussed in Table 1, these primers must also protect metal surfaces from corrosion in much the same way as metals are protected by paints. Table 10 gives a verbal description of the corrosion protection provided by the various primers used as coatings when exposed to 30 days of a salt fog environment. The thickness of primer used in these exposure panels was the same as that used in the physical property tests. As can be seen, the water based coatings provide good performance as a corrosion protective coating. For EC-3960 versus XB-3982, there is a slight edge for the solvent thinned material. For the EC-3917 versus XB-3983, there is definitely a large improvement when the water thinned primer is used. EC-3917 has been used successfully for over 20 years in the aerospace industry. We can thus assume that the protection afforded by XB-3983, will be proportionally better than EC-3917.

Part of the reason for the equivalent or improved performance of the water thinned coatings can be provided by the electron micrographs shown in Figures 1-4. Figures 1 and 3 were obtained using secondary electron imaging which gives a topographical view of the surface. Figures 2 and 4 were obtained using backscattered electron imaging which gives elemental information as well as topographical information. Darker areas in Figures 2 and 4 correspond to organic media (low atomic weight) while the lighter areas correspond to inorganic materials (higher atomic weight). As can be seen by comparison of the micrographs of the primer surfaces, the new water thinned primers provide substantially better coverage of the surface than the solvent thinned materials. Provision of a better barrier to corrosive media due to the better continuity of the coating is the probable reason for the equivalent or improved performance of XB-3982 and XB-3983 versus EC-3960 and EC-3917.

Durability of adhesive bonds made with adherends primed with the materials under discussion was evaluated in two ways; life under sustained load/high humidity/high temperature and using the wedge test. Table 11 shows the wedge test data comparing EC-3917 and XB-3983. The degree of crack extension for bonds made with both metals and both primers is essentially equivalent. The sustained load durability data

comparing EC-3960 and XB-3982 is shown in Table 12. This data demonstrates that under these loading conditions, XB-3982 provides superior durability to the solvent thinned primer. There is, however, a discrepancy between this data for EC-3960 and earlier work, i.e., EC-3960 has given sustained load durability performance in excess of 500 days in earlier tests. This matter is presently under investigation in our laboratory.

The above discussion and the data presented in Tables 3-12 indicate that the alternative to structural adhesive bonding primers containing large amounts of solvent is now available.

3. Cathodic Electrophoretically Depositable Structural Adhesive Bonding Primer (CEDSABP) (XA-3995)

a. Introduction

Electrodepositable paints have been used in industry for over 25 years. The technology of cathodic electrophoretically depositable paints has been discussed[5]. "Paints" however, differ from "structural adhesive bonding primers" because of the differences in their function. After application a "paint" does the following.

- Provides a decorative coating
- Can provide corrosion protection if so formulated; and
- Provides an adequate surface for application of subsequent topcoats.

These functions contrast those for a structural adhesive bonding primer (See Table 1). Most paints cannot conform to all the requirements listed in Table 1, especially those relating to strength and solvent resistance. There are examples of CEDSABPs in the literature[6] but these materials are useful at temperatures under 180°F (82°C). A need existed for a CEDSABP having elevated temperature resistance. 3M's proprietary knowledge of new high temperature resin systems was utilized under Air Force Contract F33615-86-R-5009 to complete development of a new high temperature resistant CEDSABP, XA-3995.

b. Experimental

I. Metallic Adherends and Surface Preparation

2024-T3 bare aluminum alloy was converted to T81 by heat soak at 375°F for 12 hours. The 2024-T81 alloy was surface prepared by the method of Table 2. Honeycomb core (5052) was also surface prepared by the method of Table 2.

II. Primer Application and Curing

Primer was applied by means of an electrodeposition cell in which the cathode was the surface prepared 2024-T81 and the anode was stainless steel. Voltages were applied by means of a Kepco regulated power supply and monitored by a Digitec Voltmeter. Various voltages were used to coat the primer until a voltage was found which gave a uniform, thin coating on the metal work piece. This voltage (20-30V) was then used throughout this work. The primer was then cured at 350°F for 2 hours.

III. Adhesive Bonding and Physical Characterization

The film adhesive used in this work was AF-143 as described in Section 2.a.III. above. The bonding and testing procedures were also described in Section 2.a.III.

IV. Durability Evaluation - Salt Fog Testing

Durability tests such as those described for XB-3982 and XB-3983 have not been completed for XA-3995. However, exposure of scribed panel and lap shear specimens to an ASTM B117 salt fog cabinet have been completed.

V. Electron Microscopy

See Section 2.a.IV.

c. Results and Discussion

Results of physical properties tests for XA-3995 are shown in Table 13. In this table we compare the performance of XA-3995 to EC-3917. The results indicate that the performance of XA-3995 either equates or exceeds the performance of EC-3917. Especially impressive is the difference in coating corrosion resistance in which XA-3995 exhibits a complete barrier to corrosion after 30 days exposure to an ASTM B117 salt fog exposure. Once again, the reasons for this improved resistance to corrosion may be due to improved coating quality. Figure 5 shows electron micrographs of the surface of XA-3995 which can be compared to Figures 1 and 2 for EC-3917. After cure, XA-3995 completely coats the metal creating an essentially pinhole free surface. The reader should also note that flatwise tension measurements were made using XA-3995. The honeycomb core and face sheets were electrophoretically coated with XA-3995 creating a thin, continuous organic coating over all of the surfaces of the honeycomb resulting in excellent flatwise tension performance. In addition to the noted excellent

performance, XA-3995 does not contain chromates and therefore reduces enviromental concerns.

4. SUMMARY

We have shown that three new water thinned structural adhesive bonding primers are now available to the Aerospace industry. XB-3982 and XB-3983 are water thinned primer that can be applied by conventional spray equipment while XA-3995 is applied by cathodic electrophoretic deposition. All three of these primers meet or exceed the performance of their solvent thinned counterparts.

5. ACKNOWLEDGMENTS

The authors would like to acknowledge the help of Mr. E. Osten who performed the electron microscopy. The authors would also like to acknowledge Air Force funding for completion of the development of XA-3995 under contract F33615-86-R-5009 administered by Wright Patterson Air Force Base, Mr. P. Tydings, Program Officer. The work was done under subcontract to Rohr Industries, Mr. R. H. Greer, Program Manager.

6. REFERENCES

1. A. V. Pocius, Proc. National SAMPE Technical Conference, 13, Azusa, CA, 1981, pp. 467-476.

2. A. V. Pocius, D. A. Wangsness, C. J. Almer, and A. G. McKown, in "Adhesive Chemistry-Developments and Trends", (L-H Lee, editor), Plenum Press, New York, 1984, pp. 617-642.

3. J. L. Cotter, in "Developments in Adhesives", 1 (W., C. Wake, Ed.), Applied Science, London, 1977, p. 1.

4. J. C. McMillan in "Bonded Joints and Preparation for Bonding", AGARD Lecture Series, No. 102, Harford House, London, 1979.

5.a. P. E. Pierce, J. Coat. Tech., 53, 52 (1981).
b. M. Wismer, P. E. Pierce, J. F. Bosso, R. M. Christenson, R. D. Jerabek, R. R. Zwack, J. Coat Tech., 54, 35 (1982).

6.a. S. L. Diener, S. J. Mels, Proc., National SAMPE Tech. Conf., 11, Azusa, CA, 1979, pp. 759-769.
b. G. T. Beckwith, T. Pollard, Proc. National SAMPE Tech. Conf., 17, Covina, CA, 1985, pp. 400-409.

Table 1

Performance Characteristics of a Structural Adhesive Bonding Primer

1. Provides protection against corrosion inside and outside of the bonded joint.

2. Provides a surface to which the adhesive can easily bond.

3. Provides protection for the surface prepared adherends during handling before bonding.

4. Exhibits resistance to aircraft fluids such as jet fuel, hydraulic fluids, solvents, etc.

5. Is capable of transferring structural load from the adherend through the surface preparation to the adhesive.

6. At appropriate thickness, displays no deleterious effects on the shear or peel properties of the adhesive bond.

Table 2

Phosphoric Acid Anodization Process

*Alkaline Degrease

Oakite 164 (180°F), 10 Minutes

*Cold Water Dip

*Cold Tap Water Rinse, 2 Minutes

*Optimized FPL Etch (155°F), 10 Minutes

*DI Water Rinse, 2 Minutes

*Phosphoric Acid Anodization

3.1 N

Room Temperature

15V for 22.5 Minutes

*DI Water Rinse, 5 Minutes

*Air Dry, 10 Minutes

*Forced Air Dry (155°F), 10 Minutes

*Prime Parts Within 72 Hours

Table 3

Physical Characteristics of Water Thinned Primers

	XB-3982	EC-3960	XB-3983	EC-3917	XA-3995
Organic Solvent Content (g/l)	114	771	56	759	44
Flash Point (°F)	75*	6**	95*	20*	120*
Viscosity (cpse)***	96	72	68	35	88
Type of Corrosion Inhibiting Pigment	Chromate	Chromate	Chromate	Chromate	Non-Chromate

*SETA FLASH - Closed Cup

**TAG-END Cup

***Brookfield LVF, Spindle 1

Table 4

Lap Shear Performance (psi) Comparing EC-3960 and XB-3982

Adhesive is AF-163-2K (0.06 wgt.)

Metal	2024-T3		7075-T6	
Product	EC-3960	XB-3982	EC-3960	XB-3982
Temperature of Test				
-67°F (-55°C)	7250 ± 320	7400 ± 70	9013 ± 612	9175 ± 519
RT (25°C)	5821 ± 324	5887 ± 133	6211 ± 114	6148 ± 75
180°F (82°C)	3471 ± 124	3468 ± 113	3432 ± 63	3497 ± 47

(Average of 6 Specimens)

Table 5

Lap Shear Performance (psi) Comparing EC-3917 and XB-3983

Adhesive is AF-143 (0.075 wgt.)

Metal	2024-T3		7075-T6	
Product	EC-3917*	XB-3983*	EC-3917*	XB-3983**
Temperature of Test				
-67°F (-55°C)	3498 ± 300	3450 ± 241	3599 ± 422	3662 ± 320
RT (25°C)	3363 ± 271	3380 ± 160	3523 ± 223	3340 ± 79
300°F (149°C)	3461 ± 151	3423 ± 258	3615 ± 291	3340 ± 79

* Average of 12 specimens

** Average of 6 specimens

Table 6

Floating Roller Peel Performance (piw) Comparing EC-3960 and XB-3982

Adhesive is AF-163-2K (0.06 wgt.)

Metal	2024-T3		7075-T6	
Product	EC-3960	XB-3982	EC-3960	XB-3982
Test Temperature				
-67°F (-55°C)	107	123	83	73
RT (25°C)	91	90	76	74

(Average of 3 specimens)

Table 7

Room Temperature

Floating Roller Peel Performance (piw) Comparing EC-3917 and XB-3983

Adhesive is AF-143 (0.04 wgt.)

Metal	2024-T3		7075-T6	
Product	EC-3917	XB-3983	EC-3917	XB-3983
RT (25°C)	6	7	4	4

Table 8

Room Temperature Floating Roller Peel Performance (piw) as a Function of Exposure to Salt Fog

Adhesive is AF-163-2K (0.06 wgt.)

Metal	2024-T3						7075-T6					
Product	EC-3960			XB-3982			EC-3960			XB-3982		
Days in Salt Fog	30	60	90	30	60	90	30	60	90	30	60	90
Peel Strength	92	92	84	92	86	96	74*	81*	81	68	71	66
% Corrosion	0	0	0	0	0	0	0	0	0	0	0	0

Each peel strength is the average of three values except those marked with an * which are an average of two specimens.

Table 9

Room Temperature Floating Roller Peel Performance (piw) as a Function of Exposure to Salt Fog

Adhesive is AF-143 (0.04 wgt.)

Metal	2024-T3						7075-T6					
Product	EC-3917			XB-3983			EC-3917			XB-3983		
Days in Salt Fog	30	60	90	30	60	90	30	60	90	30	60	90
Peel Strength	13*	14*	14*	12	18	19	10*	10*	10*	9	14	14
% Corrosion	0	0	0	0	0	0	0	0	0	0	0	0

Each peel strength is the average of three values except those marked with an * which are an average of 5 specimens.

Table 10

Description of Corrosion on Cross-Hatch "Facial" Panels Comparing Water & Solvent Thinned Primers After 30 Days Salt Fog Exposure

Metal	2024-T3		7075-T6	
Product	EC-3960	XB-3982	EC-3960	XB-3982
	No Corrosion Stain At Top	No Corrosion Med. Dark Stain At Top	No Corrosion	No Corrosion Slight Stain At Top
Product	EC-3917	XB-3983	EC-3917	XB-3983
	All Corroded Dark Color	No Corrosion Stain At Top	All Corroded Dark Colored	No Corrosion Stain At Top

Table 11

Wedge Test Crack Extensions (Inches) Comparing EC-3917 and XB-3983

Adhesive is AF-143 (0.075 wgt.)

Metal	2024-T3		7075-T6	
Product	EC-3917	XB-3983	EC-3917	XB-3983
Crack Extension	0.07 ± 0.06	0.07 ± 0.04	0.05 ± 0.03	0.04 ± 0.04

Table 12

Sustained Load Durability (Days to Failure)

Comparing EC-3960 and XB-3982

(Metal is 2024-T3 Clad Aluminum)

Adhesive is AF 163-2K (0.06 wgt.)

Sustained Load is 1800 psi @ 140°F (60°C)/100% RH

Product	Days to Failure
EC-3960	90, 414
XB-3982	362, 564, 572

Table 13

Performance Characteristics Comparing EC-3917 and XA-3995

Adhesive is AF-143

Metal is H_3PO_4 Anodized 2024-T81 Bare Aluminum

Performance Parameter	EC-3917	XA-3995
-67 Lap Shear (psi)	3401	4140
75°F Lap Shear (psi)	3501	3627
325°F Lap Shear (psi)	3272	3363
350°F Lap Shear (psi)	3189	3090
325°F Lap Shear (psi)	3480	3606
After Exposure to 200 Hrs. at 350°F		
75°F Lap Shear (psi)	3938*	4760*
After exposure to 30 Days Salt Fog		
75°F Floating Roller Peel (piw)	4	5.8
75°F Flatwise Tension (psi)	719	795
325°F Flatwise Tension (psi)	394	449
"Facial" Cross-Hatch Corrosion Test-30 Days Salt Fog Exposure	General Corrosion Over 60% of Panel	No Corrosion

*No bondline corrosion noted.

Secondary Electron Imaging of Primer Surfaces

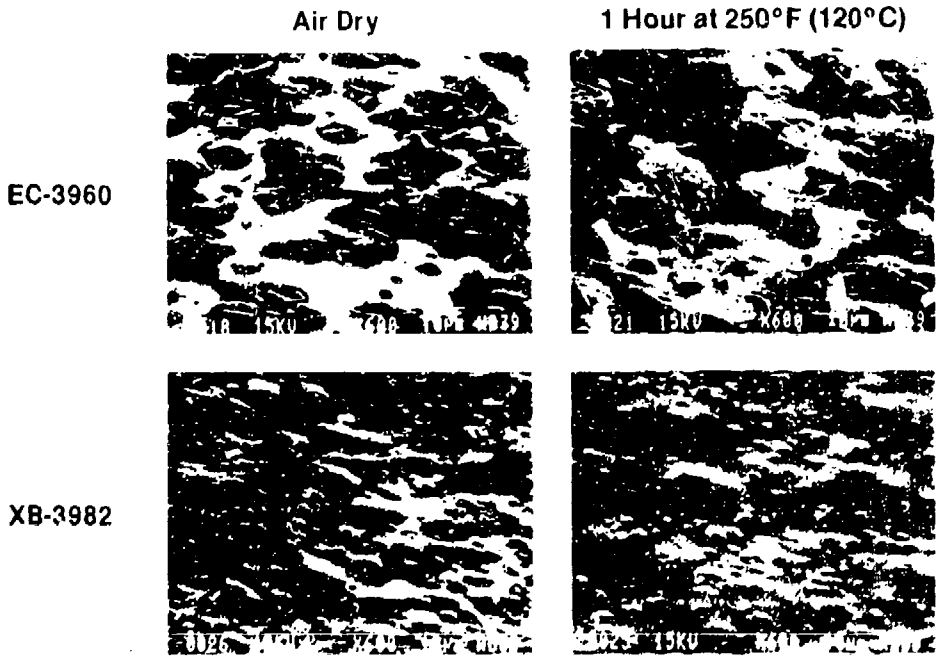

Figure 1

Backscattered Electron Imaging of Primer Surfaces

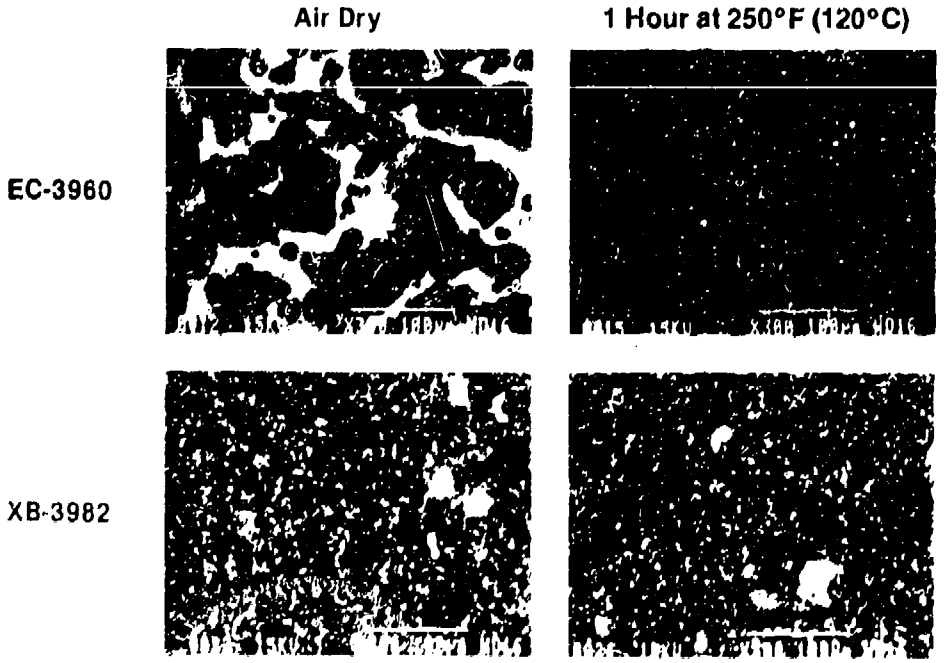

Figure 2

Secondary Electron Imaging of Primer Surfaces

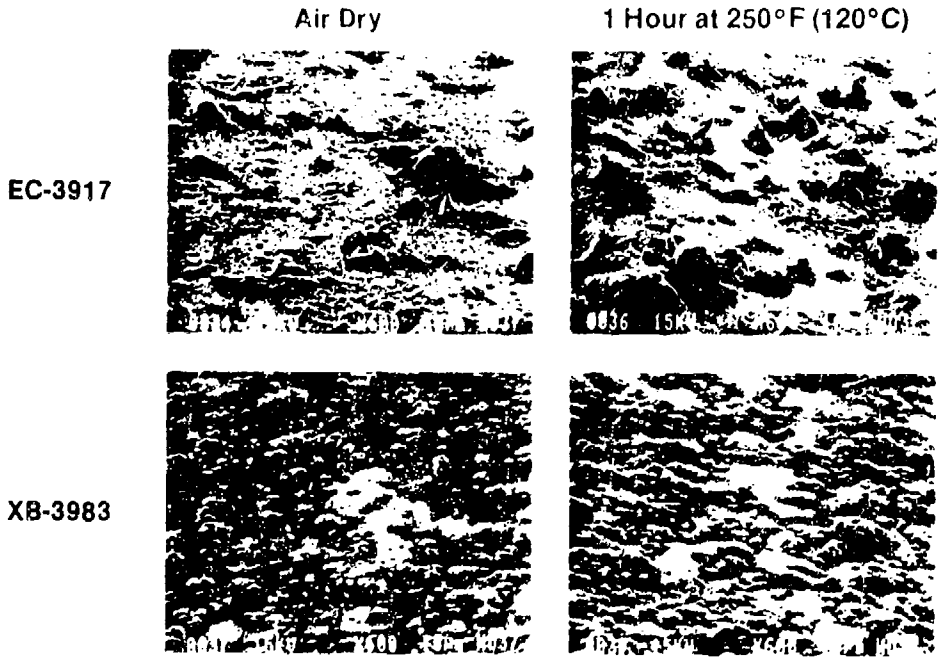

Figure 3

Backscattered Electron Imaging of Primer Surfaces

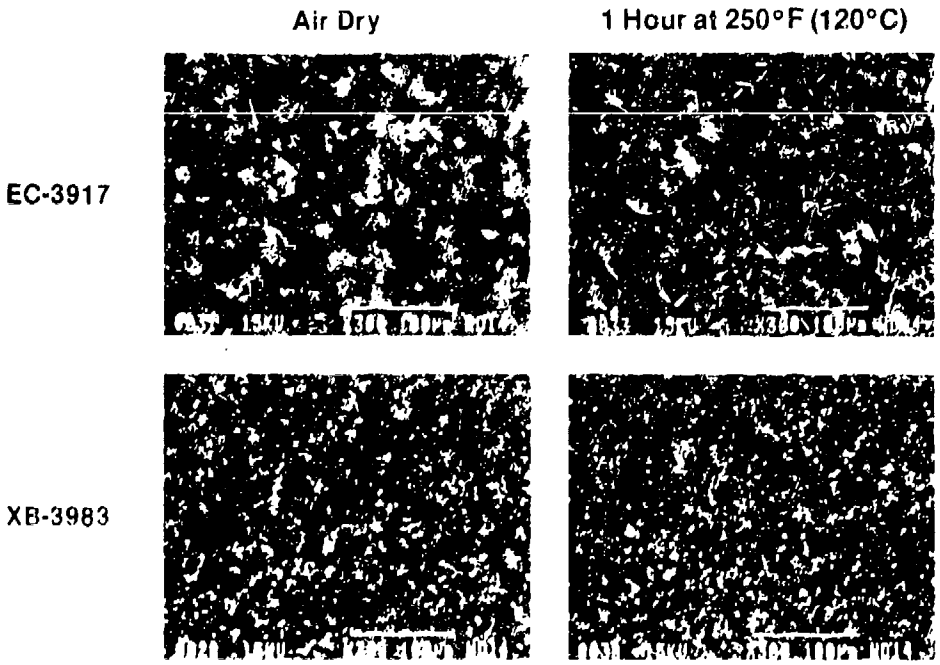

Figure 4

Electron Micrographs of Electrodispositable Primer Surface

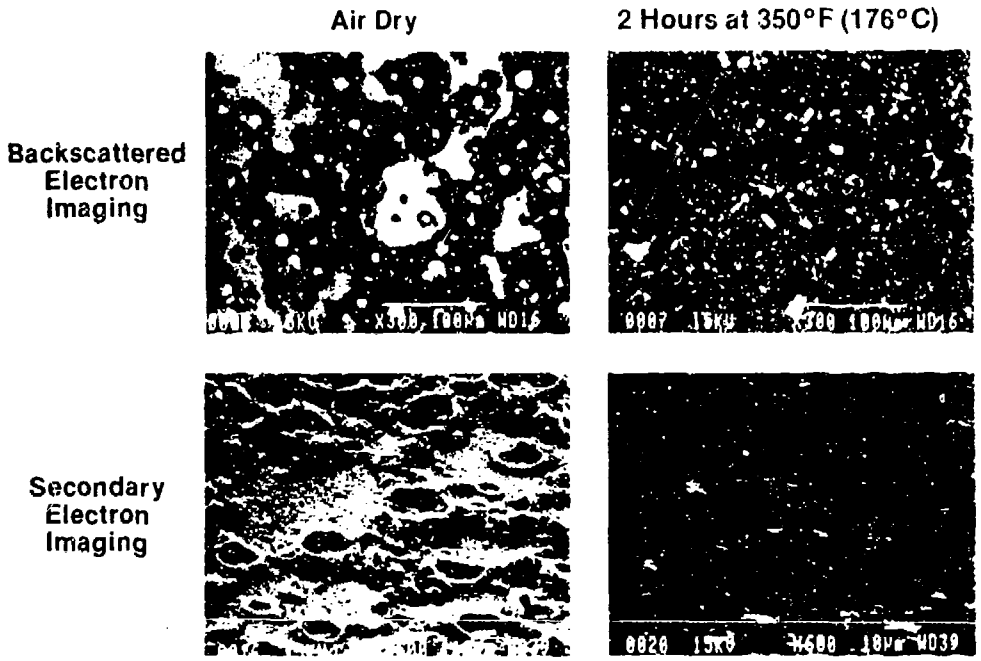

Figure 5

PREVENTING AIRCRAFT CORROSION BY PREDICTIVE CORROSION MODELING

Robert N. Miller
Lockheed-Georgia Company
Marietta, Georgia

Fred H. Meyer, Jr.
AFWAL/MLSA
Wright-Patterson AFB, Ohio

Presented at the

TRI-SERVICE CONFERENCE ON CORROSION

United States Air Force Academy
Colorado

5-7 May 1987

PREVENTING AIRCRAFT CORROSION BY PREDICTIVE CORROSION MODELING

Robert N. Miller
Lockheed-Georgia Co.
Marietta, Georgia 30063

Fred H. Meyer, Jr.
AFWAL/MLSA
Wright-Patterson AFB, Ohio 45433-6533

ABSTRACT

This is a progress report for an Air Force program to optimize aircraft maintenance scheduling through the use of a predictive corrosion model which is based on the kinetics of corrosion reactions, the degradation rates of protective systems and the environmental conditions at Air Force bases.

A VAX-11 FORTRAN computer program has been developed which enables the analysis of specific points on the C-5 aircraft and, utilizing environmental factors and the time periods an aircraft has been at various Air Force bases, gives recommended times for inspection and maintenance. The computer program includes a crack growth module which calculates the remaining flight hours until theoretical cracks grow to half their critical length, a corrosion module which computes the time for exposed aircraft alloys to corrode to a depth of 3 mils, and a coating degradation module which determines the optimum time until the next paint renewal or complete repaint operation.

The predictive corrosion model, when completed, will be used to optimize field and depot level maintenance for aircraft now in operation, inspection and maintenance schedules for new aircraft, and selection of aircraft for Analytical Condition Inspection.

1.0 INTRODUCTION

At the present time, inspection and maintenance operations are based on calendar time or flying hour intervals dictated by potential fatigue damage to structure or wear of engine parts. Any corrosion damage detected during these inspections is repaired. This maintenance scheduling procedure does not take into consideration the wide variation of environmental conditions at Air Force bases. An aircraft which operates in a dry environment requires less frequent inspections and fewer maintenance manhours than one which flys from island to island in the South Pacific.

Fatigue cracking, general corrosion and degradation of protective coating systems are strongly influenced by moisture, salt water, ultraviolet radiation and atmospheric contaminants such as sulfur dioxide, ozone and oxides of nitrogen. The aluminum, steel and magnesium alloys used in aircraft construction are affected in varying degrees. The key to this predictive corrosion modeling program is relating the kinetics of corrosion of aircraft alloys and the degradation of aircraft coating systems to the environments in which aircraft operate.

Dr. Summitt of Michigan State University(1) has developed a system for rating the corrosivity of Air Force bases. Another development of the past few years is an improved understanding of the mechanisms of corrosion of aircraft alloys. There is also a greater knowledge of the factors which cause the deterioration of paint systems. In this program much of this knowledge has been integrated into a predictive corrosion computer model which will enable accurate forecasts of corrosion problems on aircraft operating in any specific type of environment.

The initial computer program was designed for the C-5A aircraft. However, with only slight modification, it may be used for any aircraft that has a crack monitoring program. The C-141, C-130 and B-52 aircraft fleets have such programs.

2.0 OBJECTIVE AND SCOPE

2.1 Objective

The objective is to develop a corrosion prediction model which can be used to optimize:

1. Field and depot level inspection programs for existing aircraft weapons systems.

2. Analytical Condition Inspection (ACI) selection and scheduling.

3. Inspection programs for new aircraft systems entering the Air Force inventory.

2.2 Scope

This program to incorporate corrosion rate data and prediction technology into inspection and maintenance scheduling consists of the following tasks:

Task I - Review and evaluate current Air Force maintenance programs and recent work on aircraft corrosion mechanisms and fracture mechanics.

Task II - Develop corrosion rate equations for aircraft corrosion processes and degradation rate equations for aircraft coating systems and incorporate them into a corrosion prediction model.

Task III - Convert the equations and models developed in Task II into a VAX-11 FORTRAN program to establish (1) Analytical Condition Inspection selection and scheduling, (2) inspection programs for new aircraft, and (3) field and depot level inspection programs for aircraft already in operation.

Task IV - Validate the computerized corrosion forecasting models and maintenance scheduling decision logic by comparing the predictions of the model with actual corrosion histories of the C-5A and/or C-141 fleets.

Task V - Evaluate the efficiency of a new maintenance scheduling decision logic which integrates the corrosion forecasting models with Reliability Centered Maintenance's (RCM) Failure Mode Effects and Criticality Analysis (FMECA) and analytical models developed for the Aircraft Structural Integrity Program (ASIP).

3.0 PROGRAM PLAN

Figure 1 is a program road map which shows the plan for the entire program.

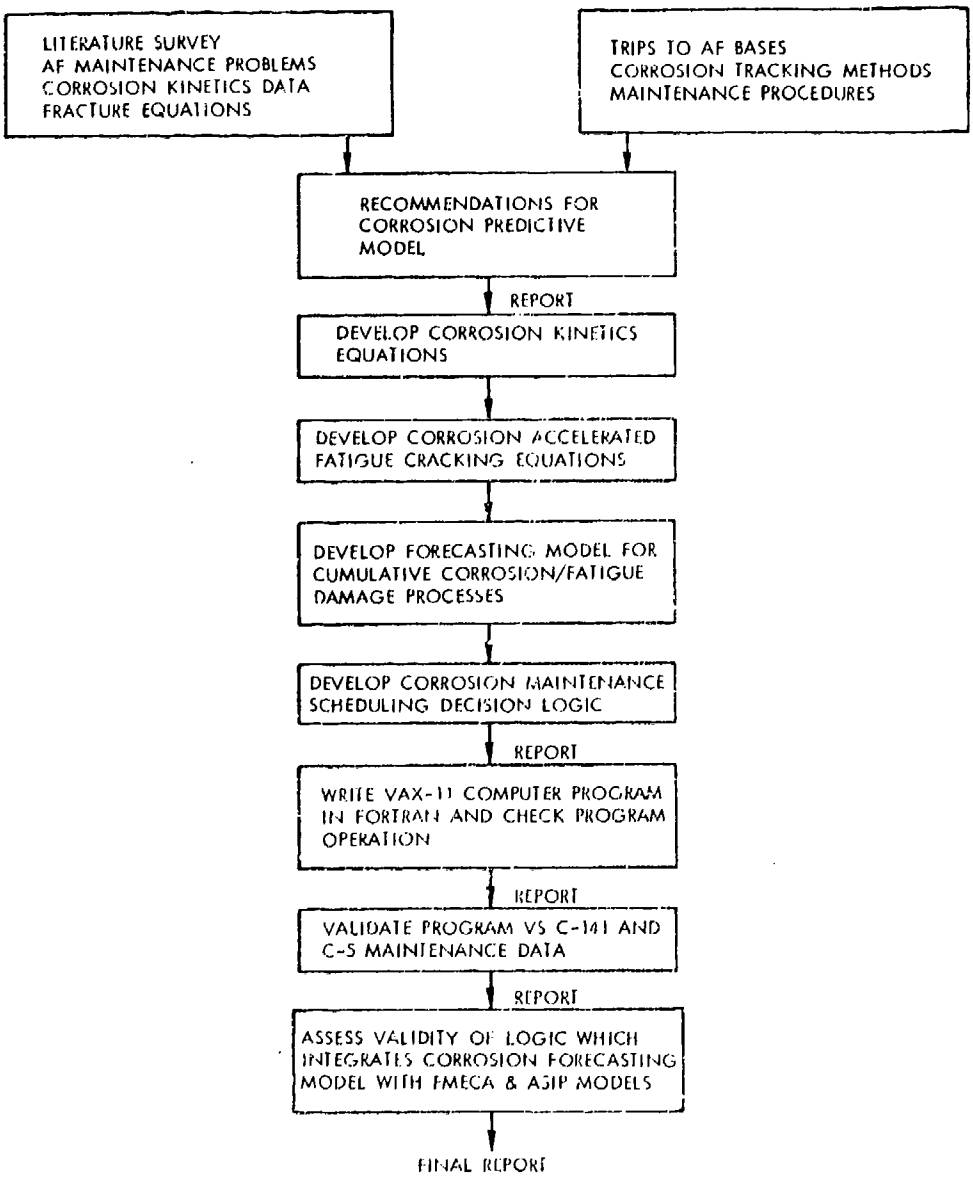

Figure 1. Program Road Map.

4.0 TECHNICAL PROGRESS

In Task III the corrosion rate equations and Air Force maintenance scheduling information obtained in Tasks I and II were integrated into a FORTRAN computer program which is compatible with existing Air Force structural analysis programs.

The logic involved and the procedures which were used are described in the following sections:

4.1 Corrosion Rate Equations

The computer program is based on the following types of corrosion and coating failure:

1. Corrosion Fatigue
2. Stress Corrosion Cracking
3. General Corrosion (including exfoliation and pitting)
4. Coating Degradation

After completing the comprehensive literature survey and reviewing scores of papers relating to fracture mechanics and corrosion rates of aircraft alloys in various environments, the equations in the following sections were selected for use in the predictive corrosion modeling program.

4.1.1. Corrosion Fatigue

The C-5 crack tracking program is based on the Forman[2] equation which takes into consideration the load ratio, R (minimum stress/maximum stress). The relationship is expressed as:

$$da/dN = \frac{C(\text{delta } K)}{(1-R)K_c - \text{delta } K}$$

where

delta K = difference between the maximum and minimum values of K

K_c = the critical stress intensity factor for fracture

C = material constant

This equation by itself is not adequate for the full range of da/dN data. The C-5 Crack Monitoring Program utilizes the Forman equation and parametric data to correct for variations in load ratios. As used in the C-5 Crack Monitoring Program, the constants in the Forman equation are based on experimental da/dN vs. delta K data obtained under conditions of 100% relative humidity.

For use in the predictive corrosion modeling computer program, the Forman equation was modified to include a Corrosivity Factor (CF).

$$da/dN = \frac{C\ (\text{delta } K)}{(1-R)K - \text{delta } K} \times CF$$

where

$$CF = \frac{da/dN\ (\text{in actual environment}}{da/dN\ (\text{obtained at } 100\%\ \text{humidity})}$$

The Corrosivity Factors were determined by plotting da/dN data vs delta K for specific aircraft alloys in dry air, distilled water, and in 3.5% NaCl solution on the same plot as illustrated in Figure 2. Then, assuming an average delta K value of 10 ksi $\sqrt{in.}$ (the average stress intensity encountered in a normal aircraft mission), the values of da/dN for each environment were read off and converted to Corrosivity Factors using the above formula. Since 3.5% NaCl is a more corrosive environment than 100% moisture, the factor for a salt/air environment would be greater than 1. Conversely, for a dry environment, the factor is less than one.

Based on the Dr. Summitt's[1] data for Air Force Bases, each base was assigned a set of Corrosivity Factors corresponding to its environmental conditions.

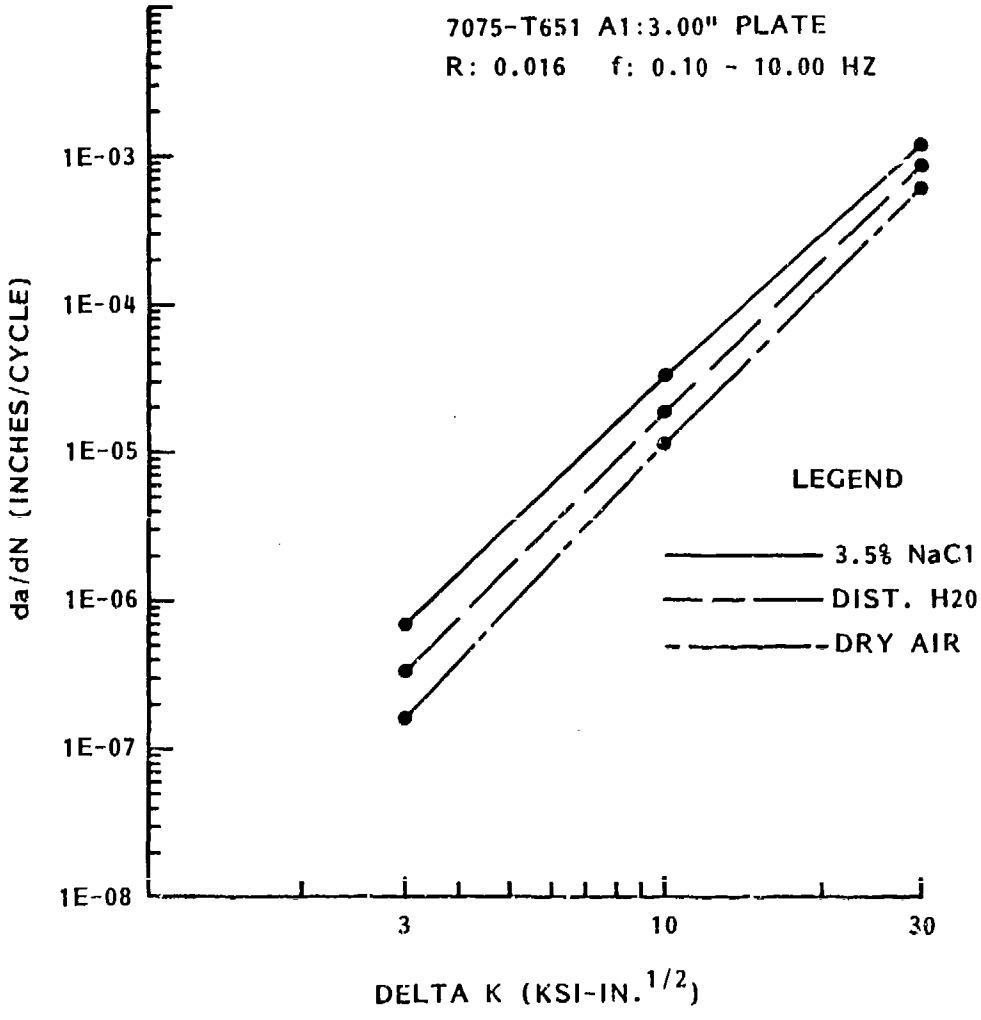

Figure 2. Crack Growth Plots for 7075-651 Aluminum.

Corrosivity Factors were calculated for 7075-T651, 7075-T73 and 7175-R73 aluminum, and for 4340 and 300M steel. The fatigue cracking data used to develop the Corrosivity Factors were obtained from the USAF Damage Tolerant Design Handbook(3).

4.1.2 Stress Corrosion Cracking

A single equation was found which defines the diverse assortment of da/dt vs. delta K curves for aluminum and steel alloys in various environments. The plots vary for each alloy and for the same alloy in various environments. Fortunately, the design handbook contains data for the more common aircraft alloys in dry, moist and salt water environments. In the predictive corrosion modeling computer program the theoretical stress intensity at each crack tip will be calculated. Whenever KIscc is exceeded, the ground time and the crack growth data from Reference 3 will be used to calculate the amount of stress corrosion cracking occurring during any given period of operation.

4.1.3 General Corrosion

Damage functions for metals in contaminated environments follow the general model

$$M = AT^B$$

where M is metal loss by corrosion (either penetration depth or weight loss), T is exposure time, and A and B are empirical constants determined by the environmental conditions, the metal involved and the type of corrosion product on the metal. The exponent B theoretically takes on the value of approximately 1/2 when corrosion is limited by the diffusion rate of the reactive species through a semi-permeable film of reaction products. This would be the case for most aluminum alloys. When the corrosion products are flocculant or soluble and offer no protection, as is generally true for steel, linear corrosion kinetics are observed and B = 1.

The Task I literature search revealed only scattered data for the corrosion of aircraft alloys in the range of environments encountered by aircraft - mild, industrial, humid, and marine. It was, therefore, necessary to conduct corrosion tests with some of the more widely used alloys in solutions with compositions simulating those of condensate and rainfall encountered by aircraft under service conditions.

In Task II, potentiostatic polarization tests were conducted with 7075-T5 and 7075-T73 aluminum and with 4340 and 300M steel in nitric and sulfurous acid solutions in the pH range of 4.0 to 6.0 and also in acid solutions containing 3 1/2% NaCl. Using linear regression mathematical techniques, these test results and the data obtained from the literature search were used to determine the constants A and B for the equations which represent the corrosion rates of specific alloys in various environments. The constants which were developed for the major aircraft alloys in mild, moderate, severe and very severe environments are summarized in Figures 3a and 3b.

The corrosion rate equations, with the appropriate constants, are being used in the predictive corrosion computer program. When a specific Air Force Base is called out, the program automatically uses the equation which corresponds to the environmental conditions at that base.

4.2 Coating Degradation

The external surfaces of most Air Force planes are completely painted. Except in the case of mechanical damage, the time required for fuselage and wing structure to corrode is the coating degradation time plus the corrosion time.

Again, the literature search did not disclose data for the deterioration of Air Force coating systems in all the types of environments which are being considered in this program. The best analysis of the complex factors involved is in Dr. Summitt's report.[1] His basic coating degradation algorithm is shown in Figure 4. The environmental factors

Environmental Constants for Corrosion Equations

Alloy	Corrosion Index							
	Mild		Moderate		Severe		Very Severe	
	A	B	A	B	A	B	A	B
7075-T6 Al	3.0E-5	.46	2.95E-5	.59	2.9E-5	.72	1.78E-3	.12
2024-T3 (CLAD)	3.6E-6	.70	4.9E-6	.77	6.3E-6	.85	1.48E-5	.70
7079-T6	1.9E-6	.89	2.05E-6	.94	2.2E-6	1.00	5.4E-9	2.00
7075-T73	3.0E-5	.46	3.6E-5	.50	9.0E-4	.50	9.3E-4	.50

Figure 3a.

Environmental Constants for Corrosion Equations (Cont'd)

Alloy	Corrosion Index							
	Mild		Moderate		Severe		Very Severe	
	A	B	A	B	A	B	A	B
AZ31B-H24	4.0E-4	.77	2.8E-4	.87	1.6E-4	.97	1.2E-4	1.30
2024-T3	5.0E-4	.30	5.3E-3	.11	1.43E-2	-.05	1.1E-3	.30
4340 Steel	3.5E-11	2.52	2.6E-8	1.40	4.11E-5	1.00	6.9E-5	1.00
300M Steel	3.5E-11	2.52	6.3E-9	2.00	7.3E-5	1.00	5.7E-4	1.00

Figure 3b.

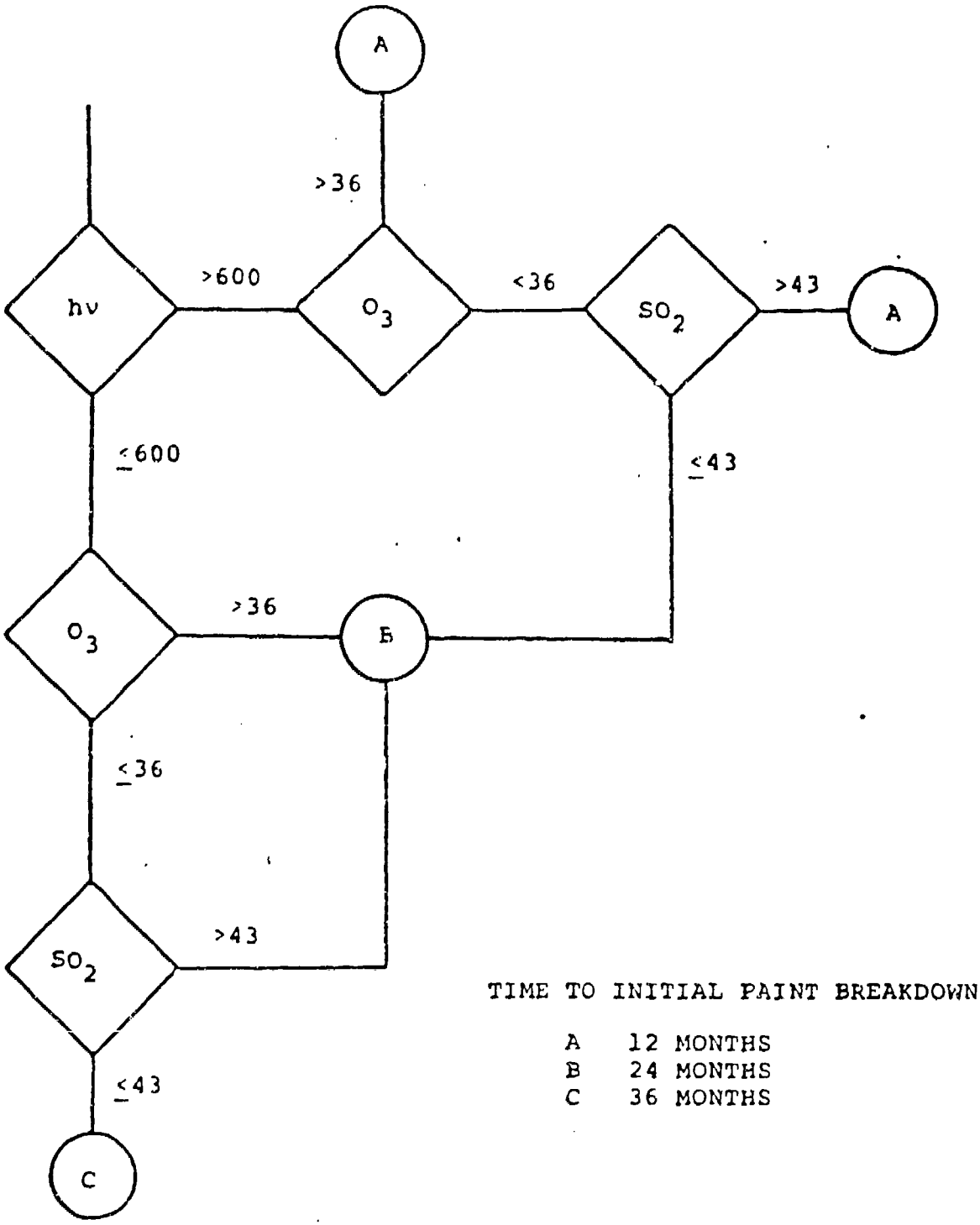

Figure 4. Paint Renewal Algorithm (1)

which cause the breakdown of coating systems are ultraviolet radiation, ozone, and sulfur dioxide. By establishing threshold values for the intensity of ultraviolet, and concentrations of ozone and sulfur dioxide, this algorithm enables bases to be rated for their effect on paint systems. An "A" rating represents high values of UV and atmospheric contaminants, a "B" rating intermediate values, and a "C" rating low values.

This algorithm provides a good basis for determining coating degradation rates and was modified to reflect Lockheed experience with the service life of various coating systems. In the predictive corrosion modeling project, the time to initial breakdown of the coating system is more important than time to repaint because the time a paint system has degraded to the point where repainting is desirable, an extensive amount of corrosion damage may have occurred.

It is recommended that a new category of paint maintenance called "Paint Renewal" be introduced. This would be a touchup and repainting of only worn or damaged areas. For the paint renewal maintenance, A, B, and C in the algorithm will represent 12, 24 and 36 months. At every fourth paint renewal interval the aircraft should be completely stripped and repainted.

4.3 Predictive Corrosion Modeling Computer Program

4.3.1 Summary of Logic

The objective of the computer program is to provide a fully integrated method of predicting crack growth, corrosion damage, or coating degradation rates for C-5 aircraft in a variety of environments. The program is designed so it may be integrated with the current structural integrity and tracking programs with a minimum of manhours and expense.

The flow diagrams for the VAX-11 FORTRAN computer program are illustrated in Figures 5 and 6. The program is designed to (a) calculate the amount or degree of corrosion or coating degradation which occurs on C-5 aircraft

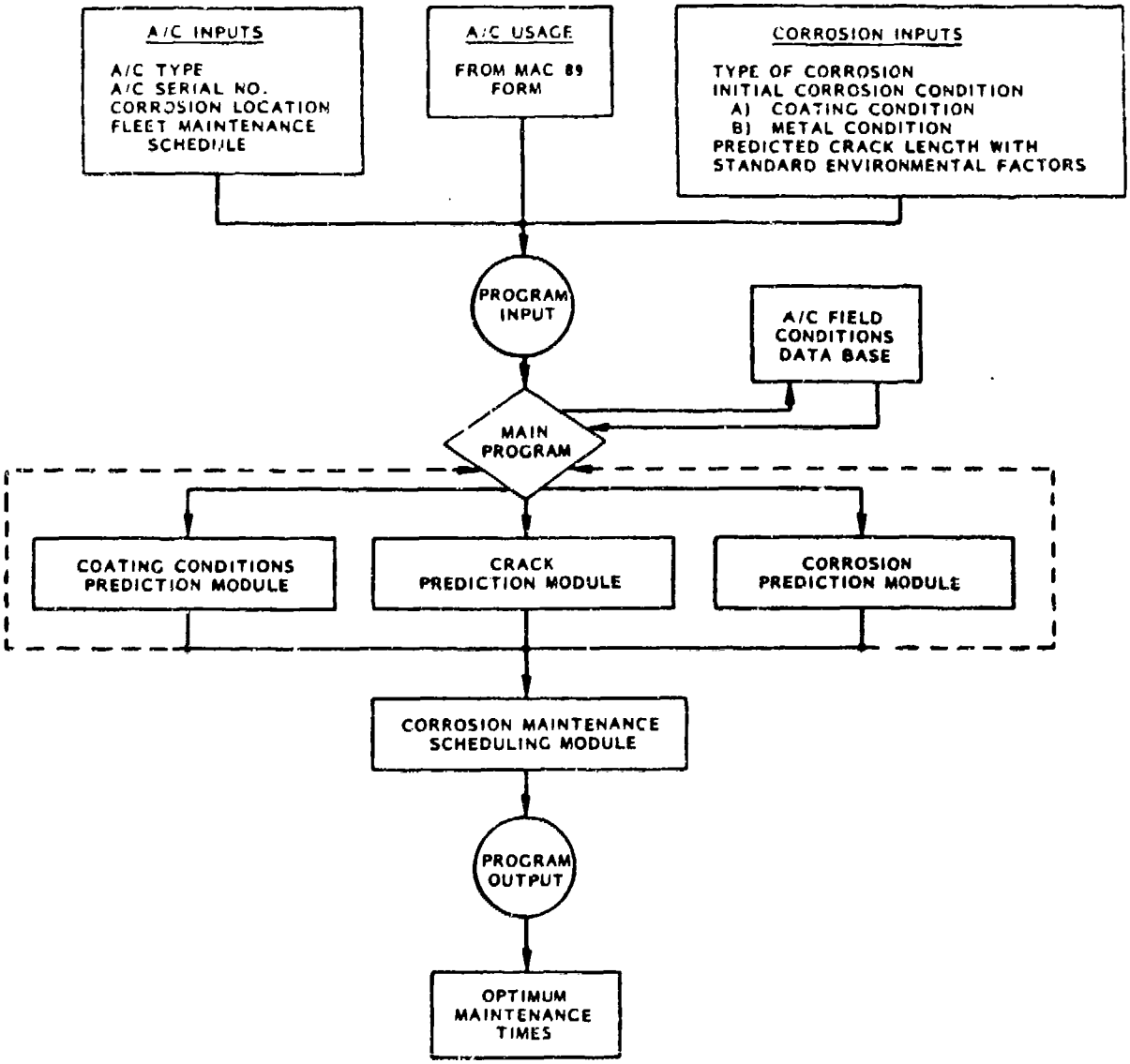

Figure 5. Flow Diagram for FORTRAN Computer Program.

Predictive Corrosion Model

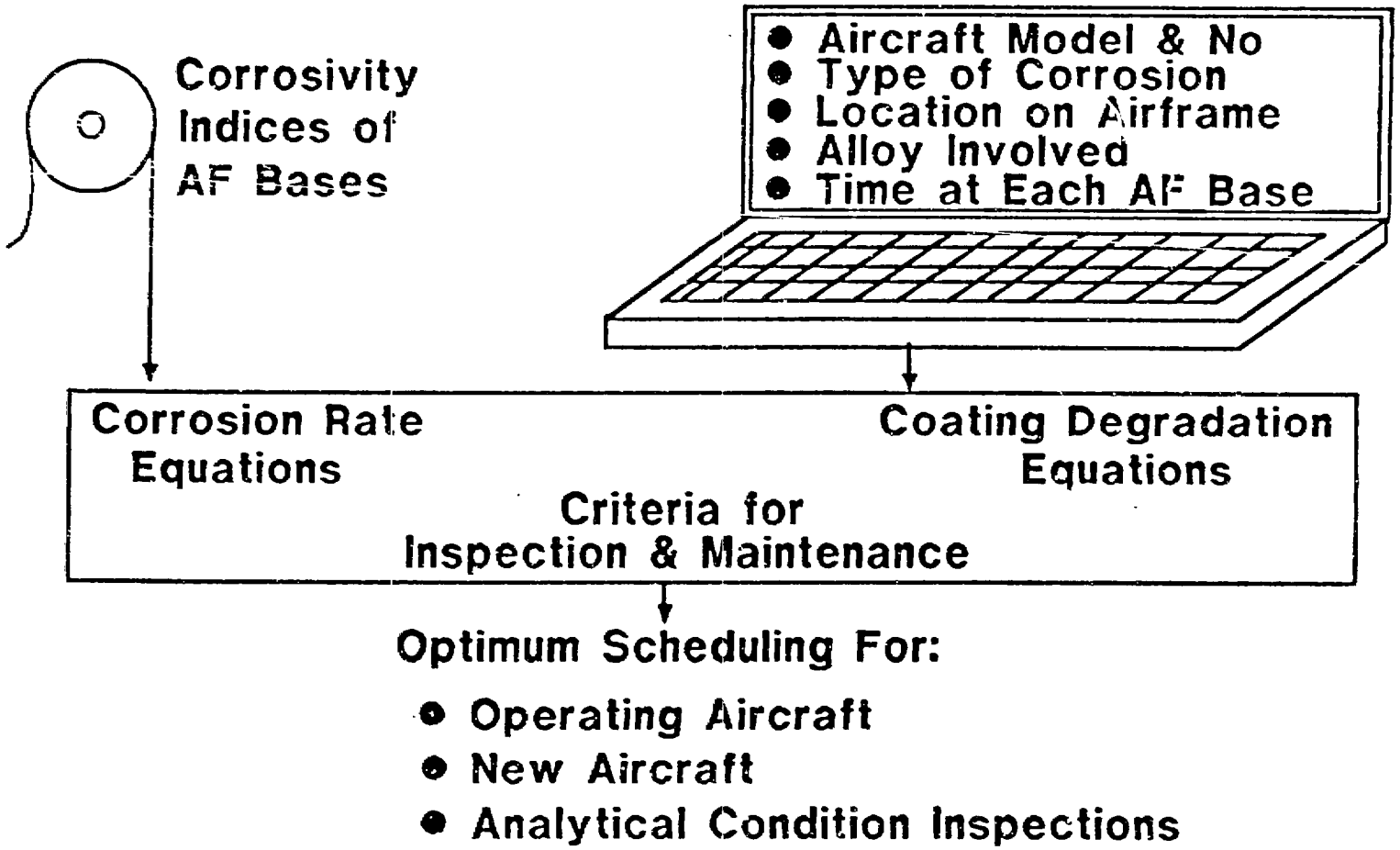

Figure 6. Flow Diagram for Computer Program.

operating in a variety of environments, (b) convert the data obtained into optimum time to next inspection, and (c) select specific scheduled maintenance times for doing the corrosion repair or paint renewal.

In its present form, the program is to be used in conjunction with the C-5 and C-141 crack monitoring programs and the C-5 and C-141 usage tapes which, for each aircraft, give a historical record of the bases of operation, the flight dates, flight durations, and the total mission hours.

Common inputs to the program are in the type of aircraft (C-5 or C-141), the tail number, the point on the aircraft which is being analyzed for corrosion or coating degradation, and the fleet maintenance schedule.

Other inputs required are the aircraft usage history from the usage tapes and information relating to protective coating system, the alloy involved, and the crack lengths predicted by the C-5 or C-141 crack programs.

The computer program contains modules for predicting fatigue and stress corrosion crack growth, for calculating the depth of corrosion of exposed metal, and for determining the degree of degradation of paint systems.

4.3.2 Crack Growth Prediction Module

Crack growth due to fatigue corrosion in flight and stress corrosion during ground standing are estimated in separate submodules. The module is not "stand alone" in that it relies on input from the C-5 or C-141 crack growth prediction programs, which calculate crack growth of an assumed inherent flaw due to fatigue corrosion for several specific analysis locations on a flight-by-flight basis. The crack growth prediction module adjusts that crack growth according to the environments at the Air Force bases from which the aircraft departs.

Inputs to the crack growth prediction module include the initial crack length, the bases transiented by the aircraft, and the number of flights, duration of each flight, 100% humidity crack growth prediction for each flight, and ground time between each flight for each base. Additional inputs include the crack location and the type of material.

Continental United States Air Force bases, including those in Alaska and Hawaii, have been classified into four corrosivity groups depending primarily on average humidity and salt water concentration. The C-5 and C-141 Crack Growth Prediction Programs estimate crack lengths based on 90-100% relative humidity conditions. The fatigue corrosion prediction submodule of the corrosion prediction program applies a correction factor to that crack growth prediction and adds the adjusted crack growth to the original crack length. In addition, the stress corrosion prediction submodule calculates any stress corrosion cracking that may occur during ground standing between flights and adds that value to the post-flight crack length before the next flight.

4.3.3 Corrosion Prediction Module

The corrosion module contains data on the corrosion rates of aircraft alloys in the environments which exist at Air Force bases. These rates were determined from the equations disclosed by literature search and from corrosion tests with aircraft alloys in simulated and actual environments. Once the specific alloy and the bases of operation of the aircraft are specified, the module automatically selects the proper equations. The corrosion module predicts the time required for aircraft alloys to corrode to a depth of 3 mils (.0762 mm) in various Air Force base environments.

The corrosion rate equations which are being used in the program are those discussed in Section 4.1. These have been selected from the literature search or developed from experimental data.

From the Corrosivity Index ratings of the Air Force bases, actual corrosion data obtained by exposing aircraft alloys at selected bases, and the results of the potentiostatic polarization tests, the corrosion rate for specific alloys at any of the Air Force bases can be calculated. In the computer program, each base is assigned a corrosion rate for each alloy. When a point on an aircraft is being analyzed the proper amount of corrosion damage is automatically allocated for the time at each base.

4.3.4 Coating Degradation Module

Primary inputs to the coating degradation prediction module include the specific coating system and the approximate coating life remaining in a moderately severe environment at the start of the simulation, the Air Force bases at which the aircraft has been stationed, and the time spent at each base. The program estimates the coating life "used" at each base. This estimate is calculated at each base, and is subtracted from the coating life remaining to result in the recommended time to the next Intensive Paint Renewal (through cleaning and touchup of degraded areas). The approximate time remaining before the next complete repaint is also calculated by assuming that a complete repaint shall be required every four Intensive Paint Renewals.

4.3.5 Crack Monitoring Points

The C-5 crack monitoring program now in use at Oklahoma City AFB tracks 46 theoretical cracks. Figure 7 shows the location of points on the wing, fuselage and tail assembly which have high stresses. A structural analysis for each of these points has been made and is available for use in this program Seven of these points have been selected for use in the initial predictive corrosion modeling computer program.

The selected points are:

1. 6290SS1 Spanwise Splice - Lower Wing Surface
2. 4250SS1 Spanwise Splice - Lower Wing Surface

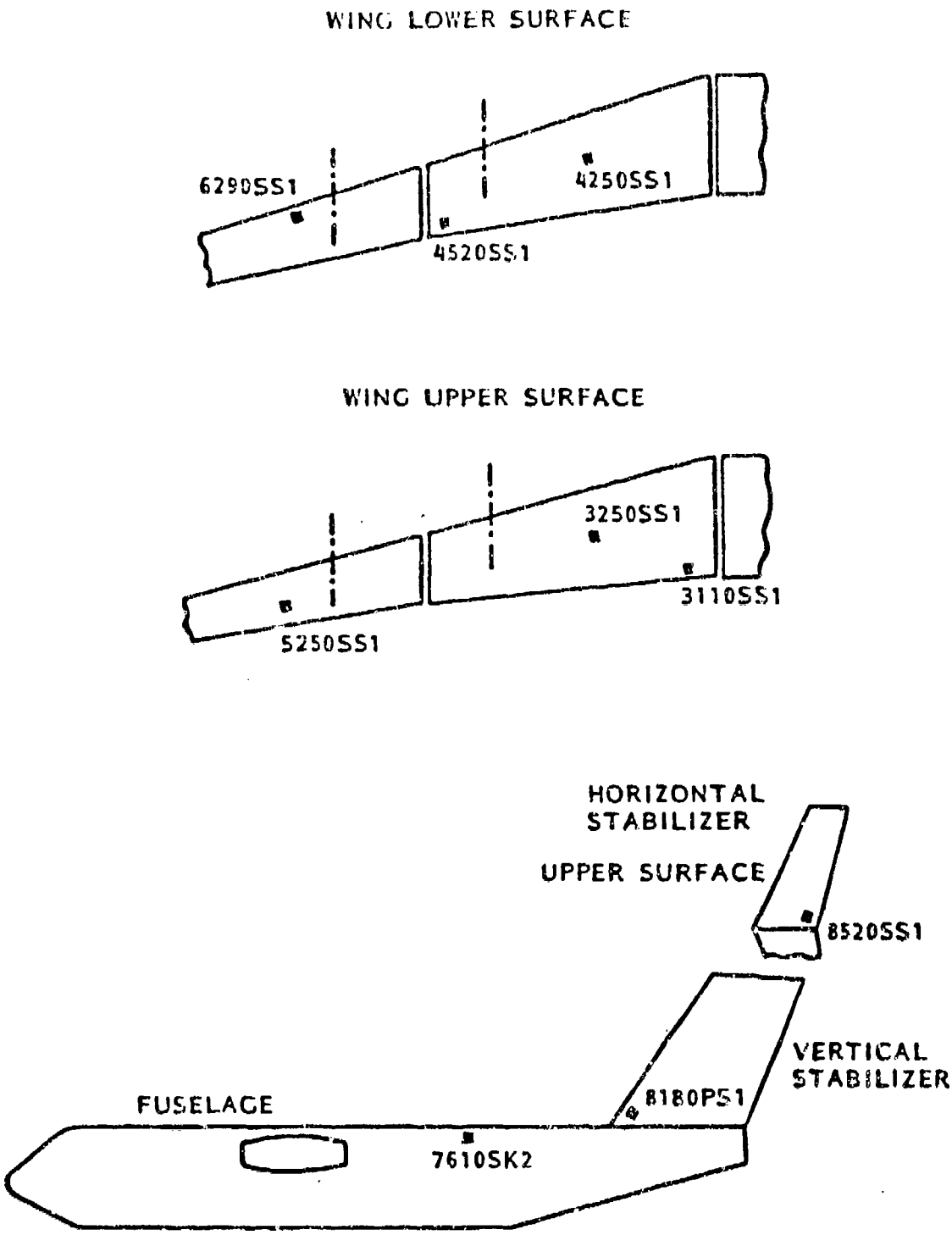

Figure 7. Location of Crack Monitoring Points on C-5A Aircraft

3. 5250SS1 Spanwise Splice - Upper Wing Surface
4. 3250SS1 Spanwise Splice - Upper Wing Surface
5. 7610SK2 Skin - Upper Fuselage
6. 8180PS1 Panel Splice - Vertical Stabilizer
7. 8520SS1 Spanwise Splice - Horizontal Stabilizer, Upper Surface

After the program has been validated by comparing predicted crack lengths with actual cracks, it will be used to track any of the 46 theoretical cracks now being monitored.

The computer program was designed so, with only minor modification, it can be used for any aircraft which already has a crack monitoring program. The C-141, C-130, and B-52 fleets have such programs.

4.3.6 Corrosion Maintenance Scheduling Module

The outputs of the corrosion, coating degradation, and crack growth prediction modules will be input to a corrosion maintenance scheduling module which will compare the upcoming maintenance schedule with the aircraft corrosion condition. The module will determine the best time to perform corrosion control maintenance items based on the aircraft condition and the capabilities of scheduled maintenance actions.

4.3.7 FORTRAN Program

The data and logic developed to date have been integrated into a FORTRAN computer program which contains essential portions of the final program.

5.0 DISCUSSION

The Predictive Corrosion Modeling Program is designed to give optimum inspection and maintenance scheduling for the major types of crack growth, corrosion damage, and coating degradation problems which may occur on C-5 aircraft. Specific aircraft can be quickly checked for potential crack growth in critical areas, for probable corrosion damage to exposed structural alloys, or for the condition of the aircraft coating system.

Even new aircraft will have areas where the protective system has been mechanically abraded and bare metal is exposed. It is, therefore, necessary to assume the existance of some bare metal and to examine the corrosion prone areas at each recommended inspection interval.

Task IV, the next task in completing the project is to validate the computer model by comparing the predictions with actual corrosion histories of C-5A aircraft. The general corrosion and coating degradation predictions will be checked by selecting specific aircraft and determining the environmental conditions in which they operated during the first few years of service. With this information as input, the predictive corrosion computer program will disclose the times at which significant amounts of corrosion damage and coating degradation should have occurred. These predictions will then be compared with a plot of corrosion control manhours for the corrosion prone areas of the aircraft.

The validation of the crack growth module of the computer program will be accomplished by comparing analytical crack growth lengths, which have been adjusted for environmental conditions during the test period, with actual cracks in the test article used in the C-5A Modified Wing Structural Test Evaluation(6). During the C-5A Modified wing test approximately 100 cracks initiated from intentional sawcuts made in the wing. A comparison of actual and predicted crack growth was performed for nineteen of these cracks representing various configurations and spanwise locations.

The final task, Task V, will be to evaluate the efficiency of a new maintenance scheduling decision logic which integrates the predictive corrosion model with the Air Force Reliability Centered Maintenance (RCM) programs. RCM currently determines inspection intervals and scheduled maintenance intervals based upon the probability of an item failing within that interval, and upon the criticality of that failure. Corrosion is a "malfunction" or "failure mode" which is experienced constantly, and a tool which can accurately predict the frequency and effect of corrosion occurrence will make an important contribution toward the objectives of Reliability Centered Maintenance programs.

As a part of the final task, the feasibility of modifying the current maintenance activity control systems to include the results of the predictive corrosion model will be investigated. If feasible, the necessary changes to the current system will be identified. The impact of making these changes will be estimated from the standpoint of cost of incorporation and cost increases/decreases of maintenance activity, as well as improvement in operational readiness of the aircraft. The operational readiness improvement aspect would come from being able to better predict corrosion problems so that preventive measures could be taken in advance or, at least, the logistical support needed (maintenance personnel, equipment, spares, etc.) would be ready and available when needed.

6.0 CONCLUSIONS

1. A VAX-11 computer program which will predict the degree of corrosion sustained by aircraft alloys, the degradation of aircraft coating systems, and the fatigue cracking of aircraft alloys in a variety of environments has been developed.

2. The predictive corrosion modeling program will enable optimum inspection and maintenance scheduling for the major types of crack growth, corrosion damage, and coating degradation problems which may occur on C-5A aircraft.

3. The predictive corrosion modeling program can be readily modified for use on the C-141, C-130, and B-52 and other aircraft fleets which have crack monitoring programs.

4. The implementation and use of the predictive corrosion modeling program will minimize unnecessary inspections and will enable corrosion damage to be prevented or repaired at minimum cost.

8.0 REFERENCES

1. R. Summitt and F. T. Fink, "PACER LIME: An Environmental Corrosion Severity Classification System," AFWAL-TR-4102, Part II, August 1980.

2. R. G. Forman, V. E. Kearney, and R. M. Engle, J. Bas Engr., 1967.

3. J. P. Gallagher, USAF Damage Tolerant Design Handbook. AFWAL-TR-82-3073, Flight Dynamics Laboratory, May 1984.

4. System Peculiar Corrosion Control Manual USAF Series C-5A and C-5B Aircraft T.O. 1C-5A-23.

5. Computer Program Documentation Report, C-5A Post Wing Modification Tracking System Status Inspection Projections, and Usage Severity Evaluations Program, LG84ER0088, September 1984.

6. E. J. Ferko, D. V. Finkle, and B. M. Payne, C-5A Modified Wing Structural Test Evaluation, Final Report, Volume II, Damage Tolerance, LG83ER0089, December 1983.

Name: Dr. Robert N. Miller

Present Affiliation:

Lockheed-Georgia Company
Dept. 72-53, Zone 319
Marietta, Georgia 30063

Title: Staff Scientist

Field of Interest/Responsbilities:

Plans, directs and conducts research programs relating to corrosion prevention, protective coatings, fatigue fracture and electrochemistry.

Previous Affiliations/Titles:

Was Associate Professor of Chemical Engineering at the Georgia Institute of Technology before coming to Lockheed-Georgia Company in 1956.

Academic Background:

B.S. in Chemical Engineering, Ohio State University
M.S. in Chemical Engineering, Ohio State University
Ph.D. in Chemical Engineering, Ohio State University

Society Activities/Offices/Awards.

National Association of Corrosion Engineers

Chairman of 1987 NACE symposium on "Corrosion and Its Control for Aerospace Structures"

Received the 1986 Frank N. Speller Award "In Recognition of Outstanding Contributions to the Practice of Corrosion Engineering". His major developments were the MIL-S-817333 Corrosion Inhibitive Sealing and Coating Compound and the MIL-P-87112 Corrosion Inhibiting Primer now in use throughout the aircraft industry.

Tau Beta Pi
Mensa

Publication/Papers

Has presented or published more than 60 papers in the fields of corrosion, protective coatings, inhibitors, electrochemistry, cryogenics and radiation effects. Has been granted 6 United States patents.

VANADIC HOT CORROSION OF GAS TURBINE BLADE COATING MATERIALS

R. L. Jones
Chemistry Division
Naval Research Laboratory
Washington, DC 20375-5000

ABSTRACT

In anticipation of possible future use of vanadium-containing fuel in Navy ship propulsion gas turbines, studies have been made at NRL on vanadium effects in the hot corrosion of CoCrAlY, a currently used metallic blade coating, and of stabilized zirconia (ZrO_2), a ceramic being developed as an advanced blade coating for gas turbines. Both materials were attacked under conditions of high V_2O_5 activity, with an outer layer of cobalt vanadate being formed on CoCrAlY which, in some instances, gave an apparent (but unreliable) "inhibition" of corrosion. Vanadic attack on zirconia caused depletion of the stabilizing oxides (i.e., Y_2O_3 or CeO_2) and degradation of the ceramic. Interestingly, the corrosion processes for both materials are similar in many respects, being in each case predominantly controlled by Lewis acid-base reactions between the molten salt/combustion gas species (Na_2O, V_2O_5, SO_3) and coating oxides (CoO, Y_2O_3, CeO_2). The paper closes with a discussion of the potential application of oxide acid-base theory to develop "corrosion-proof" stabilized zirconia coatings by, e.g., identifying new stabilizing oxides which are more resistant than Y_2O_3 to acidic (vanadic) corrosion.

INTRODUCTION

Currently US Navy ships use a distillate fuel which, because vanadium-containing compounds in crude petroleum tend to remain with the residual during distillation, has a very low vanadium content. Thus vanadic hot corrosion is not a present Navy problem. However, much of the world's remaining petroleum supply is contaminated with high levels of vanadium (500 ppm or more in some cases), and it will become increasingly expensive and difficult to insure vanadium-free fuel for future Navy needs.

While certain levels of vanadium in fuel can be tolerated by steam turbine or diesel engine ship propulsion units, vanadic hot corrosion is potentially critical for the gas turbines which power more than 100 Navy ships. The blades in these gas turbines have metal sections as thin as 0.025 in. in some areas, and they are protected against hot corrosion by CoCrAlY (a Co-based alloy containing Cr, Al, and Y) coatings which are themselves only 0.005 in. in thickness. No excess of metal thus exists in gas turbines to allow for corrosion. Also, fouling of the compressor and hot section blades must be avoided, which rules against treatment for vanadium by fuel additives that work by forming high melting vanadate deposits.

The potential seriousness of vanadium fuel contamination has been demonstrated recently by DTNSRDC burner rig tests (Ref. 1) where less than 10 ppm of vanadium added to a fuel containing 1% sulfur produced up to 5X increase in the 700C hot corrosion of specimens coated with CoCrAlY of the composition used in Navy marine gas turbines.

A strong need exists therefore both to verify and understand vanadium effects in Navy ship gas turbine hot corrosion, and to undertake the development of blade coatings that can

resist vanadate-induced, as well as sulfate-induced, hot corrosion. The ability to use vanadium-contaminated fuel would give the Navy substantial advantages including i) decreased cost and increased availability of fuel; ii) insurance against damage by accidental (or even sabotage) vanadium contamination of ship fuel; and iii) most importantly, an additional "margin of error" for wartime emergencies where fuel quality can not be controlled.

Research at NRL has been concerned with vanadic hot corrosion both of metallic CoCrAlY, i.e., the present Navy blade coating material, and of ceramic stabilized-zirconia, which is a possible future material for vanadium-resistant gas turbine blade coatings. The following article consists essentially of excerpts from NRL open literature publications which were chosen to illustrate examples of results obtained in this research.

VANADIUM CHEMISTRY

The Na-V-O system produces six compounds, including V_2O_5 (mp, 676°C) itself, which are related as shown in Table 1. Vanadium pentoxide is an acidic oxide, while Na_2O is basic. Thus as the Na_2O content of the compounds in Table 1 increases, the acidic nature of the compound decreases, going from acidic with V_2O_5 down to neutral or even basic for Na_3VO_4. The acid-base character of the different vanadate compounds affects their corrosion reactions as will be shown below. It is not sufficient therefore merely to speak of "vanadium" corrosion, but rather one must consider which vanadate species will prevail under the given corrosion conditions.

When sulfur is also present in the fuel, as usually found, SO_3 is formed which competes with V_2O_5 for reaction with Na_2O. Spacil and Luthra (Ref. 3) have shown that for Na, S, and V concentrations typical of low quality V-containing fuel and marine environments, the composition of deposits produced on the gas turbine blades will be determined by the equilibrium reaction

$$2\ NaVO_3 + SO_3 = V_2O_5 + Na_2SO_4 \qquad [1]$$

This equation predicts that increased SO_3 partial pressure in the turbine gas will increase the V_2O_5 and Na_2SO_4 activity in the blade surface deposit, while decreasing the $NaVO_3$ activity. Low melting mixed eutectic sulfates may also be formed by reaction of SO_3 and Na_2SO_4 with oxides deriving from the coating itself, such as

$$1/3\ Co_3O_4 + SO_3 + Na_2SO_4 = CoSO_4\text{-}Na_2SO_4\ (\text{mp, } 575^{\circ}C) + 1/6\ O_2 \qquad [2]$$

PREVIOUS VANADIC CORROSION RESULTS

Vanadic corrosion on boiler firesides has been a recognized problem for many years, and considerable study has been made, particularly in the period 1950-70, of vanadic corrosion in gas turbines (cf. Ref. 4). However, many questions remain unanswered, especially as regards materials and conditions relating to modern Navy ship propulsion gas turbines. In the past, laboratory tests have usually, but not always, shown $Na_2V_{12}O_{31}$ (the most acidic vanadate yet containing Na_2O) to be the "most corrosive" vanadium compound, but this fact has not been adequately explained. Similarly, the effects of SO_3 have been ambiguous, with SO_3 in the furnace gas in some cases being found to accelerate, but in other cases to slow, vanadic corrosion. Additions of V_2O_5 have also been reported in fact to inhibit sodium sulfate-

5p

induced hot corrosion of nickel and Ni-based superalloys by the formation of refractory nickel vanadate phases.

The vanadic corrosion of stabilized-zirconia ceramics has been studied only recently as a part of the development of ZrO_2 thermal barrier coatings for gas turbines and diesels (Ref. 5). Scientific understanding of this corrosion is still limited, with the previous knowledge being essentially that vanadium-containing fuels (and $NaVO_3$ in the laboratory) leached Y_2O_3 from Y_2O_3-stabilized ZrO_2, with YVO_4 usually formed, and that the presence of SO_3 accelerated the rate of attack (Ref. 6). Work at NRL has since (partly as described below) developed the idea that vanadic corrosion of stabilized-ZrO_2 is largely controlled by Lewis acid-base reactions such as

$$Y_2O_3 \text{ (basic)} + V_2O_5 \text{ (acidic)} = 2\ YVO_4 \text{ (salt)} \qquad [3]$$

and that it is possible to rank the acidic/basic character of potential stabilizing oxides for ZrO_2 so as to identify stabilizers more resistant to corrosion than Y_2O_3, and thus substantially increase the vanadic corrosion-resistant of stabilized-ZrO_2 coatings (Refs. 7,8).

VANADIC CORROSION OF CoCrAlY

In this investigation (Ref. 4), coupons of Co-35Cr-6Al-0.5Y (wgt-percent) were deposited with thin layers (3-5 mg/cm^2) of Na_3VO_4, $NaVO_3$, V_2O_5, or Na_2SO_4, or mixtures thereof. The salt-coated coupons were then exposed at 700°C in a thermobalance under flowing (25 cm/min) air, either pure or containing low concentrations of SO_3, with the corrosion rate being monitored by rate of weight gain. The original paper should be consulted for full details and results, since only two of the several findings obtained are presented here.

1. Corrosion by Pure Compounds under Air.

This is the "traditional" experiment in vanadic corrosion investigations, where metals are given a single coating of the different vanadium compounds and then simply exposed at temperature in air. However, the results here (Fig. 1) differed from those mostly reported in the past in that it was not the acidic compounds, but rather the most <u>basic</u> compound, Na_3VO_4, which gave greatest corrosion. This apparent contradiction was explained by analyses which showed that, with Na_3VO_4, the initial corrosion behavior was predominated by the <u>reaction</u>

$$2\ Na_3VO_4 + Cr_2O_3 + 3/2\ O_2 = 2\ Na_2CrO_4 + 2\ NaVO_3 \qquad [4]$$

This is an acid-base reaction where basic Na_2O from Na_2O-rich Na_3VO_4 reacts with acidic Cr_2O_3, resulting from the 35 w/o chromium content of the CoCrAlY, to produce a non-protective surface corrosion product layer containing high concentrations of the salt, Na_2CrO_4. On the other hand, attack by V_2O_5 yielded a two-layered morphology (Fig. 2) consisting of an outer cobalt vanadate phase and an inner oxide phase containing a low level of vanadium. The cobalt vanadate can also be considered as the product of an acid-base reaction, viz.,

$$2\ CoO \text{ (basic)} + V_2O_5 \text{ (acidic)} = Co_2V_2O_7 \text{ (salt)} \qquad [5]$$

Corrosion by $NaVO_3$ produced only an oxide layer (Fig. 3) containing a similar low vanadium concentration, and having much the same appearance, as the inner oxide layer resulting from

V_2O_5 attack. No cobalt vanadate phase was found with $NaVO_3$ corrosion, which indicates that the V_2O_5 activity in this case is lower than that necessary for the formation of $Co_2V_2O_7$.

Results as above suggest that one is not limited to accepting the corrosion behavior of different metals with different vanadium compounds simply as "experimental facts." Review of past investigations where the acidic vanadates gave greater corrosion than Na_3VO_4 suggests, for example, that the metals involved mostly formed oxides of a more basic nature than Cr_2O_3 (e.g., NiO), or possibly oxide films with lower Cr_2O_3 concentrations, and thus--because bases react with acids, but not other bases--were corroded more readily by vanadates with high V_2O_5 activity than those with high Na_2O activity. It may be possible therefore that vanadate/metal corrosion behaviors can be largely understood, and even to some extent anticipated, by consideration of acid-base reactions between the metal (oxides) and vanadate components, and of the likely effects of the resultant corrosion products (e.g., the formation of metal vanadate outer "barrier" layers).

2. Corrosion by Pure Compounds under Air Containing SO_3.

When CoCrAlY coupons coated with the various compounds were exposed at 700°C under air containing 13 Pa of SO_3, substantially greater corrosion occurred (Fig. 4, compare with Fig. 1) with Na_2SO_4 actually giving highest corrosion, in accord with the now well known 700°C corrosion of CoCrAlY by SO_3/Na_2SO_4. However, the most interesting behavior was shown by $NaVO_3$ in Fig. 4 where, after about 16 hours of exposure, the corrosion rate abruptly increases, but then becomes greatly reduced, or "inhibited", from 24 hours onward to the end of the test period.

An examination of the corrosion morphology both before (Figs. 5,6), and after (Fig. 7), the abrupt rise/inhibition break in the corrosion rate curve revealed that this behavior essentially results from the reaction of SO_3 with $NaVO_3$ to produce V_2O_5 and Na_2SO_4, i.e., Reaction [1]. In Fig. 5, taken after 14.5 hrs exposure, the corrosion morphology can be seen to consist of an inner oxide layer and an outer "salt" layer.
Energy dispersive x-ray analysis at higher magnification (Fig. 6) identified the medium gray phase marked by "A" in the outer salt layer
to be mostly eutectic $CoSO_4$-Na_2SO_4 (cf. Reaction [2]) containing dissolved V_2O_5 and/or $NaVO_3$, and which was molten at temperature. The white phase marked by "B" is a cobalt vanadate, probably $Co_2V_2O_7$, that is <u>precipitated</u> from the molten sulfate when the V_2O_5 activity exceeds some critical value in the melt.

After 48 hrs exposure (Fig. 7), i.e., in the "inhibition" period, the outer surface of the corrosion phase is completely capped over by cobalt vanadate (phase "B"), with the mixed $CoSO_4$-Na_2SO_4 (phases "C" and "D") being effectively buried. Thus "inibition" is achieved because i) the vanadium from the original coating of $NaVO_3$ is largely tied up in the outer cobalt vanadate layer, and ii) this cobalt vanadate layer is sufficiently covering to shield the CoCrAlY from continuing attack by the SO_3 in the air stream.

However, the cobalt vanadate outer layer is not necessarily chemically or physically stable. In Fig. 7, the outer surface of the cobalt vanadate is converting to cobalt oxide (the phase marked "A") presumably by vaporization of V_2O_5 into the air stream. Also, cracks are visible at the inner edge of the vanadate phase, suggesting that the vanadate would spall easily, and indeed a periodic building-and-spalling of an outer vanadate layer has been proposed to occur in burner rig tests of vanadic hot corrosion (Ref. 9).

Thus, as in the preceding section, it appears possible to rationalize the corrosion of CoCrAlY by vanadate/SO_3 through an understanding of the potential acid-base reactions between the metal oxides and the corrosive compound constituents (Na_2O, V_2O_5, SO_3), and of the influences the reaction products may have in continuing corrosion. Also, interestingly, the mechanism(s) of corrosion may differ between vanadium-inducted and sulfur-induced hot corrosion, since a well-defined inner oxide layer (cf. Fig. 5) is usually found with vanadic corrosion that, although it contains low, uniform levels of vanadium, gives no indication of any molten phase. This implies that oxidation/corrosion at the metal front is actually a gas-solid reaction, where vanadium, perhaps by being incorporated at low levels in the oxide structure, renders the oxide nonprotective and/or increases diffusion through the oxide layer. In contrast, sulfur-induced corrosion at 700°C is thought by many to involve a molten eutectic sulfate phase and liquid transport of the various corrodent/corrosion product species. The controversy has been briefly discussed by proponents of each theory (Ref. 9), but remains unresolved.

VANADIC CORROSION OF ZIRCONIA CERAMICS

As noted above, this research has the goal of providing scientific understanding of the vanadic hot corrosion of zirconia (ZrO_2) and other ceramics to support development of vanadic corrosion-resistant ceramic coatings for Navy ship propulsion gas turbines.

1. Acid-Base Corrosion Reaction of Zirconia Ceramics.

At first thought, ceramic oxides, being "highly stable" oxides, might not be expected to corrode. However, experience has shown that ceramic oxides do corrode, with the degradation of Y_2O_3-stabilized ZrO_2 by molten $NaVO_3$ (Fig. 8) causing Y_2O_3 to be leached from the ZrO_2 matrix and deposited as YVO_4 crystals on the ceramic surface. This process appears to be principally driven by Lewis acid-base reactions as demonstrated in NRL experiments (Ref. 7) which systematically examined reactions between the different vanadium compounds and various ceramic oxides. The results (Fig. 9) are unequivocally consistent with acid-base behavior, where, e.g., Y_2O_3 (basic) does not react with Na_3VO_4 (basic) but reacts readily $NaVO_3$ (moderately acidic) and V_2O_5 (more acidic) to produce YVO_4. The less basic oxide, CeO_2, does not react with Na_3VO_4 (CeO_2 still too basic) nor $NaVO_3$ (CeO_2 too acidic) but does react with the more acidic V_2O_5. Zirconia is apparently somewhat more acidic than CeO_2, and does not react with $NaVO_3$, and reacts only very slowly with V_2O_5: i.e., the behavior of Y_2O_3 and ZrO_2 is in excellent agreement with the degradation of Y_2O_3-stabilized ZrO_2 by $NaVO_3$ where Y_2O_3 is depleted from the ceramic with formation of YVO_4, but the ZrO_2 matrix remains essentially unattacked.

Conversely, oxides such as Ta_2O_5 are sufficiently acidic to displace V_2O_5 from the sodium vanadates, and even react with V_2O_5 itself to generate a compound that is probably a tantalate rather than a vanadate as listed in Fig. 9 (and the literature).

2. Vanadic Corrosion of Fabricated Zirconia Ceramics.

Subsequent experiments were undertaken on the corrosion of fabricated ceramics in molten $NaVO_3$ to determine i) whether the acid-base reaction characteristics of the different ceramic oxides would be retained once the oxides were processed into ceramics, and ii) whether the method of processing affects the corrosion performance of the ceramic.

As a first step in investigating these points, pieces of ceramic with different compositions and processing were exposed simultaneously in bulk molten $NaVO_3$. Surprising

results were obtained (Fig. 10) with sintered CeO_2(23w/o)-stabilized ZrO_2--which according to the data in Fig. 9 should have been "inert" since neither CeO_2 or ZrO_2 were found to react with $NaVO_3$--being depleted of CeO_2 (confirmed by SEM/EDS analysis) and showing greater depth of degradation than Y_2O_3(8w/o)-stabilized ZrO_2. A second interesting result was that the rapidly solidified (RS) and single crystal (SC) ceramics (i.e., those ceramics which had been fused) were less corroded than the sintered ceramics, even for equivalent 8(w/o) Y_2O_3-ZrO_2 compositions.

Both findings are potentially important and are being investigated further, but most emphasis to date has been placed on trying to understand the apparently anomalous corrosion behavior of CeO_2 when incorporated into ZrO_2.

3. Physical Solubility of CeO_2 in Molten $NaVO_3$.

Ceria could conceivably be leached from the zirconia matrix by simple physical solubility where no chemical reaction between CeO_2 and $NaVO_3$ occurs. To test this idea, the solubility of CeO_2 in 700-1000^oC $NaVO_3$ was determined (Ref. 8) by monitoring the weight loss suffered by solid pieces of CeO_2 equilibrated with known weights of $NaVO_3$ at the different temperatures. The solubility of CeO_2 so measured (Fig. 11) increased monotonically from about 0.1 mole-percent at 700o to 1.0 mole-percent at 1000^oC. Also, when the 1000^oC melts were quenched, CeO_2 (identified by x-ray diffraction) deposited on the crucible walls, providing further evidence that no chemical reaction occurs between $NaVO_3$ and pure CeO_2. It is difficult, however, to argue that physical solubility of this extent is solely responsible for the CeO_2 depletion, especially when other possible mechanisms have not been ruled out.

4. Reaction of CeO_2-ZrO_2 with Thin Film V_2O_5 and $NaVO_3$.

An alterative, and probably more realistic, technique for the study of vanadate/ceramic interaction is to coat the ceramic with thin films of the vanadium compound, and then examine the products and phases that are formed on the ceramic surface by exposure at temperature. For sintered CeO_2(23w/o)-stabilized ZrO_2 coated with $NaVO_3$ and exposed at 700^oC under air containing 40 Pa of SO_3, one can determine (Fig. 12) by SEM/EDXA, for example, that a molten eutectic $CeSO_4$-Na_2SO_4 phase ("1") is formed on the CeO_2-depleted ceramic surface ("2"), with $CeVO_4$ crystals ("3") then apparently being precipitated from the eutectic sulfate. This mechanism is, interestingly, very similar to the way Co_2VO_7 is precipitated from molten $CoSO_4$-Na_2SO_4 in the SO_3/$NaVO_3$ attack of CoCrAlY.

More relevant to the depletion of CeO_2 from CeO_2-ZrO_2 by $NaVO_3$, however, were tests where the surface products formed on rapidly solidified CeO_2(20w/o)-ZrO_2 by thin films of V_2O_5 at 900^oC were compared with the products formed on the same ceramic material under the same conditions by thin films of $NaVO_3$. Tests with V_2O_5 produced discrete surface crystals (Fig. 13a, "A") which contained (Fig. 13b) Ce and V, but no Zr, and which quantitative EDXA confirmed to be $CeVO_4$, i.e., the product found for reaction of pure CeO_2 and V_2O_5 in Fig. 9. Equivalent tests with $NaVO_3$ generated a surface layer of crystals (Fig. 14a), but it could be shown by x-ray mapping (Fig. 14b) that Ce was segregated into only certain crystals ("A". Fig. 14a) in this crystal layer. More significantly, quantitative EDXA established that these crystals contain about 90 a/o Ce and 10 a/o Zr, but essentially no vanadium. Thus the findings in Fig. 9 are not violated--no vanadate product has been produced by reaction of CeO_2 and $NaVO_3$--and while Ce is being segregated from the ceramic by $NaVO_3$, the final segregate is not a vanadate, but rather an oxide, albeit perhaps a mixed oxide of Ce and Zr.

5. Possible Application of Acid-Base Science from Glass Chemistry.

The chemistry of CeO_2 is thus evidently affected by its being incorporated in ZrO_2, but how the effect occurs, or how it may be predicted or quantitatively characterized, is still not known. However, concepts of acid-base chemistry in glasses, as developed by Duffy (Ref. 10), offer an intriguing possible approach to an explanation. Oxyanion glasses can be considered as formed by reaction between basic (Na_2O, CaO, etc.) and acidic (SiO_2, B_2O_3, etc.) oxides. The oxygen atoms within the resultant, e.g., silicate lattice function as Lewis bases (electron donors), whose basicity or "ability to donate negative charge" is moderated by interactions with the acidic (electron acceptor) Si^{4+} constituents of the silicate lattice, and with the other acidic cations (Na^+, Ca^{2+}, etc.) that are incorporated in the glass. As described in Ref. 10, Duffy has shown that a UV spectrometric parameter, which he terms the "optical basicity", can be obtained that "is a measure of the oxide basicity and represents the degree of negative charge residing on the oxide(-II) species." Duffy and coworkers have since determined the optical basicities for many glasses and other oxides (MgO, Al_2O_3, B_2O_3, SiO_2, P_2O_5, SO_3, etc.), and demonstrated that the optical basicity concept provides an improved explanation for many oxide reactions including acid-base reactions between oxides and oxysalts (Ref. 11).

Following this line of thinking, one can speculate that the difference in oxide lattice basicity between pure CeO_2 and a CeO_2-ZrO_2 solid solution could increase the "effective" basicity of CeO_2 (in ZrO_2) so that it could react (as Y_2O_3 does) with $NaVO_3$, possibly producing $CeVO_4$; however, such $CeVO_4$ would be unstable in the $NaVO_3$ melt, and would tend to decompose as it left the sphere of influence of the zirconia lattice, i.e., at the melt/zirconia interface. The final product on the zirconia surface would therefore be an oxide, and not a vanadate.

However, before this hypothesis is accepted as the probable cause for the unexpected depletion of CeO_2 by $NaVO_3$, at least two other possible explanations must be mentioned: i) the 10 a/o of Zr found in the CeO_2 surface crystals may not be fortuitous, but may indicate formation of a mixed Zr,Ce oxide, with the mixed oxide formation providing the driving force for the depletion of CeO_2 from the ZrO_2 matrix; and ii) Ce^{3+} is significantly more basic than Ce^{4+}, and if the Ce^{4+} in the CeO_2-stabilized ZrO_2 were reduced (as is observed under some reducing conditions), the Ce^{3+} produced could react with $NaVO_3$, but then be reoxidized to Ce^{4+} and convert to CeO_2 under oxidizing conditions in the $NaVO_3$ melt.

The reaction of $NaVO_3$ with CeO_2-stabilized ZrO_2 is thus still unexplained, but its study has identified new lines of thought and possible avenues of investigation that may be of benefit in future research on the reactions of corrosive oxysalts with zirconia and other oxide-based ceramics. Adopting Duffy's "optical basicity" technique for the study of zirconia acid-base reactions appears especially promising, although experimental difficulties may be encountered since zirconia tends to be opaque in the UV spectral region.

CLOSURE

From the work described here (and many other sources), it is evident that vanadium in the fuel has the potential to seriously increase hot corrosion in gas turbines. When multiple corrodents such as V, S, etc. are present, the corrosion reactions become complex. However, even then there appears to be a central "set" of oxide acid-base reactions between the "corrodent" oxides (Na_2O, SO_3, V_2O_5) and "material" oxides (CoO, Y_2O_3, ZrO_2, etc.) that predominantly controls the corrosion process, regardless of whether the material is metallic (CoCrAlY) or ceramic (stabilized ZrO_2). By a better understanding of these oxide acid-base reactions, we may hope, e.g., as in the present instance where oxide acid-base concepts are

being used in the search for a vanadium-resistant stabilizer for zirconia, to develop gas turbine coating materials that can withstand vanadium contaminants in fuel.

ACKNOWLEDGMENTS

The research described in this article was performed under the Gas Turbine Component Improvements Task of the NAVSEA Ship Propulsion Technology Program, and the support is gratefully acknowledged.

REFERENCES

1. L. F. Aprigliano, Paper 5, "Degraded Fuels, Selection and Testing Program," Proc. of Workshop on Gas Turbine Materials in a Marine Environment, Bath, UK, November 1984.

2. "Phase Diagrams for Ceramists," E. M. Levin et al., eds., Figs. 5126 and 5127, The American Ceramics Society, Inc. (1979).

3. K. L. Luthra and H. S. Spacil, J. Electrochem. Soc. 129, 649 (1982).

4. R. L. Jones and C. E. Williams, Matls. Sci. and Engr. 87, 353 (1987).

5. "Proceedings of the Second Conference on Advanced Materials for Alternative-Fuel-Capable Heat Engines," J. W. Fairbanks and J. Stringer, Cochairmen, EPRI RD-2369-SR, Electric Power Research Institute, Palo Alto, (1982).

6. A. S. Nagelberg, J. Electrochem. 132, 2502 (1985).

7. R. L. Jones, C. E. Williams and S. R. Jones, ibid., 133, 227 (1986).

8. R. L. Jones, "Hot Corrosion Studies of Zirconia Ceramics," to be published in Proceedings of 1987 Intl. Conf. on Metallurgical Coatings, Journal of Surface and Coatings Technology.

9. W. Moller, in "9th Intern. Congr. on Combustion Engines, Stockholm, Sweden," (1971). Paper B16.

10. J. A. Duffy and M. D. Ingram, J. of Non-Crystal. Solids 21, 373 (1976).

11. L. S. Dent-Glasser and J. A. Duffy, "Analysis and Prediction of Acid-Base Reactions between Oxides and Oxysalts using the Optical Basicity Concept," submitted to J. Chem. Soc., Dalton Trans.

TABLE 1

COMPOUNDS OCCURRING IN THE Na,V,O SYSTEM (Ref. 2)

$Na_2O + 6\ V_2O_5 = Na_2V_{12}O_{31}$	vanadium bronze I (mp, 645°C)
$Na_2O + 3\ V_2O_5 = 2\ NaV_3O_8$	vanadium bronze II (d., 548°C)
$Na_2O + V_2O_5 = 2\ NaVO_3$	sodium metavanadate (mp, 610°C)
$2\ Na_2O + V_2O_5 = Na_4V_2O_7$	sodium pyrovanadate (d., 668°C)
$3\ Na_2O + V_2O_5 = 2\ Na_3VO_4$	sodium orthovanadate (mp, 1266°C)

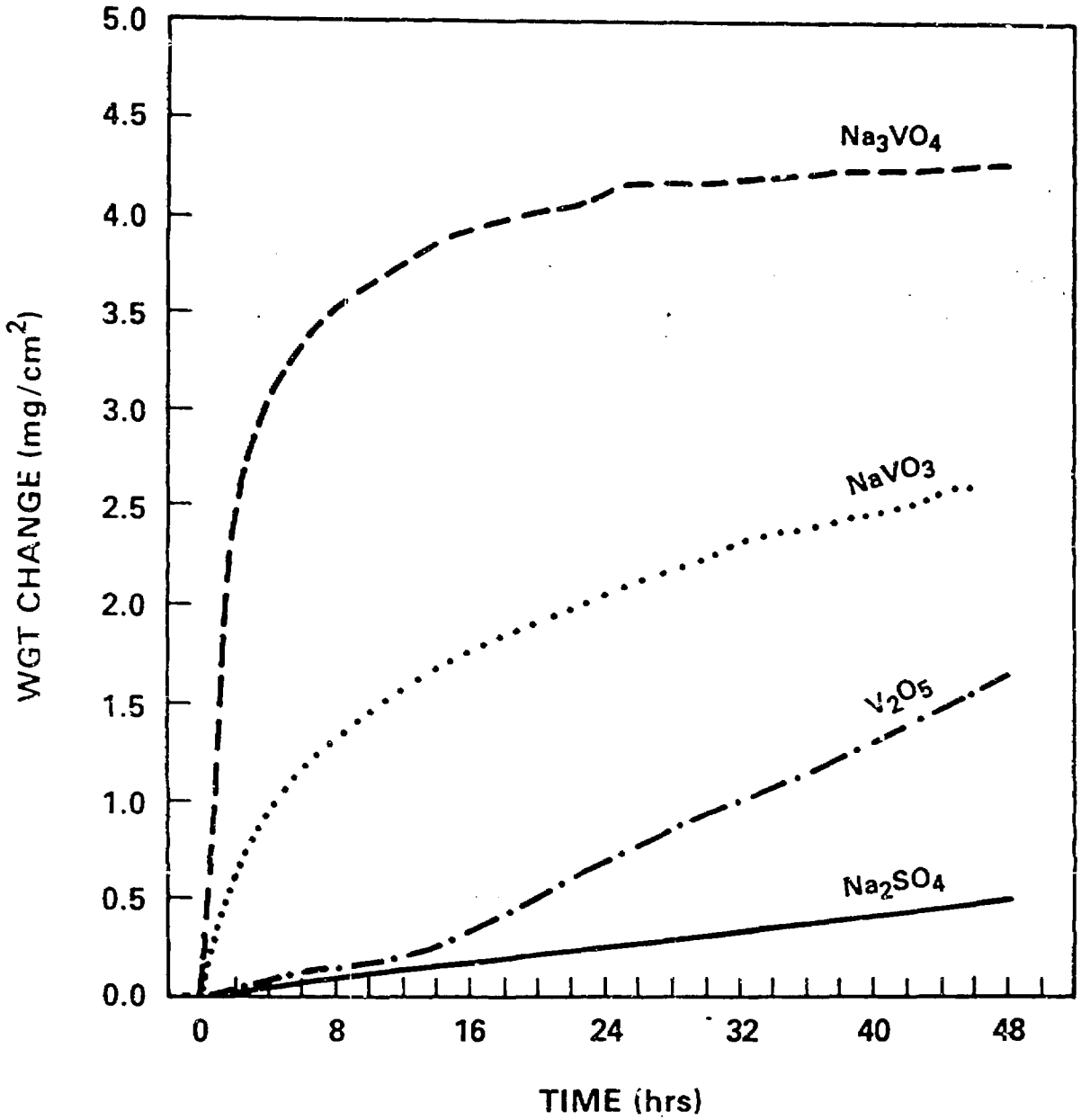

Fig. 1 Corrosion of CoCrAlY by pure compounds under flowing air at 700°C.

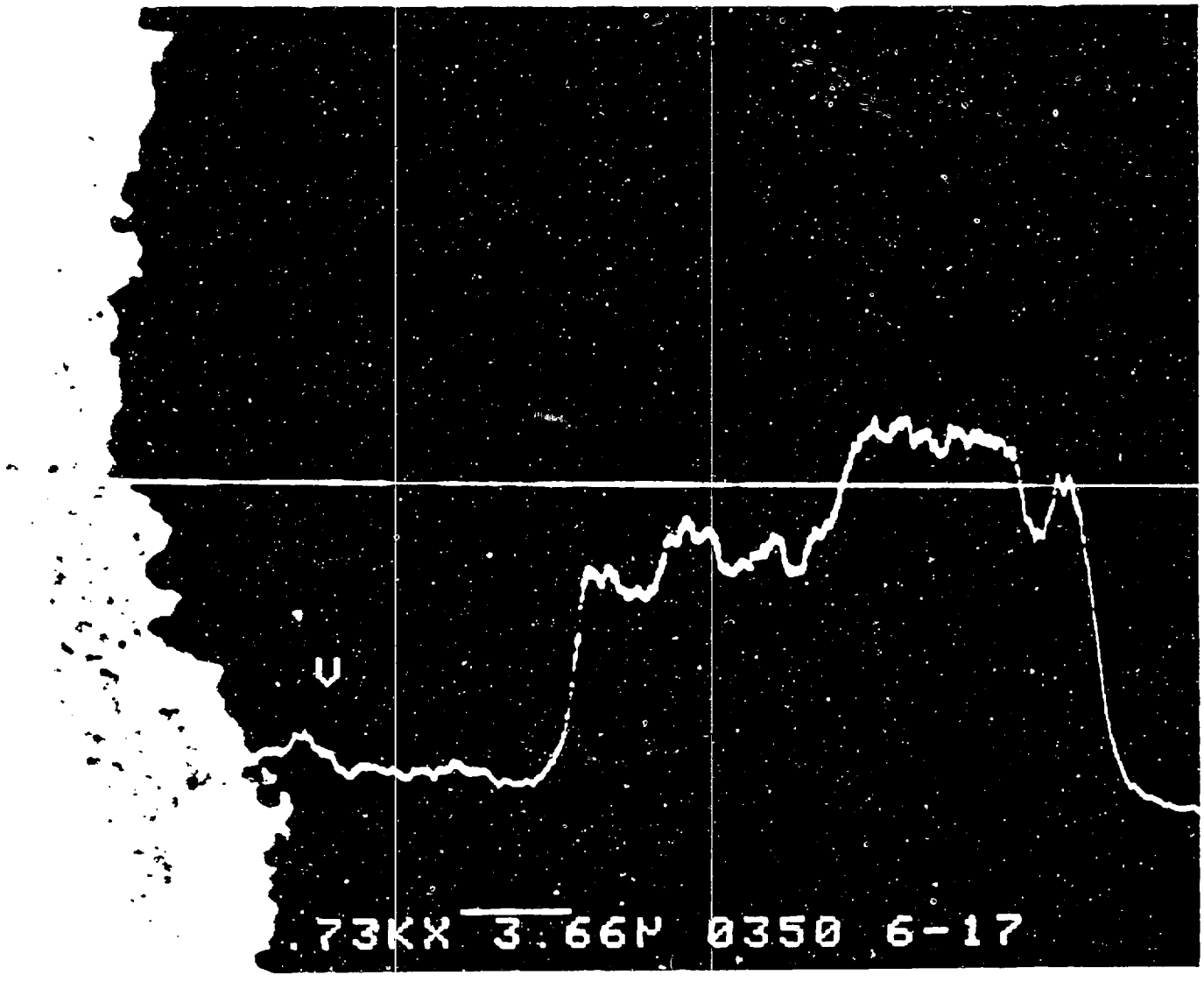

Fig. 2 Backscattered electron (BSE) micrograph with line scan x-ray analysis delineating "outer vanadate" and "inner oxide" layers in corrosion product on CoCrAlY corroded by V_2O_5 in air for 48 hrs at 700°C.

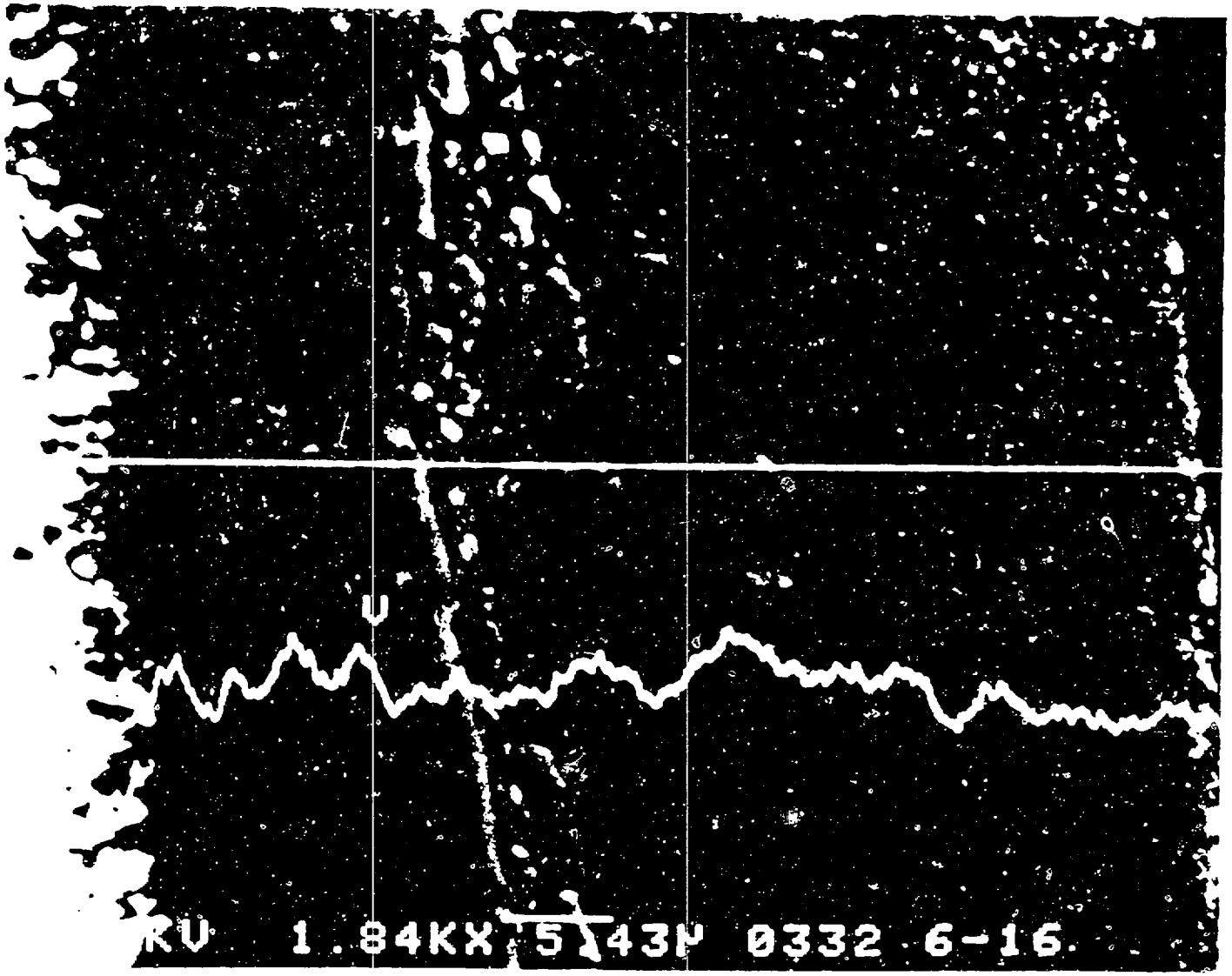

Fig. 3 BSE micrograph with line scan x-ray analysis indicating vanadium concentration in oxide layer on CoCrAlY corroded by $NaVO_3$ in air for 48 hrs at 700°C.

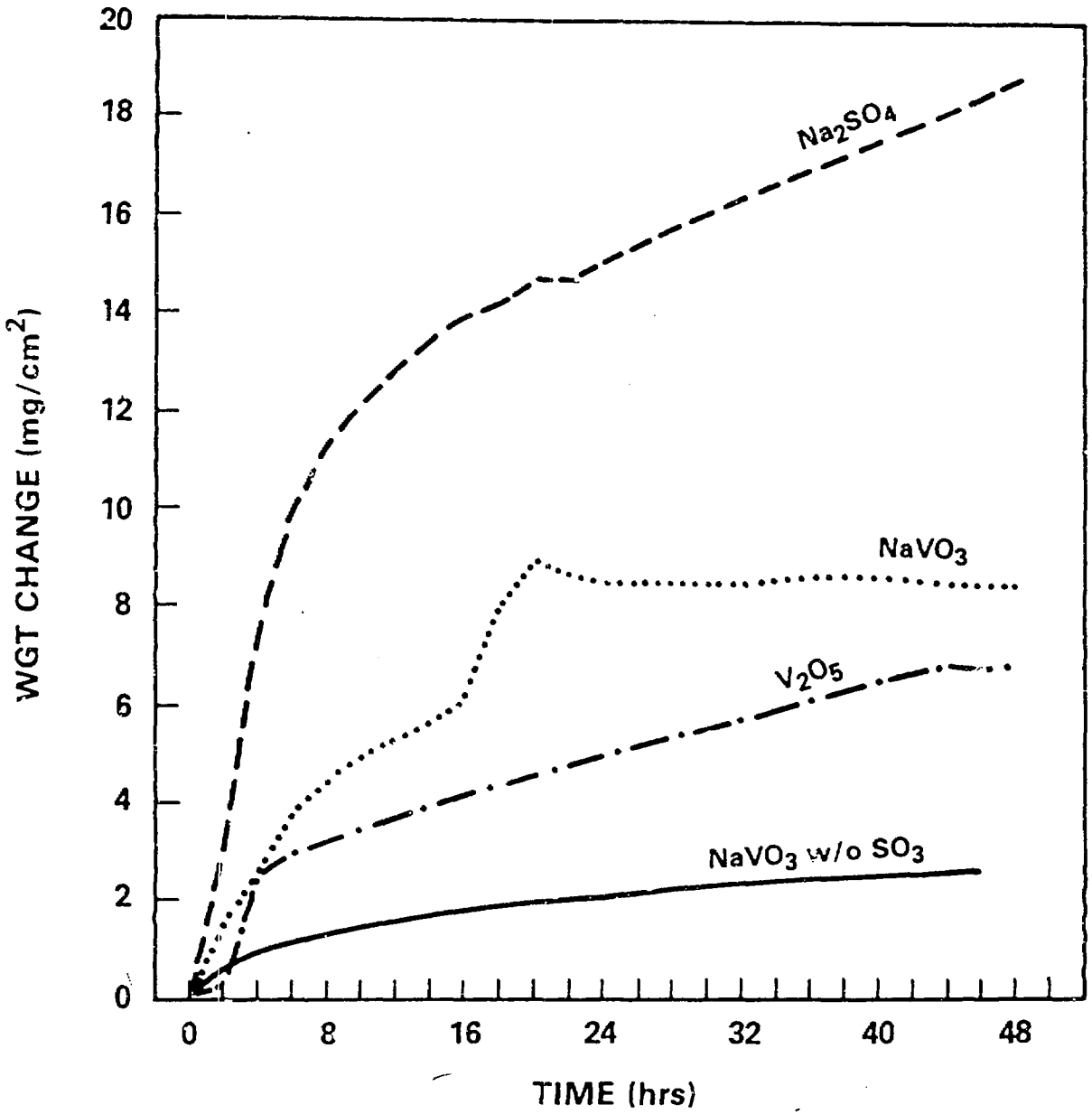

Fig. 4 Corrosion of CoCrAlY by different compounds under 13 Pa of SO_3 in flowing air at 700°C.

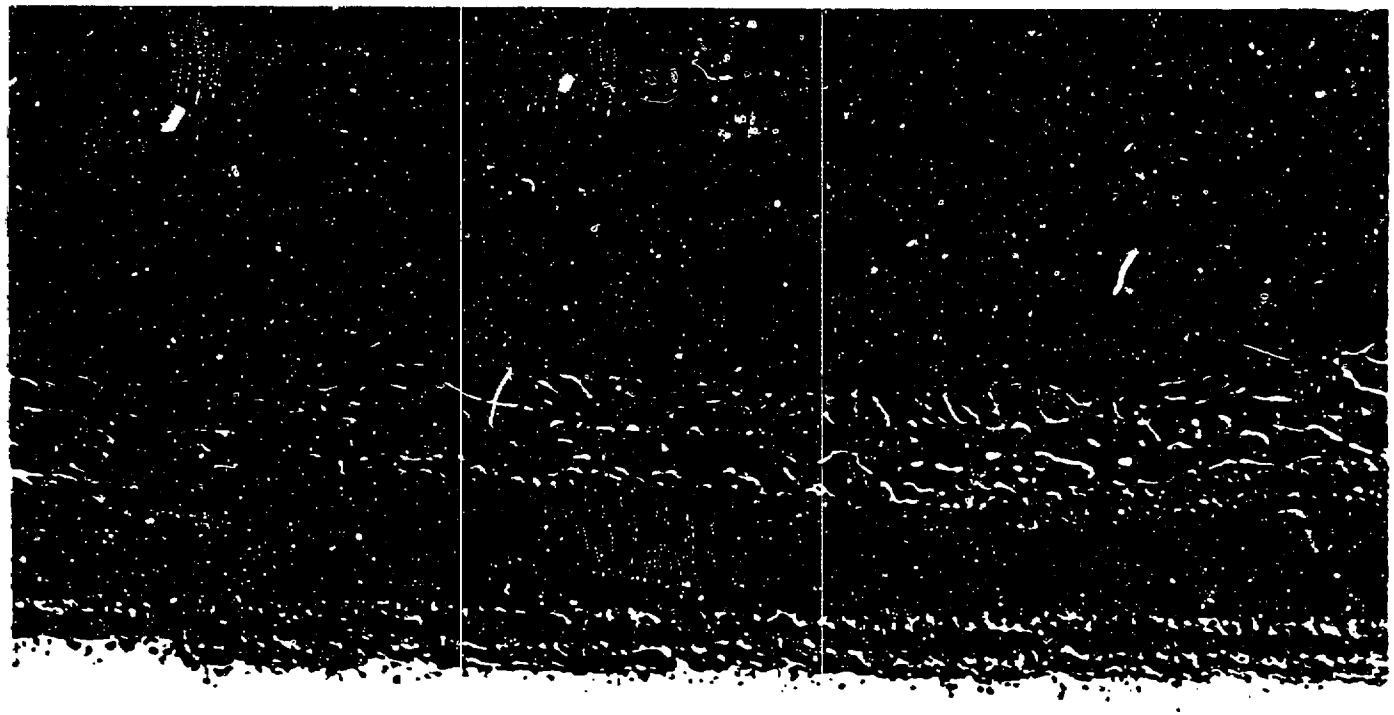

Fig. 5 Low magnification BSE micrograph showing the outer "salt" and inner oxide layers formed on CoCrAlY corroded by $NaVO_3$ under 13 Pa of SO_3 in air for 14.5 hrs at 700°C.

5

Fig. 6 Higher magnification BSE micrograph of the outer molten salt reaction layer of CoCrAlY corroded 14.5 hrs at $NaVO_3/SO_3$ (cf. Fig. 5). Indicated phases are: A, molten mixed $CoSO_4$-Na_2SO_4 containing dissolved $NaVO_3$ and V_2O_5; B, precipitating cobalt vanadate, probably $Co_2V_2O_7$; C, molten $CoSO_4$-Na_2SO_4 showing higher vanadium concentration than site A; D and E, Cr,Co,Al oxide showing trace Na,S,V.

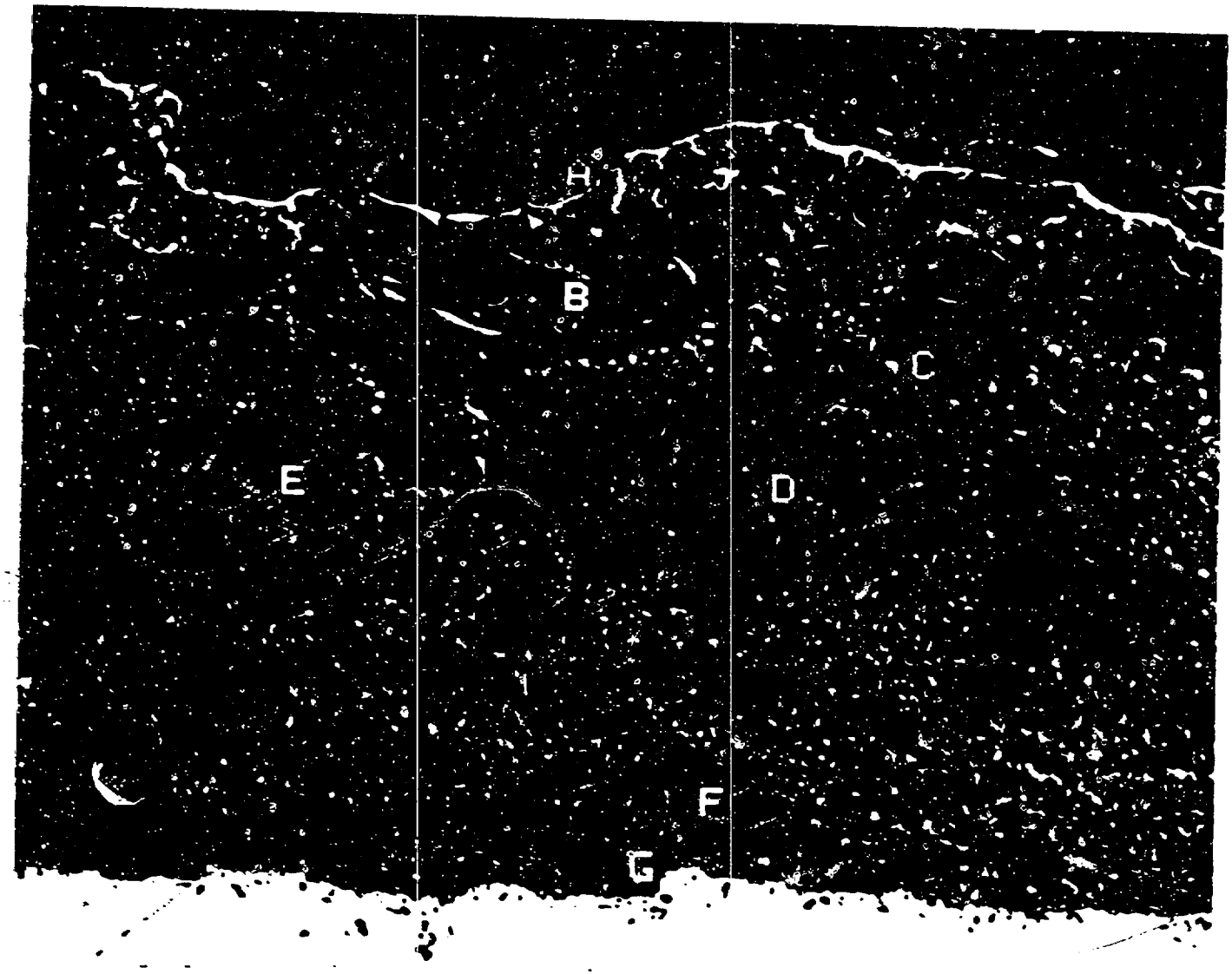

Fig. 7 BSE micrograph showing phases formed on CoCrAlY corroded by $NaVO_3$ under 13 Pa of SO_3 in air for 48 hrs at 700°C. Indicated phases are: A, Co_3O_4 produced by V_2O_5 vaporization from $Co_2V_2O_7$ phase; B, cobalt vanadate layer, probably $Co_2V_2O_7$; C, molten $CoSO_4$-Na_2SO_4, but depleted of $NaVO_3$ and V_2O_5; D, solid solution $CoSO_4$-Na_2SO_4 resulting from reduced SO_3 partial pressure in corrosion phase; E, F and G, Co,Cr,Al oxides with trace S,V.

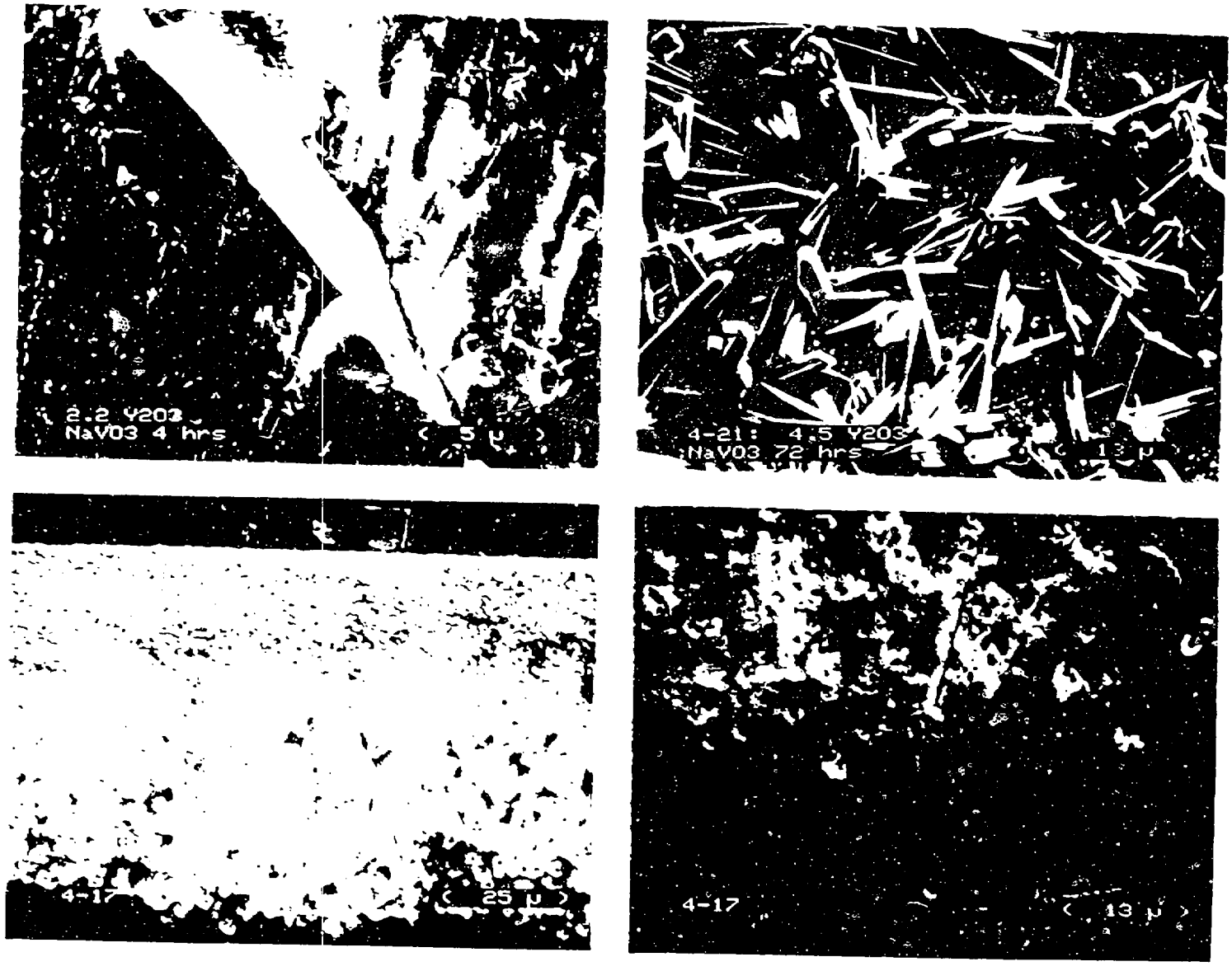

Fig 8. SEM micrographs of Y_2O_3-stabilized ZrO_2 corroded by thin film $NaVO_3$ at 700°C in air: UL, YVO_4 crystallite protruding through $NaVO_3$ film; UR, YVO_4 crystallites on ZrO_2 surface after $NaVO_3$ washed away; LL, cross-section showing zone of Y_2O_3 depletion in ZrO_2; LR, structure at front of Y_2O_3 depletion zone.

INCREASING ACIDITY →

INCREASING ACIDITY ↓	Na_3VO_4	$NaVO_3$	V_2O_5
Y_2O_3	NR	YVO_4	YVO_4
CeO_2	NR	NR	$CeVO_4$
ZrO_2	NR	NR	ZrV_2O_7 (BUT SLOWLY)
GeO_2	$Na_4Ge_9O_{20}$	$Na_4Ge_9O_{20}$ (*)	NR
Ta_2O_5	$NaTaO_3$	$Na_2Ta_4O_{11}$	α-$TaVO_5$

NR = NO REACTION

(*) AS PPT FROM H_2O SOL'N

Fig. 9. Reaction behavior of ceramic oxides with vanadium compounds at 700-900°C.

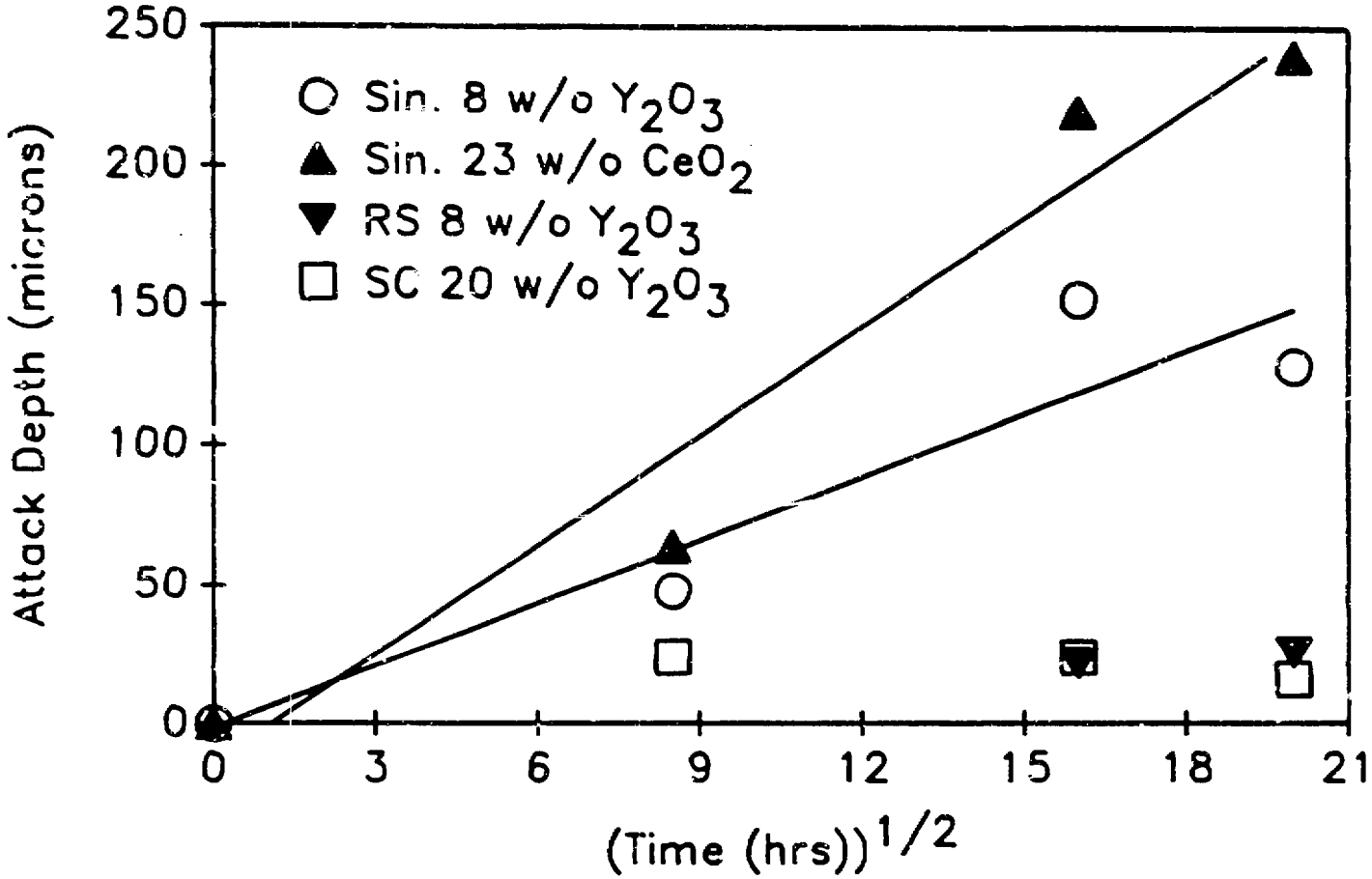

Fig. 10. Degradation of stabilized ZrO_2 ceramics in bulk $NaVO_3$ at 700°C, where ceramics were either sintered (Sin.), rapidly solidified (RS), or single crystal (SC). Solid lines are least square fits of sintered Y_2O_3- and CeO_2-stabilized ZrO_2.

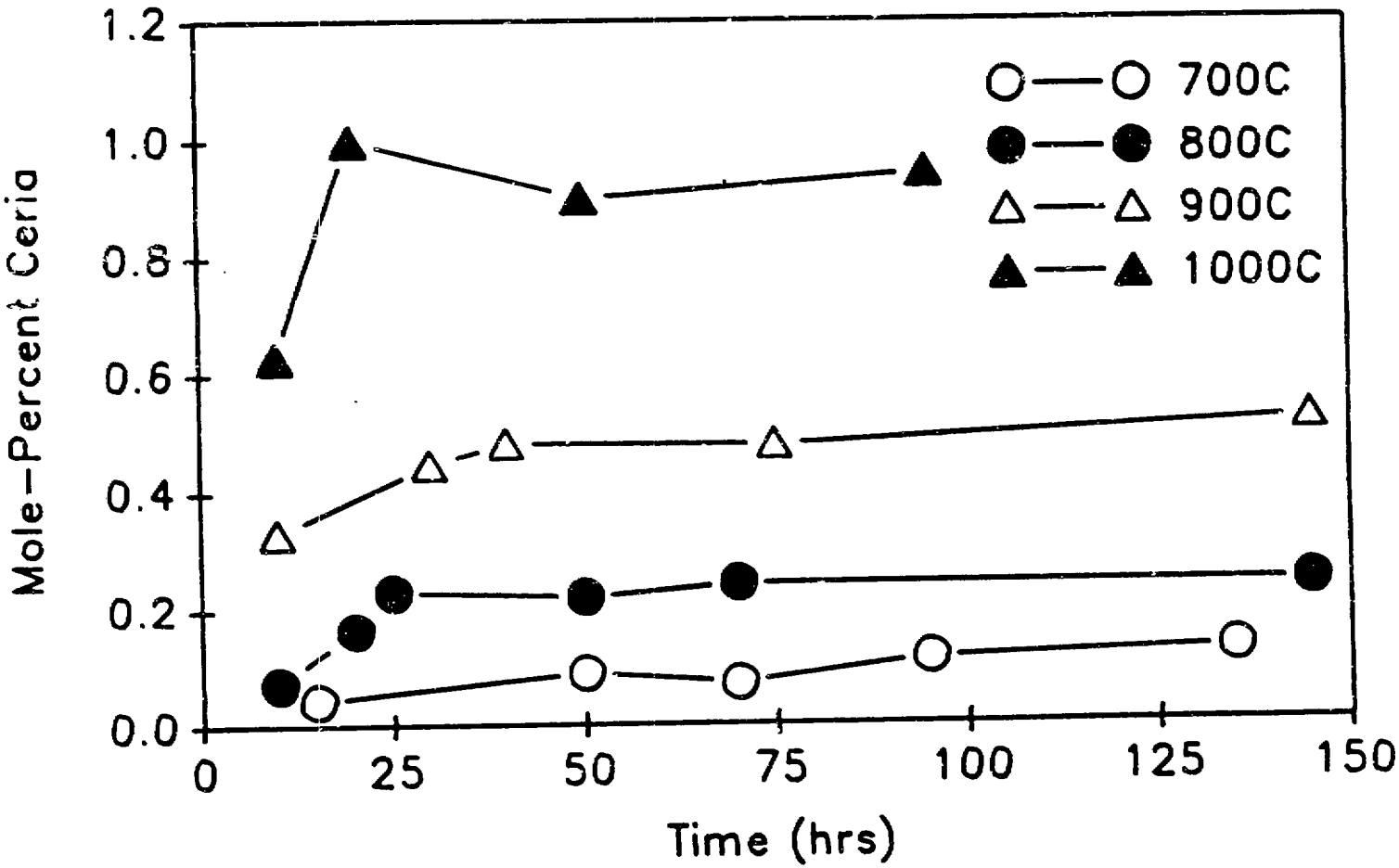

Fig. 11 Determination of the solubility of ceria (CeO_2) in $NaVO_3$ at 700-1000°C.

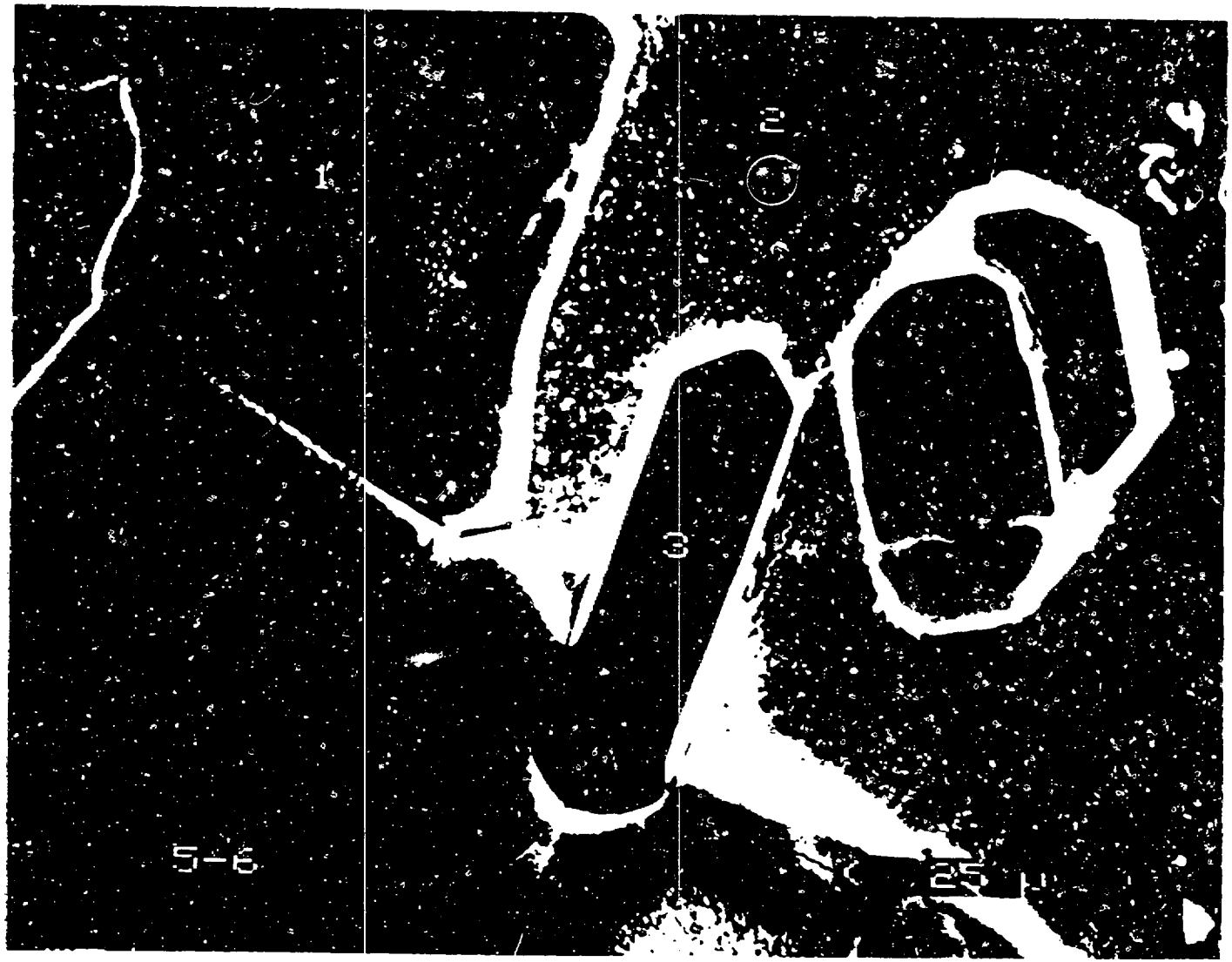

Fig. 12 Phases formed on sintered (23.5w/o)CeO_2-ZrO_2 coated with $NaVO_3$ and heated 24 hrs at 700°C under 40 Pa of SO_3 in flowing air: 1, molten eutectic Na,Ce sulfate phase; 2, CeO_2-depleted zirconia surface; 3, $CeVO_4$ crystals apparently precipitated from Na,Ce sulfate phase.

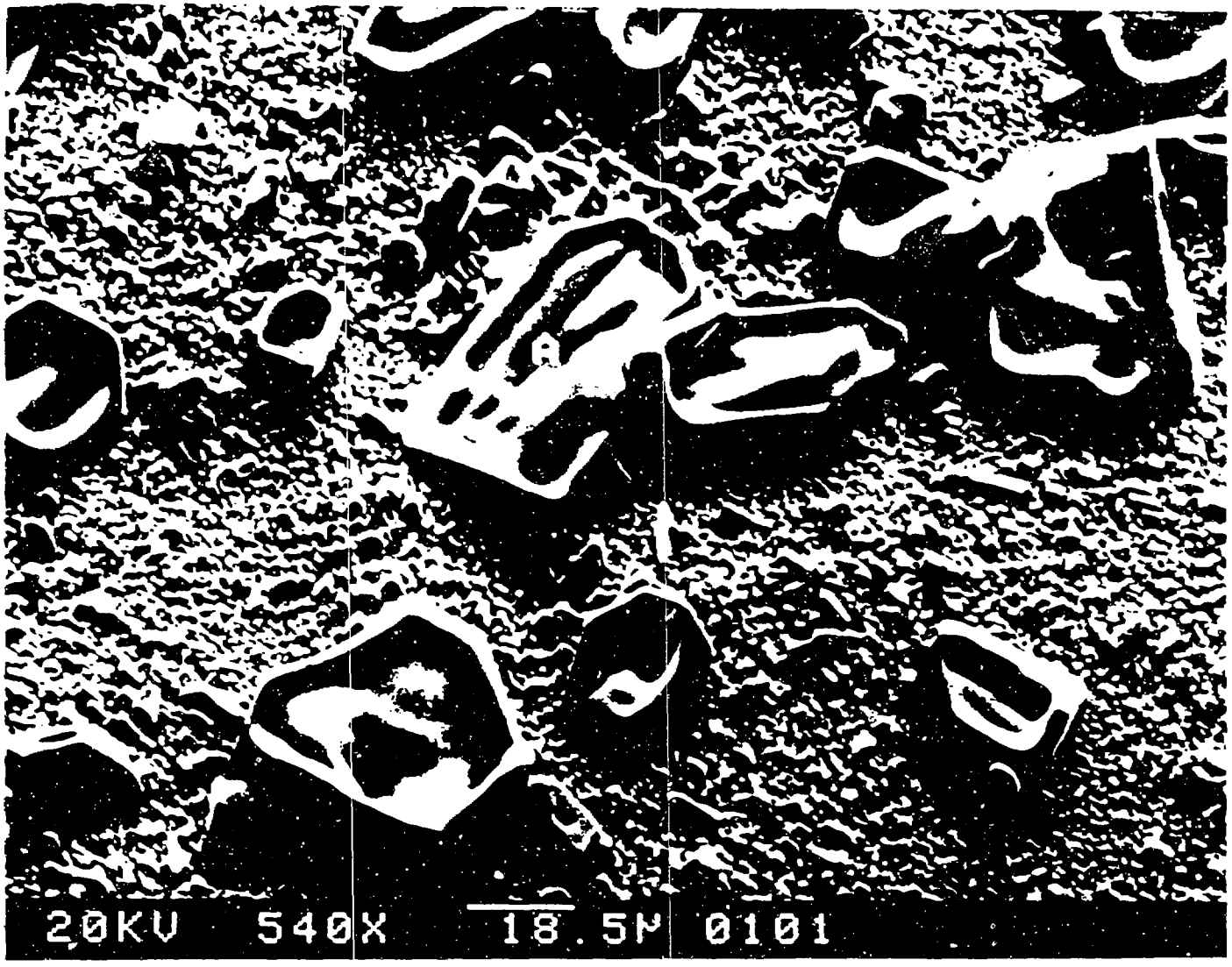

Fig. 13a. Crystals of $CeVO_4$ (marked A) from on rapidly solidified (20w/o)CeO_2-ZrO_2 coated with V_2O_5 and heated for 72 hrs at 900°C.

13a

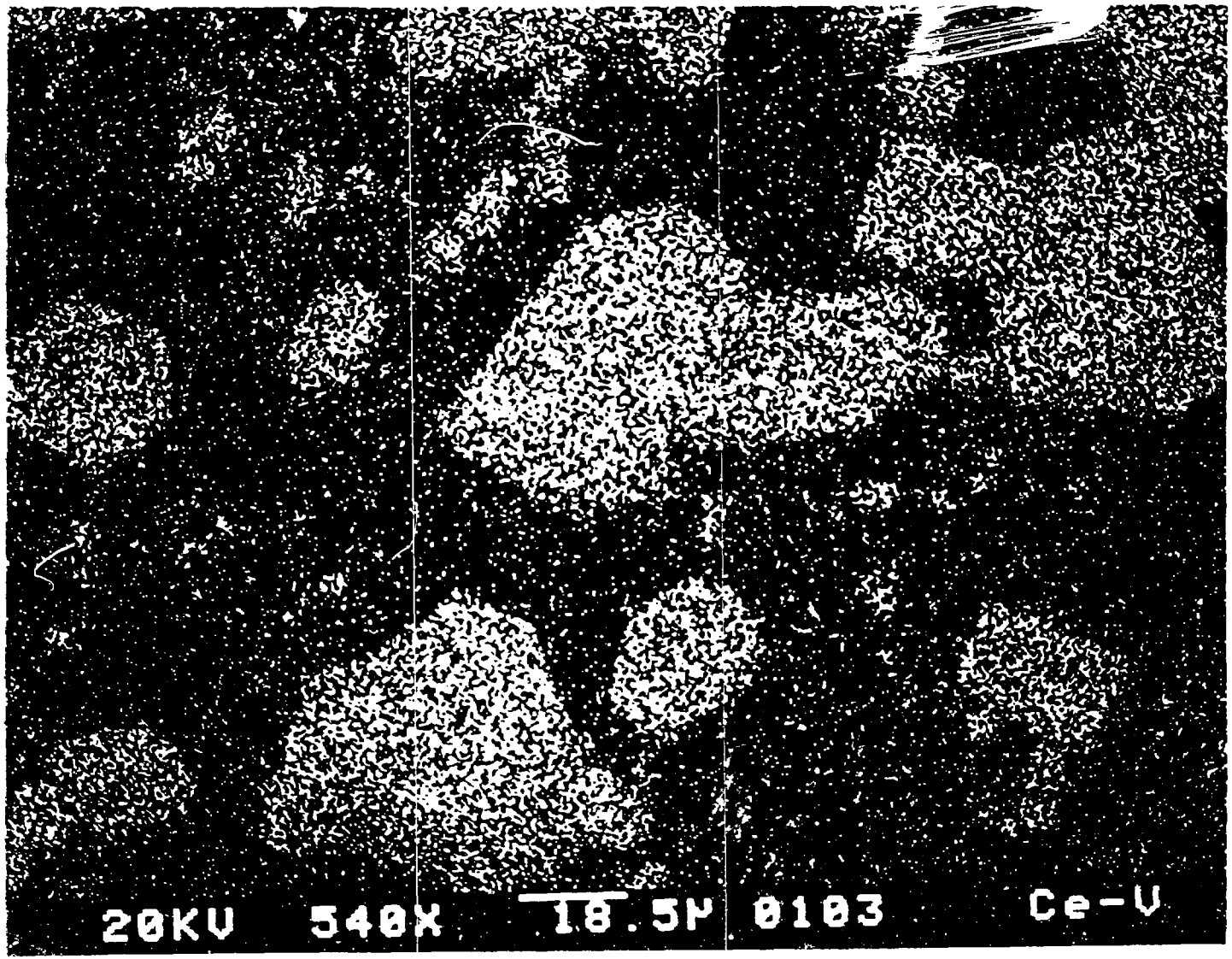

Fig. 13b. Elemental x-ray map showing Ce-V contained in surface crystals in Fig. 13a.

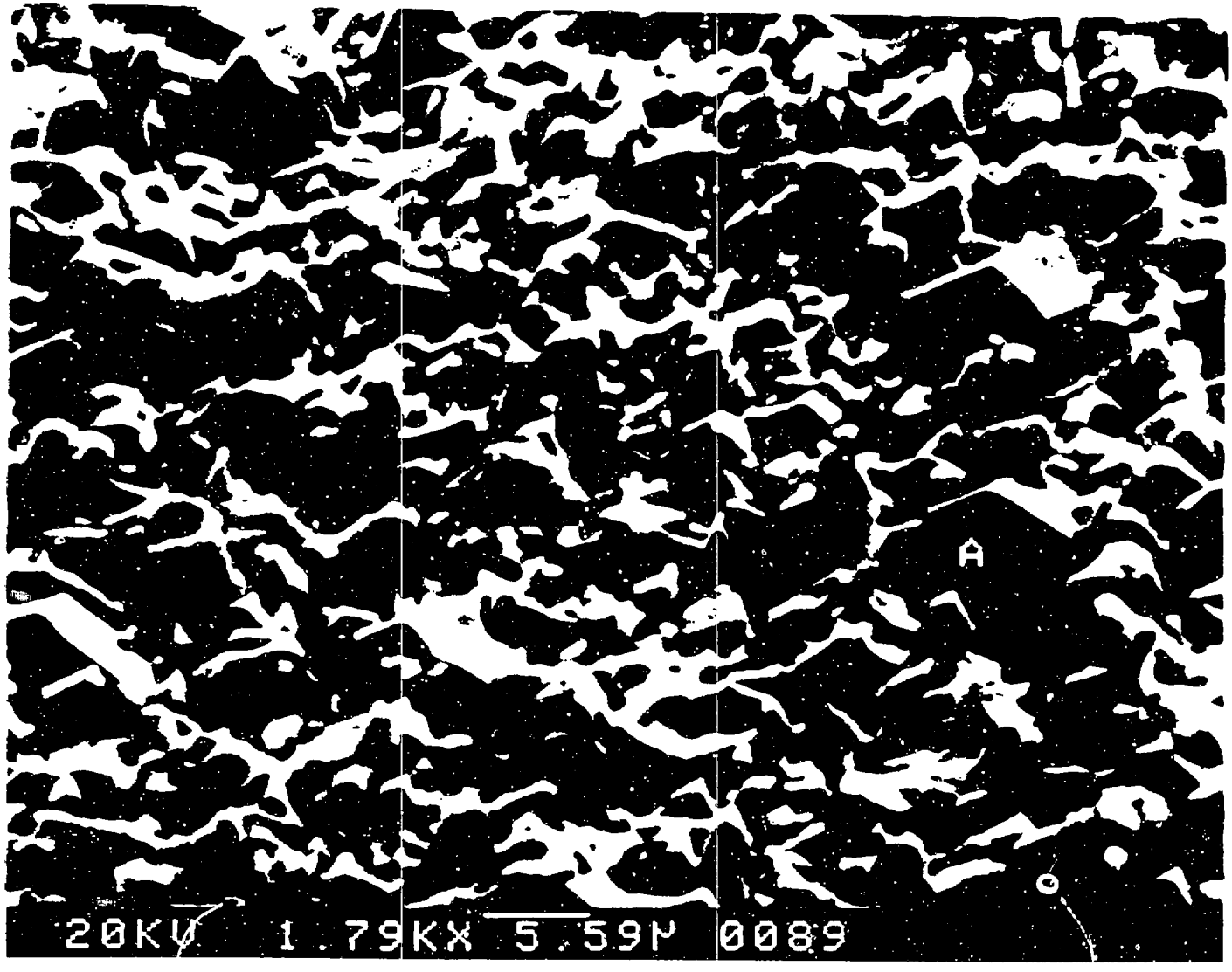

Fig. 14a. Crystal layer formed on (20w/o)CeO_2-ZrO_2 coated with $NaVO_3$ and heated for 72 hrs at 900°C, where Ce is segregated into crystals of the type marked A.

14a

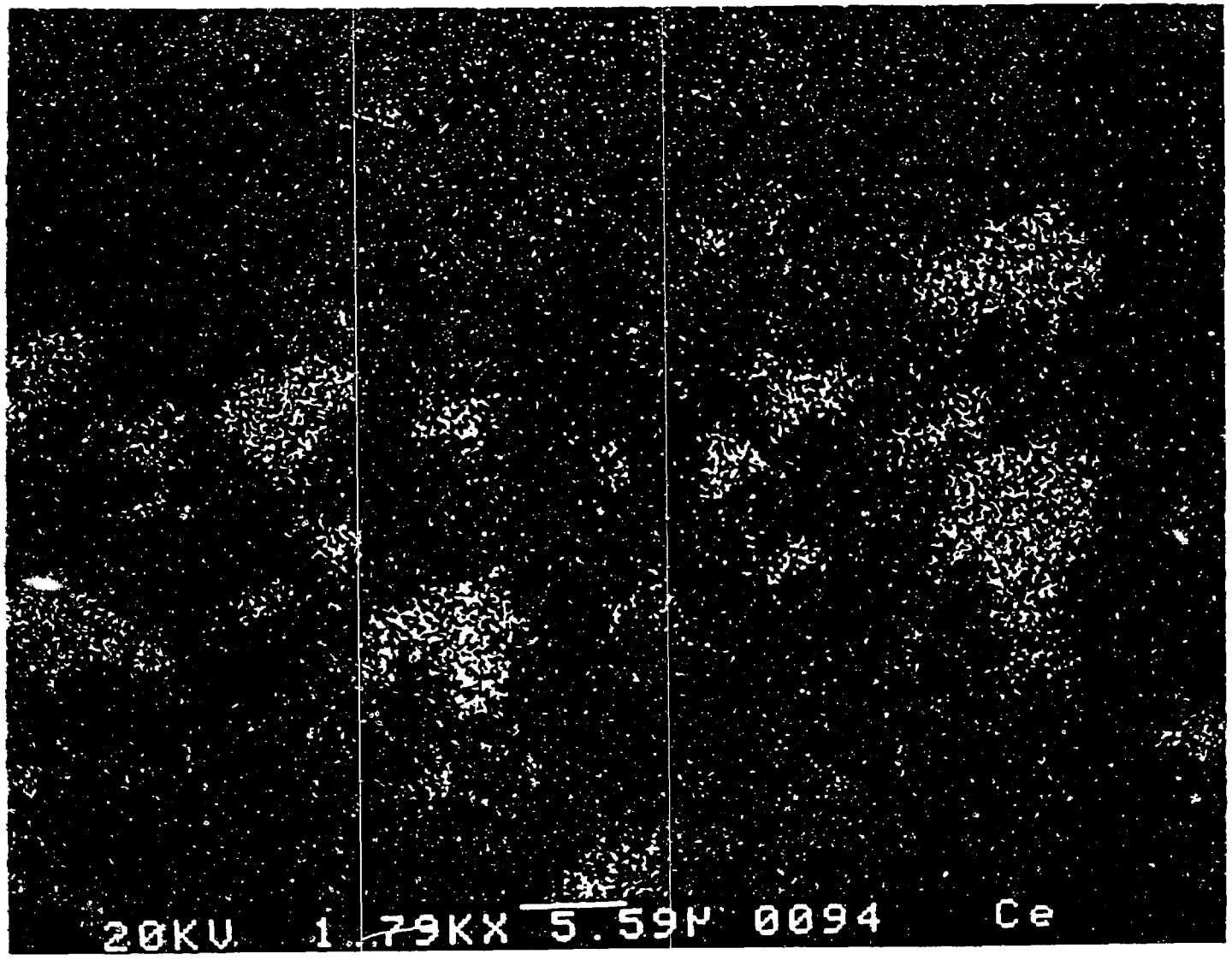

Fig. 14b. Elemental x-ray map of Fig. 14a confirming that Ce is segregated only into crystals of type marked A in Fig. 14a.

BIOGRAPHY

NAME: Robert L. Jones

PRESENT AFFILIATION: Naval Research Laboratory
Chemistry Division
Washington, DC 20375-5000

TITLE: Head, High Temperature Chemistry Section

FIELD OF INTEREST/RESPONSIBILITIES: High temperature chemistry, corrosion, molten salts, ceramics, electron microscopy

PREVIOUS AFFILIATIONS/TITLES: N/A at NRL since 1963.

ACADEMIC BACKGROUND: BS, Southern Illinois University, 1958
MS (1960) and PhD (1963) in Physical Chemistry, University of Michigan

SOCIETY ACTIVITIES/OFFICES/AWARDS: NRL Research Publication Awards (1978, 1981)
William Blum Award for Outstanding Electrochemist (Corrosion), National Capital Area Section, Electrochemical Society, (1985)
NRL Sigma Xi Applied Research Award (1986)
Gordon Conference (Corrosion) Lecturer (1970 and 197

PUBLICATIONS/PAPERS: Approximately 40 papers published in different areas of corrosion.

TRI-SERVICE CONFERENCE

ON

CORROSION

5-7 May 1987

U.S. AIR FORCE ACADEMY

Colorado Springs, CO

ATTENDANCE LIST

Preceding Page Blank

U.S. Air Force Museum
Robert Adair
Conservator
USAFM/DMC
WPAFB, OH 45433-6518
513/255-2597

Naval Air Development Ctr
Vinod Agarwala
Corrosion Scientist
Code 6062
Warminster, PA 18974
215/441-5028

U.S. Navy
Saleem Akhtar
Lt. Cdr
NPGS Monterey, 1198 8th St., #8
Monterey, CA 93940
408/646-8127

Army Materials Technology Lab
Albert Anctil
Mech. Engineer
SLCMT-MCM-MB
Watertown, MA 02172-001
617/923-5206

National Bureau Of Standards
David Anderson
Corrosion and Wear Group
Bldg 223, Room B254
Gaithersburg, MD 20899
301/975-6026

PTI
Frank Ansuini
Sr. Scientist
P.O. Box 3209
Derry, NH 03038
401/333-6112

Lockheed Missiles & Space Co
Dr.L.J. Bailin
Sr. Staff Scientist
3251 Hanover St., Bldg 204
Palo Alto, CA 94304-1187
415/424-2525

U.S. Air Force Museum
Charles Baker
Museum Tech
Collection Management
WPAFB, OH 45433-6518
513/255-2597

U.S. Army AVSCOM
Windel Baker
Gen. Engineer
4300 Goodfelow Blvd
St. Louis, MO 63122
314/263-1762

U.S. Army Materials Technology Lab
Kathleen Bamberg
Chemist
SLCMT-MSE
Watertown, MA 02172-0001
617/923-5564

Westinghouse
Jack Barnes
Engineer
Marketing Department
Pittsburgh, PA 15230
412/828-6334

Naval Surface Weapons Center
Bruce Beard
Research Chemist
10901 New Hampshire Ave, R34
Silver Spring, MD 20903-5000
202/394-3480

NAESU Detachment
Donald Beaver
Engr. Technician

Cherry Point, NC

Naval Air System Command
Subramanya Bettadapur
Sec. Head
AIR53040, GP2, Room 908
Washington, D.C. 20361-5300
202/692-6025

U.S. Air Force
Melvin Bishop
Materials Engineer Supr
WR-ALC/MMEM
Robins AFB, GA 31038
912/926-6619

NADC
John Boodey
Materials Engineer
Code 6062
Warminster, PA 18974
215/441-2811

Preceding Page Blank

Lockheed-Georgia Co
R.E. Bradley
Staff Specialist
86 S. Cobb Drive, MS53, Dept. 72-27
Marietta, GA 30063
404/424-2123

Lawrence Livermore National Lab
John Bridge
Materials Engineer
P.O. Box 808, MS/L-369
Livermore, CA 94550
415/423-3574

Sundstrand Aviation
Owen Briles
Principal Chemist
4747 Harrison Ave, Box 7002
Rockford, IL 61125-7002
815/226-2930

U.S. Army Tank-Automotive Command
George Bugarin
C, Mfg. Tech & Prod
AMSTA-TM
Warren, MI 48397-5000
313/574-5215

U.S. Army Troop Support Command
William Butler
Gen. Engineer
4300 Goodfellow Blvd, AMSTR-OE
St. Louis, MO 63120-1798
314/263-9457

Chomerics
Eric Carlson
Sr. Res. Ass.
77 Dragon Ct
Woburn, MA 01888
617/935-4850

TRW
Richard Carlston
Mgr. ICBM Corrosion
1 Space Park, MS/134/5085
RedondoBeach, CA 90278
213/217-3759

3M Company
Jospeh Claus
Specialist
3M Center, MS/251-3A-05
St. Paul, MN 55144
612/736-0137

U.S. Air Force
Ronald Clay
Chem. Engr
HQ OOALC/MMEAR
Hill AFB, UT 84056
801/777-7378

Babcock & Wilcox
Gary Clevinger
Tech Mkt. Specialist
3315 Old Forest Road
Lynchburg, VA 24506-0935
804/385-3621

U.S. Air Force
Bennie Cohen
Supv. Mgt. Engr
AFWAL/MLSA
WPAFB, OH 45433
513/255-5108

General Dynamics
Larry Collins
Proj Engr
Box 85357, MZ 94-6010
San Diego, CA 92138-5357
619/542-5718

Naval Weapon Station
Drew Courtright
Materials Engr
GS-9, WOEC, Code 331
Concord, CA 94520
415/671-5394

U.S. Navy
Joseph Crisci

David Taylor Naval Ship R&D Ctr
Annapolis, MD 21402-5067

U.S. Navy/Dept. of Defense
Chester Dacres
Research Chemist
Code R33
Silver Spring, MD 20903-5000
301/596-3507

Georgia Tech Research Institute
John Daher
Research Engineer
347 Ferst Street
Atlanta, GA 30332
404/894-3535

University of Oklahoma
Raymond Daniels
Professor
100 East Boyd
Norman, OK 73019
405/325-5811

Corpus Christi Army Depot
Larry Davis
Sr. Engineer
MS/55
Corpus Christi, TX 78419
512/939-3353

U.S. Air Force
Joseph Demers
Structures Supr
4449 MOBSS
Hanscom AFB, NM 88330
505/479-3143

U.S. Army
Ronald DeSplinter
Aero Engr
AMSAV-MEA, 4300 Goodfellow Blvd
St. Louis, MO 63120
314/263-3261

NASA Langley Research Ctr
Marcia Domack
Materials Engr
MS/188A
Hampton, VA 23665-5225
804/865-3372

Avco Systems Textron
Berj Donabedian
Materials Engineer
201 Lowell St., MS/3203
Wilmington, MASS 01887
617/657-3468

Arinc Research Corp
Patricia Donahue
Engineer, 2 Crystal Park, Ste 101
2121 Crystal Drive
Arlington, VA 22202
703/685-6100

Ocean City Research Corp.
Janes Ellor
Staff Engineer
Tennesse Ave. & Beach Thoughfare
Ocean City, NJ 08226
609/399-2417

U.S. Army
Dario Emeric
Chemist
STRBE-VC
Ft. Belvoir, VA 22060-5606
703/664-1127

Boeing Aerospace
Dewey Erlwein
Prin. Engineer
Box 3999, MS/3H-26
Seattle, WA 98124
206/657-3438

CML R&D Engineering Center
Mr. Joseph Feeney
Aberdeen Proving Ground

Edgewood, MD 21010-5423
301/671-3420/3090

Naval Surface Weapons Ctr
W.A. Ferrando
Research Physicist
10901 New Hampshire Ave, MS/R32
White Oak, MD 20903-5000
202/394-3527

NAESU Detachment
Bob Ferris
Corrosion Specialist
Box 152, NAS Cecil Field
Jacksonville, FL 32215-0152
904/778-6161

PPG Industries
Steven Fisher
Market Manager
10800 S. 13th Street
Milwaukee, WI 53154
414/639-6407

Pratt & Whitney
Robert Fishter
Chemist
MS/706-10
West Palm Beach, FL 33432
305/840-6638

Naval Air Development Center
Arthur Fletcher
Head, Materials Protection Branch
Code 6062
Warminster, PA 18974
215/441-1294

U.S. Air Force
Robert Fredell
Aerospace Engineer
AFWAL/MLSS
WPAFB, OH 45433
513/255-3370

Pennzoil Products Co
John Fu
Manager, Corrosion
P.O. Box 7569
The Woodlands, TX 77387
713/363-8077

Comnavair Dac
Robert Fusco
Corrosion Control Program Mgr
Naval Air Station, N.Island, Code 7412
San Diego, CA 92135-5100
619/437-6155

Raytheon Co
Bernard Gaffney
Materials Engr
Hartwell Rd, MS/CS1-62
Bedford, MA 01730
617/274-2970

Westinghouse Electric Corp
W.Patrick Gallagher
Sr. Matls Eng
P.O. Box 3499, MS/EE-1
Sunnyvale, CA 94088-3499
408/735-3979

Cleveland Pneumatic Co
Amal Ganguli
Director
3781 East 77th Street
Cleveland, OH 44105
216/341-1700 ext 1335

U.S. Air Force
Larry Garrett
Materials Engineer
MMEMM/ALC
Robins AFB, GA 31098
912/926-4489

Naval Air Engineering Center
Gabrielle Gerliczy
Mech. Engineer
Training Div, Code 124
Lakehurst, NY 08733
201/323-2423

Letter Kenny Army Depot
Robert Glick
Chemist
SDSLE-OAR
Chambersburg, PA 17201-5116
717/267-5486

Georgia Tech
Jan Gooch
Scientist
GTRI/EMSL
Atlanta, GA 30332
404/894-3678

Naval Sea Systems Command
Gail Goodman
Engineer
PMS 390EM
Washington, D.C. 20362
202/692-7100

Lehigh University
Richard Granata
Dr.
Sinclair Lab 7
Bethlehem, PA 18015
215/758-3574

Rockwell International
Jack Guttenplan
MTS
3370 Miraloma Ave., MS/031-GA25
Anaheim, CA 92803
714/762-3075

U.S. Navy
Harvey Hack
Metallurgist
DTNSRDC Code 2813
Annapolis, MD 21402
301/267-3502

U.S. Army Materials Tech. Lab
Elizabeth Hall
Engineer
SLCMT-MCM-CSB, Arsenal St
Watertown, MA 02172-0001
617/923-5342

Smithsonian Institute
Karl Heinzel
Museum Specialist
National Air & Space Museum
Washington, D.C. 20560
202/287-3407

SRI International
Sam Hettiarchchi
Sr. Electrochemist
333 Ravenswood Ave, PS187
MenloPark, CA 94025
415/

National Defense Headquarters
2ndLt.B. Hicks
Corrosion Specialist
101 Colonel By Dr. DAS Eng 3-4-2
Ottawa, ONTARIO K1K0P3
613/993-3926

Naval Surface Weapons Center
Scott Hoover
Engr. Tech
10901 New Hampshire Ave, MS/R32
Silver Springs, MD 20903-5000
202/394-2527

IIT Research Institute
MauriceA.H. Howes
Sr. Engineer
10 West 35 Street
Chicago, IL 60616
312/567-4200

Lockheed-Georgia Co
J.T. Huang
Specialist Engineer
86 S. Cobb, MS/Z450
Marietta, GA 30063
404/425-1745

Materials Tech. Lab
Robert Huie
Materials Engineer
SLCMT-MGM-CSB, Arsenal St
Watertown, MA 02172
617/923-5199

U.S. Army
Saul Isserow
Metallurgist
SLCMT-MCZ, Arsenal St
Watertown, MA 02172
617/923-5214

Naval Air Systems Command
David Jamieson
Logistic Manager
AIR 41121E
Washington, D.C. 20361-4112
202/692-1632

NAESU Detachment Cecil Field
Clifton Janney

369 12th Street
Atlantic Beach, FL 32233
904/778-6161

Naval Surface Weapons Center
John Jarus
Research Chemist
10901 New Hampshire Ave, MS/R32
Silver Springs, MD 20903-5000
202/394-2527

Naval Civil Engineering Lab
James Jenkins
P.E.
code 152
Port Huereme, CA 93043
805/982-4797

Naval Research Lab
Robert Jones
Chemistry Div
Code 6179
Washington, D.C. 20375-5000
202/767-2632

La Oue Corrosion Ctr
Robert Kain
Corrosion Scientist
Box 656
Wrightsville Beach, NC 28403
919/256-2271

Office of Naval Technology
James Kelly
Program Manager
800 N. Quincy St., OCNR 225
Arlington, VA 22217-5000
202/696-4791

U.S. Air Force
Richard Kinzie
Materials Engineer
WR-ALC/MMEMC
Robins AFB, GA 31098-5609
912/926-3284

General Dynamics
F.D. Kisor
Lead Engineer
Box 748, MS/2161
Ft. Worth, TX 7610[illegible]
817/777-2151

U.S. Navy
Paul Klein
Materials Engineer
DTNSRDC, Code 2813
Annapolis, MD 21042
301/267-2191

Battelle Columbus Div
Gerhardus Koch
Manager
505 King Avenue
Columbus, OH 43220
614/424-4480

U.S. Air Force
Joseph Kolek,Jr
Asst. Chief Systs Support Div
AFWAL/MLS
WPAFB, OH 45433-6523
513/255-2282

Letter Kenny Army Depot
Alex Krakovitz
Gen. Engineer
SDSLE-OAR
Chambersburg, PA 17201
717/267-5486

Westvaco
Joseph Krasowski
Res. Chemist
Johns Hopin Rd
Laurel, MD 20707
301/792-9100

Garrett Turbine Engine Co
James Laird
Engrg Spec. Sr., MS/93-391 503/4V
111 S. 34th St., Box 5217
Phoenix, AZ 85010
602/231-1613

3M Company
Robert Lamb
Mgr., Tech Serv
4032 Linden Ave. Ste 204
Dayton, OH 45432
513/253-1774

Naval Surface Weapons Ctr
Anh Le
Research Chemist
White Oak Lab
Silver Spring, MD 20903-5000
202/394-1302

U.S. Air Force Museum
Wendell Ledbetter
Museum Spec Rest.
USAFM/MH
WPAFB, OH 45433-6518
513/255-6905

U.S. Army
Milton Levy
Chief, Corrosion Science
Arsenal Street
Watertown, MA 02172-0001
617/923-5331

Swift Laboratories Inc
Charles Levy
Tech Director
P.O. Box 55
Newton, MA 02166
617/965-1254

U.S. Navy
Brenda Little
Research Chemist
Code 333
NSTL, MS 39529-5004
601/688-5494

Rockwell International
Jesse Lumsden
Group Manager
1049 Camino Dus Rios
Thousand Oaks, CA 91360
805/373-4136

COMNAVAIRLANT
Anne Lynch
LCDR
USN
Norfolk, VA 23511
804/444-7940

Martin Marietta
Edmund Lyons
Sr. Matls Engr
P.O. Box 179, L1859
Denver, CO 80201
303/971-6355

U.S. Air Force
Myron Maier
Fabrication Branch Chief
MAEME
Eglin, FL 32542-6004
904/882-8052

University of Souther California
Florian Mansfeld
Professor
Dept. Materials Science VHE 714
Los Angeles, CA 90089-0241
213/743-6424

Naval Ordnance Station
Ted Marshall
Engrg Tech
MSD/25
Louisville, KY 40214
502/364-5642

Air National Guard
Timothy McNamara
Acft. Painter
Hangar #3, MS/129 CAMS/MAFF
NAS Moffett Field, CA 94035-5006
415/966-4837

NAD Norfolk
Walter Mehaffey
Chemist
BLD V-88, 340 NESO
Norfold, VA xxxxx
804/444-8811

University of Pittsburgh
Gerald Meier
Professor
848 Benedum Hall
Pittsburgh, PA 15261
412/624-9741

Naval Ordnance Station
Stephen Meier
Metallurgist
Code 3310A
Indian Head, MD 20640-5000
301/743-4528

U.S. Air Force
Fred Meyer
Corrosion Specialist
AFWAL/MLSA
WPAFB, OH 45433-6533
513/255-5117

Smithsonian Institute
Robert Mikesh
Sr. Curator
National Air & Space Museum
Washington, D.C. 20560
202/357-2515

Lockheed-Georgia Co
Dr.Robert Miller
Staff Scientist
S. Cobb Dr., Dept 72-53, Zone 319
Marietta, GA 30063
404/424-3749

Battelle Columbus Div
Harold Mindlin
Program Manager
505 King Avenue, MCIC
Columbus, OH 43201-2693
614/424-4425

U.S. Air Force
Harvetta Mitchell
NCOIC/TSGT
4449 MOBSS
Holloman AFB, NM 88330
505/434-0738

Naval Ship Research & Development Ctr
Terry Morton
DTNSRDC
Code 2813
Annapolis, MD 21402
301/267-2843

Sermatech International
Mark Mosser
R&D Manager
155 S. Limerick Rd
Limerick, PA 19468
215/948-5100

Naval Avionics Center
Charles Myers
Material Engineer
6000 E 21st Street
Indianapolis, IN 46219-2189
317/353-3260

Naval Research Laboratory
Paul Natishan
Research Metallurgist
Code 6314
Washington, D.C. 20375
202/767-1344

University of New Mexico
Jesse Neal
Research Scienist
Campus Mail Box 25
Albuquerque, NM xxxxx
805/982-4234

Haynes International
Tony Nicholas
Reg. Rep
4650 S. Pinemont
Houston, TX 77041
713/462-2177

U.S. Air Force
John Norskog
Chem Eng.
SM-ALC/MAQCA
Sacramento, CA 95652
916/944-7031

Westinghouse
John Nurminen
Mgr, Metals Joining
1310 Beulah Rd, MS/601-1B26
Pittsburgh, PA 15235
412/256-1781

Naval Air Development Ctr
Richard Paciej
Materials Engr
Code 6062
Warminster, PA 18974-5000
215/441-7179

Babcock & Wilcox
Larry Paul
Research Engineer
1562 Beeson
Alliance, OH 44601
216/493-6906

Materials Science Group
Jeff Perkins
Professor
Naval Postgraduate School, Code 69PS
Monterey, CA 93943
408/646-2216

University of Pittsburgh
F.S. Pettit
Material Science & Engineering
848 Benedum Hall
Pittsburgh, PA 15261
412/624-9720

U.S. Air Force
Tammy Phillips
Materials Engineer
ASD/YYEF
WPAFB, OH 45433-6503
513/255-3315

3M Company
Alphonsus Pocius
Sr. Research Specialist
3M Center, Bldg 209-IW-24
St.Paul, MN 55144-1000
612/736-0287

Naval Ship Research & Development Ctr
Karen Poole
Chemist
Code 2841
Annapolis, MD 21402
301/267-2275

Naval Post Graduate School
Gary Potkay
Lieutenant
Code 34
Monterey, CA 93943
408/646-2033

U.S. Army
Gale Rahmueller
General Engineer
4700 Goodfellow Blvd, AMSTR-MET
St.Louis, MO 63120-1798
314/263-0244

Naval Training Center
Lee Reynolds
Elect. Engr
AMCPM-TND SPA
Orlando, FL 32806
308/646-4505

U.S. Air Force
Torsten Rhode
1Lt
AFWAL/MLSS
WPAFB, OH 45433
513/255-5128

U.S. Air Force
Gerald Rittinger
Museum Spec. Rest.
USAFM/MH
WPAFB, OH 45433-6518
513/255-6905

Naval Sea Systems Command
Stephen Rodgers
Head, Corrosion Control
SEA 05M1
Washington, D.C. 20715
202/692-0216

U.S. Air Force
Martin Rogers
Mat'l & Process Engineer
ASD/AFEF
WPAFB, OH 45433
513/255-5427

Martin Marietta
Nagu Satyan
Group Engineer
P.O. Box 179, L1871
Denver, CO 80201
303/971-6527

U.S. Army
August Savu
Aero. Engineer
4300 Goodfellow Blvd, AMSAV-MEA
St.Louis, MO 63120
314/263-3261

U.S. Army Materials Tech. Lab
James Scanlon
Chemical Engineer
Arsenal St, SLCMT-MCM-CSB
Watertown, MA 02172
617/923-5198

Office of Naval Research
Dr.A.John Sedriks
Scientific Officer
800 N. Quincy St., Code 1131
Arlington, VA 22217
202/696-4325

Boeing Wichita
Edward Seiwert
Engineer
K76-67
Wichita, KS xxxx
316/526-2653

Depot System Command
Jasvant Shah
General Engineer
AMSDS-O-E-T
Lexington, KY 40511-5105
606/293-4243

Arinc Research Corporation
Thomas Shanahan
Principal Engineer
2551 Riva Rd, MS/5-'89
Annapolis, IN 214[illegible]
301/266-4946

U.S. Army Materiel Command
Ira Smart
General Engineer
5001 Eisenhower Ave, AMCQA-EA
Alexandria, VA 22333-0001
202/274-8916

Naval Research Lab
J.A. Smith
Metallurgist
MS/6312
Washington, D.C. 20375
202/767-2784

Naval Aviation Engineering Serv. Unit
James Spinks,Jr
Corrosion Specialist
Marine Corps Air Station
Beaufort, SC 29904-5000
803/846-7141

U.S. Army
Jobe Statum,III
Materials Engineer
SDSAN-DOA-QSMD
Anniston, AL 36201-5030
205/235-4187

Magnesium Elektron Inc
Archie Stevenson
Tech. Mktg. Executive
6260 Howey Drive
Sal Lake City, Utah 84121
801/272-6701

Douglas Aircraft Co
Michael Stewart
Engineer/Technology
3855 Lakewood Blvd, MS/C1-E84(35-80)
Long Beach, CA 90846
213/496-7593

Brookhaven National Laboratory
Toshifumi Sugama

Building 526
Upton,LI, NY 11973
516/282-4029

Integrated Systems Analysts, Inc
Robert Sulit
Corp Tech. Dir.
740 Bay Blvd
Chula Vista, CA 92010-5254
619/422-7100

U.S. Naval Surface Weapons Center
Dr.Raymond Sutula
Branch Head
New Hampshire Ave.,Code R-33,Bl.4-171
Silver Spring, MD 20910
202/394-2472

Naval Weapon Station
Scott Sysum
Materials Engr
GS-9, WQEC Code 331
Concord, CA 94520
415/671-5394

McDonnell Douglas Astronautics Co
Andrew Tayon
Sr. Engineer
Box 516, E456/HQ/3N/MS329
St.Louis, MO 63166
314/232-6456

Arinc Research Corporation
Robert Thompson
Mgr, Materials Tech
2551 Riva Rd, MS/5-189
Annapolis, MD 21401
301/266-4933

Naval Air Development Center
James Thompson
Materials Engr
Code 6062
Warminster, PA 18974-5000
215/441-3503

Corpus Christi Army Depot
Stephen Tosto
Chemist
SDSCC-OLS MS/27
Corpus Christi, TX 78419-6040
512/939-2448

General Dynamics/Convair
Donald Treadway
Engrg Specialist
Box 85357, MZ 43-6334
San Diego, CA 92138
619/547-4933

Cortest Engineering Services
Dr.Gilbert Ugiansky
President
15200 Shady Grove Rd, Ste 350
Rockville, MD 20850
301/670-2819

Naval Surface Weapons Ctr
K.L. Vasanth
Research Chemist
U.S. Navy
WhiteOak, MD 20903-5000
202/394-3549

Naval Underwater Systems Center
Rodney Vieira
Mechanical Engineer
Bldg. 148/2
Newport, RI 02841-5047
401/841-2697

Naval Aviation Engineering Service Unit
Ishmael Villalva
Engineering Tech
Box 152, NAS Cecil Field
Jacksonville, FL 32215-0152
904/778-6161

AVCO Aerostructures
Thomas Warrion
Metallurgist
P.O. Box 210, Dept 540
Nashville, TN 37202
615/361-2989

U.S. Army Materials Tech Lab
Joe Wells
PM/CTX
SLCMT-MCZ, Arsenal St
Watertown, MA 02172-0001
617/923-5211

McDonnell Aircraft Company
Robert Williams
Engineer
Box 516, 357/33N/MS100
St.Louis, MO 63166
314/233-8674

Benet Weapons Laboratory
Donald Winegar
Mech. Engineer
Watervliet Arsenal, Bldg 40
Watervliet, NY 12289-4050
518/266-5739

Allison Gas Turbines
Sam Winters
Supervisor
Box 420, MS/T27
Indianapolis, IN 46206-0420
317/242-5117

National Research Council
Stanley Wolf
Sr. Staff Officer
2101 Constitution Ave, NW, MS/JH-406
Washington, D.C. 20418
202/334-3489

Army Materials Technology Lab
Dr.Chester Zabielski
Metallurgist
SLCMT-MCM-SB, Arsenal Street
Watertown, MA 02172-0001
617/923-5332

Battelle Columbus
Edward Zamejc
Chem. Engineer
505 King Ave, RM15-1-597
Columbus, OH 43221
614/424-4967

Belvoir Res. Dev. Eng. Ctr
Bill Zanedis
Chemist
Materials Fuels Lubs Lab
FortBelvoir, VA 22060
703/664-5374

U. S. Air Force
Gen. Gullis
AFLC
WPAFB, OH 45433

U.S. Air Force
Capt. O'Malley
AFLC
WPAFB, OH 45433

LATE PAPERS

RECEIVED AFTER

DEADLINE

THE AIR FORCE CORROSION PROGRAM - 1987

Melvin E. Bishop
Warner Robins Air Logistics Center
Robins Air Force Base, Georgia

(Viewgraph 1) Good morning. I'm Gene Bishop, the Acting Air Force Corrosion Program Manager and I'll brief the current status of Plastic Media Blasting (PMB) and its potential as an alternate method for stripping paint from aircraft.

(Viewgraph 2) Plastic Media Blasting is a method of aircraft paint stripping which can best be described as similar to sandblasting in that compressed air is used to project an abrasive, namely a thermoset plastic.

In reviewing the background of the inception of Plastic Media Blasting as an alternative to chemical stripping, one finds that there were two major reasons to search for an alternative to chemical strippers.

The first was the decreasing ability of chemical strippers to effectively remove the high technology coating systems that are applied to USAF weapon systems.

The second was the high cost of treating the voluminous liquid hazardous waste that resulted from stripping operations.

In considering Plastic Media Blasting as an alternative, evaluators found that PMB would resolve these first two problems and in addition could reduce manhours and materials costs and improve the working environment of paint stripping personnel.

(Viewgraph 3) OO-ALC in Utah was the first Air Force organization to consider Plastic Media Blasting. Initial tests at Hill AFB indicated that the process would acceptably strip aircraft having current generation coating systems. These tests also showed that the process could potentially save five (5) million dollars a year in costs associated with F-4 paint stripping operations at Hill AFB.

A test program was then initiated at AFWAL materials laboratory to determine the effects of PMB on aerospace materials of construction. This limited test program provided information that led to the approval of Plastic Media Blasting of F-4 aircraft in May of 1985. This initial approval allows each aircraft to be stripped up to four (4) times. Approval for use of Plastic Media Blasting of ground support equipment was also given at this time.

(Viewgraph 4) The Air Force Corrosion Program Manager was then tasked to investigate several mechanical aspects of Plastic Media Blasting on a variety of aircraft materials. The Battelle-Columbus Plastic Media Blasting Material Characterization Study was initiated in September 1985 and completed in July 1986. The major areas of investigation in this study were as follows:

1. Determination of changes in fatigue life properties or fatigue crack initiation characteristics in aircraft materials as a result of Plastic Media Blasting.

2. Determination, of as a result of PMB, any changes in fatigue life properties or fatigue crack initiation characteristics in aircraft materials with fasteners installed.

3. Determination of the effect of Plastic Media Blasting on the fatigue crack growth rates of aircraft materials.

4. Determination of whether the Almen Strip Test can provide reliable process control and/or research data. This test routinely provides information on the amount of residual stress that peening processes impart to metals.

5. Determination of the effect of Plastic Media Blasting on fluorescent dye-penetrant inspection techniques.

(Viewgraph 5) The Battelle-Columbus study produced two significant results. First, there was up to a 90% decrease in fatigue life for edge and center panel crack initiations. Higher density particles, such as sand inadvertently mixed with the plastic media, are the apparent cause of this decrease in fatigue life. The sand is apparently picked up from the aircraft and the blasting facility floor. Second, there was a significant increase in fatigue crack growth rates. This increase is the result of the residual stresses imparted to the metal surface as the result of Plastic Media Blasting. The mechanical effects of Plastic Media Blasting were most noticeable on thin skin test panels.

(Viewgraph 6) In order to resolve these major problems, the Air Force Corrosion Program Office contracted for a follow-on study. The follow-on study was begun on 25 Sep 86 and has a requested completion date of 30 Jun 87. Specifically, the new contract requires the contractor to:

First, confirm high density particles as the cause of fatigue life loss by blasting test specimen with clean virgin media.

Second, perform a parametric analysis using Almen strips to determine the least damaging set of parameters. Almen strips will measure damage by providing a relative index of the amount of residual stress applied to the material by the blasting process.

Third, if high density particles are causing the fatigue life loss, the contractor is to do a preliminary investigation of available separation technology and make general recommendations on the type of recovery system that might be desirable.

(Viewgraph 7) The Battelle-Columbus follow-on effort is on schedule and under budget. Battelle-Columbus laboratories has indicated that the requested 30 Jun 87 completion date will be met. The technical results from this study will be briefed to the Air Force Executive Steering Group For Nondestructive Inspection, Composites, and Corrosion in June 1987.

(Viewgraph 8) Using the results from this study, the Air Force Corrosion Program Manager will be able to make recommendations on the safest and least damaging parameters, procedures, and equipment to be used in plastic media paint stripping operations. However, we recognize that with time, the optimum parameters may change as new equipment and testing reveal even better operating procedures.

Headquarters Air Force Logistics Command MM and MA may then make a general authorization for use of the PMB process on aircraft based on the results of this test program. Individual System Program Managers will be required to make

specific authorizations for the use of Plastic Media Blasting on their respective weapon systems.

AF CORROSION PROGRAM

WR-ALC MATERIEL MANAGEMENT
WE MAKE IT HAPPEN WITH PRIDE
CENTER OF EXCELLENCE

WARNER ROBINS ALC

STATUS OF PLASTIC MEDIA BLASTING

BRIEFER: MR. GENE BISHOP

AF PLASTIC BEAD BLASTING EVALUATION PROGRAM

WARNER ROBINS ALC

WR-ALC MATERIEL MANAGEMENT CENTER OF EXCELLENCE
WE MAKE IT HAPPEN WITH PRIDE

BACKGROUND

- O PLASTIC BEAD BLASTING SIMILAR TO SAND BLASTING
- O CHEMICAL VS PBB
  - OO INEFFECTIVENESS OF CHEMICAL STRIPPERS
  - OO HAZARDOUS WASTE GENERATION
  - OO REDUCTION OF MANHOURS
  - OO LOWER MATERIAL COST
  - OO PERSONNEL SAFETY

AF PLASTIC BEAD BLASTING EVALUATION PROGRAM

- O INITIAL TESTS
  - OO PROCESS ACCEPTABLE/ECONOMICAL
- O F-4 AIRCRAFT STRIPPING
  - OO AFWAL TEST PROGRAM
  - OO F-4 PBB APPROVED - MAY 85

AF PLASTIC BEAD BLASTING EVALUATION PROGRAM

- O PLASTIC BEAD BLASTING MATERIAL CHARACTERIZATION STUDY
  - OO BATTELLE-COLUMBUS
  - OO SEPT 85 - JULY 86
- O MAJOR CONCERNS
  - OO FATIGUE LIFE
  - OO FATIGUE CRACK GROWTH RATES
  - OO ALMEN STRIP
  - OO FLUORESCENT DYE PENETRANT

AF PLASTIC BEAD BLASTING EVALUATION PROGRAM

WARNER ROBINS ALC

WR-ALC MATERIEL MANAGEMENT CENTER OF EXCELLENCE
WE MAKE IT HAPPEN WITH PRIDE

RESULTS

- O SIGNIFICANT LOSS IN FATIGUE LIFE
  - OO EDGE AND CENTER INITIATION
  - OO MECHANISM - HIGH DENSITY PARTICLES
- O SIGNIFICANT INCREASE IN FATIGUE CRACK GROWTH RATES
  - OO RESIDUAL STRESS

AF PLASTIC BEAD BLASTING EVALUATION PROGRAM

WARNER ROBINS ALC

WR-ALC MATERIEL MANAGEMENT CENTER OF EXCELLENCE — WE MAKE IT HAPPEN WITH PRIDE

- O FOLLOW-ON CONTRACT STUDY
  - OO 25 SEPT 86 - 30 JUNE 87
  - OO RESOLVE FATIGUE LIFE PROBLEM
  - OO PARAMETRIC ANALYSIS
  - OO EQUIPMENT RECOMMENDATIONS

AF PLASTIC BEAD BLASTING EVALUATION PROGRAM

WARNER ROBINS ALC

WR-ALC MATERIEL MANAGEMENT
WE MAKE IT HAPPEN WITH PRIDE
CENTER OF EXCELLENCE

STATUS

- O ON SCHEDULE
- O WITHIN BUDGET
- O RESULTS WILL BE BRIEFED JUNE 1987

SUMMARY

O HQ AFLC/MM/MA MUST PROVIDE GENERAL AUTHORIZATION

OO SPMs MUST MAKE FINAL DECISION

NAME: Melvin Eugene Bishop

PRESENT AFFILIATION: USAF, Warner Robins Air Logistics Center, Directorate of Materiel Management, Systems Engineering Division, USAF Corrosion and Materials Engineering Branch.

TITLE: Acting Chief, USAF Corrosion and Materials Engineering Branch
Chief, AF/AFLC Corrosion Programs Management Section

FIELD OF INTEREST/RESPONSIBILITIES: Prevention/ Control of Material Degradation in Aerospace Equipment.

PREVIOUS AFFILIATIONS/TITLES: Lead USAF CORROSION PROGRAM Materials Engineer for the C-5A, F-15, C-5B, ALCM, GLCM, KC-10, AND C-17.

ACADEMIC BACKGROUND: Bachelor of Chemical Engineering (1963)
Georgia Institute of Technology

SOCIETY ACTIVITIES/OFFICES/AWARDS: Member of SAE

PUBLICATIONS/PAPERS: 1985 SURVEY OF SAC CORROSION PROGRAM, Proceedings of the 1985 TRI-SERVICE CONFERENCE ON CORROSION

Validation of Nitronic 33

Stainless Steel

in

Reinforced and Prestressed Concrete

by

James F. Jenkins, PE.

Naval Civil Engineering Laboratory
Port Hueneme, California, 93043

CONTENTS

	Page
INTRODUCTION	2
PREPARATION OF TEST SPECIMENS	2
PERFORMANCE OF TESTS AND TEST RESULTS	4
Electrochemical Behavior in Mortar Extracts	4
Test Results	4
Ion Tolerance Tests	6
Test Results	6
Depassivation at Closed Cracks	6
Test Results	6
Depassivation at Open Cracks	7
Test Results	7
Repassivation at Closed Cracks	7
Test Results	7
Valuation of Prestressed Pile Specimen	8
Test Results	8
Evaluation of In-Place Specimen	8
Test Results	9
ADDITIONAL EVALUATIONS	9
REVIEW OF TEST RESULTS	10
CONCLUSIONS	11
RECOMMENDATIONS	11

INTRODUCTION

In order to reduce the magnetic signature of steel ships, periodic demagnetizing is required. This is accomplished at a shore based "deperming" pier where controlled electric currents are passed through coils surrounding the ship to neutralize the ships residual magnetic field. In order to be effective, these facilities must be constructed from nonmagnetic materials. Wood has been the traditional material for construction of these facilities. Several factors, such as the increased activity of wood destroying organisms at many Naval Activities, the increased cost of wood pilings and timbers, the requirement for longer pilings due to increased ship drafts, and improvement in the design and fabrication of prestressed concrete structures led to the consideration of prestressed concrete as a replacement for wood in such structures. However, traditional prestressed concrete uses magnetic carbon steel prestressing strand. In order for prestressed concrete to be used in the construction of deperming piers, a nonmagnetic prestressing material must be used.

Previous evaluations determined that Nitronic 33 stainless steel had appropriate mechanical, physical, and magnetic properties for use as prestressing strand. However, the long term corrosion behavior of the material in prestressed concrete was not determined. This validation was directed toward the determination of the corrosion behavior of this material in prestressed concrete.

While actual long term in situ testing of any material for a new application is highly desirable, this test program was based upon tests which can be completed in a relatively short period as construction of new deperming piers was urgently required. The tests were developed to determine the relative susceptibility of carbon steel and Nitronic 33 stainless steel to loss of passivity under various conditions which are likely to occur in an actual marine structure, and to separately assess the amounts and types of attack which are likely to occur on both carbon steel and Nitronic 33 stainless steel when, or if, active corrosion has been initiated. As both carbon steel and Nitronic 33 stainless steel were expected to behave as passive materials in concrete, the side by side comparison of the two was considered to be valid.

PREPARATION OF TEST SPECIMENS

All test specimens were cast from the same batch of concrete, representative of that to be used in construction, to reduce the effects of variation of concrete on the corrosion behavior of the embedded metal specimens. The mix design was as follows:

Cement - Type II	8.4 bags/yd
Water (W/C ratio = 0.40)	37.9 gallons/yd
Sand (San Gabriel)	1113.0 lb/yd
Coarse aggregate (San Gabriel) 3/8 inch maximum	1526.4 lb/yd
Admixture (Sika Mix 126)	200.5 fl oz/yd

Slump before admixture = 4 inches
Slump after admixture = 0 inches

The Nitronic 33 material was furnished by ARMCO Steel Corporation. All specimens were cut from the same coil of material. The wire diameter was 0.1875 inch. The chemical composition of the material, as determined by ARMCO, was as follows:

Composition of Nitronic 33 Test Wire

Element	Percent
Chromium	17.69
Manganese	12.23
Nickel	3.48
Silicon	0.50
Nitrogen	0.30
Molybdenum	0.10
Carbon	0.039
Phosphorous	0.028
Sulphur	0.002

The mechanical properties of the Nitronic 33 stainless steel wire, as determined by ARMCO, were as follows:

Ultimate Tensile Strength	136,000 psi
Yield Strength	116,000 psi
Elongation	33.3%
Reduction of Area	70.3%
Hardness	26 R_c

The stainless steel test material met the composition and strength requirements of ASTM Specification A580, Grade XM-29.

The carbon steel wire specimens were center strands from prestressing wire meeting ASTM Specification A416 (the standard specification for prestressing strand).

Both the stainless steel and carbon steel wire specimens were cast into 4- by 4- by 24-inch concrete prisms. After casting all of the specimens were placed in a steam cabinet and steam cured for 16 hours.

The 4- by 4- by 24-inch test prisms that were to be cracked were prepared by sawing a 1/2-inch deep, 3/16-inch wide "crack starter" notch in the upper "free" face of the specimen and then loading the specimen at three points as shown in Figure 1.

Eight test specimens were cut by sawing from two sections of piling furnished by ABAM Consulting Engineers, Seattle, Washington. These sections were fabricated by Concrete Technology Inc., Tacoma, Washington, and were used for previous mechanical testing of the Nitronic 33 prestressed pilings.

PERFORMANCE OF TESTS AND TEST RESULTS

Electrochemical Behavior in Mortar Extracts

Purpose of Test. To determine the chemical conditions, representative of those in marine concrete structures, which result in passivity of both carbon steel and Nitronic 33 stainless steel and to evaluate the relative stability of the passive films where they are present.

Test Procedure. Potentiostatic polarization per ASTM G61.

Test Conditions.

(pH (by dilution)

	12.1	11.6	11.2	10.0
0				
40				
400				
4000				

Extract from cured concrete was used to prepare all solutions. Chloride was from seawater.

Test Results

The electrochemical tests showed that the tolerance of Nitronic 33 stainless steel to both an increase in chloride ion and a decrease of pH was substantially greater than the tolerance of carbon steel. The electrochemical behavior for both the specimens with crevices and those without crevices was essentially identical for both the carbon steel and

Nitronic 33 stainless steel. Typical passive behavior for both the carbon steel and Nitronic 33 stainless steel as exhibited at pH 12.2 and 0 chloride is shown in Figures 2 and 3.

As the pH was lowered and/or the chloride level increased, a point was reached where the passivity of each alloy was reduced, and in the case of the carbon steel, the alloy exhibited essentially nonpassive behavior. As shown in Figures 4 and 5, the passivity of the carbon steel was reduced considerably at pH 11.6 and 200 ppm chloride, and nonpassive behavior was exhibited at pH 10.0 and 200 ppm chloride. As shown in Figure 6, the level of passivity of Nitronic 33 stainless steel retained at a pH of 10.0 and 6,000 ppm chloride was substantial.

Tables 1 and 2 summarize the results of the electrochemical tests. Fully passive behavior is indicated in the tables by a P. Marginal passivity is indicated by a M where passivity breaks down near the highest potential used in the tests. Lower levels of passivity are indicated by rupture potentials at increasingly negative potentials. Nonpassive behavior is indicated by an N.

Table 1. Electrochemical Behavior of Carbon Steel

pH (by dilution)

	12.1	11.6	11.2	10.0
0	P	P	P	P
20	P	M	+100 MV	0 MV
200	P	+100 MV	-100 MV	-200 MV
2,000	0 MV	-100 MV	-400 MV	N
6,000	-200 MV	N	N	N

Table 2. Electrochemical Behavior of Nitronic 33 Stainless Steel

pH (by dilution)

	12.1	11.6	11.2	10.0
0	P	P	P	P
20	P	P	P	P
200	P	P	P	P
2,000	P	P	P	P
6,000	P	P	M	+100 MV

Ion Tolerance Tests

Purpose of Test. To determine the relative tolerance of carbon steel and Nitronic 33 embedded in concrete to increased ionic content resulting from forced migration of seawater through the concrete.

Test Procedure. The apparatus used to determine the resistance of specimens embedded in concrete to accelerated ion migration is shown in Figure 7.

The voltage impressed across the test cell to drive the ions by electrophoresis was adjusted to give a voltage gradient of 1 volt per inch across the test specimen. Each test specimen contained one probe of Nitronic 33 stainless steel and one probe of carbon steel in order to eliminate any effects of concrete variability.

Test Results

The tolerance of Nitronic 33 stainless steel to ion migration was substantially greater than that of carbon steel. Figure 8 shows a typical potential versus time curve for an ion migration test run. After approximately 200 hours with voltage applied across the cell the carbon steel became active as indicated by an decrease in potential. The Nitronic 33 stainless steel remained passive for 1,000 hours.

After 1600 hours of testing with the potential applied, the tests were terminated and the probes were removed from the concrete blocks by crushing the blocks. As shown in Figure 9, the carbon steel showed considerable attack whereas the Nitronic 33 stainless steel showed no attack.

Depassivation at Closed Cracks

Purpose of Test. To determine the relative susceptibility of carbon steel and Nitronic 33 embedded in concrete to depassivation in the presence of a crack in the concrete that has opened and reclosed.

Test Procedure. Concrete prisms with both carbon steel and Nitronic 33 stainless steel strand cracked with crack widths of 1/64 inch, 1/32 inch, 1/16 inch, and 1/8 inch were used. The cracked specimens were exposed to seawater and then the cracks were allowed to reclose. Electrical potential measurements were used to monitor the behavior of the strand during exposure. This behavior was confirmed by visual inspection of the strands after exposure.

Test Results

Neither the carbon steel or the Nitronic 33 stainless steel depassivated at closed cracks during the duration of this test. The corrosion potential versus time for the carbon steel is shown in Figure 10 and the corrosion potential for the Nitronic 33 stainless steel versus time is shown in Figure 11.

The test bars in these specimens were removed from the test blocks after 1200 hours of exposure in the depassivation at closed crack tests. Visual inspection showed that neither the carbon steel nor the Nitronic 33 stainless steel specimens suffered any attack.

Depassivation at Open Cracks

Purpose of Test. To determine the relative susceptibility of carbon steel and Nitronic 33 embedded in concrete to depassivation in the presence of open cracks in the concrete cover of various widths.

Test Procedure. The test setup for determination of depassivation at open cracks is shown in Figure 12. Crack widths of 1/64 inch, 1/32 inch, 1/16 inch, and 1/8 inch were used.

Test Results

None of the Nitronic 33 stainless steel specimens showed depassivation during the duration of these tests. The carbon steel bars with 1-inch cover showed depassivation upon immersion for the 1/8-inch wide crack, 50 hours for the 1/16-inch crack, 150 hours for the 1/32-inch crack, and 180 hours for the 1/64-inch crack. The carbon steel bars with 2-1/4-inch cover show depassivation immediately upon immersion for the 1/8-inch wide crack but showed continued passive behavior for the 1/16-inch and tighter cracks. Figures 13 and 14 show the potential of the inner (2-1/4-inch cover) and outer (1-inch cover) bars versus time.

The test bars in these specimens were removed from test blocks to determine their surface condition. As shown in Figures 15 and 16, the Nitronic 33 stainless steel specimens were unattacked, whereas the carbon steel specimens showed considerable attack.

Repassivation at Closed Cracks

Purpose of Test. To determine the relative ability of carbon steel and Nitronic 33 embedded in concrete to repassivate in the presence of a closed crack if corrosion has initiated when the crack was open.

Test Procedure. The test setup for this series is identical to that shown for depassivation at open cracks (Figure 17). After potential readings indicate that corrosion has initiated, the cracks are allowed to close.

Test Results

Since the Nitronic 33 stainless steel did not depassivate at open cracks over the duration of the test, it was not possible to make a comparison between the carbon steel and Nitronic 33 stainless steel for the ability to repassivate. The carbon steel repassivated within 35 hours of closing of the crack as shown in Figure 18.

Valuation of Prestressed Pile Specimen

Purpose of Test. To determine the susceptibility of Nitronic 33 and carbon steel strand embedded in concrete to depassivation using specimens cut from a prestressed test piling section with cracks in the concrete cover.

Test Procedure. The piling sections were sawed into test specimens. The specimens were cracked with crack widths of 1/8 inch and 1/16 inch and immersed in seawater. The test setup for the determination of the susceptibility of carbon steel and Nitronic 33 stainless steel strand in specimens cut from test pilings is shown in Figure 19. The faces and ends of the test sections were sealed with paraffin prior to filling the reservoir with seawater.

Test Results

The corrosion potentials versus time for the carbon steel and Nitronic 33 stainless steel piling sections showed erratic behavior. This was attributed to the more complex geometry of the specimens, the presence of the spiral reinforcement which was exposed (but coated with paraffin), and the variation of cover over the strands. The potentials indicated that there may be limited corrosion activity in both the carbon steel and Nitronic 33 stainless steel prestressed specimens.

Upon completion of the potential measurements, the strand and spiral reinforcement was removed from the test specimens. As shown in Figure 20, the carbon steel strand and spiral showed considerable surface attack in the vicinity of the cracks.

The Nitronic 32 stainless steel spiral reinforcement in the piling specimens showed several areas of incipient attack. The Nitronic 33 stainless steel strand in the specimens was unattacked. The condition of the strand and spiral reinforcement is shown in Figure 21.

Evaluation of In-Place Pilings

Purpose of Test. To determine the short term (17 month) performance of prestressed pilings fabricated using both carbon steel and Nitronic 33 stainless steel exposed in a marine structure.

Test Procedure. This test was performed on two experimental pilings fabricated using Nitronic 33 stainless steel prestressing and previously installed during construction of a pier in Tacoma, Washington. Pilings prestressed using carbon steel, which were used in the remainder of the pier, were used for comparison purposes. The test pilings were evaluated using a developmental diver-held, surface-supported probe which measured the flow of current into or from the surface of the test pilings. The technique is described in Naval Civil Engineering Laboratory (NCEL) TM 52-85-01.

Test Results

No significant corrosion activity was detected in either the Nitronic 33 stainless steel or carbon steel prestressed pilings. The readings obtained on both types of pilings were similar. Small locations on the Nitronic 33 stainless steel prestressed piling where limited corrosion activity was located were correlated with carbon steel "pre-ties" used in the manufacture of the test piling. The activity associated with these "pre-ties" is evident on the potential map of one of the Nitronic 33 prestressed piles as shown in Figure 22. Examination of the piling sections obtained by NCEL for sectioning revealed that there were carbon steel tie wires in the Nitronic 33 pilings at a location and spacing equivalent to the spacing of the "hot spots" located during the inspection.

ADDITIONAL EVALUATIONS

In addition to the tests outlined previously, additional evaluations were performed. These evaluations included:

1. An evaluation of the relative amounts of corrosion product formed in the corrosion of carbon steel and Nitronic 33 stainless steel when they corrode in concrete.

2. An evaluation of the rates of propagation of corrosion of both Nitronic 33 stainless steel and Carbon Steel in concrete after the initiation of corrosion.

3. An evaluation of the effect of ion diffusion in the presence of closed cracks on the initiation of corrosion of carbon steel and Nitronic 33 stainless steel in concrete.

4. An evaluation of the effects of the types and amounts of corrosion anticipated on the structural integrity of prestressed concrete using both carbon steel and Nitronic 33 stainless steel.

5. An evaluation of the possible effects of induced electric currents on the corrosion of prestressed concrete deperming facilities.

REVIEW OF TEST RESULTS

Test Series	Results
Electrochemical Behavior	Nitronic 33 more resistant to lower pH and increased chloride.
Ion Tolerance	Nitronic 33 more resistant to ion migration.
Depassivation at Closed Cracks	Neither alloy became active.
Depassivation at Open Cracks	Carbon steel depassivated, Nitronic 33 did not depassivate.
Repassivation at Open Cracks	Carbon steel repassivated, Nitronic 33 did not depassivate.
Prestressed Piling Specimens	Potentials show carbon steel more active. Surface condition evaluation after exposure showed attack on carbon steel and no attack on Nitrnoic 33.
In Situ Piling Evaluation	No significant difference between pilings. Carbon steel in Nitronic 33 piling had become active, otherwise, no significant activity in either piling.
Propagation Rates	Carbon steel became active, uniform corrosion. Nitronic 33 remained passive.
Ion Tolerance at Closed Cracks	Nitronic 33 more resistant.
Corrosion Product Volume	Nitronic 33 did not depassivate. No comparison possible.
Structural Integrity	The structural impact of distributed localized attack of the type anticipated for the Nitronic 33 prestressed piling, should it occur, would be less serious than the more general attack which would be likely to occur on carbon steel prestressed structures of similar design.

Test Series	Results
Induced Electrical Currents	The worst case currents will be less than 1 ampere. This level is substantially below that required to cause significant corrosion activity, and can be reduced substantially by increasing the resistance of the current path by not allowing the prestressing strand to protrude from the bottom of the pilings.
Structural Integrity	The type of attack expected on the Nitronic 33, should it occur, would have less impact than that of the typical corrosion of carbon steel.
Induced Currents	The effect of induced electrical currents will be insignificant and may be easily reduced further.

CONCLUSIONS

Based upon the results of all of the tests performed in this validation, it is concluded that the resistance of Nitronic 33 stainless steel to corrosion in environments representative of those found in a prestressed or reinforced structure is superior to the corrosion resistance of the carbon steel that has been shown to give satisfactory performance in marine structures.

RECOMMENDATIONS

1. The design drawings should be carefully reviewed to insure that adequate cover is provided over all of the Nitronic 33 stainless steel.

3. Construction and construction inspection criteria should be developed for the facilities constructed using Nitronic 33 stainless steel.

4. In service inspection methods and criteria should be developed for facilities constructed using Nitronic 33 stainless steel.

5. Maintenance and repair methods and criteria should be developed for facilities constructed using Nitronic 33 stainless steel.

6. Selected test exposures of Nitronic 33 should be continued to support the recommended methods and criteria efforts and to obtain long term performance data on Nitronic 33 stainless steel.

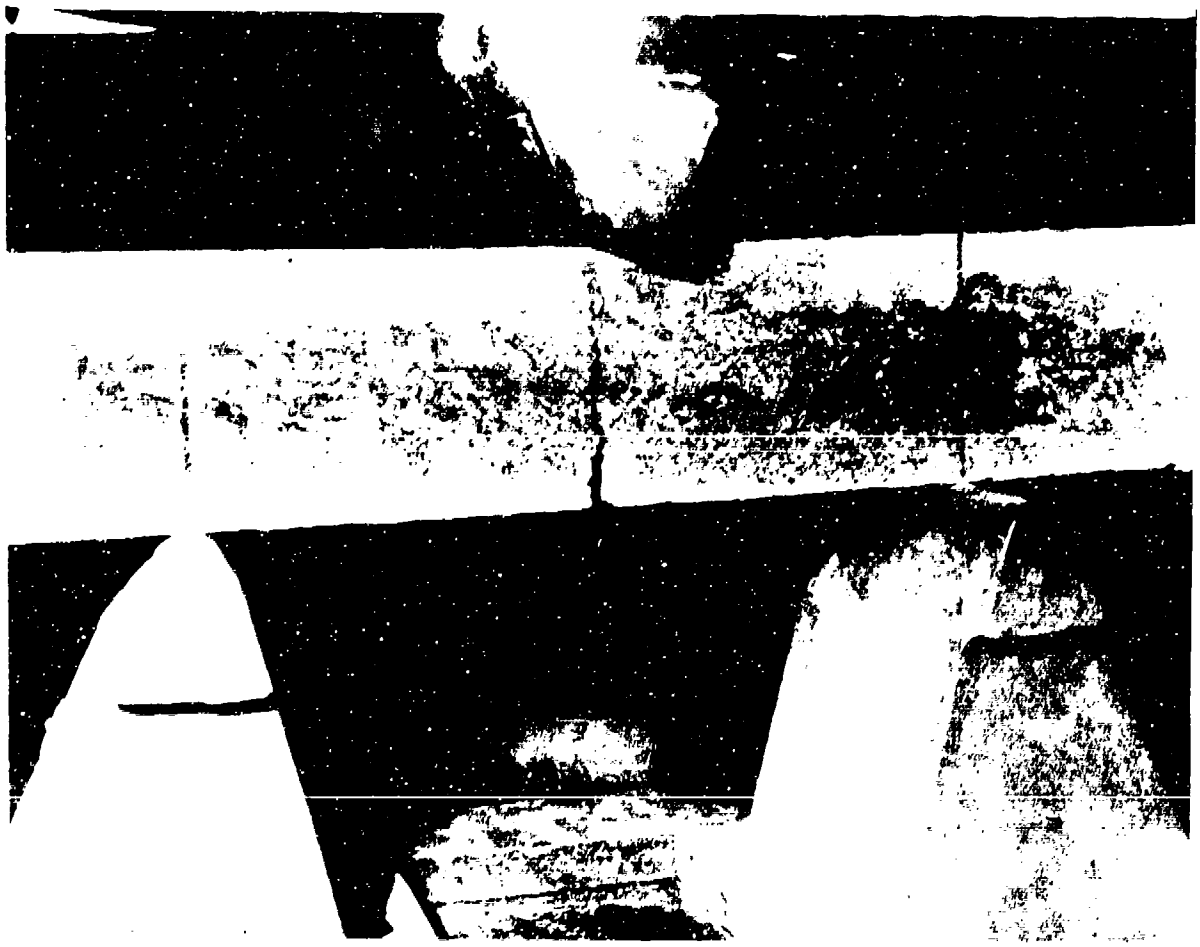

Figure 1. Cracking of 4- by 4- by 24-inch prisms.

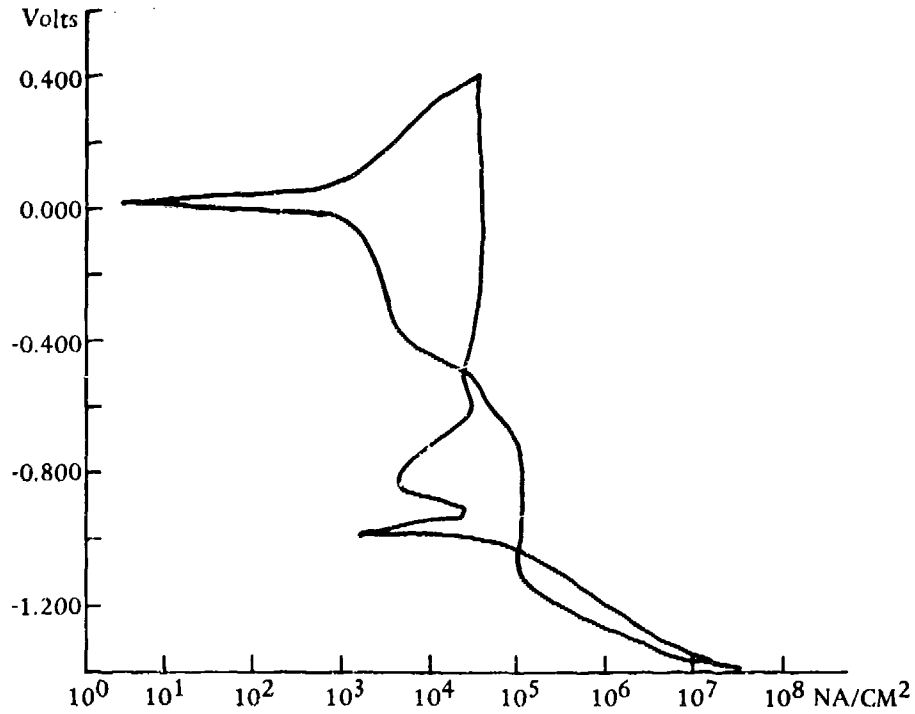

Figure 2. Polarization behavior of Nitronic 33 stainless steel - pH = 12.1, Cl^-=0.

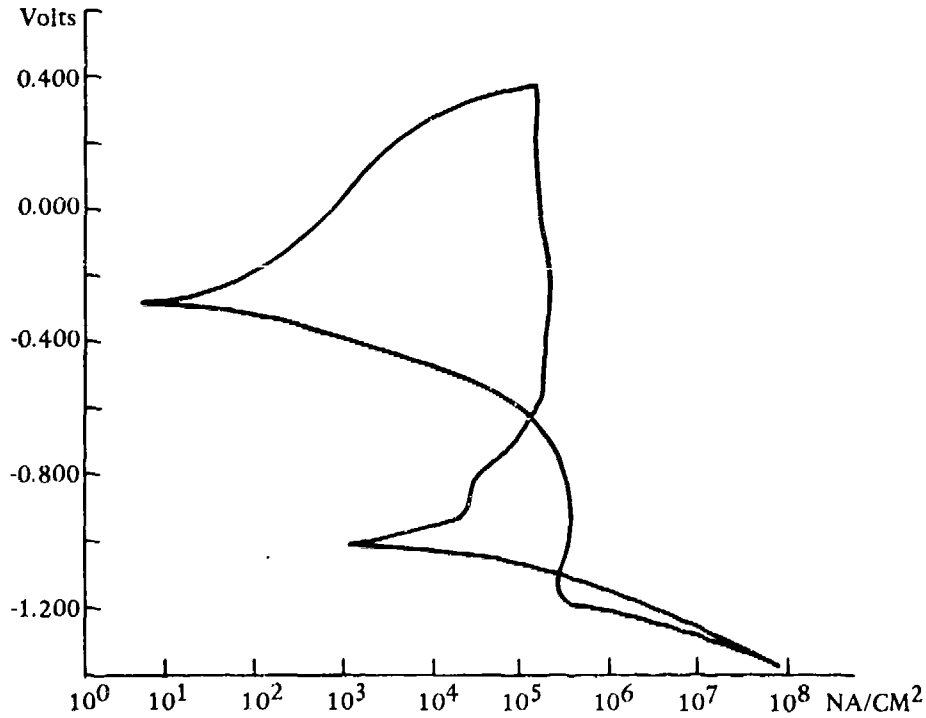

Figure 3. Polarization behavior of carbon steel - pH = 12.1, Cl^-=0.

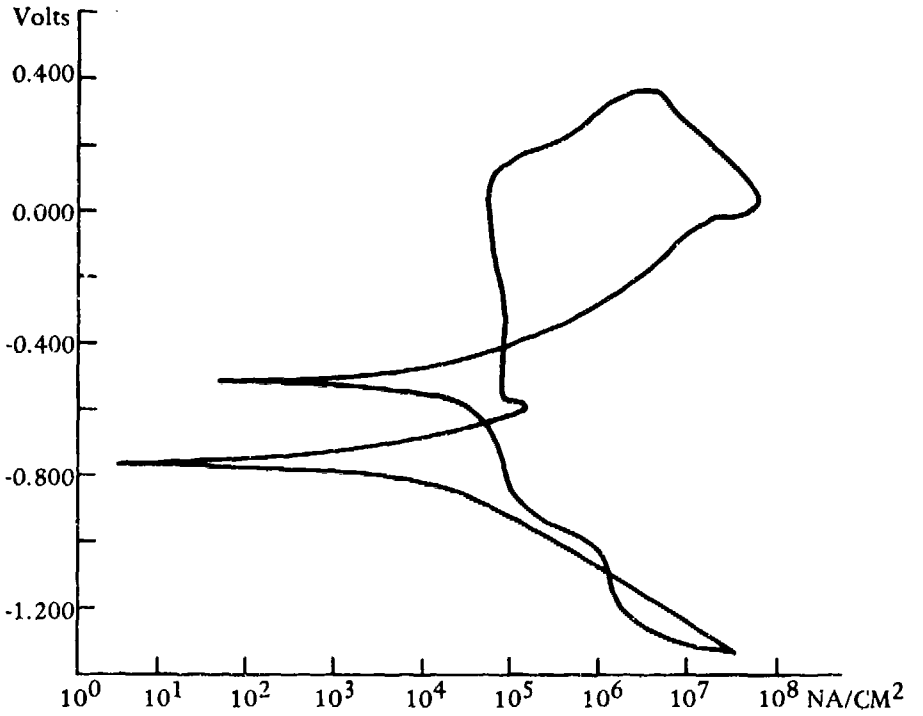

Figure 4. Carbon steel - pH=11.6, Cl^-=200 ppm.

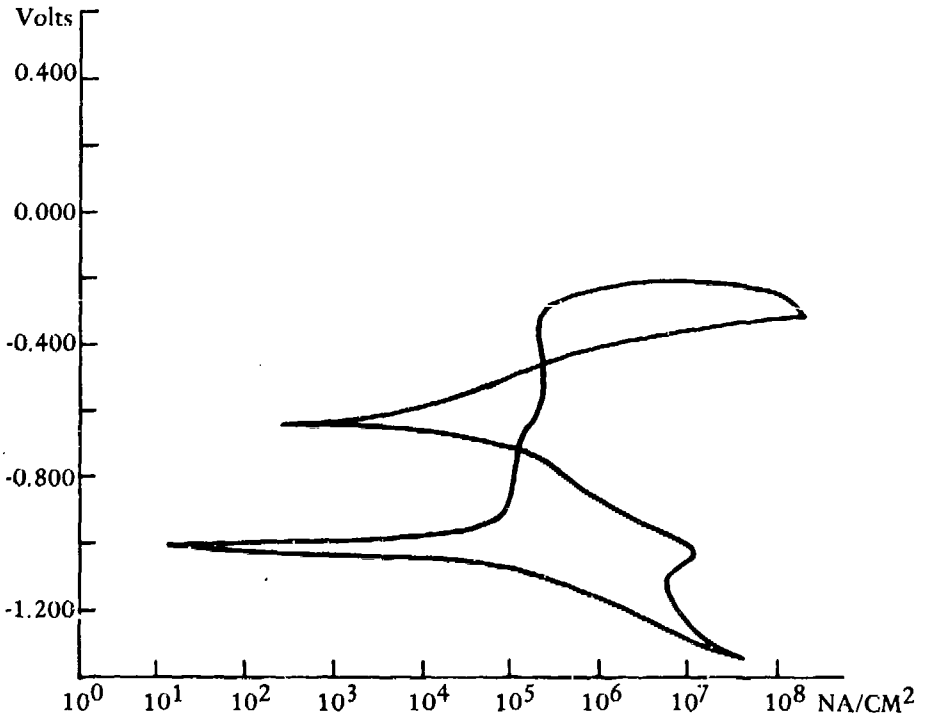

Figure 5. Carbon steel - pH=10.0, Cl^-=200 ppm.

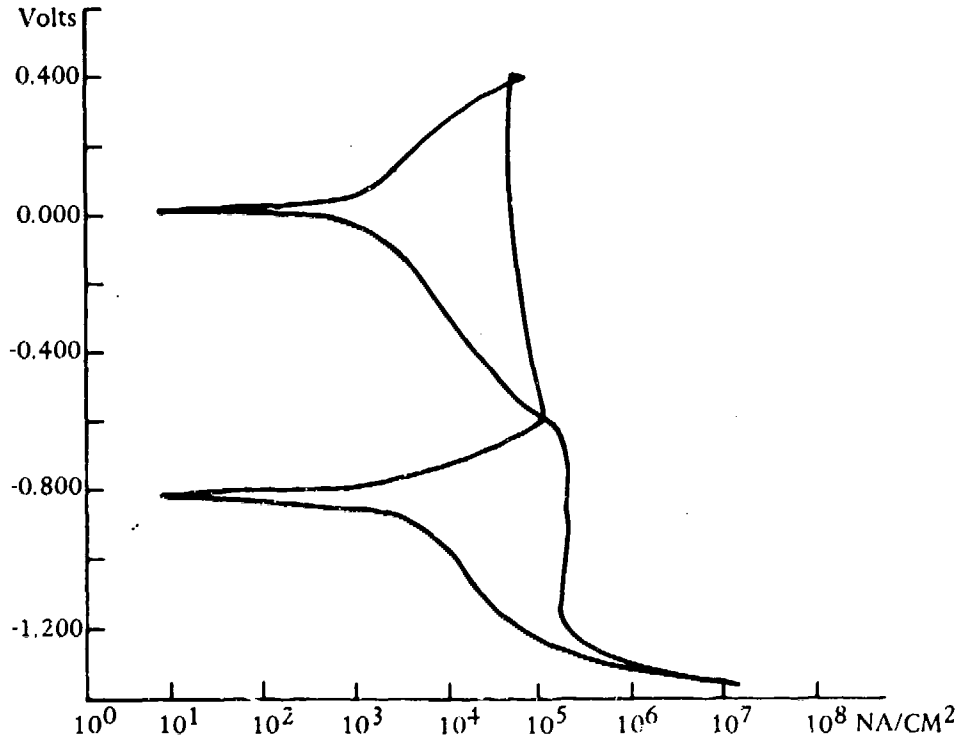

Figure 6. Nitronic 33 stainless steel - pH=10.0, Cl^-=6,000 ppm.

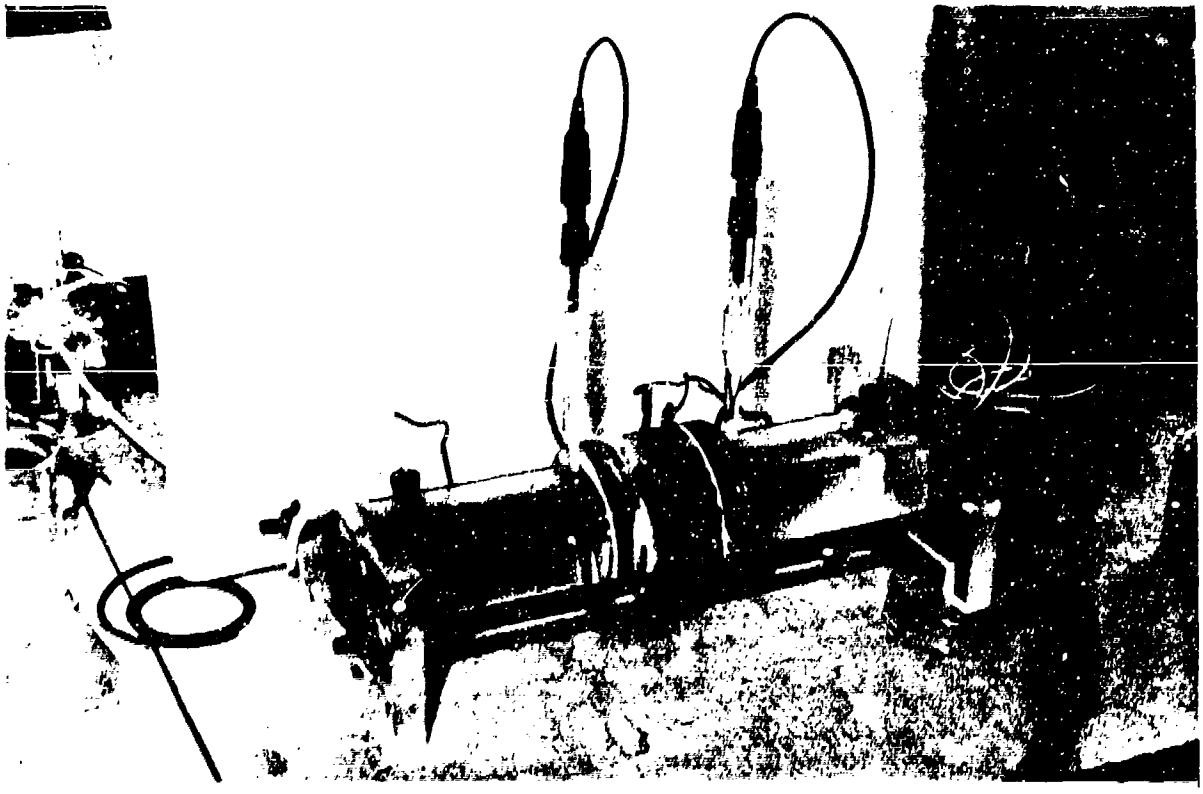

Figure 7. Apparatus for determining resistance to ion migration.

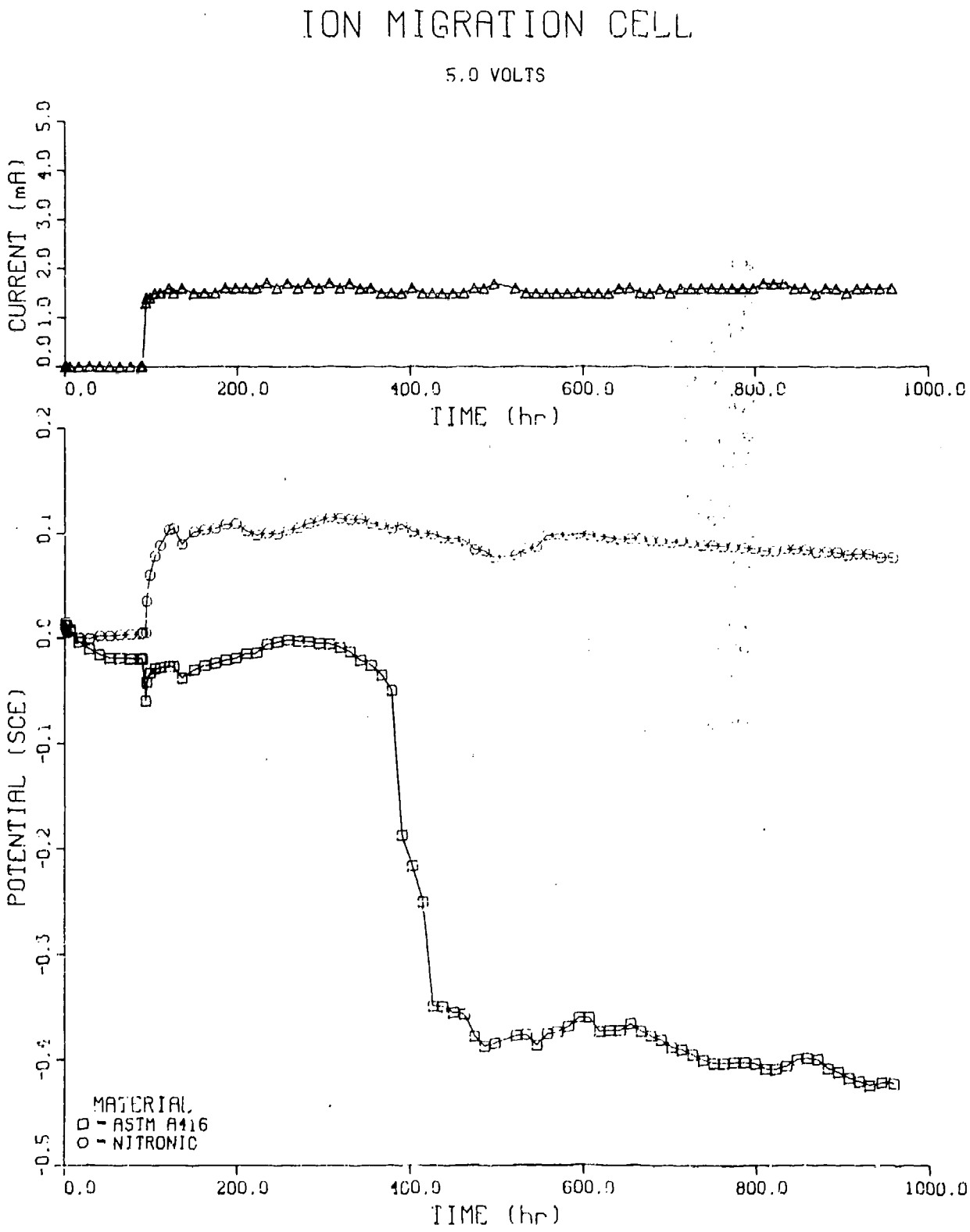

Figure 8. Tolerance of Nitronic 33 stainless steel and carbon steel to ion migration.

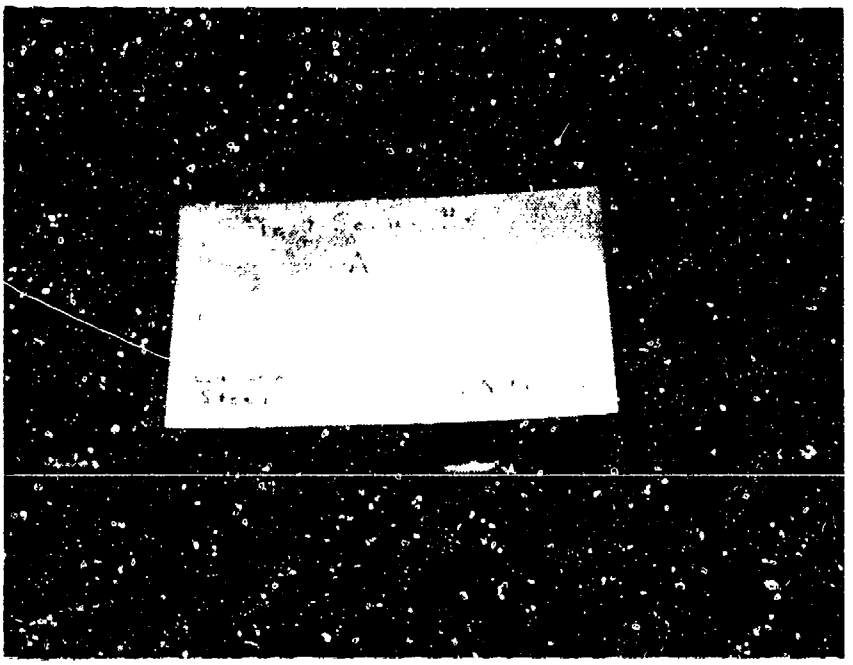

Figure 9. Tolerance of Nitronic 33 stainless steel and carbon steel to ion migration

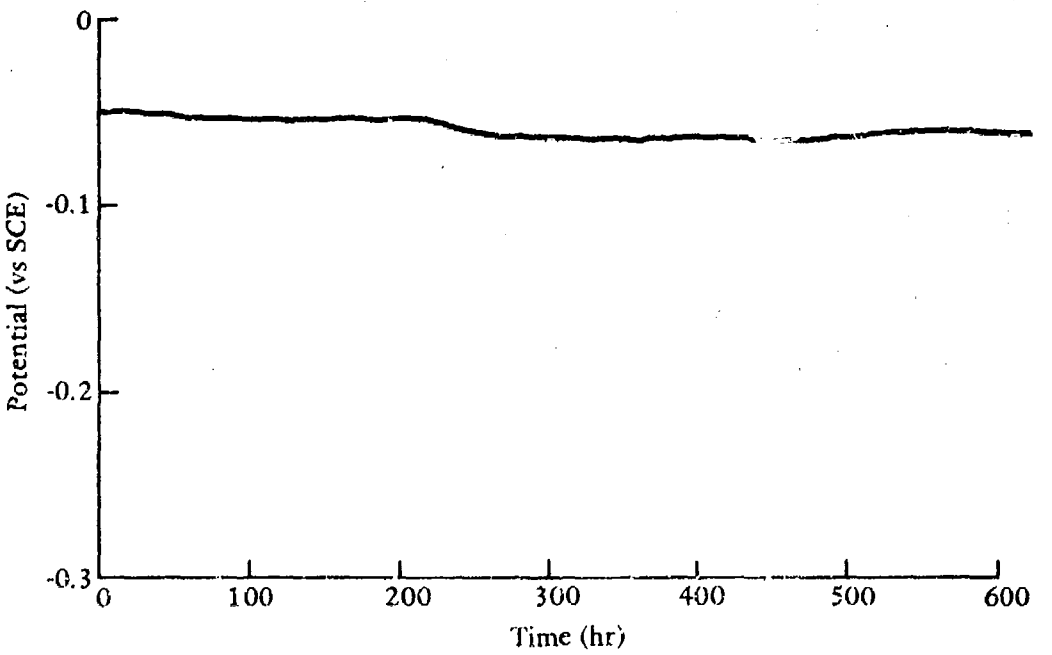

Figure 10. Corrosion potential versus time for carbon steel at a closed crack.

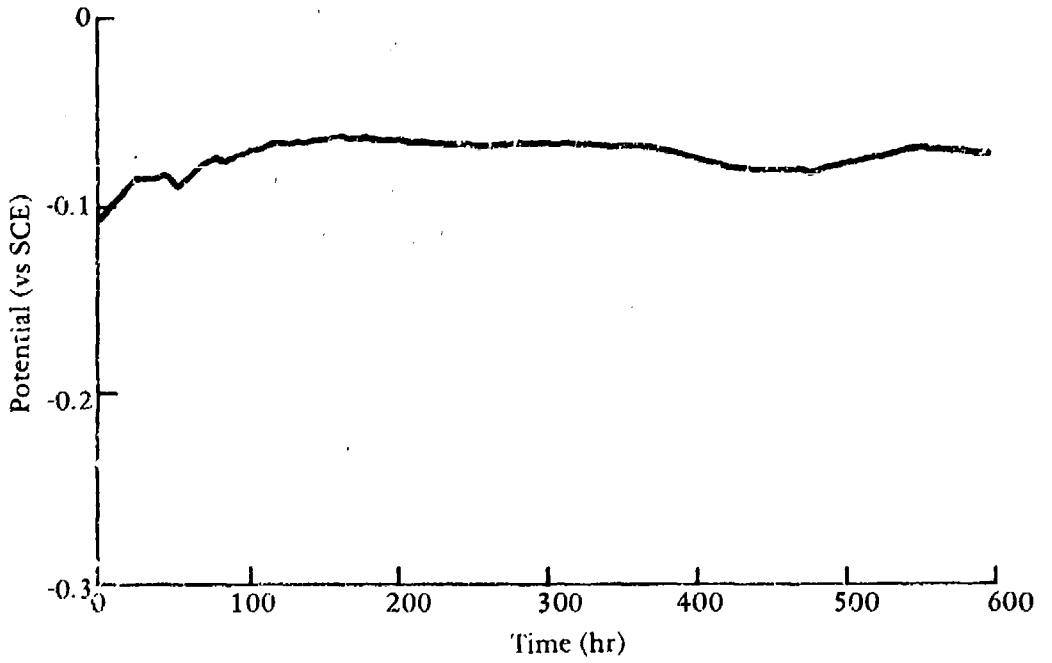

Figure 11. Corrosion potential versus time for Nitronic 33 stainless steel at a closed crack.

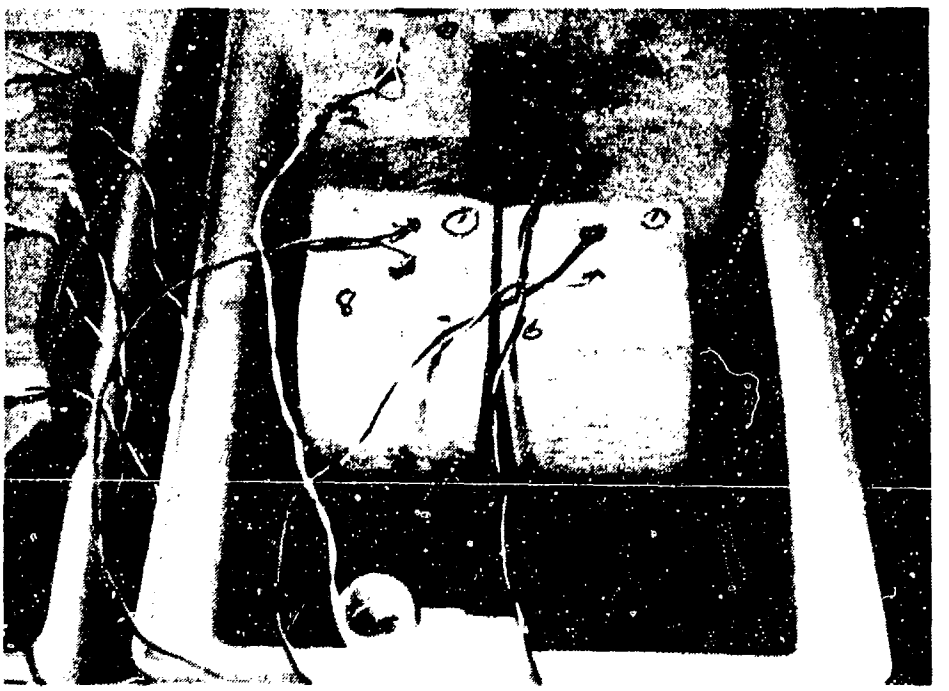

Figure 12. Setup for determination of depassivation at open cracks.

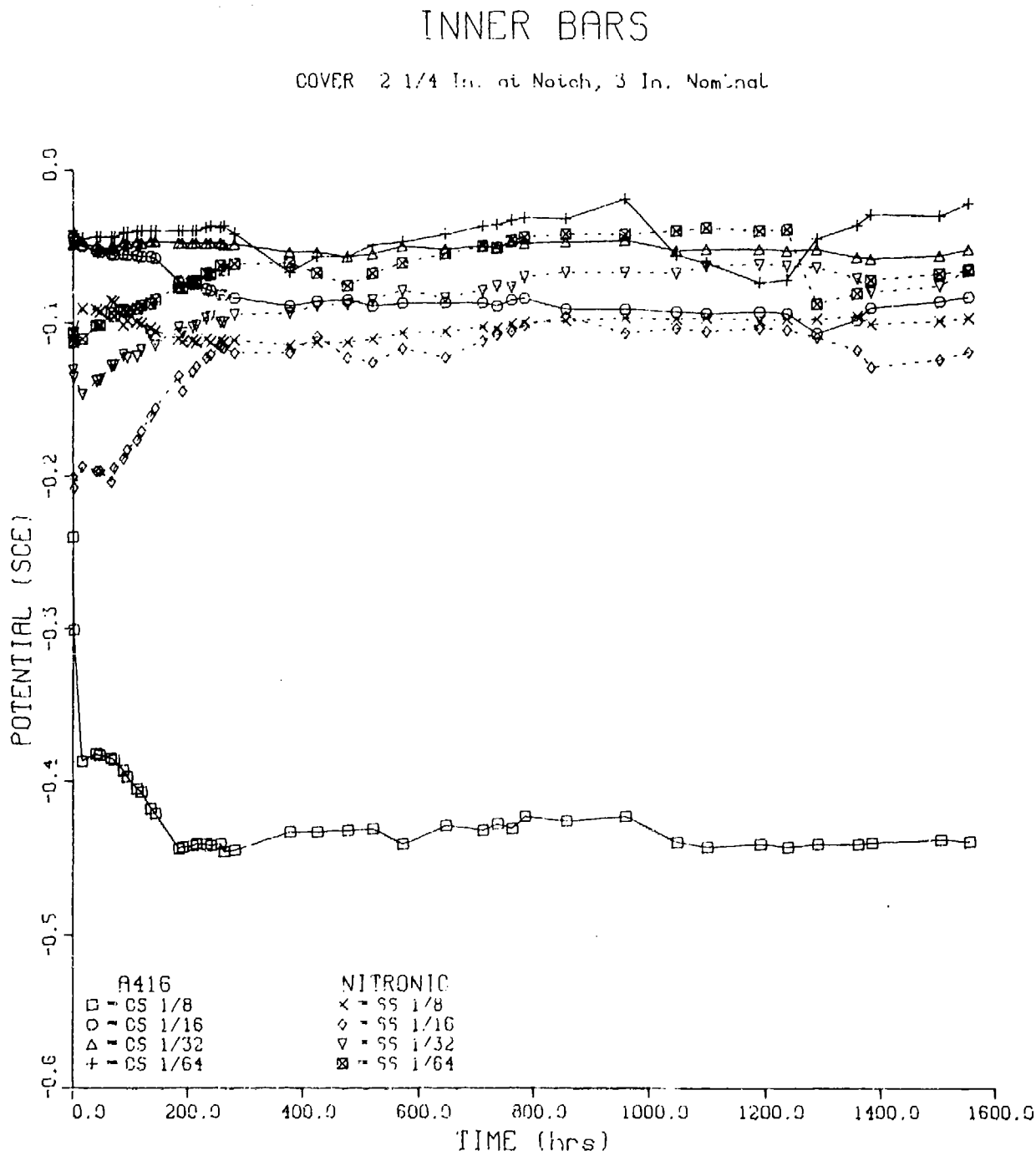

Figure 13. Potential versus time for inner bars at cracks.

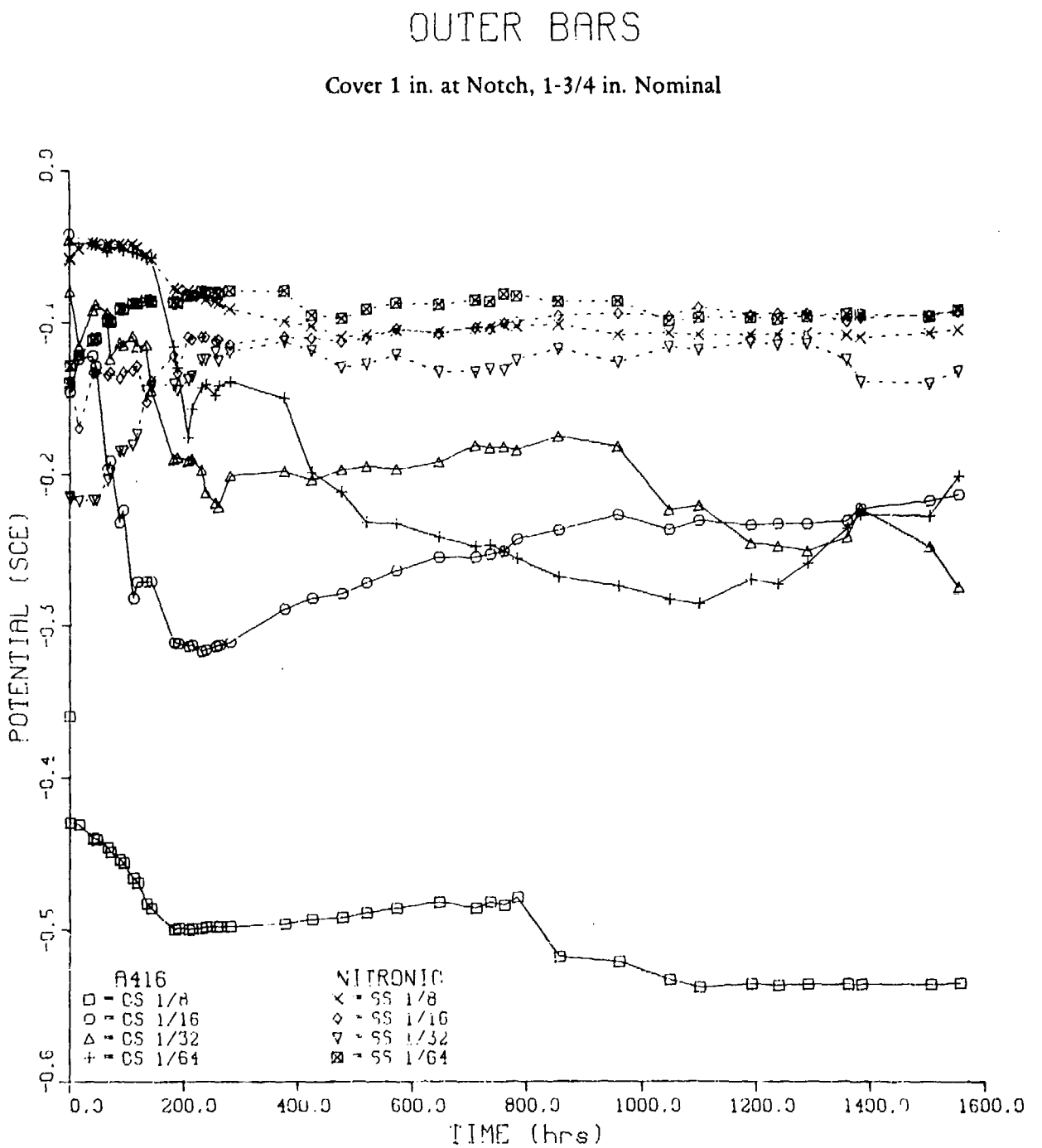

Figure 14. Potential versus time for outer bars at cracks.

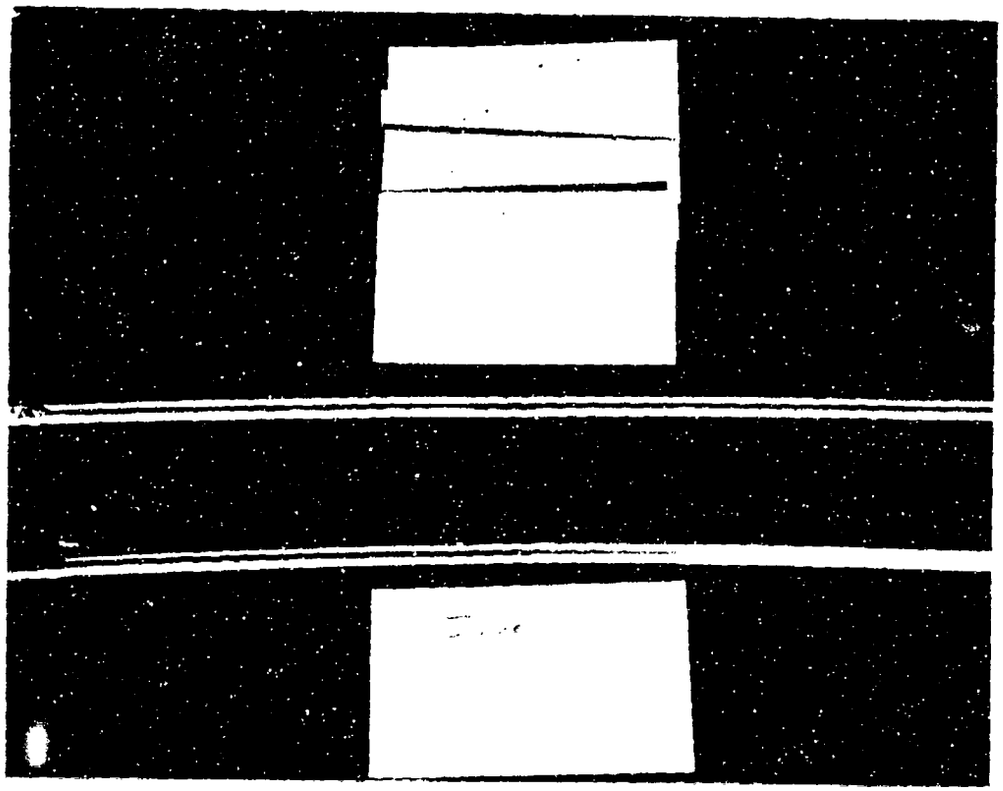

Figure 15. Nitronic 33 stainless steel bars from open crack tests.

Figure 16. Carbon steel bars from open crack tests.

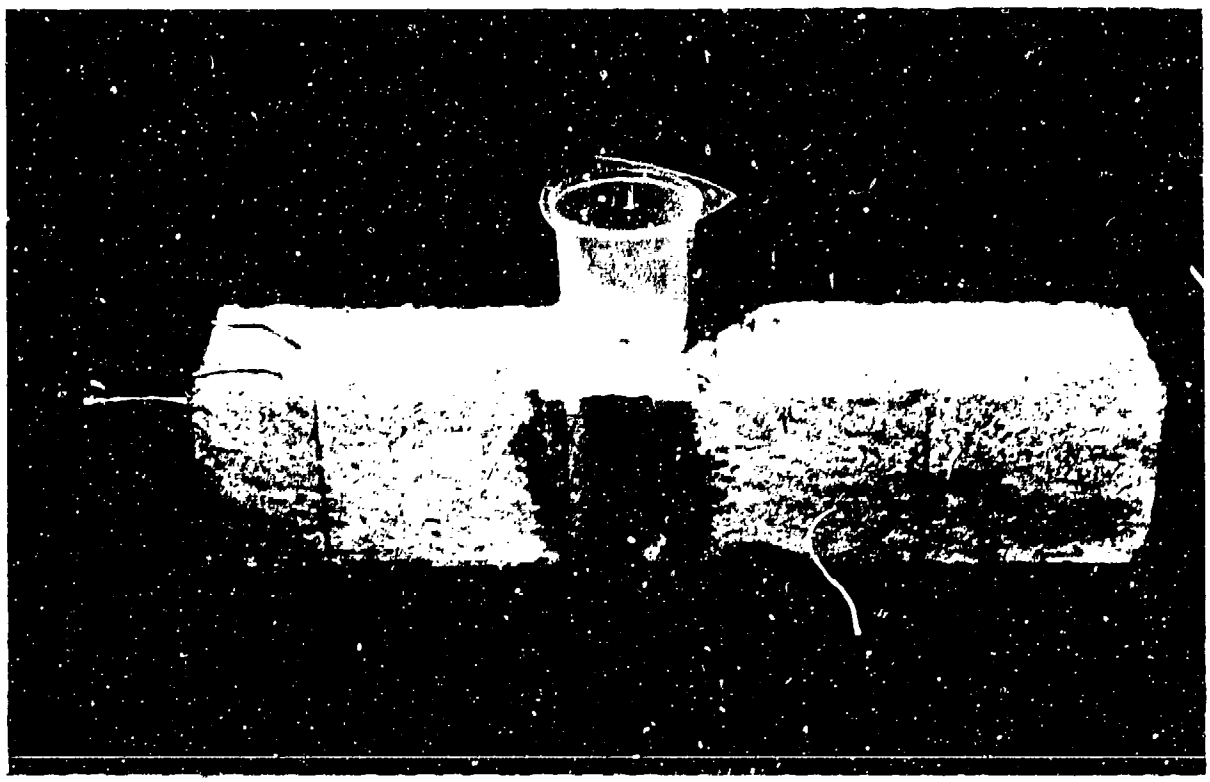

Figure 17. Test setup for depassivation at closed cracks.

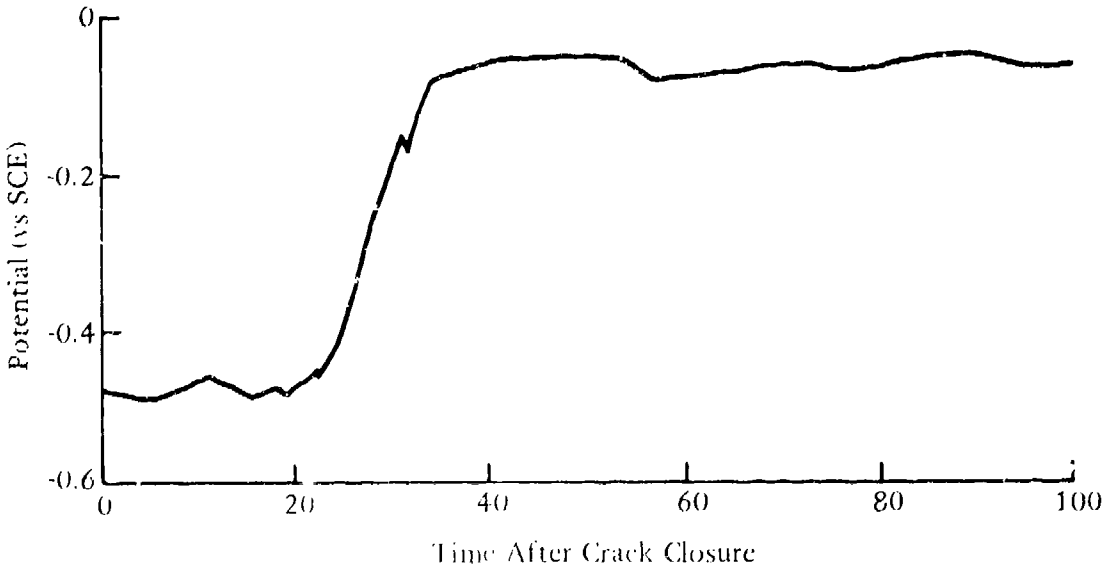

Figure 18. Repassivation of Carbon Steel after initiation of corrosion.

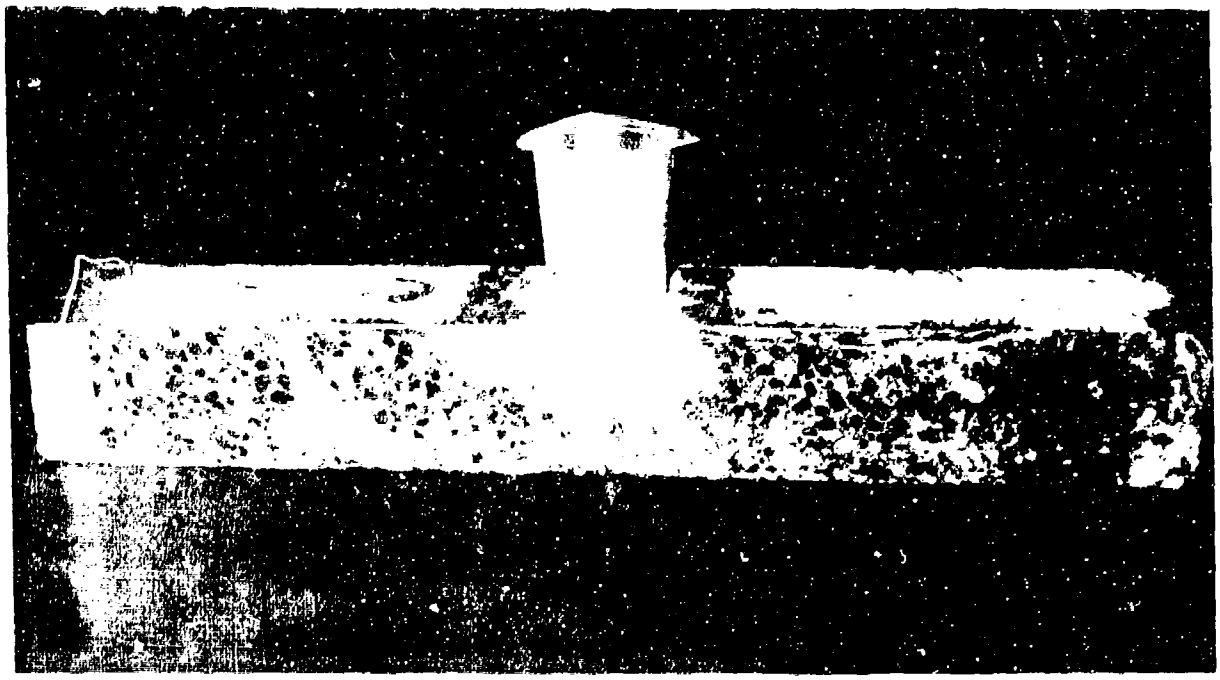

Figure 19. Test setup for the determination of the susceptibility of carbon steel and Nitronic 33 stainless steel strand in specimens cut from test pilings.

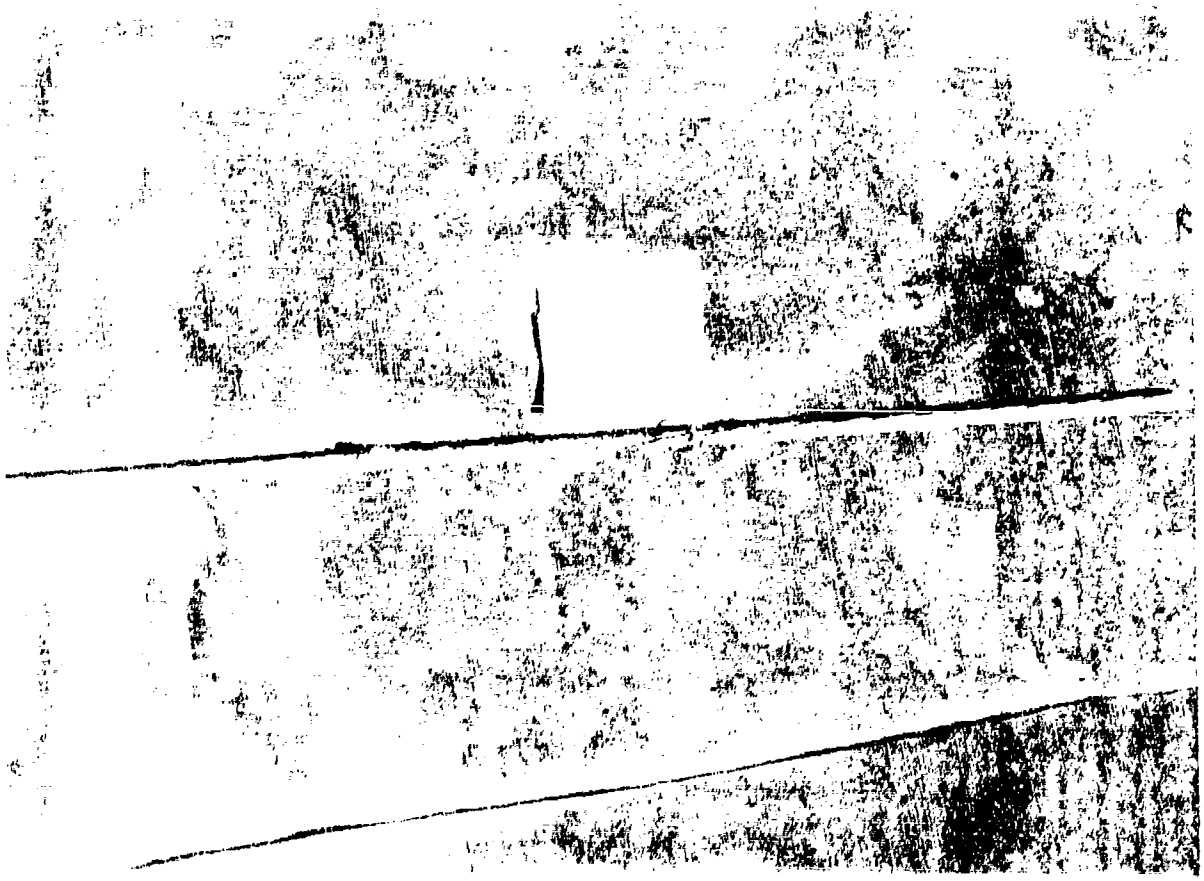

Figure 20. Carbon steel strand from piling specimen.

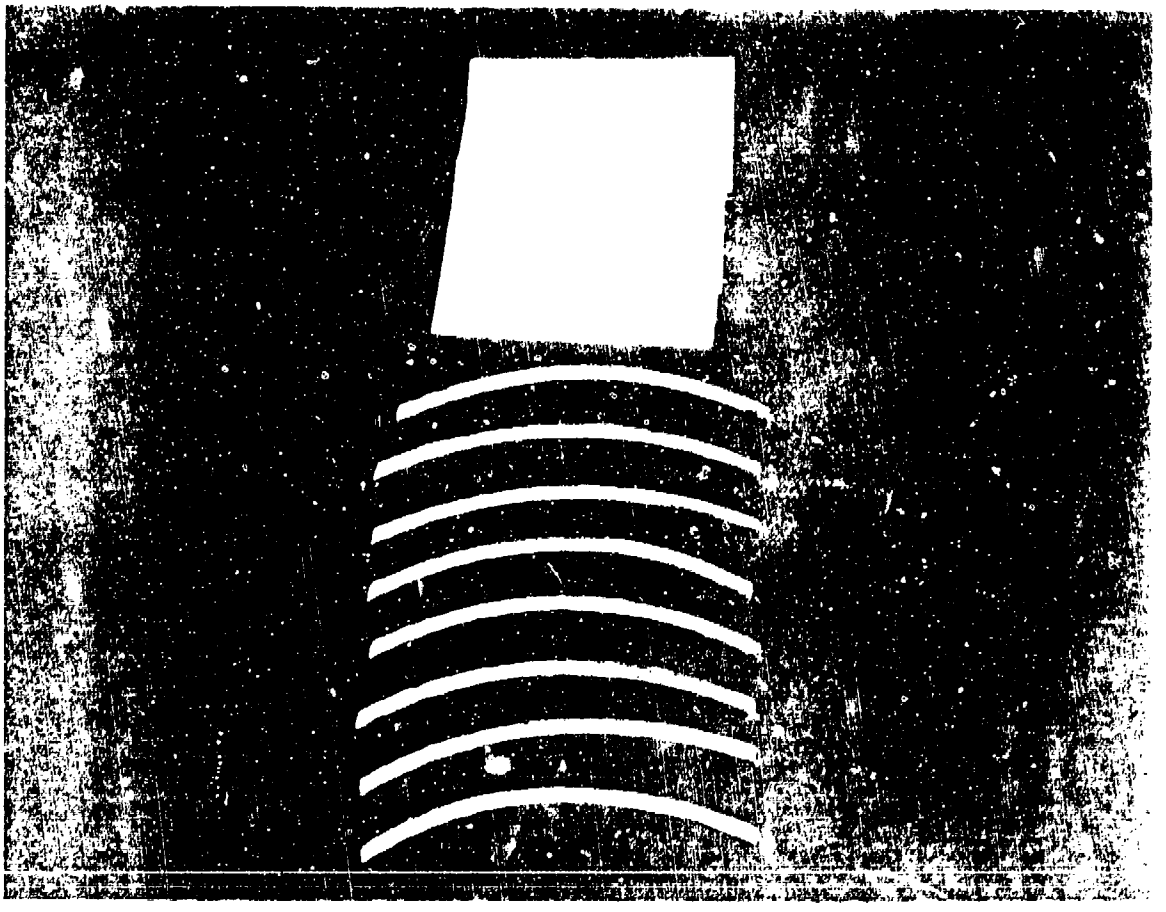

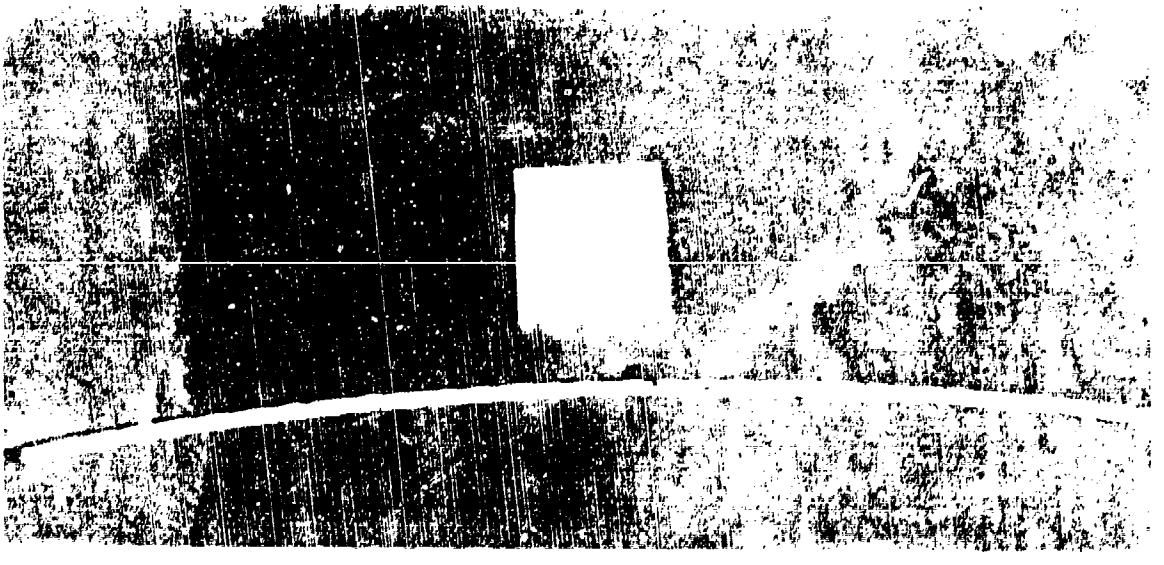

Figure 31. Nitronic 33 strand and Nitronic 33 spiral wrap from piling specimens.

NITRONIC PILE

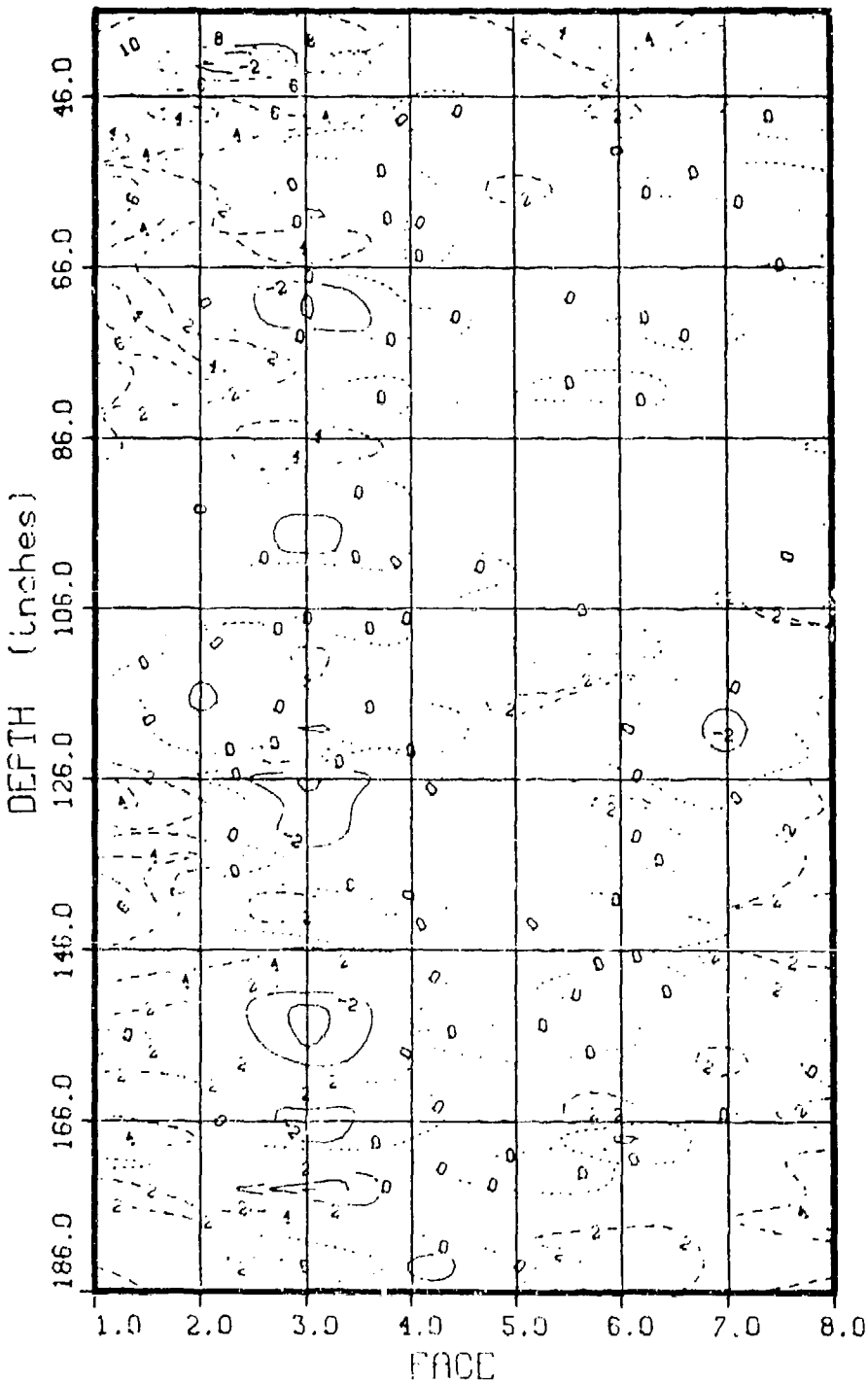

Figure 22. Current profile map - Nitronic 33 Piling.

☆ US GOVERNMENT PRINTING OFFICE 1987 - 548-054 80611